Platinum-group element mineralisation in the Shetland ophiolite complex

Thesis

Platinum-Group Element Mineralisation in the Shetland Ophiolite Complex

A thesis submitted for the degree of Doctor of Philosophy
by
Richard Alastair Lord
B.Sc. Hons. University of Bristol, 1985

Department of Earth Sciences
The Open University

May 1991

BRITISH LIBRARY

IMAGING SERVICES NORTH

Boston Spa, Wetherby
West Yorkshire, LS23 7BQ
www.bl.uk

ENCLOSURE MATERIAL NOT SCANNED BY REQUEST OF THE UNIVERSITY

Frontispiece:-

View west from the Cliff chromite quarry towards the basal thrust of the ophiolite complex, the Loch of Cliff, and the metamorphic basement gneisses beyond. Highly serpentinised chromite-rich dunite spoil from the tip in the foreground is enriched in Pd, Pt, Au and can contain up to 80 ppm Σ PGE. The highly altered serpentine matrix of such enriched chromite-bearing rocks exhibits an unusual verdant green colour when wet (e.g. below hammer head).

Abstract

The Shetland ophiolite complex exhibits the lower part of the definitive Penrose sequence, but chromitites from the Cliff locality contain levels of Pt and Pd which are unusual in ophiolites. Aspects of this mineralisation suggest both magmatic and hydrothermal concentration processes, although neither individually explain the observed paragenesis. This study examines the distribution of PGE within a representative fresh vertical section of the ophiolite stratigraphy, to assess the relative roles of such processes in the concentration and fractionation of PGE.

In the field area around Balta Sound, tectonised mantle harzburgites are overlain by a layered ultramafic cumulate sequence. Accessory Ni-Cu sulphides occur throughout these cumulates. Two stratigraphically controlled zones of chromite enrichment have been identified which mark the bases of cyclic repetitions. Such chromite enrichments lack progressive changes in mineral chemistry so repetitions within the cumulate sequence are attributed to influxes of primitive magma during open system fractionation.

The distribution of PGE and other chalcophiles show primary lithological associations, indicating a magmatic origin. Os-Ir-Ru concentrations occur in chromitites, whereas Pt-Pd-Rh concentrations occur in sulphide-bearing dunites, chromite-rich dunites, or basal pyroxenites. Stratigraphically controlled zones of PGE-enriched sulphide-bearing cumulate dunites occur close to the base of each cyclic repetition and are continuous over a strike-length of 2 km. The fractionation between PGE and other chalcophiles is consistent with magmatic processes.

The distribution and fractionation of PGE can be explained by an open system model. Negative slope patterns are produced by the precipitation of PGM from PGE saturated magmas during chromite crystallisation. This initial process buffers the PGE concentrations in each primitive magma pulse. On entering the axial chamber and mixing with the evolving resident magma, sulphide saturation occurs and the remaining PGE are partitioned into immiscible sulphide liquids. Multiple inputs result in repeated PGE enriched zones. This model explains why successive stratigraphic PGE-enriched horizons have similar positive slope patterns but progressively fractionated host silicate and sulphide compositions.

Acknowledgements

I would like to thank my supervisors Dr H. M. Prichard and Dr C. R. Neary for conceiving this project and, in particular, for their enthusiastic encouragement and searching manuscript comments respectively. I would also like to thank Professor. I.G. Gass for his continuing support of this research group and this particular aspect of ophiolite geology.

Funding for this project has come from a variety of sources and in various amounts. I began the work as a research assistant to the EEC Raw Materials Programme MSM 089 UK (H) "Development of techniques for the determination of the platinum-group elements in ultramafic rock complexes of potential economic significance: mineralogical studies". This rapidly led to a studentship, for which I thank the Open University Higher Degrees Committee and the student (I never met) from whom I inherited it.

By far the greatest part of the financial support has come from the M.I.R.O. Research Programme Contract RC 48. I thank the sponsors Riofinex North and Consolidated Goldfields and especially Dr C.J. Morrissey for his continued interest in the progress of the project. Also Mr N. Roberts and Dr S. Cribb of M.I.R.O. who originated and administered this collaboration between industry and academia. This funding provided all field work and analytical costs and a further two years research assistantship to continue the research well beyond that included in this thesis.

Finally, I thank the Open University Research Committee for my current research fellowship studying platinum in Brazil.

While at the Open University I have been helped by just about everybody at some stage but I particularly thank Ian Chaplin for thin sections, Andy Tindle for microprobe and macintosh instruction, Nick Rogers for INAA tuition, Phil Potts for ß-autoradiography and advice on analytical techniques, John Taylor for drafting the base maps and lastly John Watson for the prompt delivery of a vast number of XRF analyses.

In the course of this study I have spent over a year on Unst. While the weather is not always ideal it is always changeable. I thank Simon Tear of Riofinex for advice and practical instruction in various "industrial" techniques including pionjar sampling, diamond saw channel sampling, drill siting, drillers, graphic logging and core splitting. Thanks go to all the Shetlanders and residents of Unst for their warm hospitality and the inevitable query "Boy, ist do a RAFeen?". In particular I thank the Johnsons for accommodation, the Sandisons for flats, shipping and the loan of heavy plant, the Ritchs "O Gerratoun" for lodgings, practical crofting experience, advice on drinking and their daughter, Mike Pennington for hints on ornithology, cetaceanology and island ticking, Piffy for linguistic advice, and everybody else in "Springer's".

At home I thank my parents for financial support and continual encouragement , Anna for advice on higher degrees, all my friends for putting up with my globetrotting and sudden disappearances but especially Gords. Finally I thank Lynn for reminding me about "when you finish your thesis" and Nelson, Oölet and Tröoker for never mentioning it.

Originality

This thesis forms part of the larger M.I.R.O research project (RC 48) by Dr H.M. Prichard and R.A. Lord entitled "Platinum Mineralisation in the Shetland Ophiolite Complex". In such circumstances it is a requirement of university rules that the thesis indicates any parts which are not the candidates independent contribution to the work. These are as follows:-

Chapter 3 - Chromite Mineral Chemistry

The chromite specimens used were originally collected by H. Prichard as part of the E.E.C raw materials programme (EUR 11631).

Chapters 5 and 7 - Samples from the Cliff locality

Some of the later samples from this locality were collected jointly by Dr H.M. Prichard and R.A. Lord.and analysed within the M.I.R.O. project. These are identified as such when quoted. The interpretation of this data, in particular the suggestion of hydrothermal remobilisation of magmatic mineralisation, is an independent contribution and as such does not necessarily reflect the views of other co-workers.

Chapter 5 - Mineralogical Data

The mineralogical data presented, including that on samples from this thesis, has been compiled from the work of Dr H.M. Prichard and Dr R.A. Ixer. This data has been reinterpreted with regard to its bearing on the discrimination of hydrothermally remobilised mineralisation at Cliff.

I confirm that the above is a true statement and that, subject to any comments above, the thesis is my own, original work.

Richard Lord

Contents

List of Figures

Chapter 1

Chapter 2

Chapter 3

Chapter 4

Chapter 5

Chapter 6

Chapter 7

List of Tables

Chapter 1

Chapter 2

Chapter 3

Chapter 4

Chapter 5

Chapter 6

Chapter 7

Chapter 8

List of Plates

Chapter 2

Chapter 6

Chapter 1

Regional Geology, Previous Investigations and Aims of the Present Study

1.1 Introduction:- The discovery of platinum in Unst

The Shetland Isles lie 200 miles north of Aberdeen and 220 miles west of Scandinavia. Unst, the most northerly island of the group is on the same latitude as Bergen in Norway and Cape Farewell in Greenland (figure 1.1).

Early investigators soon recognised the potential of the chromite-rich serpentinites on Unst as suitable hosts to platinum-group element (PGE) mineralisation. The first assays, published by Hitchen in 1929, reported 1 dwt platinum metals per ton (equivalent to 1.3 ppm) in chromite concentrates taken from the chromite ore crushing mill. In addition to platinum the presence of some palladium, iridium, and "osmiridium" was established. Further assays reported lower concentrations of these metals, causing Hitchen to conclude, "platinum as being generally present in the chrome concentrates from this area but in proportions which vary very considerably".

The extent and origin of these PGE concentrations remained unconfirmed for over fifty years. During this period significant advances were made in the analytical capability for PGE and as a result knowledge of the typical geological associations of these elements increased. Concentrations of platinum and palladium were known to occur in large layered intrusions (e.g. Bushveld complex, S. A.) and in Ni-Cu sulphide-bearing mafic or ultramafic rocks from a variety of continental settings (Naldrett & Duke, 1980; Naldrett, 1981). In contrast, only minor concentrations of PGE were known in podiform chromites from ophiolite complexes (Naldrett & Cabri, 1976) within which the levels of osmium, iridium and ruthenium greatly exceeded those of rhodium, platinum and palladium (Page et al., 1982a).

Figure 1.1. Location of Unst and the study area.

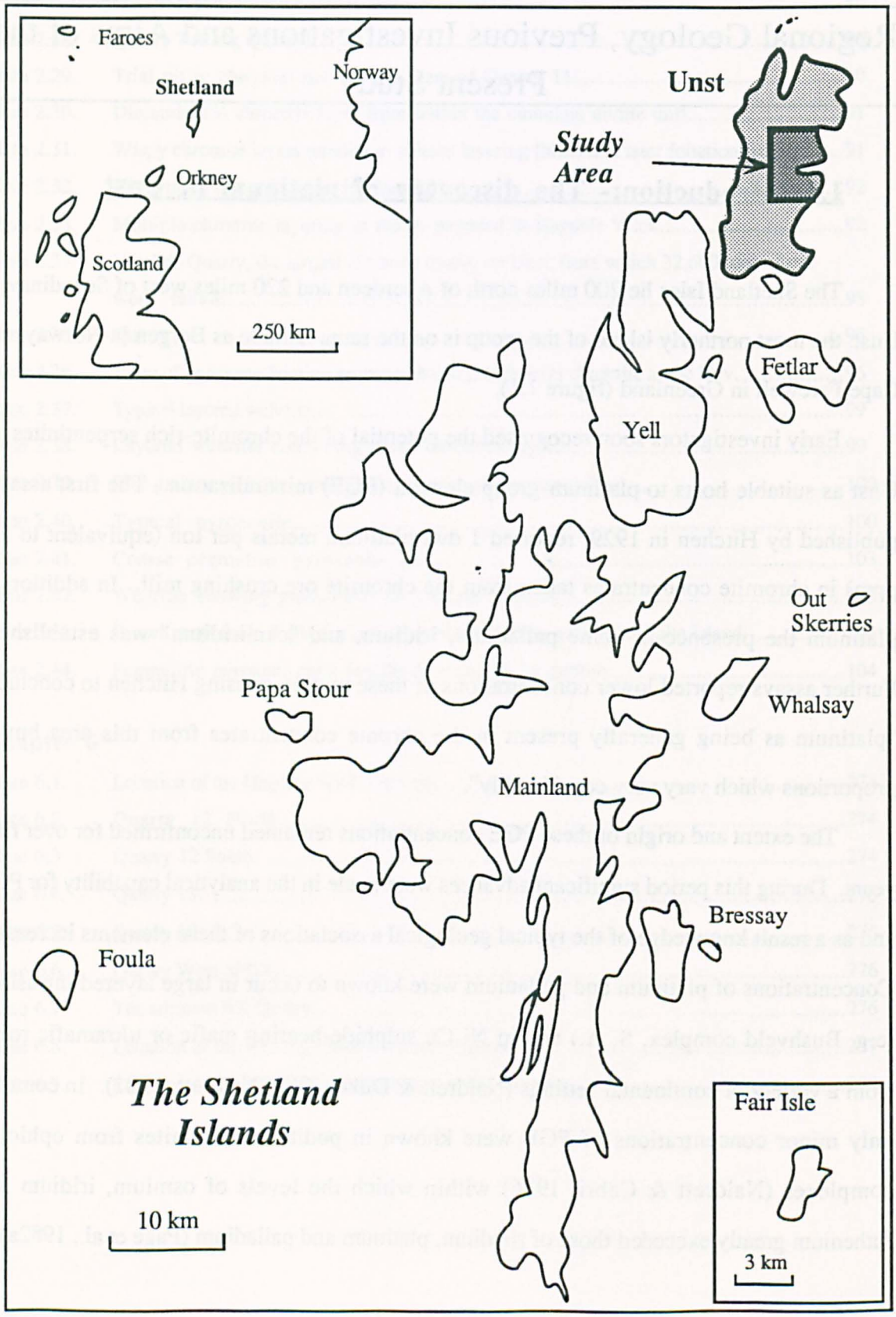

For example, Ru followed by Os and Ir were reported as the most abundant PGE in Cyprus (Constantinides et al., 1980).

The Unst basic-ultrabasic rocks where first recognised as ophiolitic in a review of the alpine-type ultramafic rocks of the Scottish Highlands (Garson and Plant, 1973). This suggestion was confirmed by re-examination of the complex (Flinn, 1985; Prichard, 1985), stimulated by renewed economic and strategic interest in the contained chromite concentrations (Gass et al., 1982). Identification of the complex as an ophiolite called into question the validity of the earlier analyses, since both the absolute and relative PGE concentrations were unusual compared with those reported in other ophiolites.

This introductory chapter considers first the geochemistry and occurrence of the PGE. The concept of an ophiolite is then defined, with a review of the published evidence that the Unst ultramafic complex is indeed ophiolitic. Recent work on PGE in the complex is considered, in particular a survey of the PGM (Prichard et al., 1986) and PGE distributions (Gunn et al., 1985). The resulting controversy regarding the origin of both the PGE concentrations and the complex are then discussed. This forms the background to the specific aims and approach of this study.

1.2 The platinum-group elements

1.2.1 General geochemistry

The six elements osmium, iridium, ruthenium, rhodium, platinum and palladium (Os, Ir, Ru, Rh, Pt, Pd) are a group of metals with similar physical properties (table 1.1). Most notable of their chemical properties is their resistance to aqueous reagents and oxygen, classifying them, together with gold, as "noble" metals (Westland, 1981). Geochemically the PGE show strong chalcophile behaviour combining with sulphur in preference to oxygen. They show siderophile character in the absence of chalcogens (Westland, 1981).

Table 1.1. Physical properties of the platinum-group elements.

Element	*Os*	*Ir*	*Ru*	*Rh*	*Pt*	*Pd*
Melting point (°C)	3050	2454	2334	1967	1768	1555
Atomic number	76	77	44	45	78	46
Relative atomic mass	190.2	192.2	101.1	102.91	195.09	106.4
Atomic radius (cm^{-8}, 12-fold coordination)	1.350	1.355	1.336	1.342	1.385	1.373
Covalent radius (cm^{-8})	1.255	1.260	1.241	1.247	1.290	1.278

(from sources quoted in Westland, 1981)

The PGE have chemical properties similar to other Group VIII transition metals including nickel, iron and cobalt. Consequently these elements are all concentrated together by geological processes (Naldrett, 1981). This includes those processes leading to the formation of the earth, during which the siderophile PGE were effectively fractionated into the core and mantle and strongly depleted from the crust (table 1.2). Transfer of PGE from the mantle may occur by tectonic emplacement of mantle material into the crust, or by melting of the mantle and crystallisation of the resulting magma in the crust (Naldrett, 1981). The formation and emplacement of ophiolites (Chapter 1.3) is therefore a suitable transfer mechanism and ophiolitic sequences represent a potential crustal source of PGE.

Table 1.2. Cosmic and terrestrial abundance of platinum-group elements (ppm).

Element	*Fe*	*Ni*	*Ir*	*Pt*	*Pd*
Carbonaceous Chondrites	184,000	10,300	0.540	1.02	0.545
Total Earth (32% core, 68 % mantle)	334,000	30,000	1.14	2.79	1.35
Earth's Crust	50,000	75	0.001	0.005	0.001
Earth's Mantle (Alpine Peridotite)	60,000	2,500	0.006	0.073	0.018
Earth's Core (Iron Meteorite)	907,000	88,000	3.53	8.45	3.82

(from sources quoted in Naldrett, 1981)

1.2.2 Classification of PGE deposits

Subsequent concentration of the PGE is required to form an orebody, since current platinum deposits are mined at levels of 5 ppm or greater, 70 times the level in the mantle (Naldrett, 1981). The strong chalcophile nature of the PGE predicts effective partitioning of these elements into immiscible sulphide droplets contained within a silicate magma, with concentration of the metals by factors of 100 to 1000 (Naldrett & Duke, 1980). As a consequence, concentrations of igneous nickel-copper sulphides also represent an important type of PGE deposit (table 1.3). Examples of these Ni-Cu sulphide dominant PGE deposits include those of Sudbury, Canada and Noril'sk, USSR.

Table 1.3. Classification of PGE deposits.

Classification	*Example*
A. PGE Dominant Deposits	
(1) Merensky-type	Merensky Reef, Bushveld
(2) Hydrothermal deposits	New Rambler, Wyoming; Messina, SA
(3) Placer deposits	Nizhnii-Tagil, Urals
B. Ni-Cu Dominant Deposits	
(I) Astrobleme	Sudbury, Canada
(II) Flood basalt/rifting related intrusions	Noril'sk, Siberia
(III) Precambrian greenstone belt magmatism	
(a) Tholeiitic intrusions	Pechenga, Kola Peninsular, USSR
(b) Komatiitic lavas & intrusions	Kambalda, WA
(IV) Phanerozoic orogenic tholeiitic intrusions	Råna, Norway

(from Naldrett 1981)

Volumetrically more important PGE-dominant Ni-Cu sulphide-bearing deposits occur in very large layered basaltic intrusions in cratonic settings. These include the Merensky and UG-2 Reefs in the Bushveld Complex, SA and the J-M Reef in the Stillwater Complex, USA. The origin of these deposits has also been attributed to the results of segregation of

immiscible sulphide liquids, although other workers have stressed the role of late-stage magmatic or hydrothermal fluids (see Naldrett & Barnes, 1986).

The action of secondary processes on a PGE-bearing igneous source may also form PGE-dominant deposits. A hydrothermal origin is suggested for the New Rambler deposit, USA (McCallum et al., 1976) and the Rathbun Lake occurrence, Canada (Rowell & Edgar, 1986). Placer deposits have been mined in the USSR, Canada, Colombia and USA derived from Alaskan- or Alpine-type ultramafic bodies (Naldrett, 1981).

Surveys of background levels of PGE in sulphide-poor igneous rocks indicate a progressive decrease in the average PGE content from ultramafic, through mafic to intermediate and felsic compositions (Crocket, 1981). Fractional crystallisation depletes Ir and probably also Os and Ru from mafic magmas more strongly than other PGE producing a fractionation trend of increasing Pd/Ir ratio with increasing evolution. A close association between concentrations of chromite and higher levels of PGE is also apparent in rocks from many different environments, including Alaskà-type complexes, ophiolites and layered stratiform mafic-ultramafic complexes, although genetic interpretation of this association is varied (Crocket, 1981).

1.2.3 PGE in ophiolite complexes

Published PGE analyses and average concentrations reported in ophiolitic rocks (up to 1985) are listed in table 1.4. There is a virtual absence of complete analyses of all six platinum-group elements. Of concern also are the relatively high detection limits particularly for Ru and Ir in the more complete analyses published by Page and co-workers. For these reasons average analyses have been calculated, where these are not already given in the source publication, and the data has been treated graphically. Figure 1.2 shows the reported concentrations of PGE in ophiolitic chromitites compared to silicate rocks. It is apparent that generally higher levels of all PGE occur in chromitites than in silicate lithologies.

Figure 1.2. Graphical comparison of the average PGE concentrations in ophiolite chromitites and silicates (data from table 1.4).

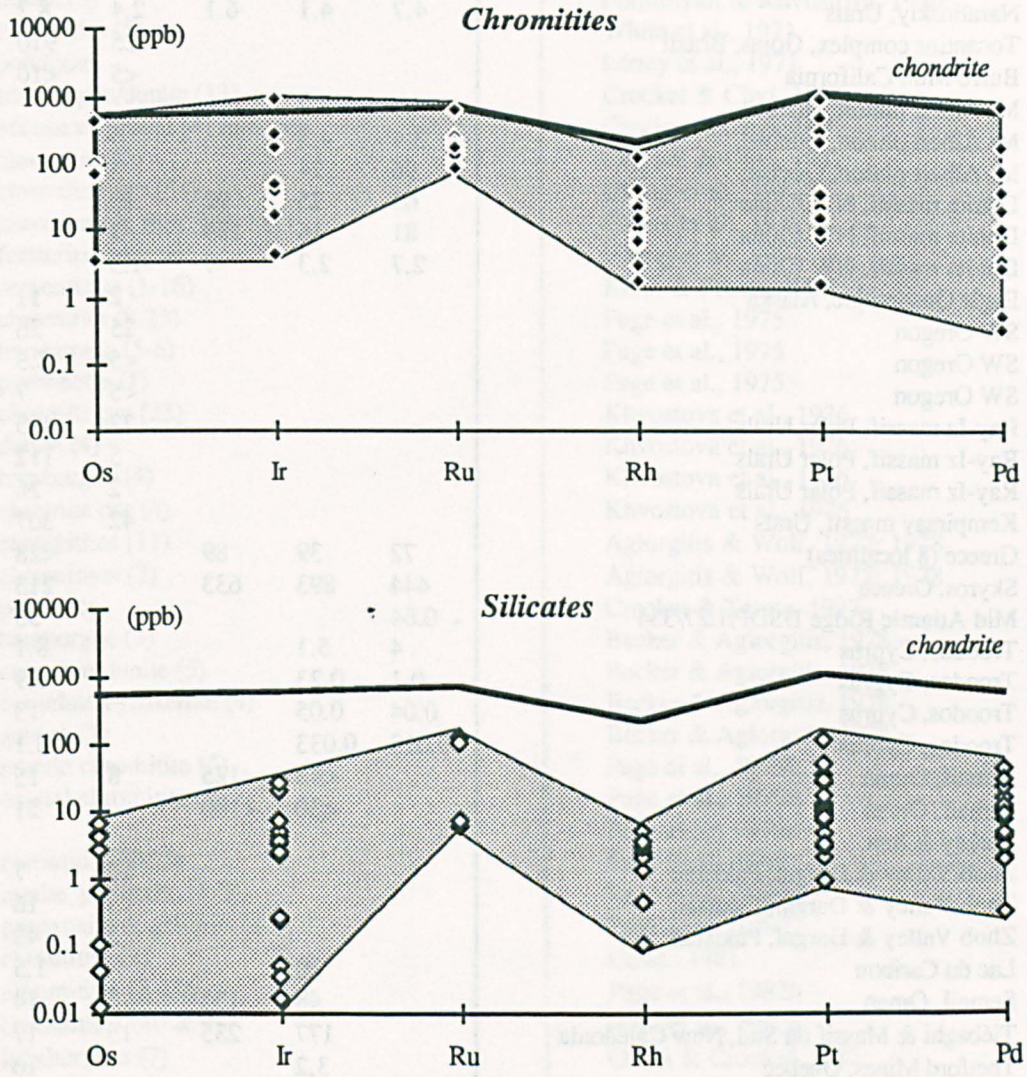

By convention, analyses of a single sample for all six PGE are normalised to chondrite and plotted on a spidergram in the order Os, Ir, Ru, Rh, Pt, Pd and Au (Naldrett et al., 1979). This procedure produces smooth patterns which are characteristic of different Ni-Cu sulphide deposits and reflect the degree of evolution of primitive magmas at the time of sulphide saturation (Naldrett & Duke, 1980). Variations in PGE tenor due to variations in sulphide ore content may be further corrected by recalculating the analysis to 100% sulphide (Naldrett et al., 1979).

Table 1.4. Average PGE concentrations reported from ophiolite complexes (up to 1985).

	Ophiolite Complex	*Os*	*Ir*	*Ru*	*Rh*	*Pt*	*Pd*
		Average PGE concentrations (ppb)					
1	Red Mtn./Cypress Is./Twin Sisters USA				<5	<10	<4
2	Naralinskiy, Urals	4.7	4.1	6.1	2.4	8.2	2
3	Tocantins complex, Goias, Brazil				125	910	170
4	Burro Mtn, California				<5	<10	<4
5	Mt Albert pluton, Quebec	6.7	2.2				9.5
5	Mt Albert pluton, Quebec	3.4	4.3				24
5	Mt Albert pluton, Quebec	96	24				0.5
6	Dunite massif, NW China	63	25	92	10		
6	Dunite massif, NW China	81	16	159	7		
6	Dunite massif, NW China	2.7	2.3	7	1.3		
7	Eagle Quadrangle, Alaska				2	11	7.5
8	SW Oregon				25	26	7.5
8	SW Oregon				<5	8.3	8.4
8	SW Oregon				<5	7	2
9	Ray-Iz massif, Polar Urals				22	475	79
9	Ray-Iz massif, Polar Urals				5	112	15
9	Ray-Iz massif, Polar Urals				2	26	4
10	Kempirsay massif, Urals				42	307	700
11	Greece (8 localities)	72	39	89		<28	<3.6
12	Skyros, Greece	444	893	633		213	38
13	Mid Atlantic Ridge DSDP/L27/334	0.64				35	41
14	Troodos, Cyprus	4	5.1			8.1	
14	Troodos, Cyprus	0.1	0.23			0.9	
14	Troodos, Cyprus	0.04	0.05			13	
14	Troodos, Cyprus	0.013	0.033			3.1	
15	Semail, Oman		<43	<125	8	15	7
15	Semail, Oman		<30	<100		21	11.5
16	Turkey & Iran						
17	Zhob Valley & Dargai, Pakistan				10	7	20
17	Zhob Valley & Dargai, Pakistan				<3	16	10
17	Zhob Valley & Dargai, Pakistan				5	48	42
18	Lac du Caribou		30			1.5	0.3
19	Semail, Oman		48	135	6	14	8
20	Tiébaghi & Massif du Sud, New Caledonia		177	235	15	17	3.2
21	Thetford Mines, Quebec		3.2			10	3.8
21	Thetford Mines, Quebec		3.6			2.1	0.29
21	Thetford Mines, Quebec		30			1.5	0.33
21	Thetford Mines, Quebec		2.4			28	21
21	Thetford Mines, Quebec		0.24			17	29
21	Thetford Mines, Quebec		0.017			4.5	3
22	Voikar-Syninsky, Polar Urals		36.8	185	1.7	7.5	3.9
22	Voikar-Syninsky, Polar Urals		48	<250	3	13.3	10.3
22	Voikar-Syninsky, Polar Urals		<20	120	0.42	9.5	11.8
22	Voikar-Syninsky, Polar Urals				<0.1	3	1.9
22	Voikar-Syninsky, Polar Urals		33	<200	7	14.4	3.6
23	Bati Kef, Guleman-Elazig, E. Turkey		35.9	80	7.2	9.5	2.7
24	All Newfoundland (8 areas)		<20	<100	3	8.2	8.7
24	All Newfoundland (8 areas)		25	<100	3.6	3.1	4.5
24	All Newfoundland (8 areas)		49	173	6.5	35	5.8
25	Josephine & Onion Mountain, SW Oregon		6.9				
25	Josephine & Onion Mountain, SW Oregon		13-1159				

Table 1.4. (continued).

	Rock type (no. samples)	*Source*
1	Dunite, peridotite	Page, 1969
2	dunite (5)	Forminykh & Khvostova, 1970
3	chromitite (5)	White et al., 1971
4	peridotite	Loney et al., 1971
5	harzburgite/dunite (13)	Crocket & Chyi, 1972
5	accessory spinel (4) min. sep.	Crocket & Chyi, 1972
5	chromitite (2)	Crocket & Chyi, 1972
6	chromitite ore (34)	Chang et al., 1973
6	chromite ore min. sep. (11)	Chang et al., 1973
6	forsteritic gangue	Chang et al., 1973
7	serpentinite (1-16)	Keith & Foster, 1973
8	chromitite (8-23)	Page et al., 1975
8	harzburgite (5-6)	Page et al., 1975
8	pyroxenite (1)	Page et al., 1975
9	chromite ore (23)	Khvostova et al., 1976
9	dunite (4)	Khvostova et al., 1976
9	harzburgite (4)	Khvostova et al., 1976
10	chromite ore (4)	Khvostova et al., 1976
11	chromitites (11)	Agiorgitis & Wolf, 1977; 1978
12	chromitites (2)	Agiorgitis & Wolf, 1977; 1978
13	peridotite	Crocket & Teruta, 1977
14	harzburgite (3)	Becker & Agiorgitis, 1978
14	cumulate dunite (5)	Becker & Agiorgitis, 1978
14	cumulate pyroxenite (4)	Becker & Agiorgitis, 1978
14	gabbro (7)	Becker & Agiorgitis, 1978
15	mantle chromitite (5)	Page et al., 1979b
15	crustal chromitite (1)	Page et al., 1979b
16		Page et al., 1979a
17	chromitite (4-25)	Page et al., 1980
17	dunite, peridotite (1-3)	Page et al., 1980
17	pyroxenite & gabbros (1-7)	Page et al., 1980
18	chromitite (2)	Oshin, 1981
19	chromitites (8-23)	Page et al., 1982b
20	chromitites (40 & 3)	Page et al., 1982a
21	harzburgites (7)	Oshin & Crocket, 1982
21	dunite pods (4)	Oshin & Crocket, 1982
21	olivine-chromitite cumulate (2)	Oshin & Crocket, 1982
21	cumulate dunite (13)	Oshin & Crocket, 1982
21	cumulate pyroxenite (12)	Oshin & Crocket, 1982
21	gabbro (4)	Oshin & Crocket, 1982
22	tectonites [incl chromitites] (4-20)	Page et al., 1983
22	mafic/ultramafic cumulates [inc. chrt] (1-20)	Page et al., 1983
22	gabbros (2-13)	Page et al., 1983
22	dykes (2-3)	Page et al., 1983
22	chromitites (14-3)	Page et al., 1983
23	chromitites (7-26)	Page et al., 1984
24	harzburgites (6)	Page & Talkington, 1984
24	dunites (9)	Page & Talkington, 1984
24	chromitites (7)	Page & Talkington, 1984
25	peridotites (9)	Stockman & Hlava, 1984
25	chromitites	Stockman & Hlava, 1984

Figure 1.3. Chondrite-normalised diagram of PGE concentrations in ophiolitic chromitites compared to stratiform chromitites (from Page & Talkington, 1984).

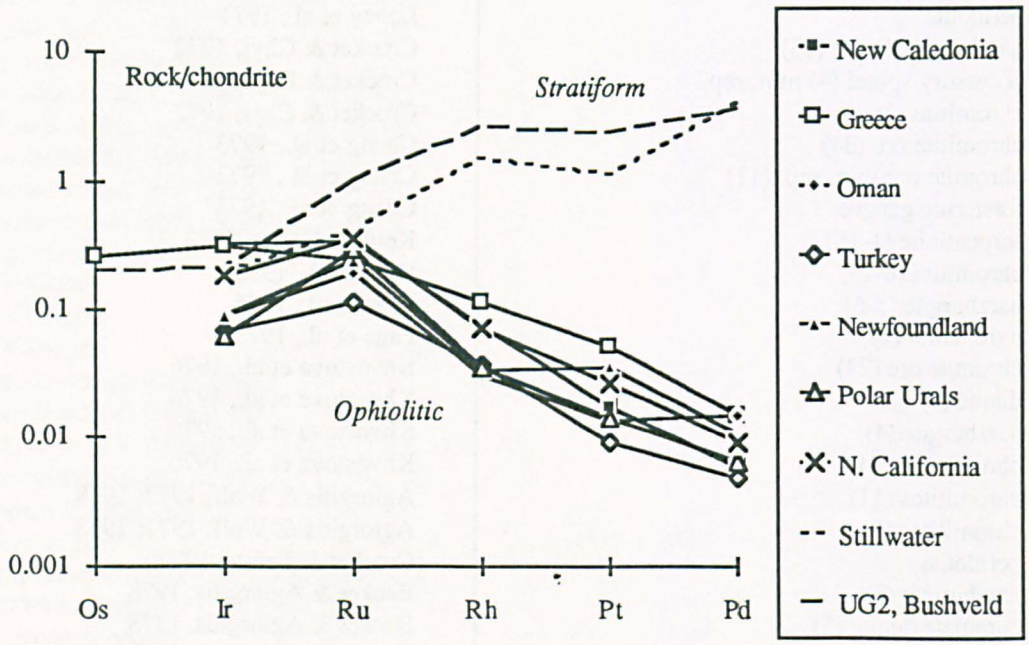

Table 1.5. PGE analyses of ophiolitic chromitites, stratiform chromitites and chondrite normalisation values.

Area	*Os*	*Ir*	*Ru*	*Rh*	*Pt*	*Pd*	*Source*
Ophiolite complexes							
New Caledonia		177	235	15	17	3.2	Page et al., 1982a
Greece	130	171	172		53	8	Agiorgitis & Wolf, 1977;1978
Oman		48	135	6	14	8	Page et al., 1982b
Turkey		36	80	7.2	9.5	2.7	Page et al., 1984
Newfoundland		49	173	6.5	35	5.8	Page & Talkington, 1984
Polar Urals		33	200	7	14.4	3.6	Page et al., 1983
N. California		100	250	14	27	5	Page et al., 1982a
Stratiform complexes							
Stillwater		109	284	299	1183	2266	Page et al., 1976
UG2, Bushveld	102	114	720	540	2460	2040	Von Gruenewaldt 1977
Normalisation values							
Chondrite	514	540	690	200	1025	545	Barnes & Naldrett, 1987

This technique of normalising to chondrite can also be used to characterise chromitites from different deposits (Page et al., 1982a; 1982b; 1983; 1984; Page & Talkington, 1984). This is shown in figure 1.3 which uses the more complete ophiolitic chromite analyses and the stratiform chromitite and normalisation values listed in table 1.5. Chromitites from ophiolitic sequences show a stronger depletion of Pt and Pd than of Ir or Ru with respect to chondrite (Page et al., 1982a). This is true for all the ophiolitic chromites examined in the studies listed above, although the relative abundances of individual platinum group elements vary slightly from area to area. Chromitites from stratiform intrusions show an inverse pattern, with enrichment of Pt and Pd and depletion of Ir and Ru with respect to chondrite. The similarity between ophiolitic chromitites from Turkey, Iran, Oman, SW Oregon, N California, New Caledonia, Greece, the Polar Urals and Newfoundland led researchers to propose that these negative slope patterns were diagnostic of ophiolitic chromitite (Page & Talkington, 1984). This interpretation was also supported by the relative abundance of Os, Ir and Ru compared to Pt, Pd or Rh in the PGM assemblages reported from ophiolitic chromitites (table 1.6). However, other ophiolitic rock types have more complex patterns and relations (Page et al., 1983; Page & Talkington, 1984).

Few complete PGE analyses of ophiolitic silicate lithologies exist in the literature (table 1.4). Average analyses of tectonites, cumulates and gabbros from the Voikar-Syninsky ophiolite complex yield negative sloping patterns similar to those of ophiolitic chromitites (figure 1.4) although these average analyses also included chromite-rich samples. The exact pattern in the region of the diagram around Ir and Ru is obscured by the lack of sensitivity of the analytical method to these elements. Samples from the gabbro unit give a positive trend from Rh to Pd reminiscent of patterns from stratiform cumulate sequences (Page et al., 1983).

Variations in the PGE patterns within the Troodos and Thetford ophiolite sequences indicate that Os, Ir and Ru are removed from the melt by fractionation of chromite, producing chromitites and dunites enriched in these elements (Agiorgitis & Wolf, 1978; 1984; Oshin & Crocket, 1982). Thus Rh, Pt and Pd are enriched in the melt and rocks subsequently crystalising from this liquid (i.e. gabbros and basalts) are more enriched in these elements (Oshin & Crocket, 1982; Barnes et al., 1985). An increase in the Pd/Ir ratio with increasing

Table 1.6. PGM reported from ophiolite chromitites (up to 1985).

Ophiolite	*Main PGM phases*	*Minor PGM phases*	*Source*
NW China	laurite [$(Ru,Os,Ir)S_2$], irarsite [IrAsS], sperrylite [$PtAs_2$]	platarsite [PtAsS], Os-Ir alloys, stibiopalladinite [$Pd_{5+x}Sb_{2-x}$]	1
N. Tibet	ruarsite [RuAsS], Os-Ir alloys, laurite [$(Ru,Os,Ir)S_2$]		2
Troodos, Cyprus	laurite [$(Ru,Os,Ir)S_2$]	erlichmanite [$(Os,Ir,Ru)S_2$]	3
White Hills, Newfoundland	laurite [$(Ru,Os,Ir)S_2$]		4
Massif du Sud, New Caledonia	rutheniridosmine [(Os,Ir,Ru)]		5
Massif de Tiébaghi, New Caledonia	laurite [$(Ru,Os,Ir)S_2$]	$(Cu,Ni)(Ir,Rh)_2S_5$	5
Guleman, Turkey	(Ru,Ir,Os) alloys		6
Fethiye, Turkey	laurite [$(Ru,Os,Ir)S_2$]		6
Al Ays, Saudi	laurite [$(Ru,Os,Ir)S_2$]		6
Troodos, Cyprus	$(Ir,Pt)S_2$	$(Ir,Pt)S_2$	6
Josephine & Onion Mountain, SW Oregon	laurite [$(Ru,Os,Ir)S_2$], Ru-Fe alloys, Ru-Os-Ir alloys, Pt-Fe alloys, Os-Ir-rich alloys	Ir-Cu-Rh sulphide, sperrylite [$PtAs_2$], Ir-Cu sulphide, Pt sulphide, Os-Ir-Ru sulphide	7
Cache Creek, British Columbia	laurite [$(Ru,Os,Ir)S_2$]		8
Vourinos, Greece	laurite [$(Ru,Os,Ir)S_2$], osarsite [OsAsS], irarsite [IrAsS], rutheniridosmine [(Os,Ir,Ru)], iridosmine [(Os,Ir)], osmiridium [(Ir,Os)]	minor Pt,Pd,Rh & Ni in main mineral phases	9

Sources:-

1 Chang et al., 1973; 2 Yu & Chou, 1979; 3 Constantinides et al., 1980; 4 Talkington, 1981; 5 Legendre & Johan, 1981; 6 Legendre, 1982; 7 Stockman & Hlava, 1984; 8 Wittaker & Watkinson, 1985; 9 Augé, 1985.

Figure 1.4. Chondrite-normalised PGE patterns from units of the Voikar-Syninsky ophiolite, Polar Urals (from Page et al., 1984).

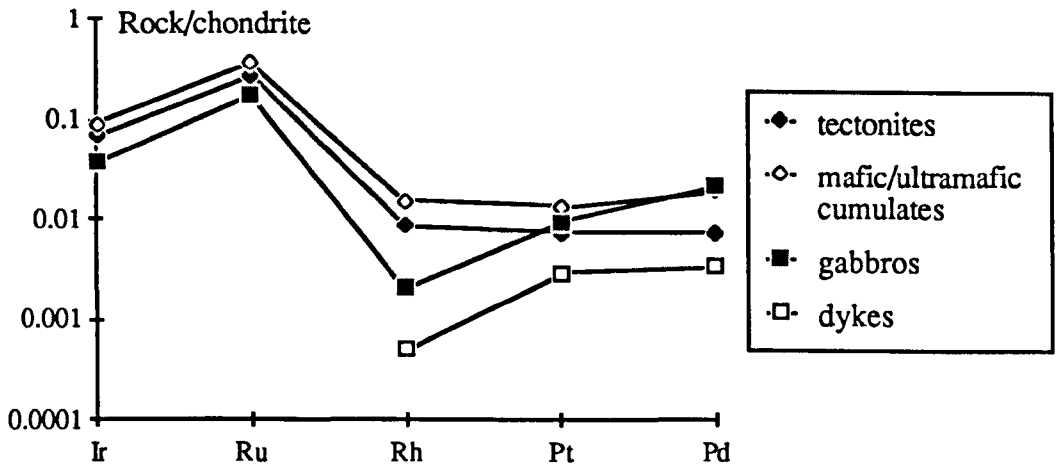

stratigraphic level is apparent in the data from Thetford and Troodos (Crocket, 1981). Furthermore, Pt partitions more strongly into silicate or oxide crystal structures than Pd, producing decreasing Pt/(Pt+Pd) ratios with increasing differentiation. In contrast Pd partitions preferentially into any sulphide phase (Oshin & Crocket, 1982).

Barnes et al. (1985) describe flat patterns in upper mantle rocks and ophiolitic harzburgites, and Os-, Ir-, Ru-enriched patterns in podiform chromitites, but note that patterns from the non-tectonised portions of ophiolites are not easily distinguishable from those of layered intrusions, ocean-floor basalts, continental flood basalts or alkaline rocks.

1.3 Definition of an ophiolite

The term "ophiolite" has been defined by a consensus statement of those present at the GSA Penrose Conference (Anonymous,1972) :-

"Ophiolite... , refers to a distinctive assemblage of mafic to ultramafic rocks. It should not be used as a rock name or as a lithologic unit in mapping. In a completely developed ophiolite the rock types occur in the following sequence, starting from the bottom and working up:-

(i) an ultramafic complex, consisting of variable proportions of harzburgite, lherzolite and dunite, usually with a metamorphic tectonic fabric (more or less serpentinised).

(ii) a gabbroic complex, ordinarily with cumulus textures commonly containing cumulus peridotites and pyroxenites and usually less deformed than the ultramafic complex.

(iii) a mafic sheeted dyke complex.

(iv) a mafic volcanic complex, commonly pillowed.

Associated rock types include:

(1) an overlying sedimentary section typically including ribbon cherts, thin shale interbeds, and minor limestones;

(2) podiform bodies of chromite generally associated with dunite;

(3) sodic felsic intrusive and extrusive rocks.

Faulted contacts between mappable units are common. Whole sections may be missing. An ophiolite may be incomplete, dismembered, or metamorphosed, in which case it should be called a partial, dismembered, or metamorphosed ophiolite. Although ophiolite generally is interpreted to be oceanic crust and upper mantle the use of the term should be independent of its supposed origin."

Figure 1.5. Diagram of processes operating at an ophiolite constructive margin (Gass & Smewing, 1981).

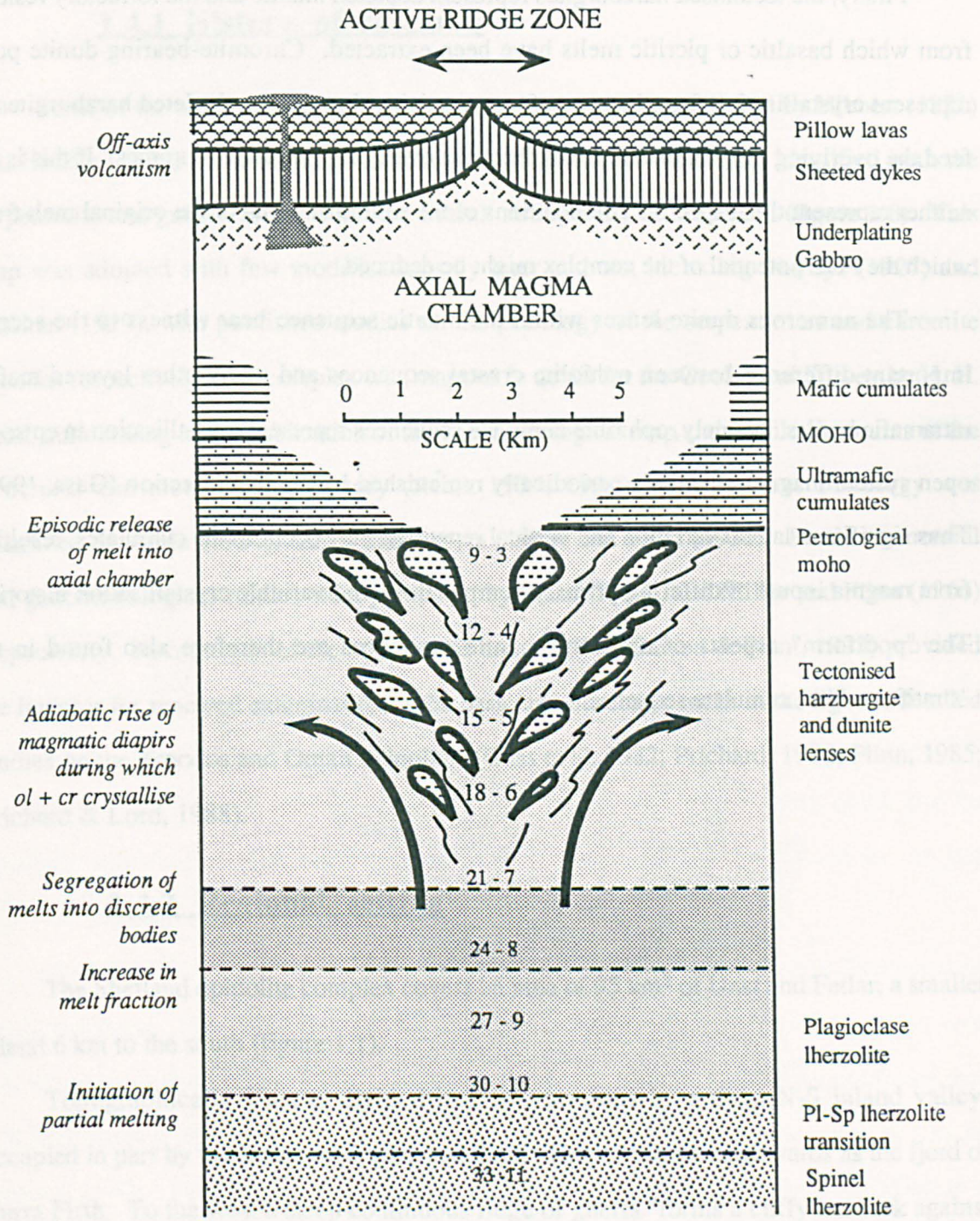

The proposal that ophiolites are on-land fragments of oceanic lithosphere (Gass, 1968) is now accepted throughout the geological world. The consensus model for their formation is shown in figure 1.5. Two aspects of this model (Gass & Smewing, 1981) are particularly relevant to the study of PGE concentrations within an ophiolite sequence.

Firstly, the tectonised harzburgites represent depleted mantle and the refractory residue from which basaltic or picritic melts have been extracted. Chromite-bearing dunite pods represent crystallisation from batches of magma rising through the depleted harzburgites to feed the overlying magma chamber and form the overlying cumulate plutonics. If this is so, neither represent the respective compositions of the source material or the original melt from which the PGE potential of the complex might be deduced.

The numerous dunite lenses within the mantle sequence bear witness to the second important difference between ophiolite crustal sequences and many other layered mafic-ultramafic bodies. Namely, ophiolite cumulate sequences represent crystallisation in episodic open system magma chambers periodically replenished by magma injection (Gass, 1990). Thus significant lateral variation and vertical repetition may occur in the cumulates, resulting from magma inputs of differing primary compositions and variable crystallisation histories. The "podiform" aspects of ophiolite mantle sequences are therefore also found in the "stratiform-like" cumulate sequence.

1.4 Evidence that the Unst basic-ultrabasic complex is ophiolitic

1.4.1 History of research

Some of the earliest observations on the geology of Unst, published by Hibbert (1821) and Heddle (1878) and including the first geological map of the island, identified both the serpentinite and gabbro units within the overall stratigraphy of the island (figure 1.6). This map was adopted with few modifications by later authors, including Phillips (1927) and Hitchen (1929), who published studies on the petrology of the serpentinites and chromite deposits respectively. The complex was mapped in detail for the Geological Survey by H. H. Read, culminating in the publication of the 1 inch geological map and detailed accounts of the structural and metamorphic history (Read, 1934; 1936). The igneous petrology was examined by Amin (1954), Curtis and Brown (1969) and Flinn (1970). Further structural and geochronological studies were published by Flinn (1958), and Miller and Flinn (1966) respectively. Recognition of the complex as an ophiolite (Garson & Plant, 1973) provided the impetus for renewed examination of the basic and ultrabasic rocks in the light of detailed studies on the Troodos and Oman ophiolites (Gass et al.,1982; Prichard, 1985; Flinn, 1985; Prichard & Lord, 1988).

1.4.2 Regional setting

The Shetland ophiolite complex covers an area of 95 km^2 of Unst and Fetlar, a smaller island 6 km to the south (figure 1.1).

Topographically Unst is divided into two portions by a deep N-S inland valley, occupied in part by the Lochs of Watlee and Cliff. This continues northwards as the fjord of Burra Firth. To the west a steep continuous ridge of gneiss "forms a cliffy bulwark against the western ocean" (Heddle 1878). The NE corner of the island is dominated by a group of steep rounded hills of schists and granite rising to over 280 m on Saxa Vord. The eastern

Figure 1.6. Heddle's (1878) geological map of Unst.

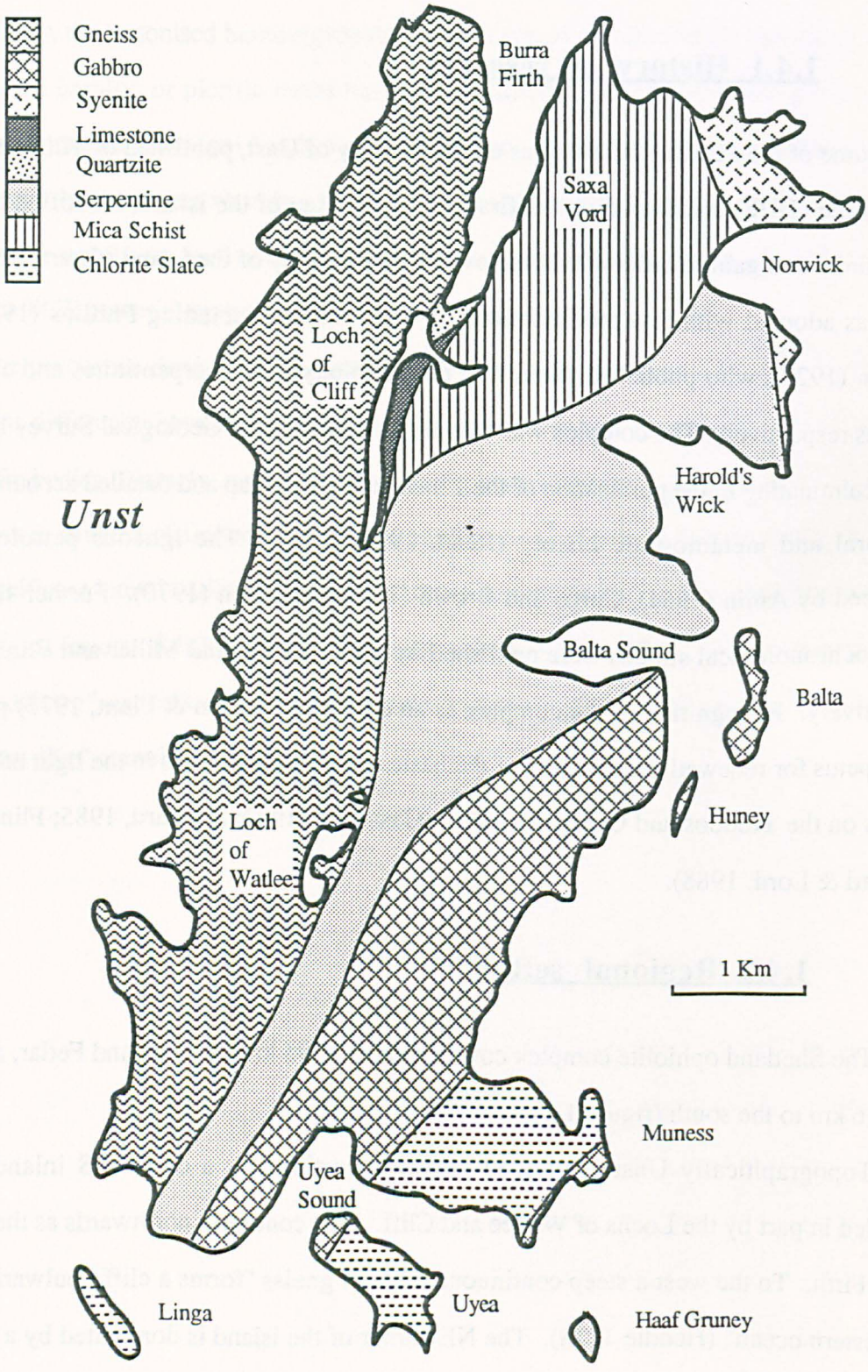

and southern areas of serpentinites and gabbros show typically low relief and undulating scenery, forming sheltered voes* at Haroldswick and Baltasound.

Reed (1934) recognised seven major tectonic units within Unst, separated by major steep to inclined N-S dislocations (figure 1.7). Movement on these structures was generally of synchronous thrusting towards the west.

Two of these blocks are composed of ophiolitic lithologies, namely the "Main and Mu Ness serpentine and greenstone block" and the "Clibberswick serpentine block". Reed describes them as having both been thrust westwards over the Valla Field gneiss and Saxa Vord schists, the former acting as a competent basement, with the later imbricated and forming a schuppen zone of disordered pods of component lithologies directly beneath the contact. The Muness Phyllite Block structurally overlies the Main Serpentine and Greenstone Block along its SE margin. Further SE greenstone and serpentine reappear from beneath the phyllites at Mu Ness. Reed recognised a partial correlation between this outcrop and a horizon in the Main Greenstone "characterised by the occurrence of large bodies of ultrabasic character", demonstrating that the phyllites occur in the core of a synform in the Main Greenstones, separated from them by a single dislocation.

Movements on the thrust boundaries between the structural blocks produced the last phase of metamorphism and juxtaposed blocks of different metamorphic history (table 1.7). The intrusion of a suite of spessartitic basic sills and dykes and the subsequent dislocation metamorphism were the only events found common to all blocks. Reed noted that the phyllites showed no relict metamorphic structures and were only affected by the last (dislocation) metamorphic event.

Flinn (1958) revised Reed's structural divisions identifying two nappes of serpentine and greenstone. This was based on new artificial exposures on Unst and correlations with the sequence on Fetlar (figure 1.10). Serpentinites of the Hamars Ness block are folded into a N-S trending synform and separated from the high grade metamorphic basement by a lower schuppen zone. The core of this synform is occupied by the Vord Hill serpentine which is in turn separated from the lower nappe by a middle schuppen zone. A third upper schuppen

---

* Small bay or creek in Shetland and Orkney.

Figure 1.7. H. H. Reed's (1934) geological map of Unst and division into seven tectonic blocks.

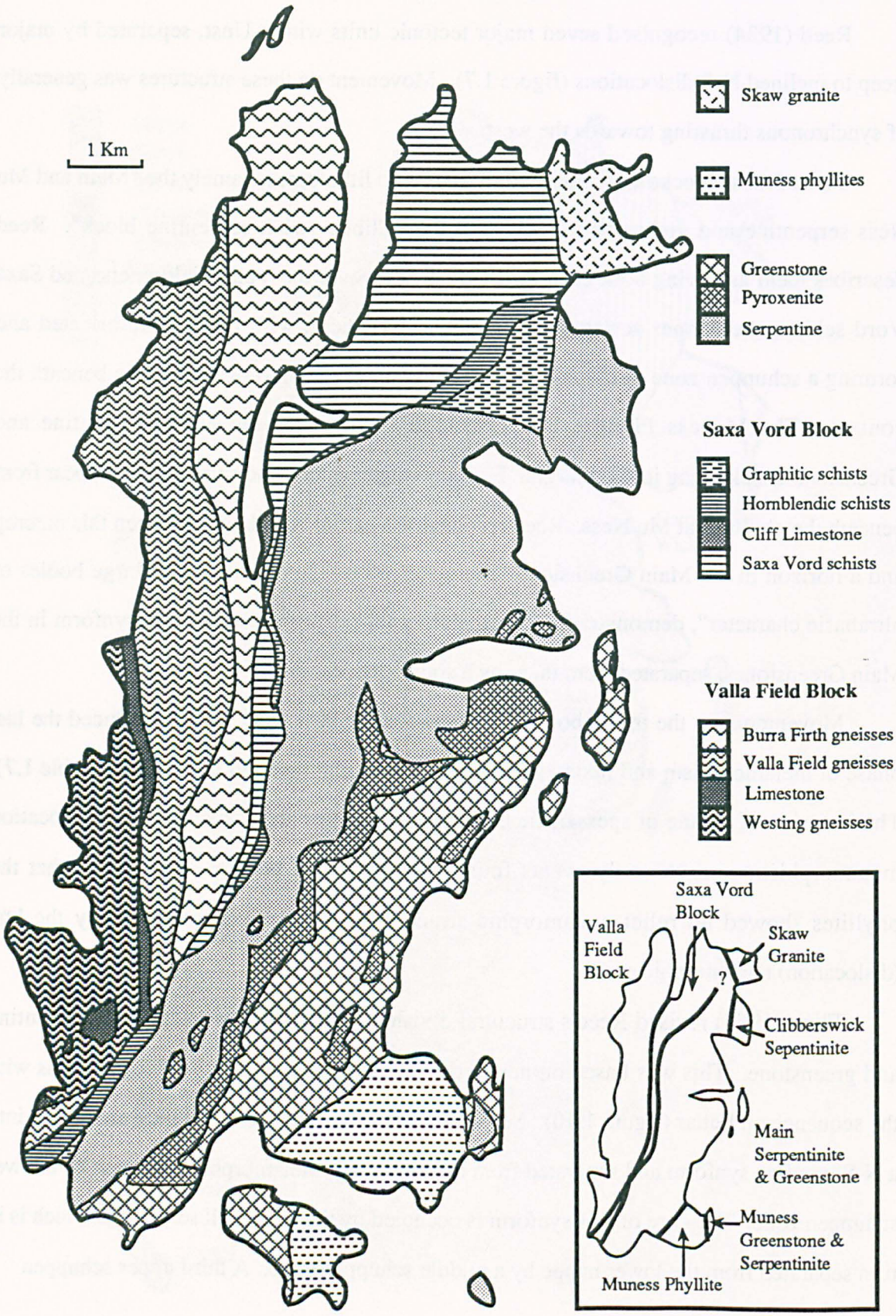

Table 1.7. Metamorphic history of the component tectonic blocks of Unst (after Reed, 1934)

Block	*Lithology*	*Structure*	*Igneous & metamorphic history*
Valla Field	Chiefly gneisses including pelitic, siliceous & feldspathic types, some granulites, schists, calc-silicate rocks & limestones	Anticlinal fold, N-S axis, S pitch. Restricted melange structure	(1) Basic & ultrabasic intrusions (2) First metamorphism St-Ky-Gt-Bi*, granitic intrusions, folding & melange (3) Second metamorphism in S Chld-Chl* (4) Spessartitic sills & dykes (5) Dislocation metamorphism formed chlorite-sericite schists
Saxa Vord	Mainly schists including hornblendic, graphitic & chloritoid-kyanite types, quartzo-feldspathic flags & limestones	Imbricate structure & partial structural succession, schuppen zone beneath serpentine blocks	(1) First metamorphism St-An-Bi-Gt* (2) Second metamorphism Ky-Chld* (3) Spessartitic sills & dykes (4) Dislocation metamorphism formed chlorite-sericite schists. Imbricate thrusting
Main & Mu Ness Serpentinite & Greenstone	Large intrusion with upper basic and lower ultrabasic parts, lowest olivine (+chromite) unit transitional to pyroxenite. Greenstone of basic plagioclase & pyroxene	Synform at Mu Ness, phyllites in core. Gabbro possibly slightly later than peridotites below	(1) Mesh texture serpentinisation. Tremolitisation & saussuritisation of gabbro (2) Spessartitic dykes (3) Dislocation metamorphism formed antigoritic zones enclosing talc schists below & on thrusts within block & around chromitites kammererite. Tremolite-zoisite schists in gabbro
Muness Phyllite	Chlorite-sericite phyllite with rare conglomeritic schist	Occupy synform in serpentine & greenstones above a thrust contact	(1) Spessartitic dykes (2) Dislocation metamorphism to chlorite-sericite with woody fabric
Clibberswick Serpentinite	Block of olivine serpentine with few enstatite & clinopyroxene crystals		(1) Mesh texture serpentinisation (2) Spessartitic dykes (3) Dislocation metamorphism formed talcose rocks on shear planes with margin of antigoritic rocks towards normal serpentine
Skaw Granite	Augen-granite with abundant xenoliths of semi-pelitic & siliceous rocks	Strong foliation cut by foliated dykes	(1) Foliation (2) Spessartitic sills & dykes (3) Dislocation metamorphism with chlorite replacing biotite in sheared margin, internal shearing out of dykes & sills

*Mineral abbreviations as follows:- Staurolite (St), kyanite (Ky), garnet (Gt), biotite (Bi), chloritoid (Chld), chlorite (Chl), andalusite (An)

zone was also recognised on Fetlar overlying the Vord Hill serpentinite. The upper and lower nappes were correlated with Reed's Main and Clibberswick serpentine blocks on Unst. The middle schuppen zone between the two was recognised on Unst by subdivision of the eastern portion of Reed's Saxa Vord block. It includes a slice of Saxa Vord schists as well as phyllites and lies between the Clibberswick and Main serpentine blocks.

1.4.3 Ophiolite sequence

Following recognition of the ophiolitic nature of the complex (D. Flinn pers. comm. in Garson and Plant, 1973), all the serpentine and greenstone blocks were re-mapped (figure 1.8) using relict mineralogy to identify the characteristic sequence of lithologies found in less altered ophiolites (Gass et al., 1982). Prichard (1985) describes the complex as incomplete and tectonically dismembered, although the characteristic lower ophiolite succession of tectonised harzburgite overlain by cumulate dunite, wehrlite, pyroxenite and gabbro is still recognisable. This is best preserved in the north of Unst. Here a SE dipping sequence is present from harzburgite, through cumulate ultramafic rocks, to gabbros in the SE (Prichard & Neary, 1982). A swarm of doleritic dykes are exposed on the east coast of Unst at the highest exposed level of the gabbro. These were interpreted as the base of a sheeted dyke complex (Prichard & Neary, 1981). The complex is terminated westwards against metasediments by a basal thrust contact running down the centre of the island. The sequence is less clear in the south of Unst where rocks are more altered and deformed (Prichard, 1985). No continuous sequence can be found on Fetlar further south, where harzburgites tectonically overly gabbros.

Identification of shear zones within the complex (Bartholomew, 1983) allowed clarification of some of the contradictions within Prichard's (1982) map. The dunite-harzburgite boundary has an E-W orientation in the east of the island but turns sharply southwards further W (figure 1.8). This N-S trend was later identified as a major shear zone, rather than a primary igneous feature (Bartholomew, 1983).

Figure 1.8. Geological map of primary ophiolite lithologies (Gass et al., 1982)

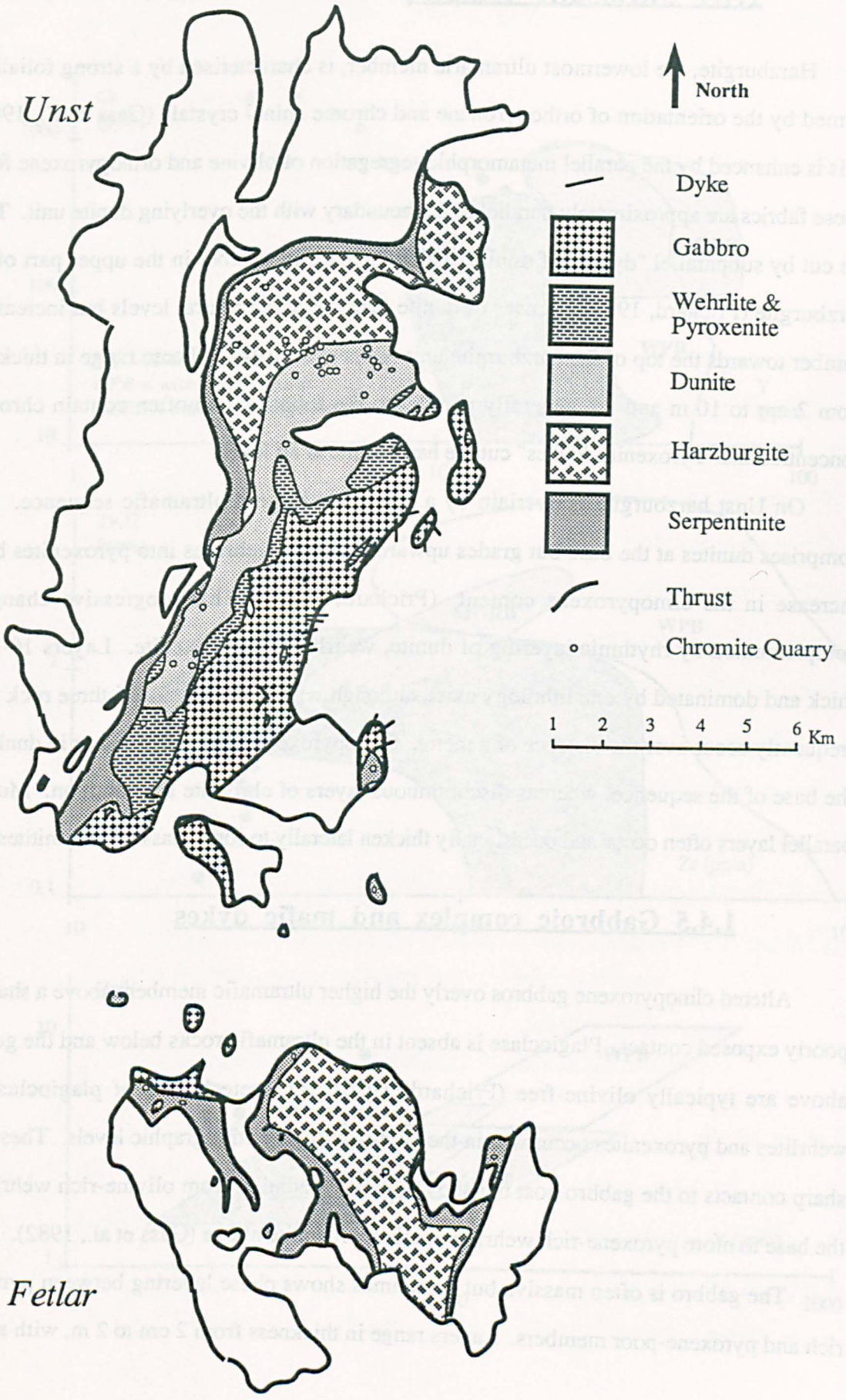

1.4.4 Ultramafic complex

Harzburgite, the lowermost ultramafic member, is characterised by a strong foliation, formed by the orientation of orthopyroxene and chrome spinel crystals (Gass et al., 1982). This is enhanced by the parallel metamorphic segregation of olivine and orthopyroxene folia. These fabrics are approximately parallel to the boundary with the overlying dunite unit. They are cut by subparallel "dykes" of dunite, which increase in number in the upper part of the harzburgite (Prichard, 1985). Lenses of dunite occur at all structural levels but increase in number towards the top of the harzburgite unit (Gass et al., 1982). These range in thickness from 2 cm to 10 m and are generally parallel to the foliation and often contain chromite concentrations. Pyroxenite "dykes" cut the harzburgite at all levels

On Unst harzburgite is overlain by a magmatic layered ultramafic sequence. This comprises dunites at the base but grades upwards through wehrlites into pyroxenites by an increase in the clinopyroxene content (Prichard, 1985). This progressive change is complemented by rhythmic layering of dunite, wehrlite and pyroxenite. Layers 10-20 m thick and dominated by one lithology exist, although within these units all three rock types frequently occur over the distance of a metre. Clinopyroxene is virtually absent in dunites at the base of the sequence, whereas discontinuous layers of chromite are common. Multiple parallel layers often occur and occasionally thicken laterally to form massive chromitites.

1.4.5 Gabbroic complex and mafic dykes

Altered clinopyroxene gabbros overly the higher ultramafic members above a sharp but poorly exposed contact. Plagioclase is absent in the ultramafic rocks below and the gabbros above are typically olivine-free (Prichard, 1985). Discrete bodies of plagioclase-free wehrlites and pyroxenites occur within the gabbro at higher stratigraphic levels. These have sharp contacts to the gabbro host but show internal gradation from olivine-rich wehrlites at the base to more pyroxene-rich wehrlite or clinopyroxenite above (Gass et al., 1982).

The gabbro is often massive but sometimes shows phase layering between pyroxene-rich and pyroxene-poor members. Layers range in thickness from 2 cm to 2 m, with sharp

Figure 1.9. Analyses of Shetland dykes plotted on the discrimination diagrams of Pearce (1980).

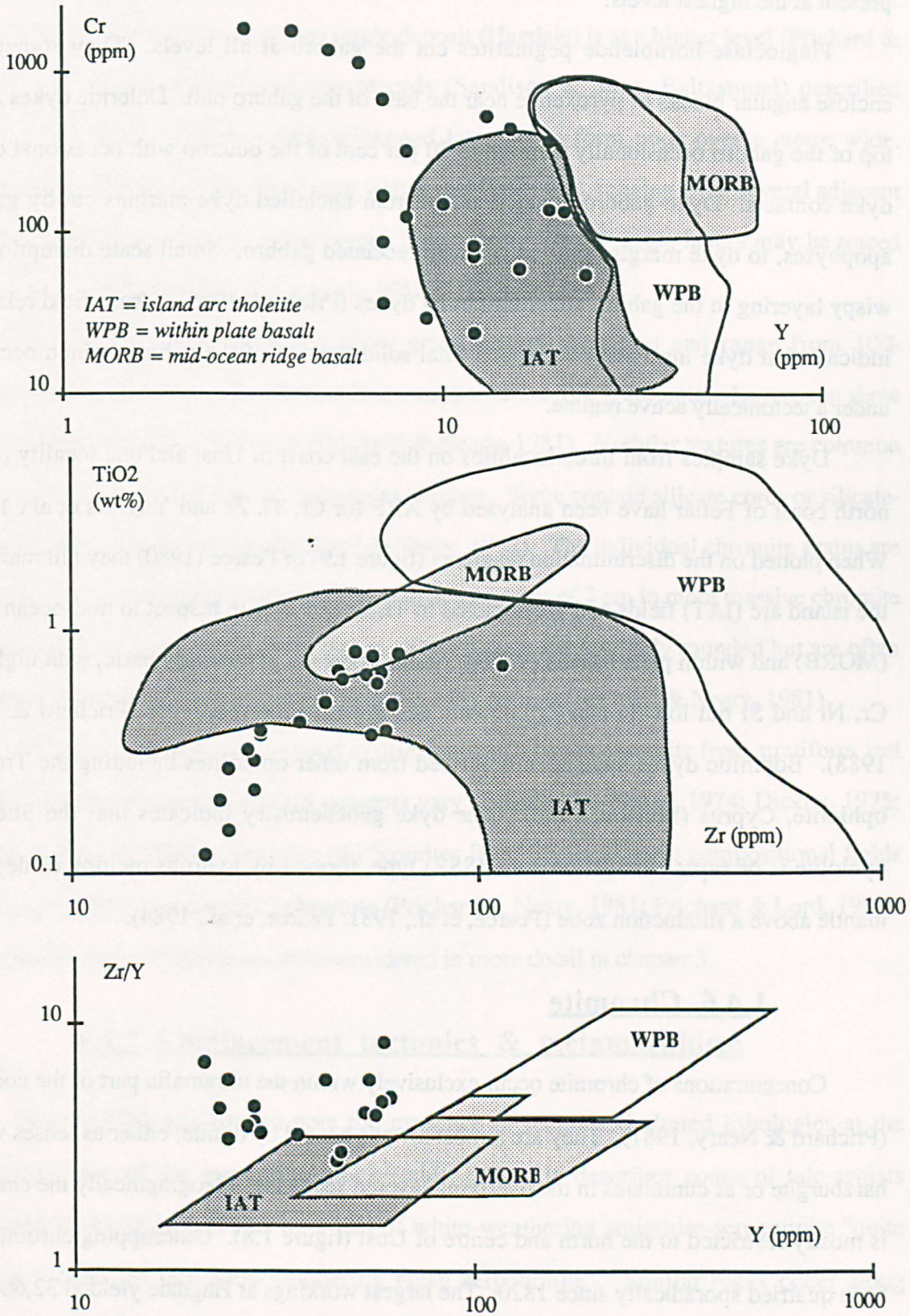

or diffuse margins and variable orientations (Prichard 1985). Wispy discontinuous layering and felsic net veining textures occur in the upper gabbro and vari-textured gabbros are present at the highest levels.

Plagioclase-hornblende pegmatites cut the gabbro at all levels. They sometimes enclose angular blocks of pyroxenite near the base of the gabbro unit. Doleritic dykes at the top of the gabbro occasionally form up to 50 per cent of the outcrop with occasional dyke-dyke contacts. Dyke-gabbro contacts range from unchilled dyke margins cut by gabbro apophyses, to dyke margins chilled against brecciated gabbro. Small scale disruptions of wispy layering in the gabbro are cross-cut by dykes (Prichard, 1985). These field relations indicate that dyke intrusion overlapped final solidification of the gabbro, which occurred under a tectonically active regime.

Dyke samples from three localities on the east coast of Unst and one locality on the north coast of Fetlar have been analysed by XRF for Cr, Ti, Zr and Y (Gass et al., 1982). When plotted on the discrimination diagrams (figure 1.9) of Pearce (1980) they fall mainly in the island arc (IAT) fields and are depleted in Ti, Zr and Y with respect to mid-ocean ridge (MORB) and within plate basalts (WPB). Some dykes are particularly basic, with high Mg, Cr, Ni and Si but low Ti and Zr contents and are therefore boninitic (Prichard & Lord, 1988). Boninitic dykes have been described from other ophiolites including the Troodos ophiolite, Cyprus (Murton, 1986). The dyke geochemistry indicates that the Shetland ophiolite is of supra-subduction zone (SSZ) type, formed by hydrous melting of depleted mantle above a subduction zone (Pearce, et al., 1981; Pearce, et al., 1984).

1.4.6 Chromite

Concentrations of chromite occur exclusively within the ultramafic part of the complex (Prichard & Neary, 1981). They are almost always hosted by dunite, either as lenses within harzburgite or as cumulates in the overlying layered sequence. Geographically the chromite is mostly restricted to the north and centre of Unst (figure 1.8). Outcropping chromite has been quarried sporadically since 1820. The largest workings at Hagdale yielded 32,600 tons of the total 50,000 tons extracted (Rivington, 1953).

Chromite concentrations occur in dunite lenses from all structural levels of the harzburgite, although not all dunite lenses contain massive chromitite or even thin chromite layers. Pods of chromite occur at all levels in the dunite unit. They are most frequent at the base of the unit, although the largest single deposit (Hagdale) is at a higher level (Prichard & Neary, 1981). Unpublished mining records (Sandison & Sons, Baltasound) described massive layers of chromite which thickened laterally to form pods over a metre wide. Discontinuous layers of chromite occur within the dunite unit, ranging from several adjacent layers 5 cm thick, to single crystal layers 10 cm long. Rarely single layers may be traced across the outcrop for 10 m (Gass et al., 1982).

The chromite concentrations show great textural variation and range from 10% disseminated chromite in a dunite matrix to nearly massive 100% chromite. Layers can show sharp, diffuse or graded junctions (Prichard & Neary, 1981). Nodular textures are common and typically ovoid with smooth or angular outlines. Some contain silicate cores or silicate-chromite intergrowth textures (Prichard & Neary, 1982). The individual chromite grains are typically 1-2 mm across but increase in size to a maximum of 2 cm in more massive chromite or in proportion to the thickness of layers. The crystals are generally rounded but are often distorted by brittle fracturing producing a pull-apart texture (Prichard & Neary, 1981).

Mineral chemistry may be used to discriminate between chromite from stratiform and ophiolitic rocks since the titanium contents vary accordingly (Neary, 1974; Dickey, 1975; Neary & Brown, 1979). Analyses of chromites from Shetland lie in compositional fields typical of podiform (ophiolitic) chromite (Prichard & Neary, 1981; Prichard & Lord, 1988). The geochemistry of the chromite is considered in more detail in chapter 3.

1.4.7 Emplacement tectonics & metamorphism

Read (1936) was first to note the presence of tectonised altered lithologies at the structural base of the serpentine block (table 1.7). He describes zones of talc-schists followed structurally upwards by a belt of white-weathering antigorite-serpentinite "quite different from the ochreous-weathering mesh serpentinite". Similar rocks occur along internal thrust zones and as talcose sheaths often containing kämmererite (Cr-rich chlorite)

Figure 1.10. Tectonic stratigraphy of Unst and Fetlar (Flinn, 1985).

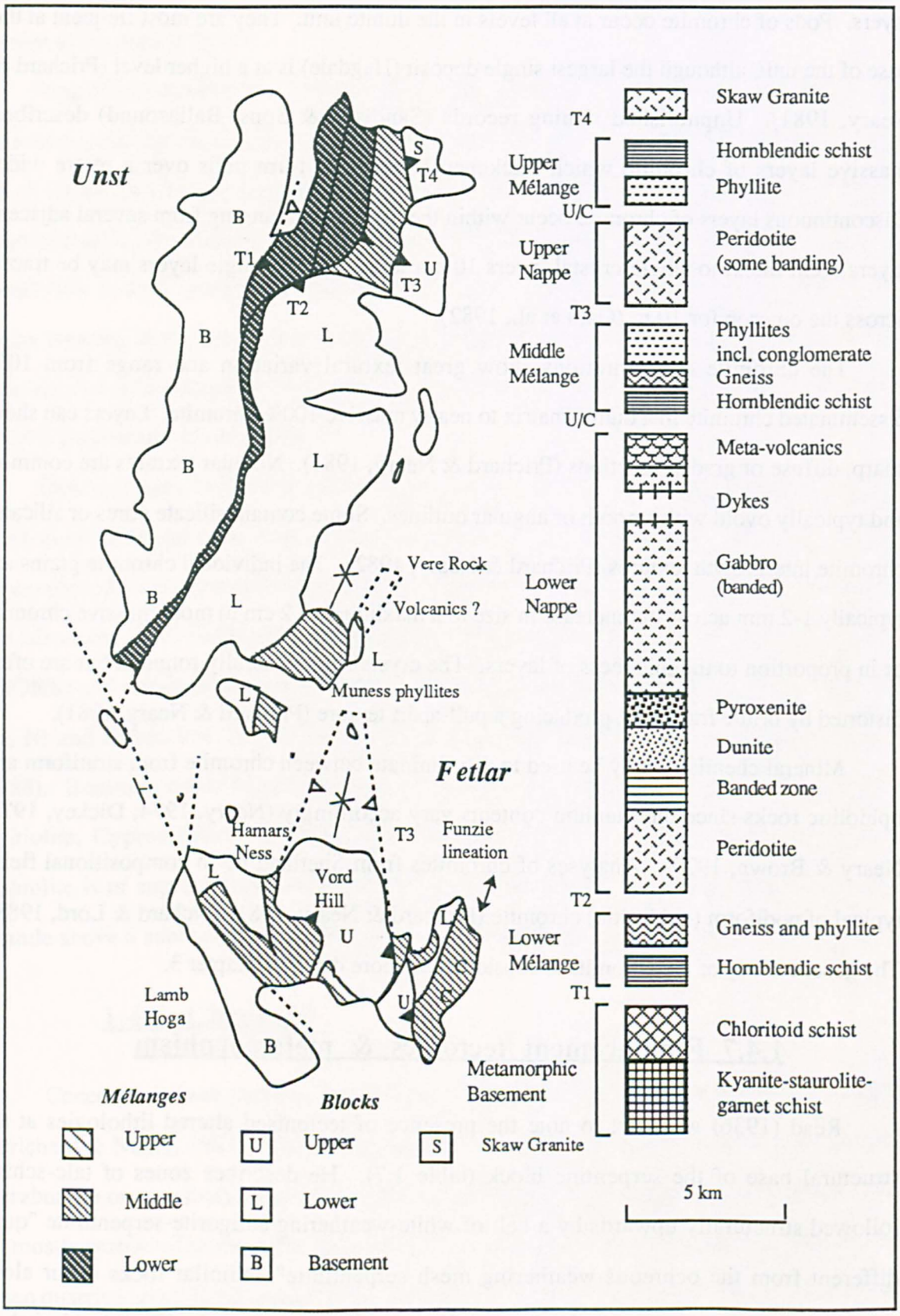

which "wrapped round" massive chromite ore-bodies. Schistose tremolite-zoisite-rocks were also found within the greenstones. These various deformed rocks were attributed to Reed's third or "dislocation" metamorphic event. This post-dated serpentinisation, tremolitisation and saussuritisation of the peridotite, pyroxenite and gabbro, and was attributed to the thrusting of the various blocks into their present positions.

Recognition of the ophiolitic origin of the two serpentinite nappes allowed re-interpretation of the phyllites and schuppen zones between and above the two nappes (figure 1.10) as melanges related to ophiolite obduction (Flinn, et al., 1979). These metamorphosed sediments contain ophiolite debris and slices of hornblendic schists and other basement metasediments (Flinn, 1985). Phyllites of the middle melange overly harzburgite on Unst and gabbros on Fetlar suggesting deposition directly onto the eroded surface of the already deformed lower ophiolite nappe (Flinn, 1958). The phyllite group has therefore been interpreted as the product of syntectonic erosion of the ophiolite nappes, continued over-thrusting deforming and metamorphosing these sediments (Flinn, 1985).

Deformation of the melanges is highly variable, ranging from very little deformation to polyphase folding (Flinn, 1985). Lineations in the phyllites and deformed conglomerates lie parallel to the fold axes, which trend NNE. This constriction is attributed to squeezing of the sediments between the more competent ophiolite nappes, the lineations representing axial elongation rather than the emplacement direction. Overturning of the generally upright folds to the WNW may indicate movement in this direction late in the emplacement of the nappes. The synformal outcrop of the Muness phyllites (Read, 1936) and the southerly trending synformal folding of the nappe pile on Fetlar (Flinn, 1958) may also indicate ESE-WNW emplacement and related or later folding (Flinn et al., 1979).

Amphibolites occur beneath the ophiolite in the south of Unst and lie directly beneath the serpentinites of the upper nappe on Fetlar (Prichard, 1985). They have been compared to those forming a metamorphic aureole beneath the Bay of Islands Complex and the White Hills Peridotite Sheet ophiolites of west Newfoundland (Williams & Smyth, 1973). On Fetlar 2-3 m of high grade garnetiferous pyroxene-bearing amphibolites grade into amphibolites and then greenschist facies metasediments and metavolcanics away from the basal contact of the ophiolite. These aureole rocks are commonly absent, with serpentinite

immediately overlying the metasediments, suggesting that later shearing has disrupted or removed them during the final stages of emplacement (Prichard, 1985). Slices of hornblendic schist between and above the two ophiolite nappes (Flinn et al., 1979) may have a similar origin (Williams & Smyth, 1973), representing ocean-floor volcanics contact-metamorphosed by over-thrust hot mantle.

The metamorphism of these sole rocks has also been studied by Spray (1988). He describes a 400 m thick thermally inverted sequence of upper amphibolite facies metabasites which grade downwards into low greenschist facies metasediments. This metamorphic sole has mid-ocean ridge basalt (MORB) geochemical "signatures" (Spray, 1988) in contrast to the supra-subduction zone (SSZ) chemistry and character of the main ophiolite complex (Prichard & Lord, 1988).

Rocks within the mélange zones have suffered greenschist facies metamorphism (Reed's third or dislocation metamorphism). This was prograde and tectonising in the unmetamorposed sediments but retrograde and non-tectonising in the incorporated slices of basement gneisses (Flinn, 1958) and aureole amphibolites (Prichard, 1985). Similar retrograde metamorphism is also found in basement rocks (Reed's second metamorphism) where they have been overridden by the nappes (Flinn et al., 1979). Both metamorphic styles have been attributed by Flinn (1985) to the burial resulting from stacking of the ophiolite nappes. Rocks within the ophiolite nappes also show signs of this greenschist facies metamorphism. Chlorite and actinolite are abundant in gabbros and dykes and magnesian chlorite commonly rims disseminated chrome-spinels. These rims are not found in other ophiolites and support the suggestion that the whole complex suffered a late regional greenschist overprint in addition to sub-oceanic greenschist metamorphism (Prichard, 1985).

Finally cataclastic retrograde metamorphism occurred in association with late thrusts and shears. This is characterised by the replacement of biotite by chlorite (Flinn, 1985).

1.4.8 Radiometric dating

A variety of rocks within the complex have been radiometrically dated. Brown hornblende from pegmatites cutting the gabbro give an Ar-Ar age of about 470 Ma (Flinn, 1985). Amphibole separates from the metamorphic sole give K-Ar ages in the range 479 ± 6

to 465 ± 6 Ma (Spray, 1988), of which the higher age is attributed to the onset of obduction. Muscovite in phyllites from between the ophiolite nappes yield K-Ar ages of 425+/-30 Ma. Similar ages have been obtained from micas in the basement metasediments (Miller & Flinn, 1966) where they have been affected by emplacement of the ophiolite nappes (Flinn, 1985). It has been suggested that this youngest age represents the regional greenschist metamorphism (Miller & Flinn, 1966) which overprints the ophiolite nappes and their aureole (Prichard, 1985), so obduction and emplacement of the ophiolite complex is constrained to between 479 and 425 Ma.

1.4.9 Conclusions

The field relations, petrology and sequence of lithologies described above compare favourably with the Penrose definition of an ophiolite and with the sequences exposed in other better preserved ophiolite complexes. It is concluded that the Unst basic-ultrabasic complex represents the lower portion of an incomplete Caledonian ophiolite (Prichard, 1985). This is confirmed both by the mineral chemistry of the chromite (Prichard & Neary, 1981; 1982) and by the geochemistry of the basic dykes, which indicate formation in a supra-subduction zone setting (Prichard & Lord, 1988).

1.5 Recent studies of PGE and PGM in Shetland

1.5.1 Introduction

Published reports of PGM in ophiolitic chromitites indicate a predominance of Os, Ir and Ru mineral phases. Typical minerals include laurite (RuS_2), Ru-Ir-Os alloys and Ru and Ir bearing arsenides (table 1.6). This reflects the greater abundance of these elements in such rocks with respect to the other PGE (section 1.2.3).

Initial mineralogical studies of Shetland chromite-rich rocks located two laurites and one iridosmine grain (Prichard et al., 1981). This prompted a more extensive mineralogical survey employing the technique of ß-autoradiography to locate mineral phases. This mineralogical survey provoked much interest in the PGE mineralisation of the Shetland ophiolite complex, largely as a result of the unusual PGM assemblages and anomalously high PGE concentrations located at the Cliff and Harold's Grave chromite quarries (Prichard et al., 1984; Neary et al., 1984). Initial analysis of PGM-rich samples by INAA revealed elevated levels of iridium averaging 1.8 g/t (18 samples) and with a maximum of 12 g/t. Samples from Cliff also contained gold levels at an average of 1.5 g/t and maximum 7 g/t. Levels of arsenic, and to a lesser extent nickel, were considered indicative of high PGE concentrations (Neary et al., 1984).

The unusual mineralisation at Cliff and Harold's Grave formed the basis for a Mineral Reconnaissance Programme by the British Geological Survey (Gunn et al., 1985; Leake & Gunn, 1985; Gunn, 1989). Further mineralogical studies documented the unusual PGM assemblages (Prichard et al., 1986; Tarkian & Prichard, 1987; Prichard & Tarkian, 1988; Prichard et al., 1989). Analyses of chromitites from Cliff (Gunn, et al., 1985; Prichard et al., 1986; Prichard et al., 1989) demonstrated the similarity of this mineralisation to that found in stratiform complexes.

The following sections first describe the results of the above studies. The various genetic interpretations placed on this evidence are then discussed (section 1.6).

1.5.2 B.G.S. Mineral Reconnaissance Programme - Structural controls and low temperature minerals

1.5.2.1 Aims and approach

The reported PGE and PGM concentrations in Unst (Neary et al., 1984, Prichard et al., 1984) were the subject of further investigation by the British Geological Survey as part of the Mineral Reconnaissance Programme (Gunn et al., 1985). The aims of this project were to evaluate the area as a potential occurrence of PGE mineralisation and to develop methods for the detection of such mineralisation.

Exploration for PGE was attempted using a combination of drainage, overburden and rock geochemistry. The collection of panned heavy mineral concentrates from overburden samples was developed as a reconnaissance technique after orientation studies at Cliff.

1.5.2.2 Drainage and overburden geochemistry

Panned concentrate samples were collected from 73 drainage sites and analysed for Ir, Au, Cr, Fe, Co, Ni, Cu and As. The results indicated generally higher levels of Ir in the harzburgite unit than in other rock types. The highest level of Ir was reported in a sample from a prominent N-S fault zone to the W of Nikka Vord which was also marked by anomalous levels of Fe, Co, Ni, Cu and As. Anomalous levels of Cr were associated with the areas of old workings (N of Baltasound) and an area of abundant drift chromite in the harzburgite unit to the SW of Quoys talc quarry (figure 1.11).

Panned overburden samples were collected as parallel traverses at 7 locations (figure 1.11). These included the known PGM localities at Cliff, Quoys and Harold's Grave, all other chromite quarries within the harzburgite unit and the dunite unit SW of Muckle Heog, and also three localities in the cumulate sequences south of Baltasound (Gerdie, Ordale and Hellier's Water).

The overburden sampling at Cliff revealed coincident Pd, Pt and Rh anomalies near to but separate from the chromite workings with known anomalous PGE contents. Low amplitude Pd and Pt anomalies were also detected in the dunite unit SW of Muckle Heog and

Figure 1.11. Location of overburden studies (Gunn et al., 1985).

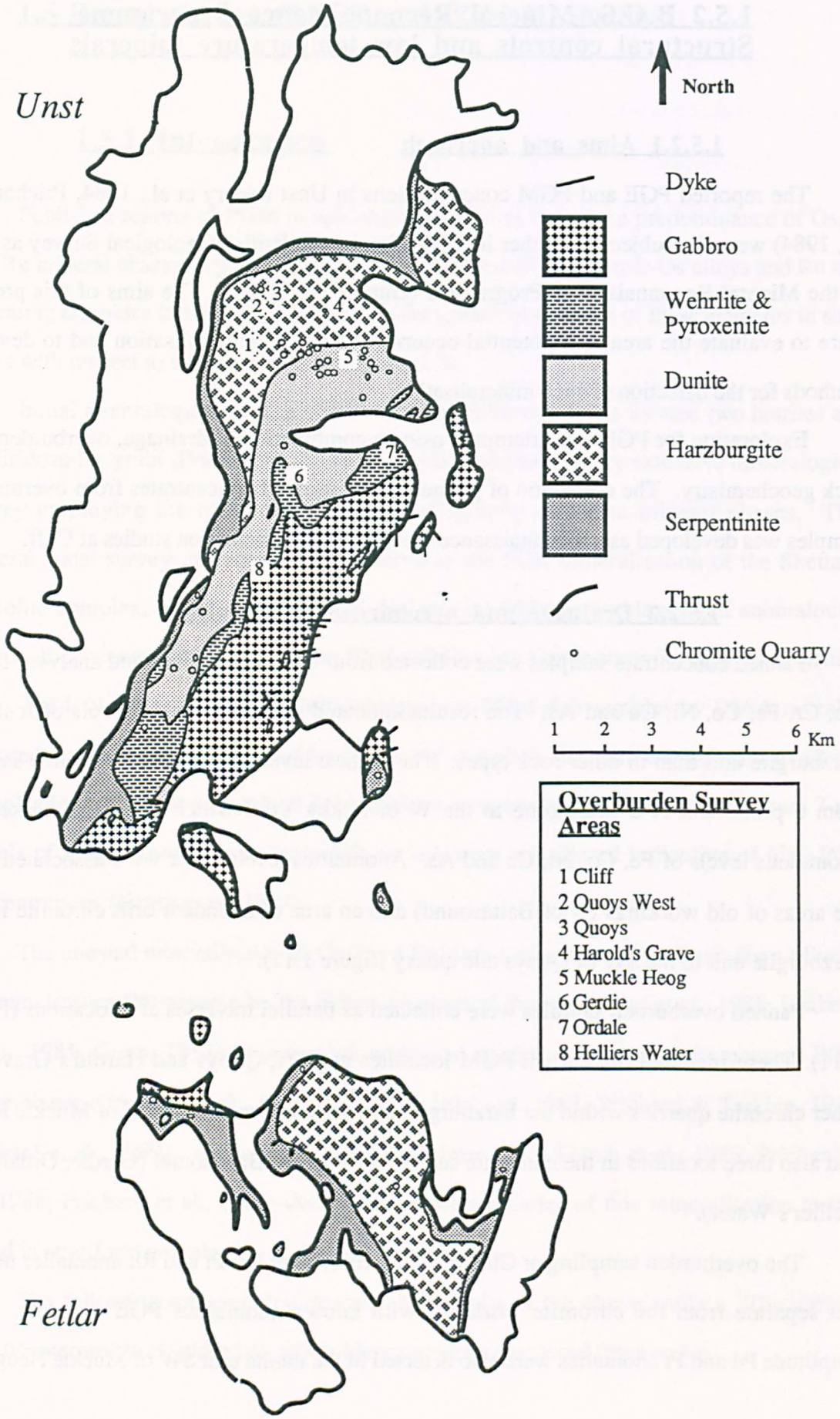

in the traverse at Hellier's Water where it crosses the prominent N-S fault zone.

Pathfinder analysis suggested some association between PGE enrichment and anomalous levels of Ni when expressed as Ni/MgO to correct for the Ni content of the olivine.

1.5.2.3 Lithogeochemistry

A total of 47 chromitites, chromite-rich dunites and associated dunites were collected covering the principal chromite occurrences and various drift chromite occurrences. Over half of these were obtained from the dumps at the Cliff quarry, with typically three samples collected from each of the remaining locations. Analysis confirmed that some chromitite samples from Cliff contain very high levels of PGE whereas others contain only background levels (table 1.8). Comparisons of adjacent dunite and chromite samples collected from each pit (figure 1.12) indicate that the dunites at Cliff generally contain lower PGE concentrations (table 1.9).

Figure 1.12. Location of chromite quarry pits and samples in the Cliff area (Gunn et al., 1985).

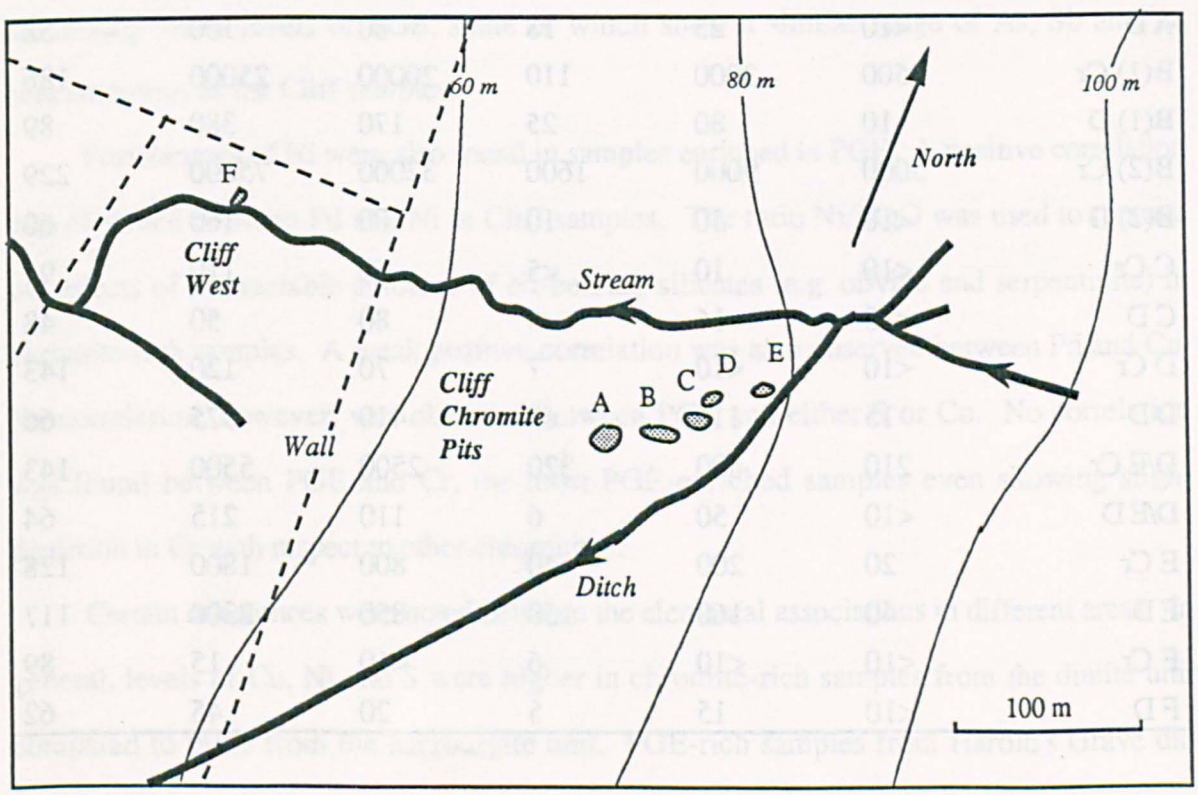

Table 1.8. PGE analyses (ppb) of chromitites and chromite-rich dunites from Cliff (Gunn et al., 1985).

Pit	*Ir*	*Ru*	*Rh*	*Pt*	*Pd*	*Ni/MgO*
A	<10	15	12	13	57	92
B (1)	3167	5733	1300	25667	46000	213
B (2)	55	600	60	3000	5000	152
C (1)	<10	10	<5	60	110	91
C (2)	400	1600	540	7000	13500	125
D/E (1)	65	317	99	948	2104	135
D/E (2)	210	800	250	3500	7500	183
F	<10	<10	6	<10	15	89

Table 1.9. PGE analyses (ppb) of adjacent dunite and chromite-rich samples from each quarry pit at Cliff (Gunn et al., 1985).

Pit, Cr/D	*Ir*	*Ru*	*Rh*	*Pt*	*Pd*	*Ni/MgO*
A Cr	<10	25	18	20	100	93
A D	<10	25	18	80	100	58
B(1) Cr	1500	3000	110	20000	25000	186
B(1) D	10	80	25	170	380	89
B(2) Cr	5000	9000	1600	32000	75000	229
B(2) D	<10	50	10	100	160	60
C Cr	<10	10	<5	60	110	91
C D	<10	16	<5	80	50	48
D Cr	<10	<10	7	70	120	143
D D	15	110	60	410	575	66
D/E Cr	210	800	320	2500	5500	143
D/E D	<10	50	6	110	215	64
E Cr	20	200	40	800	1800	128
E D	40	160	150	850	2300	117
F Cr	<10	<10	6	<10	15	89
F D	<10	15	5	20	45	62

High to moderate levels of PGE were also found in chromitites and dunites from other areas of the harzburgite unit and from the dunite unit (table 1.10), and in a few pyroxenites from the cumulate sequence (table 1.11). These concentrations show similar relative proportions of PGE to the samples from Cliff and are characterised by a predominance of Pt and Pd. There is a strong positive inter-correlation between all the PGE.

PGE-rich chromitite samples from Harold's Grave show different proportions of PGE with relatively higher Ru and Ir contents. Similar PGE ratios to those of the Harold's Grave chromitites were obtained from the panned overburden samples. This suggests that this assemblage may be regarded as a background population with localised enhancement at Harold's Grave. Significantly this type of mineralisation also shows a good correlation between Ru and Ir, with a similar Ru/Ir ratio to that found at Cliff and elsewhere (section 1.7).

Pathfinder analysis indicated that the high levels of PGE at Cliff are also associated with enrichments in Ni, Cu, As, Sb and Te. Graphical comparisons of Pd with As, Sb and Te showed positive correlations above 2 ppm Pd. This threshold effectively distinguishes between samples from Cliff and elsewhere. No correlation was observed in samples containing lower levels of PGE, some of which show a similar range of As, Sb and Te concentrations as the Cliff samples.

Enrichments of Ni were also found in samples enriched in PGE. A positive correlation was observed between Pd and Ni in Cliff samples. The ratio Ni/MgO was used to remove the effects of the variable amounts of Ni-bearing silicates (e.g. olivine and serpentinite) in chromite-rich samples. A weak positive correlation was also observed between Pd and Cu. No correlation, however, was observed between PGE and either S or Co. No correlation was found between PGE and Cr, the most PGE-enriched samples even showing slight depletion in Cr with respect to other chromitites.

Certain differences were noted between the elemental associations in different areas. In general, levels of Cu, Ni and S were higher in chromite-rich samples from the dunite unit compared to those from the harzburgite unit. PGE-rich samples from Harold's Grave did not show the associated enrichments of Ni or Cu observed at Cliff. Cumulate sequence rocks containing moderate levels of PGE in similar proportions to those from Cliff did not

Table 1.10. PGE analyses of dunites and chromite-rich dunites from other areas.

Area, Cr/D	*Ir*	*Ru*	*Rh*	*Pt*	*Pd*	*Ni/MgO*
Quoys W. Cr	10	65	15	90	115	105
Quoys Cr	24	116	6	-	15	66
Quoys Cr	<10	<10	<5	8	8	76
Quoys D	8	<10	<5	<10	4	47
H's Grave Cr	1803	4014	249	325	20	60
H's Grave Cr	831	740	129	250	19	57
Nikka Vord Cr-m	19	62	6	-	-	68
Nikka Vord Cr-l	7	16	1	<10	-	71
Muckle Heog Cr	31	81	16	250	260	180
Muckle Heog D	<10	<10	9	60	180	75
Muckle Heog Cl.D	<10	<10	<5	10	15	35
Muckle Heog D	<10	<10	<5	15	10	56
Midgarth Cr	-	48	6	<10	-	68
Hagdale Cr	<10	<10	<5	65	160	182
Watlee Cr	6	14	4	<6	-	73
Sobul Cr	39	72	9	-	-	60

Table 1.11. Average and maximum PGE concentrations in cumulate rocks.

Unit	*Av (n)*	*Ir*	*Ru*	*Rh*	*Pt*	*Pd*
Dunite	(7)	<10	9	3	13	18
Wehrlite	(3)	<10	15	5	27	27
Pyroxenite	(5)	<10	10	<5	40	58
Gabbro	(6)	<10	<10	<5	6	6
Dunite	max	<10	20	6	25	40
Wehrlite	max	<10	20	7	40	35
Pyroxenite	max	<10	18	<5	100	200
Gabbro	max	<10	17	<5	10	17

show correlations between PGE and either Ni or As, and only slight correlation with Cu. Some correlation was observed between Cr and PGE in the pyroxene-bearing lithologies. The significance of such stratigraphically controlled differences is discussed later (section 1.7).

1.5.2.4 Mineralogical studies

A mineralogical survey of samples from Cliff revealed the presence of the PGMs sperrylite ($PtAs_2$), stibiopalladinite ($Pd_{5+x}Sb_{2-x}$), hollingworthite (RhAsS), laurite (RuS_2) and possibly irarsite (IrAsS). These minerals occurred as grains generally less than 10 μm in size. Texturally the minerals were found within the chlorite haloes, magnetite rims or blackened alteration rims surrounding chromite grains, and also in the interstitial Ni-rich serpentine/carbonate intergrowths. In the dunites the PGM were found in magnetite or carbonate grains.

Associated with the PGM were an assemblage of Ni sulphides and arsenides including pentlandite ($(Ni,Fe)_9S_8$), godlevskite (Ni_7S_6), heazelwoodite (Ni_3S_2), orcellite ($Ni_{5-x}As_2$) and maucherite (Ni_3As). Pentlandite was the commonest sulphide phase occurring in grains generally hundreds of microns and up to 1mm in size. The Ni sulphides and arsenides occurred as smaller grains typically only a few tens of microns across. Both the sulphide/arsenide mineralisation and the PGM showed textural association with chlorite-carbonate-magnetite veins of a second phase of alteration, which post-dated initial serpentinisation by static hydration of olivine (section 2.5). The interpretation of these textures is discussed later (section 1.6.2).

1.5.3 A survey of PGMs in chromitites - The application of ß-autoradiography

1.5.3.1 Introduction

The technique of ß-autoradiography of polished thin sections systematically locates the minor phases containing ß-emitters (Potts, 1984). Thin sections are first irradiated with neutrons to activate the ß-emitters and after a suitable decay period exposed to a ß-sensitive film (Potts, 1986). The elements detected which are of relevance to PGM studies include Au, Ag, Ir, As, Sb and Co. PGM not principally composed of these elements may be located either by their association with other PGM in clusters and composite grains or by their content of trace amounts of these elements (Prichard et al., 1989). Since the half-lives of ß-emitters vary, so the decay intervals and exposure times for optimum detection vary. This allows distinction between the emissions of different elements. For example, Au (shorter half-live) in a specimen containing Ir, Sb and Co (longer half-lives) might be identified by comparison of images recorded at different times after irradiation (Potts & Prichard, 1986).

Sampling for the mineralogical survey was restricted to chromite-rich rocks in view of the association of PGM and chromite suggested by studies of other ophiolites (Prichard, et al. 1989). A total of 21 chromite quarry spoil tips were sampled, all those where chromite-rich spoil could be found (figure 1.13). This sampling covered the ophiolite geographically and stratigraphically, including chromite-rich rocks from both the harzburgite and dunite units. The largest quarry at Hagdale was not sampled since this was the site of the crushing mill and the origin of material was uncertain (Prichard et al., 1986). In situ samples were collected from chromite layers in dunite exposed on the coast at Hagdale Wick and from high level chromite in wehrlite in Mid Unst.

Figure 1.13. Location of chromite-rich samples for mineralogical study (Prichard et al., 1989).

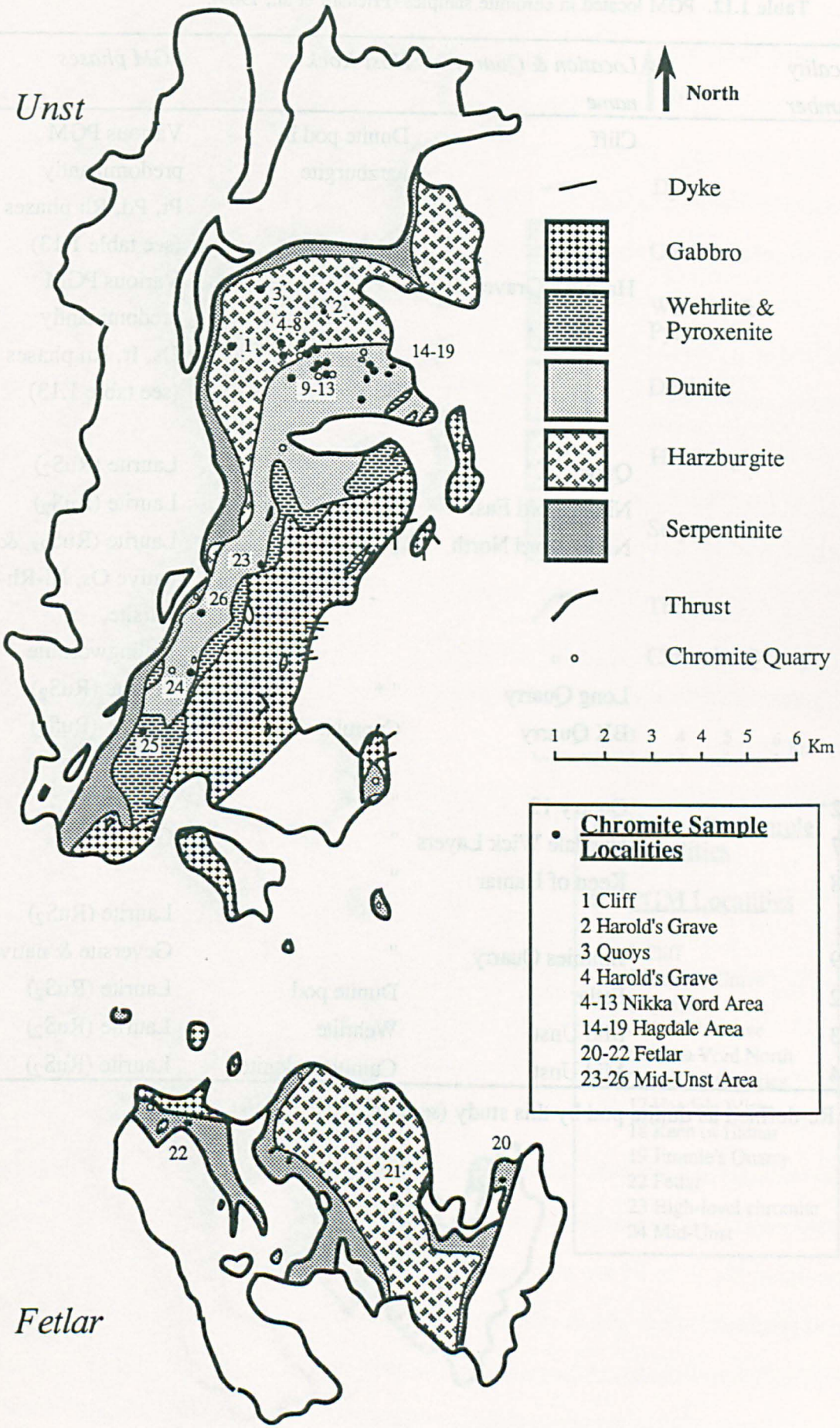

Table 1.12. PGM located in chromite samples (Prichard et al., 1989).

Locality Number	*Location & Quarry name*	*Host Rock*	*PGM phases*
1	Cliff	Dunite pod in harzburgite	Various PGM predominantly Pt, Pd, Rh phases (see table 1.13)
2	Harold's Grave	"	Various PGM predominantly Os, Ir, Ru phases (see table 1.13)
3	Quoys	"	Laurite (RuS_2)
4	Nikka Vord East	"	Laurite (RuS_2)
5	Nikka Vord North	"	Laurite (RuS_2), & native Os, Ni-Rh-Sb, irarsite, hollingworthite
7	Long Quarry	" *	Laurite (RuS_2)
9	BX Quarry	Cumulate dunite	Laurite (RuS_2)
12	Quarry 12	"	Irarsite
17	Hagdale Wick Layers	"	Os/Ir alloy
18	Keen of Hamar	"	Laurite (RuS_2)
19	Jimmies Quarry	"	Geversite & native Pt
22	Fetlar	Dunite pod	Laurite (RuS_2)
23	Mid Unst	Wehrlite	Laurite (RuS_2)
24	Mid Unst	Cumulate dunite	Laurite (RuS_2)

* Re-defined as dunite pod by this study (section 2.2.4)

Figure 1.14. Location of chromite-rich samples containing PGM (Prichard et al., 1989).

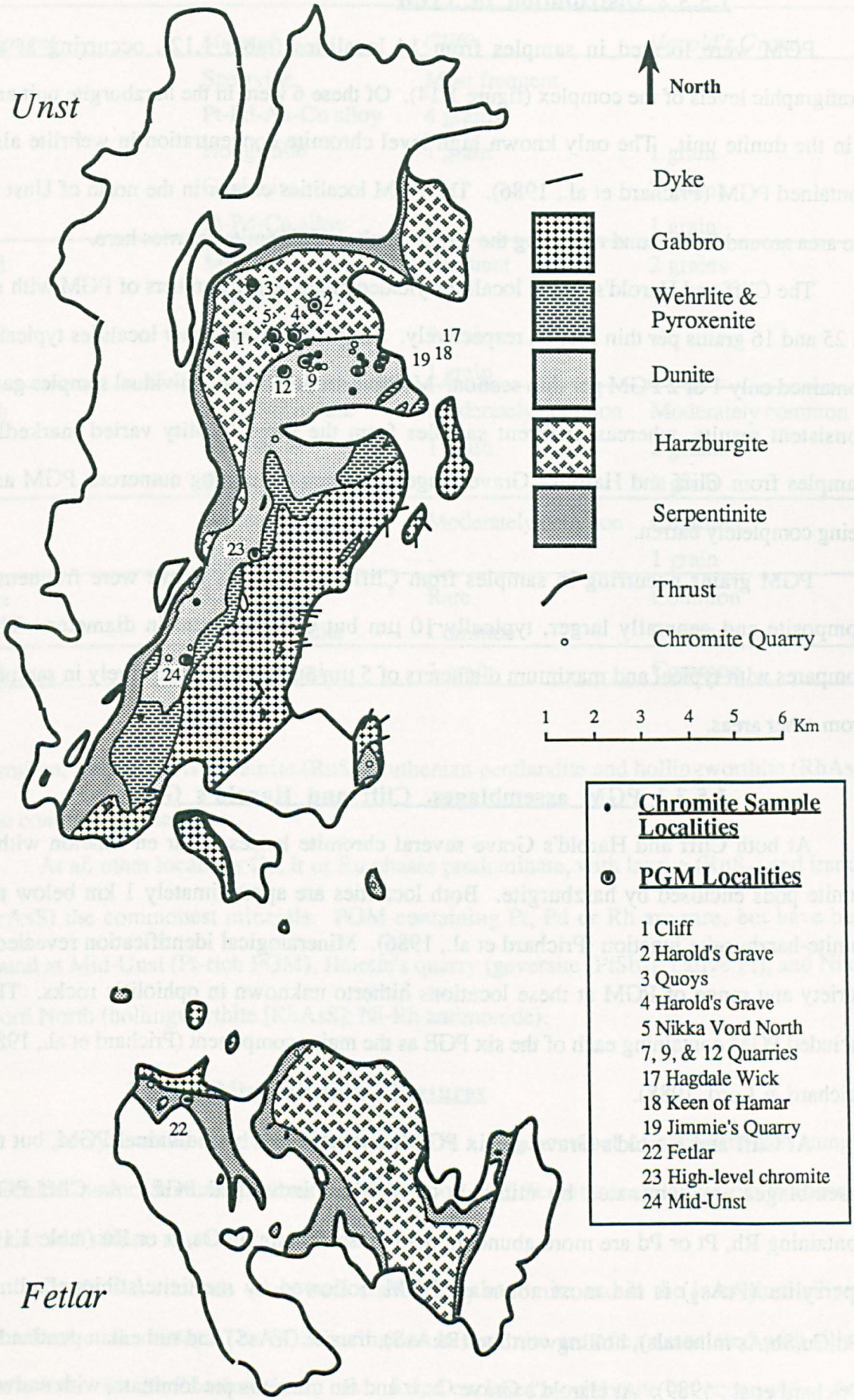

1.5.3.2 Distribution of PGM

PGM were located in samples from 14 localities (table 1.12), occurring at all stratigraphic levels of the complex (figure 1.14). Of these 6 were in the harzburgite unit and 7 in the dunite unit. The only known high level chromite concentration in wehrlite also contained PGM (Prichard et al., 1986). The PGM localities cluster in the north of Unst in the area around Baltasound reflecting the larger number of chromite quarries here.

The Cliff and Harold's Grave localities yielded much larger numbers of PGM with up to 25 and 16 grains per thin section respectively. Samples from the other localities typically contained only 1 or 2 PGM per thin section. Multiple sections from individual samples gave consistent results, whereas different samples from the same locality varied markedly. Samples from Cliff and Harold's Grave ranged between containing numerous PGM and being completely barren.

PGM grains occurring in samples from Cliff and Harold's Grave were frequently composite and generally larger, typically 10 μm but up to 250 μm in diameter. This compares with typical and maximum diameters of 5 μm and 20 μm respectively in samples from other areas.

1.5.3.3 PGM assemblages, Cliff and Harold's Grave

At both Cliff and Harold's Grave several chromite lenses occur en-échelon within dunite pods enclosed by harzburgite. Both localities are approximately 1 km below the dunite-harzburgite junction (Prichard et al., 1986). Mineralogical identification revealed a variety and range of PGM at these locations hitherto unknown in ophiolitic rocks. This included PGM containing each of the six PGE as the major component (Prichard et al., 1986; Prichard & Lord, 1988).

At Cliff and Harold's Grave all six PGE are represented by individual PGM, but the assemblages are dominated by minerals of different individual PGE. At Cliff PGM containing Rh, Pt or Pd are more abundant than those containing Os, Ir or Ru (table 1.13). Sperrylite ($PtAs_2$) is the most abundant PGM, followed by mertieite/stibiopalladinite (Pd,Cu,Sb,As minerals), hollingworthite (RhAsS), irarsite (IrAsS) and ruthenian pentlandite (Prichard et al., 1989). At Harold's Grave Os,Ir and Ru minerals predominate, with native

Table 1.13. Frequency and variety of PGM at Cliff and Harold's Grave (Prichard et al., 1989).

Element	*Mineral*	*Cliff*	*Harold's Grave*
Pt	Sperrylite	Most frequent	-
	Pt-Pd-Au-Cu alloy	4 grains	-
	Hongshiite	1 grain	1 grain
	Genkinite	-	2 grains
	Pt-Pd-Cu alloy	-	1 grain
Pd	Mertiite/ stibiopalladinite	Frequent	2 grains
	Au-Pd alloy	5 grains	-
	Potarite	1 grain	-
Rh	Hollingworthite	Moderately common	Moderately common
	Rh, Sb, S	1 grain	2 grains
	Rh, Ni, Sb	-	1 grain
Ir	Irarsite	Moderately common	Common
	Ir,Sb,S	-	1 grain
Ru	Laurite	Rare	Common
	Ru-pentlandite	Common	Common
Os	Native metal	1 grain	Common

osmium, irarsite (IrAsS), laurite (RuS_2), ruthenian pentlandite and hollingworthite (RhAsS) the commonest minerals.

At all other localities Os, Ir or Ru phases predominate, with laurite (RuS_2) and irarsite (IrAsS) the commonest minerals. PGM containing Pt, Pd or Rh are rare, but have been found at Mid-Unst (Pt-rich PGM), Jimmie's quarry (geversite [$PtSb_2$]; native Pt), and Nikka Vord North (hollingworthite [RhAsS]; Ni-Rh antimonide).

1.5.3.4 Mineralogical Textures

The systematic identification of PGMs in a large number of chromite-rich samples revealed distinct textural patterns in the position of different minerals relative to chromite grains and silicate matrix.

Os, Ir, Ru minerals occur both enclosed by chromite and in the interstitial silicates (Prichard et al., 1986). The PGM inclusions in chromite are often associated with silicate inclusions. Rh, Pt, Pd minerals are never found enclosed by chromite but occur within the

Figure 1.15. Textural position of PGM composed of different PGE with respect to chromite grains (Prichard & Tarkian, 1988).

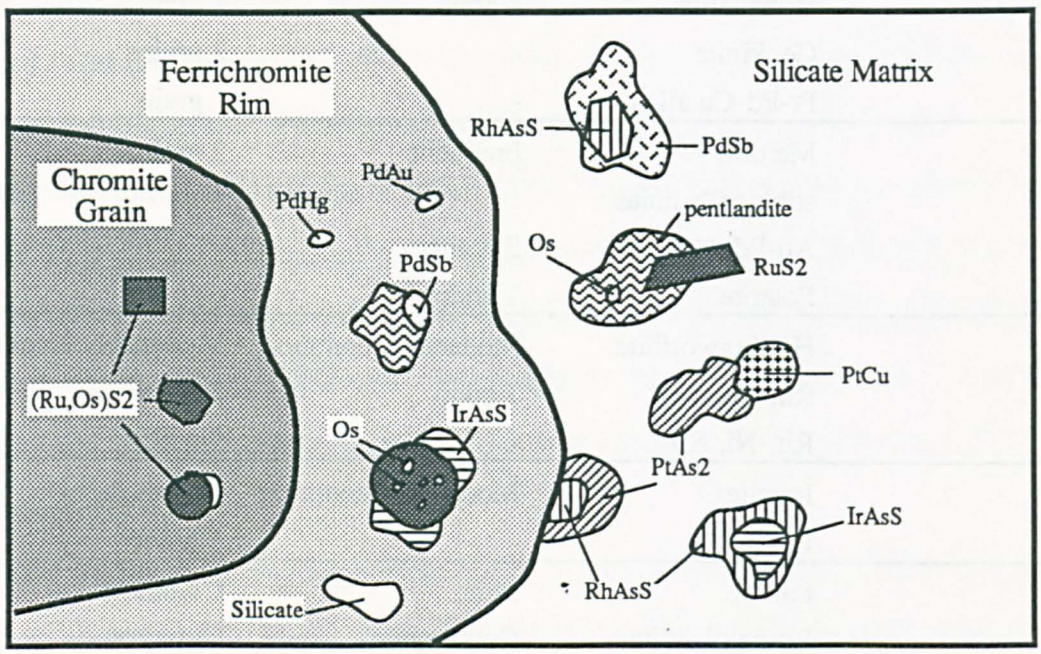

interstitial silicate matrix. Pd-bearing PGM also occur within the spongy ferrichromite alteration rims surrounding chromite grains. The shape of PGM also varies in accordance with their textural position. Enclosed PGM have angular euhedral shapes whereas PGM in the interstitial silicates are irregular. Mineral shapes vary continuously between these two extremes in sympathy with the textural position (figure 1.15).

The composition of certain PGM also varies depending on their textural position. Os,Ir,Ru minerals located in silicate contain higher levels of As (typically 2-10%) than those enclosed by chromite (generally less than 0.5%). Os-rich laurites occur within chromite, whereas laurites in the silicate matrix are Os-free but contain exsolved native osmium inclusions (Prichard et al., 1989).

Groups of PGM commonly cluster together to form composite grains. The commonest association is of native Os inclusions within laurite (RuS_2) when situated outside chromite grains. Other composite textures, in particular when one phase rims another, may indicate the order of formation of different minerals (Prichard et al., 1989). Generally As-rich

minerals surround Sb-rich phases or sulphides/sulpharsenides (e.g. irarsite (IrAsS) rimming laurites (RuS_2). Another common texture is of Rh-rich minerals rimming Ir-rich minerals (e.g. hollingworthite (RhAsS) rimming irarsite (IrAsS)). Both hollingworthite and irarsite are generally Pt-free indicating that the texturally late Pt-rich minerals were last to form. The overall textural relationships indicate crystallisation of the PGE in the order Os-Ir-Ru, Pd, Rh, Pt, with a parallel change from sulphides through antimonides to arsenides. The last PGM to form were the Pt- and Pd-rich alloys. For example hongshiite (Pt-Cu) occurs as an alteration product of sperrylite ($PtAs_2$) adjacent to a late serpentinite vein (Prichard et al., 1989).

The PGM-rich samples from Cliff also often contain nickel sulphides, arsenides and antimonides. Pentlandite, millerite and heazlewoodite occur frequently and some of these sulphides also contain Co (Prichard et al., 1989). Copper sulphides and native Cu are also common. Gold occurs as alloys with Cu or with PGE interstitially to the chromite grains. Gold-bearing minerals typically occur in association with Cu- or Pd-bearing minerals.

A few dunites from Cliff have also been found to contain PGM (Prichard & Lord, 1988; Prichard et al., 1989). These dunites are unusually fresh with only 75% serpentinisation and contain relict fresh olivine. PGM occur in association with sulphide fields consisting of clusters of heazlewoodite, millerite, pentlandite and magnetite. The PGM found in these dunites include laurite (RuS_2), hollingworthite (RhAsS) and sperrylite ($PtAs_2$).

The genetic implications of these mineralogical textures, particularly the fractionation of individual PGE with respect to the timing of chromite crystallisation, are discussed in section 1.6.1.

1.5.4 Whole-rock PGE analyses of PGM-rich samples - Stratiform and ophiolitic PGE ratios

Analyses of samples from Cliff and Harold's Grave show contrasting relative proportions of the individual PGE (Gunn et al., 1985), reflecting the different PGM assemblages at these locations (Neary et al., 1984). These differences are most apparent when the data is normalised to chondrite and plotted on a spidergram (section 1.2.3). Gunn et al. (1985) recognised the similarity between the negative slope chondrite-normalised patterns of background harzburgites and mineralisation at Harold's Grave to those reported in other ophiolites (Page & Talkington, 1984). They stressed that the positive slope patterns obtained from Cliff were more similar to those found in the Cu-Ni deposits of the Sudbury complex and the sulphide-rich rocks of the Merensky Reef in the Bushveld complex.

Subsequent analysis of ten chromitite samples (Prichard et al., 1986), including five samples from Cliff and two samples from Harold's Grave, confirmed the anomalous levels of PGE at these localities (table 1.14). Lower levels of PGE were reported in single samples of three other chromitites which included the wehrlite-hosted high level chromite in Mid-Unst.

Samples from Cliff show smooth positive slope patterns with enrichments above chondritic levels by factors of 1 to 100 (figure 1.16). Samples from Harold's Grave contain roughly chondritic levels of PGE, with flattish patterns and highly variable Pd contents. Smooth negative slope patterns were also obtained in analyses of samples from this locality (Gunn et al., 1985). The three chromitite samples from elsewhere in the complex show negatively sloping patterns with lower levels of PGE, generally depleted by factors of 10 to 100 with respect to chondrite. Such patterns are similar to those obtained from other ophiolites (section 1.2.3). Positively sloping patterns from Cliff are similar to those obtained from stratiform inclusions and were previously unknown in ophiolitic rocks (Prichard et al., 1986). Irregularities in patterns from Harold's Grave, in particular differences in the proportions of Pd relative to Pt, were attributed to the effects of hydrothermal alteration or low temperature weathering.

Figure 1.16. Chondrite-normalised diagram of Shetland chromitites compared to examples from other ophiolites and stratiform complexes (replotted from Prichard et al., 1986).

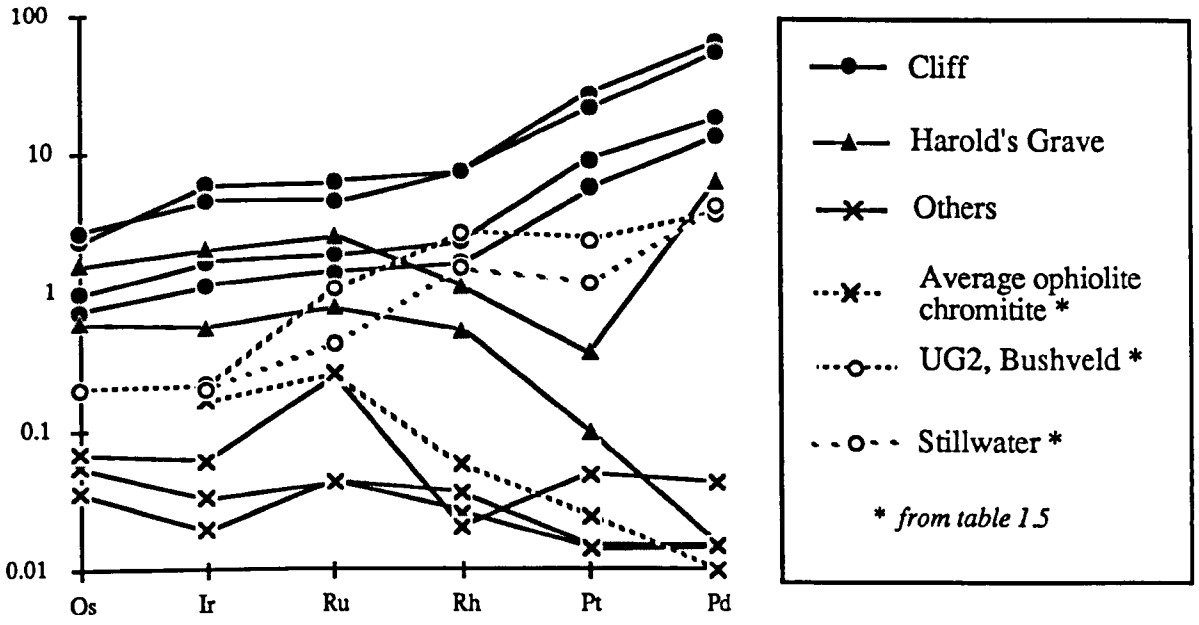

Table 1.14. PGE analyses (in ppm) of Shetland chromitites (Prichard et al., 1986).

Element	*A*	*B*	*C*	*D*	*F*	*G*	*H*	*J*	*K*
Os	1200	1400	500	370	800	302	18	28	35
Ir	3200	2500	900	600	1100	298	10	17	33
Ru	4400	3100	1300	970	1800	527	30	29	173
Rh	1500	1500	480	330	220	107	7	5	4
Pt	28000	22000	9300	5800	370	100	<15	<14	50
Pd	35000	30000	9900	7300	3400	<8	<8	<8	23
Locality	(1)	(1)	(1)	(1)	(2)	(2)	(3)	(8)	(23)

Localities:- (1) Cliff; (2) Harold's Grave; (3) Quoys; (8) Quarry 8; (23) High-level chromite (localities shown on figure 1.13)

The the chondrite-normalised patterns described above have been subjected to various interpretations (sections 1.6.1 & 1.6.2). By consensus the patterns obtained from Cliff are unusual in ophiolitic complexes but comparable to those from magmatic sulphide deposits and stratiform complexes.

1.6 The Cliff controversy - Igneous or hydrothermal, ophiolite or stratiform intrusion

In the recent studies of PGE and PGM described above various interpretations for the origin of these concentrations have been proposed. The debate centres around the unusually high grade mineralisation at Cliff which is of a type not previously known in ophiolites. The following sections summarise the various interpretative arguments as they were originally stated.

1.6.1 The hydrothermal argument (Gunn et al. 1985)

Gunn et al. (1985) proposed a hydrothermal origin for PGE mineralisation in Shetland. This hydrothermal activity may have been related to a second phase of serpentinisation during which Ni was redistributed and As, Sb and Te were introduced, probably along major N-S fault zones and other steeply dipping faults. This origin is suggested on the basis of three lines of evidence.

Firstly, although the stability fields of the PGM are poorly known, they occur in association with a sulphide assemblage indicating lower than magmatic temperatures. The minerals orcellite, maucherite, heazlewoodite and godlevskite are typically related to the serpentinisation of peridotites (Craig & Scott, 1974). Pentlandite is thought to be stable up to 610°C (Kullerud, 1963) and heazlewoodite and godlevskite to similar temperatures. Moreover the association pentlandite-godlevskite-heazelwoodite was found to be stable only below 476°C in experimental studies on the Ni-Fe-S system (Craig et al., 1968). Orcellite is formed at still lower temperatures in the range 400-450°C (Lorand & Pinet, 1984). The PGM are texturally associated with this assemblage of sulphides. Moreover, both the PGM and the sulphide/arsenide minerals show a spatial association with veining. This indicates that the PGM were stable at temperatures of less than 500°C, and suggests that they were also formed well below the range of magmatic conditions.

Figure 1.17. Triangular Rh-Pt-Pd discrimination diagram (Gunn et al., 1985).

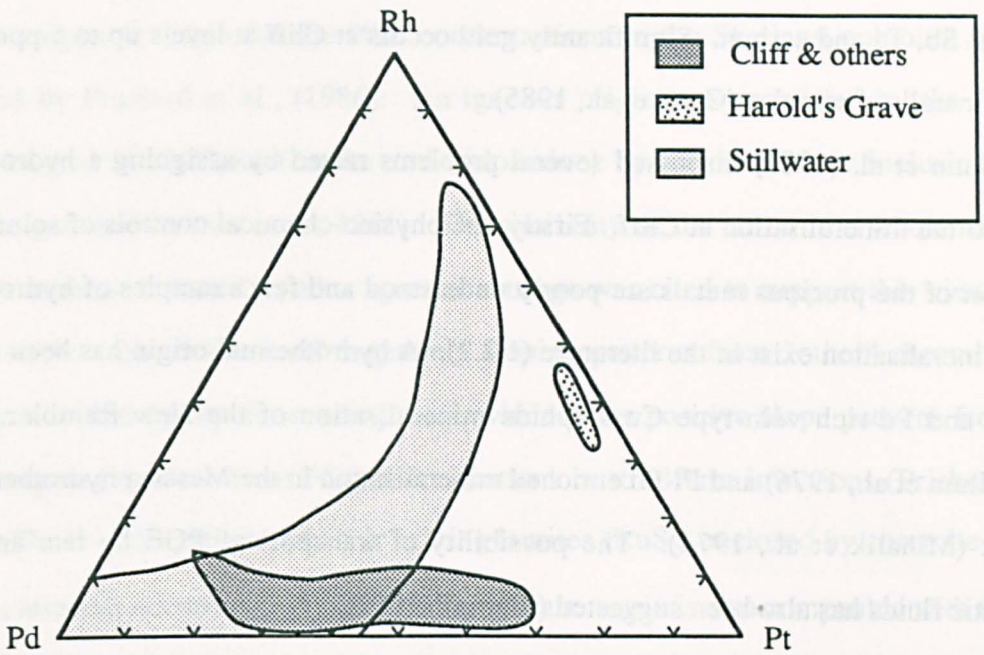

Secondly, two distinct PGE assemblages have been recognised on Unst which are discriminated on a Rh-Pd-Pt ternary diagram (figure 1.17). The first assemblage, characterised by a predominance of Os, Ir and Ru, occurs as a background population with local enrichment at Harold's Grave. This type yields a negative slope on a chondrite-normalised diagram which is similar to those of other ophiolitic chromitites (section 1.5.4). The second population is dominated by Pt and Pd and is typified by Cliff, but it is also widely found throughout the complex. This mineralisation yields a positive slope pattern on a chondrite normalised diagram similar to that observed in the Ni-Cu deposits of Sudbury and the Merensky Reef in the Bushveld (section 1.5.4). Since the mineralisation at Cliff is atypical of the sequence as a whole and is not found in other ophiolites, it is unlikely to have formed magmatically by processes intrinsic to the formation of the ophiolite.

Finally, the Cliff type of mineralisation shows some evidence of a fault-controlled distribution and is petrographically related to a second phase of serpentinisation. If the Cliff type of mineralisation is hydrothermal in origin, then the hydrothermal fluids must also have carried Ni, Cu, S, As, Sb and Te and possibly carbon. The distribution of Ni, Cu, As and PGE shows some evidence of fault control, in particular that related to a major N-S fault

zone. The Cliff area is also the focus of several groups of faults and associated hydrothermal alteration. A comparison may be drawn with the chemistry of Au transport in association with As, Sb, Te and carbon. Significantly gold occurs at Cliff at levels up to 5 ppm in the most mineralised samples (Gunn et al., 1985).

Gunn et al. (1985) discussed several problems raised by assigning a hydrothermal origin to the mineralisation at Cliff. Firstly, the physico-chemical controls of solution and transport of the precious metals are poorly understood and few examples of hydrothermal PGE mineralisation exist in the literature (1.2.2). A hydrothermal origin has been claimed for Pt- and Pd-rich vein-type Cu sulphide mineralisation of the New Rambler deposit (McCallum et al., 1976) and Pt-Pd enriched mineralisation in the Messina hydrothermal Cu deposit (Mihálik et al., 1974). The possibility of transport of PGE by late and post-magmatic fluids has also been suggested (Stumpfl, 1962).

Secondly, the close spatial association of PGE with chromite is problematical, particularly since the more chromite-rich samples are usually the most mineralised. Steep chemical gradients existing at the altering margins of chromite grains might cause preferential deposition of PGM within the altered ferrichromite haloes. Such a process would only occur in chromite mineralisation adjacent to fault zones where fluid movement was possible.

Finally, the source of PGE enrichments in the cumulate sequence is also difficult to explain. The PGE proportions are similar to those at Cliff and the sulphides pentlandite, godlevskite, heazlewoodite and maucherite have also been identified in the interstitial serpentinite of the pyroxenites. This suggests that the mineralisation occurred at the same time and under the same conditions as that at Cliff. A magmatic enrichment acting as the source of these hydrothermal concentrations was considered possible since Pt-Pd enriched PGE patterns have been observed in the mafic and ultramafic cumulate units of the Polar Urals ophiolite (Page et al., 1983) and the Thetford Mines ophiolite in Quebec (Oshin & Crocket., 1982). Since Unst appears to be "regionally enriched in PGE" the possibility of large tonnage PGE concentrations within the cumulate sequence analogous to those found in other layered intrusive complexes was suggested (Gunn et al., 1985).

1.6.2 The magmatic argument (Prichard et al., 1986)

A magmatic origin for the PGE concentrations in the Shetland ophiolite has been proposed by Prichard et al., (1986). An igneous origin was suggested by the first two PGMs located in Shetland (laurite and iridosmine) by virtue of their inclusion within chromite grains (Prichard et al., 1981). The similarity of the chromitite whole rock PGE contents to those reported in other igneous settings was cited to support this view (figure 1.16). In the case of low level negatively sloping patterns from "other" chromitites the analogy is with other ophiolite complexes, whereas the positive slope patterns from Cliff were compared to those from PGE concentrations in stratiform intrusions (Prichard et al., 1986). The textural patterns of Os Ir bearing laurites (RuS_2) enclosed by chromite and Rh, Pt or Pd minerals occurring exclusively in the silicate matrix is also compatible with the order in which PGE precipitate during fractional crystallisation (Barnes et al., 1985).

Dunite lenses within the Unst harzburgite sequence contain variable amounts of chromite (section 1.4.6). They are thought to represent in situ crystallisation from magma diapirs rising through the harzburgite to feed an overlying magma chamber (Gass & Smewing, 1981). Prichard et al. (1986) suggested, therefore, that the extremely localised variation in the absolute levels and relative proportions of individual PGE in different chromitites might result from differences in magma composition due to varying degrees of partial melting, heterogeneity of the mantle source or differing crystallisation conditions.

Two alternative hypotheses were proposed to account for the presence of arsenide and antimonide PGM phases outside chromite grains (Prichard et al., 1986). Firstly, the concentrations of these elements may have increased during progressive crystallisation. The Os,Ir,Ru bearing PGMs show a progressive increase in As content, illustrated by the As:S ratio, across the textural spectrum from enclosed to interstitial positions. Secondly, interstitial PGMs may have been locally remobilised and the mineralogy modified at a late stage and at much lower temperatures by an As- and Sb-rich fluid. The authors cite examples of studies which suggest that the introduction of As into PGMs may be related to hydrothermal alteration during serpentinisation (Jen & Teng, 1973; Whittaker & Watkinson,

1985) and that As-bearing PGM may be soluble at surface temperatures and pressures (Stumpfl & Tarkian, 1976).

Prichard et al. (1986) conclude that the whole-rock PGE chemistry suggests little bulk movement of individual PGE in Shetland (assuming smooth patterns identify magmatic concentrations), and find the textural separation of different PGE difficult to explain if the concentrations are purely hydrothermal in origin. They suggest, therefore, that this fractionation is the result of magmatic processes. However, the possibility of partial hydrothermal modification of the mineralogy of the magmatic concentrations is not precluded.

1.6.3 The late-magmatic fluid argument (Prichard & Lord 1988)

The similarity of the PGE assemblages from Cliff to those from other geological situations, most notably stratiform complexes, has been used to question the validity of the previous identification of the complex as an ophiolite. Various field relationships may be cited to support the ophiolitic theory, in particular the podiform character of the chromite concentrations and the overall stratigraphy of the complex (section 1.4). Two further lines of geochemical evidence may be used, the chromite mineral chemistry and the trace element geochemistry of the dykes (Prichard & Lord, 1988). Chromites from Shetland show the wide range of Cr/Fe ratios but limited Ti/Fe variation which is typical of other ophiolite complexes. Furthermore, chromites from Cliff and Harold's Grave containing numerous PGM have broadly similar compositions to PGM-barren chromites (Prichard & Lord, 1988). This is the subject of a later section (chapter 3). The dyke geochemistry (section 1.4.5) indicates that the ophiolite is of SSZ-type generated by hydrous melting and that the resulting magma therefore had a volatile component (Prichard & Lord, 1988).

There is considerable debate concerning the role of magmatic volatiles in processes controlling the distribution of PGE in stratiform complexes (Ballhaus & Stumpfl, 1985). Much of this debate is relevant to the origin of PGE concentrations in Shetland. However, it is difficult to assess the relative roles of magmatic and magmato-hydrothermal processes as a result of the superimposition of secondary fluid alteration (Prichard & Lord, 1988). All

ultramafic rocks in the complex have been serpentinised to some extent, but fresh primary olivine, clinopyroxene, orthopyroxene and chrome spinels are usually present. In contrast the chromite-rich lenses are always situated in highly altered zones, and silicate minerals interstitial to the chromite grains are always totally altered to serpentine and chlorite. This may be a consequence of the rheological contrast between dunite and chromitite, which during deformation created pathways for fluids and facilitated preferential alteration. In addition to serpentinisation there is evidence of a hydrothermal alteration event, possibly linked with acid igneous activity and talc formation (Neary & Prichard, 1985).

Recent mineralogy has also revealed the presence of PGM in dunites surrounding the PGM-rich chromitites at Cliff (Prichard et al., 1989). These include laurite (RuS_2), hollingworthite (RhAsS) and sperrylite ($PtAs_2$). Whole-rock INAA analysis of these samples returned Ir concentrations of up to 15 ppm. These dunites are some of the least altered rocks in the area and contain abundant fresh olivine (Prichard & Lord, 1988). This was used as evidence that PGE concentrations are not solely related to alteration zones or secondary processes, but may be a primary association within the chromite-rich dunite pod. It was suggested that late magmatic fluids may also influence PGE mobility and that the hydrous melting conditions proposed for the origin of SSZ ophiolite complexes may therefore be important for PGE concentration (Prichard & Lord, 1988).

1.7 Discussion of genetic models

The previous sections have summarised the published arguments for the origin of PGE concentrations in the Shetland ophiolite by magmatic, hydrothermal and late-magmatic fluid processes. These accounts are now critically assessed.

The association at Cliff of PGM with a sulphide assemblage controlled by veining and characteristic of formation at temperatures below 500°C, prompted Gunn et al. (1985) to suggest a hydrothermal origin. It is not implicit from these observations that the PGM were formed at these low temperatures since the stability of the PGE phases is poorly known. For example, an original magmatic assemblage may have remained stable during hydrothermal alteration of the associated sulphide phases. Two other lines of evidence were provided.

Firstly, two distinct populations of PGE mineralisation were recognised throughout the ophiolite indicating two different origins (Gunn et al., 1985). Mineralisation dominated by Os, Ir and Ru occurred as a background throughout the harzburgite unit with local enrichment at Harold's Grave and was thought to be generally magmatic. The distinct, Pt, Pd dominant mineralisation found at Cliff and elsewhere, was thought to be hydrothermal. Clearly there is no obvious source for hydrothermal Pt or Pd within the ophiolite in this model unless magmatic concentrations occur elsewhere in the sequence. Concentrations of Pt and Pd in the layered cumulate sequence were thought to be magmatic by analogy with those in the Polar Urals and Thetford Mines ophiolites (Page et al., 1983; Oshin & Crocket, 1982). The concentrations in the Unst cumulates contained the same PGE ratios and were associated with a similar sulphide assemblage to that at Cliff. Furthermore, both the Cliff and Harold's Grave types of mineralisation were found to have identical constant ratios of Ru and Ir. This strongly suggests a genetic link between the two populations.

The second argument for a hydrothermal origin centred around the fault control patterns in the distribution of the PGE and their pathfinder elements Ni, Cu and As. Gunn et al. (1985) noted that PGE-bearing chromitites from the dunite unit generally contained higher levels of Cu and Ni compared to chromitites from the harzburgite unit containing similar levels of PGE. This observation could equally be interpreted as a distribution of pathfinder elements under stratigraphic control, which is more likely to be magmatic than hydrothermal in origin. Correlations between PGE and the other pathfinder elements (As, Sb and Te) were only observed in the anomalously high concentrations found exclusively at Cliff and are therefore not generally applicable. This also suggests that the results of mineralogical studies of samples from Cliff are similarly limited, and may not represent the true assemblage elsewhere.

Prichard et al. (1986) suggested a magmatic origin based on two lines of evidence. Firstly, the similarity of the smooth chondrite-normalised PGE patterns from Cliff to those found in other igneous settings. Considerable debate exists surrounding the extent to which magmatic processes are responsible for these concentrations (Stumpfl & Tarkian, 1976). The often cited example of the greater mobility of Pd compared to Pt (Fuchs & Rose, 1974) relates to surface weathering in soils and may not be relevant to the hydrothermal alteration of

magmatic rocks. The modification of magmatic PGE ratios during hydrothermal remobilisation by virtue of their differential solubilities has been suggested (Keays et al., 1982; McCallum et al., 1976; Rowell & Edgar, 1986; Hulbert et al., 1988) although large increases in Pd/Pt ratios have not always been found where magmatic concentrations are upgraded (e.g. Talkington & Watkinson, 1984; Boyd et al., 1988).

Secondly, some PGM occur enclosed by chromite grains of compositions typical of ophiolitic magmatic chromite. However these minerals only represent the assemblage and proportions of PGE which are typical of ophiolite chromitites. An entirely different PGM assemblage occurs interstitially to and surrounding the chromite grains. The proposed paragenetic sequence of early enclosed and late interstitial PGM, separated by the crystallisation of chromite, is compatible with the order of crystallisation of the PGE during magmatic fractionation. This does not preclude the possibility that Pt-Pd-Rh concentration were formed by an entirely separate magmatic process to the Os-Ir-Ru concentrations and owe their present concentration at chromite grain boundaries to hydrothermal remobilisation.

The predominance of antimonide and arsenide minerals in the interstitial PGM assemblage is also problematical, providing evidence of low temperature processes, perhaps modifying magmatic assemblages. Moreover, certain Pd minerals occur within the altered ferrichromite rim surrounding the chromite grain. The origin of ferrichromite rims on chromite grains is itself controversial (Bliss & Maclean, 1975) but is often related to serpentinisation (Ulmer, 1974; Haggerty, 1976). More recently a link has been established between the formation of ferrichromite and the alteration of chromite by a mineralising hydrothermal fluid (Wylie et al., 1987).

Prichard and Lord (1988) suggested that late magmatic fluids might also influence PGE mobility or concentration. The presence of a volatile component in the magma is indicated by the SSZ origin of the complex. This model was suggested to reconcile the magmatic origin of the PGE suggested by the inclusions in chromite with the hydrothermal characteristics of the mineralisation in the silicate matrix. If the remaining PGE partitioned into a high temperature immiscible fluid phase, then the resulting mineralisation would not necessarily be associated with the dunite pod which represents the silicate magma phase. The presence of PGM in partially fresh dunites at Cliff is also contradictory, since auto-alteration and

serpentinisation would be expected during mineralisation by this fluid at the temperatures suggested by the sulphide assemblage.

The fluid-rich nature of the SSZ melting environment is more likely to play a role in the generation of silicate magmas containing significant PGE contents. This can be seen by analogy with suggested multi-stage mantle melting to generate PGE-enriched boninitic magmas and the compositionally similar parental magmas for the Bushveld complex (Hamlyn & Keays, 1986). It follows from the chalcophile behaviour of PGE that during the generation of sulphur saturated initial melts these elements will remain in the mantle (Hertogen et al., 1980). Subsequent remelting of this refractory source produces sulphur deficient PGE-enriched magmas (Hamlyn et al., 1985; Hamlyn & Keays, 1986).

More recently Hulbert et al. (1988) have suggested that the PGE concentrations at Cliff may have resulted from the hydrothermal remobilisation of an original magmatic concentration. Chemical studies indicate that PGE become mobile as thiosulphate complexes only during the initial stages of serpentinisation and thus move with the associated redox front. Interaction with an introduced As-bearing fluid provides a mechanism of effectively fixing Pt since the arsenide (sperrylite) is more insoluble than the sulphide. In this model the association of PGE mineralisation with chromite is again linked to the development of dilational brittle fractures in the more competent chromitite body, compared to the ductile expanding serpentinite, acting as a focus for mineralising fluids.

Perhaps the greatest criticism of all the recent studies of the Cliff mineralisation is that, while noting an association between chromite content and high PGE concentrations, they fail to adequately demonstrate the distribution of PGE with respect to the different primary silicate lithologies. Magmatic concentrations would only be found within the dunite pod and the surrounding harzburgites would be PGE-poor. Conversely hydrothermal concentrations might cross-cut the igneous structure or be related to the degree of alteration of the igneous lithologies. If PGE precipitation is controlled by an interaction with chromite then the chromite-bearing harzburgites should contain similar levels of PGE as the chromite-poor dunites (C. R. Neary, pers. comm.). The spatial arguments centring around the development of void spaces would similarly be related to the distribution of chromite-rich and chromite-poor primary lithologies. Finally the effects of secondary alteration on an

original magmatic concentration would be best quantified by locating and establishing the distribution of PGE within another magmatic chromite-rich pod well away from the basal thrust or other internal alteration zones.

1.8 Outline of problem

In conclusion, at the outset of this study considerable debate still surrounded the origin of PGE concentrations in the Shetland ophiolite, in particular the unusually high concentrations of Pt and Pd found at Cliff. Contradictory evidence exists of both magmatic and hydrothermal processes although neither alone can fully explain the patterns of PGE concentration described. Additional detailed work is required to establish the character, distribution and genetic controls of mineralisation and thereby quantify the roles of magmatic and hydrothermal processes both spatially and temporally in the whole of the ophiolite complex. The specific problems which this study aims to answer are summarised below in the order in which the appear in subsequent chapters:-

(1) Can a complete primary lithological stratigraphy be recognised in the complex? (Ch 2)

(2) Do chromitites from the PGM-rich localities, Cliff and Harold's Grave, have distinctive or non-ophiolitic chromite compositions? (Ch 3)

(3) Do chromite-rich rocks from other localities also contain unusual levels or ratios of PGE? (Ch 4)

(4) Do concentrations of PGE occur in chromite-poor lithologies? (Ch 4)

(5) What is the overall pattern of concentration of PGE in the complex? (Ch 4)

(6) Do PGE levels show any patterns of association with particular igneous lithologies indicating primary concentration processes? (Ch 4)

(7) Can the controls of PGE mineralisation be recognised in hand specimen in the field? (Ch 4)

(8) Can a model be devised predicting the occurrence of PGE in other complexes? (Ch 4)

(9) Can pathfinder elements* for the PGE concentrations be identified? (Ch 5)

(10) Do high levels of pathfinder elements uniquely define PGE concentrations? (Ch 5)

(11) What are the patterns of distribution and concentration processes of any pathfinder elements? (Ch 5)

(12) Do differences in these patterns for different elements indicate different geochemical behaviour? (Ch 5)

(13) Can stratigraphically controlled horizons of PGE enrichment be recognised? (Ch 6)

(14) What are the relative concentrations of the individual PGE? (Ch 7)

(15) Can differences in the internal ratios of the six PGE be related to different associations or processes? (Ch 7)

(16) Can magmatic fractionation processes be seen? (Ch 7)

(17) Are non-magmatic processes required to fully account for the patterns of PGE mineralisation identified? (Ch 5, Ch 7, Conclusions)

---

*a pathfinder is an element which has a similar distribution as the sought element but which is cheaper or easier to detect

Chapter 2

Field Relations, Petrology and Structure of the Ophiolite Sequence

2.1 Introduction

Field work began with detailed field mapping of the characteristic primary rock units in the ophiolite sequence. Production of a detailed lithological base map was also a prerequisite for the accurate location of samples, in order to show the geographical distribution of PGE concentrations in relation to the ophiolite stratigraphy. To facilitate this mapping a relatively small (8 km^2), well exposed study area was chosen, which contained a representative vertical section of the ophiolite.

The area selected, around Baltasound in the centre of Unst (figure 2.1), lies in the NE corner of the main (lower) ophiolite nappe exposure. Previous reconnaissance mapping of this area (Gass et al., 1982), indicated a vertical NE-striking stratigraphy, with an apparently complete sequence from harzburgite in the NW to gabbro in the SE.

Topographically this area is undulating and gently sloping except for a prominent east-west ridge, formed by Nikka Vord, Little Heog and Muckle Heog, which rises to 140 m above sea level. Southwards the ground slopes gently towards Balta Sound, rising again eastwards towards the vertical sea cliffs on the Keen of Hamar (plate 2.1).

The eastern promontory of Swinna Ness and also the Ordale area south of Balta Sound both show a conspicuous ridged topography with a NE-SW grain.

The topography of the area closely reflects the underlying geology. Harzburgites occupy the higher ground to the north, the E-W trending junction with the dunite unit forming a prominent scarp feature above the lower ground around Baltasound. Alternating layers of pyroxenite in wehrlite and dunite impart the NE-SW grain in the areas of the Keen

Figure 2.1. Geography and topography of study area.

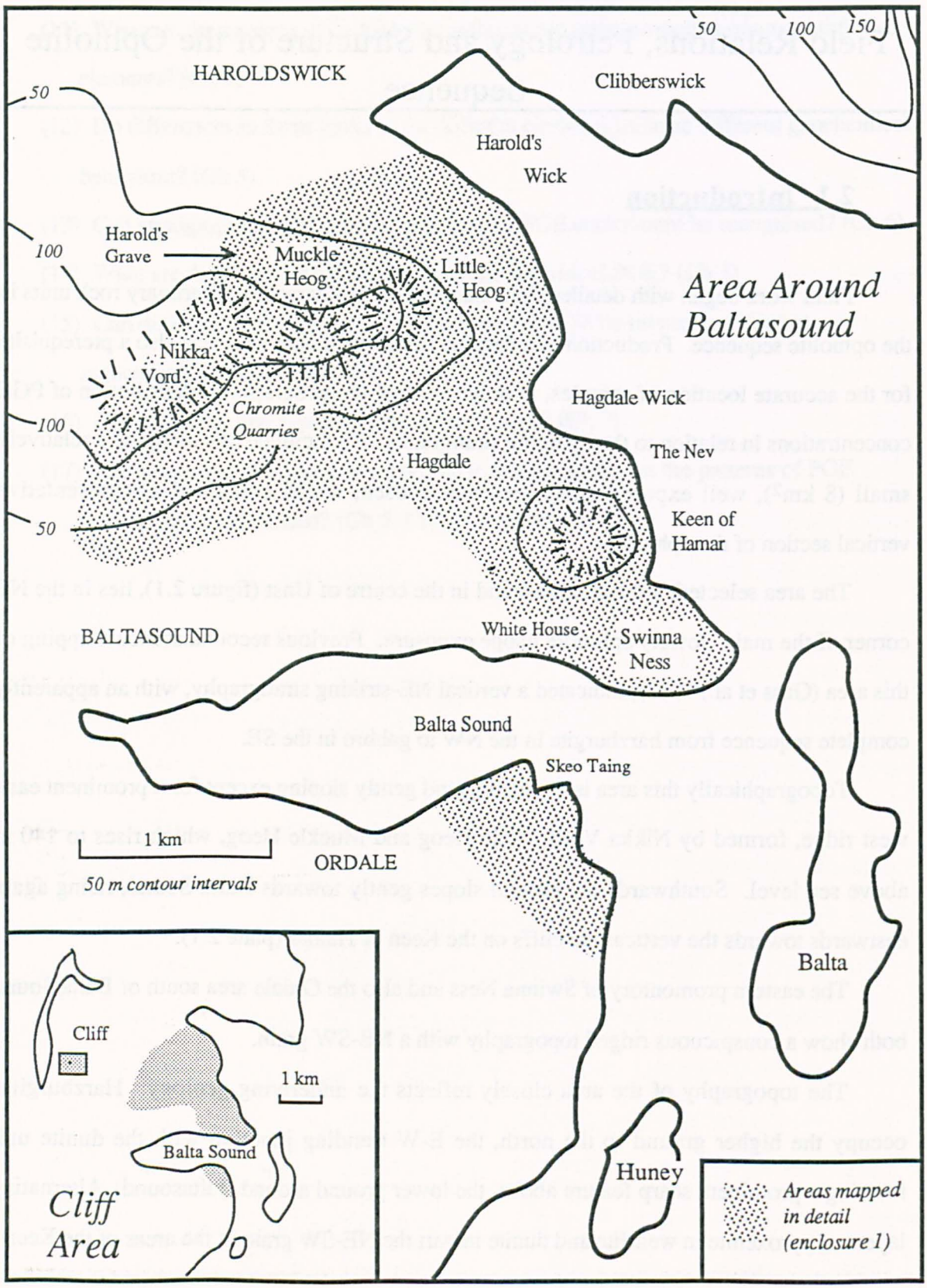

Plate 2.1. View to SE from Little Heog showing the ophiolite stratigraphy.

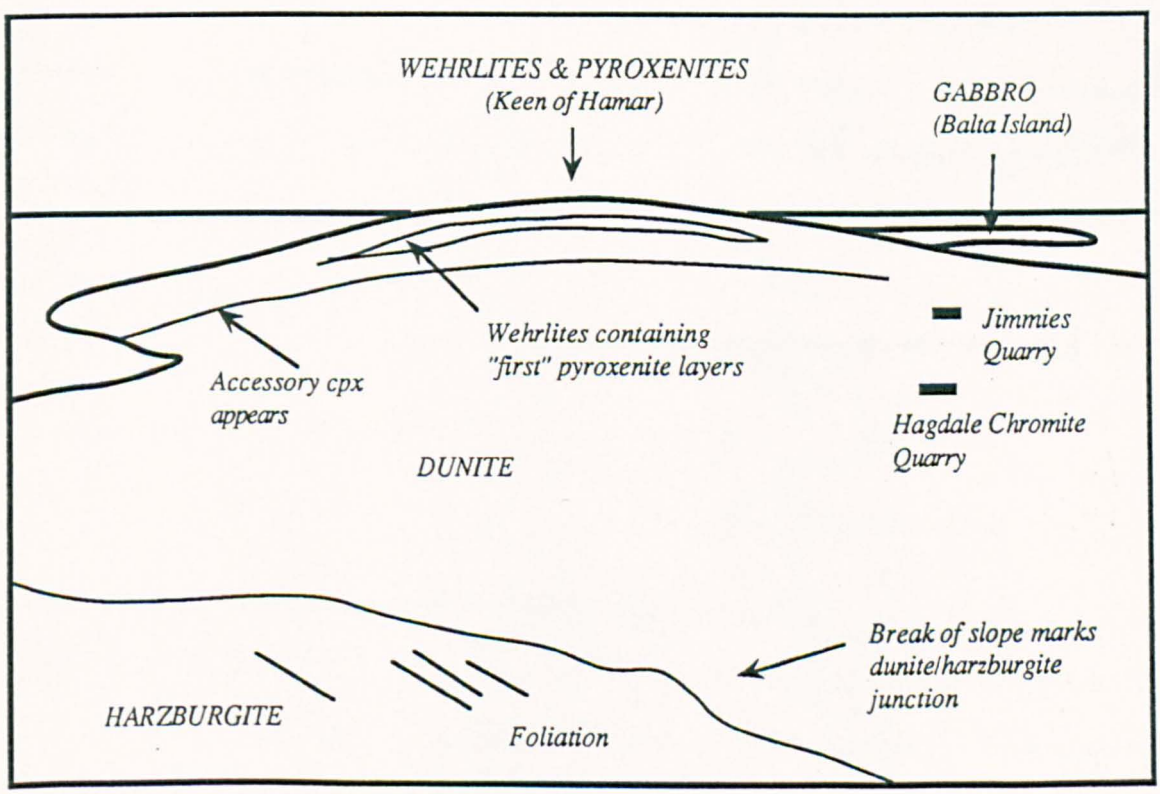

of Hamar and Ordale, with a sharp junction to gabbros further south east and on Balta island.

Exposure is best on the higher ground to the north. Here it is always patchy, with upstanding areas approaching 50% exposure surrounded by poorly exposed low lying areas. Elsewhere exposure is generally poor apart from scattered ridges of good exposure and near complete coastal sections along the low cliffs of the eastern shore.

In the course of this study the area was re-mapped in detail using air photograph enlargements at a scale of 1:4500. The results of this mapping are shown in detail on enclosure 1 and summarised in figure 2.2. In view of the virtual absence of transgressive structures in previous maps of the ophiolite, particular attention was paid to the identification of internal faults and shear zones, in order to establish the tectonic disruption of the sequence and detailed igneous stratigraphy. Using air photographs allowed much fine-scale lithological detail to be recorded. Due to stereoscopic distortions, however, this method does not facilitate the recording of complex petrofabrics. Representative foliations are shown on enclosure 1 which were recorded using an early version as a base map.

The following sections describe the field appearance of each lithological unit of the sequence together with any field relations observed during mapping. These are compared to those known from the literature where contradictions occur. A summary of previous petrological investigations is also included.

2.2 Mantle sequence

2.2.1 Harzburgite

Harzburgites are typically yellowish-brown in colour with a characteristic rough weathered surface and a blocky appearance in outcrop (plate 2.2). Mineralogically they are composed of varying proportions of relict olivine and pyroxene or serpentine and chlorite pseudomorphs after these minerals. The original mineralogy was predominantly olivine with subsidiary orthopyroxene and accessory chromite and clinopyroxene. According to Brzozowski (1977) the original composition of the Unst harzburgite was 60% olivine,

Figure 2.2. Summary geological map of the area around Balta Sound. The Cliff area is shown as an inset at the same scale. For the location of both areas see figure 2.1.

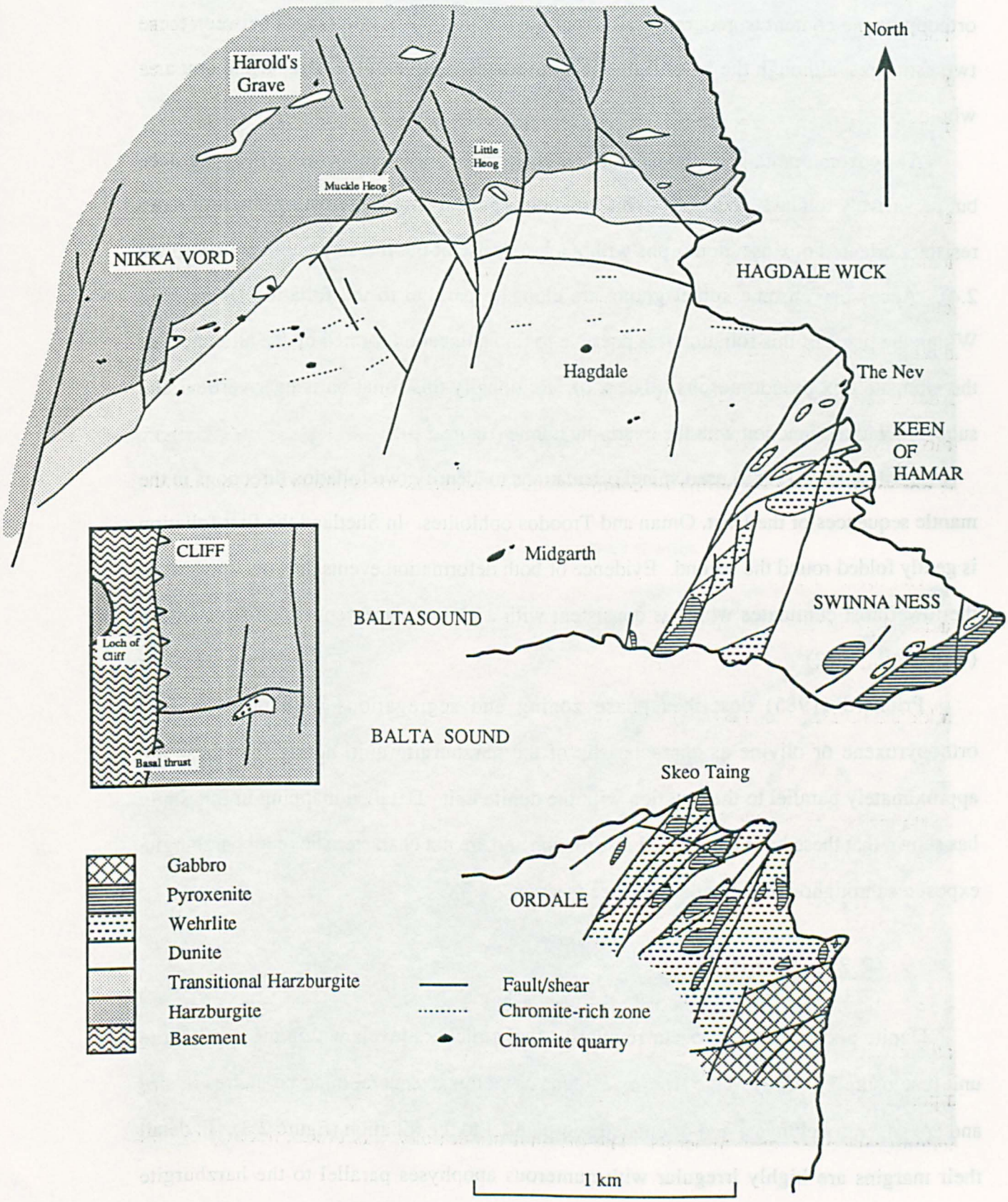

30-35% enstatite, 5% chrome spinel and up to 5% diopside. Prichard (1985) reports orthopyroxene constituting at maximum only 15% of the harzburgite and olivine compositions uniformly of Fo 90.5. Field observations in this study indicate that the orthopyroxene content is geographically variable (section 2.2.3) and ranges between these two estimates, although the latter figure is more representative of the harzburgite unit as a whole.

Away from dunite pods the harzburgite is typically very homogeneous in appearance but pervasively foliated (plate 2.3). This foliation is picked out by alternating layers of more resistant oriented opx pseudomorphs within a less resistant olivine-serpentine matrix (plate 2.4). Accessory chrome spinel grains are elongate parallel to the foliation (plate 2.5). Within the plane of this foliation it is possible to find a lineation formed by the alignment of the elongate opx pseudomorphs (plate 2.6). Regionally this foliation is near vertical and subparallel to the junction with the overlying dunite (figure 2.3).

Bartholomew (1983) used spinel orientations to identify two foliation directions in the mantle sequences of the Unst, Oman and Troodos ophiolites. In Shetland the first foliation is gently folded round the second. Evidence of both deformation events dies out upwards in the lowermost cumulates which is consistent with a pre-emplacement ocean-floor origin (Gass et al., 1982).

Prichard (1985) describes phase zoning and segregations with more or less orthopyroxene or olivine as characteristic of the harzburgite unit, noting that these are approximately parallel to the junction with the dunite unit. Detailed mapping in this study has shown that these have a restricted distribution and are not characteristic of all harzburgite exposures throughout the mantle sequence (section 2.2.3).

2.2.2 Dunite pods

Dunite pods (plate 2.7) occur regularly at all structural levels within the harzburgite unit (enclosure 1). They range from a few tens of metres to several hundred metres in size and are generally elongate and orientated sub-parallel to the foliation (figure 2.3). In detail their margins are highly irregular with numerous apophyses parallel to the harzburgite foliation. Frequent satellite lenses suggest that these dunite bodies have a complex three-

Plate 2.2. Typical outcrop of homogeneous harzburgite.

Plate 2.3. Mantle foliation cutting homogeneous harzburgite.

Plate 2.4. Outcrop/foliation lineation. Layers of opx defining foliation (close-up of plate 2.2).

Plate 2.5. Spinel elongation direction parallel to foliation (close-up of plate 2.4).

Figure 2.3. Map of dunite pods in harzburgite around Muckle Heog and Little Heog.

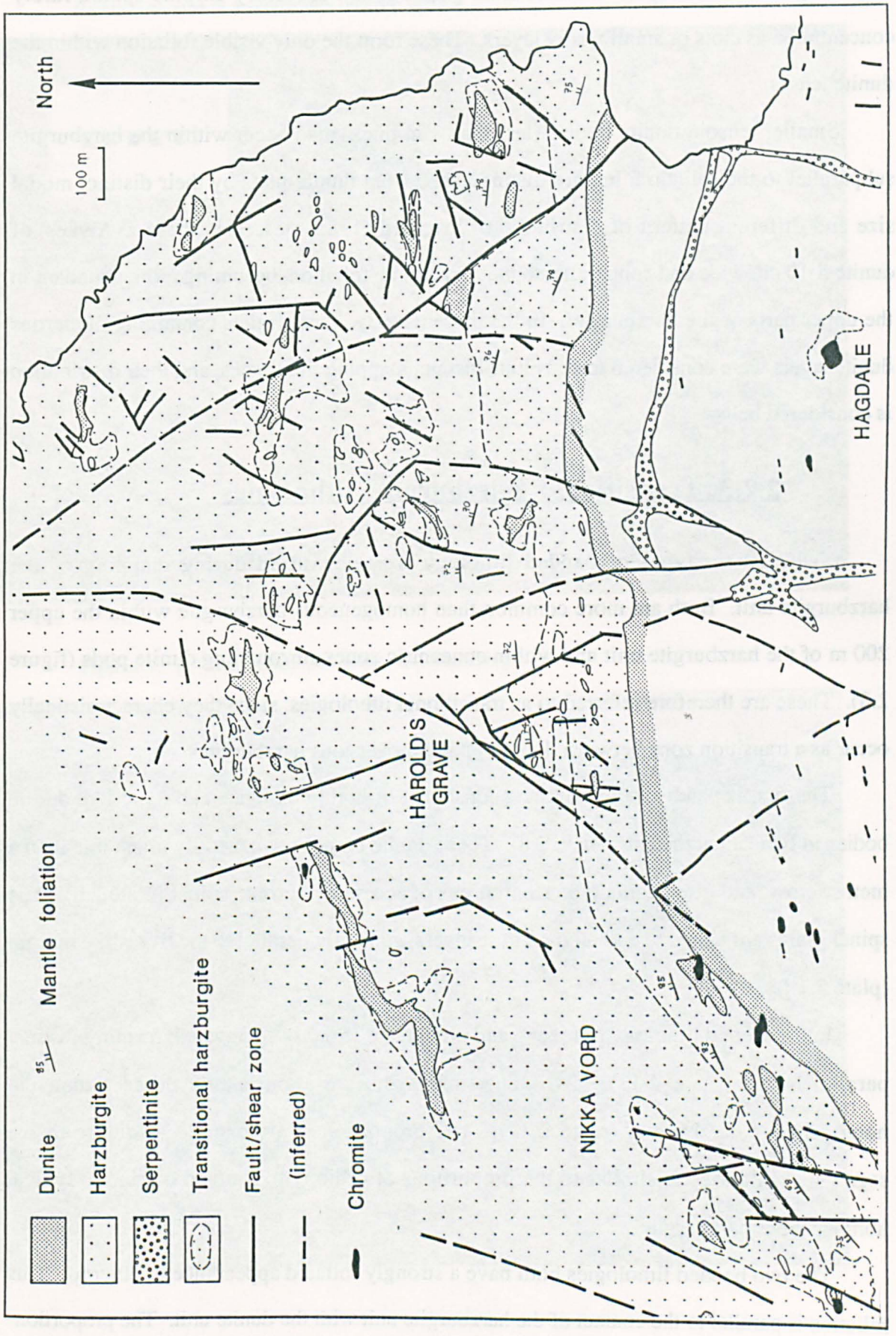

dimensional structure. Their margins are sharp and locally cross-cut or truncate the foliation of the adjacent harzburgite. Dunites from pods contain accessory chrome spinel, rarely concentrated as clots or small wispy layers. These form the only visible foliation within the dunite lenses.

Smaller lensoid dunite bodies (less than 1 m thick) also occur within the harzburgite subparallel to the foliation, but are distinguished from dunite pods by their distinct modal size and different pattern of distribution. Prichard (1985) describes these as 'dykes' of dunite 5-10 cm wide and subparallel to the harzburgite foliation, becoming more abundant in the upper parts of the harzburgite. In the present study, harzburgites containing numerous dunite layers were considered to constitute distinct mapping lithologies, and their distribution is considered below.

2.2.3 Transitional harzburgite lithologies

Two distinct types of banded lithology were identified during mapping of the harzburgite unit. Both are more common than homogeneous harzburgite within the upper 200 m of the harzburgite unit and within concentric zones surrounding dunite pods (figure 2.3). These are therefore referred to as transitional lithologies, since they characteristically occur as a transition zone between dunites and homogeneous harzburgites.

The first is patchy in appearance, consisting of highly elongate and dyke-like dunite bodies in typical harzburgite (plate 2.8). These dunite bodies are generally much less than a metre across, and often contain concentrations of accessory chrome spinel (plate 2.9). The spinel grains are elongate and aligned in stringers, generally parallel to the dyke-like margin (plate 2.10).

In the second lithology pyroxene and olivine are strongly segregated, forming distinct parallel layers (plate 2.11). Pyroxene-rich layers are significantly coarser than the homogeneous harzburgite (plate 2.12). The proportion of pyroxenite to dunite in the segregated lithology is similar to the proportions of orthopyroxene and olivine in typical homogeneous harzburgite.

The two banded lithologies both have a strongly foliated appearance in outcrop. This foliation is parallel to the contact of the harzburgite unit with the dunite unit. The proportion

Plate 2.6. Elongate opx pseudomorphs defining a lineation direction in the plane of the foliation as seen in a subparallel outcrop surface.

Plate 2.7. A small dunite pod north of Little Heog.

Plate 2.8. Outcrop of "patchy" transitional harzburgite. Lenses of dunite in otherwise typical harzburgite.

Plate 2.9. Chromite stringers in dunite layer (close-up of plate 2.8).

Plate 2.10. Close up of plate 2.9 showing elongation of chromite grains. Note the variable lineation directions.

Plate 2.11. Outcrop of "segregated" transitional harzburgite adjoining typical homogeneous harzburgites above the hammer.

Plate 2.12. Close-up of segregations showing the coarser crystals in the pyroxenite folia compared to those in the harzburgite (left of pen).

Plate 2.13. Pyroxenite "dykes" cutting harzburgite subparallel and oblique to the foliation.

of transitional harzburgite increases towards this junction and predominates over homogeneous harzburgite in the upper 200 m of the unit. In addition to zones surrounding dunite pods these lithologies also occur as irregular isolated patches within typical harzburgite well away from any outcropping dunite pods. These are probably marginal zones associated with dunite pods above or below the present erosional plane.

Thin "dykes" of pyroxenite (now totally serpentinised), typically less than 10 cm across, occur cutting all lithologies of the harzburgite unit. These are common near dunite pods, where they often cross other foliations (plate 2.13). Pyroxenite "dykes" occasionally cross-cut other "dykes" (plate 2.14). Very rarely single dyke-like dunite bodies can be traced cutting the harzburgite unit over distances of several tens of metres. (plate 2.15).

The banded lithologies and minor intrusions described above are typical features of ophiolite mantle sequences (Gass & Smewing, 1981). The gneissose banding, referred to here as "segregated transitional harzburgite" results from the metamorphic segregation of olivine and orthopyroxene into separate folia, enhancing the harzburgite foliation (Gass, 1980). Minor concordant dunite layers typical of the "patchy transitional harzburgite" may be explained as infolded or more deformed examples of the larger more discordant "dunite pods". These are generally regarded as the olivine precipitating from magma diapirs rising from a lower lherzolitic melting zone through the previously depleted harzburgites (Allen, 1975; Gass & Smewing, 1981). The similar range of Cr/Al variation in chromite from harzburgites and intra-harzburgitic dunites has led others to suggest that dunite bodies were formed by metasomatic-like processes involving orthopyroxene instability related to relatively high water pressures (Johan and Augé, 1986).

Compared to other ophiolites the dyke-like minor intrusions cutting the Unst harzburgite show a limited range of compositions. In a study of the Semail peridotite Gregory (1984) reported a pseudo-stratigraphy within the minor intrusions, with dunite and pyroxenite dykes throughout but gabbroic dykes only in the upper levels. More evolved compositions were related to greater assimilation of the wall-rocks as a function of the geometry of the conduit (figure 2.4). With low melt/rock ratios in large fast flowing conduits olivine is precipitated and the melt evolves along the olivine control vector. Melts in small low flow anastomosing conduits assimilate more wall rock and evolve rapidly to

cotectic assemblages. The absence of gabbroic intrusions in Shetland indicates a regime of high flow rates, thus maintaining high melt/rock ratios and minimizing reaction with the wall rock harzburgites.

Figure 2.4. Phase diagram illustrating the effects of melt/rock ratios on the evolution of picritic melts during ascent through the upper mantle (from Gregory, 1984). With high melt/rock ratios in large fast flowing conduits olivine is precipitated and the melt evolves along the olivine control vector. Melts in small low flow anastomosing conduits assimilate more wall rock and rapidly evolve to cotectic assemblages.

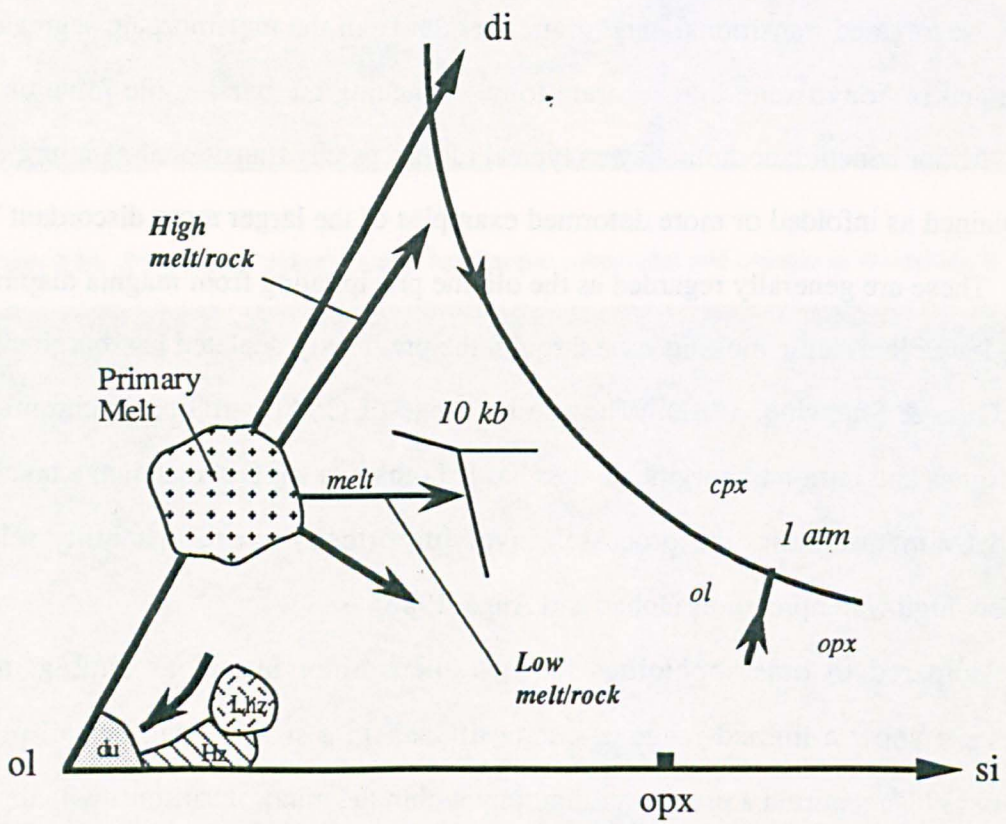

Plate 2.14. Cross-cutting conjugate pyroxenite "dykes".

Plate 2.15. Dyke-like dunite body (light yellow, immediately to right of hammer) with parallel pyroxenite "dyke" along right hand margin.

Plate 2.16. Nikka Vord South chromite quarry. The chromite orebody is surrounded by a thin margin of dunite (poorly exposed), surrounded in turn by harzburgites

Plate 2.17. Layered Quarry north of Quarry 12. A group of small pits from which well layered chromite-rich dunite spoil can be found.

2.2.4 Chromite concentrations

Several chromite bodies occur within the harzburgite unit (figure 2.5). These include the Cliff and Harold's Grave localities (figure 2.2) which are considered in more detail later (section 2.2.5). Chromitite has also been worked at four locations on Nikka Vord (plates 2.16 - 2.19)*. In all cases the workings are located in dunite pods or their surrounding envelope of transitional lithologies. Three other relatively large chromite workings are located close to the junction with the dunite unit to the south of Nikka Vord (plates 2.20, 2.21 & 2.28). Previous reconnaisance mapping (Prichard & Neary,1982) located these within the dunite unit. Detailed re-mapping has established that these lie just within the upper part of the harzburgite, in one case (quarry 7 or Long Quarry) enclosed by a dunite pod impinging on the dunite unit (figure 2.5).

A full range of chromite textures is typically represented in the spoil from each quarry. These include disseminated, layered and near massive varieties. Occasionally nodular or olivine intergrowth textures occur. The textures of chromite concentrations in the Shetland ophiolite and their significance have been discussed by previous workers (Gass et al. 1982, Prichard & Neary 1982). Of particular interest is the occurrence of nodular chromite textures in both the harzburgite and dunite units. Nodular chromite textures are characteristic of 'Alpine' (now ophiolitic) occurrences (Thayer 1960, 1969) and have not been found in stratiform complexes. The origin of nodules is disputed, but may involve immiscible liquids developed in the presence of a volatile component (see discussion in Prichard & Neary 1982).

---

* Plates of all the disused chromite quarries from which any samples were collected are included in chapters 2 and 6 so as to allow correct future identification of different localities.

Figure 2.5. Map of chromite occurrences in the area around Baltasound.

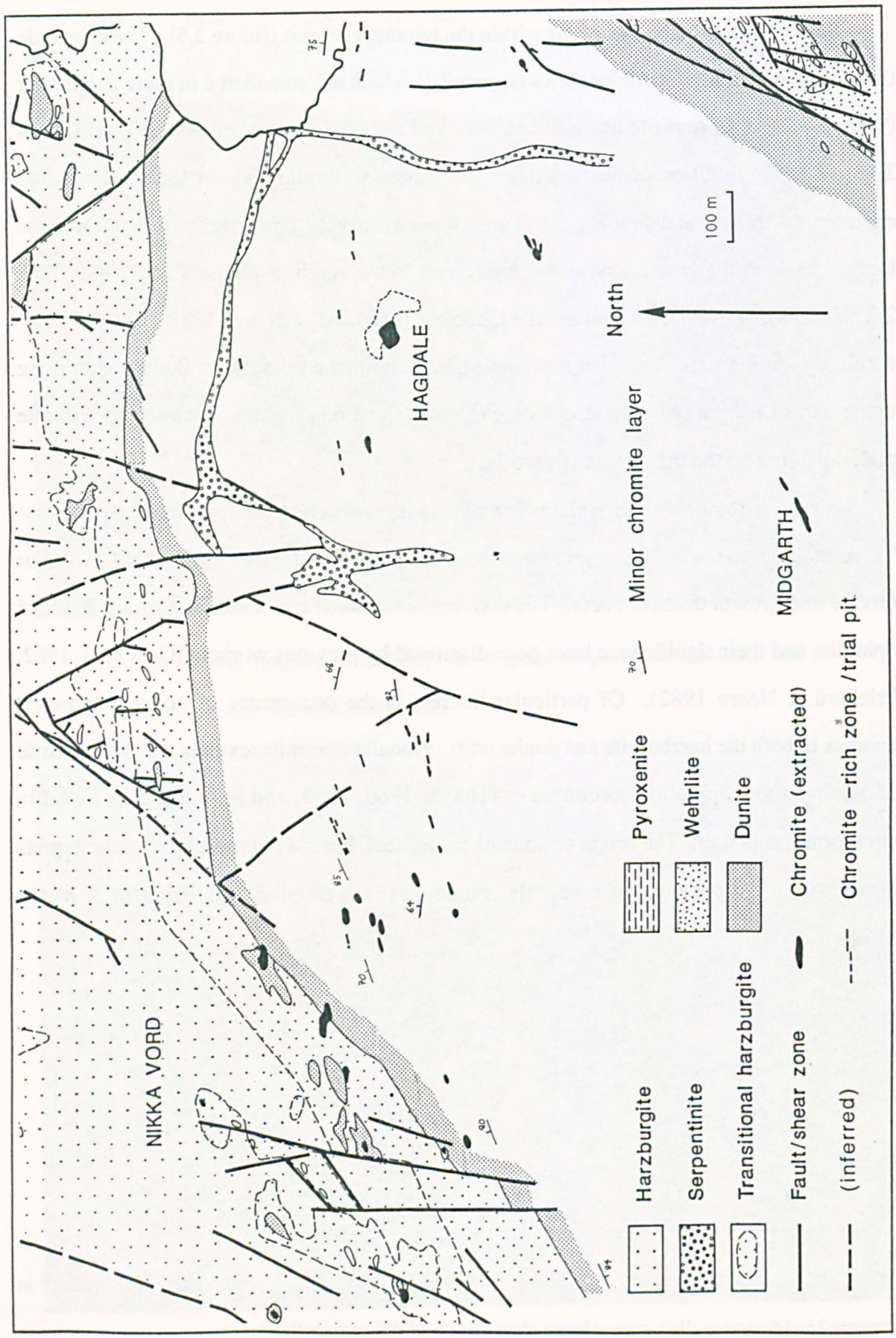

Plate 2.18. Nikka Vord North chromite quarry.

Plate 2.19. Nikka Vord East chromite quarry.

Plate 2.20. Quarry 8 West.

Plate 2.21. Quarry 8.

2.2.5 Cliff and Harold's Grave

The nature of the chromite occurrences at Cliff and Harold's Grave are of particular relevance to this study in view of the large number and variety of PGMs recorded from these localities (section 1.5). Both Cliff and Harold's Grave chromite workings are relatively small and associated with dunite pods (figure 2.1). The Harold's Grave workings are located in the NW corner of the present study area, 1 km N of the dunite/harzburgite junction (figure 2.3). The Cliff workings, approximately 5 km W of Harold's Grave, were also mapped in detail to allow comparisons with the area around Baltasound (figure 2.6).

At Cliff five elongate pits, each less than 10 m in length, occur in a NE trending array, close to the SW tip of the enclosing dunite pod (plate 2.24), which has a similar orientation (figure 2.6). The Cliff quarries lie 300 m east of the basal thrust of the ophiolite, which in this area strikes NNE and dips approximately 45° ESE (plate 2.22). A parallel structure passing close to the edge of the workings is suggested by a sharp break in exposure westwards (plate 2.23). This is slightly offset sinistrally by a NE trending shear zone occupying poorly exposed ground immediately N of the workings. Foliated harzburgites indicate that this later structure dips very steeply SE, and forms the N margin of the dunite pod.

Spoil tips at Cliff contain both near massive chromitites and disseminated chromite-rich dunites. In particular, disseminated chromite-rich dunites from this locality often have a characteristic green serpentinite matrix (plate 2.25).

At Harold's Grave a single E-W elongate pit approximately 20 m long occurs in transitional harzburgite. It is close to an unusually large ENE trending dunite pod or line of dunite pods 500 m in length (figure 2.3). The limited exposure indicates that this dunite pod is continuous for at least 200 m. The dunite pod and transitional harzburgites are truncated by a NNW trending near vertical shear zone passing 40 m E of the workings (plate 2.26).

Spoil at Harold's Grave typically consists of cm scale irregular layers of near massive chromite in a matrix of brown dunite. Chromite layers swell and coalesce into massive chromite.

Figure 2.6. Map of the Cliff Quarry area.

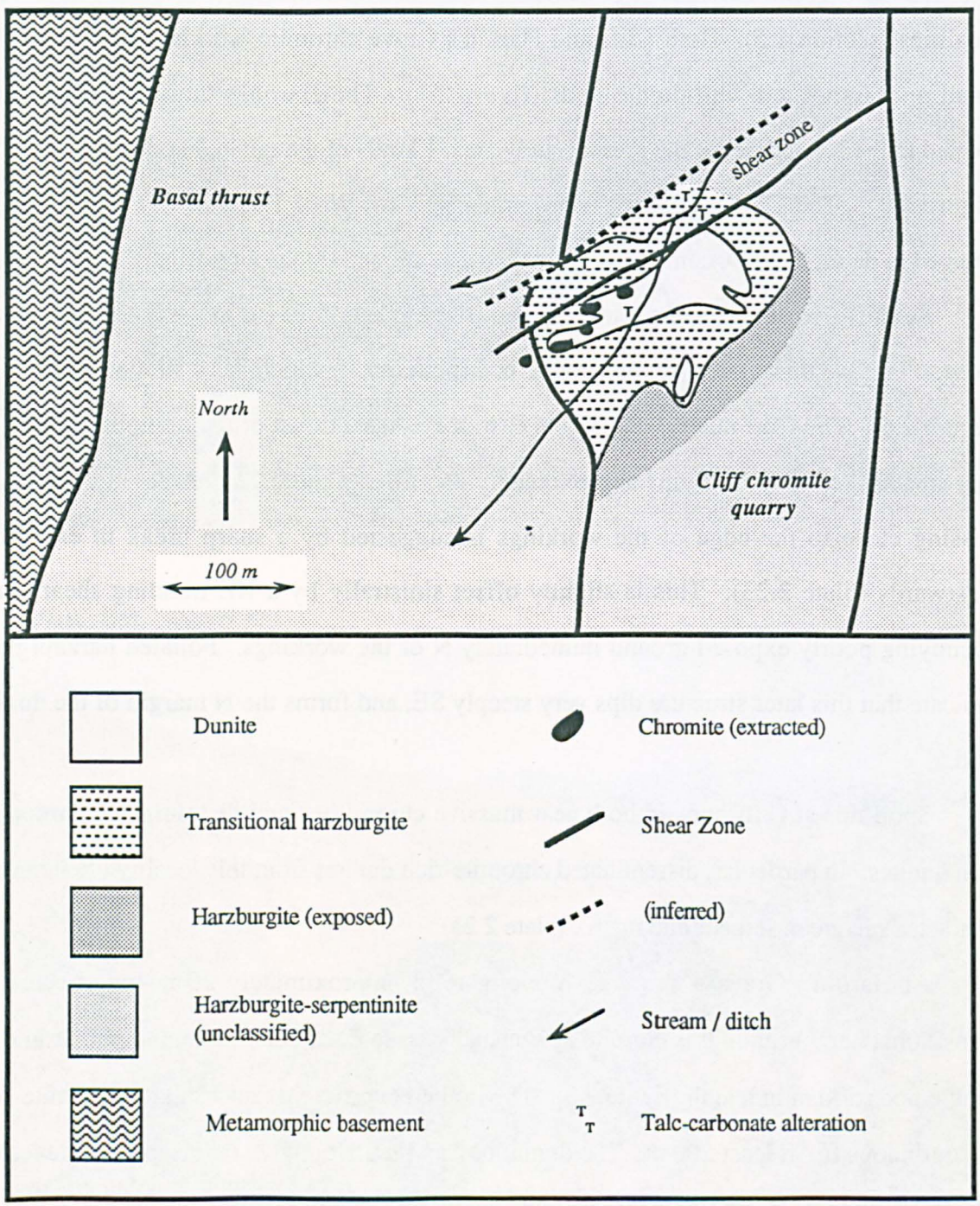

Plate 2.22. View west from main Cliff chromite pit towards the ophiolite basal thrust, which runs parallel to the wall.

Plate 2.23. View west from the lower (western) Cliff chromite pit showing area of poor exposure.

Plate 2.24. The main chromite pit at Cliff is hosted in dunite and transitional harzburgite close to the margin of the dunite pod.

Plate 2.25. Distinctive green serpentinite matrix typical of PGE enriched disseminated chromite-rich dunites from Cliff.

Prichard (et. al 1986) considered the Cliff quarry to lie directly along strike from Harold's Grave, parallel to the harzburgite foliation and therefore 1 km below the petrological moho. Recognition of the structural complexity of the ophiolite (this study), sheds considerable doubt on this interpretation. The Cliff area is bounded by major shear lineaments, running parallel to the basal thrust zone, on which the horizontal displacement is unknown. The progressive sinistral offset of the primary E-W layering further W in the complex (section 2.6) suggests that the Cliff area may represent a deeper level in the stratigraphy than its present position indicates (figure 2.7).

Figure 2.7. Sketch map showing stratigraphic positions of the Cliff and Harold's Grave localities.

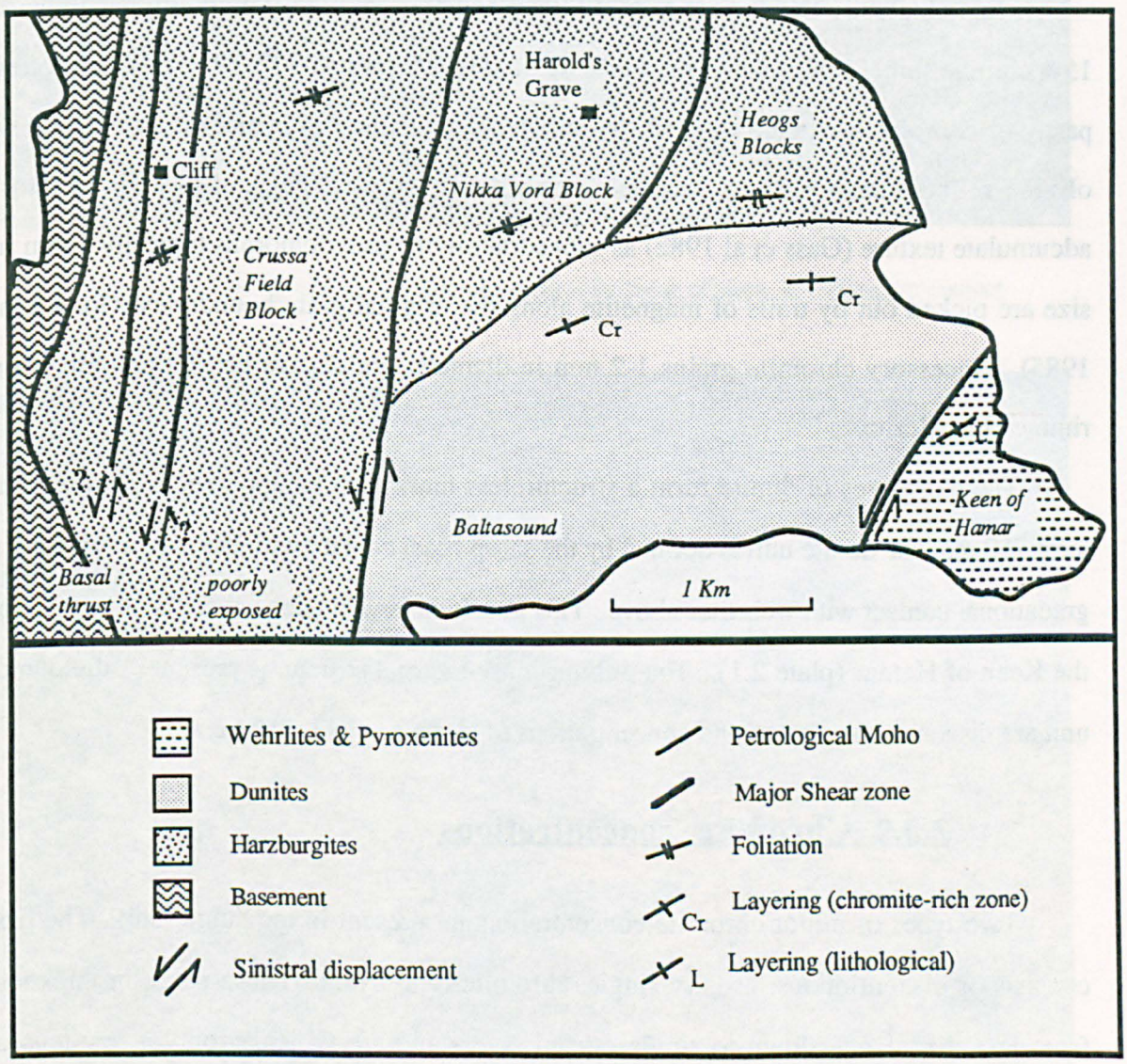

2.3 Crustal sequence

2.3.1 Dunite unit

Weathered dunite outcrops are typically honey coloured and characteristically have smooth irregular surfaces. They are generally poorly exposed and have been preferentially eroded compared with the adjacent harzburgites. This has resulted in the formation of a prominent scarp feature at the contact between the dunite unit and the harzburgite unit in the area south of Muckle Heog (plate 2.27).

Mineralogically the dunites were originally composed of 85-95% olivine, with up to 15% chrome spinel and minor interstitial sulphides (Brzozowski 1977). The olivine is often partly or completely altered to mesh serpentine, chlorite, tremolite and magnetite. Fresh olivine relicts occur in most samples, rarely up to 40%. The dunites show a ghost adcumulate texture (Gass et al 1982) as subhedral olivine pseudomorphs typically 1 mm in size are picked out by trails of magnetite along the original grain boundaries (Gunn et al 1985). Accessory chromite grains 1-2 mm in diameter are always present and are often rimmed by chlorite.

The exposures of dunite form a structureless mass with an apparent thickness of at least 750 m. The dunite unit is defined by the sharp basal contact with the harzburgite and a gradational contact with wehrlites above. This transition is well exposed on the north side of the Keen of Hamar (plate 2.1). The only primary internal structures present in the dunite unit are discontinuous layers and concentrations of chrome spinel (plate 2.30).

2.3.2 Chromite concentrations

Two types of minor chromite concentration are present in the dunite unit. The first consists of discontinuous, usually single, chromite-rich layers. These range in thickness from less than 1 cm, down to single crystal layers and are typically only a few tens of centimetres in length (plates 2.31, 2.32). Very rarely single layers may be traced across

Plate 2.26. View north from Harold's Grave. These relatively small trial workings are close to a major NNW fault which forms the break of slope just beyond the quarry.

Plate 2.27. View of dunite unit showing prominent break of slope at harzburgite contact below Muckle Heog.

Plate 2.28. Quarry 7 (Long Quarry).

Plate 2.29. Trial pit in chromite-rich zone 1, east of Quarry 11.

Plate 2.30. Disseminated chromite layer from within the cumulate dunite unit.

Plate 2.31. Wispy chromite layers parallel to silicate layering (blue pen) and later foliation (red pen).

Plate 2.32. Close up of chromite layer in plate 2.31. Note that the spinel elongation is oblique to the phase layering.

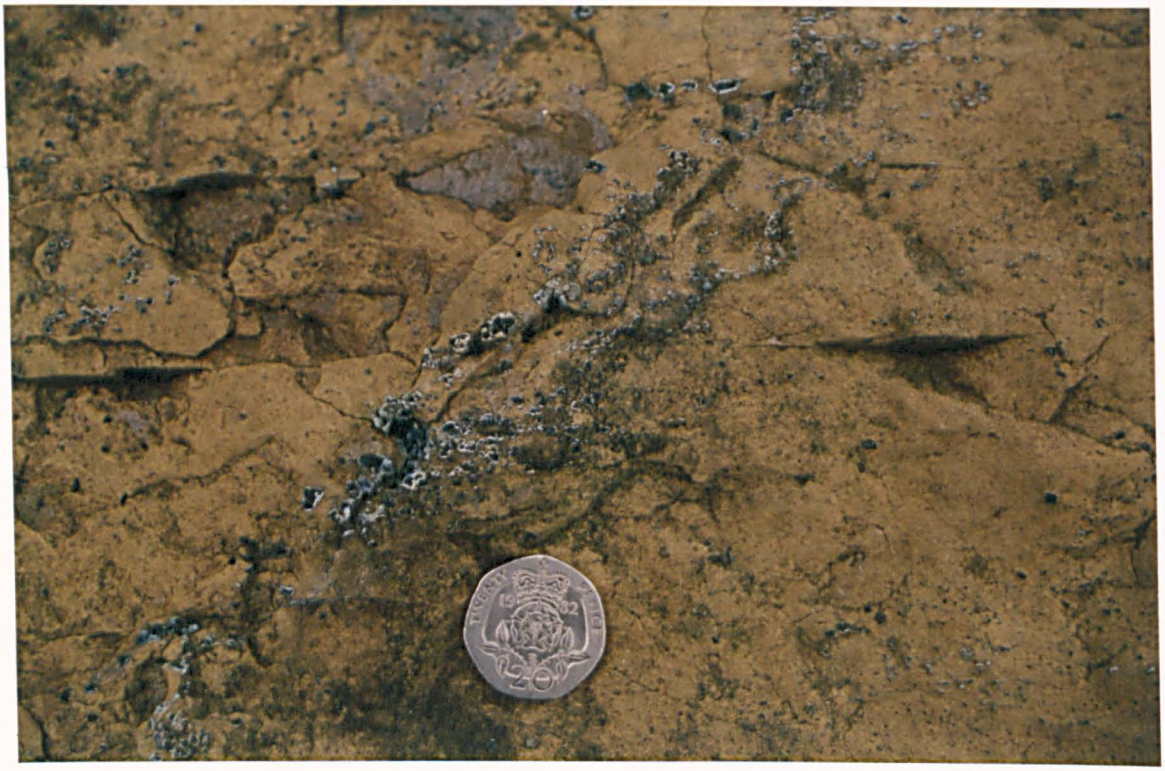

Plate 2.33. Multiple chromite layering in dunite exposed in Hagdale Wick. A younging direction towards the top of the photograph is suggested by slump structures deforming the sharp bases of layers.

Figure 2.8. Location of chromite quarries within stratigraphically controlled chromite-rich zones.

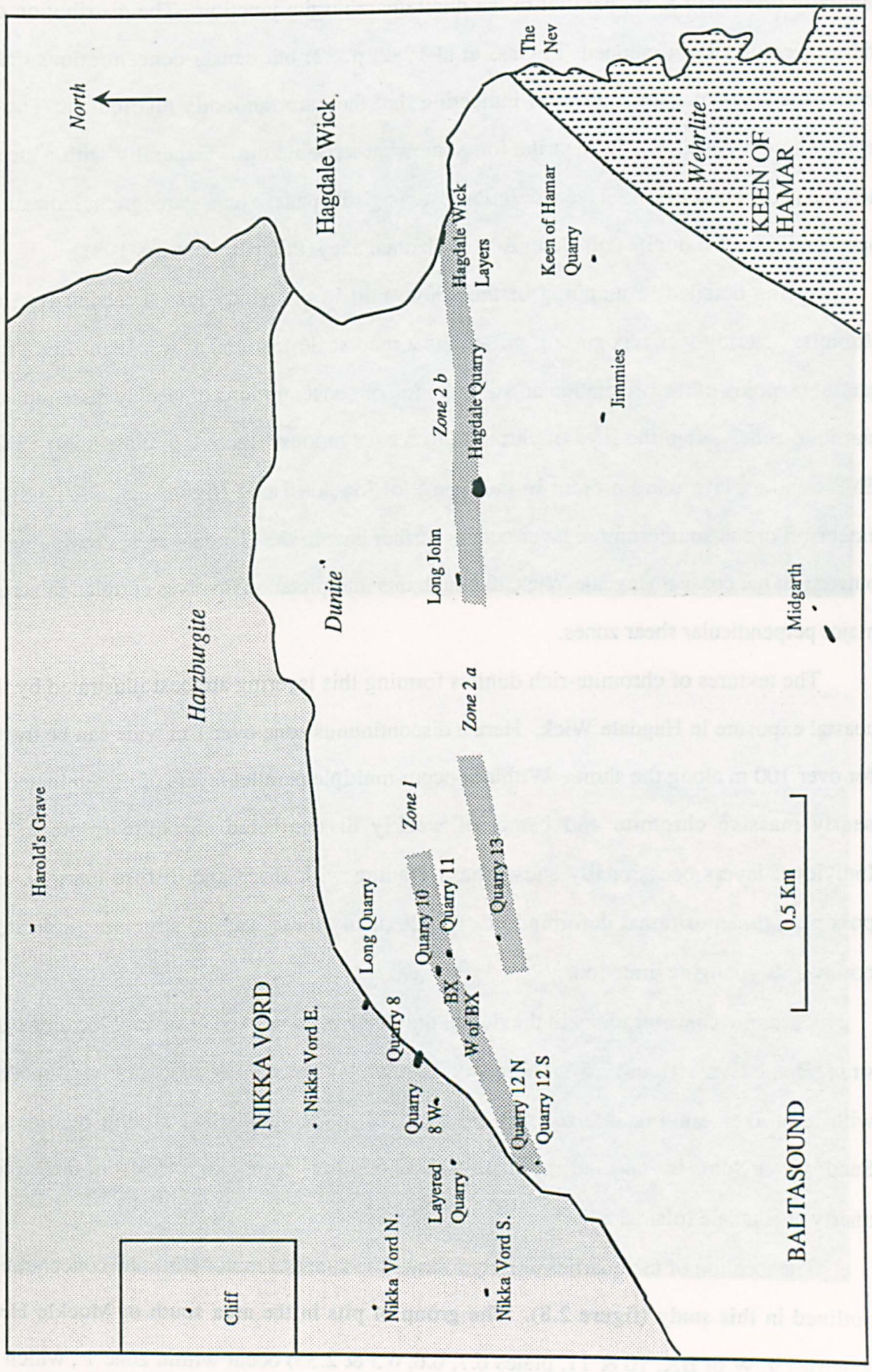

outcrop, in one case for 10 m. These layers occur randomly throughout the unit, and are generally orientated E-W, parallel to the dunite/harzburgite junction. The distribution of these layers has been mapped (in Gass et al 1982, p. 22) but denser concentrations only reflect the areas of good exposure, indicating that they are randomly distributed. These layers show a consistent E-W strike but somewhat variable dip. Generally with a steep northerly dip, poles to these layers describe a weak girdle pattern on a stereogram, indicating open folding of the dunite unit along E-W horizontal axes (Prichard & Neary 1981).

During detailed re-mapping of the dunite unit in this study area a second type of chromite layering was recognised, present as a map scale feature. It was identified after careful mapping of the orientation and distribution of concentrations of weakly disseminated chromite zones, often the sites of chromite trial excavations (figure 2.5, plate 2.29). Two ENE trending layers are present in the area S of Muckle Heog (figure 2.8). A possible extension of the southernmost layer occurs further east in the Hagdale area, continuing to outcrop on the coast at Hagdale Wick, although this interpretation involves correlation across major perpendicular shear zones.

The textures of chromite-rich dunites forming this layering are best illustrated by the coastal exposure in Hagdale Wick. Here a discontinuous zone over 1 m wide can be traced for over 100 m along the shore. Within it occur multiple parallel layers of disseminated or nearly massive chromite and bands of weakly disseminated chromite (plate 2.33). Individual layers occasionally show phase grading with sharp and diffuse margins and possible syn-depositional deformation. Paradoxically these way up structures indicate a northwards younging direction.

Chromite concentrations in the dunite unit have been worked at several locations and stratigraphic levels (figure 2.5). These workings are typically elongate in an ENE direction, with long axes ranging in size from 50 m to 10 m. Unpublished mining records (C. Sandison & Sons, Baltasound) indicate that 32,600 tons were extracted from the largest quarry at Hagdale (plate 2.34).

The location of the quarries closely follows the zones of minor chromite concentration outlined in this study (figure 2.8). The group of pits in the area south of Muckle Heog (quarries 9, W of BX, 10 & 11, plates 6.7, 6.6, 6.5 & 2.35) occur within zone 1 , which

Plate 2.34. Hagdale Quarry, the largest chromite quarry on Unst, from which 32,600 tons of ore were taken.

Plate 2.35. Quarry 11.

Plate 2.36. View of pyroxene-bearing sequence hosting high level chromite at the Nev. Disseminated and massive chromite layers occur sporadically in the lowermost 1-2 m of the upper dunite layer.

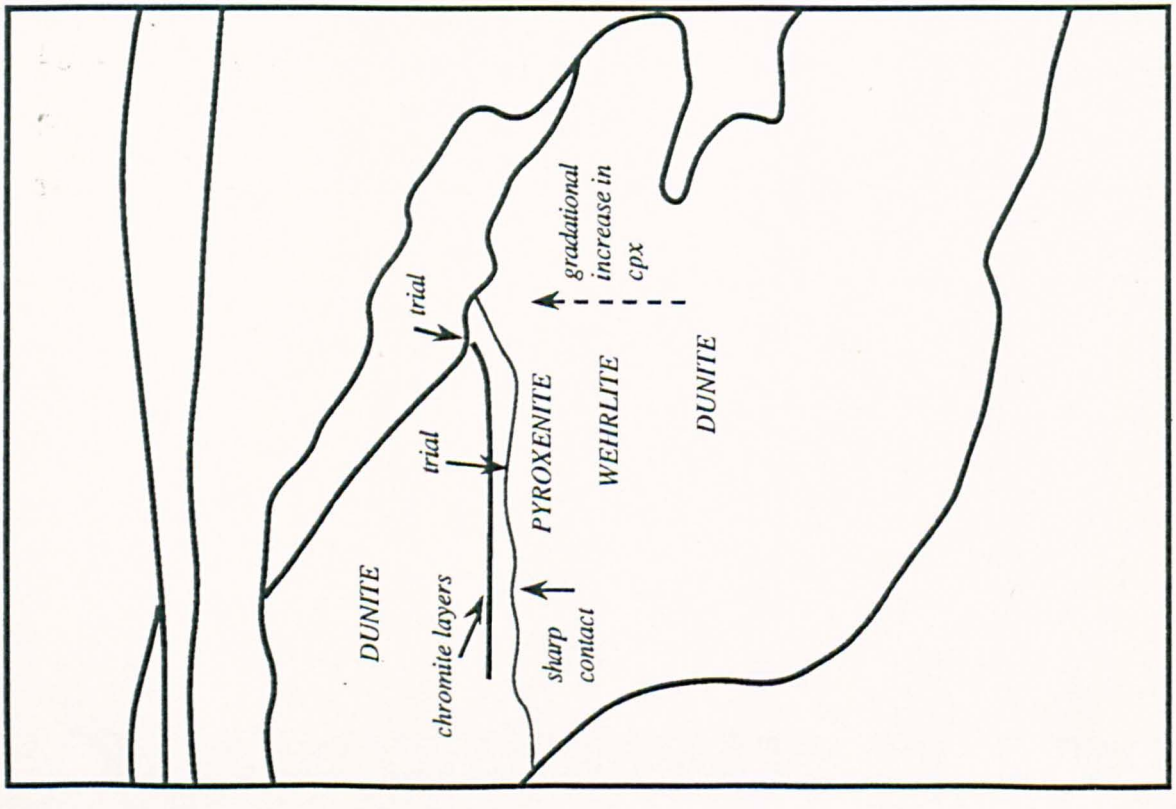

possibly extends west to quarries 12 & 12 S (plates 6.2 & 6.3). Quarry 13 is located close to zone 2 a, the southernmost layer in this area (plate 6.4). Zone 2 b further west includes quarries 14 (Long John) & 16 (Hagdale), and the coastal chromite locality (17) in Hagdale Wick. Air photographs showing the positions of backfilled workings indicate a further zone (zone 3) to the south of Hagdale extending to Jimmies Quarry (quarry 19) and workings on the Keen of Hamar (quarry 18).

During this study another chromite working, which includes exposures of in situ chromite, was located on the cliffs of the Keen of Hamar in the east of the area (the Nev). This concentration is distinct in that it is located within a pyroxene-bearing cumulate sequence (figure 2.9), and is therefore a new high level chromite occurrence (plate 2.36).

Spoil tip material indicates that the textures of chromite-rich rocks from the dunite unit are similar to those from dunite pods, with a variety of layered, disseminated and near massive chromite typically present.

The stratigraphically controlled horizons of chromite enrichment described above indicate that other unexposed podiform chromitite bodies may occur along strike. As part of a chromite exploration program Rivington (1953) suggested that the distribution of known concentrations could be explained as ore zones which might provide drilling targets for additional ore bodies. In this study a single "ore bearing zone" was proposed running ESE through quarries 8, 10 & 11. This zone is at 40° to the regional strike and the stratigraphic horizons described above and was largely disproved by the subsequent drilling program (Rivington 1953).

2.3.3 Wehrlites and pyroxenites

A layered sequence consisting of various proportions of dunite, wehrlite and pyroxenite occurs south and west of the dunite unit on the Keen of Hamar, Swinna Ness and Ordale (figure 2.9). These rocks show a range of colours in sympathy with their differing contents of grey-green pyroxene and yellow-brown weathering olivine. The olivine weathers preferentially to the pyroxene resulting in a characteristic rough surface (plate 2.37). This greater resistance of pyroxene-rich lithologies also results in a ridged topography, with well exposed crests of pyroxenite and poorly exposed troughs of wehrlite or dunite. In the proximity of shear zones, altered examples of pyroxenite or wehrlite all weather to a characteristic pink colour.

Mineralogically the rocks are composed of various proportions of olivine and clinopyroxene, with minor amounts of chrome spinel (plate 2.38) and altered plagioclase (plate 2.39). The clinopyroxene is usually very fresh and has a subhedral cumulus texture in pyroxenites. Pyroxene first appears as an intercumulus phase in the uppermost dunites (Prichard, 1985).

Clinopyroxene grains show a range of sizes, but individual grains in a single rock are generally of a similar size, resulting in a well sorted appearance. In pyroxenites the grain size is typically a few millimetres (plate 2.40), although coarser variants containing crystals several centimetres across produce a pegmatitic rock (plate 2.41).

Two types of layering fabrics occur in the wehrlites. The first consists of discrete layers of pyroxene in olivine (plate 2.37). The second consists of continuous gradation in the proportion of these two phases (plate 2.42). Layering occurs on a variety of scales. Microscale layering may be seen in hand specimen, and mesoscale layering in single outcrops. Macroscale layering occurs on a map scale, with units tens of meters in thickness. In practice mapped pyroxenite units, for example, may contain small amounts of dunite and wehrlite, but are defined on the basis of a predominance of pyroxenite (> 50 % as a definition, but typically >>70 %).

Plate 2.37. Typical layered wehrlite. Discrete wispy layers of euhedral pyroxene.

Plate 2.38. Layered wehrlite containing small chromite layer. Note the whitish green chlorite rims surrounding most chromite grains.

Plate 2.39. Fine grained wehrlite containing accessory plagioclase (white).

Plate 2.40. Typical pyroxenite.

Figure 2.9. Geological map of the Keen of Hamar, Swinna Ness and Ordale.

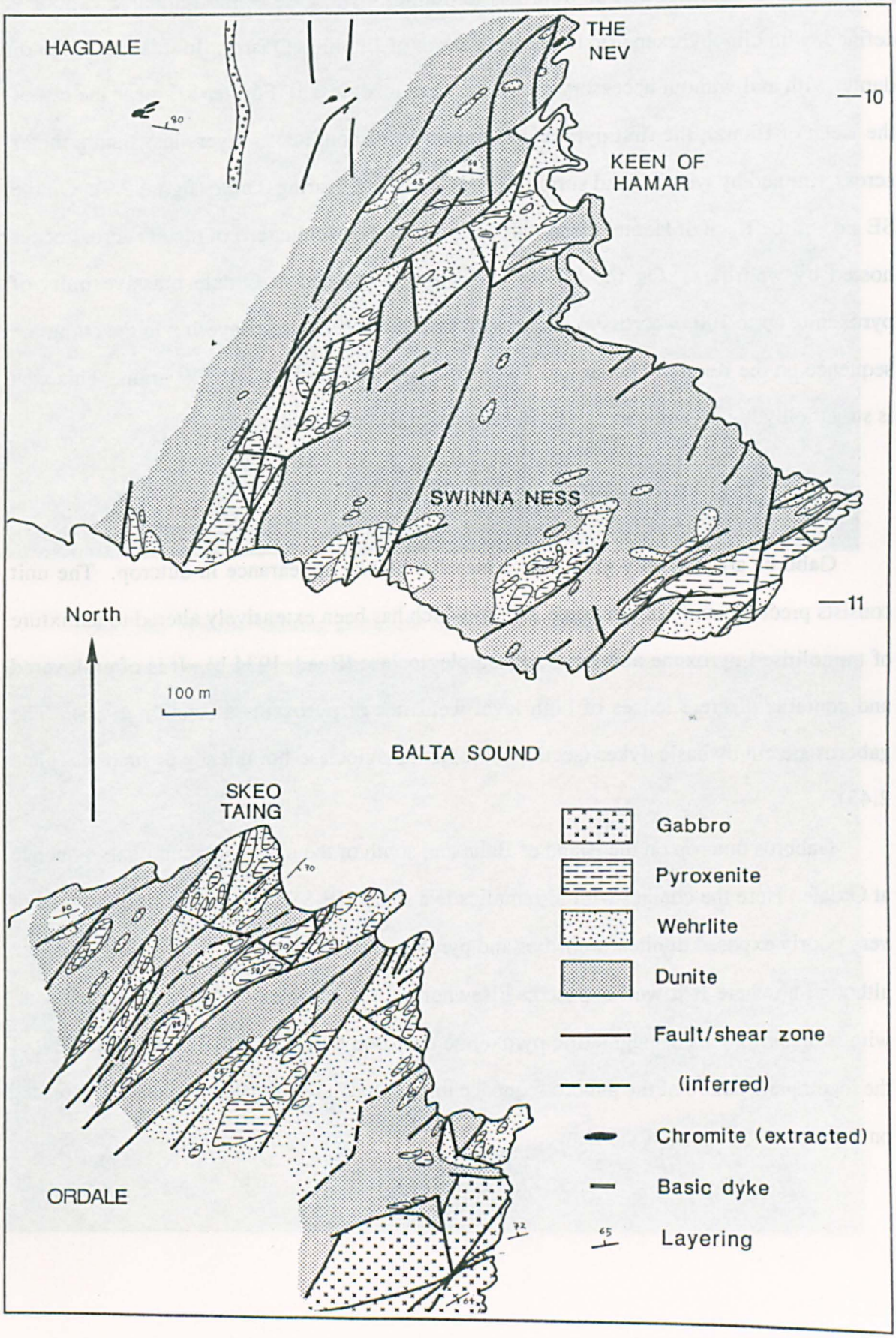

The cumulate sequence as a whole shows an upwards increase in the proportion of pyroxenites to wehrlites and of wehrlites to dunites. The base of the sequence is poorly defined, with clinopyroxene first appearing south of Jimmie's Quarry. In this area units of dunite with and without accessory pyroxene were recognised. Further SE, near the top of the Keen of Hamar, the first pyroxenites appear as discontinuous layers less than a meter across, rimmed by wehrlite and surrounded by pyroxene-bearing dunite (figure 2.9). On the SE side of the Keen of Hamar discontinuous pods of pyroxenite tens of meters across occur hosted by wehrlites. On the SE tip of Swinna Ness and at Ordale massive units of pyroxenite up to 100 m across alternate with wehrlite and dunite. Layering in the cumulate sequence on the Keen of Hamar and Swinna Ness shows a strong NE-SW grain. This area is structurally highly complex, and will be discussed later (section 2.5).

2.3.4 The gabbro unit

Gabbros are typically grey with a massive blocky appearance in outcrop. The unit consists predominantly of pyroxene gabbro which has been extensively altered to a mixture of tremolitised pyroxene and saussuritised plagioclase (Reed, 1934 b). It is often layered and contains discrete lenses of high level wehrlites or pyroxenites (section 1.4.5). The gabbros are cut by basic dykes (section 1.6.5) and plagioclase-hornblende pegmatites (plate 2.43).

Gabbros outcrop on the island of Balta and south of the ultramafic cumulate sequence at Ordale. Here the contact with ultramafics is a sharp NE-SW feature, south of an area of very poorly exposed dunites, wehrlites and pyroxenites. This junction is probably tectonic, although nowhere is it well exposed. Elsewhere in the complex intrusive contacts occur, with irregular blocks of pegmatitic pyroxenite enclosed by gabbro (plate 2.44). In view of the incomplete nature of the gabbro sequence in this study area, greater emphasis was placed on the ultramafic succession below.

Plate 2.41. Coarse pegmatitic pyroxenite.

Plate 2.42. Wehrlite showing gradational ratio phase layering.

Plate 2.43. Brown amphibole & plagioclase pegmatite intruding gabbro on Balta Island.

Plate 2.44. Pegmatitic pyroxene rafts (outlined) enclosed by gabbro.

2.4 Distribution of sulphides

During fieldwork particular attention was paid to observations of the presence or absence of accessory sulphides in hand-specimen, in view of their possible significance to PGE mineralisation (section 1.2). This has allowed the distribution pattern of accessory sulphides in the complex to be deduced. Accessory sulphides commonly occur in most lithologies but are less common in the mantle sequence than in the crustal sequence. In particular, harzburgites typically contain no visible sulphide. Rarely sulphides occur in the olivine-rich portions of transitional harzburgites. However, they often occur in the dunite pods and in chromite-rich dunites or dunite spoil from chromite quarries in this setting. In contrast, accessory sulphides are usually present in all varieties of ultramafic cumulates at all levels in the crustal sequence. They are particularly common at the base of the dunite unit and in dunites spatially associated with former chromite concentrations, now exposed as the wallrocks and spoil of the disused workings.

During field sampling (section 4.2) all 251 reconnaissance samples were classified according to rock type. The relative quantity of accessory sulphide which they contained was also recorded. This information provides further evidence of the distribution of sulphides in the complex. In figure 2.10 the samples have been grouped according to rock type. Samples from chromite quarries within the harzburgite or dunite units and dunites from dunite pods or the main cumulate dunite unit have been further subdivided accordingly. The "highly altered" category includes various samples which were too sheared or serpentinised for the original primary lithology to be deduced. The percentage of samples from each category which contained sulphides has been calculated and is shown as a histogram. This diagram confirms that most cumulate rock types contain sulphides, whereas harzburgites are sulphide-barren. Dunites and chromite-rich dunites from pods within the harzburgite unit often contain sulphides, as do the more olivine-rich transitional harzburgites.

Further samples were collected in traverses across sulphide-bearing zones at the base of the dunite unit and exposures in chromite quarry walls (sections 6.2 & 6.3). These

samples were classified in the field according to the relative amount of accessory sulphide they contained. This relative scale ranges from sulphide-barren to very sulphide-rich, although the sulphide content of samples falling in the latter category rarely exceeds a few percent. This information has been used to calculate the percentage of the samples from each setting which contain each level of accessory sulphide. A similar proportion of samples from the two situations contain sulphides, since in both cases just less than 20 % were sulphide-barren. The relative amount of sulphide, however, is greater in dunites close to chromite concentrations than in dunites from the base of the dunite unit (fig 2.11).

Figure 2.10. Histogram showing the distribution of sulphides through the ophiolite sequence. The percentage of samples of each lithological category which contained sulphides is shown in approximate stratigraphic order. Mantle sequence lithologies light tone, crustal sequence dark tone. Total of 251 samples.

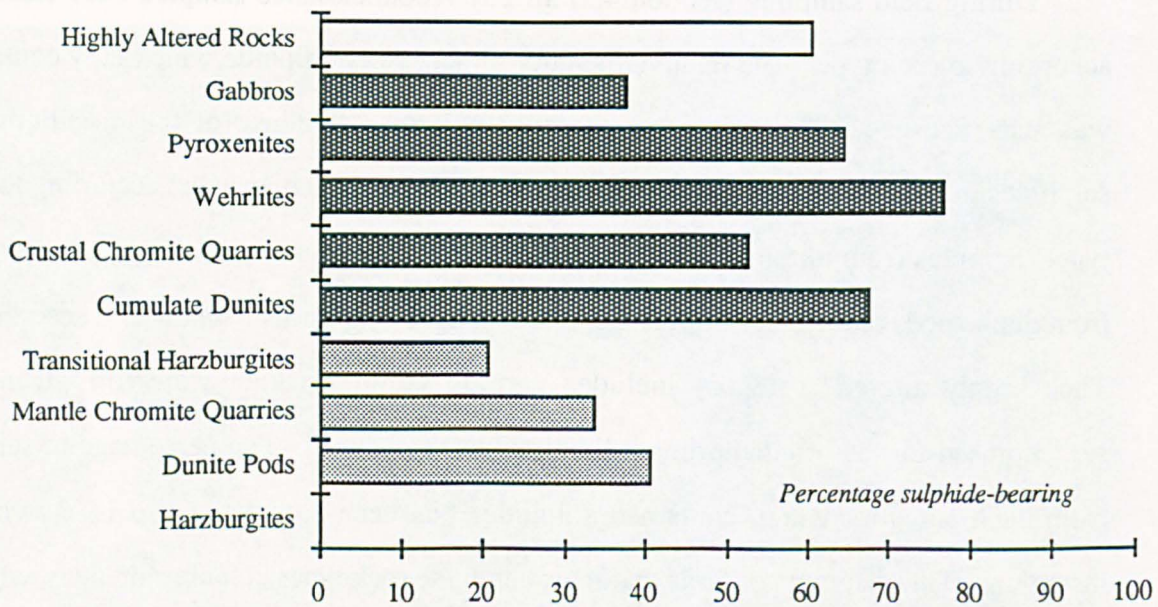

Figure 2.11. Bar charts showing the relative quantity of accessory sulphide in samples from traverses (a) across the basal dunites and (b) across the chromite quarries within the dunite unit. Sulphide barren (No S), sulphide-bearing (SB), moderate sulphide (Mod.S), sulphide-rich (SR) and very sulphide-rich (VSR) denote relative sulphide content from zero to a maximum of a few percent.

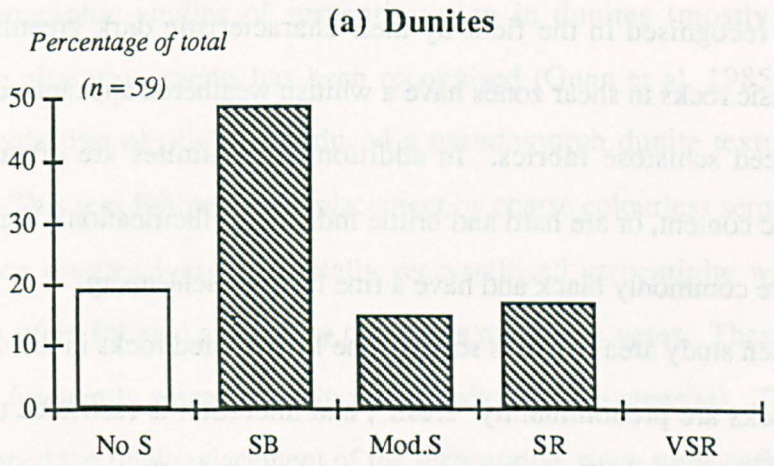

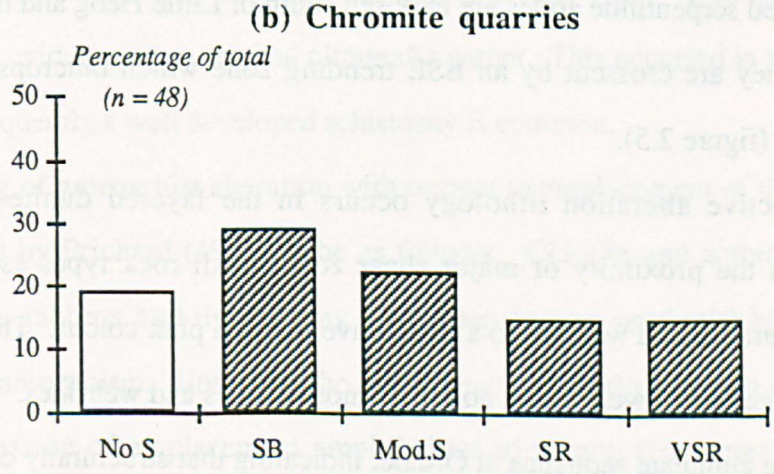

2.5 Alteration

In view of the importance of shear zones as fluid pathways and foci for hydrothermal action, with possible implications for PGE mineralisation (section 1.6.4), particular attention was paid to the identification of such zones during mapping .

All fresh ultramafic rocks in the complex show petrological evidence of serpentinisation (sections 2.2 & 2.3). More highly serpentinised rocks associated with shear zones may be recognised in the field by their characteristic dark greenish-black colour. Altered ultrabasic rocks in shear zones have a whitish weathered appearance, and commonly have pronounced schistose fabrics. In addition, serpentinites are often soapy to touch indicating a talc content, or are hard and brittle indicating silicification. Very highly sheared serpentinites are commonly black and have a fine lustrous schistosity.

The chosen study area contains some of the least altered rocks in the ophiolite. Within this area all rocks are predominantly "fresh", and alteration is restricted to the immediate vicinity of shear zones. These zones are characteristically unexposed, forming low topographic features in all rock types except dunites. Within the dunite unit two N-S trending sheared serpentinite zones are exposed south of Little Heog and north of the Keen of Hamar. They are crosscut by an ESE trending zone which outcrops on the coast in Hagdale Wick (figure 2.5).

A distinctive alteration lithology occurs in the layered dunites, wehrlites and pyroxenites in the proximity of major shear zones. All rock types assume a uniform wehrlitic appearance and weather to a distinctive mottled pink colour. This contrasts with the 'fresh' orange brown weathering colour of most dunites and wehrlites. Pink alteration is prevalent in the cumulate sequence at Ordale, indicating that structurally controlled passive alteration becomes progressively more extensive further south across the study area.

Highly serpentinised dunite samples are also common in chromite quarry spoil tips. The dunite matrix in disseminated chromite-rich samples is usually totally serpentinised and it ranges in colour from yellow to bright green. In some layered specimens this alteration follows the chromite layers. This indicates that olivine adjacent to chromite preferentially

alters to serpentine. Altered chromite-rich samples also commonly contain chlorite in the matrix. In dunites the accessory chromite grains are often rimmed by greenish white chlorite haloes.

The alteration associated with internal shear zones has been compared to that seen in the basal serpentinised zone of the ophiolite (Gass et al. 1982). Here serpentinisation is often total, with chrome spinel the only relict mineral. Any pseudomorph textures are also destroyed by shearing. Silicified, carbonated or talcose serpentinites are also common. The common pink colouration is attributed to impregnation by carbonates.

From petrographic studies of serpentinisation in dunites (mostly from Cliff) a sequence of five alteration events has been recognised (Gunn et al. 1985). The first of these, a static hydration of olivine, produced a pseudomorph dunite texture outlined by magnetite trails. This was followed by replacement by coarse colourless serpentinite, first as veinlets, and then progressively to a totally recrystallised serpentinite with no primary textures. This is often foliated and cut by numerous magnetite veins. These recrystallised serpentinites are frequently veined or replaced by carbonates (magnesite). This carbonation probably overlapped the final replacement of the serpentinite, since some carbonate veins are crosscut by later serpentinite veins. In the extreme case carbonation produced a talc magnesite rock, obliterating evidence of the primary rock type. Relict chrome spinels provide the only evidence of an original ultramafic parent. This occurred in relation to shear zones and consequently a well developed schistosity is common.

The timing of greenschist alteration with respect to emplacement of the ophiolite has been considered by Prichard (1985) to be as follows. Chlorite and actinolite, which are abundant in the gabbros and dykes, may have been in part produced by oceanic crust greenschist metamorphism. However, the occurrence of chlorite rims on chromite grains and the retrogression of emplacement amphibolites to greenschist facies (section 1.4.7) indicate that the complex was also overprinted by later regional greenschist metamorphism.

The production of talc has also been assigned to a post-emplacement event, possibly the result of hydrous fluids emanating from a local acid intrusion (Neary & Prichard 1985).

2.6 Structural pattern and disruption of sequence

Detailed mapping of the primary magmatic sequence in this area has revealed a previously unrecognised degree of structural complexity.

Stereo air photographic interpretation (figure 2.12) indicated strong NE to NNE trending and subordinate NW to NNW trending sets of high angle lineaments. Comparison of the interpretation with the geological map (figure 2.2) reveals that the lineament textures vary between different rock types. The harzburgite unit is characterised by a blocky pattern with a strong development of both sets of structures. Only the most prominent lineaments extend into the dunite unit, in part due to the poorer exposure of this lithology. Layered cumulate rocks on the Keen of Hamar and at Ordale exhibit a very intense set of NE to NNE lineaments. The gabbro unit contains a few well developed spaced lineaments.

Field mapping confirmed that these lineaments are shear zones or fault zones disrupting the ophiolite stratigraphy. Offsets of the E-W line of the dunite/harzburgite boundary indicate a horizontal component to movements on these structures. This displacement has a predominantly sinistral sense on NE trending structures and a dextral sense on NW trending structures. The best example of sinistral offset occurs on the major NE-SW shear zone west of Nikka Vord which forms the NW boundary of the study area (figure 2.7). The dunite/harzburgite junction is truncated westwards against harzburgite which extends at least as far south as the road (offset of at least 0.5 km). Vertical displacements are generally unknown because most primary foliations are vertical and because the shear planes and any kinematic microstructures are usually not exposed.

The highly serpentinised N-S and ESE shear zones which cross the dunite unit (section 2.5) are deformed by and apparently pre-date the NW or NE trending structures. These serpentinite zones are disjointed and offset by the later shear zones (e.g. north of Muckle Heog), and have a possible folded outcrop pattern (figure 2.3).

Figure 2.12. Stereo air photographic interpretation (compare with geology map fig. 2.2 p 65).

Disruption of the primary stratigraphy varies systematically across the area. In the north of the area an E-W primary foliation is preserved in the harzburgites. In the dunite unit ENE trending stratigraphic zones of chromite concentration have been recognised (section 2.3.2). Further SE on the Keen of Hamar the sequence is progressively more disrupted by an increasing number of NW trending structures. Short sections of ENE to NE primary layering are preserved in slices bounded by NE trending shear zones. The culmination of this increasing deformation by NE trending shear zones is seen at Ordale. Here fault bounded deformed slivers of wehrlite and pyroxenite show sub-parallel NNE to NE internal lithological layering in an essentially tectonic pseudo-stratigraphy.

To summarise, deformation in the area around Balta Sound is due to sinistral movements on vertical NE trending shear zones. The harzburgite and gabbro units behaved competently and deformation was concentrated in the zone of ultramafic cumulates between. The dunites and wehrlites behaved incompetently, allowing progressive rotation of the more competent pyroxenite layers into parallelism with the numerous NE-SW shear zones (figure 2.13).

Other workers have considered the contradictory E-W layering directions found within NE striking lithological units in the south of Unst. An example occurs in the Watlee area, which was considered to result from the rotation of an originally NNE striking block (Gass et al. 1982). Gunn et al. (1985) considered this layering direction to be an original feature against which cumulate and gabbro units were discordantly emplaced. Extrapolation of the mapping at Ordale suggests that the NE-SW striking grain of the ophiolite may be a tectonic pseudo-stratigraphy, with the original E-W primary layering preserved only rarely within less sheared blocks (Lord & Prichard 1989).

Table 2.1. Thickness of basal cumulate dunites in different ophiolites.

Ophiolite	*Thickness (m)*	*Reference*
Unst, Shetland	1000 - 1600	This study
Troodos, Cyprus	200 - 400	Gass, 1980
Semail, Oman	Laterally variable	Browning, 1982
(a) Al Maydah	c. 1000* (3 km ultramafics)	
(b) Wukuabah	750 (0.75 km ultramafics)	
(W. Rustaq Block)		

*Subdivision of an olivine-rich upper part of the mantle sequence (or transition zone) reduces the maximum thickness of the basal cumulate dunite unit at Al Maydah to 200 m (I.G. Gass, pers. comm.)

Figure 2.13. Equal area projection showing poles to mantle foliations, chromite layers and pyroxene layers. The orientations are consistent with original near vertical northerly dipping primary foliations which are rotated by drag on NE trending shear zones

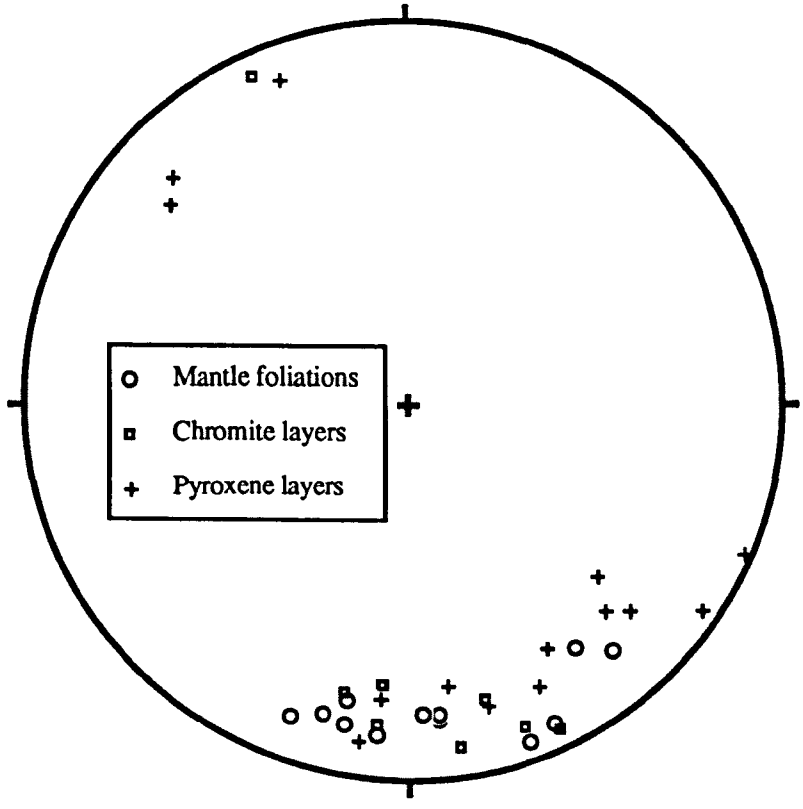

2.7 Discussion and conclusions

Field mapping has confirmed that the area around Balta Sound contains the lower parts of the Penrose ophiolite sequence. Tectonised mantle sequence harzburgites are overlain by a layered crustal sequence in which dunites grade upwards, with cyclic repetition, through wehrlites into clinopyroxenites. Above this is a gabbroic unit which encloses discrete high-level wehrlite and pyroxenite bodies and is intruded by a dyke swarm at the highest exposed level. The sequence is thus complete only within the ultramafic units. The overlying gabbros are separated by a tectonic junction and comparisons with other more complete ophiolite sequences indicate that a cumulate sequence of layered olivine gabbros is missing.

Small scale mapping on air photographs has allowed much detail of the tectonite and layered sequences to be recorded. This allows samples to be accurately located and places them in context within the igneous stratigraphy. Any systematic variations in PGE content with lithology or stratigraphic level will therefore be apparent.

One new aspect of the ophiolite sequence revealed by this detailed mapping is the continuity of stratigraphically controlled zones of chromite enrichment. Podiform chromitite bodies and disseminated chromite concentrations occur sporadically along these stratiform horizons. This is highly relevant to the present study in view of the frequent association of PGE mineralisation with chromite concentrations found in a variety of geological settings (section 1.2). At least two zones are present within the cumulate dunite unit in the area north of Balta Sound (figure 2.8). This unit is unusually thick in comparison to the dunite units of other ophiolites (table 2.1). The origin of this thickness, whether a true magmatic thickness or tectonically repeated, is considered in the following chapter which describes variations in chromite chemistry between the different chromite-rich horizons.

Chapter 3

Chromite Mineral Chemistry

3.1 Introduction

The analytical study described in this chapter was carried out using a suite of chromitite samples collected during the E.E.C Raw Materials Programme project "Development of Techniques for the determination of PGE in ultramafic rock complexes of potential economic significance: mineralogical studies" (Prichard et al., 1989). This preceded the discovery of extensive new PGE concentrations described later in this thesis, so its usefulness to the study of the origin of the PGE concentrations is restricted. However, it is appropriate to review and re-interpret this data for two reasons:

First, it contributed to the understanding of the PGM-rich chromitites within the complex. These show ophiolitic compositions indistinguishable from PGM-barren chromitites (Prichard & Lord, 1988). This information formed the background to the new sampling programme.

Second, these analyses may shed light on possible geographical and stratigraphical variations in chromite mineral composition. The analytical data are considered in the light of new mapping, in particular the recognition of stratigraphic zones linking the podiform chromite concentrations (section 2.3.2).

3.2 Data collection

Details of the 31 EEC chromite samples are listed in table 1 and the 17 localities within the present study area from which these were collected are shown in figure 3.1. The locality numbers refer to the chromite quarry numbering system of Prichard et al. (1989). The suite includes samples from nearly all locations where chromite-rich spoil occurs and includes

Table 3.1. Details of chromite samples.

Locality Number	*Location & Quarry name*	*Sample Number*	*Texture & Chromite Content*
1	Cliff	CL1	Disseminated 60 %
1	Cliff	CL3	Nodular 60 %
1	Cliff	CL7	Disseminated 40 %
1	Cliff	1349	Disseminated 30 %
2	Harold's Grave	Q1	Disseminated 60 %
2	Harold's Grave	Q2	Massive 85 %
2	Harold's Grave	Q3	Massive 85 %
2	Harold's Grave	Q3PX	Disseminated 60 %
3	Quoys	210	Disseminated 70 %
4	Nikka Vord East	NEV2	Disseminated 50 %
5	Nikka Vord North	1312	Disseminated 40 %
6	Nikka Vord South	1301	Nodular 60 %
7	Long Quarry	1408	Massive 80 %
8	Quarry 8	1316	Massive 80 %
8	Quarry 8	109	Massive 85 %
9	BX Quarry	1392	Disseminated 50 %
11	Quarry 11	3683	Disseminated 60 %
12	Quarry 12	1332	Disseminated 70 %
12	Quarry 12	1320	Massive 70 %
12	Quarry 12	1386A	Disseminated 50 %
13	Quarry 13	1400	Disseminated 30 %
13	Quarry 13	1395	Disseminated 30 %
14	Long John Quarry	1333B	Disseminated 70 %
15	Midgarth Quarry	MID 1	Disseminated 60 %
17	Hagdale Wick Layers	U83	Disseminated 20 %
17	Hagdale Wick Layers	U403	Disseminated 50 %
18	Keen of Hamar	1364	Nodular 60 %
18	Keen of Hamar	1361	Disseminated 40 %
18	Keen of Hamar	1365	Disseminated 50 %
18	Keen of Hamar	1366	Disseminated 20 %
19	Jimmies Quarry	1368	Disseminated 70 %

Figure 3.1. Location of analysed chromite samples.

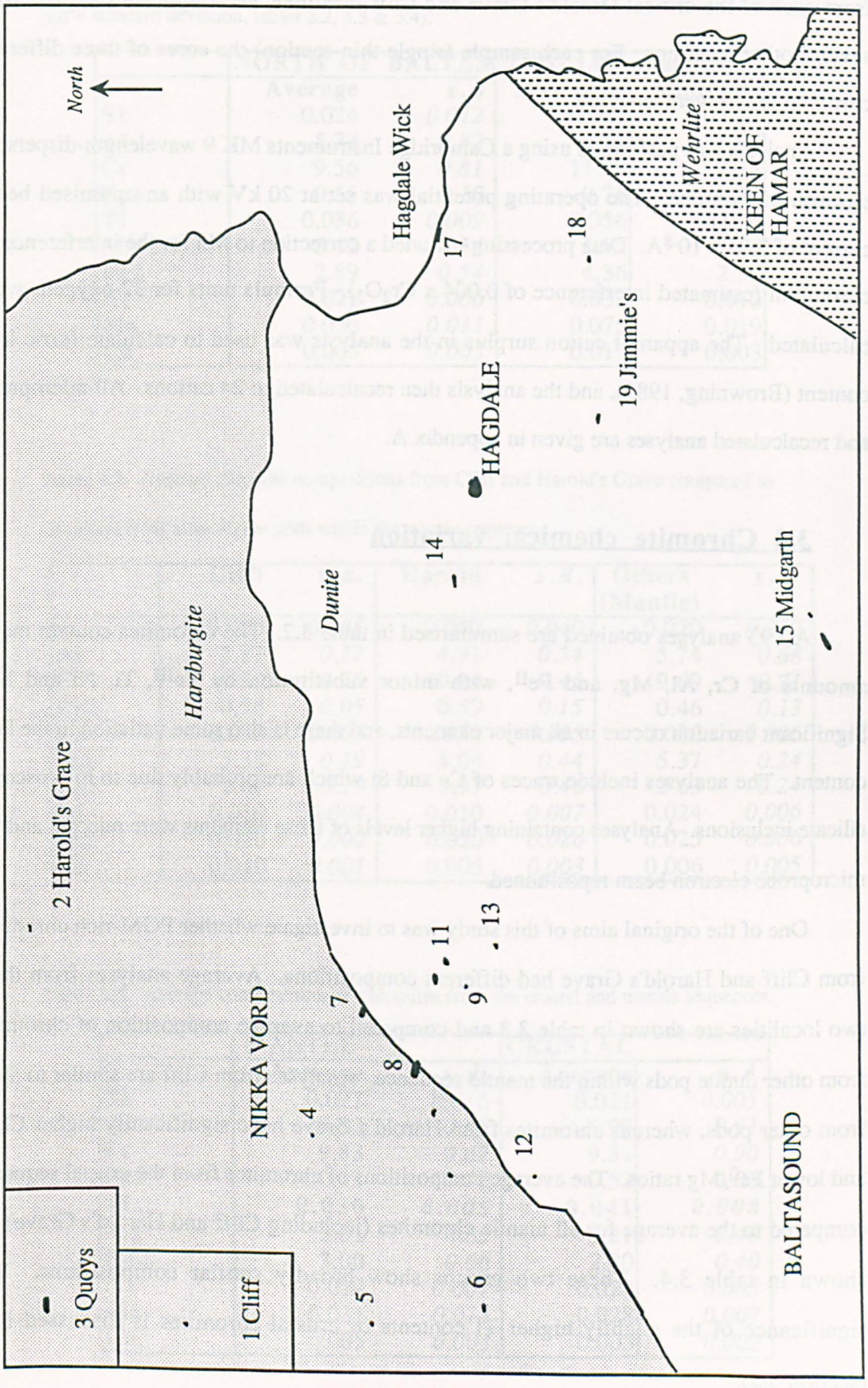

nodular, disseminated and massive (or pull-apart) textures. Four samples were obtained from each of the critical Harold's Grave and Cliff localities, and duplicate samples from several other locations. For each sample (single thin-section) the cores of three different chromite grains were analysed.

Analysis was performed using a Cambridge Instruments MK 9 wavelength-dispersive electron microprobe. The operating potential was set at 20 kV with an optimised beam current of 3.05 x 10^{-8}A. Data processing included a correction to Mn for the interference of chromium (estimated interference of 0.004 x Cr_2O_3). Formula units for 32 oxygens were calculated. The apparent cation surplus in the analysis was used to calculate ferric iron content (Browning, 1982), and the analysis then recalculated to 24 cations. All microprobe and recalculated analyses are given in appendix A.

3.3 Chromite chemical variation

All 93 analyses obtained are summarised in table 3.2. The chromites contain major amounts of Cr, Al, Mg, and Fe^{II}, with minor substitution by Fe^{III}, Ti, Ni and Mn. Significant variation occurs in all major elements, and there is also some variation in the Fe^{III} content. The analyses include traces of Ca and Si which are probably due to microscopic silicate inclusions. Analyses containing higher levels of these elements were rejected and the microprobe electron beam repositioned.

One of the original aims of this study was to investigate whether PGM-rich chromites from Cliff and Harold's Grave had different compositions. Average analyses from these two localities are shown in table 3.3 and compared to average composition of chromites from other dunite pods within the mantle sequence. Analyses from Cliff are similar to those from other pods, whereas chromites from Harold's Grave have significantly higher Cr/Al and lower Fe^{II}/Mg ratios. The average compositions of chromites from the crustal sequence compared to the average for all mantle chromites (including Cliff and Harold's Grave) are shown in table 3.4. These two groups show broadly similar compositions. The significance of the slightly higher Ti contents of crustal chromites is discussed later (section 3.5).

Table 3.2. Variations in chromite chemistry in all samples from the area around Balta Sound (s.d = standard deviation, tables 3.2, 3.3 & 3.4).

	NORTH OF BALTASOUND (All analyses)			
	Average	*s.d*	Maximum	Minimum
Si	0.024	*0.012*	0.067	0.012
Al	5.77	*0.82*	7.71	3.97
Cr	9.56	*0.81*	11.29	7.74
Fe3	0.55	*0.10*	0.76	0.31
Ti	0.036	*0.009*	0.056	0.024
Mg	5.12	*0.54*	5.72	3.64
Fe2	2.89	*0.54*	4.36	2.30
Ni	0.021	*0.006*	0.032	0.010
Mn	0.030	*0.011*	0.075	0.019
Ca	0.005	*0.003*	0.015	0.003

Table 3.3. Average chromite compositions from Cliff and Harold's Grave compared to chromites from other dunite pods within the mantle sequence.

	Cliff	*s.d.*	Harold	*s.d.*	Others (Mantle)	*s.d.*
Si	0.020	*0.005*	0.040	*0.040*	0.020	*0.009*
Al	5.77	*0.12*	4.91	*0.54*	5.74	*0.68*
Cr	9.57	*0.16*	10.34	*0.45*	9.69	*0.71*
Fe3	0.56	*0.05*	0.59	*0.15*	0.46	*0.13*
Ti	0.030	*0.002*	0.030	*0.005*	0.030	*0.006*
Mg	5.34	*0.19*	4.04	*0.44*	5.37	*0.24*
Fe2	2.67	*0.19*	3.97	*0.46*	2.63	*0.24*
Ni	0.010	*0.004*	0.010	*0.007*	0.024	*0.006*
Mn	0.020	*0.006*	0.050	*0.020*	0.025	*0.006*
Ca	0.010	*0.001*	0.005	*0.003*	0.006	*0.005*

Table 3.4. Average compositions of chromites from the crustal and mantle sequences.

	MANTLE		CRUSTAL	
	Average	*s.d.*	Average	s.d.
Si	0.027	*0.016*	0.021	*0.005*
Al	5.53	*0.65*	5.99	*0.91*
Cr	9.83	*0.62*	9.31	*0.90*
Fe3	0.52	*0.12*	0.57	*0.08*
Ti	**0.030**	***0.005***	**0.041**	***0.008***
Mg	5.01	*0.65*	5.21	*0.40*
Fe2	3.00	*0.66*	2.80	*0.40*
Ni	0.019	*0.007*	0.022	*0.005*
Mn	0.031	*0.015*	0.028	*0.007*
Ca	0.005	*0.004*	0.005	*0.002*

Table 3.5. Analyses of chromites from Cliff and Harold's Grave.

CLIFF CHROMITES (three grains analysed from each of four samples)												
	CL1a	CL1b	CL1c	CL3a	CL3b	CL3c	CL7a	CL7b	CL7c	1349a	1349b	1349c
Si	0.020	0.012	0.012	0.027	0.019	0.012	0.027	0.020	0.020	0.020	0.019	0.027
Al	5.63	5.58	5.60	5.74	5.79	5.83	5.88	5.79	5.76	5.90	5.90	5.85
Cr	9.81	9.85	9.79	9.58	9.55	9.48	9.43	9.51	9.48	9.39	9.46	9.45
Fe3	0.47	0.49	0.52	0.57	0.57	0.60	0.57	0.59	0.66	0.60	0.53	0.59
Ti	0.028	0.028	0.028	0.028	0.027	0.027	0.031	0.031	0.028	0.031	0.031	0.028
Mg	5.51	5.38	5.32	5.27	5.58	5.64	5.18	5.22	5.42	5.19	5.37	4.97
Fe2	2.50	2.62	2.68	2.74	2.43	2.38	2.84	2.79	2.60	2.83	2.65	3.05
Ni	0.020	0.018	0.014	0.012	0.014	0.008	0.020	0.012	0.008	0.012	0.014	0.008
Mn	0.018	0.024	0.031	0.034	0.025	0.013	0.028	0.026	0.026	0.026	0.019	0.027
Ca	0.003	0.008	0.003	0.003	0.003	0.003	0.003	0.003	0.003	0.003	0.003	0.003
HAROLD'S GRAVE CHROMITES (three grains analysed from each of four samples)												
	Q1a	Q1b	Q1c	Q2a	Q2b	Q2c	Q3a	Q3b	Q3c	Q3Pa	Q3Pb	Q3Pc
Si	0.020	0.013	0.020	0.029	0.049	0.104	0.159	0.021	0.020	0.020	0.028	0.021
Al	5.61	5.61	5.72	4.35	4.78	4.49	4.32	4.30	4.40	5.16	5.12	5.07
Cr	9.79	9.77	9.65	10.48	10.52	10.52	10.78	10.99	10.94	10.20	10.20	10.27
Fe3	0.49	0.54	0.52	1.04	0.53	0.73	0.51	0.59	0.53	0.53	0.55	0.55
Ti	0.032	0.028	0.028	0.029	0.035	0.025	0.037	0.041	0.040	0.034	0.035	0.035
Mg	4.58	4.49	4.62	3.74	3.62	3.55	3.46	4.06	4.24	4.60	3.89	3.67
Fe2	3.43	3.50	3.38	4.23	4.38	4.48	4.66	3.95	3.77	3.42	4.11	4.31
Ni	0.018	0.018	0.014	0.029	0.002	0.013	0.006	0.008	0.014	0.020	0.012	0.012
Mn	0.026	0.034	0.033	0.070	0.075	0.080	0.064	0.044	0.040	0.020	0.047	0.061
Ca	0.003	0.003	0.003	0.008	0.008	0.011	0.008	0.003	0.003	0.003	0.003	0.003

Chromite analyses from Cliff and Harold's Grave are shown in table 3.5. The analyses of three different chromite grains from each specimen indicate that chemical variation within each sample is small. Slightly larger variations occur between different samples from the same locality but these are small in comparison to the compositional differences between the two localities.

By convention variations in spinel major element chemistry are shown as projections within the spinel prism (Stevens, 1944). The relevant parts of these projections are shown in figure 3.2 with metal ratios expressed as percentages. Analyses obtained from Cliff, Harold's Grave, other mantle and crustal chromites are shown by different symbols.

The Unst chromites show a wide variation in Cr/(Cr+Al) (45-75%) and in Mg/(Mg+Fe^{II}) [40-75%], but a very restricted variation in Fe^{III}/(Cr+Al+Fe^{III}) [1-5%]. In addition, Cr/(Cr+Al) and Mg/(Mg+Fe^{II}) show an inverse correlation. Analyses from Cliff and Harold's Grave plot as separate groups, the latter characterised by higher Cr/(Cr+Al)

and Harold's Grave plot as separate groups, the latter characterised by higher Cr/(Cr+Al)

Figure 3.2. Shetland chromite analyses shown on projections within the spinel prism (Stevens, 1944), (a) Cr/(Cr+Al) v Mg/(Mg+Fe^{II}), (b) Fe^{III}/(Cr+Al+Fe^{III}) v Mg/(Mg+Fe^{II}). Analyses from Cliff (open triangles), Harold's Grave (open squares), other mantle chromite pods (closed diamonds) and crustal chromites (closed squares).

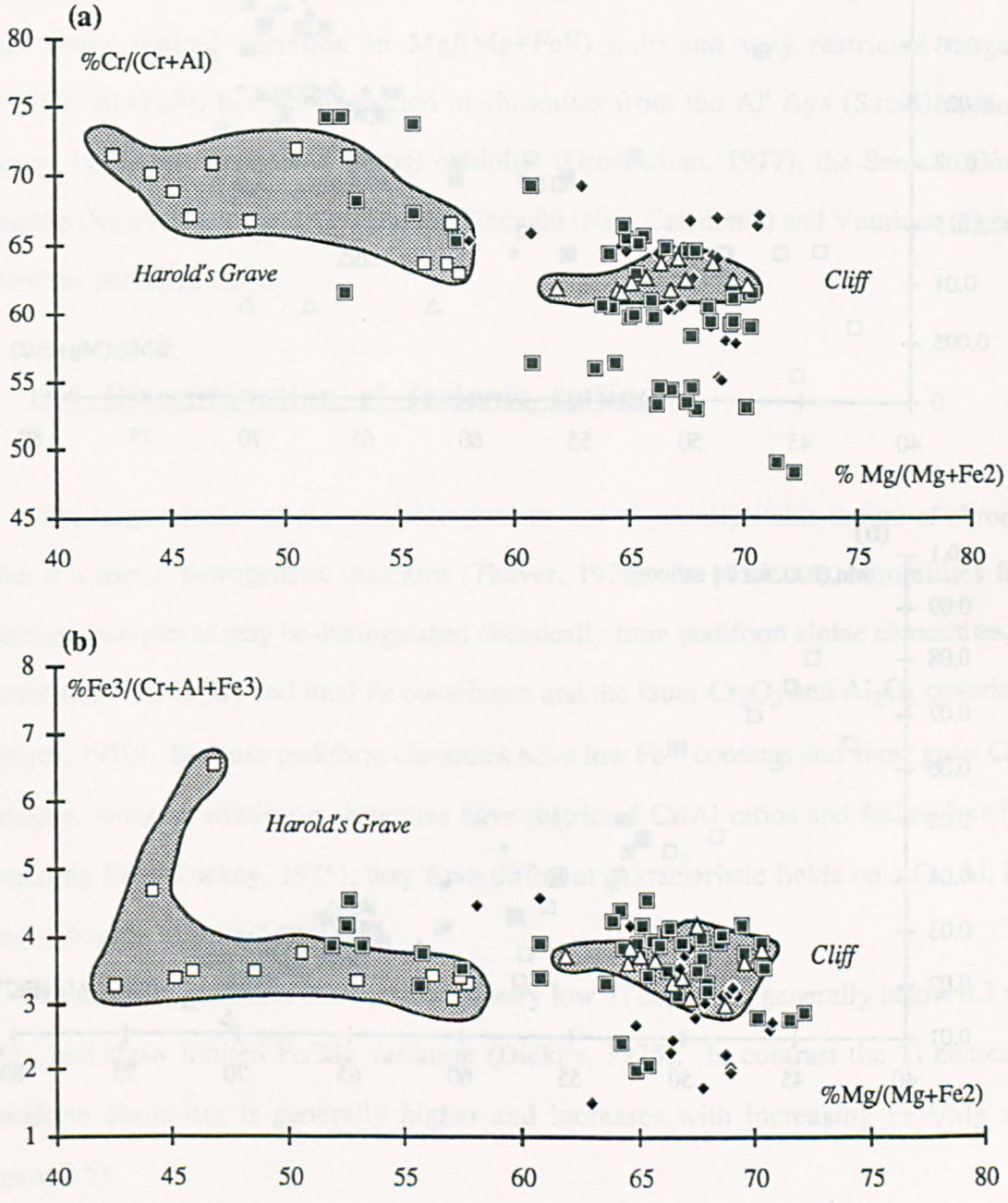

Figure 3.3. Correlations between minor elements and covariant major element ratios (a) $Mg/(Mg+Fe^{II})$ v Ni, (b) $Mg/(Mg+Fe^{II})$ v Mn. Analyses from Cliff (open triangles), Harold's Grave (open squares), other mantle chromite pods (closed diamonds) and crustal chromites (closed squares).

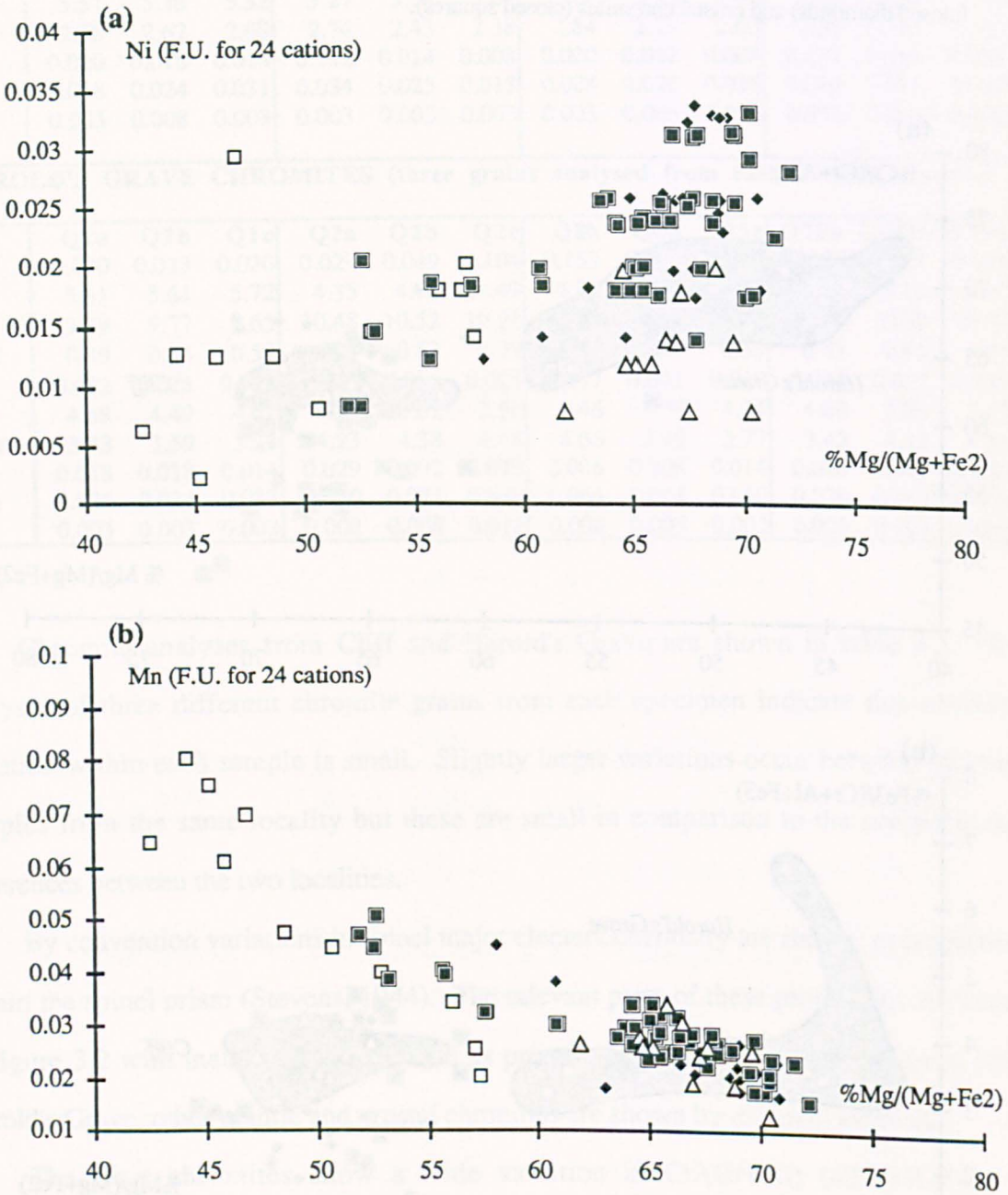

and lower $Mg/(Mg+Fe^{II})$. These groups overlap the compositional range of the other chromites.

Analyses of the minor elements Ni and Mn were found to vary systematically with the covariant major element ratios. The best correlations are with $Mg/(Mg+Fe^{II})$ indicating substitution in tetrahedral sites. A good inverse correlations is shown with Mn and a weak positive correlation with Ni (figure 3.3).

The chemical variation of Unst chromites is similar to that generally observed in podiform chromite deposits (Dickey, 1975). In particular, the wide range in Cr/(Cr+Al) ratio, more limited variation in $Mg/(Mg+Fe^{II})$ ratio and very restricted range of $Fe^{III}/(Cr+Al+Fe^{III})$ has been reported in chromites from the Al' Ays (Saudi) ophiolite (Neary, 1974), the Troodos (Cyprus) ophiolite (Greenbaum, 1977), the Semail (Oman) ophiolite (Neary & Brown, 1979) and the Tiébaghi (New Caledonia) and Vourinos (Greece) ophiolites (Roberts, 1986).

3.4 Discrimination of tectonic setting

The large number of chemical components and physically stable nature of chromite make it a useful petrogenetic indicator (Thayer, 1970). In particular, chromitites from stratiform complexes may be distinguished chemically from podiform alpine chromitites, the former showing Cr_2O_3 and total Fe covariance and the latter Cr_2O_3 and Al_2O_3 covariance (Thayer, 1970). Because podiform chromites have low Fe^{III} contents and show great Cr/Al variation, whereas stratiform chromites have restricted Cr/Al ratios and follow trends of increasing Fe^{III} (Dickey, 1975), they have different characteristic fields on a Cr, Al, Fe^{III} ternary diagram (figure 3.4).

In addition, podiform chromites have very low Ti contents, generally below 0.3 wt% TiO_2, and show limited Fe/Mg variation (Dickey, 1975). In contrast the Ti content of stratiform chromites is generally higher and increases with increasing Fe^{II}/Mg ratio (figure 3.5).

Figure 3.4. Ternary Cr, Al, Fe^{III} chromite discrimination diagram (from Dickey, 1975).

The lower figure shows the area of interest enlarged with Shetland analyses plotted and classified according to their setting.

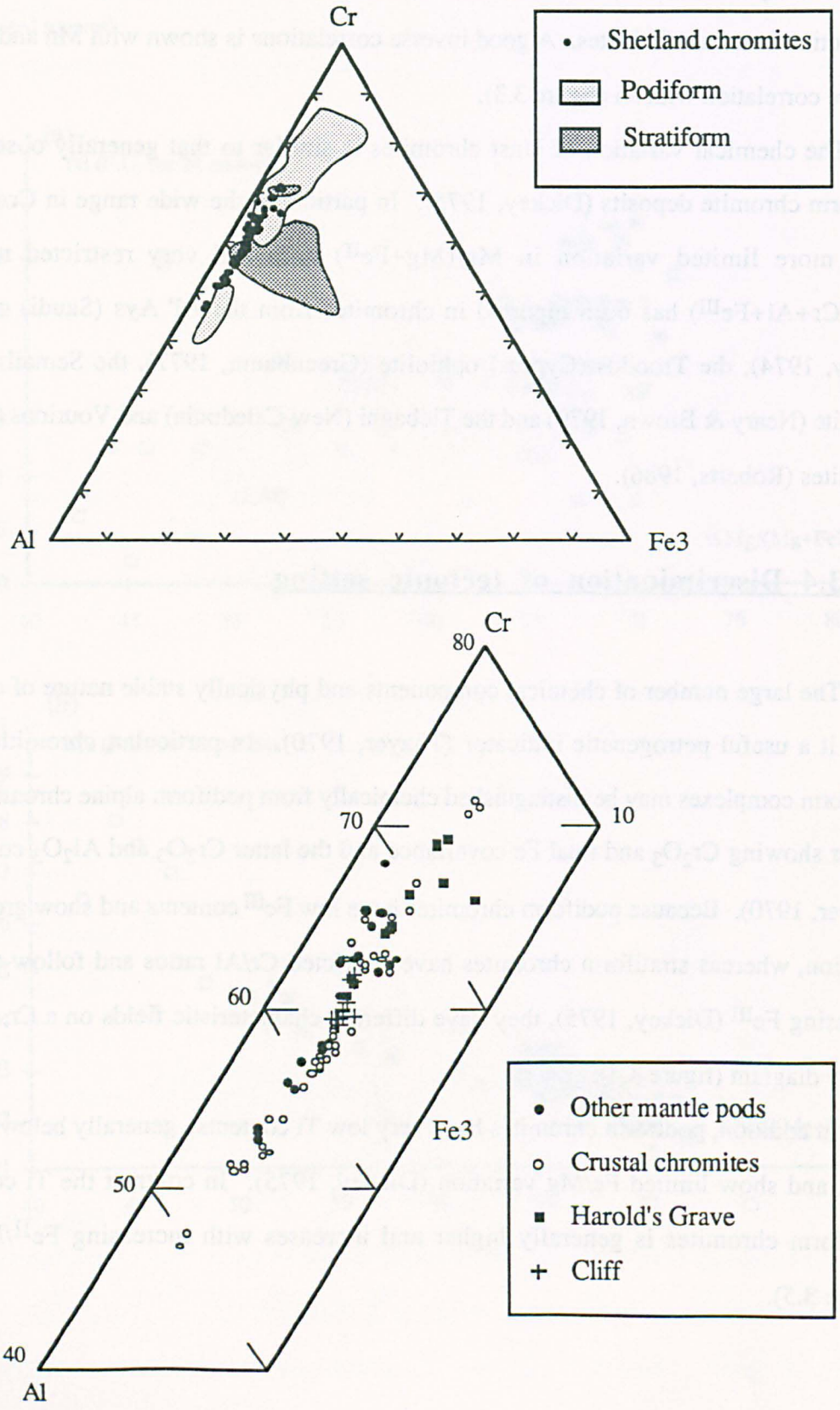

Figure 3.5. Fe^{II}/Mg v TiO_2 (wt%) chromite discrimination diagram (from Dickey, 1975).

The enlarged lower figure shows the Shetland analyses classified according to their setting.

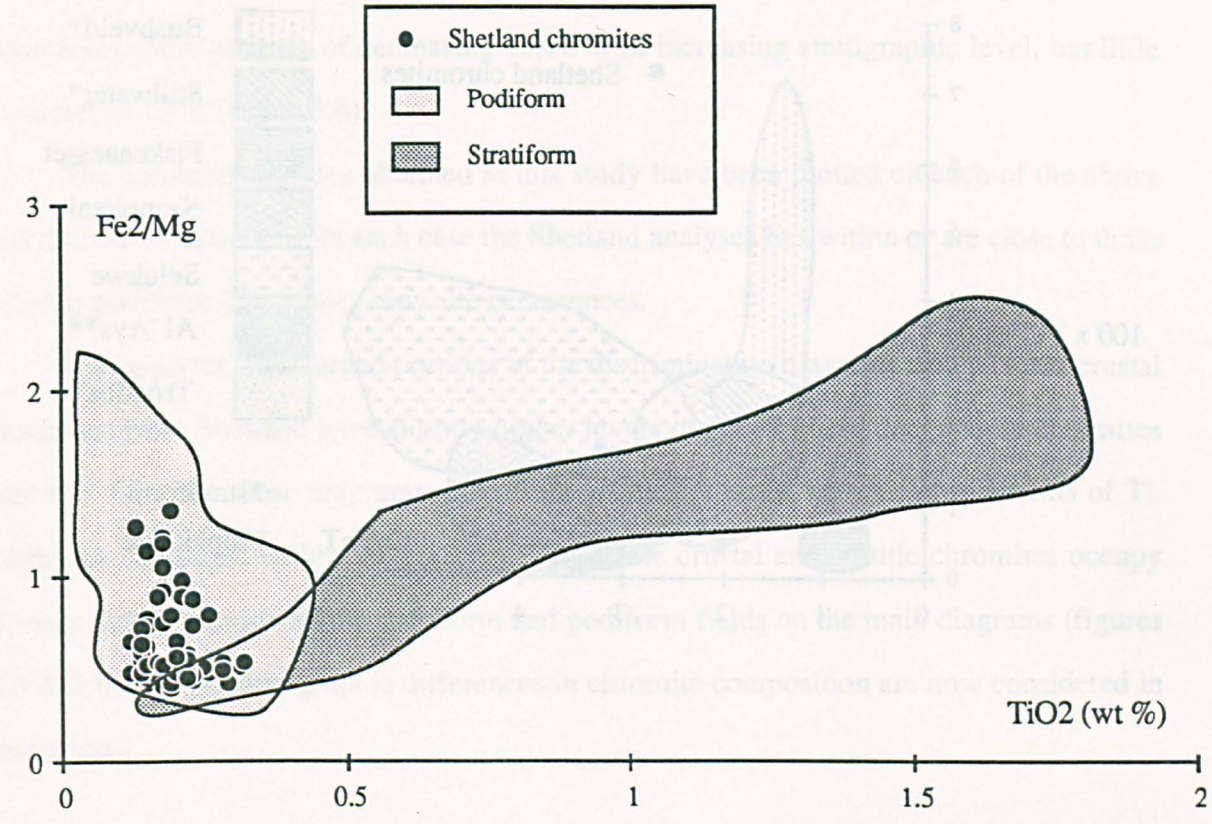

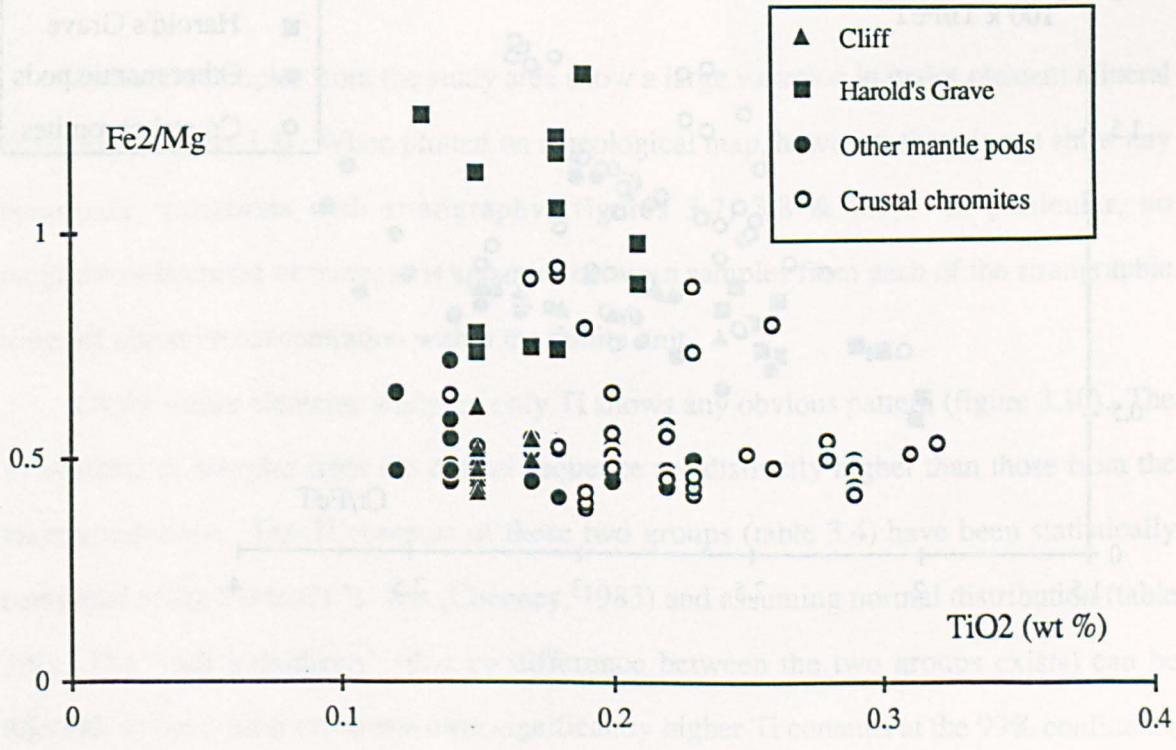

Figure 3.6. Cr/Fe^T v Ti/Fe^T chromite discrimination diagram (from Neary & Brown, 1979).

The enlarged lower figure shows the Shetland analyses classified according to their setting.

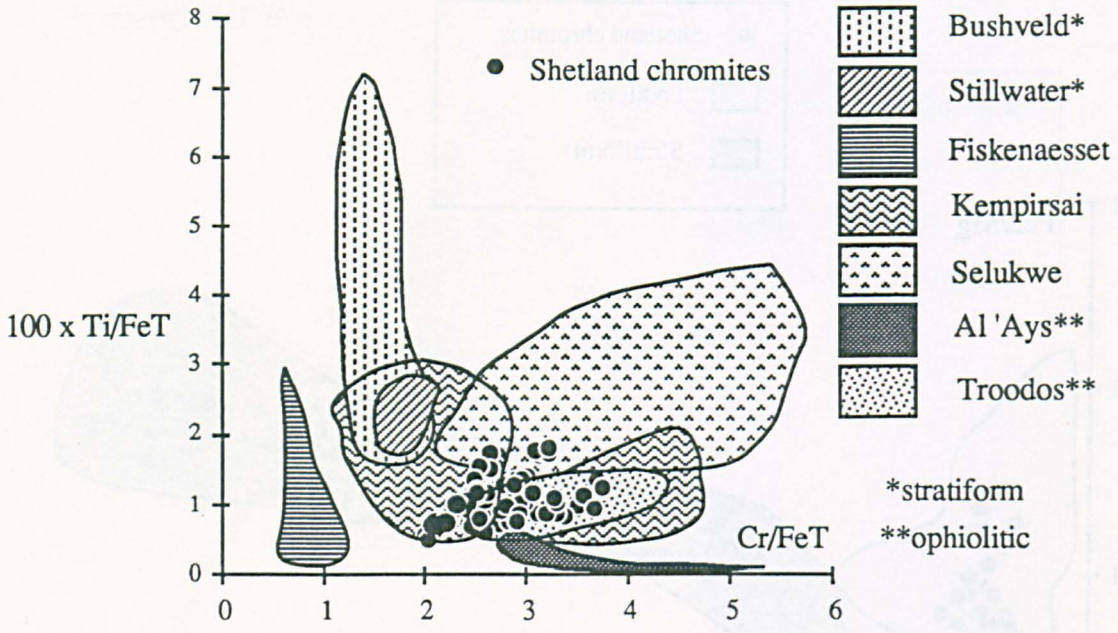

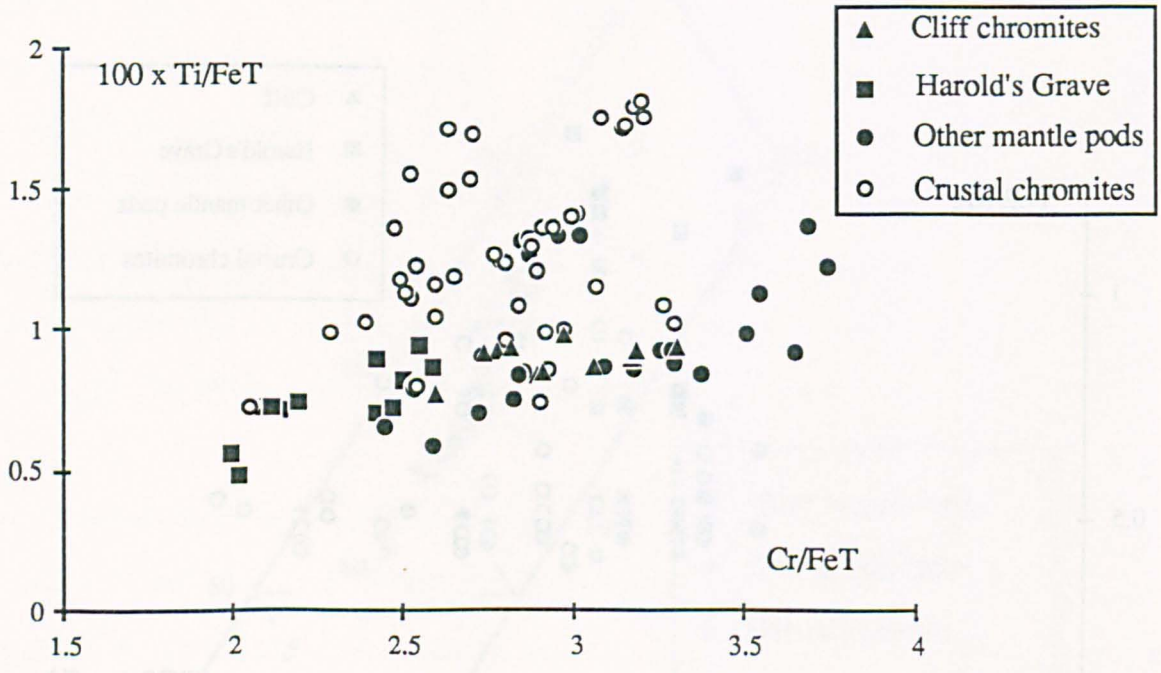

Suites of chromite samples from different environments also show different trends on a Cr/Fe v. Ti/Fe diagram (Neary & Brown, 1979). Stratiform complexes show patterns of increasing Ti/Fe with stratigraphic level but constant Cr/Fe. Conversely ophiolitic complexes show patterns of decreasing Cr/Fe with increasing stratigraphic level, but little variation in Ti/Fe (figure 3.6).

The chromite analyses obtained in this study have been plotted on each of the above discrimination diagrams. In each case the Shetland analyses lies within or are close to those of other podiform (ophiolitic) chromite occurrences.

It is apparent on enlarged portions of the discrimination diagrams using Ti that crustal chromites from Shetland have slightly higher levels of this element than mantle chromites (section 3.5). On these diagrams, stratiform chromites show variable enrichments of Ti. Although contained within the podiform fields, the crustal and mantle chromites occupy distinct fields, mimicking the stratiform and podiform fields on the main diagrams (figures 3.5 & 3.6). These stratigraphic differences in chromite composition are now considered in more detail.

3.5 Stratigraphic variation

Chromite samples from the study area show a large variation in major element mineral chemistry (section 3.3). When plotted on a geological map, however, they do not show any systematic variations with stratigraphy (figures 3.7, 3.8 & 3.9). In particular, no progressive decrease or increase is apparent between samples from each of the stratigraphic zones of chromite concentration within the dunite unit.

Of the minor elements analysed only Ti shows any obvious pattern (figure 3.10). The Ti contents of samples from the crustal sequence are distinctly higher than those from the mantle sequence. The Ti contents of these two groups (table 3.4) have been statistically compared using Student's "t" test (Cheeney, 1983) and assuming normal distribution (table 3.6). The "null hypothesis" (that no difference between the two groups exists) can be rejected, so the crustal chromites have significantly higher Ti contents at the 99% confidence level. The Ti content does not, however, show any progressive increase or decrease with

Figure 3.7. Map of chromite sample localities with sample numbers.

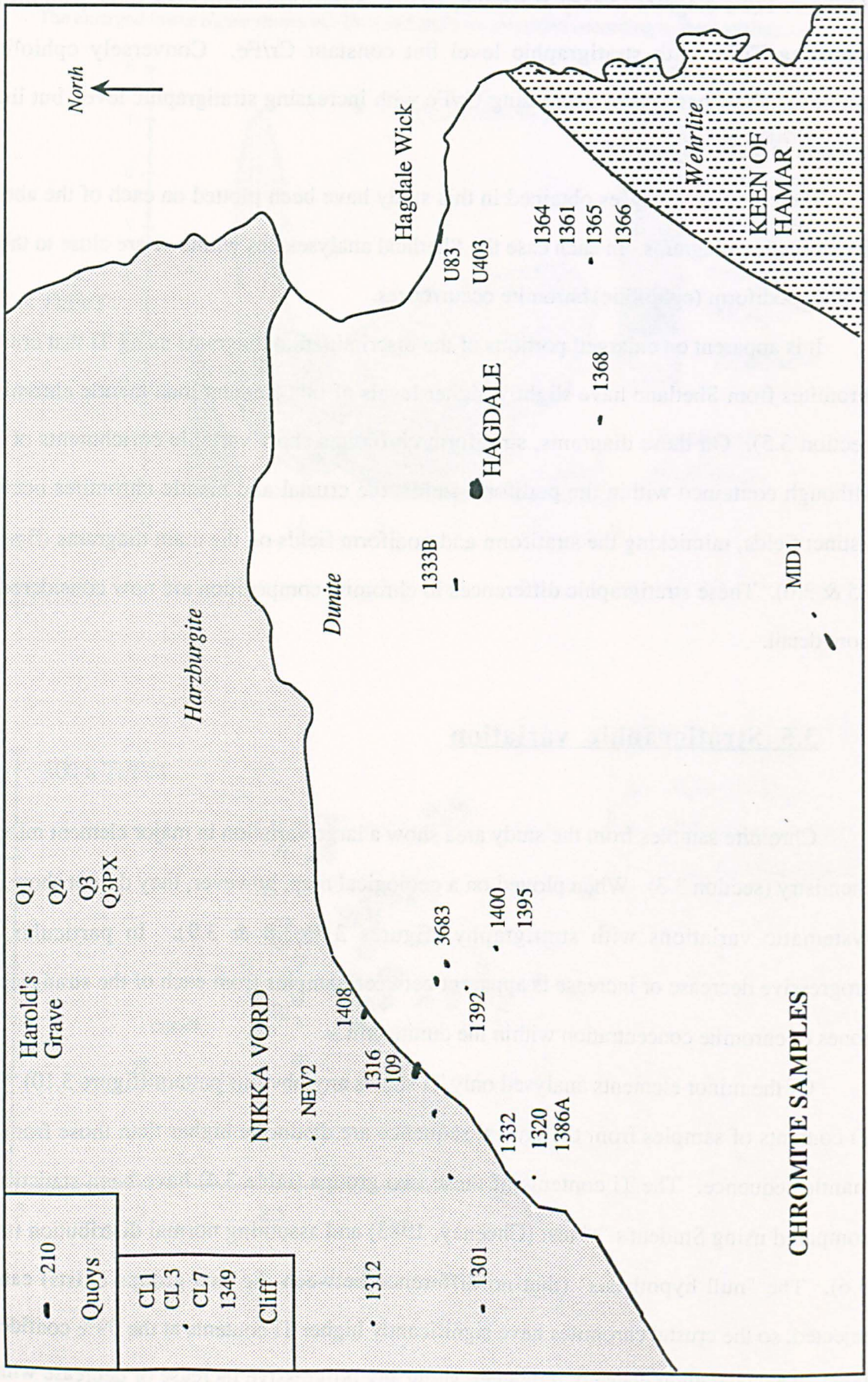

Figure 3.8. Map of chromite sample localities and average Cr/(Cr+Al) ratios.

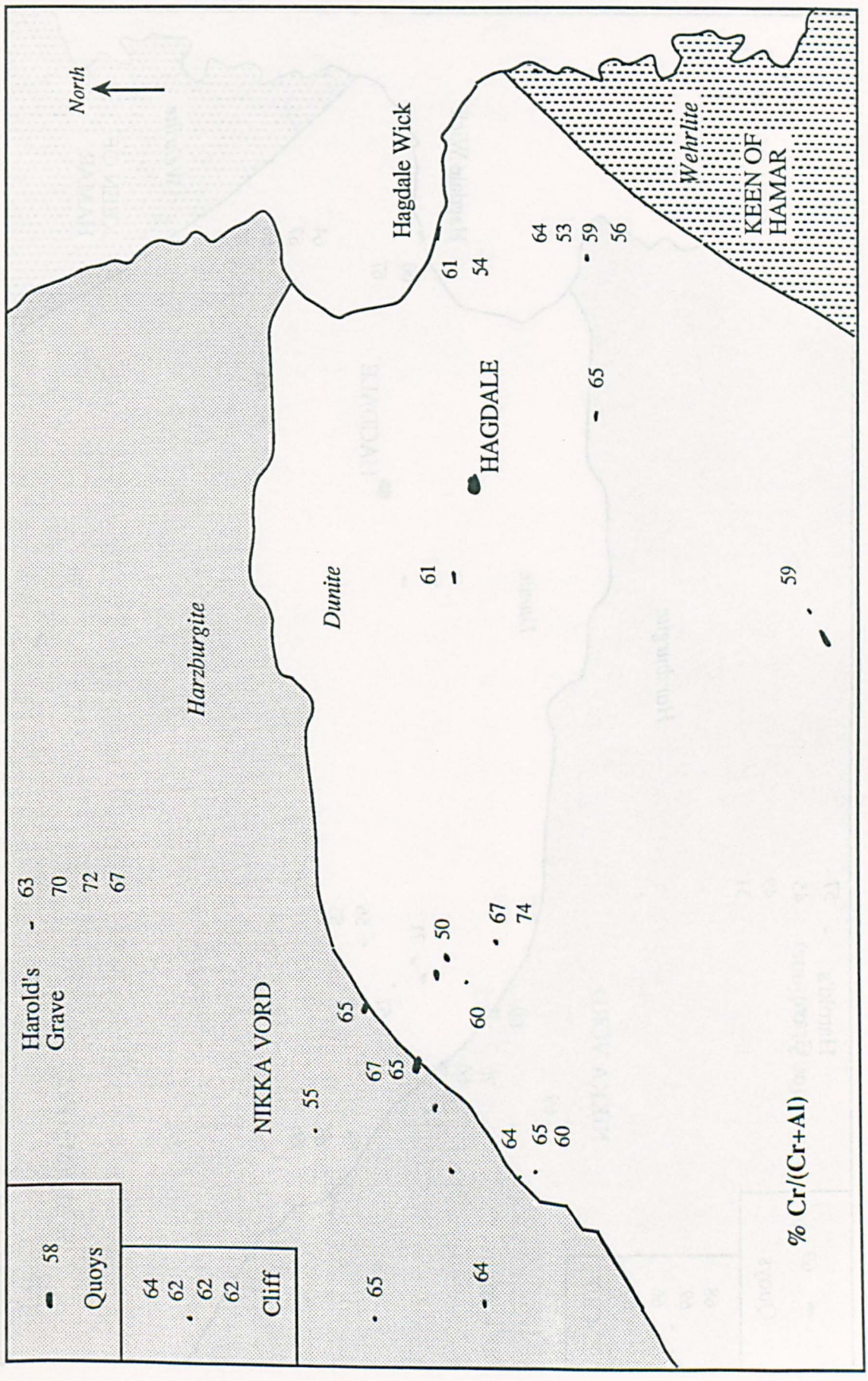

Figure 3.9. Map of chromite sample localities and average $Mg/(Mg+Fe^{II})$ ratios.

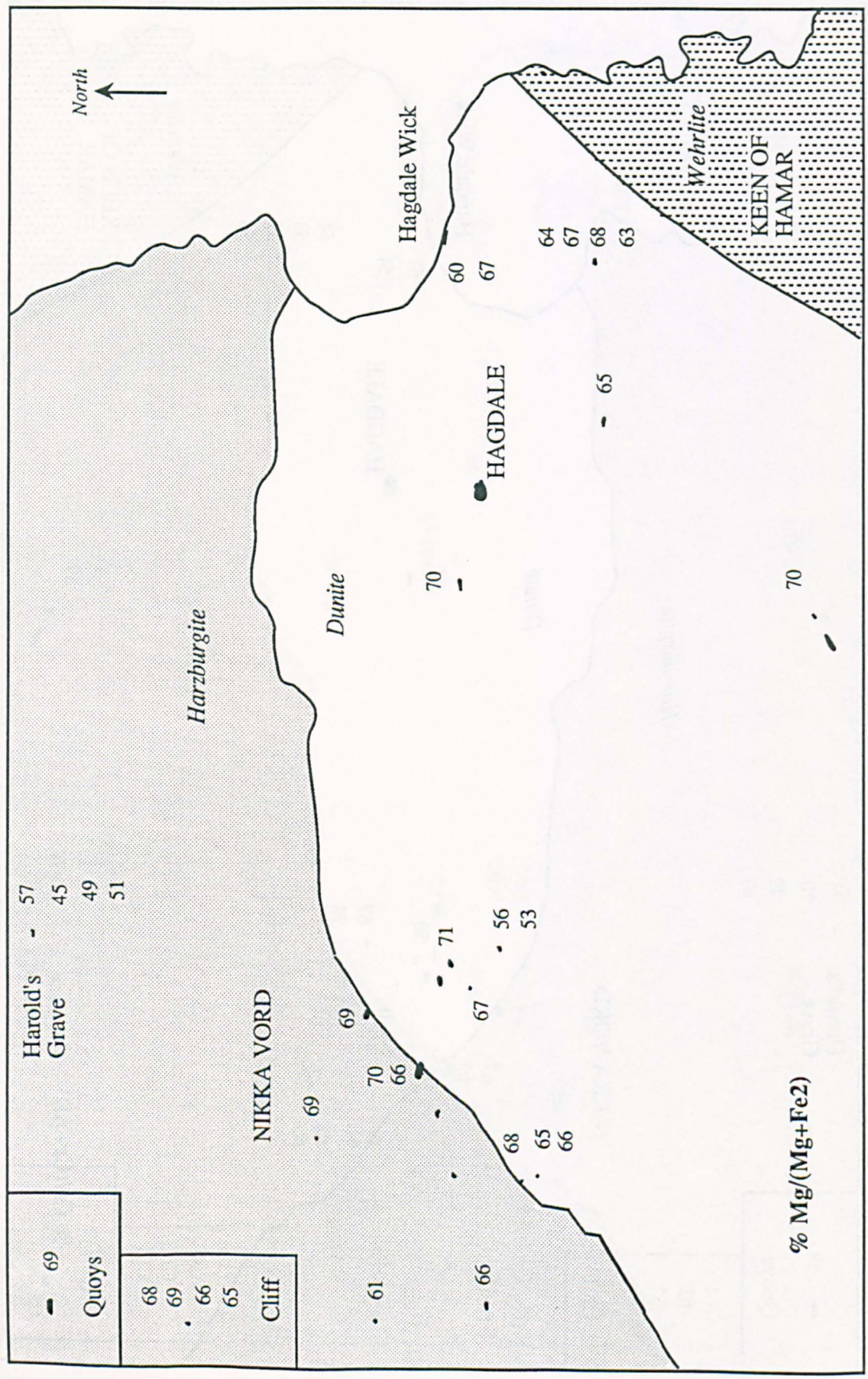

Figure 3.10. Map of chromite sample localities and average Ti contents.

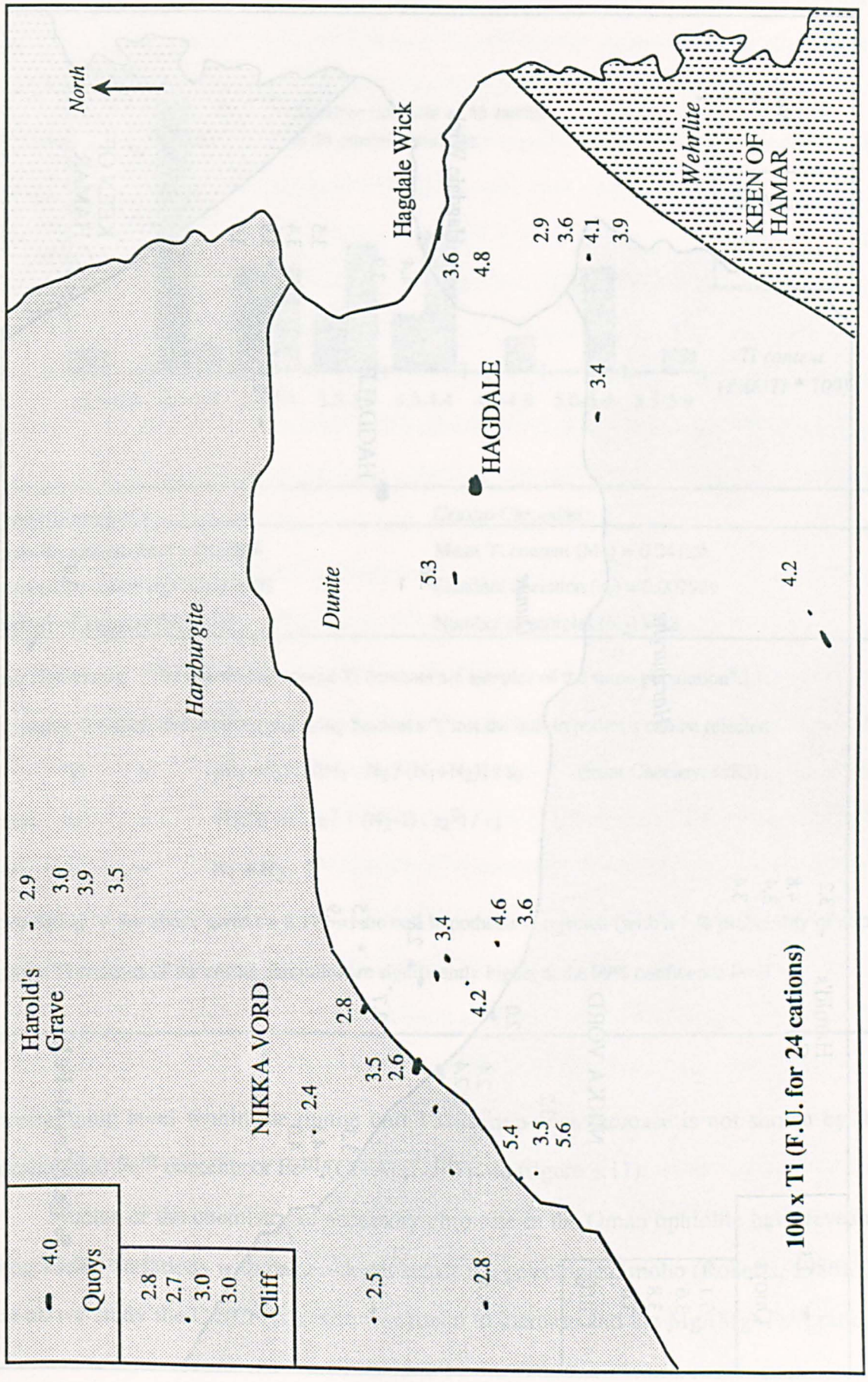

Figure 3.11. Map of chromite sample localities and average $Fe^{III}/(Cr+Al+Fe^{III})$ ratios.

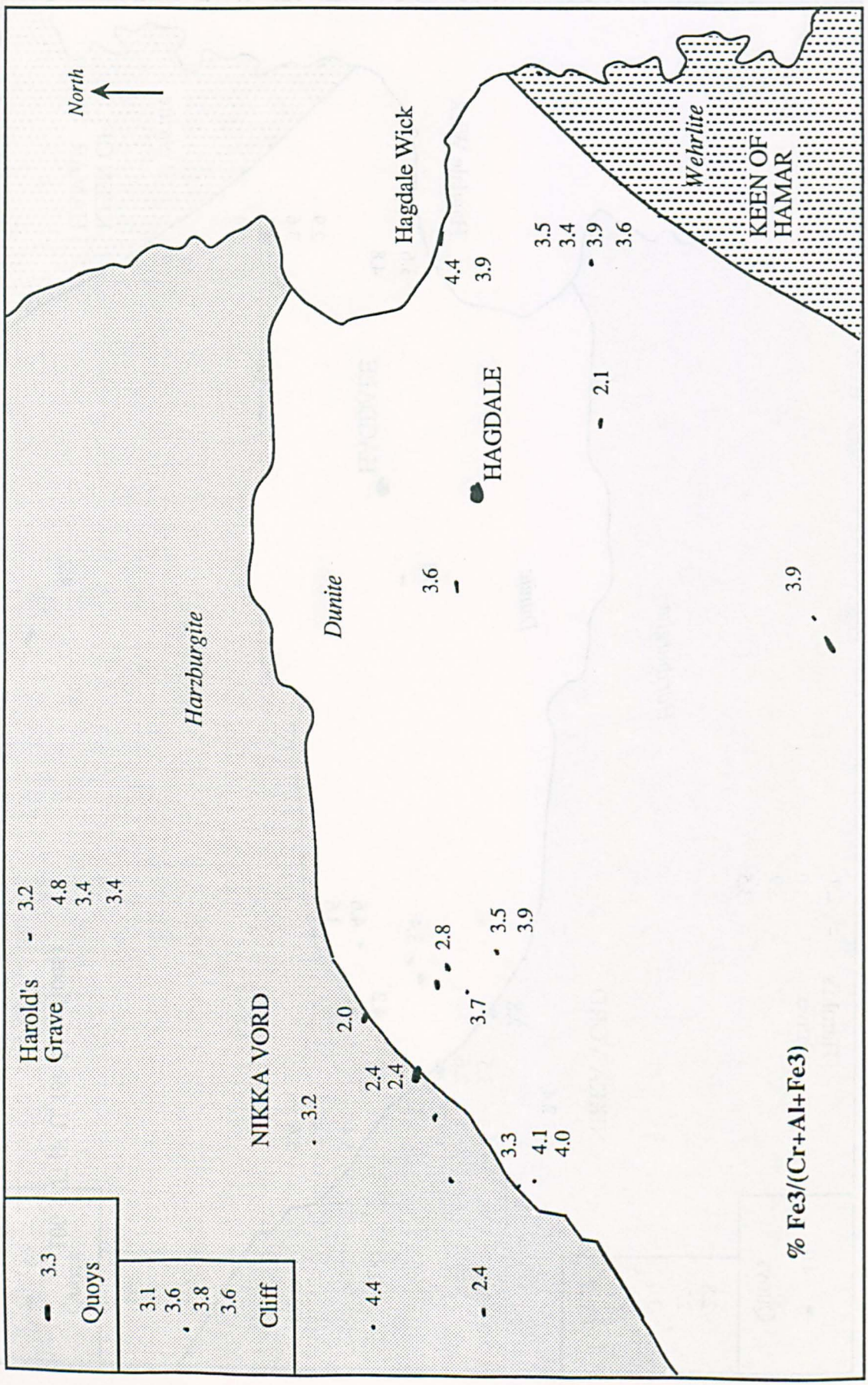

Table 3.6. Statistical testing of different Ti contents of crustal and mantle sequence chromites.

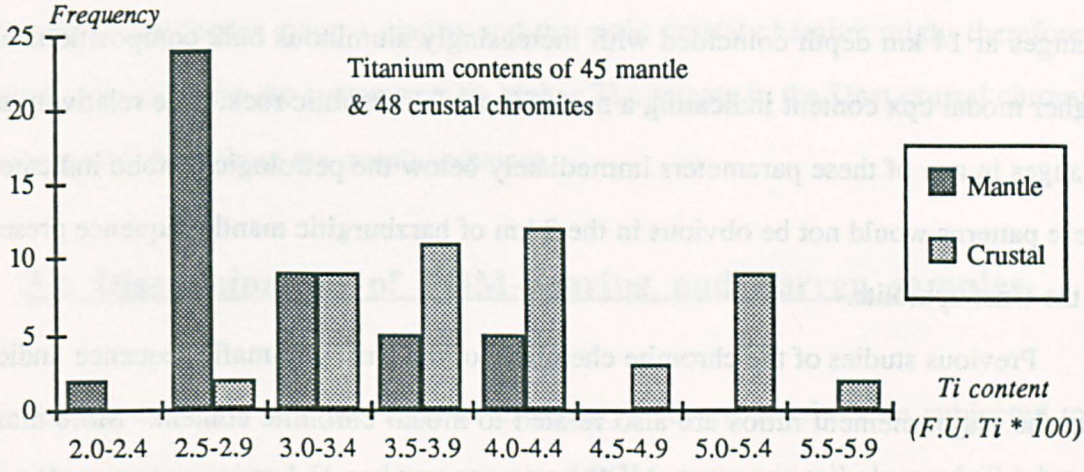

Mantle Chromites:-	*Crustal Chromites:-*
Mean Ti content (M_1) = 0.03003	Mean Ti content (M_2) = 0.04129
Standard deviation (s_1) = 0.004792	Standard deviation (s_2) = 0.007989
Number of samples (N_1) = 45	Number of samples (N_2) = 48

Null Hypothesis: "The mantle and crustal Ti contents are samples of the same population".

Assuming Gaussian distributions and using Student's "t"test the null hypothesis can be rejected

$$\text{"t"} = (M_1-M_2) \cdot \sqrt{[N_1 \cdot N_2 / (N_1+N_2)]} / s_0 \quad \text{(from Cheeney, 1983)}$$

where $$s_0 = \sqrt{\{[(N_1-1) \cdot s_1^2 + (N_2-1) \cdot s_2^2] / \nu\}}$$

and $$\nu = N_1 + N_2 - 2$$

Calculating "t" for above gives t = 8.175 so the null hypothesis is rejected (with a 1 % probability of error) and the Ti contents of the crustal chromites are significantly higher at the 99% confidence level.

stratigraphic level within the dunite unit. This step-wise increase is not shown by the recalculated Fe^{III} contents or $Fe^{III}/(Cr+Al+Fe^{III})$ ratio (figure 3.11).

Studies of the chemistry of accessory chromite in the Oman ophiolite have revealed progressive variations with palaeo-depth below the petrological moho (Roberts, 1986). In the above study the Cr/(Cr+Al) ratio was found to increase and the $Mg/(Mg+Fe^{II})$ ratio to

decrease slightly down to a depth of 14 km. At greater depths The Cr/(Cr+Al) ratio decreased sharply and the $Mg/(Mg+Fe^{II})$ ratio increased rapidly. The trace elements Ti and Ni showed patterns similar to Cr/(Cr+Al) and $Mg/(Mg+Fe^{II})$ respectively. The sharp changes at 14 km depth coincided with increasingly aluminous bulk compositions and a higher modal cpx content indicating a more "fertile" lherzolitic rock. The relatively small changes in any of these parameters immediately below the petrological moho indicate that these patterns would not be obvious in the 2 km of harzburgitic mantle sequence preserved in the Unst ophiolite.

Previous studies of the chromite chemistry of the Unst ultramafic sequence indicated that the major element ratios are also related to modal chromite content. More massive chromites yielded higher $Mg/(Mg+Fe^{II})$ ratios than disseminated chromites, and nodular chromites had higher Cr/(Cr+Al) ratios than other chromites from the same locality (Prichard & Neary, 1982). This study suggested progressive decreases in TiO_2 content and $Fe^{III}/(Cr+Al+Fe^{III})$ ratio with depth in both disseminated and massive chromite. These patterns were reported over the region of the petrological moho, which included the uppermost 2 km of the mantle sequence and lowermost 1 km of the crustal sequence. Inspection of the graphical data from which these conclusions were drawn (fig. 4, Prichard & Neary, 1982) indicates that the scatter of the analyses is too great to distinguish between a progressive stratigraphic increase in Ti and a step-wise increase across the petrological moho, particularly for the more chromite-rich samples. Clearly some analyses from the dunite unit contain more TiO_2 than most from the harzburgite unit. This is consistent with postulated higher Ti threshold levels in the crustal sequence than in the mantle sequence which is the interpretation drawn from the present study.

Factors influencing the Ti content of chromites have been discussed by Neary (1974), and include the original composition and degree of fractionation of the magma and also the crystallisation conditions, in particular the oxygen fugacity. In the Oman mantle sequence greater TiO_2 enrichment was found in the disseminated accessory spinels from dunite pods compared to those from harzburgites (Augé & Roberts, 1982). This indicates that these dunite pods are unlikely to represent a residue of partial melting, but result from crystal precipitation from a magma. This supports the established view that chromite bodies

contained within the mantle sequence of ophiolites represent early crystallisation in feeder conduits beneath the main crustal magma chamber (Menzies & Allen, 1974; Neary & Brown, 1979; Gass & Smewing, 1981). Only differences between the crystallisation conditions in the feeder magma diapirs and the main crustal chamber might therefore be invoked to account for the systematically higher Ti contents in the Unst crustal chromites compared with those from the mantle sequence.

3.6 Discrimination of PGM-bearing and barren samples

All the chromite samples used in this study had previously been subjected to ß-autoradiography (section 1.5) and any contained PGMs systematically located (Prichard et al., 1989). All the minerals identified are listed in table 3.7. Originally this data was used to classify the samples as follows:-

(i) Samples from Cliff (all containing many Pt, Pd & Rh minerals)

(ii) Samples from Harold's Grave (all containing many Os, Ir & Ru minerals)

(iii) Other PGM-bearing samples (mostly laurites)

(iv) Barren samples from the same localities as (iii)

(v) Samples from PGM-barren localities.

This classification of samples allows comparisons between the compositions of PGM-bearing and PGM-barren chromites. In figure 3.12 these categories are shown separately on enlarged portions of the three diagrams which discriminate between ophiolitic and stratiform chromite (i.e. figures 3.4, 3.5 & 3.6). Chromites from Cliff and Harold's Grave are also distinguished on the graphs of major element variation (figure 3.2). All these diagrams indicate that there is nothing unusual about the compositions of the PGM-rich ophiolitic chromites and that they cannot be distinguished from PGM-barren chromites using the host mineral chemistry.

Subsequent studies of the distribution of PGE concentrations in this area (chapter 4) have largely revised the above classification of chromite quarries according to PGM content. The compositional comparisons between Cliff and Harold's Grave are still valid, however, since chromitites from these two localities are known to contain large numbers of small

Table 3.7. Minerals located in chromite samples using ß-autoradiography (Prichard et al., 1989).

Locality Number	*Location & Quarry name*	*Sample Number*	*PGM phases*
1	Cliff	CL1,CL2, CL7, 1349	Various PGM predominantly Pt, Pd, Rh phases
2	Harold's Grave	Q1, Q2, Q3, Q3PX	Various PGM predominantly Os, Ir, Ru phases
3	Quoys	210	Laurite (RuS_2)
4	Nikka Vord East	NEV2	Laurite (RuS_2)
5	Nikka Vord North	1312	Laurite (RuS_2), & native Os
		[others]	[Ni-Rh-Sb & hollingworthite]
6	Nikka Vord South	1301	—
7	Long Quarry	1408	Laurite (RuS_2)
8	Quarry 8	1316, 109	—
			—
9	BX Quarry	1392	Laurite (RuS_2)
11	Quarry 11	3683	—
12	Quarry 12	1332	—
		1320	Irarsite
		1386A	—
13	Quarry 13	1400,	—
		1395	—
14	Long John Quarry	1333B	—
15	Midgarth Quarry	MID 1	—
17	Hagdale Wick Layers	U83,	—
		U403	Os/Ir alloy
18	Keen of Hamar	1364,	—
		1361	—
		1365	—
		1366	Laurite (RuS_2)
19	Jimmies Quarry	1368	Geversite & native Pt

Figure 3.12. Enlarged portions of the three chromite discrimination diagrams (figures 3.4, 3.5 & 3.6) showing analyses of samples with and without PGM.

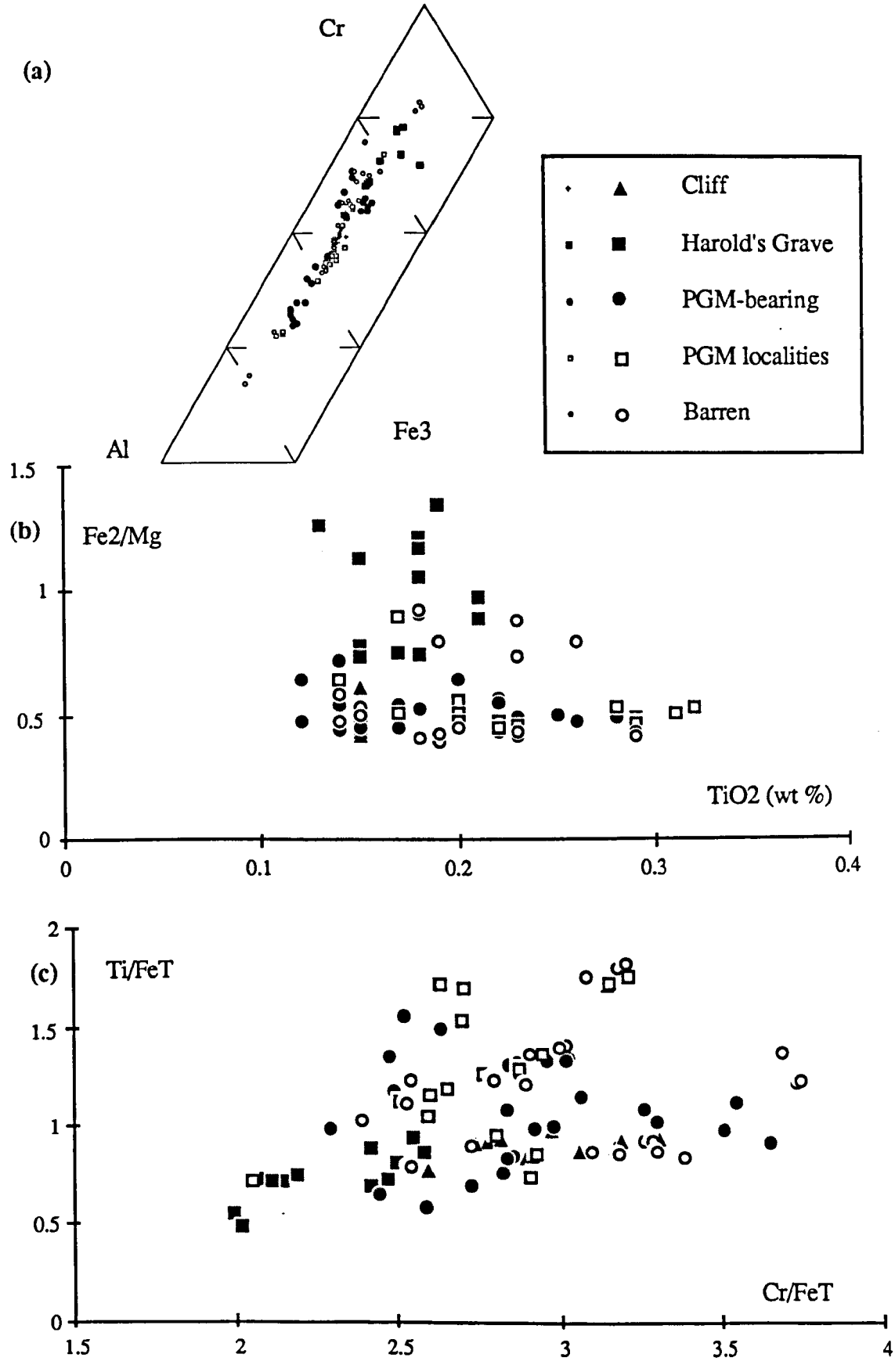

Table 3.8. Estimate of the number of thin sections (2 x 4 cm) which must be examined to be certain of finding a minor phase inclusion of the specified size (Potts, 1984). Assumes homogeneous distribution of cubic PGM of dimension x in chromite with whole-rock PGE abundance W.

Size of cube	*Number of thin sections required at given PGE concentration (W)*		
(x)	*W = 1 ppb*	*W = 10 ppb*	*W = 100 ppb*
1 μm	5	0.5	(many per section)
2 μm	22	2	(few per section)
5 μm	139	14	1

Table 3.9. Calculations of the minimum grade required for representative "analysis" of rock thin sections (after Clifton et al., 1969). The necessary sample size increases with decreasing tenor or increasing grain size.

Density of chromite = 5.09 g/cm3
Thin section dimensions = 2cm x 3 cm

(Mineral diameter = thickness of sample)

Mineral diameter	*Mass of sample*	*Required grade**
(a) 4 microns	12 mg	1 ppm
(b) 8 microns	24 mg	4 ppm
(b) 16 microns	49 mg	16 ppm

** The grade of gold required to ensure representative analysis, defined as the expected analysis of 20 gold particles. Model uses randomly distributed gold spheres (Clifton et al., 1969)*

PGM and anomalous levels of PGE (Prichard et al., 1986). The usefulness of a mineralogical technique in identifying localities containing lower levels of PGE is questionable as a result of the "nugget" effect* (table 3.8 & 3.9). Significant whole-rock PGE analyses have since been obtained from several of the above "PGM-barren" localities.

3.7 Discussion

The Unst chromites show the wide variations in Cr/(Cr+Al) and Mg/(Mg+Fe^{II}) and low Ti or Fe^{III} contents which are characteristic of podiform chromitites. With the exception of subtle changes in Ti content, these differences in major and minor element chemistry are unrelated to stratigraphic level or PGE content. In particular, no chemical uniformity is apparent between podiform chromite concentrations from the same horizon. The stratigraphic continuity of these zones has been established by detailed field mapping (section 2.3.2). This suggests that individual chromitite bodies may result from magmas with different original compositions or with differing degrees of fractionation. Alternatively the variations in major element ratios may purely reflect differing degrees of equilibration with bulk silicate composition dependent on differing modal chromite contents. The lack of progressive chemical changes between successively higher chromite horizons suggests that these represent different magma inputs, rather than reversals in a single evolving magma.

The Ti contents of the chromite do vary in a manner systematically related to stratigraphic level. The Ti content of chromites from the crustal sequence are significantly higher than those from the mantle sequence. Since chromitites in dunite pods in the mantle sequence represent crystallisation from pockets of magma feeding the overlying chamber, only differences in the physical conditions of crystallisation might produce such a pattern. In the case of the Ti content of chromite, this is possibly related to changes in oxygen fugacity as batches of magma enter the main magma chamber and mix with the resident melt.

---

* The effect on analytical sampling size of the occurrence of Au or PGE as particulate native metal or discrete PGM phases (see also section 4.3).

In conclusion, mineral chemistry distinguishes between chromites from stratiform complexes and ophiolitic complexes. It does not, however, distinguish between ophiolitic chromites containing the positive slope (Pt-, Pd-, Rh- dominant) and negative slope (Os-, Ir-, Ru-dominant) PGE mineralisation, even though these different assemblages are typical of each respective paragenesis. The chromitites from Unst all conform to ophiolitic compositions but may contain either type of PGE concentration. It is apparent that different processes control the composition of the host chromite from those influencing the type of PGE assemblage. The close spatial association between chromite and PGE concentrations is described in the following chapter.

Chapter 4

The Distribution of PGE and Gold in the Ophiolite Complex

4.1 Introduction

Stream sediment, overburden and lithogeochemical sampling by the British Geological Survey (Gunn et al., 1985) indicated that widespread PGE mineralisation occurred within the ophiolite sequence described in chapter 2 (section 1.5.2). A hydrothermal origin was proposed for the unusual Pt-, Pd-rich mineralisation at Cliff on various lines of evidence (section 1.6.1). Lower grade Pt and Pd mineralisation in the pyroxene-rich cumulate sequence was thought to be magmatic, as was the Os-Ir-Ru mineralisation within the harzburgite unit, which was considered typical of that found in other ophiolite complexes (Gunn et al., 1986). The possibility of other magmatic PGE concentrations in the complex, perhaps acting as a source of Pt and Pd for hydrothermal mineralisation, therefore cannot be precluded (section 1.7).

Previous work at the Open University (Prichard et al., 1989) suggested a magmatic origin for all PGE mineralisation by comparisons with similar concentrations in igneous parageneses. This study included a detailed survey of the PGM associated with chromitites in the complex (section 1.5.3) but included Pt and Pd whole rock analyses of only ten chromite-rich samples (section 1.5.4). Further sampling and analysis was therefore required.

In order to show the distribution of PGE in the complex an extensive sampling program with routine analysis for PGE was initiated. This was to include all silicate lithologies as well as chromite-rich rocks, so as to establish the distribution of PGE in the complex as a whole. Through the recognition of primary igneous rock types and accurate stratigraphic positioning of samples this would indicate whether PGE mineralisation was

related to the primary lithologies in a manner indicative of magmatic processes. Conversely, by the collection of the various alteration lithologies spatially associated with shear zones the importance of hydrothermal action could be established.

This chapter begins with the details of the sampling program and the analytical methods. This is followed by descriptions of the PGE distribution and the genetic controls of mineralisation. In the conclusions a model is proposed accounting for the occurrence of PGE concentrations in ophiolites.

4.2 Sampling program

A total of 388 samples were collected representing all the primary rock types and alteration styles present in the complex. Of these, 121 were collected from disused chromite quarries, chromite trial pits and in situ chromite mineralisation. These included the known sites of PGE mineralisation at Cliff and Harold's Grave. A further 130 samples were collected covering the field area geographically and including samples from all recognised primary lithological units. The remaining 137 samples were collected as measured traverses during follow-up sampling of areas shown to be of interest by the initial reconnaissance sampling. The location of all samples is shown on enclosure 2.

4.2.1 Orientation studies at Cliff and Harold's Grave

Field examination and sampling of anomalously PGE-rich chromitites at Cliff and Harold's Grave (section 2.2.5) formed an orientation study on which the sampling of the other chromite quarries was based.

At the Cliff chromite quarry high levels of PGE and numerous PGMs had been located in a sparsely disseminated chromite-rich dunite (H. M. Prichard pers. com.) with a peculiar lime-green serpentinite matrix (plate 2.26). Nickel sulphides and arsenides had been observed in thin sections of samples from this locality (Prichard et al. 1986). It was found that the presence of sulphide phases could be recognised in the field with the aid of a hand lens.

In contrast, the chromite-rich dunites from Harold's Grave were found to have a distinctly different field appearance. Here chromite typically occurred in more massive layers in a brown dunite matrix. No sulphide phases were observed in any chromite-rich dunite samples from this locality.

The above differences in appearance indicated that it might be possible to distinguish in the field between chromite-rich samples or localities containing Os-Ir-Ru or Pt-Pd-Rh dominant PGE concentrations. The latter assemblage is characteristic of samples from Cliff (section 1.5.4), possibly as a result of the accessory sulphide content. In contrast chromitites from Harold's Grave, which do not contain visible sulphide, yield only the former PGE assemblage which is more typical of ophiolitic chromitite (section 1.2.3). This theory was subsequently tested by collecting a suite of sulphide-bearing and sulphide-poor samples from all the other chromite quarries.

4.2.2 Chromite quarry sampling

Samples were collected from all known locations of chromite mineralisation in the study area (figure 4.1). This included a number of disused chromite quarries and trial excavations (table 4.1). Samples of any remaining in situ chromite mineralisation were collected from these pits, together with representative specimens from the adjacent spoil tips. Unexploited small scale in situ mineralisation was also sampled from within a dunite pod in the harzburgite unit (locality 13, figure 4.1), from the dunite unit (localities 13 & 24) and from high-level mineralisation within the pyroxene-bearing cumulate sequence (locality 27).

At each locality a suite of samples representing the different lithologies was collected, including massive chromitites, dunites and disseminated or layered chromite-rich dunites. Every sample was examined for sulphide phases in detail. Ideally samples of each lithology were selected both with and without accessory sulphide. Variants showing the characteristic green serpentinite matrix noted at Cliff were also collected, together with any unusual chromite textures or alteration styles. Harzburgites and wehrlites were sampled when they were present in the spoil tip. All samples are shown classified by chromite content and by the presence or absence of visible sulphide in table 4.1.

Figure 4.1. Location of chromite quarry samples.

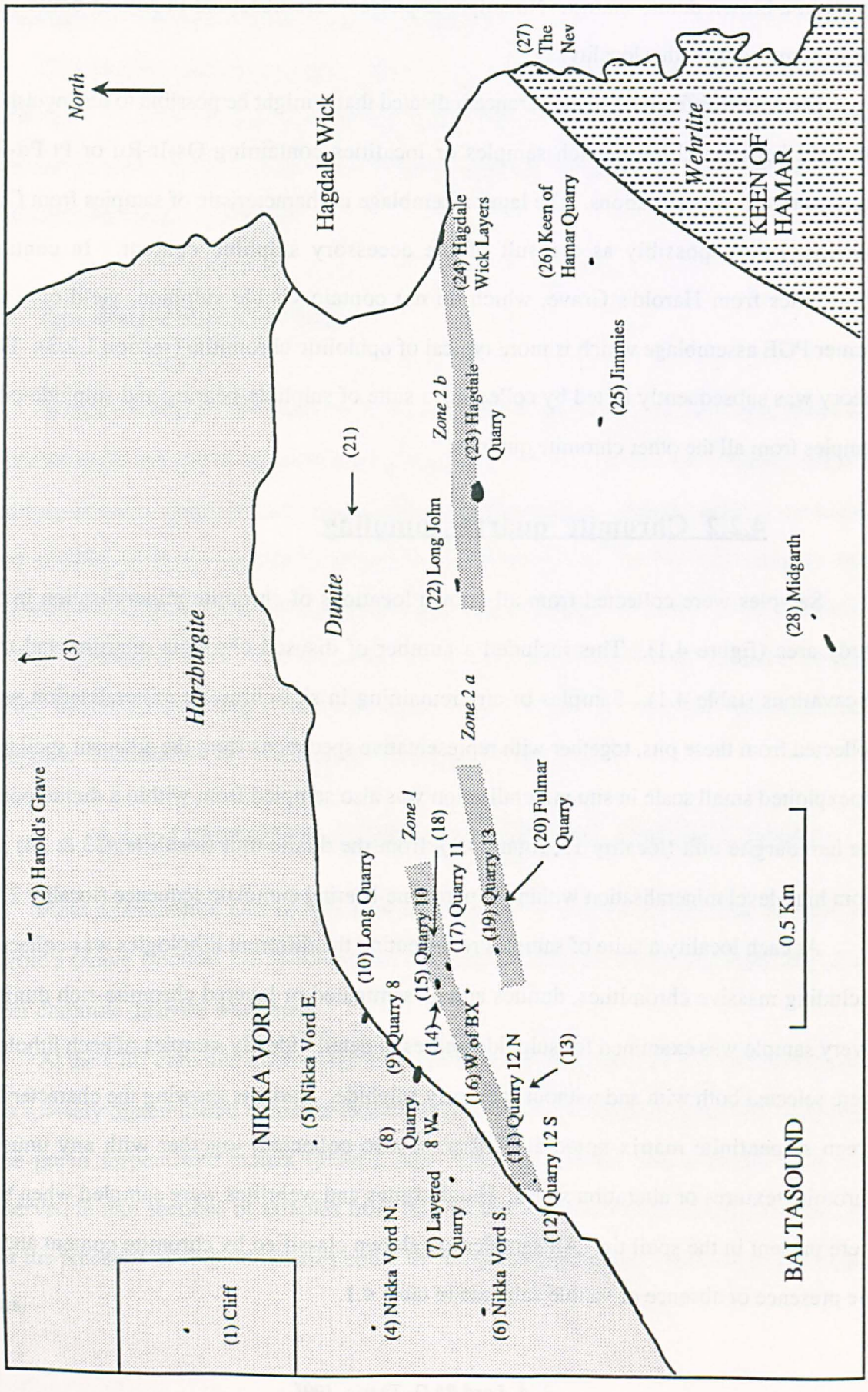

Table 4.1. Details of chromite quarry samples.

Locality figure 4.1	*Location*	*Number of samples*	*Sulphide-bearing samples**	*Sulphide-barren samples**
1	Cliff Quarry	5		CR, CR, DC, DC, DC
2	Harold's Grave Quarry	6	DU	CR, CR, CR, DC, DU
3	In situ chromite in dunite pod	2		DC, DC
4	Nikka Vord North Quarry	7	DU, DU, CR	A, CR, DC, DU
5	Nikka Vord East Quarry	6		DC, DU, CR, A, H, DC
6	Nikka Vord South Quarry	7	DU, DC, CR, DC	H, DC, DC
7	Layered Quarry	3	DC	DC, DC
8	Quarry 8 W	5	CR, DU, DU	CR, DC
9	Quarry 8	6	CR, DC, A, A	CR, DC
10	Long Quarry	4	DU, CR	CR, DU
11	Quarry 12 N	5	DC, DC, DC, DC	DC
12	Quarry 12 S	7	DC, DU, CR, DU	DC, DC, DC
13	In situ chromite in stream	2	DC	DC
14	Trial pit	2	DC	DC
15	Quarry 10	4	DC, CR	DC, CR
16	Quarry W of BX	3	DC, DC, DU	
17	Quarry 11	7	DU, DC, CR, CR, DC, DU	DC
18	Trial pit & drift chromite	2		DC, CR
19	Quarry 13	3	DU	DC, DC
20	Fulmar Quarry	5	DU, DU	DC, DC, DC
21	Trial pit	1	CR	
22	Long John Quarry	1	DU	
23	Hagdale Quarry	2	DU, DU	
24	In situ layers, Hagdale Wick	5		DC, CR, CR, DC, CR
25	Jimmie's Quarry	6	DC, W, DU, DC, DU	CR
26	Keen of Hamar Quarries	8	CR, DU	DC, DC, DC, DC, DC, DC
27	The Nev in situ high level chromite.	3	A, CR	CR
28	Midgarth Quarry	4	DU	DC, DC, CR

* Key:- Chromitite (CR), chromite-rich dunite (DC), dunite (DU), harzburgite (H), wehrlite (W), serpentinite (A).

Figure 4.2. Location of silicate samples.

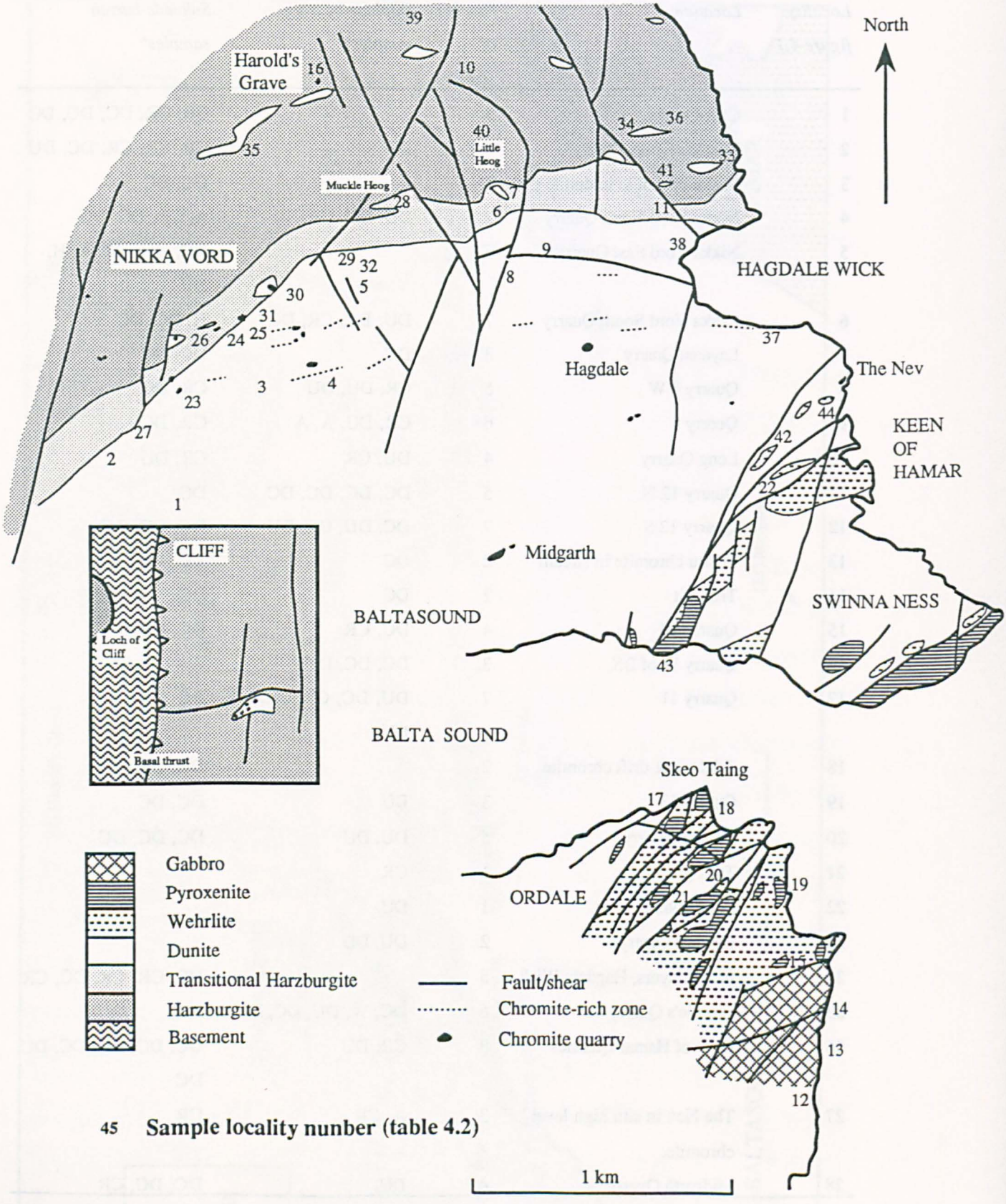

Table 4.2. Details of silicate samples.

Lithology	*Locality (number of samples)*
MANTLE SEQUENCE	
(a) Typical harzburgites (Harold's Grave)	16 (9)
(b) Transitional dunite/harzburgite around a dunite pod (Little Heog)	7 (14), 6 (3)
(c) Dunites from chromite-poor dunite pods (Little Heog)	40 (4), 41 (1), 33 (1), 34 (2), 16 (1), 35 (1)
(d) Pyroxenite veins & host harzburgites	36 (2), 37 (1), 38 (3), 39 (2)
CRUSTAL SEQUENCE	
(1) Dunite Unit (North of Baltasound)	
(a) Typical dunites with variable accessory chromite and/or sulphide	1 (3), 2 (3), 3 (3), 4 (2), 5 (7)
(b) Basal dunites with anomalous accessory sulphide	23 (1), 29 (1), 30 (1), 31 (1), 32 (2), 25 (1), 24 (1), 26 (1), 27 (1), 28 (1)
(2) Pyroxene-bearing cumulates	
(a) Basal pyroxenite/wehrlite layers (Keen of Hamar)	42 (7)
(b) Sulphide-bearing basal pyroxenite bodies (Keen of Hamar)	44 (5)
(c) Wehrlite dominant layered sequences (Keen of Hamar & Ordale)	22 (7), 20 (5)
(d) Pyroxenite dominant layered sequences (Keen of Hamar & Ordale)	43 (5), 21 (3)
(3) Gabbro Unit (SE of Ordale)	
(a) Altered, mafic and sulphide-bearing gabbros	12 (1), 13 (2), 14 (1), 15 (1)
(b) High-level pyroxenites and wehrlites	14 (3)
ALTERED LITHOLOGIES	
(a) Serpentinites from shear zones cutting harzburgites & dunites	8(1), 9 (3), 10 (1), 11 (1)
(b) Pervasively altered pyroxenites & wehrlites (Skeo Taing)	17 (3), 18 (4)
c) Gossans from shear zones in gabbros (SE of Ordale)	14 (1)
(d) Fault breccias & serpentinites within pyroxenites	17 (1), 19 (1), 15 (1)

4.2.3 Representative stratigraphic sampling

The location of all groups of silicate samples is shown on figure 4.2. These sample localities cover the study area geographically, particularly the better exposed regions on the high ground around the Heogs and along the eastern coast. These two regions provide good sections which are respectively parallel and perpendicular to the ophiolite stratigraphy.

Sampling was preceded by detailed lithological mapping (chapter 2). This allowed selection of the best exposed areas of each characteristic stratigraphic unit. All these samples have been grouped thematically (table 4.2).

Within the mantle sequence harzburgites were collected from the vicinity of the PGE-enriched chromite-rich dunite pod at Harold's Grave. This was complimented by extensive sampling of a well exposed chromite-poor dunite pod and its marginal transitional harzburgites outcropping on Little Heog. Dunites were also collected from several other chromite-poor pods throughout the area, including both major transgressive and minor subparallel types. These dunites were selected with particular attention to the amount of accessory chromite and or sulphide they contained. Finally, a few pyroxenite veins and their host rocks were sampled.

Within the crustal sequence dunites were selected containing variable amounts of accessory chromite and sulphides. Significantly the ultramafic samples with highly anomalous sulphide contents were mostly restricted to the basal region of the cumulate sequence (section 2.4).

Representative sampling of the pyroxene-bearing portion of the cumulate sequence was difficult because of the the complexity and differing scales of igneous layering. In view of the overall trend that had been recognized, from dunites, through wehrlites, to pyroxenites, the layered sequence was sampled at several different stratigraphic levels. Both the Keen of Hamar and the Ordale areas were sampled in this manner. Dunite/wehrlite and wehrlite/pyroxenite sequences were sampled in each area, including the first small scale pyroxenite layers (table 4.2). Two discrete pyroxenite bodies were sampled by detailed traverses, close to the first appearance of this rock type in the sequence. Pyroxenites from

within gabbro were sampled in the extreme south of the Ordale area. These may represent high-level pyroxenites and wehrlites, since a considerable stratigraphic break is postulated across the tectonic contact north of the first gabbro exposures (figure 2.9).

All the sampling described above was carried out in the least altered areas. These areas were selected as being most representative of the primary igneous lithologies. In addition, a variety of samples were also collected from shear zones cutting the sequence, although these features are rarely well exposed. At Ordale the shearing is noticeably more intense and has resulted in pervasive alteration. Here specimens were collected from lithologies showing a variety of unusual altered textures and colours. This included the characteristic "pink" wehrlites (section 2.5).

The result of the sampling program described above was to provide a suite of specimens of a wide geographical spread which are representative of all the primary lithologies and alteration styles present in the complex. Field descriptions and details of all samples are given in appendix B.

4.3 PGE Analysis

The PGE analytical program was designed to allow screening of a large number of reconnaissance samples by low cost routine analysis. These qualitative analyses would then be used to select a subset of samples of interest for high quality quantitative re-analysis.

Two peculiarities of PGE analysis severely limit the quality of whole-rock analyses. Firstly, the elements occur at very low concentrations (typically at the ppb level). They often also occur in a difficult analytical matrix (e.g. chromite). Preconcentration is therefore required to allow detection by most analytical methods and this constitutes an additional source of error. The analytical techniques are also operating close to the limit of their useful range, which in turn affects the precision and accuracy of the analysis. Internal standardisation may be used to assess the quality of the data obtained.

Secondly, the PGE are known to occur as discrete mineral grains. This can lead to sampling problems generally known as the 'nugget effect'. Samples must therefore be adequately homogenised and sufficiently large to contain a statistically representative number

of PGM particles (e.g. 20, Clifton et al., 1969). The sample size required thus increases with decreasing grade or increasing particle size. The relatively large sample sizes used for fire-assay preconcentration (typically 50 g) tends to compensate for these effects (Potts 1987).

4.3.1 Laboratory sampling procedure

Throughout the sampling program 1-2 kg field samples were collected and subjected to "total sample" preparation by the analytical laboratory. This involved pulverisation of 1 kg of material and homogenisation. This powder was then sub-sampled for analysis by riffling, thus avoiding biased sampling of heavy phases (i.e. PGM). Good comparison between repeated quantitative analyses indicate that this procedure adequately homogenised the material for 50 g sub-samples (table 4.3).

4.3.2 Internal standardisation

Only one international reference material was available for use as an internal standard. This material (SARM-7, formerly called PTO-1) is platinum ore derived from the Merensky Reef (table 4.4). The matrix of this standard is a gabbro pegmatoid, containing clinopyroxene, plagioclase, chromite, precious metals and sulphides (Steele et al., 1975). This standard is thus significantly different in bulk composition from the majority of the Shetland samples. Furthermore, SARM-7 contains only 74 ppb Ir, which is considerably lower than the expected Ir content of some Shetland samples (section 1.6.1). No other high Ir international reference material is available.

For these reasons, three Shetland chromite-rich samples were prepared for use as standards. Sample CX was a disseminated chromite-rich dunite from Cliff which was known to contain anomalous levels of all six PGE, particularly Rh, Pt and Pd. Sample HGX was a chromitite from Harold's Grave known to contain anomalous levels of Os, Ir and Ru. Sample BX was a disseminated chromite-rich dunite from a quarry in the dunite unit north of Baltasound. No PGMs had been found at this locality and the sample was therefore thought to be barren of PGE.

Table 4.3. Duplicated analyses (in ppb) by NiS-FAP & ICP-MS (by Analytical Services) for a range of PGE tenors and a variety of matrix compositions, indicating adequate homogenisation and sampling procedures.

Lithology	*Repeat*	*Os*	*Ir*	*Ru*	*Rh*	*Pt*	*Pd*	*Au*
Dunite	(a)	< 2	2	15	1.5	2	5	58
	(b)	< 2	3	13	1.5	5	7	54
Dunite	(a)	8	12	19	11	74	130	72
	(b)	8	12	17	11	72	120	74
Dunite (S)*	(a)	12	21	33	27	150	290	72
	(b)	10	19	36	26	140	290	74
Dunite (S)*	(a)	20	37	80	50	210	520	100
	(b)	22	40	78	47	200	510	95
Chromitite	(a)	6	9.5	29	2.5	9	8.5	68
	(b)	10	10	31	4.5	10	10	70
Pyroxenite	(a)	4	5	21	4	22	37	210
	(b)	2	4.5	20	3.5	20	35	200
Serpentinite	(a)	4	4.5	14	4	13	21	46
	(b)	4	4.5	14	4.5	13	20	48

*(S) indicates samples contain accessory sulphide phases

Table 4.4. Certified values of PGE concentrations in SARM-7, based on the analytical results of 38 laboratories (Steele et al., 1975).

Element	*Certified value (ppm)*	*95 % Confidence Limits*
Pt	3.74	± 0.045
Pd	1.53	± 0.032
Au	0.31	± 0.015
Ag	0.42	± 0.040
Rh	0.24	± 0.013
Ru	0.43	± 0.057
Os	0.063	± 0.0068
Ir	0.074	± 0.012

The three standard powders were then circulated to a number of laboratories and analysed as unknowns. The results of these analyses were used to select a suitable laboratory and to propose a consensus value for the PGE content of the three standards (table 4.5).

Comparison of the analyses of CX, HGX and BX returned by the various laboratories illustrates the difficulties of obtaining precise PGE assays. The analyses returned for iridium are in particularly poor agreement, probably due to the loss of insoluble residues (P. J. Potts, pers. comm.). All labs show moderately good agreement on the Pt and Pd content of all three standards over this wide range of concentrations (50 ppm to 0.2 ppm).

4.3.3 Reconnaissance analysis

For the reconnaissance program commercially available analysis was chosen on the grounds of cost effectiveness and short turn-around time. An initial two batches (batch 1A & 1B) totalling 195 samples were analysed for Pt, Pd and Ir by Caleb Brett, St Helens. This lab used nickel sulphide collection fire-assay preconcentration (NiS-FAP) and an inductively-coupled plasma atomic emission spectroscopy analytical finish (ICP-AES), for which a detection limit of 20 ppb was claimed. Caleb Brett also analysed these samples for Au by a separate lead fire-assay. A further two batches (batch 2A & 2B) totalling 193 samples were analysed for Pd and Pt by Anamet Services, Avonmouth. This laboratory also uses NiS-FAP with an ICP-AES finish and claims a detection limit of 10 ppb.

4.3.4 Instrumental neutron activation analysis

All samples submitted to Caleb Brett (batches 1A & 1B) were also analysed by instrumental neutron activation analysis (INAA) at the Open University. This analysis was initiated to quantify the potential pathfinder elements Co and Sb (section 5.2.2) but also provided comparative analyses of Ir and Au.

The standard INAA procedures for the determination of rare earth elements (Potts et al., 1985) were modified to allow screening of a large number of samples. Capsules containing 0.3 g of rock powder were irradiated in an epithermal neutron flux for 24 hours

Table 4.5. Reported analyses of three Shetland chromite-rich internal standards circulated to several analytical laboratories using various analytical techniques and the proposed value derived from these.

Standard	*Element*	*Laboratory & Method **					
		1	*2*	*3*	*4*	*5*	*6 §*
CX	Pt	40.23	39.9	35	42.7	34	40
	Pd	52.82	52.1	54	54.45	27	53
	Ir	12.53	4.17	-	< 0.02	3.7	12
HGX	Pt	0.177	0.29	0.28	0.19	0.29	0.28
	Pd	0.167	0.144	0.32	0.4	0.22	0.22
	Ir	3.51	< 0.02	-	< 0.02	0.15	3
BX	Pt	0.183	0.4	0.4	0.3	0.22	0.3
	Pd	< 0.02	0.068	0.07	0.51	< 0.037	?
	Ir	< 0.02	0.88	-	< 0.02	0.82	?

* Laboratory	Method
(1) Anamet, Avonmouth	NiS-FAP & ICP-ES
(2) Caleb Brett, St Helens	NiS-FAP & ICP-ES
(3) Omac, Loughrea	Pb-FAP & Graphite Furnace AAS
(4) Alfred H. Knight, St Helens	NiS-FAP & Graphite Furnace AAS
(5) Nuclear Activation Services, Ontario	NiS-FAP & INAA
(6) Proposed value	

§ (P. J. Potts, pers. comm.)

Table 4.6. Sample breakdown and analytical laboratories.

Sample Group	*Caleb Brett (Pt, Pd, Ir)*	*Anamet (Pt, Pd)*	*Total Samples*
Chromite Quarries	99	22	121
Silicate Lithologies	96	34	130
Measured Traverses	-	137	137
Total Samples	195	193	388

(0° facility, Imperial College Reactor, Ascot). Iron foils, normally used during REE determination to make corrections for flux variations due to sample position (±30%), were not included in order to streamline sample preparation and data correction procedures.

Calibration was achieved by including a sample of the standard OUPG-3, which is Ailsa Craig microgranite doped with known concentrations of PGE (table 4.7). In addition to this primary calibration standard a sample of CX was also included with every batch as a secondary standard to check for batch to batch fluctuations (table 4.10). Gamma spectra were recorded after decay intervals of 9 - 12 days in order to optimise the simultaneous detection of Ir, Au, Sb and Co (P.J. Potts pers. com.). The calculation of detection limits for this type of analysis according to Poisson statistics is shown in table 4.8).

4.3.5 Analysis for all six PGE

Samples containing significant Pt, Pd or Ir concentrations were reanalysed for all six PGE and Au by Analytical Services, Willetton, Western Australia. This laboratory uses nickel sulphide fire assay preconcentration with an inductively-coupled plasma mass spectrometry analytical finish (NiS-FAP & ICP-MS). This technique has lower detection limits, higher precision and greater accuracy than ICP-AES but is currently more expensive. The detection limit claimed by this laboratory is 0.5 ppb for Ir, Ru, Rh, Pt, Pd and 2 ppb for Os and Au. Gold analyses are unreliable below 500 ppb because of limitations of the nickel sulphide fire assay method.

4.3.6 Assessment of analytical data

The international standard SARM-7 and the internal chromite-rich standards were submitted as unknowns to all laboratories. The analyses reported by the various analytical methods are summarised in tables 4.9 and 4.10.

The poor agreement between the analyses of the Shetland chromite-rich standards returned by Caleb Brett and the proposed value (or their initial analysis) was cause for concern regarding the reliability of the analytical method (table 4.10a). These analyses are moderately consistent for Pt and Pd at the extremely high levels found in CX (ppm levels).

Table 4.7. INAA analytical details and calibration using standard OUPG-3.

Element	*Y-Emission (KeV)*	*OUPG-3 Doped concentration (ppm)*	*Gross counts*	*Back-ground counts*	*Net counts*	*Sensitivity § (counts/ppm)*
		c	N	B		s
Ir	468	1.021	3039	1338	1701	1666
Au	411.8	4.17	38074	2236	35838	8594
Sb*	564	10.42	4110	1072	3038	103
	1691		283	76	207	7.3
Co*	1332	20	1372	549	823	41.4
	1173		1628	697	931	46.6

* Determination from two spectral lines averaged to calculate final concentration

§ Calibration factor used in table 4.8 calculated as $s = c/(N-B)$

Table 4.8. Calculation of detection limits for Ir, Au, Sb and Co using standard OUPG-3 (chromite-rich matrix).

Element	*Y-Emission (KeV)*	*Gross counts*	*Background counts*	*Net counts*	*Detection limit (ppm) (3 sigma) ¶*
		Nc	Bc		Lc
Ir	468	22400	2916	19484	0.097
Au	411.8	31102	4283	26819	0.023
Sb	564	7536	1897	5639	1.3
	1691	349	28	321	2.2
Co	1332	8334	189	8145	1
	1173	9779	547	9232	1.5

¶ From Poisson counting statistics the detection limit $Lc = k\sqrt{Bc}/s$ where s is the calibration factor from table 4.7 and k =3 (Currie, 1968)

Table 4.9. Analyses as unknowns of PGE standard SARM-7 by the various analytical laboratories and methods.

(a) Caleb Brett (ICP-ES).

Element	*Certified value (ppm)*	*Confidence limit (95%)*	*Analyses submitted anonymously*			
		SARM-7	*1*	*2*	*3*	*4*
Ir	0.074	±0.012	0.03	<0.02	<0.02	<0.02
Pt	3.74	±0.045	0.74	0.76	1.48	3.16
Pd	1.53	±0.032	0.68	0.7	0.33	1.76
Au	0.31	±0.015	0.24	0.21	0.36	0.26

(b) Anamet (ICP-ES).

Element	*Certified value (ppm) SARM-7*	*Confidence limit (95%)*	*Analyses submitted anonymously*	
			1	*2*
Pt	3.74	±0.045	3.55	3.52
Pd	1.53	±0.032	1.46	1.44

(c) Analytical Services (ICP-MS).

Element	*Certified value (ppm)*	*Confidence limit (95%)*	*Analyses submitted anonymously*		
			1	*2*	*3*
Os	0.063	±0.0068	0.058	0.042	0.040
Ir	0.074	±0.012	0.086	0.23	0.21
Ru	0.24	±0.057	0.38	0.57	0.56
Rh	0.43	±0.013	0.21	0.46	0.43
Pt	3.74	±0.045	3.2	3.1	3.2
Pd	1.53	±0.032	1.5	2.5	2.4
Au	0.31	±0.015	0.28	0.39	0.41

Table 4.10. Analyses as unknowns of Shetland chromite-rich standards by the various analytical laboratories and methods.

(a) Caleb Brett (ICP-ES).

Standard	*Element*	*Proposed value (ppm)*	*Initial analysis*	*Analyses submitted anonymously*			
				1	*2*	*3*	*4*
CX	Pt	40	39.9	19.1	20	26.5	20.4
	Pd	53	52.1	44.2	47	48.6	45.3
	Ir	12	4.17	0.7	1.14	2.7	2.24
	Au	2.7	-	3	3.3	2.99	2.89
HGX	Pt	0.28	0.29	<0.02	0.18	0.15	0.19
	Pd	0.22	0.144	<0.02	0.34	0.17	0.19
	Ir	3	<0.02	0.08	<0.02	<0.02	0.12
	Au	?	-	0.036	0.03	0.039	0.039
BX	Pt	0.3	0.4	0.08	0.22	0.26	0.24
	Pd	?	0.068	0.02	0.1	0.03	<0.02
	Ir	?	0.88	0.44	0.42	0.63	0.58
	Au	0.03	-	0.021	<0.01	<0.01	0.019

(b) Open University (INAA).

CX (GMX Detector)

Element	*Analysis as unknown*				
(ppm)	*1*	*2*	*3*	*4*	*5*
Ir	8.5	10.3	11.1	9.3	10.9
Au	3.1	3.3	3.1	2.9	2.9

CX (GEM Detector)

Element	*Analysis as unknown*						
(ppm)	*1*	*2*	*3*	*4*	*5*	*6*	*7*
Ir	12.0	11.1	11.1	16.1	12.6	12.5	11.1
Au	3.2	3.9	2.8	3.1	2.8	3.2	2.8

(c) Analytical Services (ICP-MS).

Element	*Os*	*Ir*	*Ru*	*Rh*	*Pt*	*Pd*	*Au*
CX (ppm)	1.4	2.9	3.9	2.2	27	38	1.9

However, Pt is systematically under-reported compared with the proposed value and the initial analysis. Analyses at the lower levels of Pt and Pd found in BX and HGX (200-300 ppb) are less consistent. Analyses for Ir in both CX and HGX (ppm levels) are highly inconsistent and significantly lower than for the initial analysis. The problems of Ir analysis are discussed later.

The source of these fluctuations in the Pt and Pd analyses is not necessarily just at the analytical stage. Although all possible care had been taken during preparation of the Shetland chromite-rich materials to achieve homogenisation, this procedure was not as exhaustive as that required for preparation of an international standard (Steele et al., 1975). Inhomogeneity effects, particularly variation between different pots of powders were unknown. The analyses of the international reference material SARM-7 indicate some component of purely analytical variation (table 4.9a).

A different analytical laboratory (Anamet Services, Avonmouth) was therefore chosen to analyse the second batches of reconnaissance samples (2A & 2B). Anamet returned Pt and Pd analyses of SARM-7 showing moderately good agreement with the certified values (table 4.9b). These batches were not analysed for Au and Ir because of the respective low levels and analytical problems which were encountered in the analysis of batches 1A & 1B for these elements.

The analyses of SARM-7 by Analytical Services were in moderate agreement with the certified values of Os, Ir, Ru, Rh, Pt, Pd and Au (table 4.9c). Since the Australian analyses were performed on a subset of samples also analysed by Anamet, Caleb Brett and the Open University they can be used as reference point against which to assess the performance of the other laboratories. Samples analysed by Analytical Services from batch 1 and 2 are listed in tables 4.11 and 4.12 together with the analyses reported by the other laboratories. Graphical comparisons (figures 4.3, & 4.4) reveal a general agreement only on the order of magnitude of Pt and Pd concentrations. Fields of data points are produced, rather than the ideal linear relationship, illustrating the degree of imprecision inherent in this type of analysis. Any inaccuracies are thus difficult to see, although the analyses of Pd by Anamet are noticeably low. This discrepancy was also apparent on geological grounds, since the analyses did not always show the pattern of coincident anomalous Pt and Pd, with Pd

Table 4.11. Comparison between Pt, Pd, Ir and Au analyses by Caleb Brett (C.B.), Analytical Services (A.S.), and the Open University.

Sample	*Pt A.S.*	*Pt C.B*	*Pd A.S.*	*Pd C.B*	*Ir A.S.*	*Ir C.B*	*Ir O.U.*	*Au A.S.*	*Au C.B*	*Au O.U.*
Batch 1B										
RL050	4.5	<20	4	<20	1	<20	<100	28	42	46
RL060	95	70	160	120	0.5	<20	<100	2	<10	<
RL069	170	80	24	<20	180	130	300	<2	<10	<
RL070	330	180	56	30	550	350	1200	<2	<10	<
RL104	44	50	42	30	5	200	<100	2	<10	<
RLM002	210	80	310	160	66	60	180	10	12	<
RLM003	35	50	24	<20	97	70	220	<2	<10	<
RLM004	330	170	650	330	50	90	100	18	33	<
RLM006	3.5	<20	5	<20	16	<20	<100	<2	29	<
RLM007	870	580	2100	1060	120	90	300	130	135	120
RLM008	22	<20	48	30	4	<20	<100	2	15	<
RLM009	170	90	29	<20	90	50	200	<2	15	<
RLM011	160	80	29	<20	35	20	100	4	<10	<
RLM029	250	160	420	290	50	40	190	62	72	<
RLM030	8.5	<20	5.5	<20	.11	<20	<100	<2	23	<
RLM040	27	30	36	20	6.5	<20	<100	10	19	<
Batch 1B										
RLM059	40	50	73	80	7.5	<20	<100	<2	10	<
RLM063	370	360	700	640	77	<20	190	8	21	<
RLM064	250	260	390	400	52	<20	160	6	17	<
RLM065	140	180	260	300	23	<20	<100	20	33	30
RLM066	390	460	260	320	81	<20	360	6	17	<
RLM067	440	410	710	800	57	<20	170	22	38	30
RLM068	120	140	230	360	16	<20	<100	26	49	130
RLM069	360	280	800	590	82	<20	290	<2	32	30
RLM070	140	170	340	420	22	<20	<100	<2	66	50
RLM071	12	20	30	40	4	<20	<100	8	13	30
RLM082	270	300	410	340	48	<20	190	20	41	60
RLM087	240	300	380	420	28	80	<100	18	28	<
RLM088	73	700	120	1180	11	170	<100	6	<10	<
RLM096	200	160	190	190	47	<20	240	4	<10	<
RLM097	120	80	190	150	22	<20	<100	110	96	<
RLM098	9	<20	10	<20	14	<20	100	2	<10	<
RLM099	21	<20	33	<20	17	<20	<100	4	<10	<

Table 4.12. Comparison between Pt and Pd analyses by Anamet (AN.) and Analytical Services (A.S.).

		Pt *A.S*	*Pt* *AN.*	*Pd* *A.S*	*Pd* *AN.*
Batch 2A	RLA025	73	90	130	140
	RLA028	17	10	23	30
	RLA032	14	20	17	30
	RLA033	6	20	21	40
	RLA034	14	20	20	30
	RLA040	25	40	36	60
	RLA041	25	50	25	40
	RLA042	13	20	21	30
	RLA078	49	30	40	10
	RLA079	4	<10	6.5	<10
	RLA080	2.5	<10	6.5	<10
	RLA081	15	<10	20	<10
	RLA082	250	150	410	230
	RLA083	170	110	340	200
	RLA084	52	20	78	50
	RLA085	33	20	49	20
	RLA086	31	10	50	50
	RLA087	21	10	36	20
	RLA088	27	<10	110	10
	RLA089	8.5	<10	12	<10
Batch 2B	RLA096	76	130	86	10
	RLA097	180	20	470	<10
	RLA098	110	140	260	20
	RLA099	230	280	670	160
	RLA100	210	550	520	1070
	RLA101	180	200	250	190
	RLA103	270	320	620	550
	RLA104	150	160	290	280
	RLA105	6.5	<10	15	<10
	RLA106	3.5	<10	6	<10
	RLA149	32	30	99	80
	RLA151	10	10	26	20
	RLA152	13	20	36	10
	RLA153	40	20	48	20
	RLA156	35	70	110	190
	RLA171	40	<10	21	<10
	RLA172	2	<10	2.5	<10
	RLA173	13	<10	9.5	<10
	RLA176	16	<10	17	<10

Figure 4.3. Graphical comparison between analyses by Caleb Brett (C.B.) and Analytical Services (A.S.) for Pt, Pd, Ir and Au (ppb).

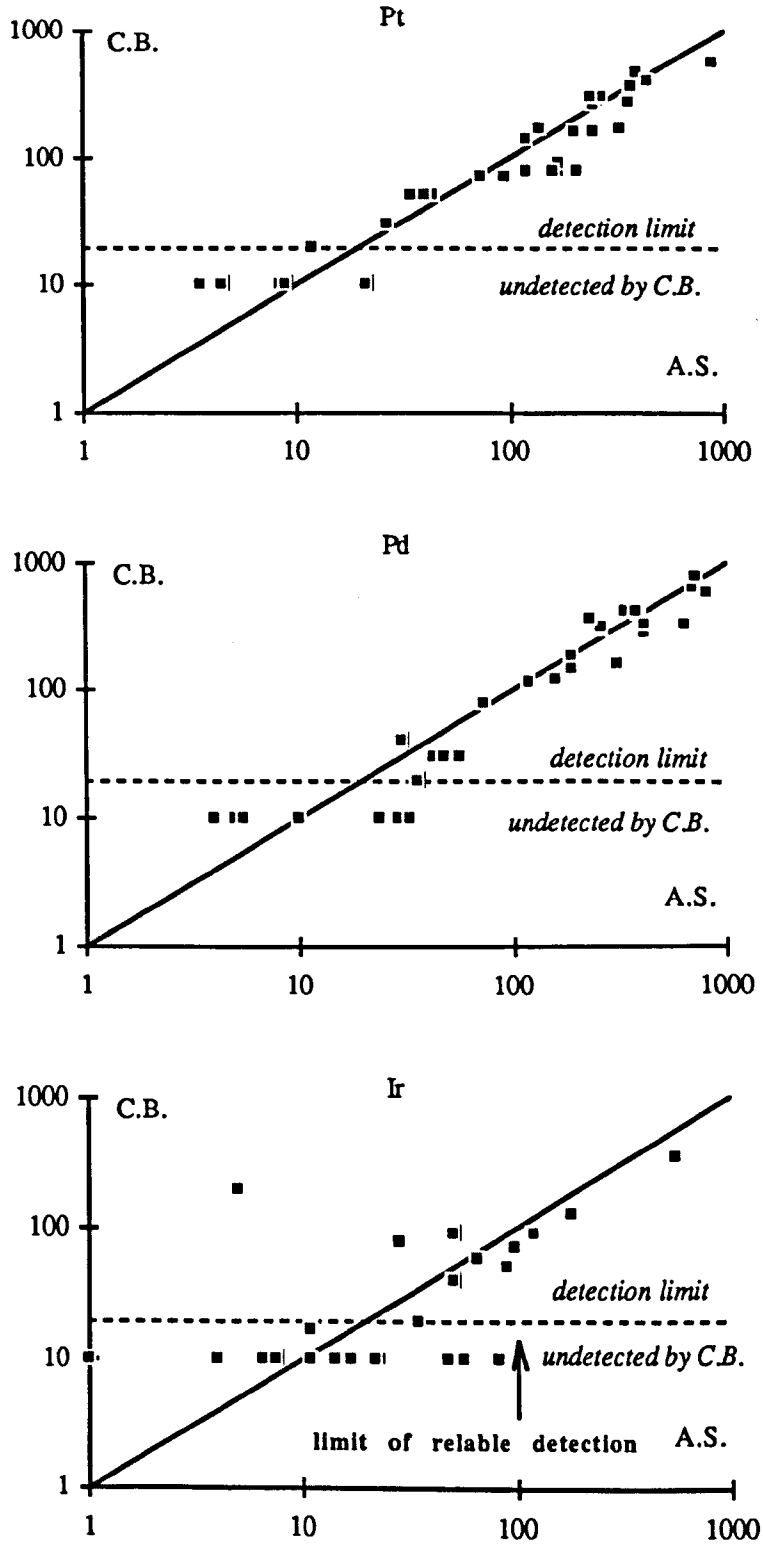

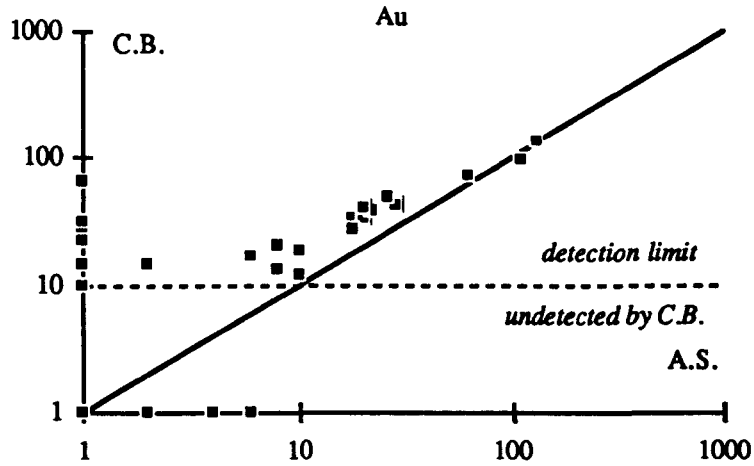

Figure 4.4. Graphical comparison between analyses by Anamet (AN.) and Analytical Services (A.S.) for Pt and Pd (ppb).

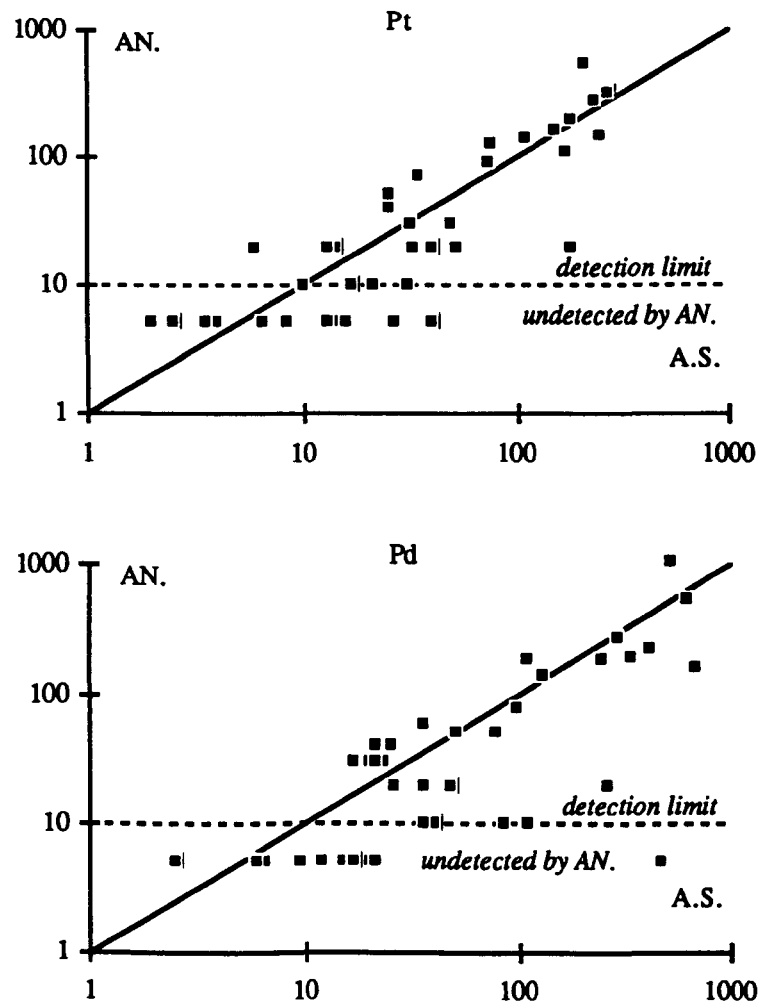

Figure 4.5. Graphical comparison between analyses by the Open University (O.U.) and Analytical Services (A.S.) for Ir and Au (ppb).

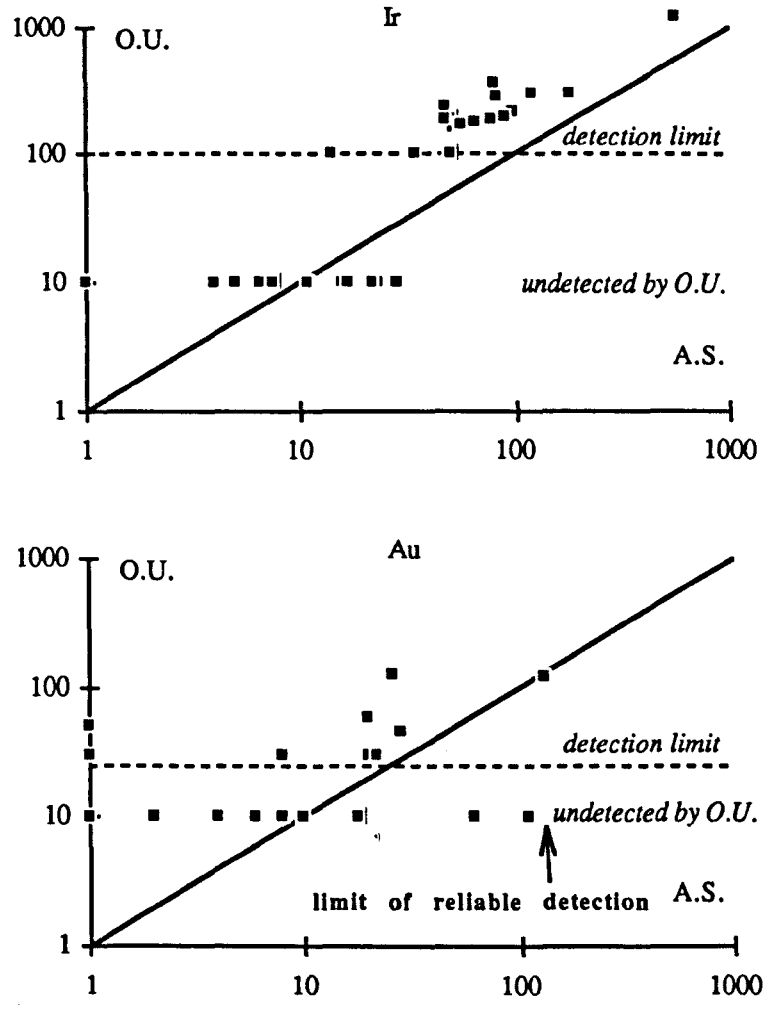

typically greater than or equal to Pt, which had been recognised in most other samples.

The analyses of Ir by Caleb Brett also show very poor agreement with the reference analyses. In particular, the limit of reliable detection of Ir by this laboratory is around 100 ppb (figure 4.5). Furthermore, both Caleb Brett and Analytical Services returned much lower Ir analyses of CX than the proposed value (table 4.10). The proposed level of 12 ppm Ir in CX was suggested by previous INAA analyses of this material and was supported by the initial analysis by Caleb Brett (table 4.5). This value was obtained consistently from samples of CX included as secondary standards during INAA analysis (table 4.10 b), as were consistent Au analyses close to the proposed value. Comparison between the reference analyses and the Ir determinations by INAA illustrates the systematically higher analyses of Ir obtained by this technique compared to fire-assay methods (figure 4.5). The relatively high detection limits for Ir and Au (0.5 ppm and 100 ppb respectively) by this method are also apparent.

Several possible explanations can be suggested to account for the differences in the Ir analyses which are described above. In the absence of a high Ir reference material these remain unresolved.

(a) INAA produces unrealistically high Ir analyses (e.g. due to enhancement of Ir peaks in overlapping multi-element gamma spectra).

(b) Fire assay procedures systematically under-report Ir analyses (e.g. by loss of insoluble residues.

(c) The unusually high Ir contents of Shetland material are beyond the usual calibration ranges, which are incorrectly calibrated in the absence of high Ir reference material (note good agreement for low level Ir content of SARM-7 analysed as an unknown by Analytical Services).

(d) The effects of the chromite-rich matrix of high Ir materials compared to SARM-7.

In conclusion, the imprecision and inaccuracy of the reconnaissance Pt, Pd, Ir and Au analysis is such that the absolute concentrations of PGE reported do not merit rigourous interpretation. These data do, however, indicate the relative quantity of PGE in different samples and allow a qualitative geological interpretation of their patterns of distribution, since at least the correct order of magnitude of PGE concentrations is consistently reported.

4.4 The Distribution of PGE and gold

The reconnaissance analytical program detected an unexpectedly large number of whole rock Pt, Pd, Ir and Au concentrations (table 4.13). Of the 250 samples analysed, 96 contained Pt and 88 contained Pd at levels above 20 ppb (38% and 35% respectively). From the subset of 195 samples, 71 contained Au and 24 contained Ir above the respective detection limits of 10 ppb and 20 ppb (36% and 12% respectively). The following sections describe the range of PGE concentrations and their geographical distribution in the complex.

Table 4.13. Percentage of samples containing detected PGE and Au.

Element	*Samples analysed*	*Detection limit*	*Detected samples*	*Percentage*
Pt	250	20 ppb	96	38
Pd	250	20 ppb	88	35
Ir	195	20 ppb	24	12
Au	195	10 ppb	12	36

4.4.1 Distribution of detected levels of Pt, Pd, Ir and Au

The reconnaissance samples were all classified in the field according to their primary rock types. This classification has been used to construct histograms showing the percentage of samples from each lithological unit which contain detected Pt, Pd, Ir or Au (figure 4.6). These diagrams indicate that detected levels of these four elements occur in most rock types. The proportion of mineralised samples varies, however, between different lithologies in a consistent manner for the four elements.

Samples from the Cliff quarry all contain detected Pt, Pd and Ir and most also contain Au. A large number of samples from other chromite localities also contain PGE and Au. This includes quarries both in dunite pods within the harzburgite unit and those within the dunite unit. The "pyroxenites & wehrlites" category, which includes cpx-bearing dunites,

Figure 4.6. Histograms showing the percentage of samples of different lithological units containing Pt, Pd, Ir and Au at or above 20 ppb (10 ppb for Au).

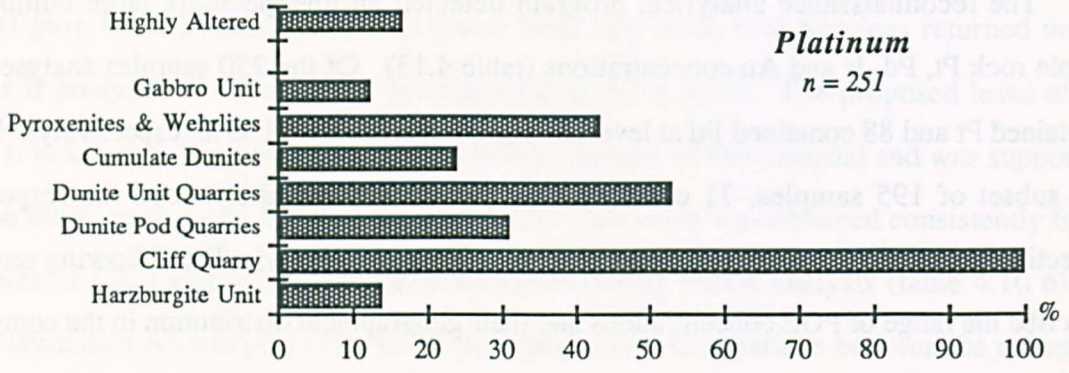

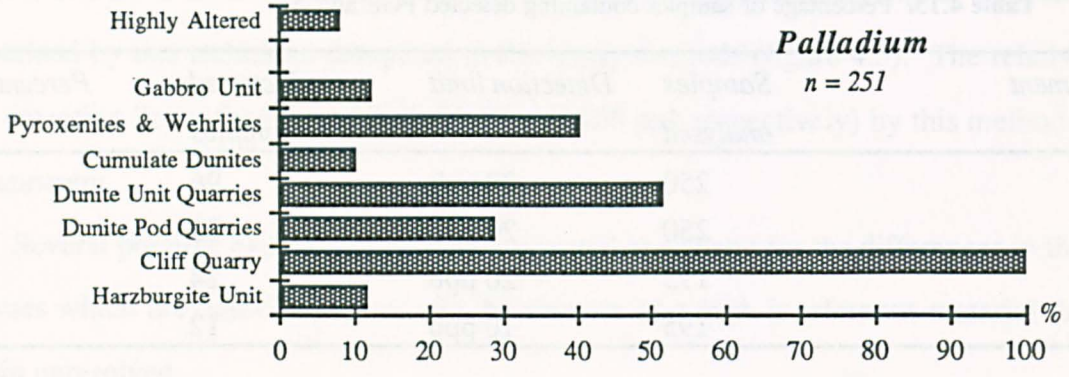

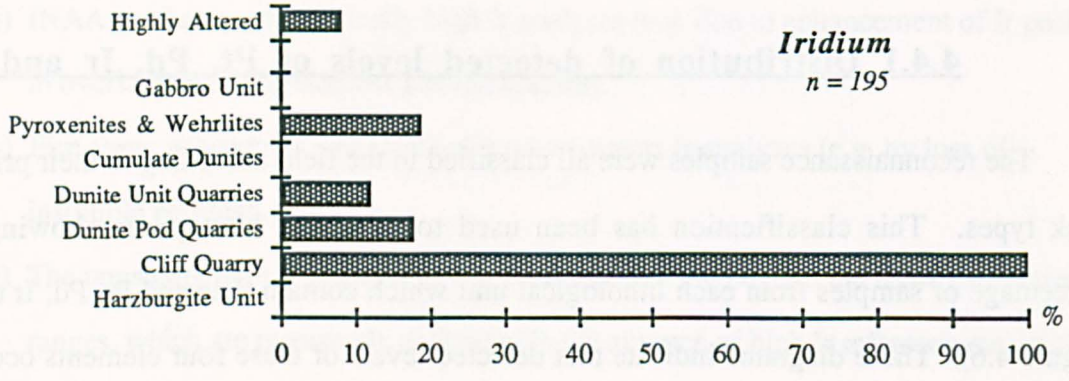

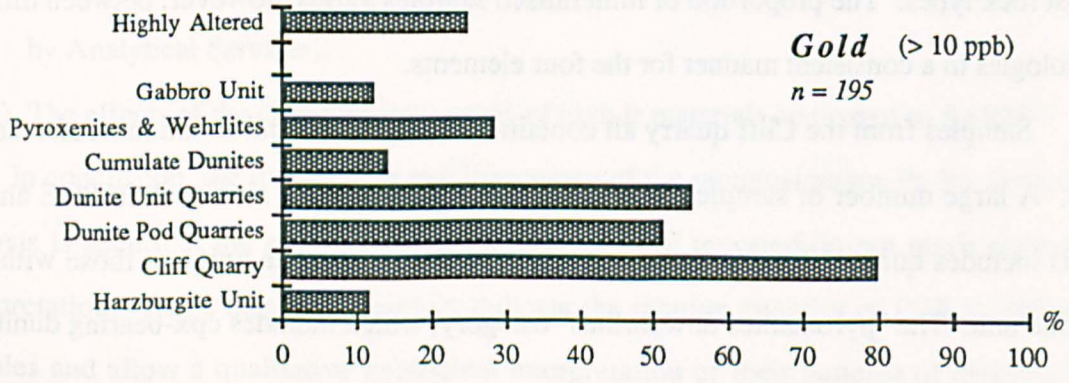

also contains a large number of PGE-bearing samples. Very few gabbros, harzburgites or highly altered samples contain detected levels of precious metals.

The consistent lithological distribution patterns shown by Pt, Pd, Ir and Au suggest that concentrations of these different metals have a common origin. Furthermore, the variation in the frequency with which detected levels occur in different rocks indicates that the mineralisation is lithologically controlled.

4.4.2 Range of PGE and Au concentrations

So far comparisons have been made between samples containing concentrations of PGE above and below the analytical detection limit. In order to achieve a better comparison between the relative levels of PGE and Au it was necessary to examine the statistical distribution of the analytical data and thereby achieve a suitable definition of anomalous or background levels of each element.

Figure 4.7 shows the cumulative frequency and relative frequency distribution patterns for analyses of each element. Because these all show logarithmic distributions the logarithm of each concentration was calculated before grouping the data. Labels on the horizontal axes refer to the mid point of each group interval, for which the antilogarithm has been calculated to allow reading of concentrations directly in ppb or ppm. The relative frequency (or the percentage of samples falling within each class interval) has also been plotted on each cumulative frequency chart. The relative frequency has been multiplied by a suitable factor to increase the size of the histogram. Open squares indicate the percentage of samples falling below the detection limit (a majority in all cases). Arrows indicate the threshold values between critical groups, again recalculated to the actual concentrations.

All four elements show similar frequency distributions. Most detected concentrations fall within a single population but very highly anomalous concentrations of each element also occur. Platinum and palladium show very similar patterns which are essentially single statistical populations with the bulk of the concentrations falling below the 398 ppb and 631 thresholds respectively. Above these thresholds the patterns are modified by a few very highly anomalous concentrations which range up to 10.4 ppm Pt and 64.9 ppm Pd. Iridium

Figure 4.7. Concentration ranges and frequency distributions for Pt, Pd, Ir and Au.

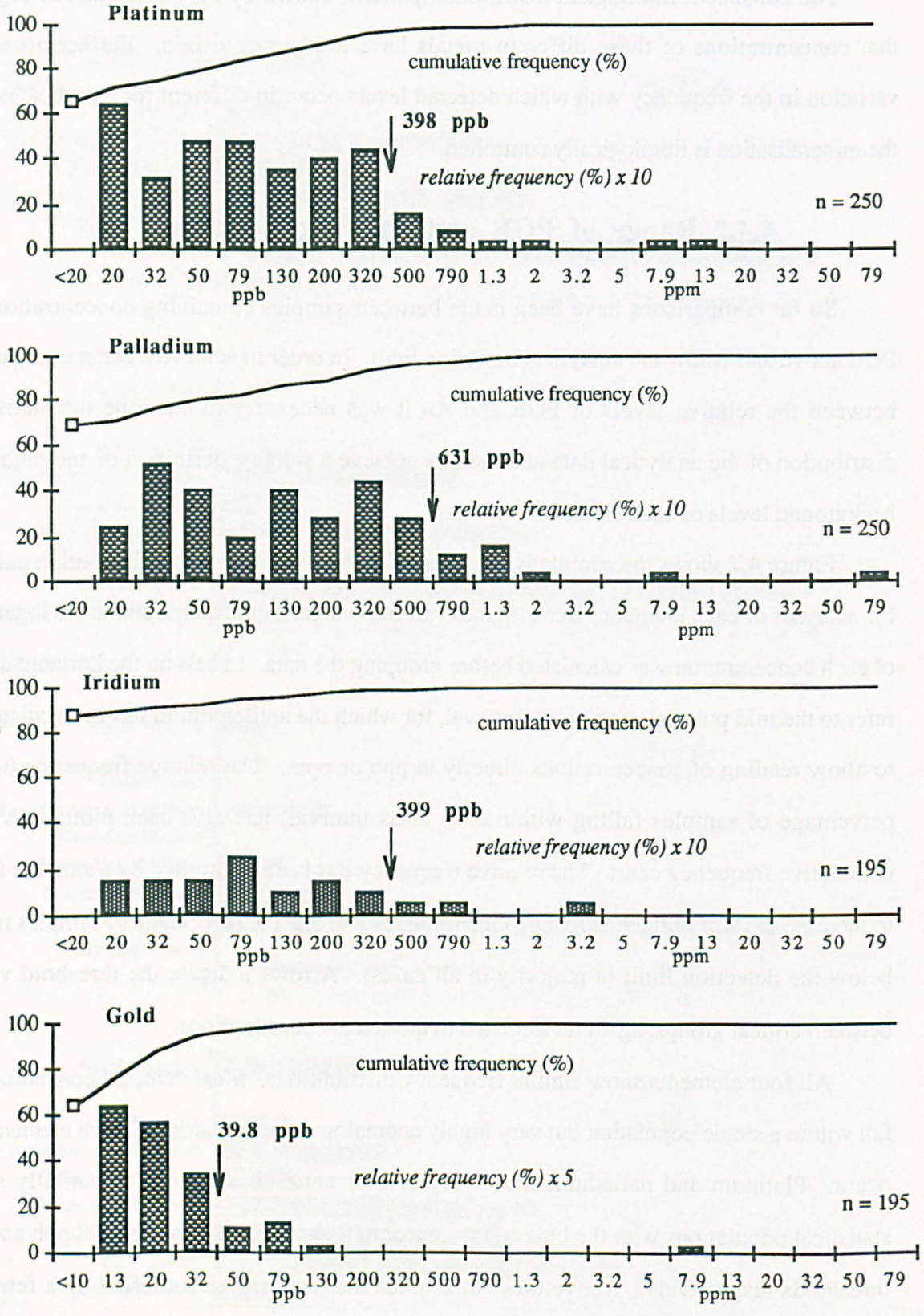

and gold show patterns comparable with those of Pt or Pd, but the concentration ranges are broader and narrower in each case. The bulk of the samples contain Ir and Au levels below the thresholds of 399 ppb and 39.8 ppb respectively. Anomalous Ir and Au concentrations range up to maxima of 2.7 ppm and 3.9 ppm. The origin of very highly anomalous concentrations in certain samples is considered later (section 5.7).

4.4.3 Distribution of anomalous levels of PGE and Au

Inspection of the analytical data indicates that the absolute levels of PGE and Au are also related to the type of host rock. The highest concentrations occur in chromitites, chromite-rich dunites and dunites collected from disused chromite quarries (up to 3.7 ppm total Pt + Pd). Exceptionally high levels (up to 75 ppm total Pt + Pd) occur in similar samples from the Cliff quarry. Moderately high levels of PGE were also found in samples of pyroxenites and wehrlites collected from close to the base of the pyroxene-bearing cumulate sequence (up to 720 ppb total Pt + Pd) and from discrete high-level ultramafic bodies in the gabbro unit (up to 190 ppb total Pt + Pd).

In order to show this pattern of concentration distribution three threshold levels were selected for each of the four elements concerned (table 4.14). The highest of these corresponds to the visual cut-off points noted in the frequency distributions (figure 4.7). Samples containing concentrations above these cut-off points are considered to be very highly anomalous. The two lower thresholds were selected to correspond with the minimum concentrations defining the upper 10 and 20 percentile groups of each statistical population. Samples containing concentrations above these two thresholds are considered to be highly anomalous and anomalous respectively.

Table 4.14. Threshold values defining anomalous mineralisation.

Mineralisation	*Definition*	*Pt*	*Pd*	*Ir*	*Au*
Very highly anomalous	Frequency cut-off	398	631	398	39
Highly anomalous	Upper 10 percentile	200	295	35	27.5
Anomalous	Upper 20 percentile	65	65	* ≥20	18.5

* Only 12 % of samples contained Ir concentrations above the detection limit of 20 ppb

Figure 4.8. Distribution of anomalous Pt concentrations.

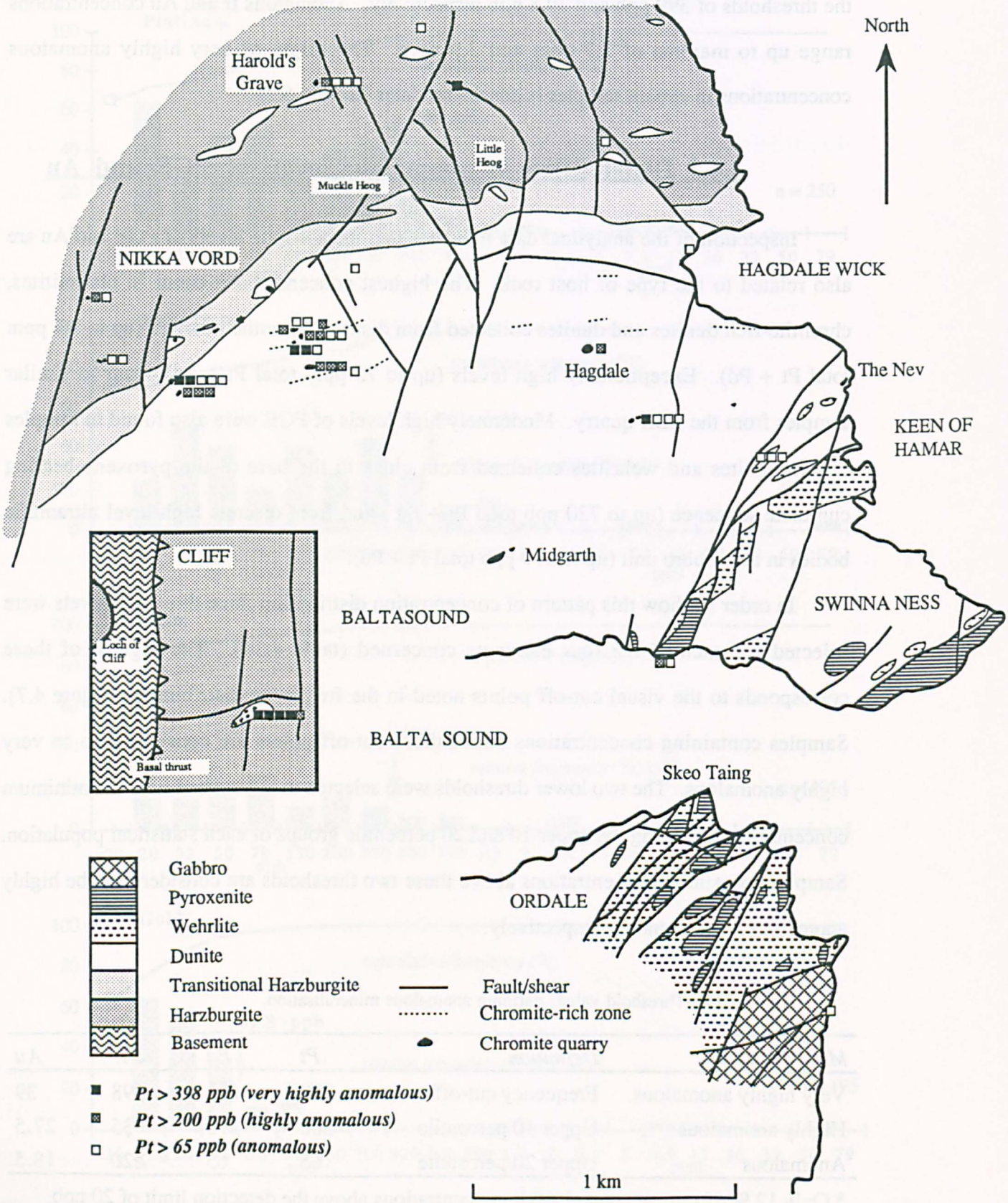

Figure 4.9. Distribution of anomalous Pd concentrations.

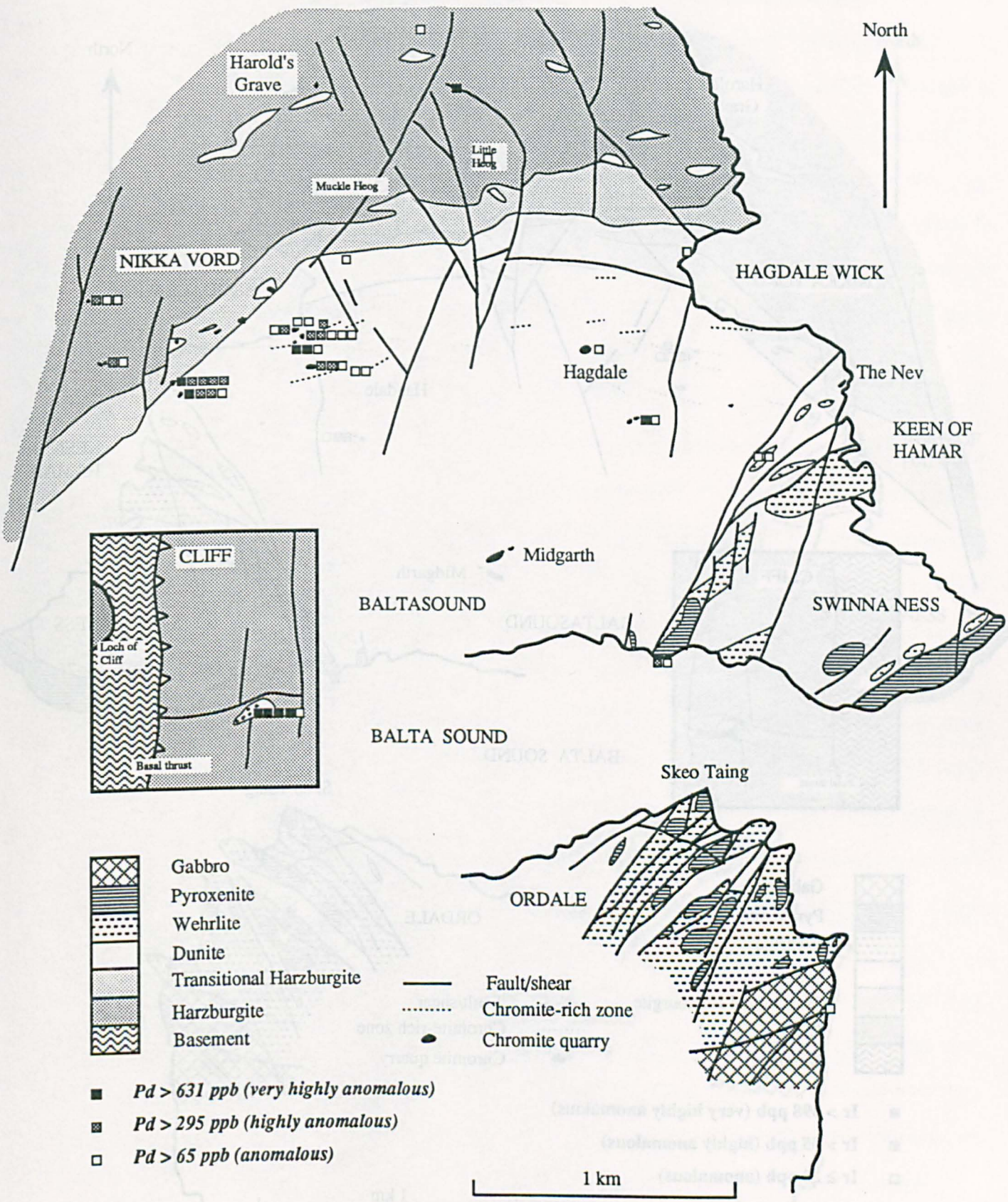

Figure 4.10. Distribution of anomalous Ir concentrations.

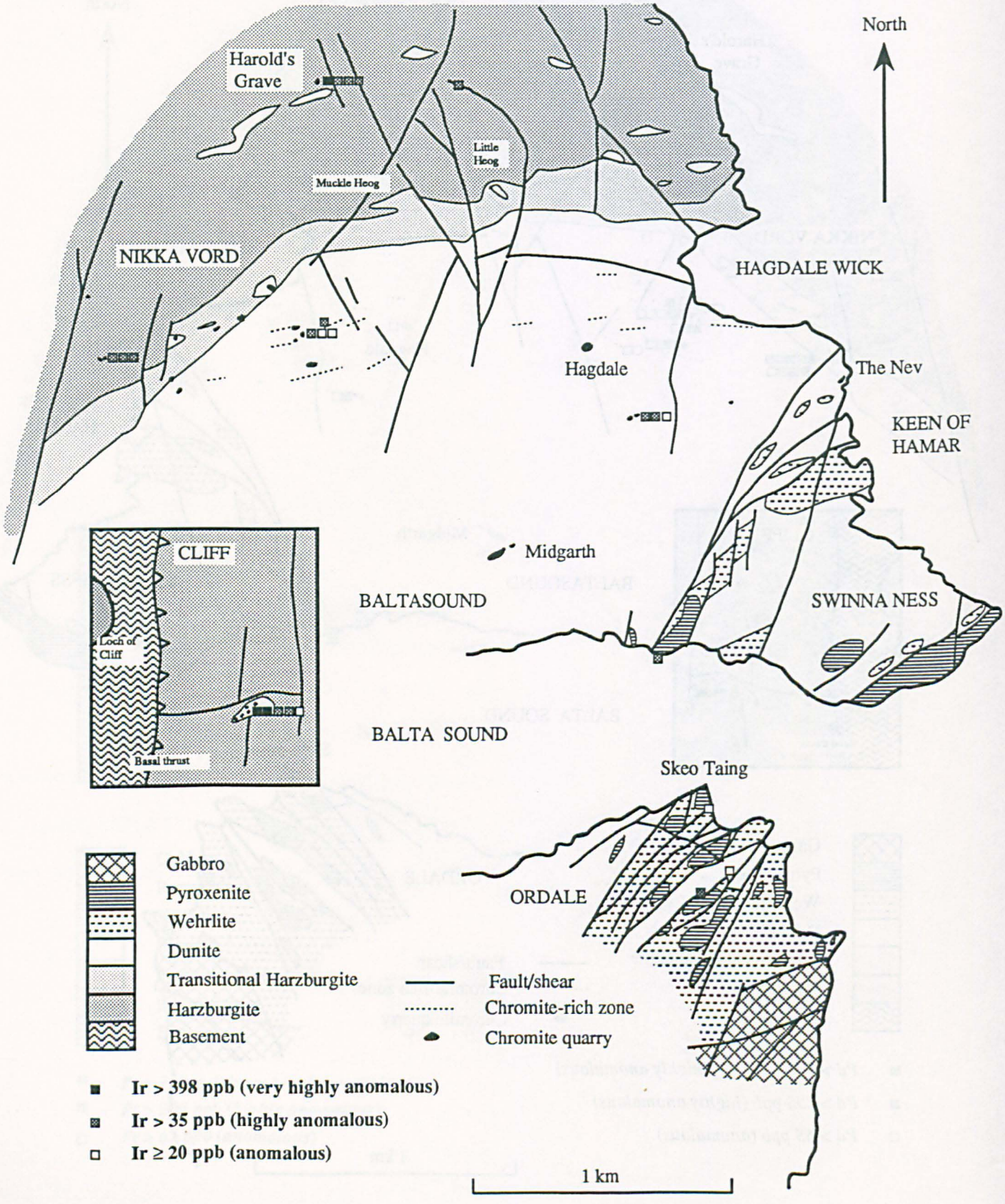

Figure 4.11. Distribution of anomalous Au concentrations.

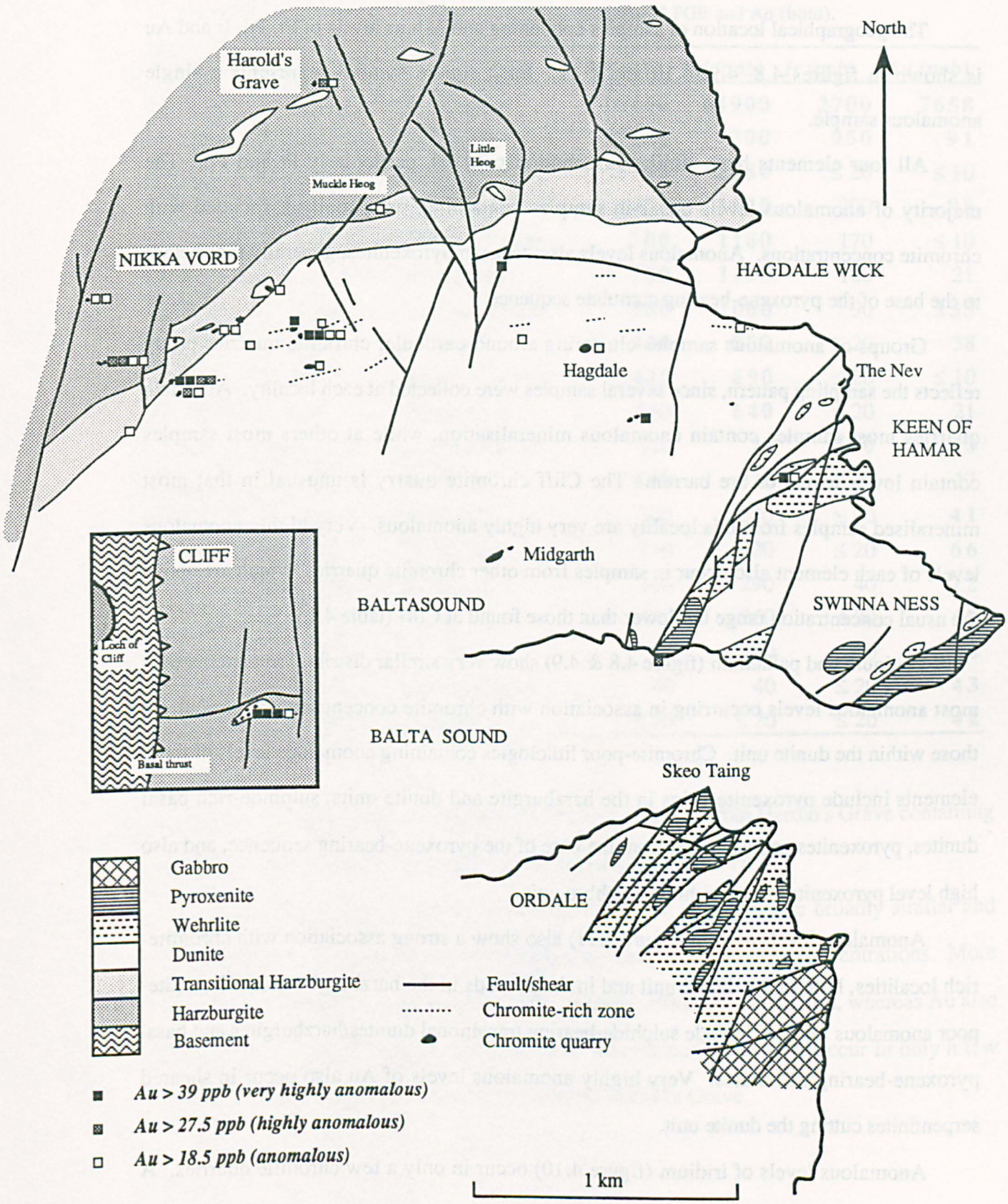

4.4.3.1 Geographical distribution

The geographical location of samples containing anomalous levels of Pt, Pd, Ir and Au is shown in figures 4.8, 4.9, 4.10 and 4.11. Each square symbol represents a single anomalous sample.

All four elements have similar distribution patterns, particularly Pt and Pd. The majority of anomalous levels occur in samples containing, or spatially associated with chromite concentrations. Anomalous levels also occur in pyroxenites, generally those close to the base of the pyroxene-bearing cumulate sequence.

Groups of anomalous samples clustering around particular chromite quarries partly reflects the sampling pattern, since several samples were collected at each locality. At certain quarries most samples contain anomalous mineralisation, while at others most samples contain lower levels or are barren. The Cliff chromite quarry is unusual in that most mineralised samples from this locality are very highly anomalous. Very highly anomalous levels of each element also occur in samples from other chromite quarries, which are above the usual concentration range but lower than those found at Cliff (table 4.15).

Platinum and palladium (figure 4.8 & 4.9) show very similar distribution patterns with most anomalous levels occurring in association with chromite concentrations, particularly those within the dunite unit. Chromite-poor lithologies containing anomalous levels of these elements include pyroxenite veins in the harzburgite and dunite units, sulphide-rich basal dunites, pyroxenites and wehrlites from the base of the pyroxene-bearing sequence, and also high level pyroxenites from within the gabbro unit.

Anomalous levels of gold (figure 4.11) also show a strong association with chromite-rich localities, both in the dunite unit and in dunite pods in the harzburgite unit. Chromite-poor anomalous samples include sulphide-bearing transitional dunites/harzburgites and basal pyroxene-bearing cumulates. Very highly anomalous levels of Au also occur in sheared serpentinites cutting the dunite unit.

Anomalous levels of iridium (figure 4.10) occur in only a few chromite quarries. A few scattered samples from the layered pyroxenite and wehrlite sequences also contain anomalous levels. Both the Harold's Grave and Cliff quarries contain very highly

Table 4.15. Samples containing "very highly anomalous" PGE and Au (bold).

Sample	*Lithology*	*Locality*	*Pt (ppb)*	*Pd (ppb)*	*Ir (ppb)*	*Au (ppb)*
RLM086	dunite/chr	Cliff Quarry	**10400**	**64900**	**2700**	**7658**
RLM084	dunite/chr	Cliff Quarry	**7480**	**7200**	**950**	**91**
RLA122	dunite/chr	Quarry W of BX	**1700**	**2080**	≤ 20	≤ 10
RLM085	dunite/chr	Cliff Quarry	**1450**	**1520**	200	**88**
RLM088	chr/mnt	NW Little Heog	**700**	**1180**	170	≤ 10
RL001	chromitite	Cliff Quarry	**760**	**1120**	120	21
RLM007	dunite/chr	Jimmie's Quarry	**580**	**1060**	90	**135**
RLM067	dunite/chr	Quarry 12	**410**	**800**	≤ 20	38
RLA124	dunite	Quarry W of BX	**440**	**690**	≤ 20	≤ 10
RLM063	dunite	Quarry 12 S	360	**640**	≤ 20	21
RL068	chromitite	Harold's Grave	310	20	**560**	≤ 10
RLM066	dunite/chr	Quarry 12	**460**	320	≤ 20	17
RLM082	dunite/chr	Quarry 11	300	340	≤ 20	**41**
RLM070	dunite/chr	Quarry 12	170	420	≤ 20	**66**
RLM029	dunite/chr	Quarry 11	160	290	40	**72**
RLM068	dunite/chr	Quarry 12	140	360	≤ 20	**49**
RLM097	chromitite	Quarry 10	80	150	≤ 20	**96**
RLM014	wehrlite	Keen of Hamar	40	40	≤ 20	**43**
RL050	serpentinite	Little Heog	≤ 20	≤ 20	≤ 20	**42**

anomalous levels of iridium. Unlike the Cliff area, samples from Harold's Grave containing highly anomalous levels of Ir and Pt do not contain significant Pd.

In conclusion, the distribution patterns of Pt, Pd, Ir and Au are broadly similar and indicate that anomalous levels are spatially associated with chromite concentrations. More frequently Pt and Pd occur associated with chromite within the dunite unit, whereas Au also occurs with chromite in the harzburgite unit. Anomalous levels of Ir occur in only a few chromite quarries, particularly those at Cliff and Harold's Grave.

Table 4.16. Classification of samples according to lithological unit and tenor of Pt, Pd, Ir or Au mineralisation.

Lithological Unit	*Number of samples*	*Number of samples containing levels above each threshold*		
Platinum	n = 250	> 65 ppb	> 200 ppb	> 398 ppb
Harzburgite Unit	43	2	0	0
Cliff Quarry	5	5	5	4
Dunite Pod Quarries	48	9	3	0
Dunite Unit Quarries	68	27	15	5
Cumulate Dunites	29	2	0	0
Pyroxenites & Wehrlites	37	5	1	0
Gabbro Unit	8	1	0	0
Highly Altered	12	1	1	1
Palladium	n = 250	> 65 ppb	> 295 ppb	> 631 ppb
Harzburgite Unit	43	2	0	0
Cliff Quarry	5	5	4	4
Dunite Pod Quarries	48	6	3	0
Dunite Unit Quarries	68	29	16	5
Cumulate Dunites	29	2	0	0
Pyroxenites & Wehrlites	37	4	1	0
Gabbro Unit	8	1	0	0
Highly Altered	12	1	1	1
Iridium	n = 195	≥ 20 ppb	> 35 ppb	> 398 ppb
Harzburgite Unit	34	6	0	0
Cliff Quarry	5	5	4	2
Dunite Pod Quarries	45	8	8	1
Dunite Unit Quarries	49	6	3	0
Cumulate Dunites	21	0	0	0
Pyroxenites & Wehrlites	21	4	2	0
Gabbro Unit	8	0	0	0
Highly Altered	12	1	1	0
Gold	n = 195	> 18 ppb	> 27 ppb	> 39.8 ppb
Harzburgite Unit	34	2	0	0
Cliff Quarry	5	4	3	3
Dunite Pod Quarries	45	12	4	0
Dunite Unit Quarries	49	16	9	6
Cumulate Dunites	21	1	0	0
Pyroxenites & Wehrlites	21	4	2	1
Gabbro Unit	8	0	0	0
Highly Altered	12	1	1	1

Figure 4.12. Histograms showing the lithological control of Pt, Pd, Ir and Au mineralisation and the association of anomalous levels with chromite concentrations.

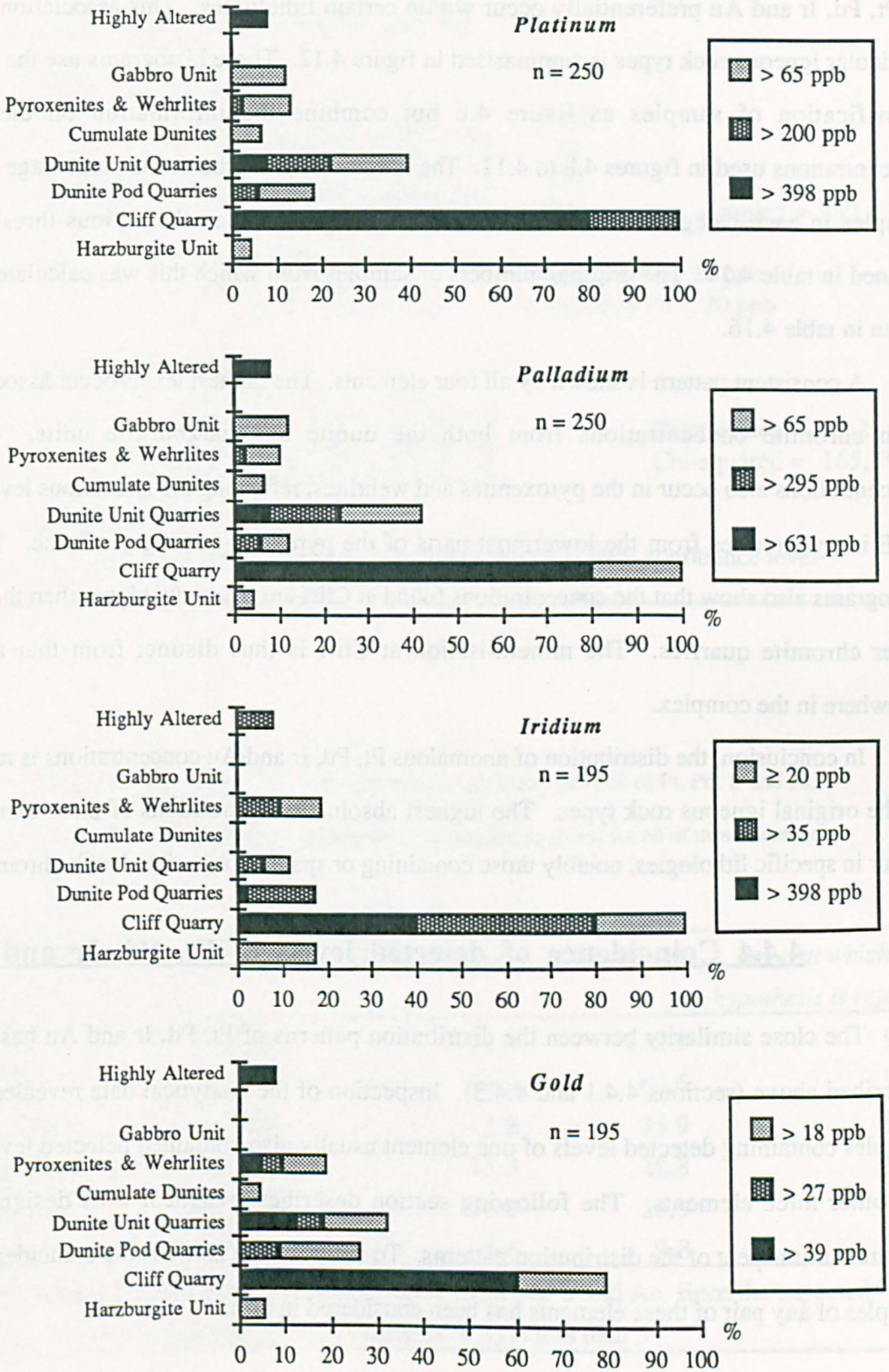

4.4.3.2 Lithological distribution of anomalous PGE and Au

The geographical distribution patterns (section 4.4.3.1) indicate that anomalous levels of Pt, Pd, Ir and Au preferentially occur within certain lithologies. This association with particular igneous rock types is summarised in figure 4.12. These histograms use the same classification of samples as figure 4.6 but combine the information on element concentrations used in figures 4.8 to 4.11. The horizontal scale shows the percentage of all samples in each category containing concentrations greater than the various thresholds defined in table 4.14. The original numbers of samples from which this was calculated are given in table 4.16.

A consistent pattern is shown by all four elements. The highest levels occur associated with chromite concentrations from both the dunite and harzburgite units. High concentrations also occur in the pyroxenites and wehrlites, reflecting the anomalous levels of PGE in pyroxenites from the lowermost parts of the pyroxene-bearing sequence. These histograms also show that the concentrations found at Cliff are markedly higher than those at other chromite quarries. The mineralisation at Cliff is thus distinct from that found elsewhere in the complex.

In conclusion, the distribution of anomalous Pt, Pd, Ir and Au concentrations is related to the original igneous rock types. The highest absolute concentrations of these elements occur in specific lithologies, notably those containing or spatially associated with chromite.

4.4.4 Coincidence of detected levels of Pt, Pd, Ir and Au

The close similarity between the distribution patterns of Pt, Pd, Ir and Au has been described above (sections 4.4.1 and 4.4.3). Inspection of the analytical data revealed that samples containing detected levels of one element usually also contained detected levels of the other three elements. The following section describes statistical tests designed to illustrate this aspect of the distribution patterns. To simplify calculations the coincidence in samples of any pair of these elements has been considered in turn.

Figure 4.13. Contingency table for the coincidence of detected Pt and Pd in all 250 samples.

Coincidence of detected Pt and Pd

Observed Frequencies

	Pt	~Pt	Totals
Pd	73	6	79
~Pd	15	156	171
Totals	88	162	250

No. samples = 250

where Pt signifies Pt ≥ 20 ppb ~Pt signifies Pt < 20 ppb
Pd signifies Pd ≥ 20 ppb ~Pd signifies Pd < 20 ppb

Expected Frequencies

	Pt	~Pt
Pd	27.8	51.2
~Pd	60.2	110.8

Discrepancy = 45.2
Chi-squared = 165.7*

*Null hypothesis:-
"Pt and Pd are not positively associated" rejected at 99% confidence level

Table 4.17. Summary table of the association of binary pairs of of Pt, Pd, Ir and Au concentrations greater than 20 ppb for the 195 samples analysed for all of these elements.

Coincident elements	*Association*	*Discrepancy*	*Chi-squared*	*Level at which null hypothesis is rejected*
Pt & Pd	positive	32.1	132.9	99 %
Pt & Ir	positive	16.9	64.6	99 %
Pd & Au	positive	13.8	33.9	99 %
Pt & Au	positive	13.3	28.8	99 %
Pd & Ir	positive	10.8	23.9	99 %
Ir & Au	positive	5.6	9.8	*

* Chi-squared cannot be used to test the coincidence of Ir and Au, since the expected number of samples containing both elements (4.4) is less than 5

The coincidence or otherwise of two attributes is best illustrated by the use of contingency tables (Cheeney, 1983). In this case the two attributes are the occurrence of detected concentrations of different PGE. The contingency table quantifies the degree of coincidence of the two attributes which is present in the dataset. From simple probability theory the expected coincidence of the two variables, assuming they are independent events, can also be calculated. The difference between these two tables indicates whether the two attributes occur together more frequently than expected and is expressed numerically by calculation of the discrepancy value. A large positive discrepancy indicates that the two attributes show a positive association and preferentially occur together. The statistical significance of such observations can be tested using chi-squared which is a measure of the departure of observation from expectation (Cheeney 1983). The value of chi-squared in this case is calculated from the information given in the observed and expected contingency tables. If the calculated value of chi-squared is greater than the critical value of 6.635 (for one degree of freedom) then the null hypothesis that "the observed discrepancy is due to random fluctuation" may be rejected at the 99% confidence level.

As an example the contingency tables for the coincidence of Pt and Pd at or above 20 ppb in all reconnaissance samples is shown in figure 4.13. The contingency table of expected frequencies is calculated assuming that Pt and Pd mineralisation are statistically independent events. The observed frequency of coincident Pt and Pd shows a large positive discrepancy from the expected frequency, indicating that these elements show a strong positive association. The value of chi-squared exceeds the critical value and so this result is statistically valid.

Table 4.17 shows the calculated discrepancies and values of chi-squared from contingency tables for all possible binary combinations of elements for the subset of 195 samples analysed for Pt, Pd, Ir and Au. All combinations of elements show positive associations. Pt and Pd show the strongest association, followed by Pt and Ir, and then Pd and Au, Pt and Au and finally Pd and Ir. The null hypothesis was rejected at the 99% confidence level for all pairs of elements except Ir and Au.

The close association between Pt, Pd, Ir and Au concentrations and the resultant similarity in the distribution patterns of these elements strongly suggests a common genetic

link. Furthermore, the association of anomalous mineralisation with particular primary lithologies indicates that igneous processes are most relevant when considering what are the likely factors controlling this type of PGE mineralisation.

4.5 Controls of PGE & gold mineralisation

The preceding section has described the close spatial association between chromite concentrations and higher PGE levels, a pattern recognised in rocks from a variety of different geological settings (section 1.2.2). The chalcophile behaviour of PGE indicates that Ni-Cu sulphide phases also have a significant effect on mineralisation in igneous environments. The following section examines the relative importance of chromite and accessory sulphide phases on the distribution of PGE in ophiolite complexes.

The reconnaissance samples included a suite of 121 samples collected from all the known chromite concentrations in the study area (section 4.2.2). These samples contained variable amounts of chromite and were all classified in the field accordingly (table 4.18). The presence or absence of accessory sulphide was also recorded in the field. All 121 samples were analysed for Pt and Pd, and a subset of 99 were also analysed for Ir and Au. Orientation studies at Cliff and Harold's Grave (section 4.2.1) had suggested that Pt, Pd and Au mineralisation occurred in chromite-rich rocks which contained sulphide. This suite of samples allows this hypothesis to be rigourously tested.

Table 4.18. Classification of chromite quarry samples according to chromite content.

Category	*Lithology*	*Number analysed for Pt, Pd, Ir, Au*	*Number analysed for Pt & Pd only*
CR	Chromitite	26	30
DC	Disseminated chromite-rich dunite	48	57
DU	Dunites, dunite host rock	20	26
A	Others, including highly altered samples	5	8
TOTAL		99	121

Figure 4.14. Histograms showing the percentage of samples from chromite quarries containing detected Pt, Pd, Ir or Au, grouped according to the chromite content of the host. Chromitite (CR), chromite-rich dunite (DC), dunite (DU) and serpentinite (A).

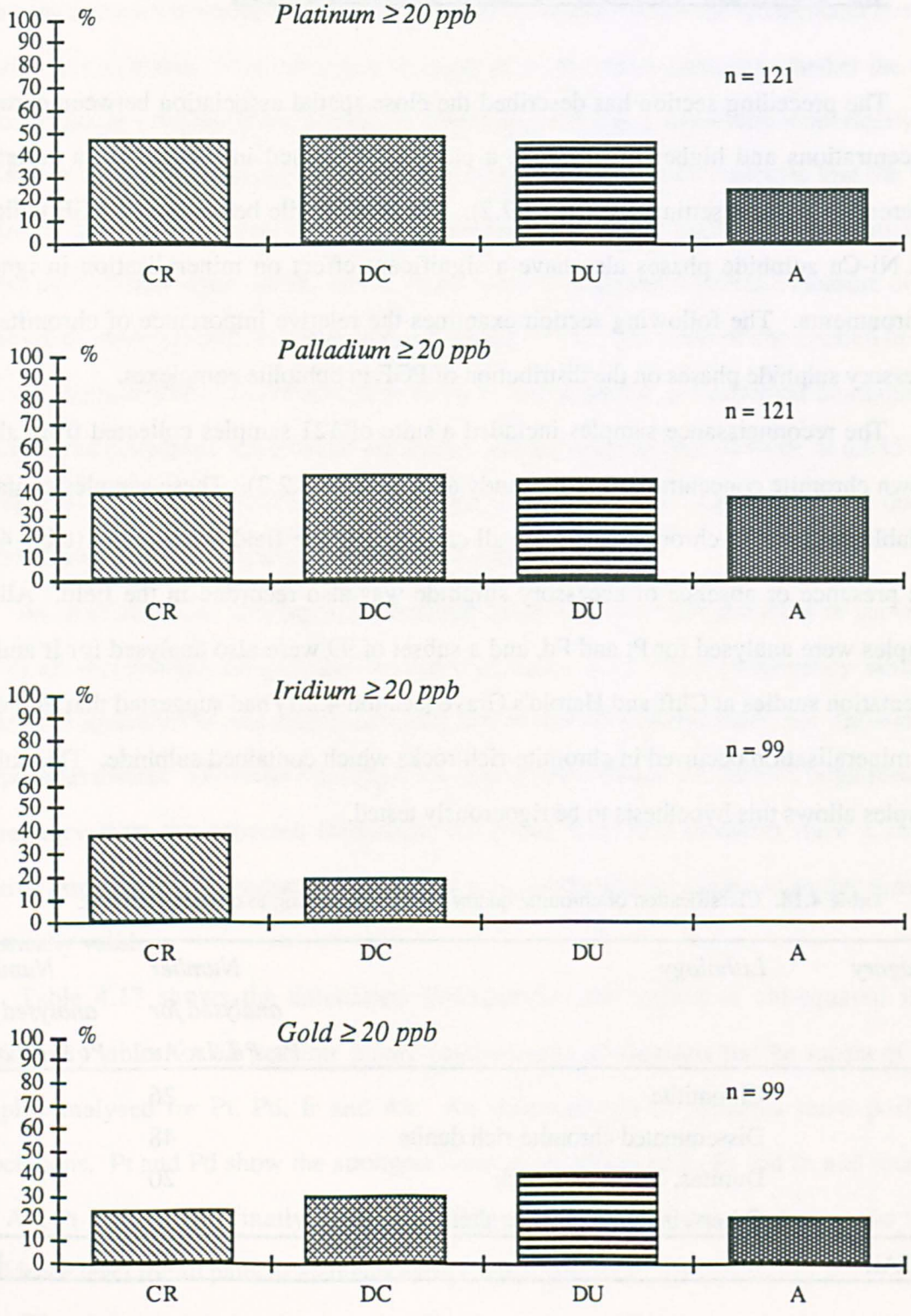

4.5.1 Chromite content

The classification of chromite quarry samples according to chromite content is shown in table 4.18. The category CR includes only massive chromitites or the more massive disseminated chromites, and category DC the disseminated chromite-rich samples. Category DU includes dunites collected from the chromite quarry spoil tips and quarry faces, which are therefore spatially associated with the chromite concentrations. The category A includes the few other rocks with peculiar alteration styles which were also collected from spoil tips.

Histograms in figure 4.14 show the percentage of samples in each chromite content category which contain detected PGE. The percentage of samples containing either Pt or Pd is apparently unrelated to the chromite content of the host lithology. In contrast, Ir is more commonly found in the more chromite-rich samples. Gold shows a complimentary pattern, occurring in all rock categories but more commonly in those containing less chromite.

Contingency tables have been used to test for any association between higher chromite contents and the occurrence of detected levels of PGE. The attribute of higher chromite content was assigned to all samples in the CR category in the first instant, and then to all samples in either the CR or DC categories. The values of discrepancy and chi-squared were calculated in each case for the occurrence of Pt, Pd, Ir and Au at levels of 20 ppb or more (table 4.19).

Ir and massive chromite show a positive association which is statistically significant (figure 4.15). This coincidence is also apparent when the massive and disseminated chromite-rich dunites are grouped together but in this case cannot be tested using chi-squared. The other elements show no statistical discrepancy and their occurrence in samples is apparently independent of the amount of chromite they contain.

Figure 4.15. Contingency table showing the preferential occurrence of iridium in chromitites.

Coincidence of detected Ir and massive chromite

Observed Frequencies

	Ir	~Ir	Totals	
Cr	10	16	26	
~Cr	9	64	73	
Totals	19	80	99	No. samples = 99

where Cr signifies CR* ~Cr signifies DC, DU or A*
Ir signifies Ir ≥ 20 ppb ~Ir signifies Ir < 20 ppb

Expected Frequencies

	Ir	~Ir	
Cr	5.0	21.0	Discrepancy = 5.0
~Cr	14.0	59.0	Chi-squared = 8.4

Null hypothesis "detected Ir and massive chromite are not associated" rejected at 99 % confidence level

* Categories defined in table 6.6

Table 4.19. Summary table of the association of detected Pt, Pd, Ir and Au concentrations or sulphide phases with chromitites and chromite-rich rocks.

Chromite content	*Number of samples*	*Element*	*Association*	*Discrepancy*	*Chi-squared*	*Level at which null hypothesis is rejected*
CR or DC	121	Pt	none	1.7	0.5	Not rejected
CR or DC	99	Pt	none	3.9	3.2	Not rejected
CR or DC	121	Pd	none	0.2	0.005	Not rejected
CR or DC	99	Pd	none	2.4	1.2	Not rejected
CR or DC	99	Ir	positive	4.8	7.9	*
CR or DC	99	Au	none	-1.7	0.7	Not rejected
CR only	99	Ir	positive	5.0	8.4	99%

* Chi-squared cannot be used to test the coincidence of Ir and chromite, since the expected frequency of an Ir-bearing chromite-poor sample (DU or A) is less than 5

4.5.2 Accessory sulphide content

Figure 4.16 shows the percentage of chromite quarry samples which contain accessory sulphide, subdivided according to their chromite content. Sulphides are common in all categories but most frequently occur in the dunites spatially associated with the chromite. Separate histograms have been plotted for both databases used in this section which show very similar patterns. The negative association between sulphides and chromite enrichments has been statistically tested using contingency tables. (table 4.20)

Contingency tables have also been calculated for the occurrence of detected Pt, Pd, Ir or Au in quarry samples with and without visible accessory sulphide (table 4.21). Pt, Pd and Au all show strong positive associations with sulphide which are statistically significant. This is illustrated by the histograms in figure 4.17 which combine the information on PGE mineralisation, sulphide content and chromite content (figures 4.14 and 4.16). Each of the

Figure 4.16. Histograms showing the percentage of samples from chromite quarries containing accessory sulphide, grouped according to chromite content.

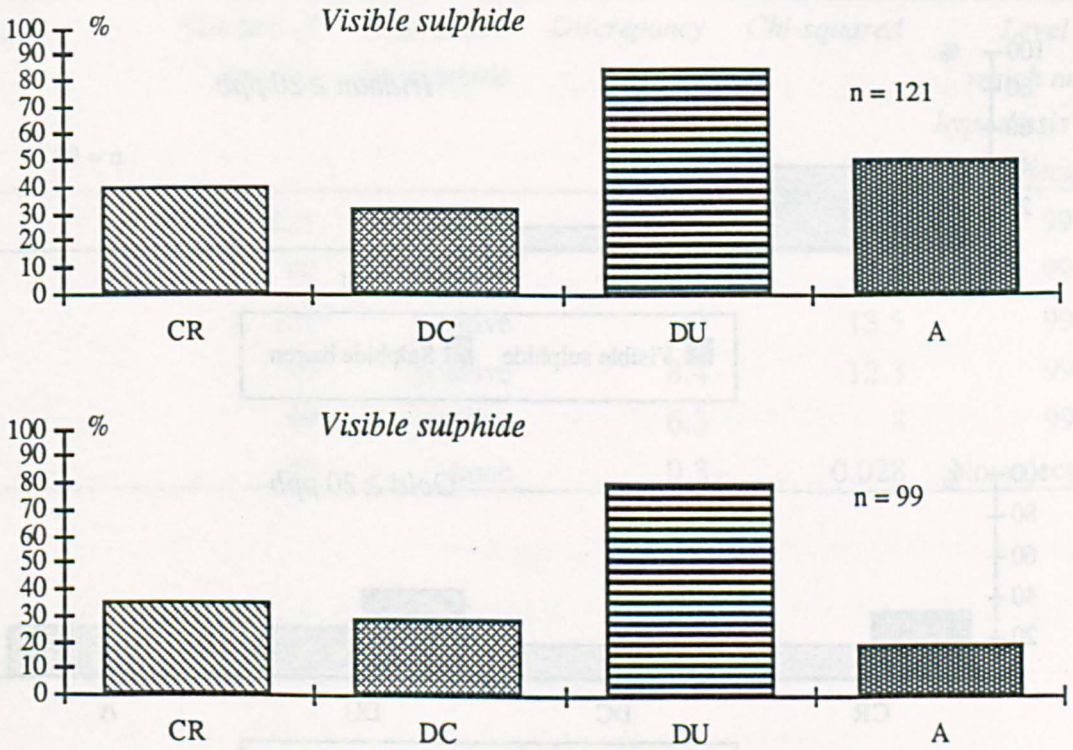

Figure 4.17. Histograms showing the percentage of quarry samples containing detected levels of PGE and Au, classified according to their chromite and accessory sulphide contents.

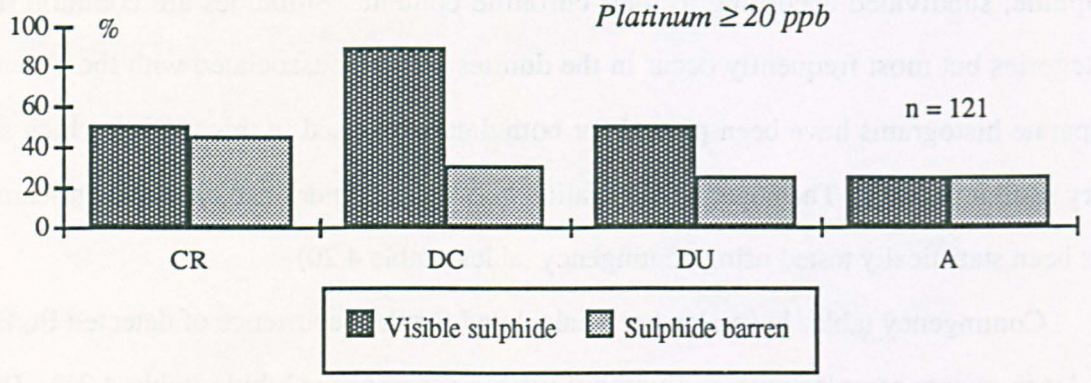

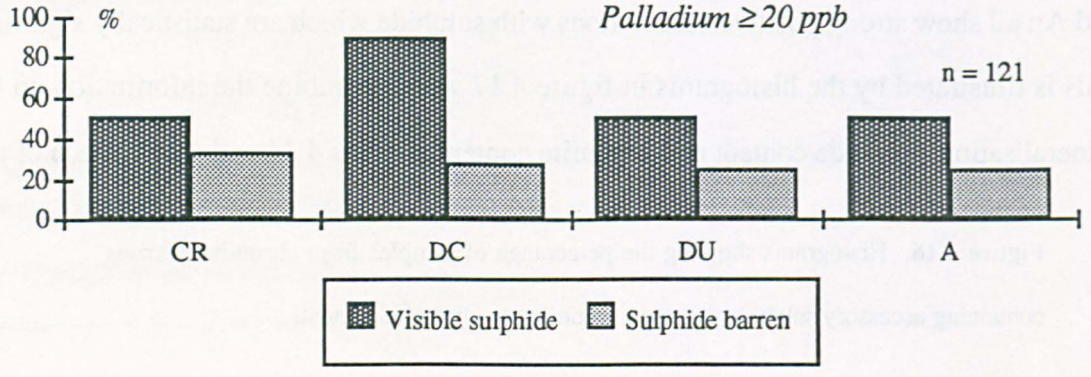

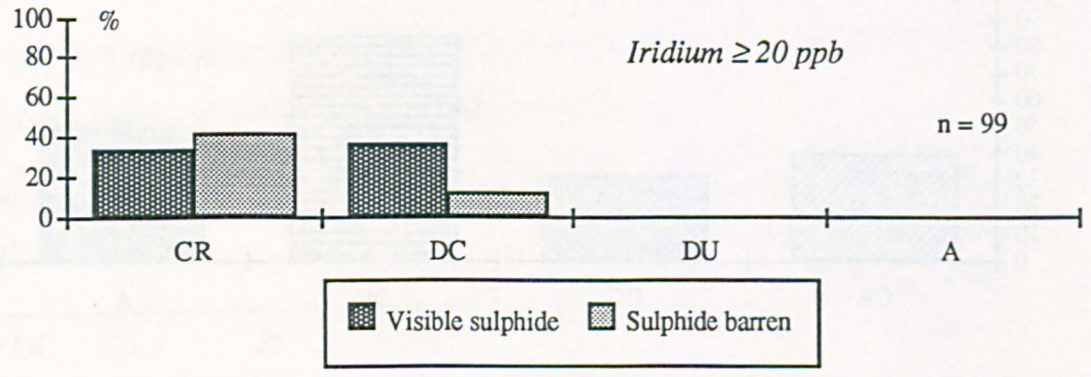

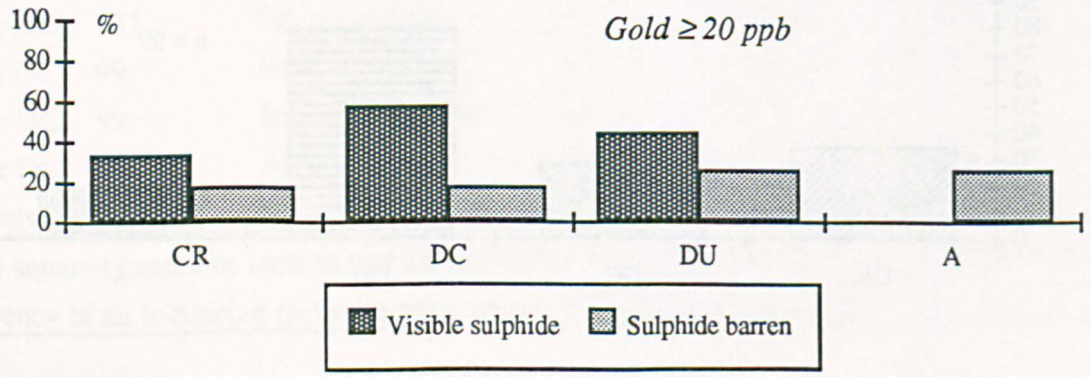

Table 4.20. Summary table of the association of accessory sulphide phases with chromite-rich rocks.

Chromite content	*Number of samples*	*Association with accessory sulphide*	*Discrepancy*	*Chi-squared*	*Level at which null hypothesis is rejected*
CR or DC	121	negative	-10.3	17.3	99 %
CR or DC	99	negative	-6.9	10.6	99 %
CR only	121	none	-1.9	0.6	not rejected
CR only	99	none	-1.5	0.5	not rejected

Table 4.21. Summary table of the association of detected PGE concentrations with accessory sulphide phases.

Element	*Number of samples*	*Association with sulphide*	*Discrepancy*	*Chi-squared*	*Level at which null hypothesis is rejected*
Pt	121	positive	8.1	8.7	99%
Pt	99	positive	6.6	7.5	99%
Pd	121	positive	10	13.5	99%
Pd	99	positive	8.4	12.3	99%
Au	99	positive	6.3	8	99%
Ir	99	none	0.3	0.028	Not rejected

chromite categories have been subdivided into those samples with and without visible accessory sulphide. The vertical scale shows the percentage of each type which contain PGE. A similar pattern is shown for Pt, Pd and Au. Detected levels of these elements more commonly occur in sulphide-bearing lithologies regardless of their chromite content. Concentrations of these three elements are particularly common in sulphide-bearing chromite-rich dunites but also frequently occur in sulphide-bearing chromitites or dunites. The preferential occurrence of Pt, Pd and Au in sulphide-bearing samples is most pronounced in chromite-rich dunites, even though sulphides are commonest in the associated dunites (figure 4.16). In contrast Ir most commonly occurs in chromitites and is independent of their sulphide content.

The above patterns indicate that Pt, Pd and Au concentration is controlled by sulphide phases whereas Ir concentration is controlled by chromite. Furthermore, concentrations of Pt, Pd and Au most commonly occur with sulphide when it is spatially associated with chromite.

4.5.3 Relationship between chromite, sulphide and PGE concentrations

The geographical distribution of both detected and anomalous levels of PGE and Au (sections 4.4.1 and 4.4.3) indicated that PGE concentrations most commonly occur spatially associated with chromite concentrations. In apparent contradiction, the occurrence of Pt, Pd and Au is clearly controlled by the presence of sulphide phases, and not the amount of contained chromite (section 4.5.1 and 4.5.2). Furthermore, the distribution of Pt, Pd and Au is not entirely similar to the distribution of sulphides in the complex (section 2.4).

Sulphides commonly occur in most lithologies, but are less common in the mantle sequence than the crustal sequence, although PGE occur with chromite in both of these settings (section 4.4.1). Accessory sulphide is usually present in most ultramafic cumulate rocks at all levels in the sequence, although anomalous levels of PGE are restricted to certain lithological groups (section 4.4.3). The relative quantity of sulphide is highest in the basal dunites, particularly those exposed in the chromite quarry walls (section 2.4).

Within samples from chromite quarries the occurrence of sulphide is antithetic to that of chromite (figure 4.16). The associated dunites are therefore more frequently visibly sulphide-bearing or contain greater quantities of sulphide than the chromitites. This indicates that the sulphide phases occur within the olivine-rich matrix of disseminated chromite-rich dunites.

It has been shown from the suite of quarry samples that Pt, Pd and Au more frequently occur in sulphide-bearing lithologies (figure 4.17). This distinction between the percentage of sulphide-bearing and sulphide-barren samples which contain PGE is greatest within the disseminated chromite-rich dunites. For example, approximately 90 % of the sulphide-bearing chromite-rich dunites contained detected levels of Pt, compared to only 50 % of the associated sulphide-bearing dunites. These observations indicate that Pt, Pd and Au are fractionated into the sulphide phases which are spatially closest to chromite concentrations. The behaviour of Ir is similar in this respect, since this element only occurs in chromite-rich lithologies. Any model to explain the concentration of PGE in this environment must consider why sulphides associated with chromite in particular indicate a probable anomalous PGE content.

4.6 Conclusions and genetic model

The extensive sampling and analytical program described in this chapter has revealed the widespread occurrence of anomalous PGE concentrations in the ophiolite complex. Anomalous levels of PGE which were previously known at Cliff and Harold's Grave have been located in other chromite-rich dunite pods from within mantle harzburgite. More significantly, concentrations of PGE have also been found associated with stratigraphically controlled chromite concentrations within the cumulate dunite unit. These PGE concentrations contain high levels of platinum and palladium, and occur not only in chromitites, but also in the associated dunites and chromite-rich dunites. PGE concentrations have also been located in other chromite-poor rocks within the crustal sequence, including wehrlites and pyroxenites. Anomalous levels of Pt and Pd occur in sulphide-bearing pyroxene-rich lithologies from close to the base of the pyroxene-bearing

layered sequence, and also in sulphide-bearing pyroxene-rich ultramafic bodies within the gabbro unit.

The distribution of Pt, Pd, Ir and Au concentrations through the ophiolite stratigraphy is summarised in figure 4.12. They show similar distribution patterns and concentrations of the four elements occur together indicating a common origin by a single genetic process. The distribution patterns are not related to alteration zones but are lithologically controlled, with PGE concentrations occurring more frequently in certain igneous rock types. Such lithological association is indicative of primary igneous processes with concentration of the PGE occurring at the same time as the formation of the enclosing silicate rock.

Hand specimen description of samples and observation of their accessory sulphide content has provided further evidence of the controls of PGE mineralisation. Anomalous levels of Pt, Pd and Au occur preferentially in sulphide-bearing disseminated chromite-rich dunites, and in sulphide-bearing dunites which are spatially associated with chromite concentrations. Anomalous levels of Ir most commonly occur in chromitites and chromite-rich rocks. These two controls (i.e. chromite and accessory sulphide) form visual pathfinders for PGE mineralisation which can be recognised in the field. The differences in behaviour between Ir and Pt or Pd also indicate internal fractionation within the platinum group of elements.

Anomalous levels of PGE preferentially occur together with sulphides spatially associated with chromite concentrations. These chromite concentrations generally occur close to the base of the layered crustal sequence and in dunite pods within the harzburgite. Within the consensus ophiolite model (Gass, 1980) these pods represent magma diapirs feeding the overlying magma chamber. At least two stratigraphically controlled parallel layers of chromite concentration have been mapped in the dunite unit (section 2.3.2). The lack of progressive changes in chromite mineral chemistry between successive stratigraphically higher chromite horizons (section 3.5) indicates that they represent different magma inputs. It is suggested that the chromite enrichments mark the base of each cyclic repetition in the cumulate sequence. The distribution of chromite concentrations indicates that they were formed early in the crystallisation history of the magma. The sulphides associated with the chromite concentrations thus represent the earliest sulphide phases

forming within the cumulate sequence. In the case of cyclic repetitions these are the first sulphides segregating from each batch of primitive magma.

A genetic model for the occurrence of PGE in ophiolites may now be suggested, namely that PGE concentrations occur associated with the first sulphide segregating from the evolving magma. In the Shetland ophiolite this occurred at the same time as, or immediately after, chromite crystalised. PGE concentrations therefore occur close to the base of layered cumulate sequences. Repetitions occur representing fresh inputs of magma during open system fractional crystallisation.

The three subsequent chapters consider the evidence for and implications of themes developed in this chapter. Chapter five examines the association of PGE and sulphides by describing the distribution of other associated metals and their use as pathfinder elements. Chapter six considers the nature of the PGE concentrations and their pathfinder elements in more detail using the results of follow-up sampling and geochemical traverses. Chapter seven investigates the fractionation of different elements within the platinum group and the overall fractionation and concentration of the PGE within the ophiolite complex.

Chapter 5

Trace Element Distributions and Pathfinder Analysis

5.1 Introduction

The preceding chapter described the results of an extensive sampling and analytical program with the aim of establishing the distribution of PGE and Au in the complex. Included in the descriptions of the analytical methods was a discussion of the potential difficulties of obtaining low cost routine analyses of the PGE concentrations typically found in silicate rocks. These problems were to a large extent confirmed by the results of the various standardisation procedures used to assess the analytical data.

An alternative method of locating anomalous PGE concentrations in future sampling programs might include using pathfinder element analysis. This technique relies on analysing for another element which has a similar distribution to the sought element but is easier and or cheaper to determine. For example, if Pt and As occurred exclusively as sperrylite ($PtAs_2$) these elements would have similar distribution patterns and since As may be readily analysed by relatively cheap methods (e.g. by XRF) it would be a useful pathfinder for PGE mineralisation.

In chapter 4 it was shown in that the distribution of PGE in the complex is related to the primary rock types. Such patterns of lithological association are indicative of concentration by igneous processes. The chemical behaviour of PGE and studies of their distribution in a variety of other igneous settings would indicate that immiscible sulphide liquids are likely to have acted as a concentration mechanism during formation of the primary ophiolite sequence (section 1.2). Confirmatory evidence of this is provided by the association of detected Pt, Pd and Au concentrations with visible sulphide phases (section 4.5). This suggests that sulphur and the chalcophile metals Ni, Cu and Co may show similar distribution patterns as Pt, Pd and Au, representing potential pathfinder elements in

this geological setting. The association of of Ir with chromite-rich rocks indicates that Cr may have a similar use for this particular element.

Previous studies of samples from Cliff indicated that the anomalous levels of PGE at this locality are associated with enrichments in Ni, Cu, As, Sb and Te (Gunn et al., 1985). Mineralogical studies support these findings since the PGM-rich chromitites contain Ni-Cu sulphides, native Cu, Ni arsenides and Ni antimonides (Prichard et al., 1989). Furthermore the PGM assemblage, particularly those minerals containing Pt or Pd, is dominated by arsenide and antimonide phases. It was argued by Gunn (et al., 1985) that the elements As, Sb and Te were introduced during the low temperature hydrothermal activity responsible for the PGE mineralisation (section 1.6). However, these three elements were not found to be good pathfinders for the PGE mineralisation elsewhere in the complex.

Differences were noted between the elemental associations in different areas (Gunn et al., 1985). PGE-rich samples from Harold's Grave did not show the associated enrichments of Ni or Cu observed at Cliff. Higher levels of Ni and Cu were found in PGE-bearing samples from the dunite unit compared with similar rocks from the harzburgite unit. In the cumulate sequence no correlation was found between PGE and either Ni or As, and only a weak correlation with Cu. Some correlation was observed between Cr and PGE in the pyroxene-bearing lithologies.

From the discussion above it is apparent that the pathfinder elements for PGE mineralisation in this environment are far from clear. The studies of mineralisation from the Cliff area contradict the association of PGE with chalcophile elements suggested by this study. Since the suite of reconnaissance samples were all analysed for PGE they provide a means of assessing the usefulness of various trace elements as pathfinders. For the reasons given above it is necessary to consider both the Ni, Cu, Co, S and the As, Sb groups of elements as well as Cr and other elements indicative of the host rock mineralogy.

This chapter begins with descriptions of the trace element analysis methodology. This data is then used to show the geographical and lithological distribution of various concentrations of the different trace elements. This allows comparisons with the distribution patterns of PGE to be made and their usefulness as pathfinder elements to be assessed.

Finally the relation between sulphide, sulphur and chalcophile element concentrations is discussed.

5.2 Trace element analysis

Several analytical techniques were needed in order to analyse for the required range of trace elements. Multi-element energy-dispersive x-ray fluorescence analysis (ED-XRF) provided Ni Cu, As and Cr as well as approximate major element data and was therefore used routinely. This was augmented by INAA analysis for Co or Sb and also some commercial analysis of sulphur. These techniques were only performed on selected subsets of samples.

5.2.1 XRF analysis for Ni, Cu, As and Cr

All 388 samples were analysed as powder pellets by ED-XRF at the Open University using a silver x-ray tube. The standard analytical and correction procedures are described in Potts et al. (1984). This method provides analyses of a wide range of trace elements with excitation conditions optimised for the determination of Ni, Cu, Zn, Ga, Rb, Sr, Y, Zr, Nb, Pb and Th. The analyses of As, Mo and U are also satisfactory and are only limited by the lack of reliable calibration standards. Of these trace elements, Ni, Cu and As were most relevant to this study. The technique is not optimised for V, Cr, Co or Ba, which are therefore only determined for 'order of magnitude' information. Since the Shetland ultramafic rocks all contain accessory spinel the typical Cr analyses are comparatively high and provide a good indication of the relative chromite content. Approximate major element analyses are also provided by ED-XRF analysis of pellets, primarily for mass correction procedures. These major element analyses are effected to various degrees by matrix effects but provide an indication of the original rock type where this is uncertain. Analysis for S and Cl is affected by scattered l-lines from the silver tube. Accessory amounts of sulphides cannot therefore be quantified by this method.

Figure 5.1. Graphical comparison of ED- and WD-XRF analyses for Ni and Cu.

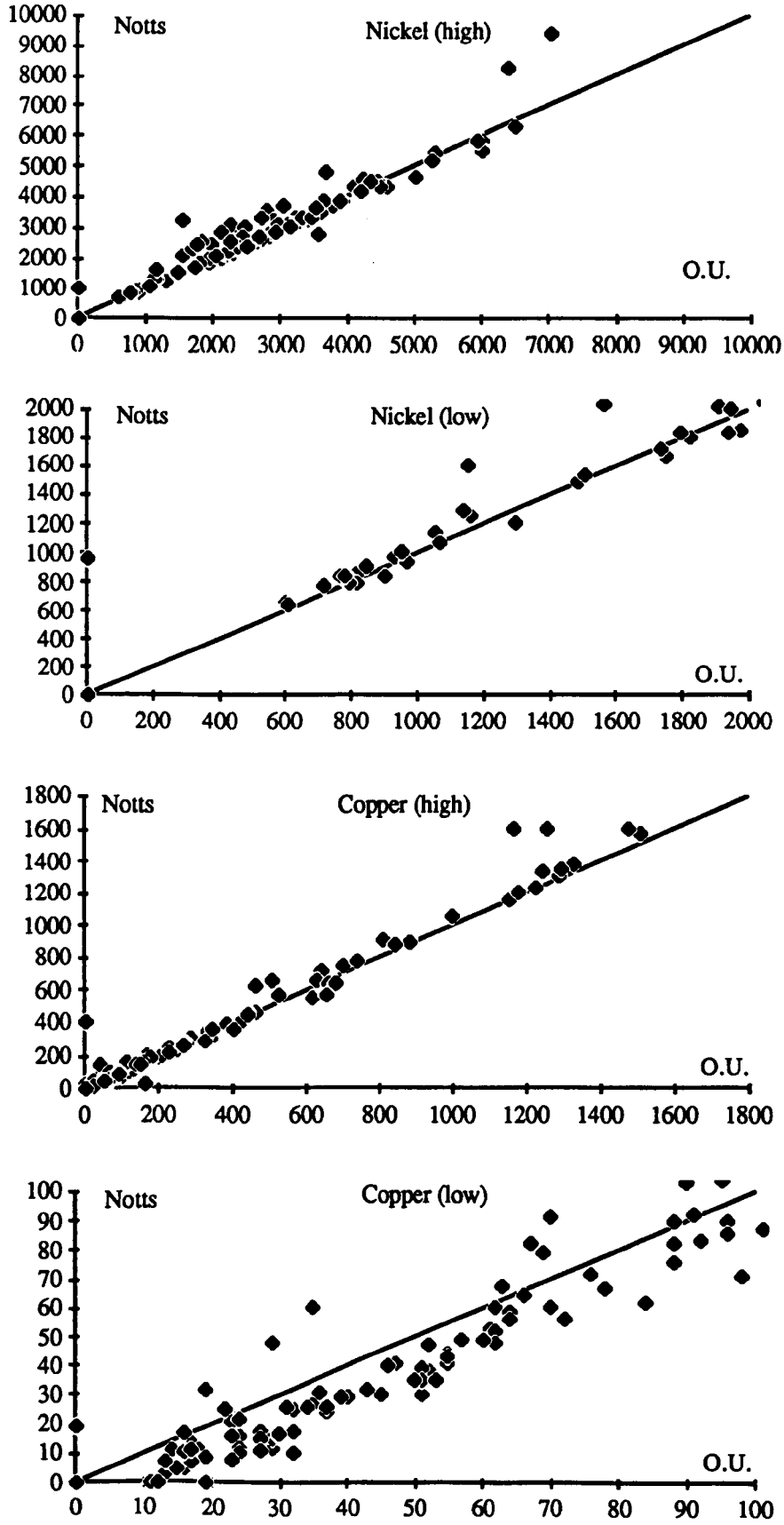

Figure 5.2. Graphical comparison of ED- and WD-XRF analyses for Cr and As.

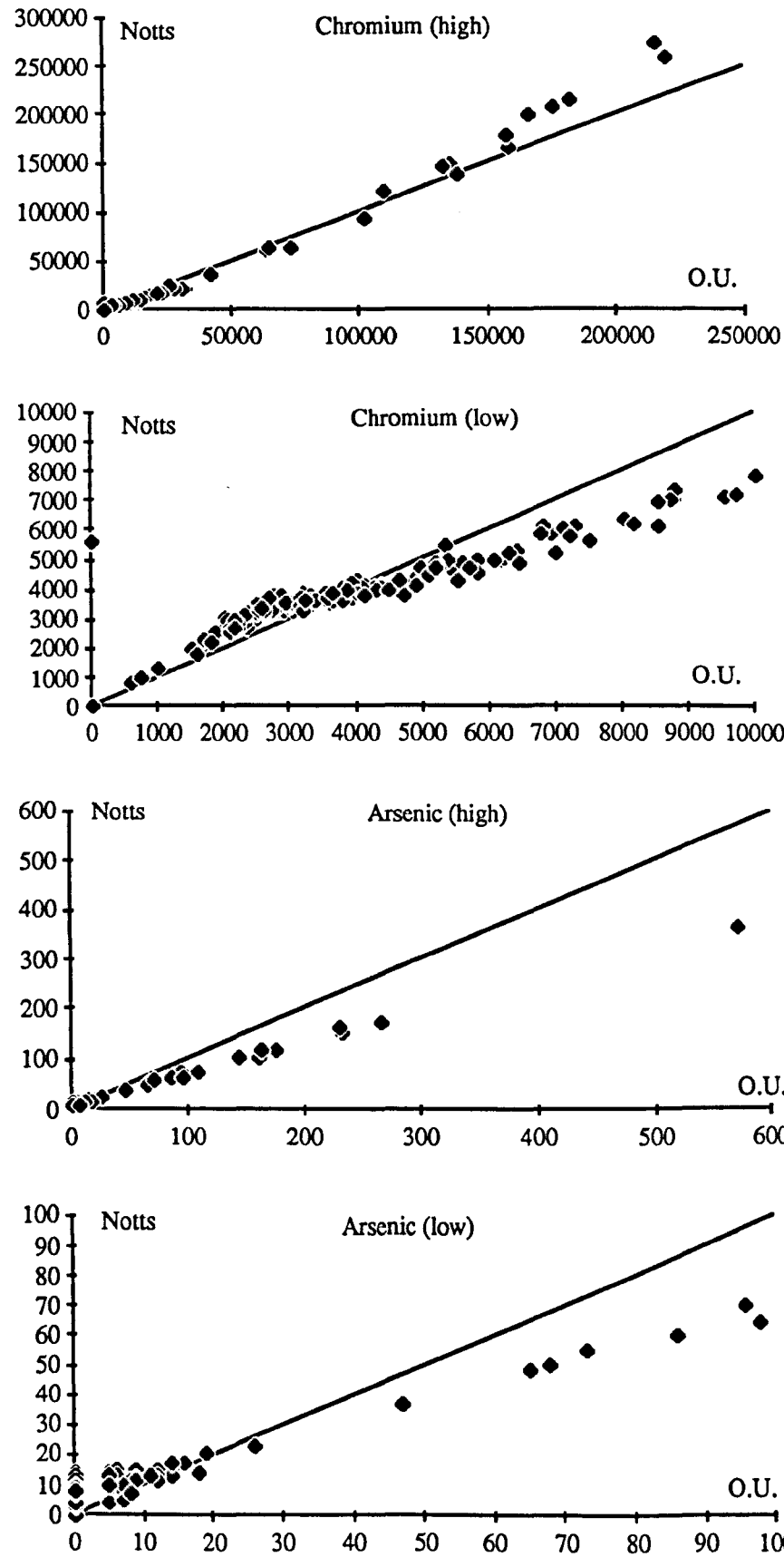

5.2.2 INAA analysis for Co and Sb

A subset of 195 samples were analysed by INAA at the Open University in order to obtain reliable Sb and Co analyses. The analytical procedure has been described previously (section 4.3.4). Calculations of detection limits from counting statistics indicate that the analyses of Co and Sb are reliable at levels above 1 - 2 ppm (table 4.8).

5.2.3 Commercial analysis of sulphur

A subset of 33 samples were analysed for sulphur by Analytical Services, Willetton, Western Australia. This laboratory uses a hydrofluoric-based mixed acid digest and an ICP-OES analytical finish. A detection limit of 0.01 wt % sulphur (i.e. 100 ppm) is claimed for this method.

5.2.4 Assessment of trace element analytical data

A range of secondary standards were routinely included with the unknowns during ED-XRF analysis so as to check each batch of data. These standards included a dunite (NIM-D), a granodiorite (GSP-1) and a Hawaiian basalt (BHVO-1). Many of the Shetland samples, however, contained levels of Cr, Ni and Cu beyond the range of these standards. A subset of 191 samples were re-analysed for Ni, Cu, As and Cr using wavelength-dispersive XRF at Nottingham University. Direct comparison of these analyses with the ED-XRF analyses from the Open University allows the performance of the analytical techniques to be investigated over the unusual range of concentrations and matrix compositions.

Graphical comparisons of the EDS and WDS analyses of Ni and Cu are shown in figure 5.1. The two different analyses of these elements show excellent agreement, as would be expected, since the analytical conditions are optimised for their determination. Ni is reliably detected down to ~600 ppm and Cu to 10 ppm. Comparison of the two analyses for Cr and As indicate systematic departures from a 1:1 ratio (figure 5.2). This pattern suggests differences in the calibrations between laboratories, which are exaggerated because

Figure 5.3. Comparison of Co analyses by INAA and ED-XRF.

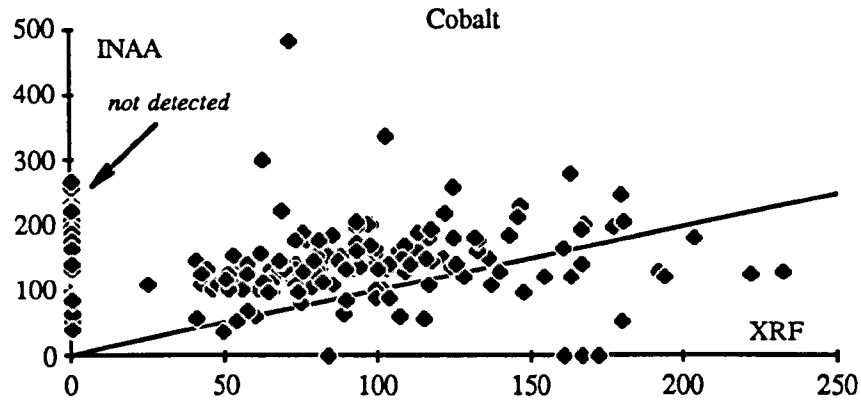

Figure 5.4. Comparison of Co analyses by INAA and ED-XRF with Cr contents.

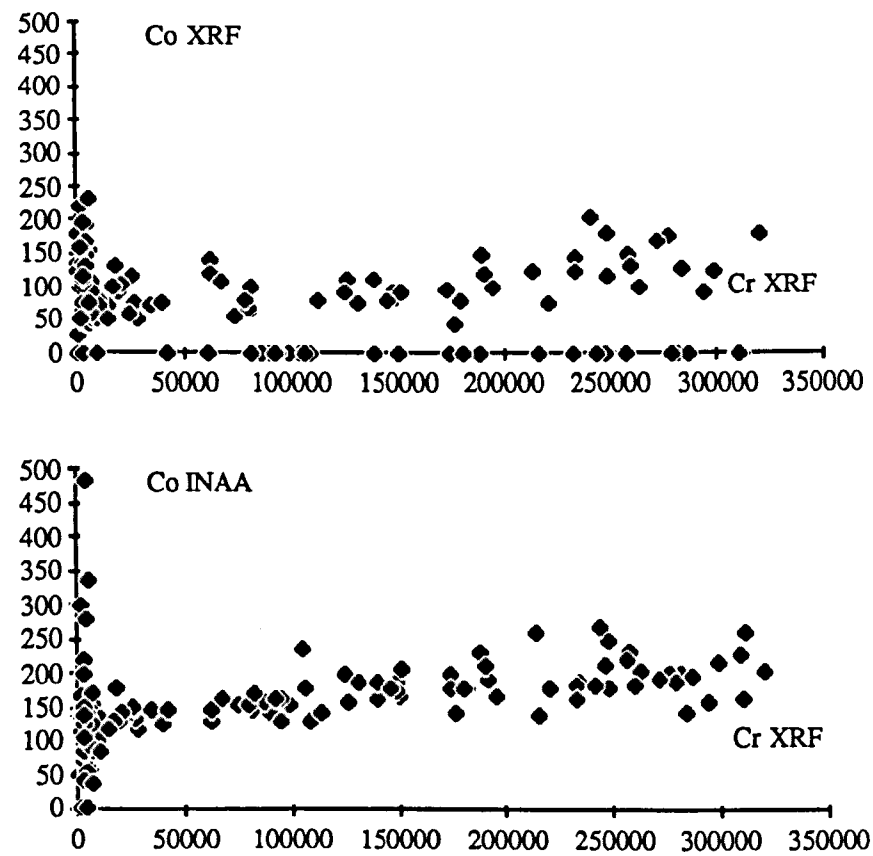

both elements are present at concentrations beyond the usual calibration ranges. Detection of chromium is reliable down to 500 ppm and arsenic to below 10 ppm.

ED-XRF also produces analyses of Co, although the procedure is not optimised. These analyses have been compared to those obtained using INAA (figure 5.3). The analyses show poor agreement, with non-detection by XRF over the full range of concentrations determined by INAA (points plotting on vertical axis). This problem is confirmed by comparisons of the Co and Cr concentrations, since a good correlation is expected between Co and Cr in chromite-rich rocks (section 5.5.2). The ED-XRF analyses of Co show random non-detection across the range of observed Cr (and hence chromite) concentrations. For these reasons, only Co analyses produced by INAA are used in the following discussion, although these were only performed on a limited number of samples.

The preceding discussion indicates that the trace element analyses are sufficiently precise and accurate to observe possible correlations with the PGE. To avoid problems of data incompatibility the Open University ED-XRF analyses are used throughout the following study. This allows valid comparison of the relative magnitude of trace elements concentrations between samples from different areas. The lower useful limits of the analytical determinations used in this chapter are summarised in table 5.1.

Table 5.1. Working limits of trace element analyses.

Element	*Laboratory*	*Method*	*Useful limit*
Ni	Open University	ED-XRF	600 ppm
Cu	Open University	ED-XRF	10 ppm
Cr	Open University	ED-XRF	500 ppm
As	Open University	ED-XRF	10 ppm
Co	Open University	INAA	1 ppm
Sb	Open University	INAA	1 ppm
S	Analytical Services	HF, ICP-OES	100 ppm

5.3 The distribution of trace elements

The routine analysis of a representative suite of samples from the ophiolite sequence for a range of potential pathfinder elements also allows the distribution of these trace elements in the complex to be investigated. In the following section similar diagrams and maps have been produced for Ni, Cu, Cr, Co, As and Sb as were used to show the distribution of PGE in the complex (section 4.4).

5.3.1 Range of Ni, Cu, Cr, Co, As and Sb concentrations

The range of trace element concentrations is shown by cumulative and relative frequency histograms in figure 5.5. The elements Ni, Co, Cr and Cu all have different concentration frequency patterns from those shown by PGE and Au (figure 4.7). The Ni, Cr and Co distributions each contain distinct populations at particular concentration levels. These populations have been identified by comparison of the analytical data with the field observations and consist of particular igneous lithologies or amounts of accessory sulphide. Table 5.2 lists the ten samples with the highest overall levels of Ni, Co, Cu, As and Sb as examples of the most anomalous lithologies.

The concentration of nickel in a particular sample is apparently related to its olivine and sulphide content. Dunites contain intermediate levels indicating substitution of Ni in olivine (2000-3000 ppm). Olivine-poor lithologies contain significantly lower concentrations. Anomalously high levels of Ni occur in sulphide-bearing dunites, due to the Ni content of both the olivine and the sulphide phases (table 5.2).

Concentrations of Co show a similar pattern, indicating substitution of the element into olivine. Dunites therefore form a distinct population at intermediate concentration levels (100-200 ppm), with lower concentrations occurring in olivine-poor rocks. High concentrations of Co occur in some sulphide-bearing rocks, and also in chromitites, due to substitution of this element into chromite (table 5.2). Although Co was not routinely analysed during microprobe studies of chromite composition (chapter 3), Co ß-activity from

Figure 5.5. Concentration range and frequency distributions for Ni, Co, Cr, Cu, As and Sb.

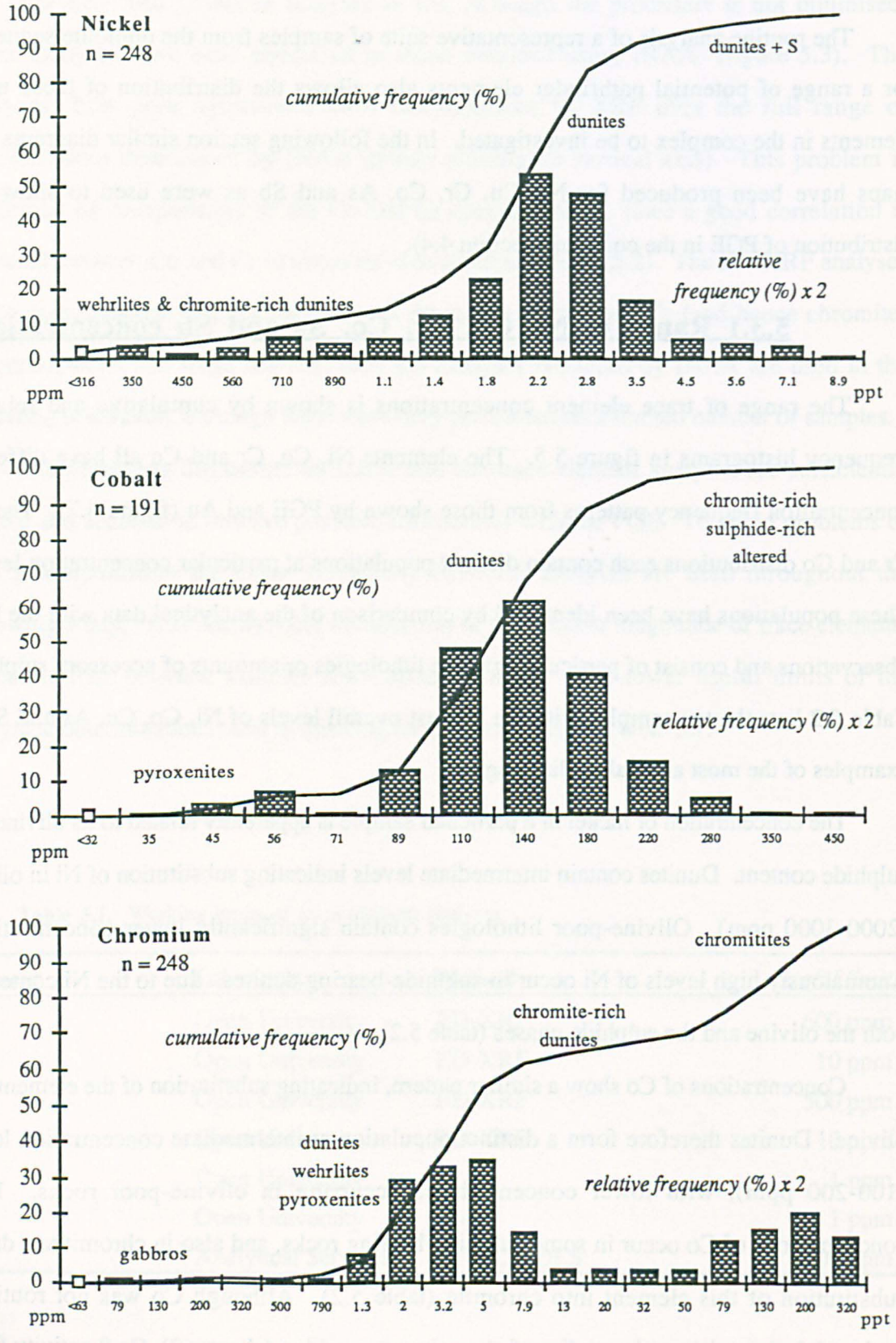

Figure 5.5 (cont.).

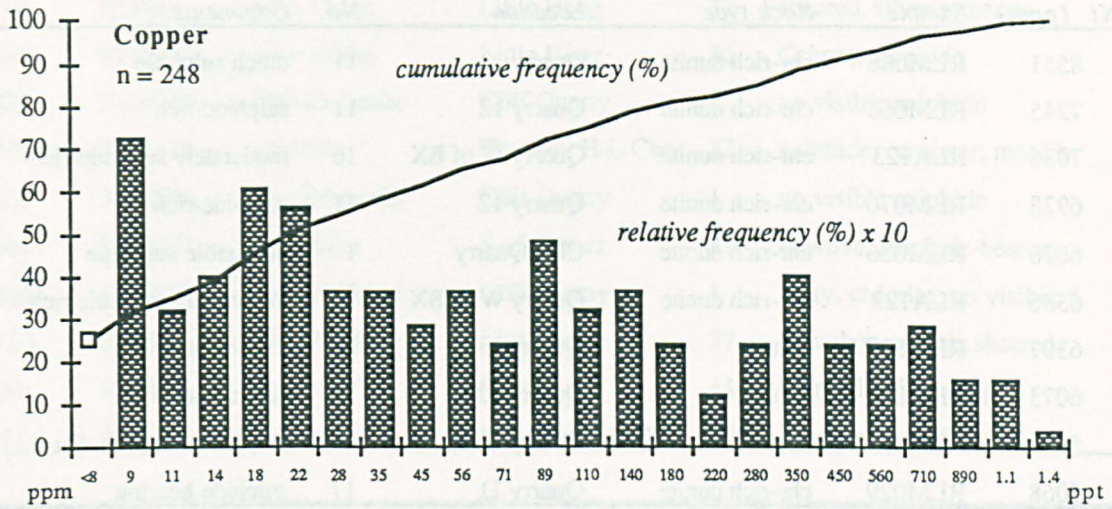

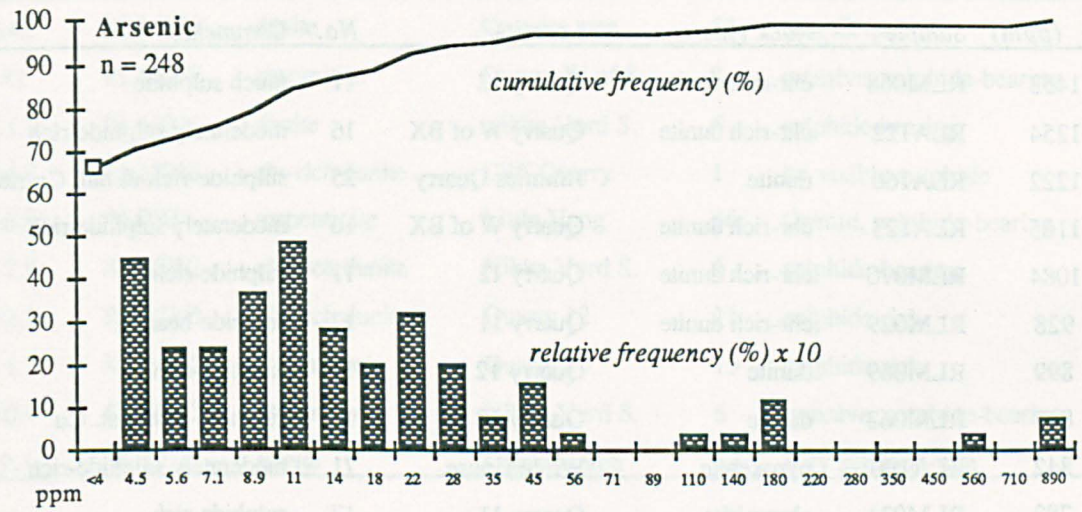

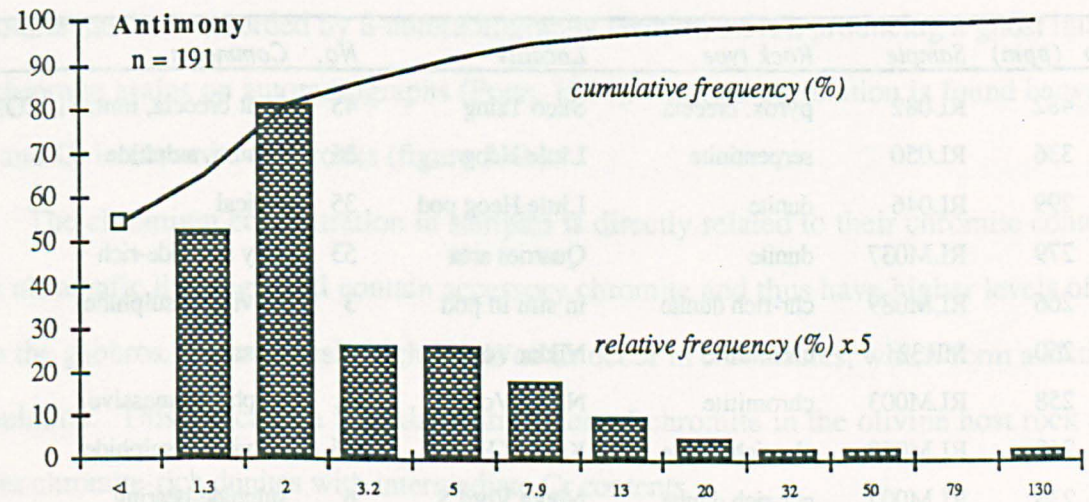

Table 5.2. Details of the ten samples containing the highest levels of Ni, Cu, Co, As & Sb.

Ni (ppm)	*Sample*	*Rock type*	*Location*	*No.*	*Comments*
8551	RLM068	chr-rich dunite	Quarry 12	11	much sulphide
7245	RLM065	chr-rich dunite	Quarry 12	11	sulphide-rich
7036	RLA123	chr-rich dunite	Quarry W of BX	16	moderately sulphide-rich
6928	RLM070	chr-rich dunite	Quarry 12	11	sulphide-rich
6676	RLM086	chr-rich dunite	Cliff Quarry	1	no visible sulphide
6386	RLA122	chr-rich dunite	Quarry W of BX	16	moderately sulphide-rich
6307	RLM079	dunite	Quarry 13	19	sulphide-rich
6073	RLM069	dunite	Quarry 12 S	12	sulphide-rich
5670	RLM063	dunite	Quarry 12 S	12	sulphide-rich, nat. Cu
5068	RLM029	chr-rich dunite	Quarry 11	17	sulphide-bearing

Cu (ppm)	*Sample*	*Rock type*	*Locality*	*No.*	*Comments*
1453	RLM068	chr-rich dunite	Quarry 12	11	much sulphide
1254	RLA122	chr-rich dunite	Quarry W of BX	16	moderately sulphide-rich
1222	RLA160	dunite	Jimmies Quarry	25	sulphide-rich & nat. Cu rich
1165	RLA123	chr-rich dunite	Quarry W of BX	16	moderately sulphide-rich
1084	RLM070	chr-rich dunite	Quarry 12	11	sulphide-rich
928	RLM029	chr-rich dunite	Quarry 11	17	sulphide-bearing
899	RLM069	dunite	Quarry 12 S	12	sulphide-rich
847	RLM063	dunite	Quarry 12 S	12	sulphide-rich, nat. Cu
842	RLA190	pyroxenite	White House	71	moderately sulphide-rich
782	RLM031	chromitite	Quarry 11	17	sulphide-rich

Co (ppm)	*Sample*	*Rock type*	*Locality*	*No.*	*Comments*
482	RL082	pyrox. breccia	Skeo Taing	45	fault breccia, mnt, Si, CO3
336	RL050	serpentinite	Little Heog	36	Cr/mnt, sulphide
299	RL046	dunite	Little Heog pod	35	typical
279	RLM037	dunite	Quarries area	53	very sulphide-rich
266	RLM089	chr-rich dunite	in situ in pod	3	no visible sulphide
260	MR32	chromitite	Nikka Vord N.	4	massive
258	RLM003	chromitite	Nikka Vord S.	6	sulphide, massive
248	RLM058	chr-rich dunite	Keen of Hamar	26	no visible sulphide
236	RLM002	chr-rich dunite	Nikka Vord S.	6	sulphide-bearing
232	RL068	chromitite	Harold's Grave	2	weathered surface

Table 5.2 (cont.).

As(ppm)	*Sample*	*Rock type*	*Locality*	*No.*	*Comments*
900	RL064	serp. / harz.	Little Heog	37	sheared, silver minerals
848	RL050	serpentinite	Little Heog	36	Cr/mnt, sulphide
525	RLM086	chr-rich dunite	Cliff Quarry	1	no visible sulphide
195	RLA171	chr/mnt	The Nev H L Chr.	27	sulphide, on shear, mnt/Cr
181	RLM084	chr-rich dunite	Cliff Quarry	1	no visible sulphide
164	RLA047	chromitite	S of Setters	21	massive, sulphide-bearing
126	RLM085	chr-rich dunite	Cliff Quarry	1	rusty, chlorite, no visible S
110	RL066	serp. / harz.	Little Heog	37	S, carbonate-rich, sheared
54	RL054	dyke	Ordale	41	tourmaline? bearing
42	RLA173	chromitite	The Nev H L Chr.	27	massive, top of layer

Sb(ppm)	*Sample*	*Rock type*	*Locality*	*No.*	*Comments*
142	RLM039	dunite	Quarries area	54	near Cr quarry
41	RLM020	chromitite	Quarry W of 8	8	massive, sulphide-bearing
25.7	RLM001	dunite	Nikka Vord S.	6	sulphide-bearing
24.8	RLM086	chr-rich dunite	Cliff Quarry	1	no visible sulphide
16.9	RL050	serpentinite	Little Heog	36	Cr/mnt, sulphide-bearing
12.9	RLM002	chr-rich dunite	Nikka Vord S.	6	sulphide-bearing
12.7	RLM065	chr-rich dunite	Quarry 12	11	sulphide-rich
11.3	RLM097	chromitite	Quarry 10	15	sulphide-rich
10.7	RLM003	chromitite	Nikka Vord S.	6	massive, sulphide-bearing
9.4	RLM038	dunite	Quarries area	52	very sulphide-rich

chromite has been recorded by ß-autoradiography (section 1.5.1), producing a ghost image of chromite grains on autoradiographs (Potts, 1984). A good correlation is found between Co and Cr in chromite-rich rocks (figure 5.4b).

The chromium concentration in samples is directly related to their chromite content. The ultramafic lithologies all contain accessory chromite and thus have higher levels of Cr than the gabbros. Anomalously high levels of Cr occur in chromitites, which form a distinct population. This indicates a bimodal distribution of chromite in the olivine host rock and fewer chromite-rich dunites with intermediate Cr contents.

Copper levels show a simple pattern, with a single population spanning a wide range of concentrations. The highest Cu concentrations occur in sulphide-bearing lithologies. These often also contain visible native Cu (table 5.2).

The cumulative and relative frequencies histograms for As and Sb are also shown in figure 5.5. Concentrations of these two elements show frequency distributions similar to those of PGE and Au. Both elements exhibit a main population at low and intermediate levels but these are modified by a few very highly anomalous concentrations. Anomalous levels of both elements occur in sulphide-bearing samples of chromitites, chromite-rich dunites or dunites, particularly those from Cliff. The most As-rich samples occur in shear zones and contain concentrations almost an order of magnitude higher than those found in chromite quarries (table 5.2).

In conclusion, concentrations of Ni, Co and Cr are affected by the primary mineral phases and are hence related to the igneous rock types. Concentrations of the chalcophile elements Ni, Cu and Co are also controlled by the sulphide content of these lithologies. Arsenic shows dual behaviour, since anomalous levels are associated with primary chromite concentrations but far higher levels occur in secondary altered lithologies within shear zones.

5.3.2 The geographical and lithological distribution of anomalous levels of Ni, Cu, Co, As and Sb

To illustrate the distribution of anomalous levels of Ni, Cu, Co, As and Sb in the complex, threshold values corresponding to the upper 10 and 20 percentile groups were calculated (table 5.3). These were used to define anomalous and highly anomalous concentrations in the same manner as for PGE and Au (section 4.4.3). The geographical distribution of samples falling above these thresholds is shown in figures 5.6 to 5.10 The percentage of samples from each lithological unit containing anomalous concentrations of these elements are shown in figure 5.11.

All five elements show similar distribution patterns which are analogous to those of PGE and Au. Anomalous levels cluster around the disused chromite quarries in the area

Figure 5.6. Distribution of anomalous Ni concentrations.

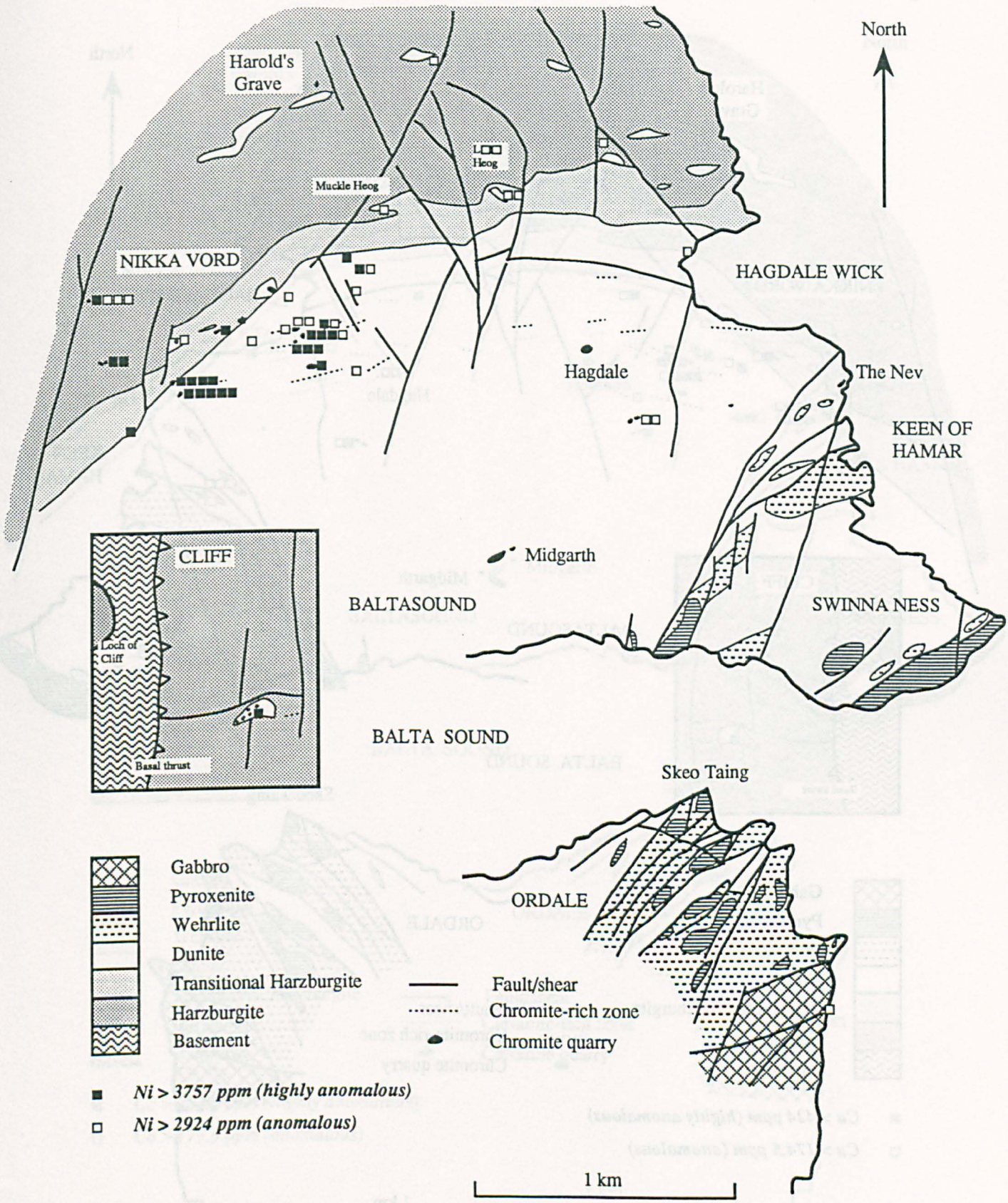

Figure 5.7. Distribution of anomalous Cu concentrations.

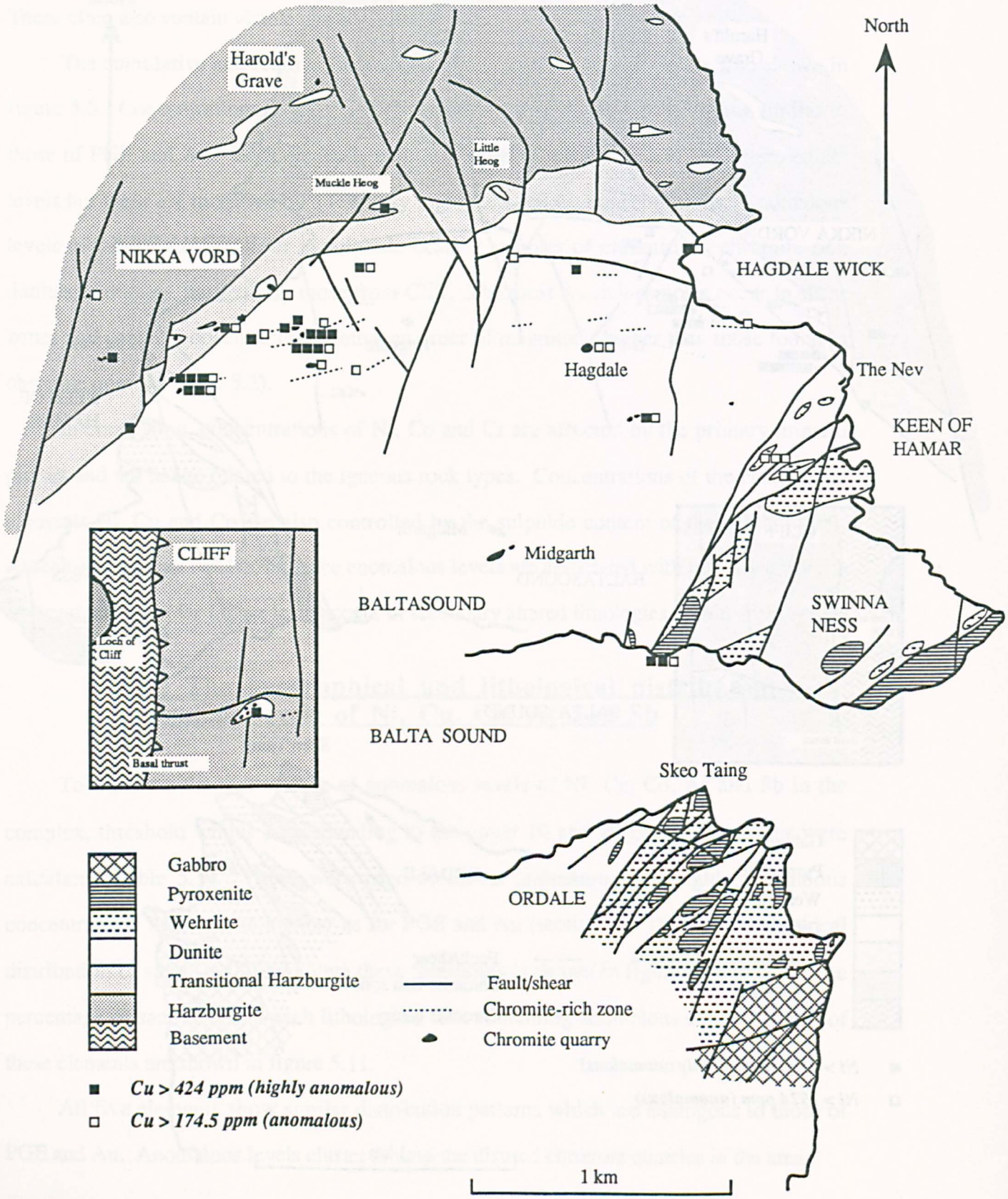

Figure 5.8. Distribution of anomalous Co concentrations.

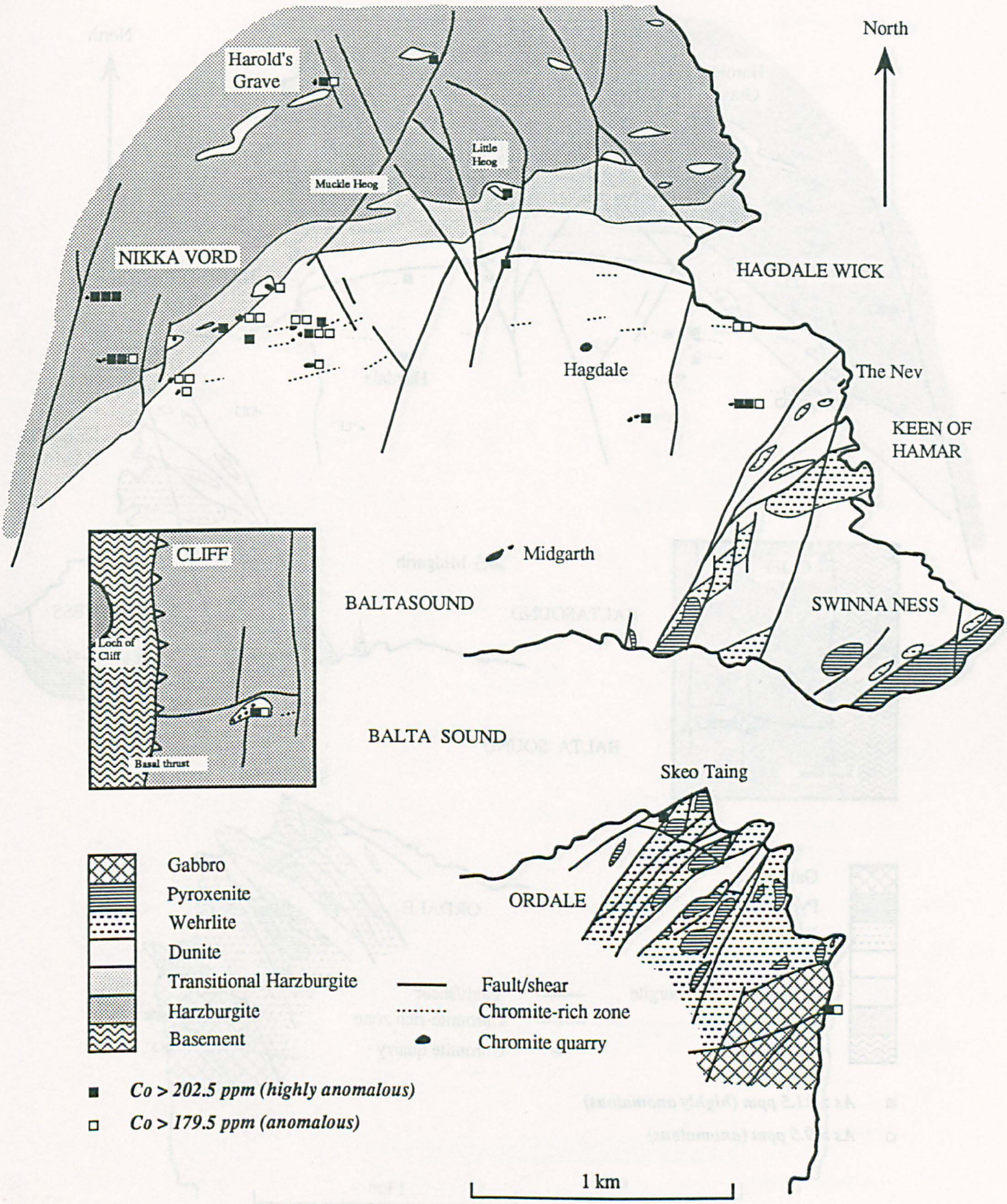

Figure 5.9. Distribution of anomalous As concentrations.

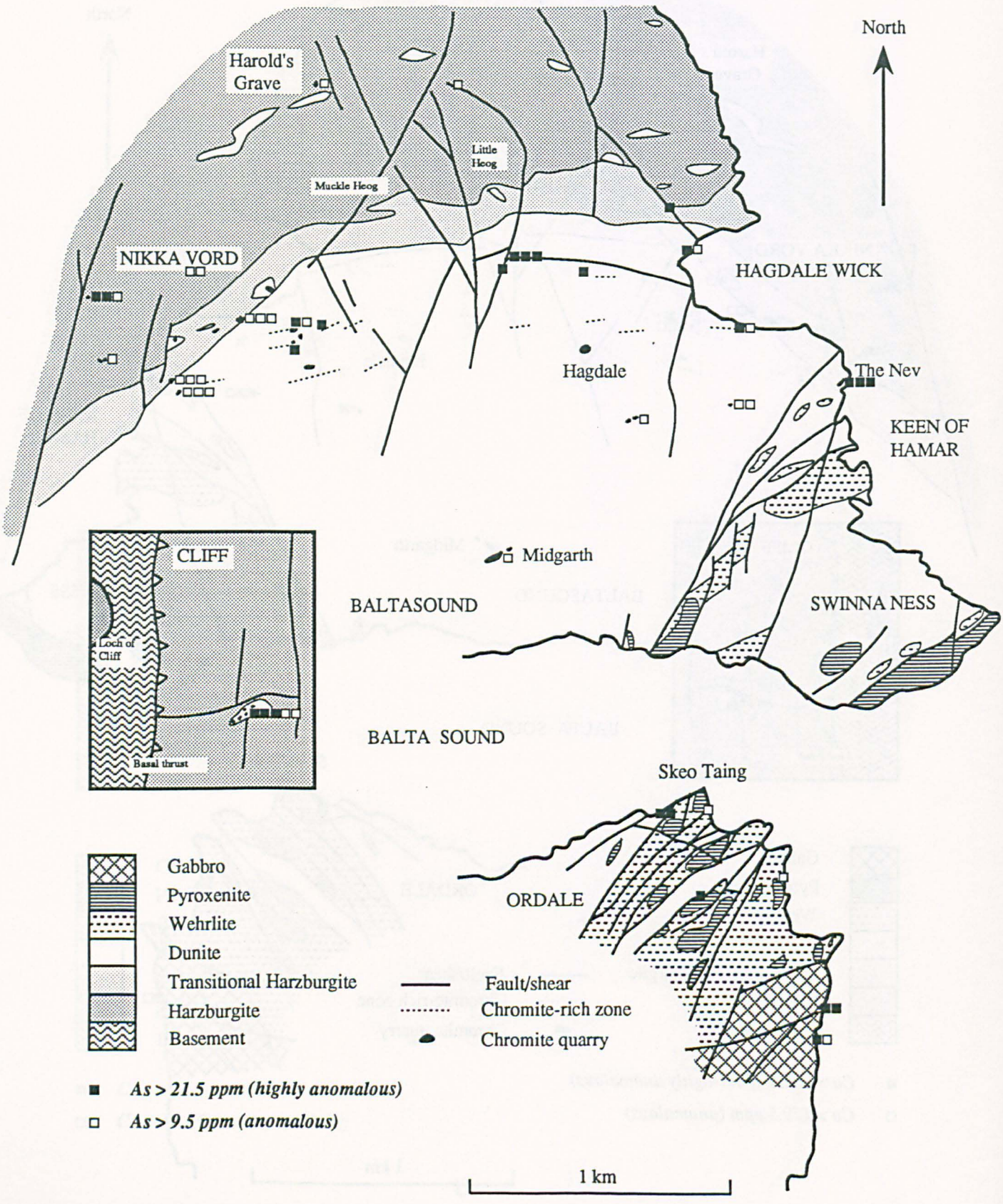

Figure 5.10. Distribution of anomalous Sb concentrations.

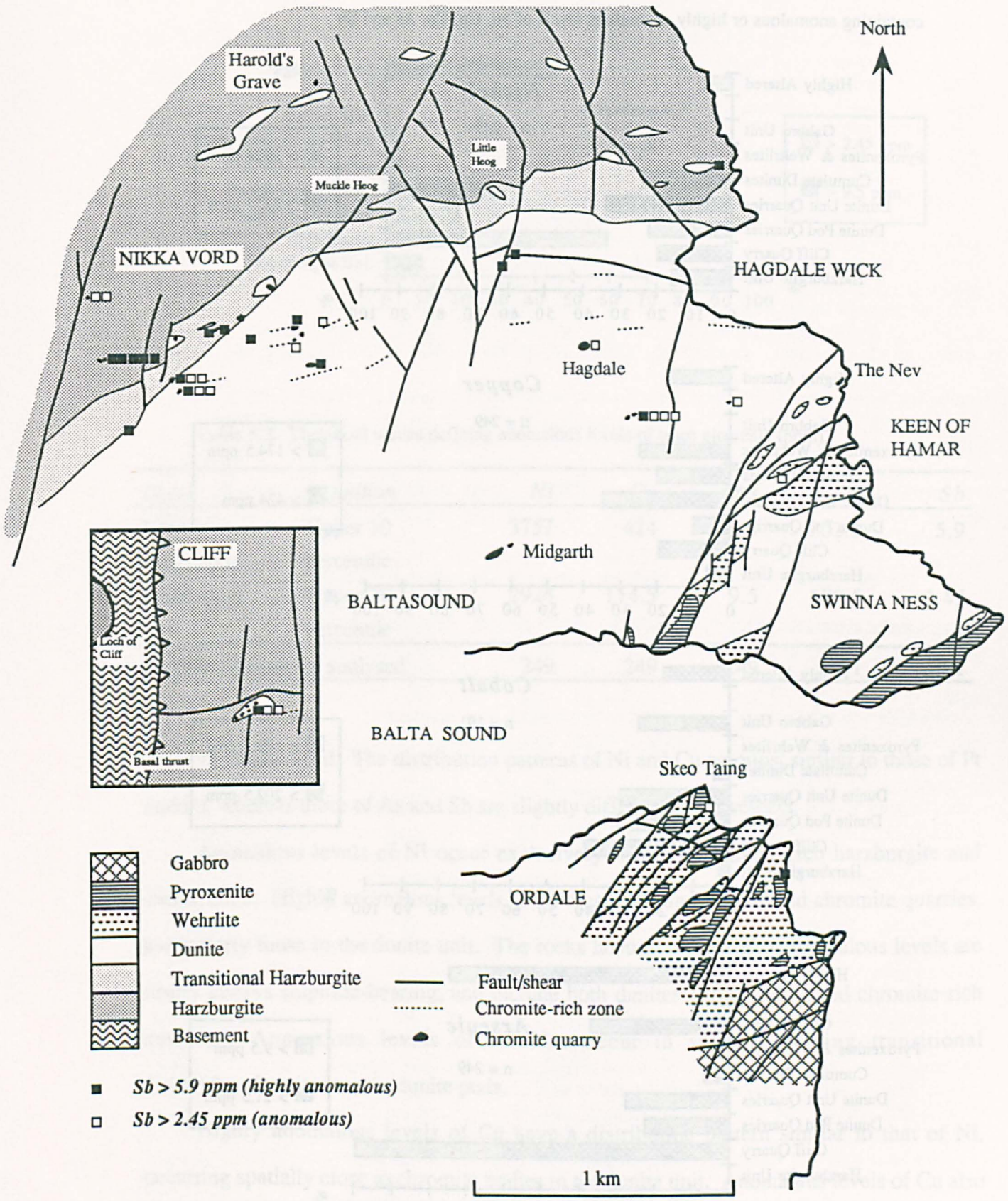

Figure 5.11. Histograms showing the percentage of samples of different lithological units containing anomalous or highly anomalous levels of Ni, Cu, Co, As and Sb

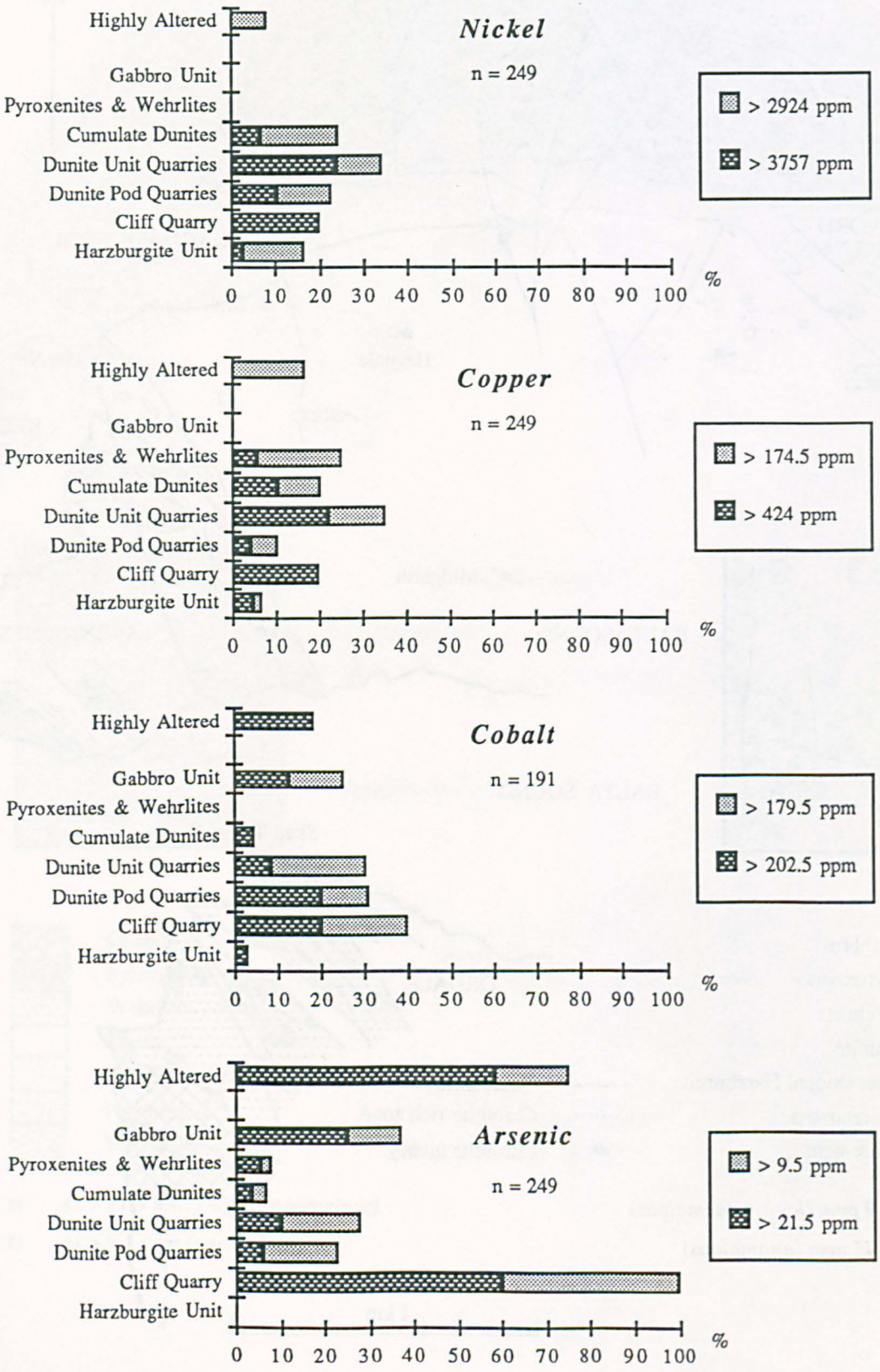

Figure 5.11 (cont.).

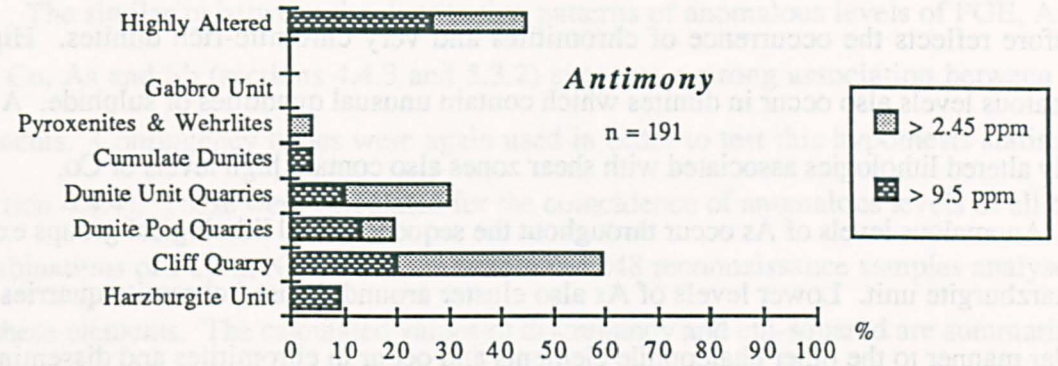

Table 5.3. Threshold values defining anomalous levels of trace elements (ppm).

Level	*Definition*	*Ni*	*Cu*	*As*	*Co*	*Sb*
Highly anomalous	Upper 10 percentile	3757	424	21.5	202.5	5.9
Anomalous	Upper 20 percentile	2924	174.5	9.5	179.5	2.45
Number of samples analysed		249	249	249	191	191

south of Nikka Vord. The distribution patterns of Ni and Cu are most similar to those of Pt and Pd, whereas those of As and Sb are slightly different in this respect.

Anomalous levels of Ni occur exclusively within the olivine-rich harzburgite and dunite units. Highly anomalous levels of Ni cluster around the disused chromite quarries, particularly those in the dunite unit. The rocks hosting these highly anomalous levels are nearly always sulphide-bearing, and include both dunites and disseminated chromite-rich dunites. Anomalous levels of Ni also occur in sulphide-bearing transitional dunites/harzburgites and in dunite pods.

Highly anomalous levels of Cu have a distribution pattern similar to that of Ni, occurring spatially close to chromite bodies in the dunite unit. Anomalous levels of Cu also occur at higher levels in the pyroxene-bearing sequence, however, and are generally absent

from the harzburgite unit. Anomalous levels hosted by pyroxenites and wehrlites occur close to the base of the pyroxene-bearing layered sequence.

Anomalous levels of Co occur mostly in chromite-rich lithologies and their distribution therefore reflects the occurrence of chromitites and very chromite-rich dunites. Highly anomalous levels also occur in dunites which contain unusual quantities of sulphide. A few highly altered lithologies associated with shear zones also contain high levels of Co.

Anomalous levels of As occur throughout the sequence in all lithological groups except the harzburgite unit. Lower levels of As also cluster around disused chromite quarries in a similar manner to the other chalcophile elements and occur in chromitites and disseminated chromite-rich dunites. In contrast, highly anomalous levels of As are most prevalent in samples from the Cliff quarry and in serpentinites and other highly altered lithologies throughout the sequence. These samples generally contain As concentrations one to two orders of magnitude higher than the threshold values calculated for the top 10 and 20 percentile groups (table 5.2).

The distribution pattern of Sb is analogous both to that of As and to that of the other chalcophile elements. Highly anomalous levels cluster around chromite quarries, including the Cliff quarry. Highly anomalous levels of Sb are also common in highly altered lithologies from the dunite and pyroxene-bearing layered sequence.

In conclusion, the distribution of anomalous levels of Ni, Cu, Co, As and Sb shows similarities to that of PGE and Au, in particular the pattern of association with sulphide-bearing chromite-rich lithologies (section 4.4.3). The primary lithological control of Ni, Cu and Co concentrations is indicative of a predominantly igneous distribution in the ophiolite sequence. Moderate levels of As and Sb show a similar pattern but highly anomalous levels occur in association with shear zones and highly altered lithologies. This is indicative of transport and concentration by a secondary fluid during the related alteration of the host rock. Highly anomalous levels of As occur at Cliff, which in other respects is similar to the other chromite quarries, since Cliff also contains highly anomalous levels of PGE, Ni, Cu, Co and Sb.

5.4 Associations of trace elements

The similarity between the distribution patterns of anomalous levels of PGE, Au, Ni, Cu, Co, As and Sb (sections 4.4.3 and 5.3.2) suggests a strong association between these elements. Contingency tables were again used in order to test this hypothesis statistically (section 4.4.4). These were calculated for the coincidence of anomalous levels of all binary combinations of Pt, Pd, Ni, Cu and As within the 248 reconnaissance samples analysed for all these elements. The calculated values of discrepancy and chi-squared are summarised in table 5.4, and indicate a statistically significant positive association between most pairs of elements.

Similar contingency tables have been calculated for the subset of 191 samples analysed for Pt, Pd, Ir, Au, Ni, Cu, Co, As, Sb and Cr (table 5.5). Anomalous levels of each element were again defined as those within the upper 20 percentile of the concentration range. Threshold values for Pt, Pd, Ni, Cu and As were recalculated for this new smaller database (table 5.6).

The associations with all other trace elements have been listed in order of decreasing discrepancy for each of Pt, Pd, Ir and Au (table 5.7). In all cases Pt, Pd, Ir and Au show the strongest association with other precious metals, although differences exist in the order of associations with other trace elements. Ir shows a strong association with the elements indicative of chromite content (i.e. Co and Cr). Pt, Pd and Au show strongest associations with the chalcophile elements indicative of sulphide content (i.e. Ni and Cu) and also with antimony. Certain combinations of trace elements also show strong positive associations (e.g. Co and Cr, Ni and Cu), the result of their common occurrence in particular mineral phases (i.e. chromite and sulphide respectively). This suggests that the associations with PGE and Au have a similar mineralogical significance. In particular, the strong association with Sb indicates that Pt, Pd and Au often occur as antimonides in this environment. This has been confirmed by recent mineralogical studies of material from the area around Balta Sound (see section 5.7). Differences in the order of trace element associations may indicate differences in the dominant mineralogy of each platinum-group element.

Table 5.4. Summary table of the associations of Pt, Pd, Ni, Cu and As in 248 samples at the anomalous levels defined in table 5.3.

	Pt	Pd	Ni	Cu	As
Pt	XXXXX	**32.5**	**14.5**	**15.5**	**7.1**
Pd	*160*	XXXXX	**18.9**	**13.9**	**6.5***
Ni	*31.9*	*55.7*	XXXXX	**20.9**	[3.5]
Cu	*36.4*	*30.2*	*68.1*	XXXXX	[1.5]
As	*7.4*	*6.4**	*1.9*	*0.3*	XXXXX

Chi-squared values (italic) **Discrepancy values (bold)**

A discrepancy value greater than one indicates a positive association between elements.
A value of chi-squared greater than 6.635 indicates that the null hypothesis "the observed discrepancy is due to sampling fluctuation" is rejected at the 95 % confidence level.
**A value of chi-squared greater than 3.841 indicates that the null hypothesis is rejected at the 95 % confidence level.*
Non-significant discrepancy values are shown in brackets.

Table 5.5. Summary table of the associations of Pt, Pd, Ir, Au, Ni, Cu, Co, Cr, As and Sb in 191 samples at the anomalous levels defined in table 5.6.

	Pt	Pd	Ir	Au	Ni	Cu	Co	As	Sb	Cr
Pt	XXX	**23.4**	**15.4**	**13.0**	**11.6**	**8.6**	**8.8**	**7.0**	**11.8**	**8.6**
Pd	*113.4*	XXX	**9.1**	**14.6**	**15.2**	**12.2**	**6.4**	**7.6**	**10.4**	**5.2***
Ir	*71.9*	*24.3*	XXX	**5.5**	[2.2]	[2.2]	**6.4**	[3.5]	**4.4***	**4.2***
Au	*37.2*	*45.2*	*9.3*	XXX	**10.8**	**11.8**	[3]	**5.2***	**13.0**	[2.8]
Ni	*28.5*	*47.0*	*1.5*	*25.2*	XXX	**15.4**	[1.6]	[1.8]	**10.6**	[2.4]
Cu	*15.7*	*30.3*	*1.5*	*30.1*	*49.1*	XXX	[1.6]	[1.8]	**9.6**	[1.4]
Co	*16.7*	*8.6*	*12.3*	*2.0*	*0.6*	*0.6*	XXX	[4]	[3.8]	**18.6**
As	*10.8*	*12.3*	*3.8*	*6.1*	*0.7*	*0.7*	*3.6*	XXX	**7.0**	[3.8]
Sb	*30.0*	*22.5*	*5.8*	*37.2*	*23.8*	*19.5*	*3.2*	*10.8*	XXX	[3.6]
Cr	*15.7*	*5.6*	*5.3*	*1.7*	*1.2*	*0.4*	*73.1*	*3.2*	*2.8*	XXX

Table 5.6. Concentration thresholds defining anomalous levels of Pt, Pd, Ir, Au, Ni, Cu, Co, Cr, As and Sb within the subset of 191 samples.

Element	*Pt*	*Pd*	*Ir*	*Au*
Threshold (ppb)	60	35	≥ 20	19.5

Element	*Ni*	*Cu*	*Co*	*As*	*Sb*	*Cr*
Threshold (ppm)	2822	100	179.5	10.5	2.45	149471

Table 5.7. Ranked summary table of the association of Pt, Pd, Ir and Au with other trace elements.

Element	*Associated elements (listed in order of decreasing discrepancy value)*
Pt	Pd, Ir, Au, Sb*, Ni*, Co*, Cu* & Cr*, As*.
Pd	Pt, Ni*, Au, Cu*, Sb*, Ir, As*, Co*, Cr*.
Ir	Pt, Pd, Co*, Au, Sb*, Cr*.
Au	Pd, Pt & Sb*, Cu*, Ni*, Ir, (As)*

* Potential pathfinder elements
(As) indicates null hypothesis only rejected at 95% confidence level.

5.5 Element ratios and pathfinders

A consequence of the strong positive association between PGE and other trace elements is that these elements form potential pathfinders for the precious metals. For example, if platinum occurred exclusively as sperrylite ($PtAs_2$) and no other As-bearing phases were present, As and Pt would show a constant ratio in mineralised samples. Alternatively, if sperrylite was again the only platinum-bearing phase and occurred together with a variety of As-rich phases, then areas or samples containing anomalous levels of As might identify areas or samples containing anomalous Pt concentrations. These examples indicate the type of information on the occurrence or origin of mineralisation which can be inferred from the relationship with pathfinder elements. The assumptions used in the examples given above also indicate the difficulties of pathfinder analysis for the type of mineralisation described in this study, due to its complex mineralogy (section 1.5.3) and the mutual association of a large number of elements, some of which occur in several different phases (section 5.4).

The following section considers the graphical relationships between Pt, Pd, Ir, Au, Ni, Cu, Co, As, Sb and Cr concentrations within the database of 191 samples analysed for all of these elements.

5.5.1 PGE and Au ratios

The mutual association of Pt, Pd, Ir and Au is in most cases stronger than the associations with other trace elements (table 5.7). This is indicated by higher positive values of discrepancy coefficients between combinations of Pt, Pd, Ir and Au (table 5.5). Graphical comparisons between these elements are shown in figure 5.12. In each graph samples from Cliff (open squares) and Harold's Grave (open circles) are distinguished from the other samples (closed circles). In all cases undetected concentrations (i.e. < 20 ppb) plot along the axes (= 1 ppb)

Platinum and palladium concentrations follow a simple linear relationship. The majority of samples have Pt/Pd ratios between 0.25 and 3. Samples from Harold's Grave

(open circles) form a distinct field outside this range with Pt/Pd ratios greater than 3. Samples from Cliff (open squares) lie within the range of the other samples with one exception. This sample (RLM086) is enriched in Pd with respect to other samples from Cliff and, significantly, also contains the overall highest concentrations of Pt and Pd.

Graphs of Ir against Pt and Ir against Pd both show similar patterns. Most data points follow a linear relationship with Pt/Ir ratios between 1 and 10 and Pd/Ir ratios between 2 and 12. In contrast samples from Harold's Grave have Pt/Ir and Pd/Ir ratios less than one and occupy a separate field. They are also significantly enriched in Ir compared to the main field of samples (excluding Cliff). Certain other samples show similar Ir enrichment, including RLM003. Like the Harold's Grave samples this is also a chromitite from a pod within the harzburgite unit (Nikka Vord South Quarry).

Comparisons of Au against Pt, Pd and Ir all generate similar patterns. Au concentrations are apparently independent of the Ir, Pt or Pd concentrations. Consequently many samples contain concentrations of only one element or the other and plot along the axes of these graphs. Sample RLM086 is again anomalous, since it has higher Au/Pt and Au/Ir ratios than the other samples from Cliff. This is consistent with the selective enrichment of Au and to a lesser extent Pd.

In conclusion, most mineralised samples show a weak linear dependence between Pt, Pd and Ir, although ratios of these elements vary widely between individual samples. This is consistent with mineralogical evidence since PGM often contain more than one PGE and usually several PGM occur together. Chromitites from Harold's Grave and some other chromite-rich samples exhibit different PGE ratios and are relatively more enriched in Ir. This indicates that Ir-rich mineralisation of the type found at this locality is distinct and the behaviour of this element is significantly different from that of Pt and Pd. Samples from Cliff usually show similar PGE ratios to other mineralised samples from north of Baltasound but are distinguished by much higher absolute levels of PGE. The exception contains the highest overall levels of PGE. The ratios of individual PGE indicate that this sample is

Figure 5.12. Graphical comparisons of Pt, Pd, Ir and Au analyses.

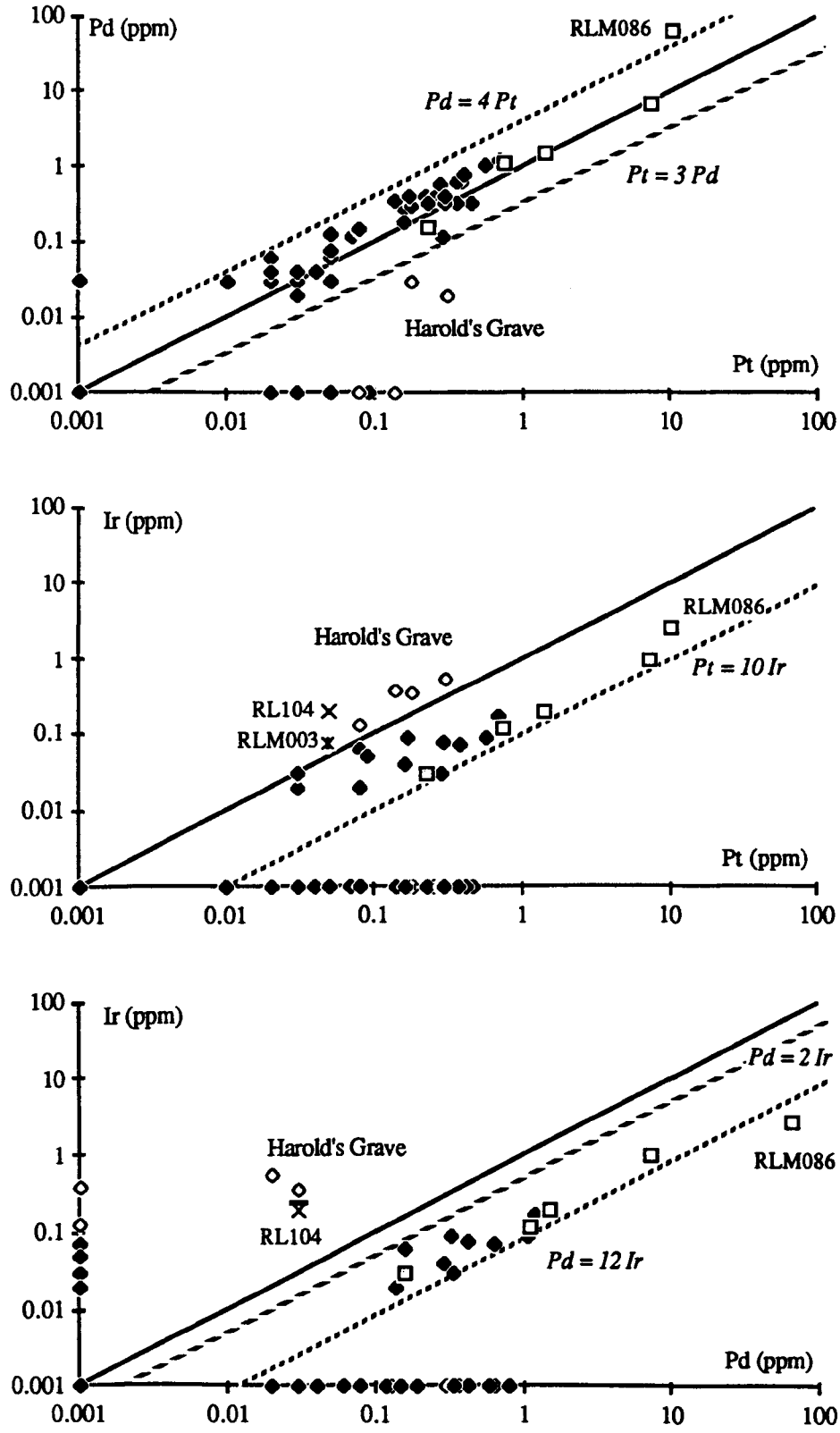

Figure 5.12 (cont.).

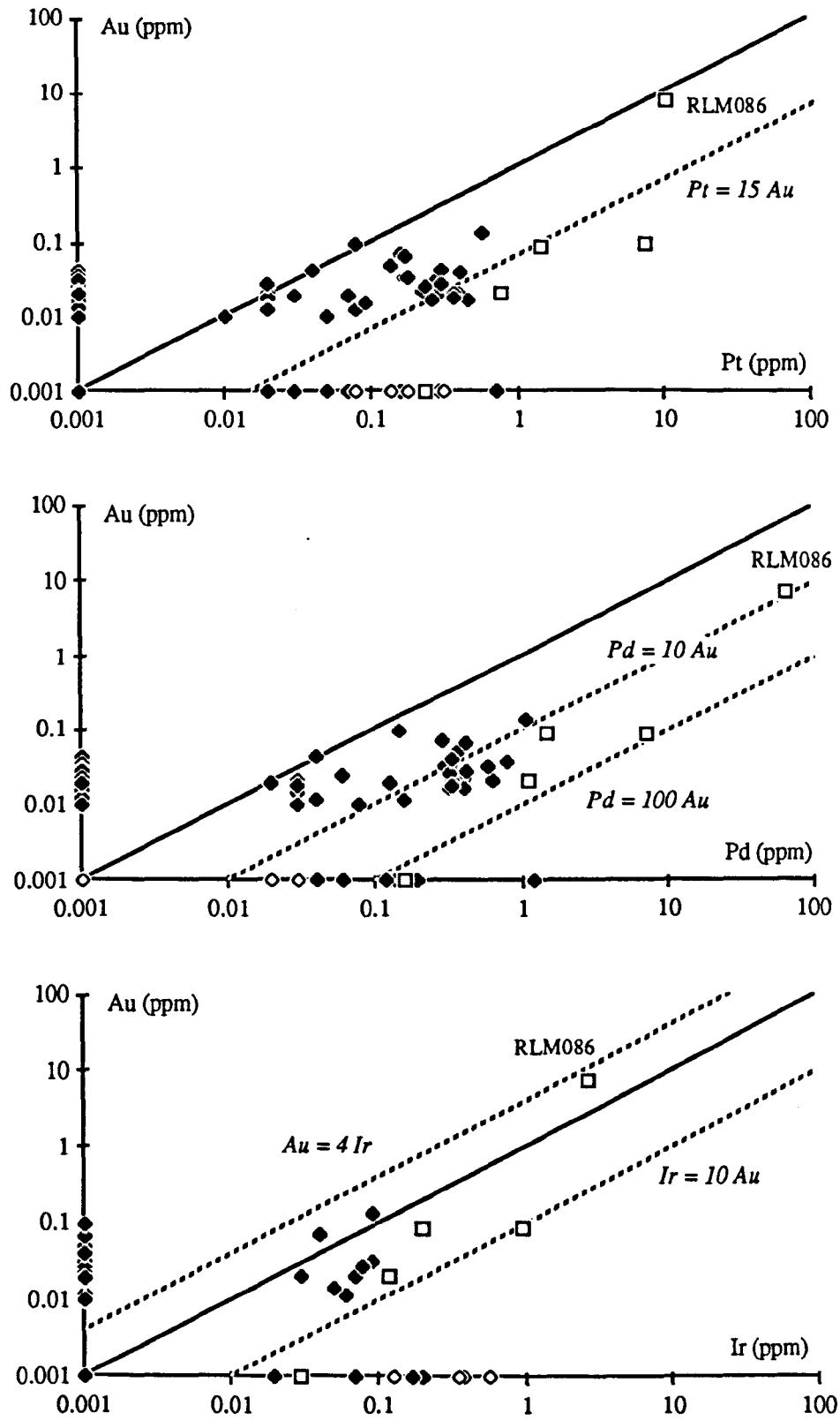

enriched in Pd and to a greater extent Au. This disseminated chromite-rich dunite was selected as the best example of the unusual green serpentinite matrix found at Cliff (section 4.2.1). This indicates that the possibility of secondary remobilisation of PGE at this locality cannot be ignored.

5.5.2 Trace element ratios

Statistical analysis revealed strong positive associations between certain pairs of trace elements (table 5.7). Of all such combinations Cr and Co showed the highest discrepancy value. Graphical comparisons of the concentrations of these elements (figure 5.4) indicates a strong positive correlation for samples containing high levels of chromium. This is probably due to the substitution of Co in chromite. Certain other low chromium samples also contain anomalous levels of Co, which is attributed to the Co content of some sulphide-phases.

A strong association was also noted between anomalous levels of Ni and Cu. High concentrations of these chalcophile elements are indicative of significant accessory sulphide contents. Many sulphide-bearing samples which contain high levels of nickel also contain high levels of copper, although no linear correlation is apparent and hence Ni/Cu ratios are not constant (figure 5.13a). Most samples have Ni/Cu ratios greater than 5. The relationship between sulphide content and nickel concentration is complicated by the substitution of Ni in olivine, reaching approximately 3500 ppm in whole rock analyses of dunites (section 5.3.1). This would increase the overall Ni/Cu ratio, and has greatest effect in olivine-rich, sulphide-poor specimens.

A graphical comparison between As and Sb concentrations (figure 5.13b) clearly shows the anomalousness of the higher As concentrations. These are found in samples from the Cliff quarry, serpentinites and other highly altered lithologies. These As-rich samples often also contain anomalously high levels of Sb, although a linear relationship between the two elements is not apparent. The majority of samples plot within the field defined by As < 60 ppm and Sb < 15 ppm.

Figure 5.13. Graphical comparisons between trace elements.

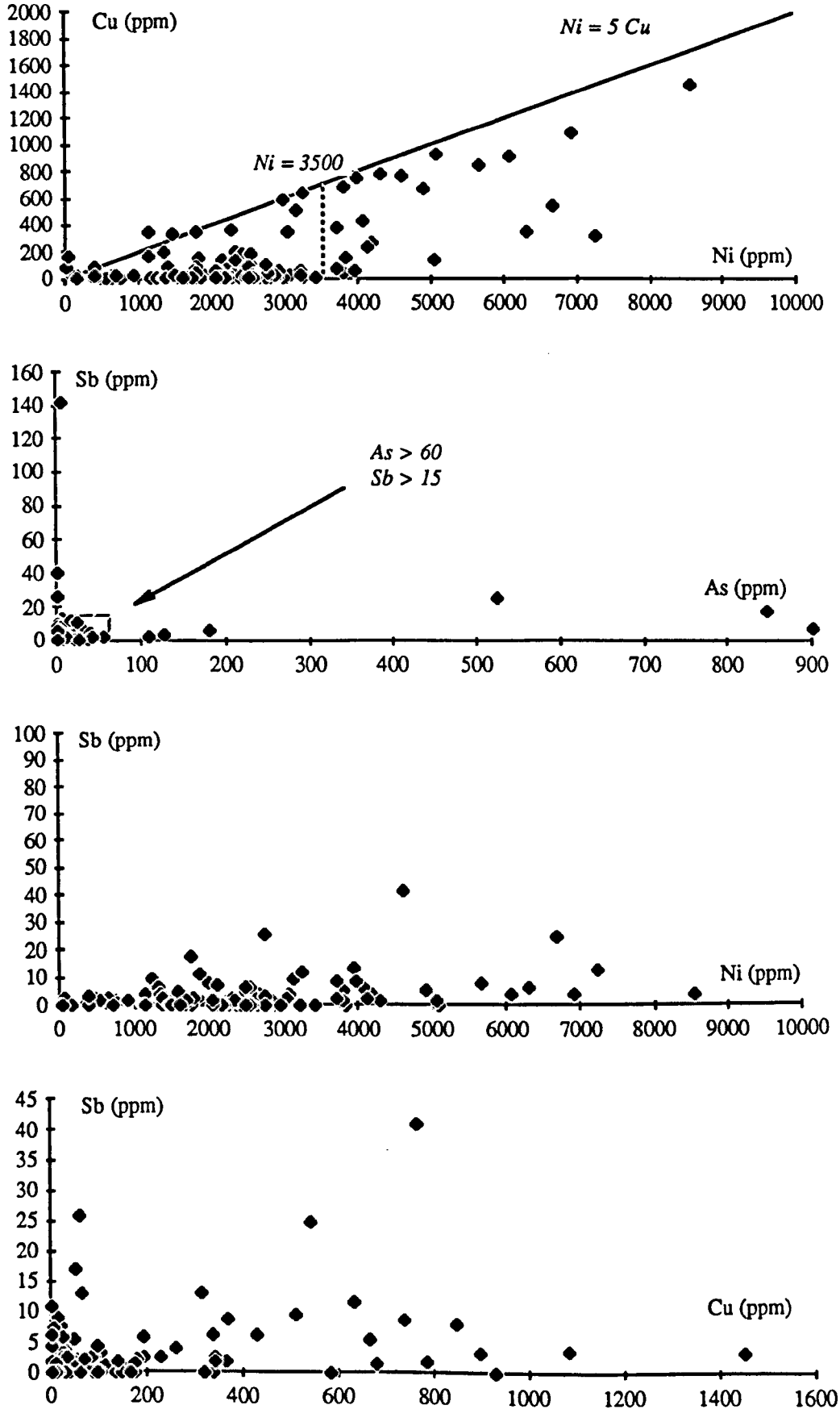

Calculations also suggested an association between Sb and both Ni and Cu. No obvious correlation exists between these two pairs of elements (figure 5.13c and d), although most samples containing high levels of Cu or Ni also contain significant levels of Sb.

5.5.3 Ratios between trace elements and PGE or Au concentrations

It has been suggested earlier that if constant ratios exist between Pt, Pd, Ir or Au and particular trace elements they might form useful pathfinders for PGE which could replace direct analysis. In figures 5.14 to 5.17 Pt, Pd, Ir and Au have each been plotted against Ni, Cu, Co, Cr, As and Sb. In view of the higher levels of PGE, As and Sb in samples from Cliff, compared with mineralised samples from other areas, these have been identified on each graph (open squares).

No element shows a clear linear correlation with Pt, Pd, Ir or Au for all mineralised samples. In all cases the bulk of the data points, samples from the area north of Baltasound, show a grouped distribution over a wide range of concentrations. Samples from Cliff are distinguished in each graph by their generally higher levels of PGE and Au. Differences in the form of these data fields divide the elements into three groups, namely the chalcophile elements (Ni and Cu), the two elements found in chromite (Cr and Co) and lastly the two PGM forming elements (As and Sb). The relation with Ir is also distinct from that of Pt, Pd or Au in several cases.

Levels of Ni and Cu are generally higher in samples containing detected Pt, Pd or Au, compared to samples in which PGE were not detected (points plotting on vertical axes). Within the field of data from around Balta Sound there is in each case an overall increase in the concentration of the pathfinder element in the more PGE-rich samples. Although samples from Cliff contain elevated levels of PGE the Ni and Cu contents do not increase in proportion and are within the range of other mineralised samples. No obvious relation between Ir and Ni or Cu occurs in either data set. These findings are consistent with the observed association of anomalous Pt, Pd and Au concentrations with higher levels of chalcophile elements (section 5.4). The lack of a reasonable correlation and the scatter

Figure 5.14. Nickel concentrations as an indication of Pt, Pd, Ir and Au contents.

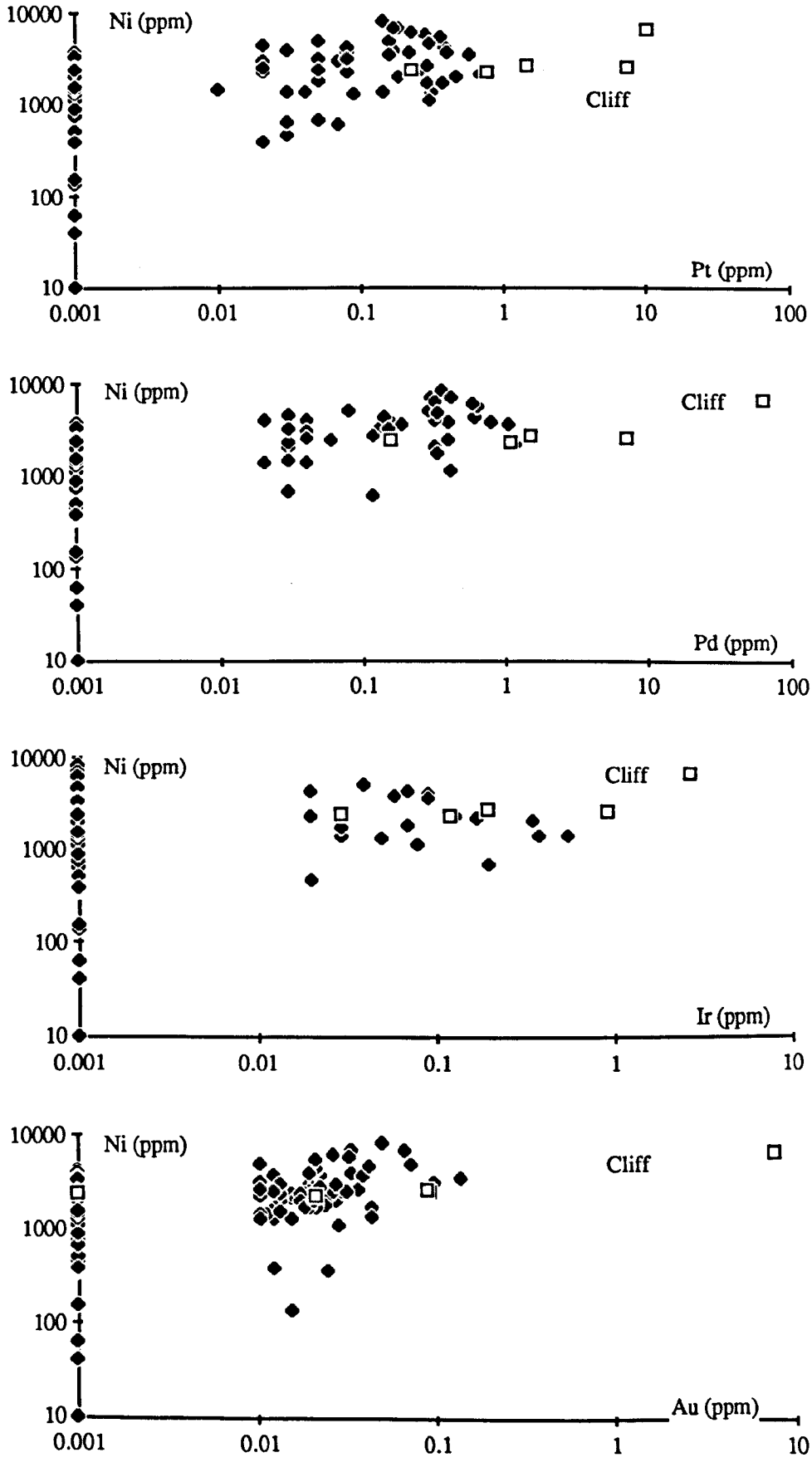

Figure 5.15. Copper concentrations as an indication of Pt, Pd, Ir and Au contents.

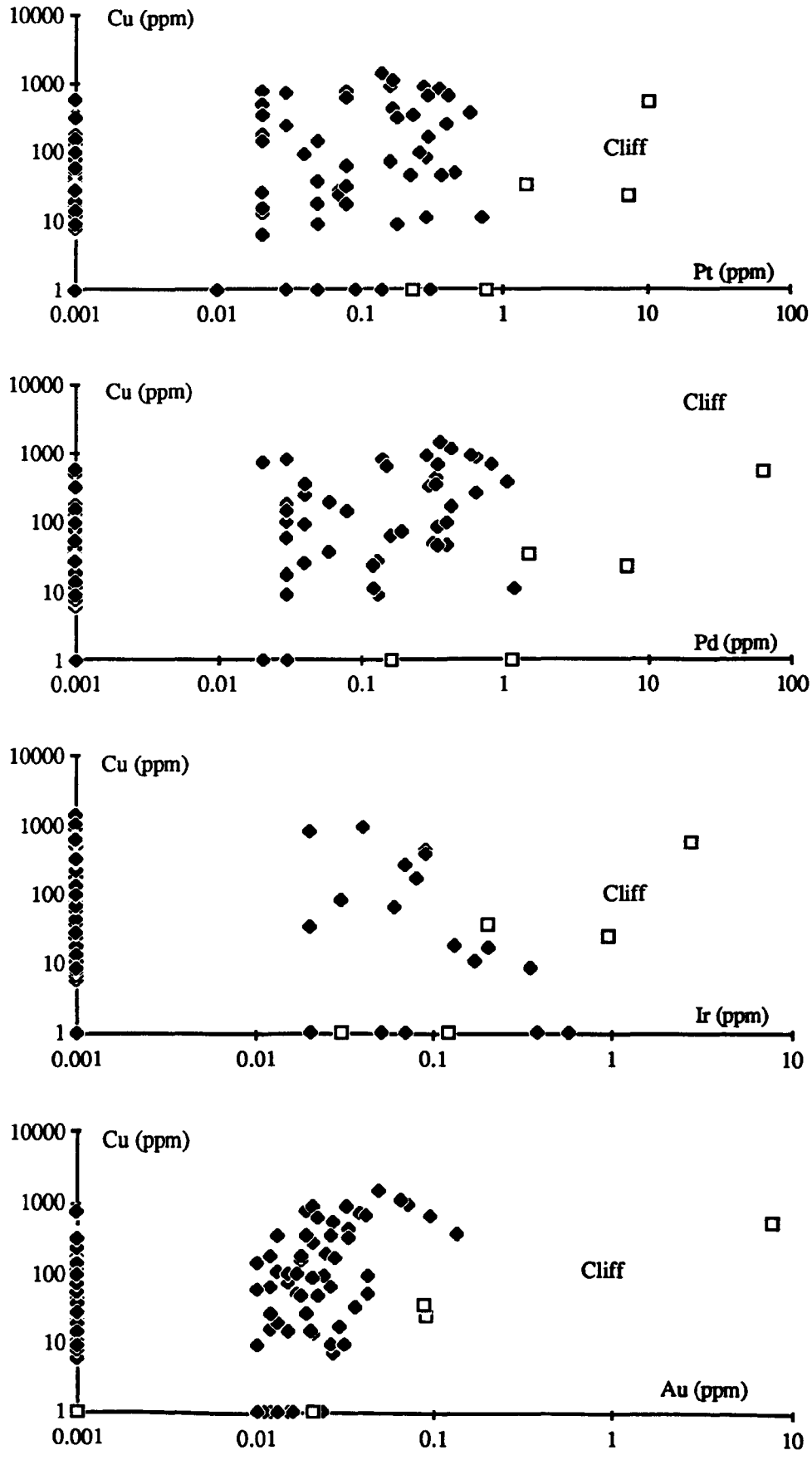

Figure 5.16. Cobalt concentrations as an indication of Pt, Pd, Ir and Au contents.

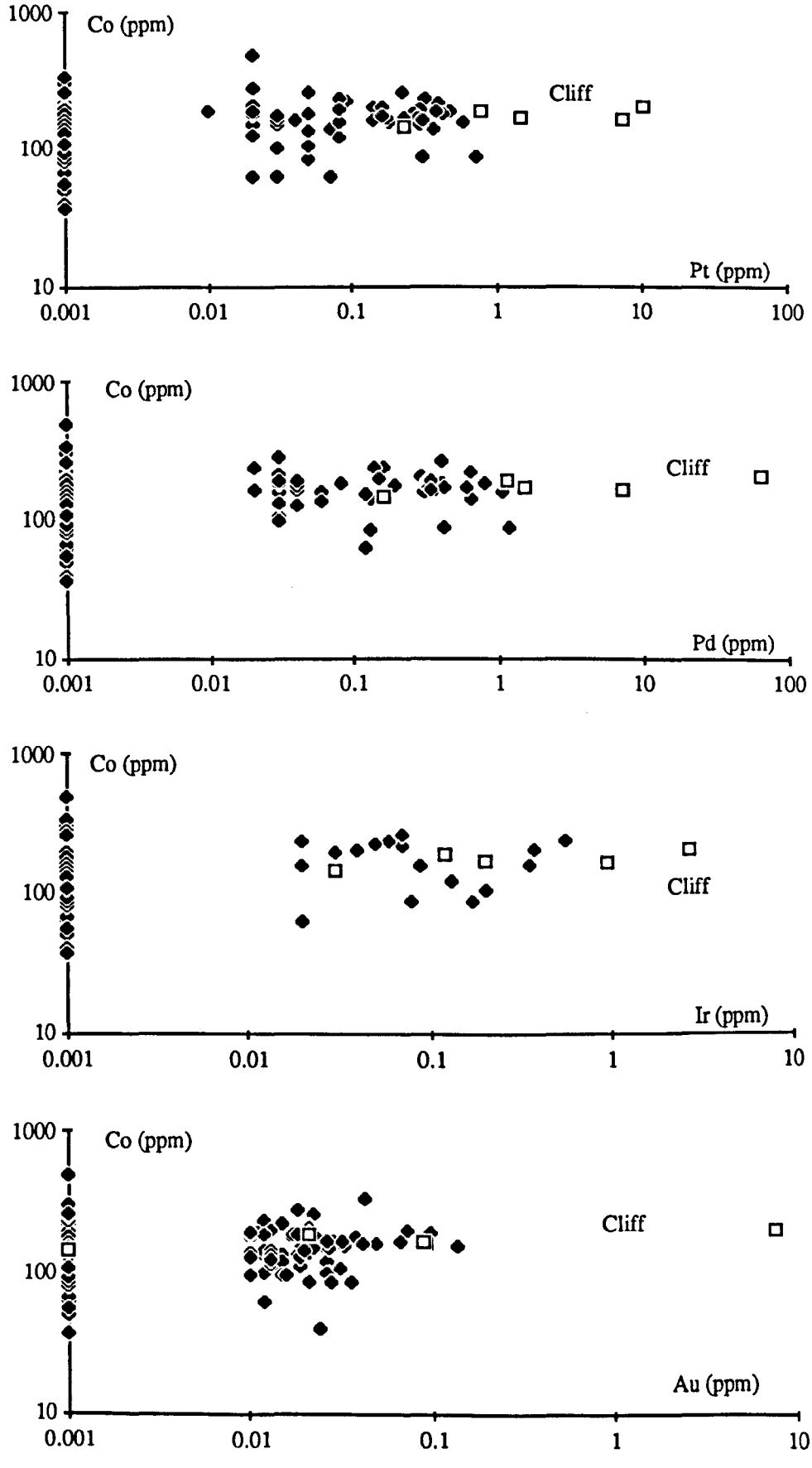

Figure 5.17. Chromium concentrations as an indication of Pt, Pd, Ir and Au contents.

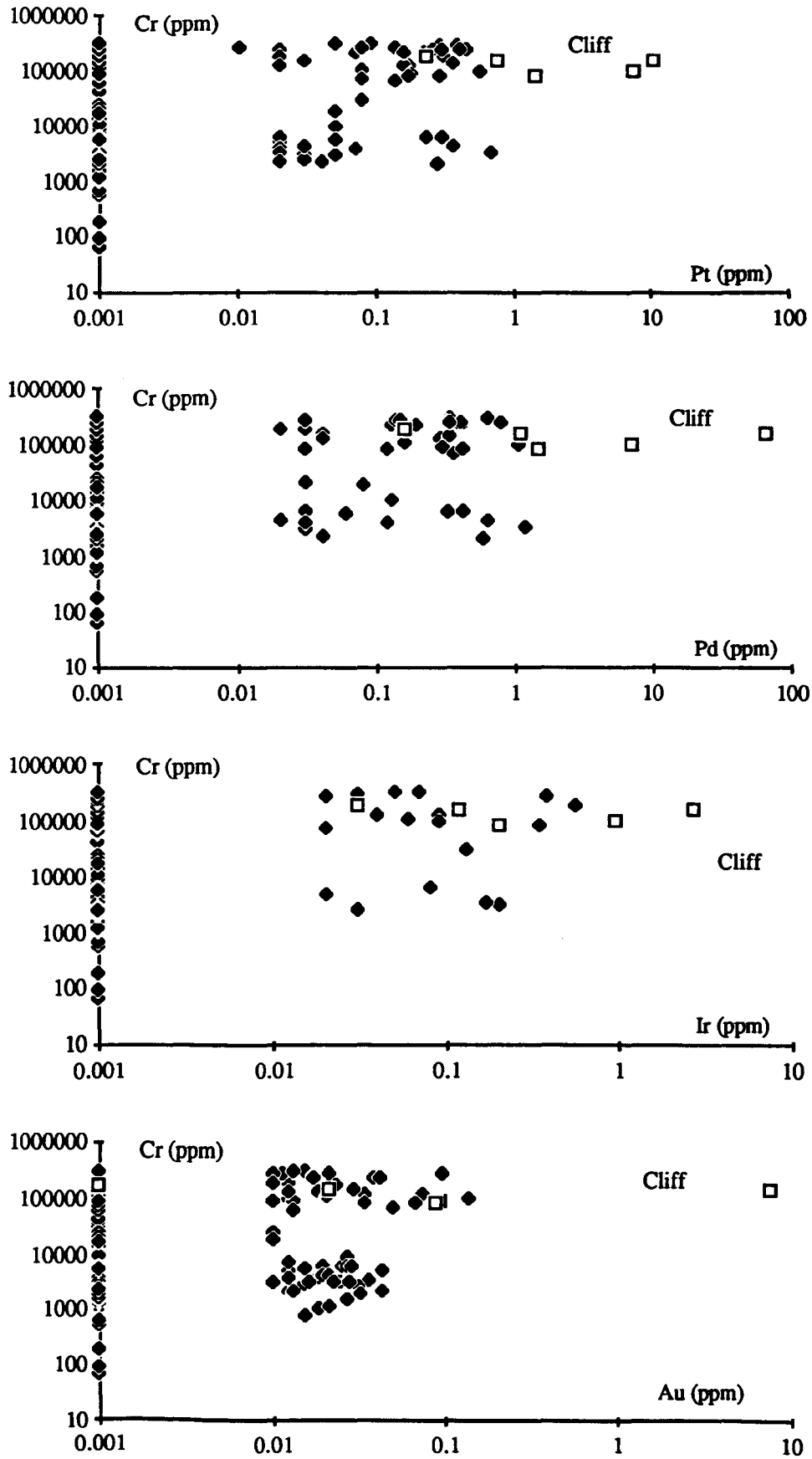

Figure 5.18. Arsenic concentrations as an indication of Pt, Pd, Ir and Au contents.

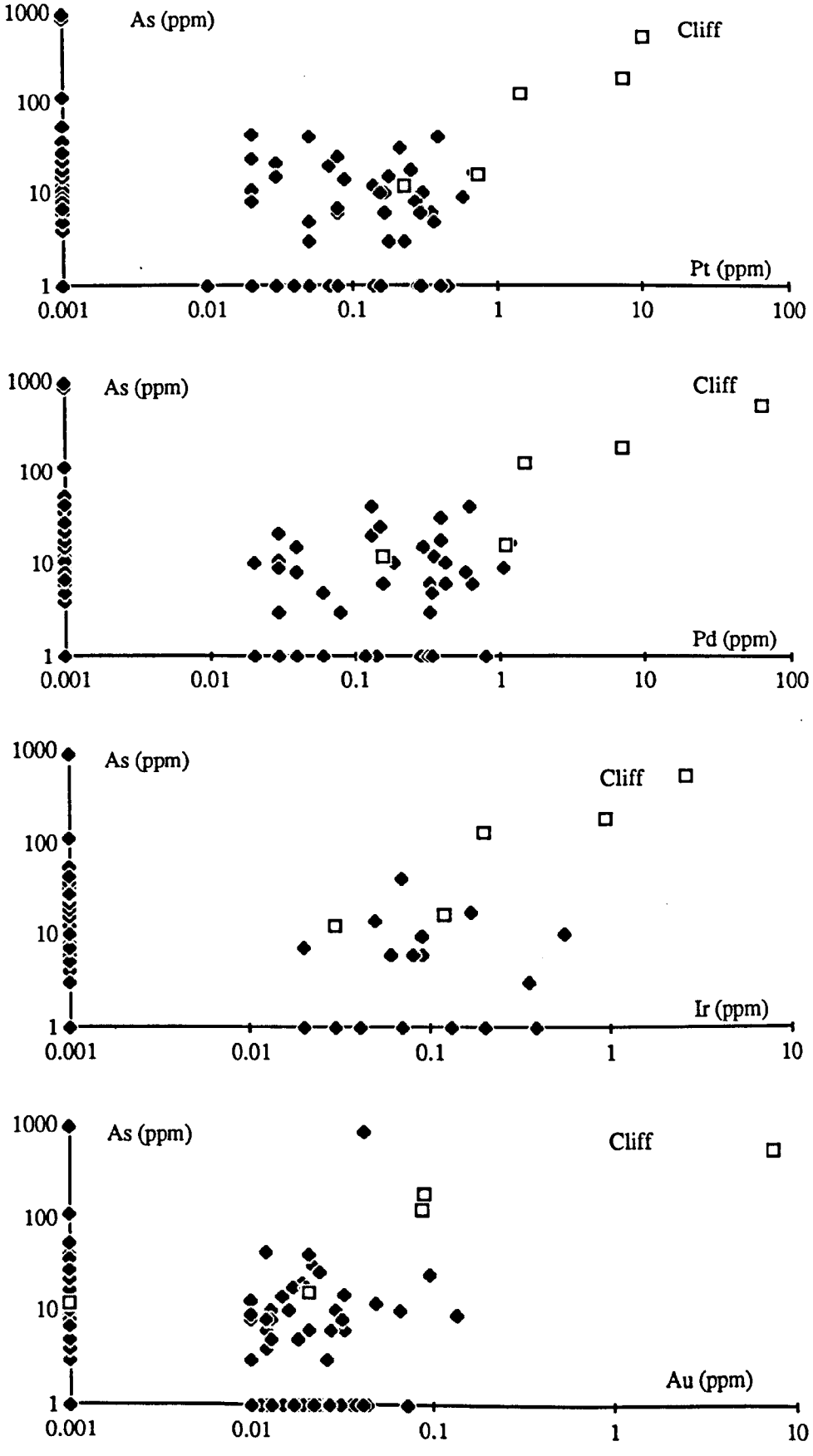

Figure 5.19. Antimony concentrations as an indication of Pt, Pd, Ir and Au contents.

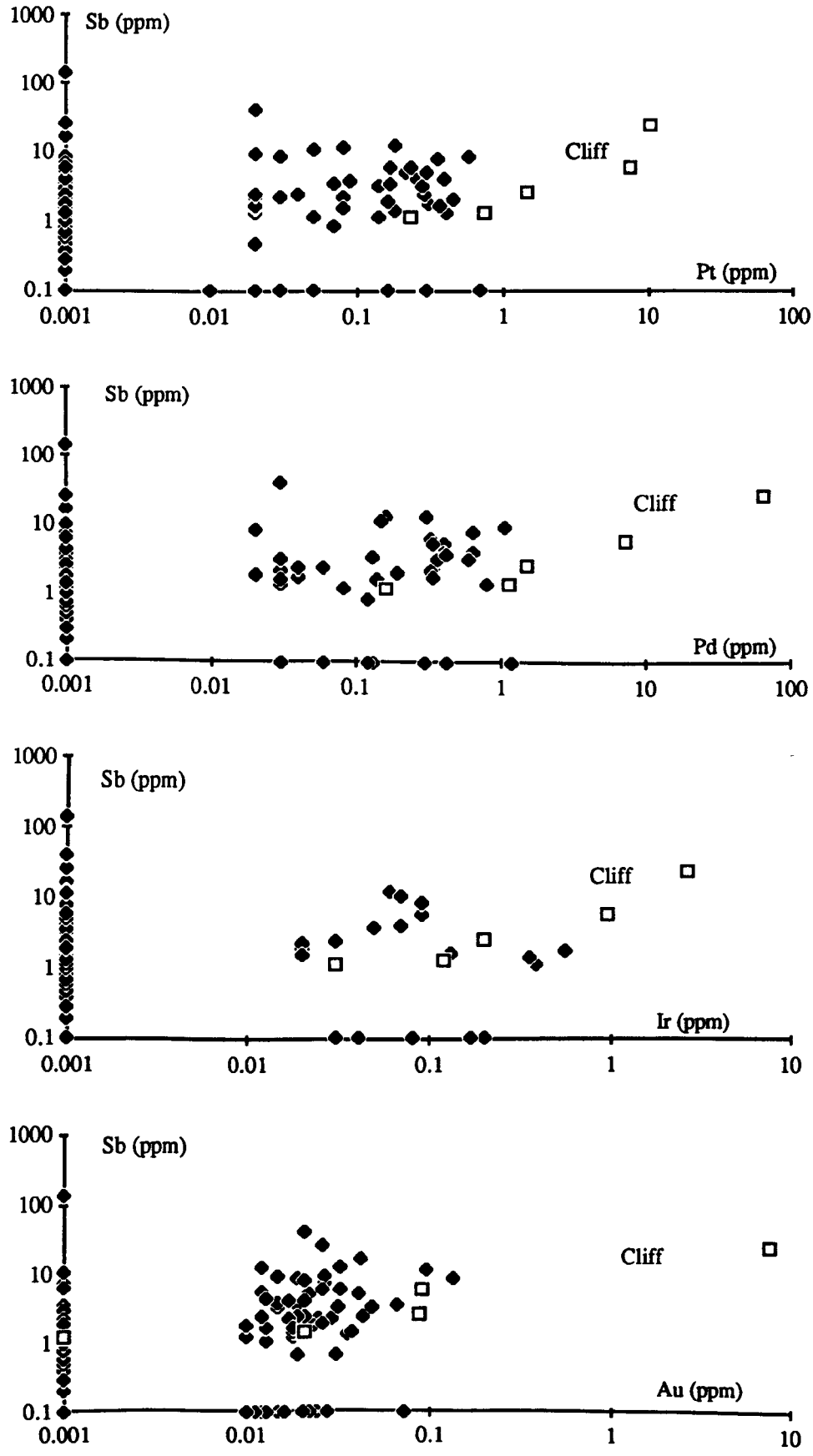

within the data fields imply that levels of Ni and Cu would not be a reliable indication of the absolute PGE contents of samples.

Levels of Co and Cr are invariant over the range of Pt, Pd, Ir and Au concentrations. This is shown by the horizontal arrays of data points (figures 5.16 and 5.17). Comparisons between the range of concentrations in samples with and without PGE indicate that mineralised rocks generally contain moderate to high levels of Cr (i.e. dunites and chromite-rich dunites). This pattern is particularly noticeable for Ir, which is only found in chromite-bearing rocks (section 4.5.1).

No correlation is seen between levels of PGE and As or Sb concentrations in samples from the area around Balta Sound (figures 5.18 and 5.19). These form a horizontal group of data points (closed circles) at low or moderate levels of As and Sb compared to the overall range (vertical axes). This is illustrated by the large numbers of PGE-bearing samples containing undetected levels of As or Sb (plotting along horizontal axes). In sharp contrast samples from Cliff show a good linear dependence between PGE or Au levels and concentrations of As and Sb. Rocks containing higher levels of Pt, Pd, Ir and Au contain progressively higher levels of As and Sb. The combination of higher Pt, Pd, Ir, Au, As and Sb concentrations effectively discriminates between the mineralisation at Cliff and that elsewhere in the study area.

5.5.4 Conclusions

The investigation of inter-elemental ratios described above indicates that no suitable pathfinder elements exist which might be analysed as a substitute for the direct analysis of PGE. Although anomalous levels of PGE are associated with sulphide phases and with anomalous levels of Ni or Cu, only a weak linear dependence is observed between the precious metals and the chalcophile elements. The complex relationship between sulphides and chalcophile element concentrations is considered in the next section.

Consideration of the inter-element ratios has also suggested certain differences between the associations of elements in different areas. The different PGE ratios in mineralisation from the Harold's Grave and Cliff areas are known to correspond to differences in the mineralogical assemblage and its paragenesis (section 1.5.3). By analogy,

the strong geochemical association between elevated Pt, Pd, As and Sb concentrations at Cliff and the virtual absence of this association elsewhere in the complex, indicates that the well documented Cliff mineralogical assemblage may not be representative of all the other Pt-, Pd-rich mineralisation in the ophiolite complex. Mineralogical studies of samples from the extensive new PGE concentrations located in this study are summarised in section 5.7 The different geochemical association at Cliff and its bearing on the genesis of the mineralisation at this locality is also the subject of a later section (section 5.8).

5.6 Sulphur and chalcophile element concentrations as an indication of sulphide content

A small subset of samples were analysed for sulphur (section 5.2.3), in order to establish the connection between sulphides and chalcophile elements. Field observations indicated that anomalous levels of Ni and Cu occurred in samples containing visible sulphide phases.

The sulphur analyses are listed in order of magnitude for each rock category (table 5.8). This compensates for variations in Ni threshold levels between different lithological groups due to their variable olivine contents. Dunites, chromitites and chromite-rich dunites all show a general increase in Ni and Cu levels with increasing sulphur concentrations.

Graphically both Ni and Cu show statistically significant correlations with sulphur and also a strong mutual correlation (figure 5.20). The graph of Ni against sulphur indicates that samples other than chromitites (circles), dunites (black squares) and chromite-rich dunites (triangles), contain less Ni at the same levels of sulphur. These other lithologies (open squares) are mostly pyroxene-bearing cumulates but also include a serpentinite and a transitional harzburgite. This is consistent both with the lower olivine content of the pyroxene-rich samples and with the possibly lower Ni tenor of olivine and sulphide phases at higher stratigraphic levels. Sample RLM003, a chromitite from the Cliff quarry, also shows an anomalously low Ni content considering its sulphide tenor. In figure 5.20 b these samples have been excluded from the regression analysis, which gives a better correlation with a higher coefficient and an intercept (2556 ppm Ni) which is consistent with the

Figure 5.20. Correlations between chalcophile element concentrations and sulphur contents.

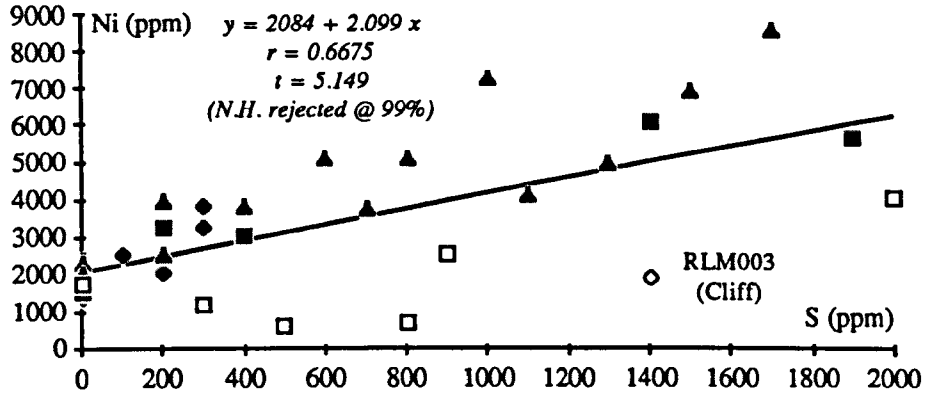

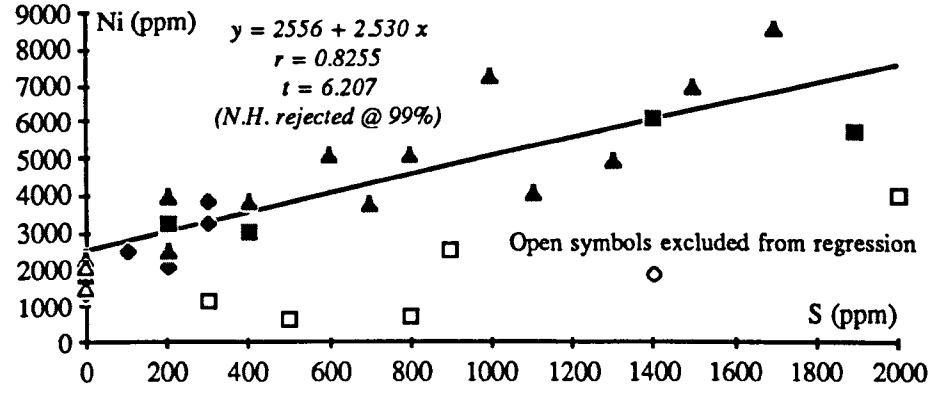

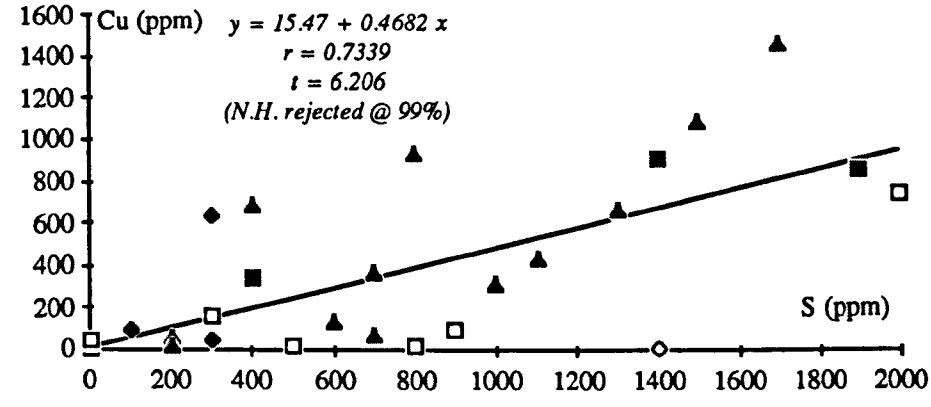

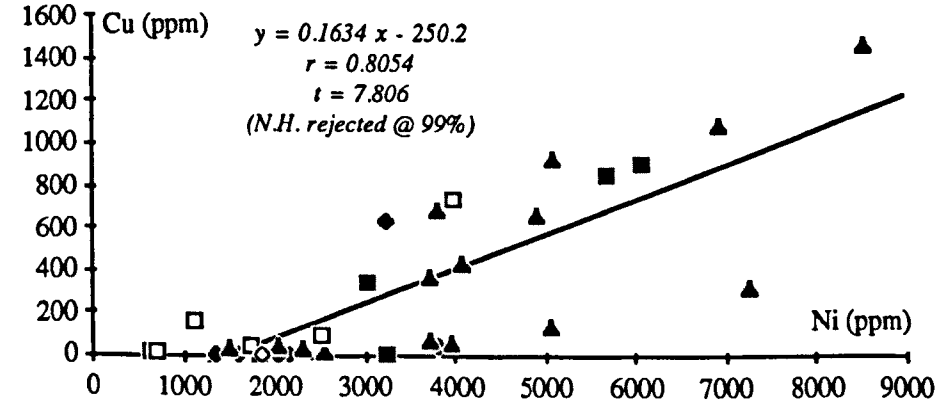

Table 5.8. Sulphur and chalcophile element concentrations (ppm).

Sample	*Rock type*	*S*	*∑PGE*	*Ni*	*Cu*	*Co*	*As*	*Sb*
RLM088	chr/mnt	0	2.05	2172	11	87	17	0
RLM009	chromitite	0	0.16	1344	0	225	14	3.8
RLM099	chromitite	0	0	1607	0	164	0	0
RLM064	chromitite	100	0.68	2478	95	180	18	4.1
RL070	chromitite	200	0.56	2039	9	156	3	1.5
RLM097	chromitite	300	0.33	3229	633	192	25	11.3
MR32	chromitite	300	0.64	3800	47	260	31	5.3
RLM003	chromitite	1400	0.12	1869	0	258	0	10.7
MR33	dunite	200	0.18	3243	9	84	40	0
RLM071	dunite	400	0.07	3038	343	125	8	1.7
RLM069	dunite	1400	0.90	6073	899	167	8	3.3
RLM063	dunite	1900	1.02	5670	847	142	6	7.8
RL069	dunite/chr	0	0.21	2346	18	119	0	1.7
RLM011	dunite/chr	0	0.1	2323	33	154	7	2.3
RLM030	dunite/chr	0	0.02	1838	0	179	0	1.8
RLM066	dunite/chr	0	0.80	2048	49	186	0	2.2
RLM098	dunite/chr	0	0	1498	28	182	0	0
RLM002	dunite/chr	200	0.31	3941	63	236	6	12.9
RLM006	dunite/chr	200	0.03	2539	17	168	10	2.2
RLM067	dunite/chr	400	1.25	3794	680	181	0	1.4
RLM059	dunite/chr	600	0.14	5039	140	179	3	1.2
RLM007	dunite/chr	700	1.87	3720	371	154	9	8.7
RLM096	dunite/chr	700	0.35	3718	70	177	10	2
RLM029	dunite/chr	800	0.56	5068	928	199	0	0
RLM065	dunite/chr	1000	0.51	7245	315	158	15	12.7
RLM004	dunite/chr	1100	0.62	4057	427	159	6	6
RLM082	dunite/chr	1300	0.68	4903	666	161	0	5.2
RLM070	dunite/chr	1500	0.66	6928	1084	169	10	3.6
RLM068	dunite/chr	1700	0.55	8551	1453	163	12	3.3
RLM040	dunite/harz.	2000	0.07	3983	739	161	0	8.4
RL060	H.L.pyrox.	500	0.19	627	23	61	0	0.85
RLM087	pyroxenite	300	0.83	1130	164	85	6	0
RL050	serpentinite	0	0.04	1754	50	336	848	16.9
RL104	wehrlite	800	0.28	697	17	103	0	0
RLM008	wehrlite	900	0.05	2509	99	95	0	3.2

Table 5.9. Stratigraphically controlled variation in the Ni contents of olivine-rich sulphide-poor rocks.

Sample	*Locality*	*Cu (ppm)*	*Ni (ppm)*
Dunite pod in harzburgite unit			
RLO41	Little Heog	8	2718
RL046	Little Heog	0	2793
Dunite pods in harzburgite unit with chromite concentration			
RLM036	Harold's Grave	9	2563
RLM042	Nikka Vord East	0	2592
Basal dunite unit			
RL004a	North of Baltasound	31	2041
RL007	North of Baltasound	0	1793
RL019	North of Baltasound	23	2231
RL023	North of Baltasound	13	2224
RL029a	North of Baltasound	16	2394
Dunite near high-level chromite in pyroxene-bearing layered sequence			
RLA169	Keen of Hamar (27)	37	2200
Pyroxene-bearing dunites from pyroxene-bearing layered sequence			
RL096	Ordale (48)	0	1663
RL099	Ordale (48)	0	1393
RL102	Ordale (48)	0	1519

background olivine Ni content inferred from analyses of sulphide barren dunites (table 5.9). The analyses of dunites containing no visible sulphide indicate that the Ni content of olivine is variable and decreases systematically at higher levels in the cumulate sequence. Furthermore, disseminated chromite-rich dunites contain similar concentrations of nickel as dunites with comparable sulphide contents (figure 5.20b). This indicates that the olivine or sulphides in chromite-rich lithologies contain higher levels of nickel than those in dunites.

Assuming that the regression intercept coefficient in figure 5.20b corresponds to the average background from Ni contained in olivine, then the gradient coefficient corresponds to the average Ni/S ratio of the sulphide phases. This is significantly higher than the Ni/S ratio of the reported mineral phases (table 5.10). Taking a "worst case" model with Ni also occurring as maucherite (Ni_3As) and breithauptite (NiSb) only in the most sulphide-rich

Table 5.10. Nickel mineral assemblages and modelling of bulk Ni/S ratios.

Mineral	*Formula**	*Ratio*	*Comments*	*Reference*
Nickel sulphide assemblage		**Ni/S**		
Pentlandite	$4[(Ni,Fe)_9S_8]$	0.66-0.41	Fe/Ni 0.7-1.4	[1], [2], [3]
Millerite	3[NiS]	1		[2], [3]
Heazlewoodite	$[Ni_3S_2]$	1.5		[1], [2], [3]
Godlevskite	Ni_7S_6	1.2		[1]
Nickel arsenide assemblage		**Ni/As**		
Orcellite+	Ni_2As	2	$(Ni_{5-x}As_2)$	[1]
Maucherite	Ni_3As	3		[1]
Nickel antimonide		**Ni/Sb**		
Breithuaptite	2[NiSb]	1		[3]
Nickel-rich alloy		**Ni/Fe**		
Awaruite	4[Ni,Fe]	1.5		[4]

[1] Gunn et al., 1985
[2] Prichard et al., 1989
[3] Ixer & Prichard, 1989
[4] J. Maynard pers. comm.
*Formulae from Hey, 1975
+Formula from Embrey & Fuller, 1980

Nickel sulphide assemblage only

(ppm)	Intercept	Maximum	
S	0	2000	*Ni sulphide with Ni/S = 2.53*
Ni	2556	7616	*(from figure 5.24)*

Nickel sulphide, arsenide, antimonide assemblage

(ppm)	Intercept	Maximum	
S	0	2000	*Ni as arsenide = 120 ppm*
Ni	2556	7616	*Ni as antimonide = 13 ppm*
As	0	40	*Sulphide Ni/S ratio = 2.46*
Sb	0	13	

(Assuming all As as maucherite and all Cu as native metal)

samples and in amounts equivalent to As and Sb levels of 40 ppm and 13 ppm respectively (the maximum levels recorded in this data set), only reduces the average Ni/S ratio of the sulphide phases to 2.46. This calculation also assumes that all Cu is present only as native metal, whereas copper sulphides are known to occur (Prichard et al., 1989; Ixer & Prichard, 1989). This excess of nickel indicates that nickel-rich non-sulphide phases should also occur e.g. awaruite (Ni-Fe alloy), which has also been observed mineralogically (J. Maynard, pers. comm.).

The numerical modelling above indicates a general deficiency in sulphur with respect to chalcophile elements, even when the effects of olivine Ni content and possible replacement by As or Sb is considered. This suggests remobilisation and a net loss of sulphur. The sulphur-poor nickel mineral assemblage described above has been related to the effects of serpentinisation under low fO_2 conditions, liberating reducing Fe, free H_2 and then H_2S, thus allowing remobilisation and loss of sulphur (Ramdohr, 1967). Further sulphur mobility and loss is possible by oxidation during supergene alteration. Oxidising conditions are indicated by the alteration of Pd antimonides to Pd ochre and of sperrylite ($PtAs_2$) along its cleavage to Pt, Fe, Cu, Ni oxides (Ixer & Prichard, 1989). Evidence of this further loss of sulphur is provided by the green oxide alteration rims which were observed around sulphides in hand specimens. Such Ni-rich oxides are probably the cause of the characteristic green colouring of the serpentinite matrix in weathered chromite-rich dunites from Cliff and elsewhere (section 4.2.1).

In conclusion, anomalous levels of Ni and Cu are related to the original sulphide contents of the ultramafic lithologies. Present day sulphur concentrations mostly retain a correlation with chalcophile elements. However, mineral assemblages, calculations of bulk sulphide Ni/S ratios and field observations of green sulphide alteration rims or Ni-rich serpentinites all indicate substantial remobilisation and a net loss of sulphur. For these reasons whole-rock chalcophile element analyses provide a better indication of original igneous sulphide contents than direct measurements of sulphur concentrations.

5.7 Platinum-group mineral assemblages in the crustal ultramafic cumulate sequence

The extensive mineralogical surveys which formed the basis of the present study (Prichard et al., 1981; Neary et al., 1984; Gunn et al., 1985; Leake & Gunn, 1985; Prichard et al., 1986; Tarkian & Prichard, 1987; Prichard & Tarkian, 1988; Prichard et al., 1989) were concerned only with chromitite or chromite-rich dunites and were predominantly of material from the Cliff locality (all results summarised in section 1.5). In the course of the present study extensive new Pt-, Pd-rich concentrations have been located in chromite-poor crustal lithologies including sulphide-bearing dunites or pyroxenites. Moreover, the strong geochemical association between elevated Pt, Pd, As and Sb concentrations at Cliff is virtually absent elsewhere in the complex (section 5.5). This indicates that the well documented Cliff mineralogical assemblage may not be representative of all other Pt-, Pd-rich mineralisation in the ophiolite complex.

The Cliff mineralisation has also been the subject of a further comprehensive mineralogical study which included characterisation of the associated sulphide assemblage (Ixer & Prichard, 1989). This work is summarised in table 5.11 for comparison. Mineralogical characterisation of As-poor mineralisation from sulphide-bearing cumulate dunites and pyroxenites is still at a preliminary stage but all currently available published and unpublished work is summarised in table 5.12.

The most striking difference between the PGM assemblage in other areas compared to that found at Cliff is the predominance of Pt or Pd-antimonides (geversite, stibiopalladinite) and the scarcity of sperrylite ($PtAs_2$). Sperrylite is the main platinum phase at Cliff but elsewhere it has only been found in the altered matrix of pyroxene-bearing cumulates. Both of these pyroxene-rich samples are from highly tectonised areas of the ophiolite sequence (section 2.6). It has been shown that more altered lithologies from such zones are characterised by higher levels of As (section 5.3) since these structures allowed access to As-bearing hydrothermal fluids emanating from the basal thrust of the ophiolite (Lord &

Table 5.11. Mineralogical assemblages and paragenetic sequence of Pt, Pd, Au, Ag and base metal mineralisation at Cliff (from Ixer & Prichard, 1989).

Host Rock	*PGM Assemblage*	*Paragenesis*
Chromite-rich dunites & dunites	(1) Pt, Pd & Au tellurides	(1) Earliest assemblage, as < 2 μm grains within rows or clusters of 5-20 μm Ni-Fe, Ni or Cu sulphide inclusions in chromite
Chromite-rich dunites & dunites	(2) Native Au, Au-Pd, Au-Cu, sperrylite, geversite, Pd antimonide	(2) Main PGM carrier, found with pentlandite-heazlewoodite-millerite & minor Cu sulphide assemblage, nickel arsenides, breithauptite and Ir-, Rh- and Os-bearing PGM, in silicate infilled fractures cutting chromite, voids in ferri-chromite rims and most extensively within altered silicate matrix
Silicates	(3) Native Au & Ag	(3) High fineness Ag-poor Au with Au-Cu rims. Native Ag intergrown with native Cu in Cu sulphide or heazlewoodite
Chromite-rich dunites & dunites	(4) PGE ochres (oxides)	(4) Pd antimonides alter to Pd ochre and sperrylite alters along cleavage to Pt, Fe, Cu, Ni oxides as a result of supergene alteration

Prichard, 1989). The presence of sperrylite seems diagnostic, therefore, of the hydrothermal alteration of PGE mineral assemblages (see section 5.8).

Where magmatic PGE concentrations are not affected by such hydrothermal processes Pt or Pd antimonides are spatially related to altering Ni-Fe sulphides (H. Prichard, pers. comm.) mirroring the geochemical and lithological associations between PGE concentrations and sulphide-bearing rocks or anomalous chalcophile element concentrations (sections 4.5 & 5.4). This textural pattern suggests that PGE are released from immiscible sulphide droplets during solidification or later during serpentinisation and the related alteration of the original sulphide minerals. Such sulphide-bearing dunites commonly contain a variety of base and precious metal alloy phases (table 5.12), as well as amorphous PGE oxides (ochres). Similar alloys and ochres are also found in the Cliff assemblage, where they have been related to in-situ alteration during serpentinisation (Prichard & Tarkian, 1988), and to supergene alteration respectively (Ixer & Prichard, 1989).

Table 5.12. Recent mineralogical studies of crustal sequence mineralisation from the Balta Sound area or analogous areas (Prichard & Lord, 1989; Prichard et al., in prep.*).

Locality	*Lithology*	*PGE Phases*	*Comments*
South Unst (locality 25 figure 1.13)	Over 350 grains within a single pyroxene crystal in wehrlite sample MR 45	(1) Pd-Cu sulphides ± trace Au, Pt. Pd-Pb alloy ± trace Au, Pt (2) Pd-As and Pd-Sb, & lesser Pt-As with rare Pd-Cu-Au & Au-Ag-Pd alloys & Pd-Te	(1) As 0.5-3 μm circular blebs enclosed by fresh pyroxene in rows along two perpendicular pairs of sub-parallel annealed fracture planes oblique to all 3 pyroxene cleavages. Often Pd-S grains occur within circular Fe-, Ni- and Cu-bearing sulphide blebs (2) Where altering cleavage crosses above zones, with resultant serpentine & magnetite, and as continuation into serpentinised matrix. Larger (< 15 μm) elongate or lath-shaped grains orientated along cleavage zones, associated with Fe-poor Ni-Cu sulphides
Balta Sound chromite Quarries area (Quarry W of BX, locality 16, figure 4.1)	Sulphide-bearing dunite (RLA126)	Pt-bearing antimonides (geversite?)	Two Pt-Sb grains identified around 200 μm relict pentlandite grain now partially altered to heazlewoodite (± millerite)
Ordale coast (midway between RL097 &RL098, see enclosure 2)	Sulphide-bearing (highly altered) pyroxenite (NA25)	Pt-As (sperrylite?) & Pd-Sb, probably stibiopalladinite, native Pt	Cluster of PGM around 100 μm Ni-, Fe- and Cu-bearing sulphide field in serpentine & chlorite after olivine interstitial to fresh pyroxene crystals. Larger (5 μm) Pt-As grains circling sulphide & smaller (< 1 μm) grains at chlorite/pyroxene margin. Native Pt and Pd-Sb enclosed by magnetite in altered sulphide field
Balta Sound Quarries area	Sulphide-bearing dunites with native Cu in veins (drillcore)	Pd-Sb, Pd-Cu-Sb, native Pd, Pt-Ni ochre, Pt-Fe-Cu alloy, PtSb	Pd & Pt antimonides alloys & ochres located close to Ni-Cu sulphides, including pentlandite altering to heazlewoodite ± millerite, native Cu, Ni-Fe alloys, breithauptite (Ni-Sb) and Ni-Pb alloy, with native Cu/Ag intergrowth and Ag-Hg amalgam. Rare Ni-As, sperrylite totally absent

*The data given in this table result from the mineralogical studies of Dr H.M. Prichard and are taken from the unpublished final report of the MIRO project RC48 (Prichard & Lord, 1990).

Further evidence of an original magmatic association between PGE and Fe-Ni-Cu sulphides has been provided by studies of a single pyroxene crystal from a "typical" wehrlite sample from South Unst (table 5.12). Over 350 small PGM have been qualitatively identified, occurring as 0.5-15 μm grains along four annealed fracture planes crossing a fresh pyroxene and its serpentinite matrix (H. Prichard, pers. comm.). Where surrounded by fresh pyroxene the PGMs are Pt and Pd-bearing Ni, Cu, Au sulphides and Pb alloys (Prichard & Lord, 1989). Where the linear array crosses the serpentinised (olivine) matrix or serpentinised cleavage zones the PGE-bearing phases exhibit recrystallised textures and are chiefly Pd-As, Pd-Sb or Pt-As minerals. The origin of the sulphide inclusions is problematical since their composition is different from that expected if early magmatic sulphide droplets were included by a growing pyroxene (A. J. Naldrett, pers. comm.). Instead it seems likely they were injected along fractures and the pyroxene subsequently annealed (H. Prichard, pers. comm.). The bulk geochemical signature of this sample exemplifies those of high-level pyroxene-rich cumulates which represent evolved late magmatic sulphide segregations (see section 7.7.4). Nevertheless these relict inclusions provide evidence of an early high temperature PGE sulphide assemblage which was poor in both As and (more significantly) Sb. Serpentinisation of the interstitial olivine and along the pyroxene cleavage allowed the ingress of later As-, Sb-bearing hydrothermal fluids and subsequent recrystallisation to the usual arsenide-antimonide PGM assemblage (Prichard & Lord 1989).

In conclusion, the recent mineralogical studies of areas other than Cliff have revealed that Pt and Pd occur principally as antimonides (geversite and stibiopalladinite respectively). Moreover, these minerals are spatially associated with altering sulphide phases. Relict inclusions within fresh pyroxene provide evidence of a Ni-Fe-Cu-Pb-Pt-Pd sulphide assemblage as a possible precursor. The formation of arsenide PGM can be related to the later interaction of As-bearing hydrothermal fluids. Furthermore $PtAs_2$ (sperrylite) is the principal Pt-bearing phase at Cliff in sharp contrast to the Pt antimonide (geversite?) found elsewhere. The significance of this As enrichment to the genesis of the anomalously high PGE concentrations at Cliff is now considered.

5.8 Hydrothermal reconcentration of pre-existing magmatic PGE concentrations at Cliff

The strong geochemical association between elevated Pt, Pd, As and Sb concentrations at Cliff and the virtual absence of this association elsewhere in the complex (section 5.5) indicates genetic differences in the mineralisation at this locality. These differences have been born out by recent mineralogical studies of mineralisation in other areas (section 5.7). In particular it appears that platinum antimonide is the typical Pt-rich phase in all areas unaffected by hydrothermal alteration. In contrast $PtAs_2$ (sperrylite) is the main platinum mineral at Cliff. The high levels of As at Cliff have been attributed to a hydrothermal overprint by As-rich fluids introduced along the basal thrust of the the ophiolite (Lord & Prichard, 1989). The chromite-rich dunites from Cliff contain Pt and Pd concentrations one to two orders of magnitude higher than those found in "fresh" magmatic mineralisation elsewhere in the complex (section 4.4.3). The aim of this section is to assess whether hydrothermal processes are responsible for this enrichment.

5.8.1 The distribution of anomalous PGE concentrations at Cliff

To allow the best possible interpretation of the origin of the mineralisation at Cliff all available Pt, Pt, Ir, Au, As and Sb analyses of mineralised material from this locality have been compiled (table 5.13). The location of these samples is shown on figure 5.21 using the Cliff quarry map of Gass et al. (1982). The approximate concentrations in PGE-bearing samples are also given, expressed as Σ Pt + Pd (ppm). Samples shown in boxes are chromite-rich and dunite samples collected from each of the chromite pits (A-E) or their adjacent spoil tips (Gunn et al., 1985). Analyses of in situ mineralisation are shown in bold type (Prichard & Lord, unpublished data). The location of PGE-barren in situ silicate samples is also shown.

Anomalous PGE concentrations show the following distribution pattern (figure 5.21). Firstly, concentrations greater than 1 ppm Σ Pt + Pd occur in chromite-rich material from all

Figure 5.21. Compilation map showing samples locations and PGE grades at Cliff. Quarry map modified from Gass et al. (1982).

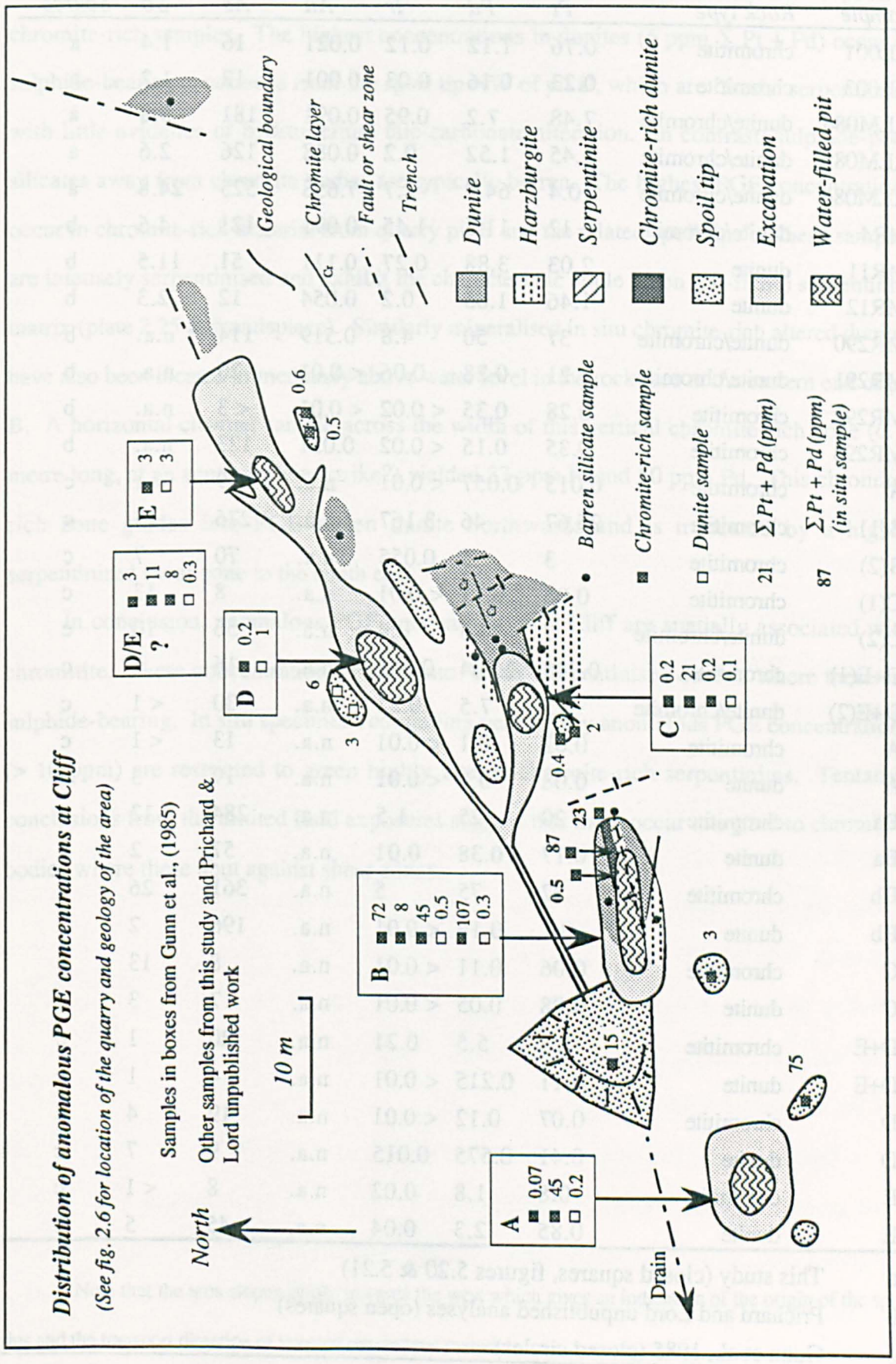

Table 5.8. Compilation of all available analyses (in ppm) of material from the Cliff quarry.

Sample	*Rock type*	*Pt*	*Pd*	*Ir*	*Au*	*As*	*Sb*	*Source*
RL001	chromitite	0.76	1.12	0.12	0.021	16	1.4	a
RL003	chromitite	0.23	0.16	0.03	0.001	12	1.2	a
RLM084	dunite/chromite	7.48	7.2	0.95	0.091	181	5.8	a
RLM085	dunite/chromite	1.45	1.52	0.2	0.088	126	2.6	a
RLM086	dunite/chromite	10.4	64.9	2.7	7.658	525	24.8	a
MR4	dunite/chromite	12	11.5	1.45	0.091	121	4.6	b
MR11	dunite	2.03	3.88	0.27	0.111	51	11.5	b
MR12	dunite	1.46	1.65	0.2	0.054	12	2.3	b
MR290	dunite/chromite	37	50	4.8	0.519	114	n.a.	b
MR291	dunite/chromite	0.21	0.28	0.06	< 0.01	20	n.a.	b
MR292	chromitite	0.28	0.35	< 0.02	< 0.01	< 3	n.a.	b
MR293	chromitite	0.35	0.15	< 0.02	0.031	123	n.a.	b
A	chromitite	0.013	0.057	< 0.01	n.a.	19	< 1	c
B(1)	chromitite	25.67	46	3.167	n.a.	276	15	c
B(2)	chromitite	3	5	0.055	n.a.	70	7	c
C(1)	chromitite	0.06	0.11	< 0.01	n.a.	8	13	c
C(2)	dunite/chromite	7	13.5	0.4	n.a.	56	10	c
D+E(1)	chromitite	0.948	2.104	0.065	n.a.	16	1	c
D+E(2)	dunite/chromite	3.5	7.5	0.21	n.a.	30	< 1	c
A	chromitite	0.02	0.1	< 0.01	n.a.	13	< 1	c
A	dunite	0.08	0.1	< 0.01	n.a.	19	3	c
Ba	chromitite	20	25	1.5	n.a.	284	12	c
Ba	dunite	0.17	0.38	0.01	n.a.	57	2	c
Bb	chromitite	32	75	5	n.a.	361	26	c
Bb	dunite	0.1	0.16	< 0.01	n.a.	196	2	c
C	chromitite	0.06	0.11	< 0.01	n.a.	8	13	c
C	dunite	0.08	0.05	< 0.01	n.a.	7	3	c
D+E	chromitite	2.5	5.5	0.21	n.a.	20	1	c
D+E	dunite	0.11	0.215	< 0.01	n.a.	4	1	c
D	chromitite	0.07	0.12	< 0.01	n.a.	19	4	c
D	dunite	0.41	0.575	0.015	n.a.	9	7	c
E	chromitite	0.8	1.8	0.02	n.a.	8	< 1	c
E	dunite	0.85	2.3	0.04	n.a.	45	5	c

a This study (closed squares, figures 5.20 & 5.21)

b Prichard and Lord unpublished analyses (open squares)

c Gunn et al., 1985 (closed circles)

five quarry pits. Dunites which were spatially close to chromite concentrations (now found in spoil tips) are also frequently mineralised, albeit at lower levels than the respective chromite-rich samples. The highest concentrations in dunites (6 ppm Σ Pt + Pd) occur in sulphide-bearing specimens from the spoil tip NW of pit D, which are "fresh" serpentinites with little evidence of hydrothermal talc-carbonate alteration. In contrast, sulphide-poor silicates away from chromite bodies are typically barren. The highest PGE concentrations occur in chromite-rich material from quarry pit B and the related spoil tips*. These samples are intensely serpentinised and exhibit the characteristic apple green (Ni-rich?) serpentinite matrix (plate 2.25 & frontispiece). Similarly mineralised in situ chromite-rich altered dunites have also been located immediately above water level in the rock face at the eastern end of pit B. A horizontal channel sample across the width of this vertical chromite-rich zone (c. 1 metre long, at an acute angle to strike?) yielded 37 ppm Pt and 50 ppm Pd. This chromite-rich zone grades into PGE-barren dunite northwards and is truncated by a highly serpentinised shear zone to the south east.

In conclusion, anomalous PGE concentrations at Cliff are spatially associated with chromitite. These concentrations extend into "fresh" serpentinised dunites where these are sulphide-bearing. In situ specimens containing very highly anomalous PGE concentrations (> 10 ppm) are restricted to green highly altered chromite-rich serpentinites. Tentative conclusions from the limited field exposures suggest that these occur marginal to chromitite bodies where these abut against shear zones.

---

* Note that the area slopes gently towards the west which gives an indication of the origin of the spoil tips and the transport direction of rejected ore-gangue material

5.8.2 The significance of As and Sb enrichment at Cliff

The linear relationships between PGE and As or Sb concentrations in samples from Cliff (section 5.5.3) suggest that these elements might be pathfinders for the unusual levels of PGE mineralisation found at this locality. Gunn et al. (1985) described correlations between Pd and As, Sb or Te in samples containing over 2 ppm Pd (section 1.5.2.3). To substantiate these findings all the available analyses of Pt, Pd, Ir, Au, As and Sb in chromitites dunites or chromite-rich dunites from Cliff have been compiled (table 5.13). Graphs of PGE plotted against pathfinder elements are shown in figures 5.22 and 5.23. The various symbols refer to the different data sources (table 5.13).

Both Pt and Pd show good correlations with As and Sb. Similar correlations occur with Ir and Au, although fewer complete analyses are available for these elements. To statistically test these correlations, best fit lines have been calculated by regression analysis. The correlation and regression coefficients are summarised in table 5.14. The statistical significance of the correlations has been tested using Student's t test, which allows rejection of the null hypothesis that "no correlation exists" (Cheeney, 1983). All correlations were found to be statistically valid (table 5.14).

Two patterns emerge from this data. Firstly the regression constants involving As are significantly higher than the As/PGE ratios of typical PGM phases (e.g. sperrylite $PtAs_2$). Together with the large positive intercept constant, this indicates a large excess of As over PGE. Secondly, ranking the combinations in order of their correlation coefficient produces the same order of PGE for both As and Sb (i.e. Au, Pd, Ir, Pt). This is close to the order of relative mobility in hydrothermal environments, generally Au > Pd > Pt > Os, Ir, Ru (Hulbert et al., 1988). If As is present in the system then Pt mobility is further suppressed by the low solubility of sperrylite .

Upon close inspection the graphs of Pt and Pd against As or Sb can be divided into two portions. Below about 500 ppb Pt or Pd no clear correlation is seen with As or Sb (figure 5.22). This is within the range of PGE concentrations seen in the samples from around Balta Sound, in which no correlation with As or Sb was observed (section 5.5.3). A few of the Cliff samples plot within this range but they contain anomalously high levels of

Figure 5.22. Graphical relationships between Pt, Pd, As and Sb in samples from Cliff.

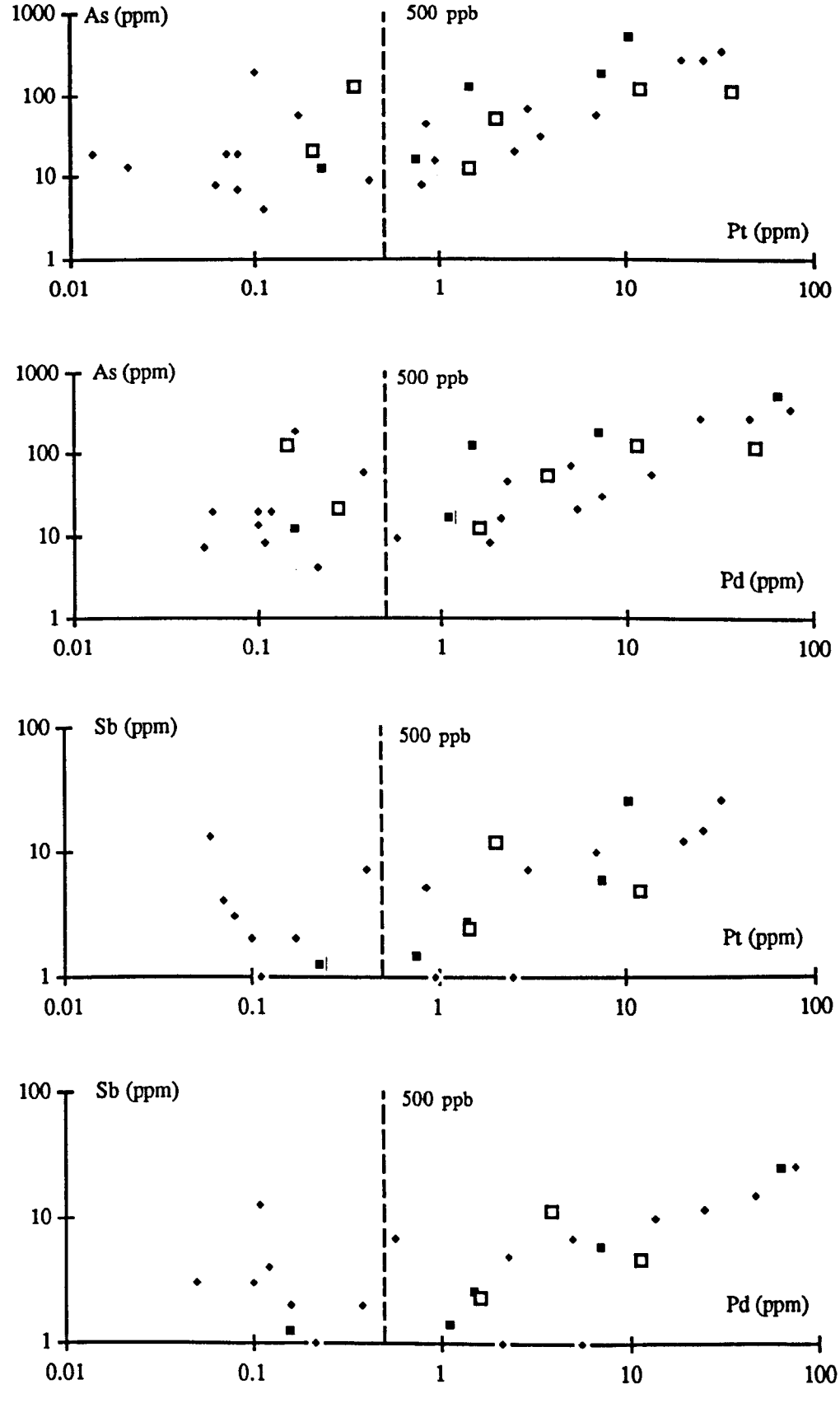

Figure 5.23. Graphical relationships between Au, Ir, As and Sb in samples from Cliff.

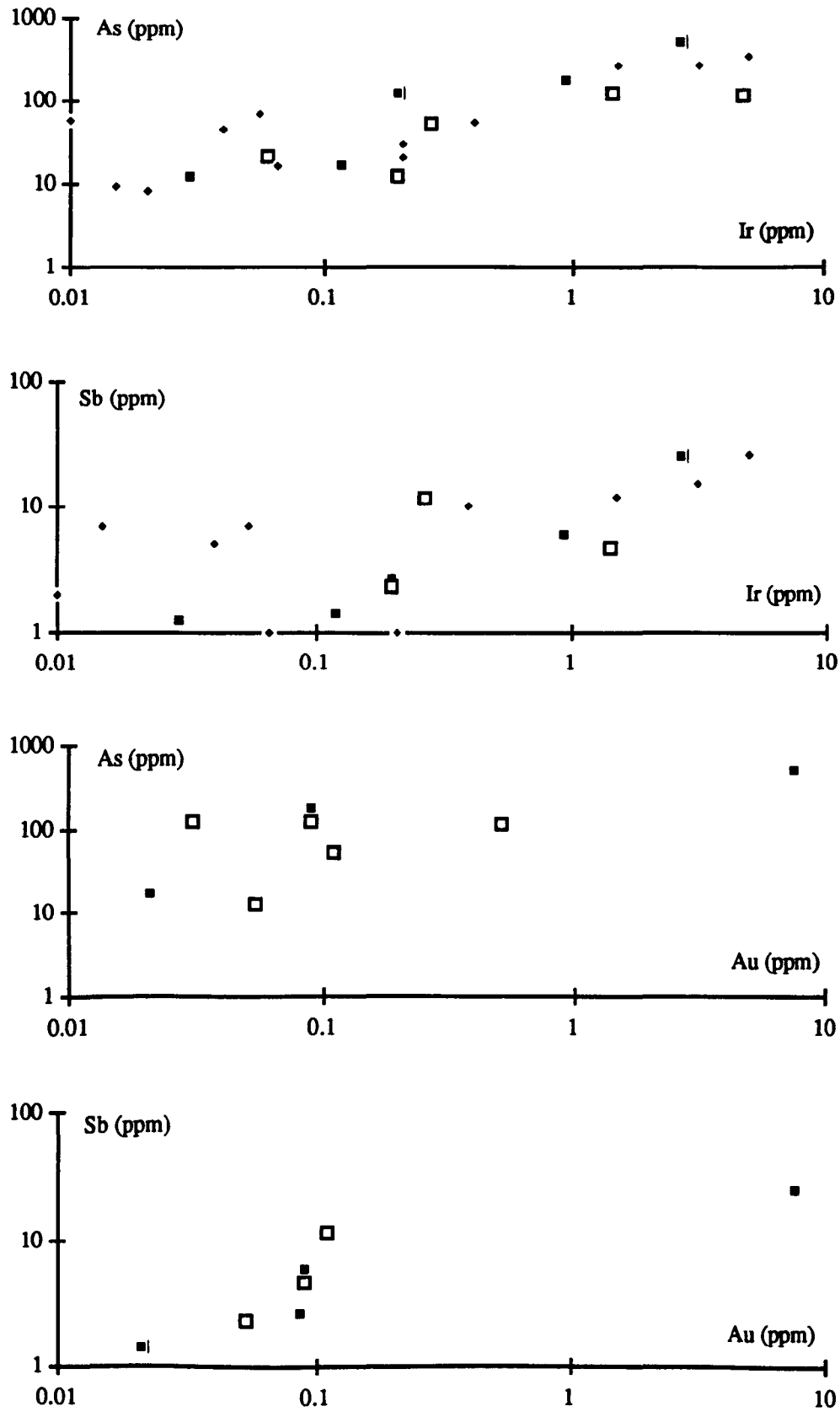

Table 5.14. Regression analysis of correlations between PGE and As or Sb in samples from Cliff.

Element combination (x & y)	*Regression intercept (a)*	*Regression slope (b)*	*Pearson's correlation coefficient (r)*	*Student's t*	*Rejection level of null hypothesis*
Au & As	85.7	57.4	0.93	7.0	99%
Pd & As	35.9	5.1	0.83	8.2	99%
Ir & As	46.2	62.9	0.71	4.5	99%
Pt & As	46.6	7.8	0.62	4.4	99%
Au & Sb	4.5	2.7	0.92	5.1	99%
Pd & Sb	4.0	0.3	0.86	8.0	99%
Ir & Sb	3.5	4.7	0.86	6.7	99%
Pt & Sb	4.2	0.6	0.70	4.7	99%

Figure 5.24. Discrimination of different mineralisation styles at Cliff using Pt and As.

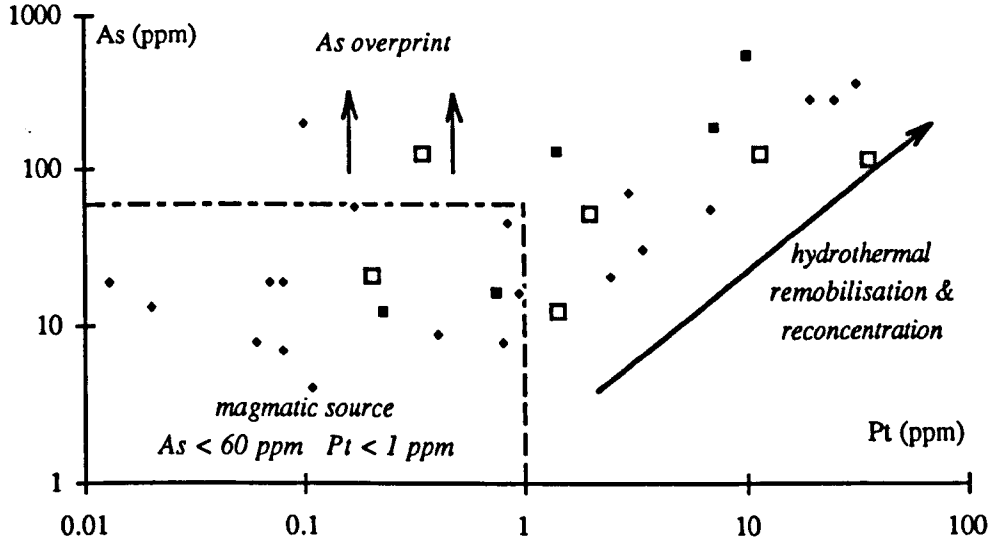

As or Sb. Above the 500 ppb threshold a strong correlation is seen between PGE and As or Sb. These very highly anomalous levels of PGE are only found at Cliff.

The high levels of As at Cliff have been attributed to a hydrothermal overprint by As-rich fluids introduced along the basal thrust of the ophiolite (Lord & Prichard, 1989). The Cliff quarry is close to the basal thrust of the ophiolite and at the focus of several other shear zones (section 2.2.5). The correlations between PGE and As or Sb indicate that the very high levels of PGE found here are the result of local remobilisation and reconcentration by these fluids. There is good evidence for a magmatic PGE source at Cliff, since it fulfils the general requirements of Ni-Cu sulphides associated with chromite (section 4.6). Some samples from Cliff plot within the field defined by As < 60 and PGE < 1 ppm, which is typical of magmatic mineralisation elsewhere in the ophiolite. Enhanced levels of As or Sb with typical magmatic PGE contents can be attributed to a passive overprint by an As-bearing fluid. Extreme hydrothermal action might result in remobilisation and reconcentration of PGE in association with As and Sb mineralisation. This model is shown for Pt and As in figure 5.24. This model is consistent with the observed mineralogical assemblage (section 5.7) and indicates genetic differences between the PGE concentrations at Cliff and those elsewhere in the complex.

5.8.3 Discussion of hydrothermal remobilisation mechanisms

Gunn et al. (1985) proposed a purely hydrothermal origin for PGE the mineralisation at Cliff, suggesting that this occurred during serpentinisation of the ultramafic host rocks (section 1.6.1). This model raises several problems, most notably the source of the Pt, Pd and Rh (section 1.7). Hulbert et al. (1988) have revised the hydrothermal model to include possible pre-concentration of PGE by magmatic processes, evidence of which is provided by certain relict magmatic textures (Prichard et al., 1986) and the association of PGE with a primary chromite-rich pod and its surrounding dunite envelope (Prichard and Lord, 1988).

The silicate reactions (table 5.15) relevant to the solution of PGE during progressive serpentinisation by a low salinity fluid have been considered by Hulbert et al. (1988). They point out that the net effect of the initial reaction (1) is to cause the pore fluid to become more

Table 5.15. Mineral-solution reactions during serpentinisation of harzburgite (after Hulbert et al., 1988).

Initial Reactions			
(1)	$2Mg_2SiO_4 + 2H^+ + H_2O$ *Forsterite*	=	$Mg_3Si_2O_5(OH)_4 + Mg^{++}$ *Serpentine*
(2)	$3MgSiO_3 + 2H_2O$ *Enstatite*	=	$Mg_3Si_2O_5(OH)_4 + SiO_2$ (aq) *Serpentine*
Subsequent Reactions			
(3)	$3Mg_2SiO_4 + SiO_2$ (aq) $+ 4H_2O$ *Forsterite*	=	$2Mg_3Si_2O_5(OH)_4$ *Serpentine*
(4)	$2MgSiO_3 + Mg^{++} + H_2O$ *Enstatite*	=	$Mg_3Si_2O_5(OH)_4 + 2H^+$ *Serpentine*
(5)	$Mg^{++} + 2H_2O$	=	$Mg(OH)_2 + 2H^+$ *Brucite*
(6)	$3Mg^{++} + 4SiO_2$ (aq) $+ 4H_2O$	=	$Mg_3Si_4O_{10}(OH)_2 + 6H^+$ *Talc*

alkaline. Such an alkaline pore fluid is capable of dissolving a sufficient quantity of sulphur (>>30 ppm) to allow dissolution of the entire sulphide component of a normal ultramafic rock. Under alkaline conditions the sulphur is present in solution as HS^- so the fluid will be capable of dissolving Pt and Pd as thiosulphate or bisulphide complexes.

The potential of thiosulphate or bisulphide ligands as complexing agents for PGE has been considered by Mountain & Wood (1988). Although thiosulphate may be metastable at low temperatures it is unlikely to persist at typical hydrothermal temperatures. For these reasons the bisulphide ligand is a more likely candidate although the stability constants for complexes with Pt or Pd complexes have not been measured. Minimum estimates of these solubility constants indicate that solution is feasible and may be greater for mixed ligand

Figure 5.25. Schematic diagram showing the reaction profile for progressive serpentinisation of a harzburgite in terms of ion concentrations in the pore fluid and the relative proportion of relict primary and secondary minerals (from Hulbert et al., 1988).

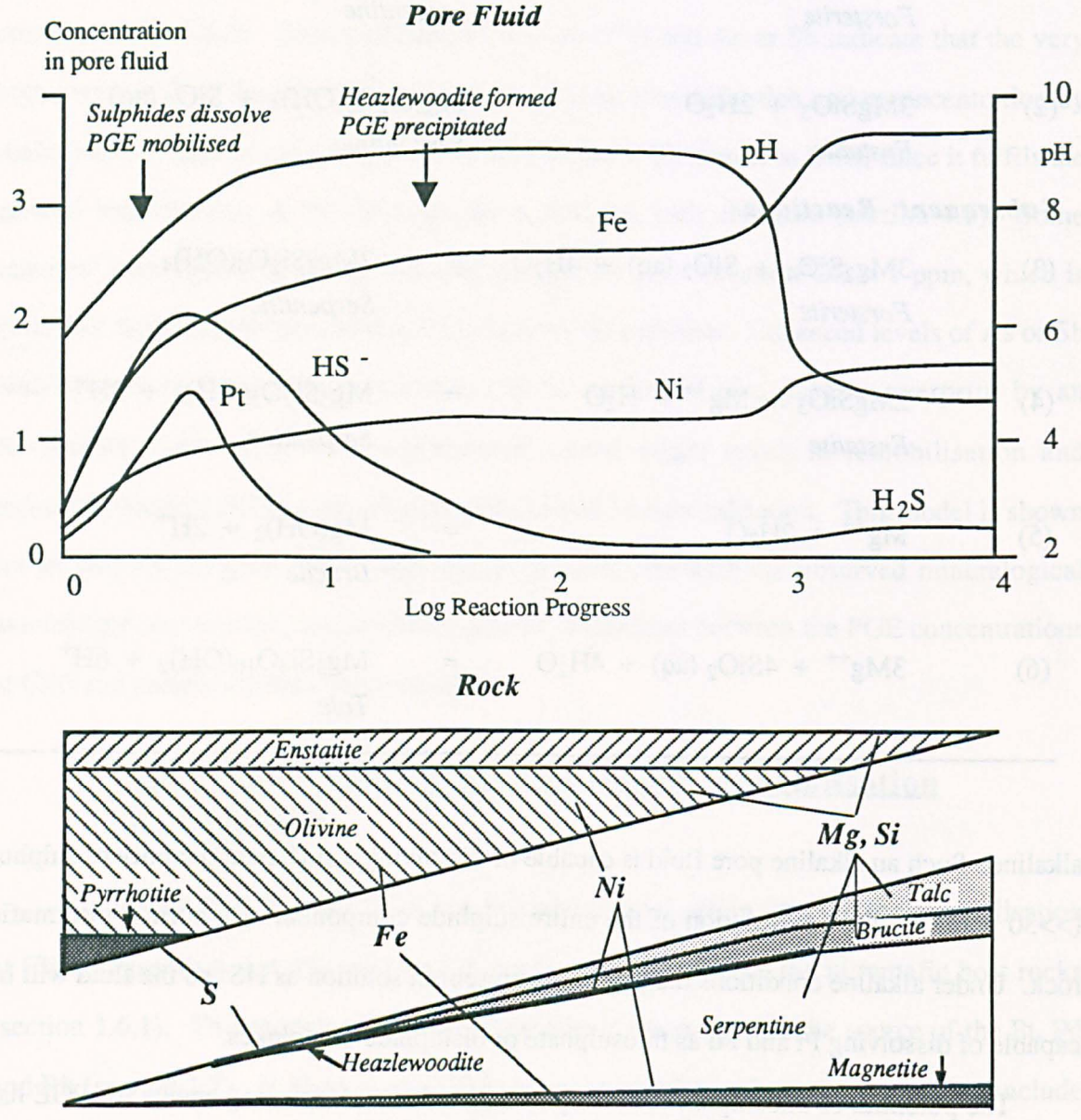

complexes in alkaline solutions. Moreover, the estimated solubilities of Pt and Pd as tetrabisulphide complexes are very similar indicating that the elements will move in equal proportions.

Thus PGE mobilisation as bisulphide complexes is possible when HS^- concentrations in the pore fluid are high (Hulbert et al., 1988). These conditions only occur during the

early stages of serpentinisation (figure 5.25). As the serpentinisation of olivine progresses, Ni and Fe are released from olivine, heazlewoodite becomes saturated and progressively removes sulphur, so the concentration of HS^- drops. As the concentration of sulphur in the fluid falls, so magnetite is formed from the iron released by serpentinisation. Also reactions (3) to (6) cause progressive acidification of of the pore fluid. By analogy with the behaviour of gold, neutral to acidic fluids in equilibrium with magnetite will not allow solution as thio-complexes.

The above discussion indicates that PGE mobility in a low salinity fluid is possible during the early stages of serpentinisation but is inhibited as serpentinisation proceeds (Hulbert et al., 1988). This behaviour provides a mechanism for the dissolution, transport and reprecipitation of the precious metals. The zone of PGE mobility will follow the serpentinisation front. Since serpentinisation involves an increase in volume and serpentine behaves in a ductile fashion, it is likely that this fluid will be expelled along brittle fractures in the fresh ultramafic rock.

The remobilisation mechanism of Hulbert et al. (1988) which is described above can be readily applied to the Cliff occurrence. As has been discussed earlier (section 5.8.1) anomalous PGE concentrations (1 - 6 ppm Σ Pt + Pd) occur in chromite-rich rocks and the spatially associated sulphide-bearing dunites. This spatial association between PGE and chromite has been recognised throughout the ophiolite complex and is thought to reflect magmatic processes and the formation of primary concentrations (section 4.6). This situation is shown in figure 5.26 (a) for a hypothetical chromite body similar to that originally present at Cliff. At the Cliff locality highly anomalous PGE concentrations (up to 87 ppm Σ Pt + Pd) occur in the highly altered chromite-rich serpentinite margin of chromitite bodies near to shear zones. Several aspects of the serpentinisation model allow explanation of this apparent enhancement of the original concentrations.

Serpentinisation is known to follow chromitite bodies producing a totally altered matrix in the marginal chromite-rich dunites (Prichard and Lord, 1988). Moreover, pull-apart fractures are developed in the chromitite body as a result of the volumetric expansion of the surrounding serpentinite host. By the combination of these factors serpentinising fluids are allowed access to the PGE-bearing chromitite body and fluid mobility within it is

Figure 5.26. Diagram showing a mass balanced model for the hydrothermal reconcentration of magmatic PGE concentrations at Cliff.

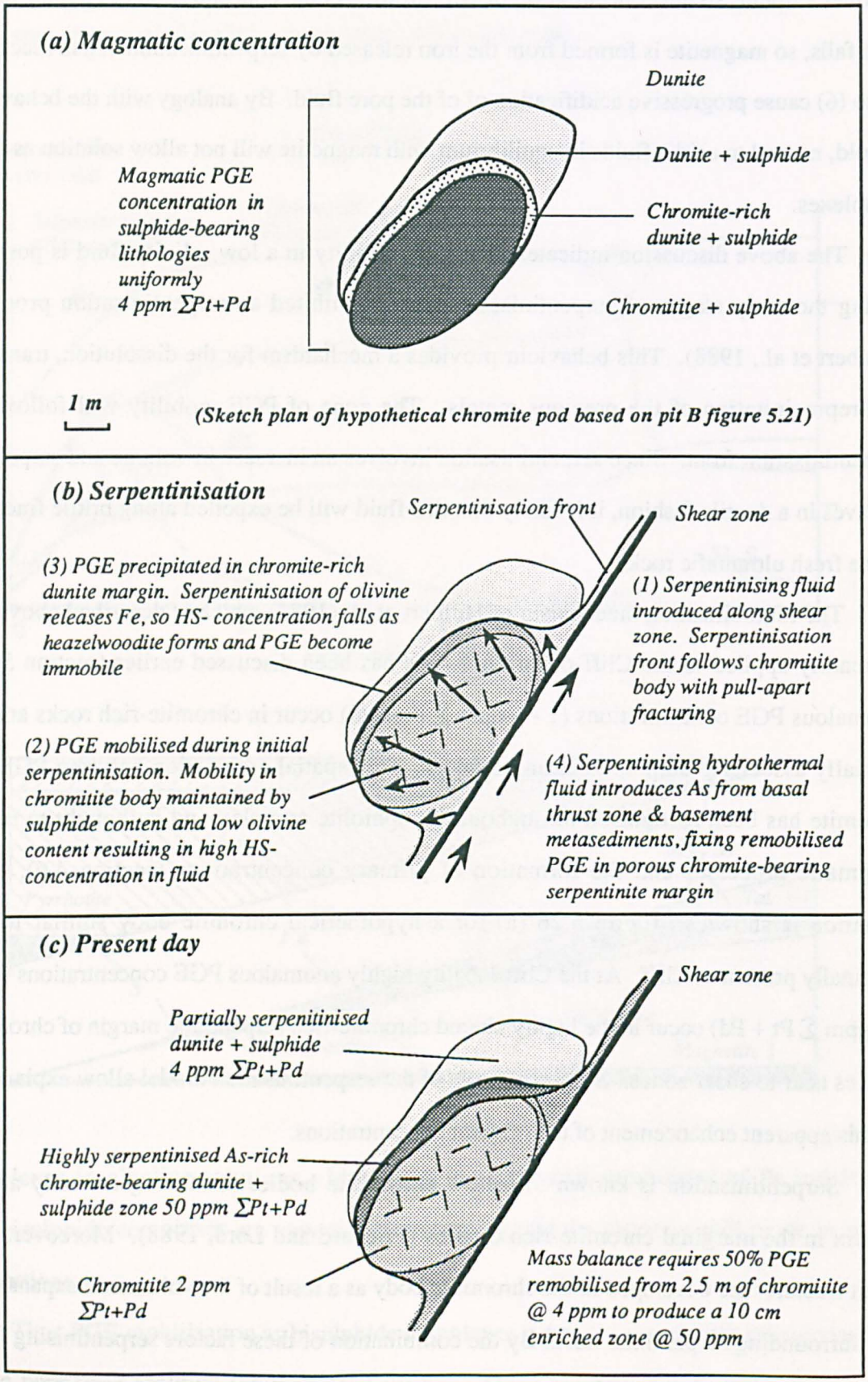

enhanced (figure 5.26 b). Moreover the presence of sulphide phases within the chromite or the dunite will chemically promote PGE mobility by contributing bisulphide ligands to the pore fluid during their dissolution. It is exactly these areas where anomalous magmatic PGE concentrations occur. Furthermore, the mobility of PGE is inhibited by the progressive serpentinisation of olivine. Thus PGE mobility is facilitated in regions with higher sulphide/olivine ratios such as within a sulphide-bearing dunite or a sulphide-bearing chromitite pod. At the margins of these zones sharp chemical gradients will exist and in particular the release of nickel from olivine will promote precipitation of secondary sulphides (e.g. heazlewoodite), a corresponding fall in the HS^- concentration of the fluid, and the consequent reprecipitation of PGE. The margins of the chromitite body are likely to develop void spaces due to the volumetric expansion of the surrounding serpentinite. In the case of disseminated chromite-rich dunite it is possible that a sponge-like system of void spaces will occur around each chromite grain. These factors provide an explanation why remobilised PGE are reconcentrated at the margins of chromite bodies (e.g. figure 5.21) and their mineralogical textures often indicate PGM formation within the altered margins of chromite grains (see section 1.7).

If the above mechanism constitute a viable means of PGE remobilisation such enhancements would be expected to occur around all serpentinised PGE-bearing chromitite bodies. Whereas such chromite-rich dunites often contain higher levels of PGE than their equivalent chromitites, enhancements on the scale found at Cliff are unknown elsewhere in the complex. These enrichments are related to the unique geological setting of Cliff, where a magmatic PGE concentration is overprinted by an As-bearing hydrothermal fluid. The importance of this fluid to the reconcentration and upgrading of remobilised magmatic PGE concentrations is illustrated by the pathfinder studies, where correlations have been observed between the higher levels of As and the highest PGE grades. In apparent contradiction, an As-bearing fluid is an unlikely agent for the initial serpentinisation and release of PGE. Although the stability constants for PGE complexes with ligands involving As, Se and Te are unknown, it is likely that these metals have a very strong capacity to immobilize PGE because of the greater stability of arsenide, telluride and selenide minerals compared with the corresponding sulphides (Mountain & Wood, 1988). Thus the role of the As-bearing fluid

at Cliff is to effectively precipitate remobilised PGE from solution (figure 5.26 b). The highest PGE tenors are expected to form where the serpentinising fluids mix with later As-bearing oxidising fluids. Again this will occur in serpentinite at the margin of the chromitite body, according to the source area, volumetric expansion and void space arguments discussed above. This model explains why hydrothermal enrichments occur where magmatic concentrations abut against shear zones, whereas the serpentinites from the shear zones are themselves PGE-poor.

The structural pattern in the area around Cliff (figure 2.6) is relevant to a discussion of the origin of the As-bearing fluid. Sedimentary rocks beneath the ophiolite basal thrust are the most likely source of the As. It can be seen that the Cliff quarry lies at the junction of N-S and (later?) NE-SW shear zones (figure 2.6). The internal N-S shear zones parallel to the basal thrust are commonly sinistral, as is shown by offsets of the ophiolitic layering (figure 2.7). The general orientation of the NE-SW shear zone and the slight offset along it, suggests that this is a conjugate dextral structure (figure 2.6). These two structural directions in combination allow access to As-bearing hydrothermal fluids emanating from the basal thrust and circulating through the underlying metasediments. By virtue of the serpentinisation reaction fresh dunites will be impervious to hydrous fluids. Thus it is only when serpentinisation is well advanced that hydrothermal circulation is possible and an exchange of As between basement and ophiolitic serpentinites occurs. For these reasons it is likely that hydrothermal As-bearing fluids reached the Cliff area slightly later than the initial serpentinisation. These fluids provided a potent mechanism for fixing the dissolved PGE remobilised by the initial serpentinisation of a sulphide-bearing magmatic PGE concentration.

The model suggested here explains why unserpentinised sulphide-bearing dunites from Cliff contain magmatic levels of PGE (1-4 ppm), whereas the highly serpentinised chromite-rich margin of the chromitite body contain hydrothermally enhanced levels (10-100 ppm). This material formed the gangue of the historical chromitite mining operations and as a consequence is well represented in the surrounding spoil tips (plate 2.26). Although experimental data are lacking, the formation of bisulphide complexes is a possible means of dissolution and remobilisation of magmatic PGE concentrations during serpentinisation.

Interaction with a later As-bearing fluid derived from the basal thrust provides an effective means of fixing any remobilised PGE. It should be stressed that a large scale hydrothermal system scavenging background levels of PGE from silicate lithologies is not envisaged. Instead it is thought that the PGE are sourced locally from an existing magmatic concentration. It is the nature of such a magmatic concentration, namely the presence of sulphide phases within chromite-rich rocks, which itself allows such remobilisation and enhancement of typical magmatic concentrations. Simple calculations indicate that mass balance can be obeyed while producing the type of enrichments seen at Cliff. The implications of this model from an exploration viewpoint are that such concentrations, although very high grade, are likely to be small. Their location will be controlled by the distribution of magmatic source concentrations, rather than evidence of hydrothermal alteration alone. The combination of processes envisaged at Cliff also suggests that they may be rare geologically. Further work on the spatial distribution of PGE mineralisation at Cliff using drill-core (work in progress) will allow this predicted model to be tested.

5.8 Discussion and conclusions

The trace elements Ni, Cu, Co, and Cr show an igneous distribution in the ophiolite sequence. This is illustrated by their patterns of primary lithological association and mineralogical control. Anomalous levels of these elements are associated with chromite-rich lithologies in a similar manner as anomalous Pt, Pd Ir and Au concentrations (chapter 4). Moderate levels of As and Sb show a similar distribution, although superimposed on this pattern are highly anomalous concentrations one or two orders of magnitude higher. These occur in highly altered lithologies associated with shear zones, which is indicative of secondary concentration processes during alteration by hydrothermal fluids.

The chalcophile elements are fractionated by magmatic processes. This is illustrated by the different relative concentrations of Ni and Cu at different stratigraphic levels in the cumulate sequence. Enrichments of Ni occur in basal olivine-rich lithologies but Cu enrichments also occur in the stratigraphically higher pyroxene-rich rocks. This earlier depletion of Ni is mirrored by decreases in the Ni content of olivine and possibly of the sulphide phases at higher stratigraphic levels.

Anomalous levels of PGE and Au are associated with anomalous levels of Ni, Cu, Co, Cr, As and Sb. The relative strength of these associations is different for each platinum-group element, indicating internal fractionation within the group. Ir shows a particularly strong association with Co and Cr, since both occur in chromite. Pt Pd and Au show a strong association with Ni and Cu, reflecting their connection with sulphide phases.

The relationship between Pt, Pd, Au and chalcophile elements described above suggests that Ni and Cu are potential pathfinders for PGE mineralisation. Graphically only a weak linear dependence is observed between PGE and chalcophile elements when the whole database is considered. Possible reasons for such a poor correlation are as follows:-

(1) The precision of the PGE analyses is too low, obscuring any linear pattern by random fluctuation.

(2) An original primary dependence has been obscured by secondary processes and remobilisation.

(3) Ratios of PGE to pathfinder elements vary with stratigraphic level and rock type reflecting igneous fractionation processes.

The first and last factors are considered in the following chapters by detailed investigation of single mineralised horizons and by re-analysis using a technique with superior precision. The possibility of significant secondary remobilisation can be dismissed for all areas other than Cliff since primary lithological associations and mineralogical controls are preserved. Furthermore, the bulk of the mineralisation does not contain the highly anomalous levels of As and Sb which geochemically fingerprint rocks substantially altered by secondary fluid related processes.

This is not the case for mineralisation from the Cliff quarry. Chromitites, disseminated chromite-rich dunites and sulphide-bearing dunites from this locality contain anomalous levels of Ni, Cu and Sb and highly anomalous levels of Pt, Pd, Ir, Au and As. The high levels of As have been attributed to a hydrothermal overprint by As-rich fluids as a consequence of the proximity of the Cliff area to the basal thrust of the ophiolite (Lord & Prichard, 1989). The PGE mineralisation at Cliff shows all the attributes of other mineralised areas, namely an association with Ni-Cu sulphides and chromite. However, the absolute concentrations of PGE at Cliff are one to two orders of magnitude higher than those found elsewhere. Furthermore, the higher concentrations of Pt, Pd, Ir and Au show statistically significant correlations with As and Sb. This suggests that the original primary PGE concentrations have been remobilised and enhanced by serpentinisation and interaction with As-rich hydrothermal fluids.

For these reasons it is suggested that the extremely high grades found at Cliff are due to the secondary hydrothermal remobilisation and enhancement of an existing igneous concentration. A general feature of hydrothermal PGE deposits is that they contain concentrations of Pd >> Pt >> other PGE and are Au-rich, reflecting the differing solubilities of each element (Hulbert et al., 1988). Consideration of the PGE inter-elemental ratios alone provides little evidence of the modification of the original magmatic concentrations (section 5.5.1). The sample from Cliff with the highest overall grade does shows an enrichment in Pd and Au relative to Pt or Ir, when compared to other samples from Cliff but these latter samples exhibit similar inter-elemental ratios to mineralised rocks

from elsewhere. These problems are considered in the final chapter where high precision analyses of Cliff material for all six PGE are discussed.

Chapter 6

Stratigraphically Controlled PGE Mineralisation

6.1 Introduction

The reconnaissance sampling and analytical program described in chapters four and five indicated that PGE and chalcophile elements have retained an igneous distribution in the ophiolite sequence. These elements are fractionated by the magmatic processes producing this sequence and anomalous concentrations occur at certain stratigraphic levels in distinct lithological associations.

Anomalous levels of Pt and Pd occur principally in sulphide-bearing dunites spatially associated with chromite. Subsidiary concentrations also occur in sulphide-bearing pyroxenites from the basal regions of the layered pyroxene-rich sequence. Multiple chromite-rich horizons testify to cyclic repetitions within the cumulate sequence which are attributed to influxes of primitive magma during open-system fractionation. Initial results indicate that anomalous levels of PGE are associated with each of these horizons. The occurrence of PGE in the basal regions of cyclic units indicates that PGE were concentrated in the first sulphide phases segregating from the evolving resident magma soon after each primitive input. This genetic model predicts that PGE concentrations might also occur in sulphide-bearing horizons in the poorly exposed region close to the base of the dunite unit.

This chapter describes the results of follow-up sampling and analysis of rocks collected in areas containing, or expected to contain, anomalous mineralisation. The aims of this sampling were threefold:- Firstly to establish the form and vertical extent of mineralisation. Secondly to establish the lateral continuity of mineralised horizons between different exposures and finally to investigate progressive fractionation at successively higher stratigraphic levels. This was achieved by collecting closely spaced samples along traverses perpendicular to the silicate layering. The results of this surface sampling were encouraging

and prompted a drilling program with the aim of intersecting lateral continuations of this mineralisation under poorly exposed areas.

Details of all the traverses are given in table 6.1 and their locations are shown in figure 6.1. The 137 new samples were all analysed for Pt and Pd by Anamet Services and for a range of trace elements by ED-XRF at the Open University. This included the potential pathfinder elements Ni, Cu, Cr and As. The analytical procedures were identical to those of the reconnaissance program (sections 4.3.3 and 5.2.1 respectively). The traverses collected from within the basal dunites, the chromite quarries and the basal pyroxenites are now described in turn.

Table 6.1. Details of rock sample traverses.

Traverse	*Location*	*Number of samples*	*Maximum Pt (ppb)*	*Maximum Pd (ppb)*
Basal dunites				
T2	Hagdale Wick	36	90	140
T3	Muckle Heog East	9	50	80
T4	Muckle Heog West	8	40	70
T5	Trench	9	120	90
Chromite quarries				
T10	Quarry 12	4	290	630
T11	Quarry 12 S	10	380	700
T8	Quarry 10	11	150	220
T9	Quarry W of BX	4	780	1810
T7	Quarry 13	12	550	1070
T1	Fulmar Quarry	7	30	40
Pyroxene-bearing cumulates				
T13	Hagdale Coast	5	340	580
T12	The Nev high level chromite	10	250	450
T6	White House	12	150	230

Figure 6.1. Location of rock sample traverses.

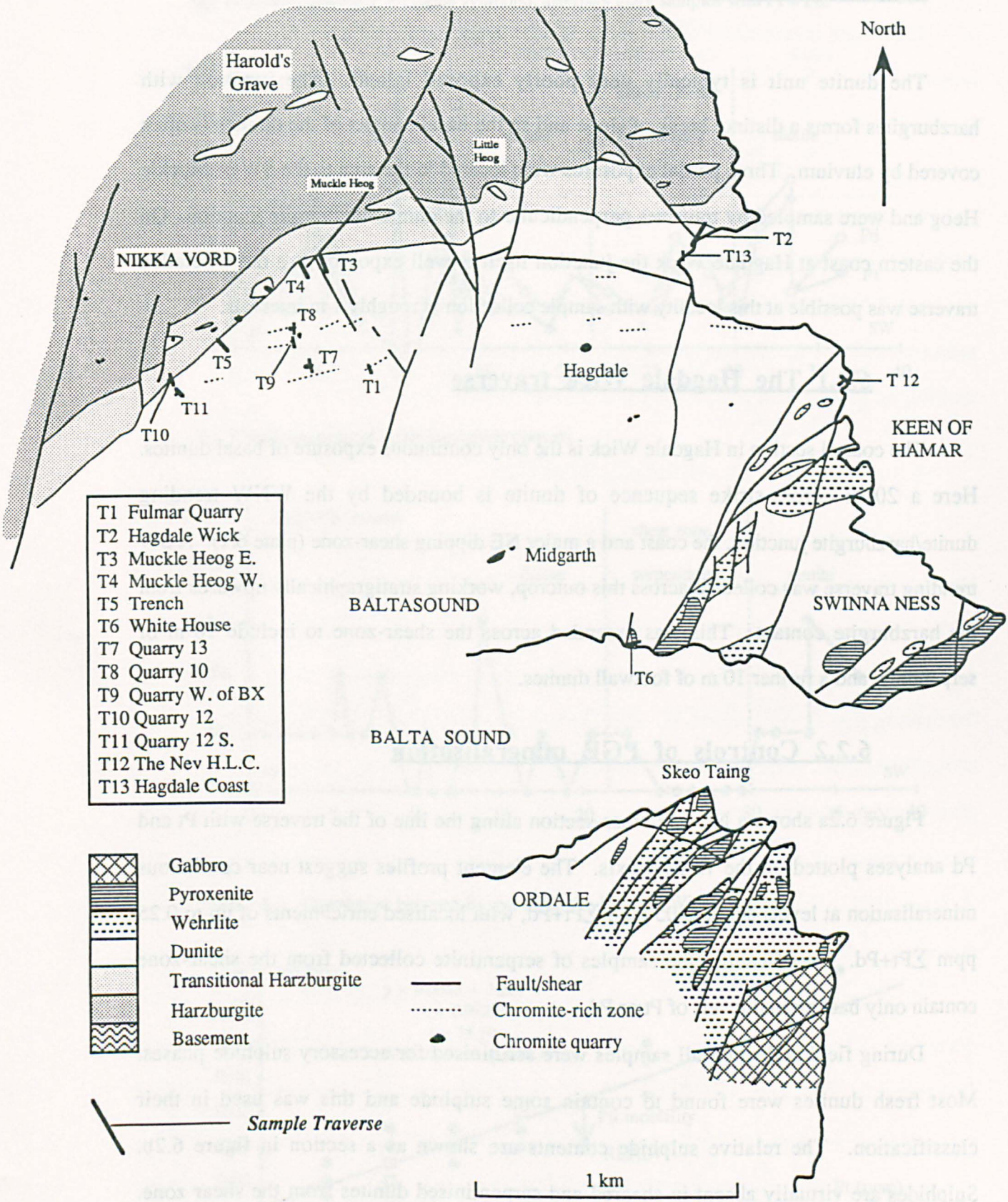

6.2 Basal dunites

The dunite unit is typically very poorly exposed inland. The junction with harzburgites forms a distinct break of slope and so the basal contact of the dunites is often covered by eluvium. Three partial exposures were located in the area to the SW of Muckle Heog and were sampled by traverses perpendicular to the dunite/harzburgite junction. On the eastern coast at Hagdale Wick the junction itself is well exposed, so a more detailed traverse was possible at this locality with sample collection at roughly 1 m intervals.

6.2.1 The Hagdale Wick traverse

The coastal section in Hagdale Wick is the only continuous exposure of basal dunites. Here a 20 m across-strike sequence of dunite is bounded by the WNW trending dunite/harzburgite junction, the coast and a major NE dipping shear-zone (plate 6.1). A SW trending traverse was collected across this outcrop, working stratigraphically upwards from the harzburgite contact. This was extended across the shear-zone to include 10 m of serpentinite and a further 10 m of footwall dunites.

6.2.2 Controls of PGE mineralisation

Figure 6.2a shows a NE-SW cross-section along the line of the traverse with Pt and Pd analyses plotted on the vertical axis. The element profiles suggest near continuous mineralisation at levels above 0.05 ppm ΣPt+Pd, with localised enrichments of up to 0.25 ppm ΣPt+Pd. Significantly, the samples of serpentinite collected from the shear-zone contain only background levels of Pt or Pd.

During field collection all samples were scrutinised for accessory sulphide phases. Most fresh dunites were found to contain some sulphide and this was used in their classification. The relative sulphide contents are shown as a section in figure 6.2b. Sulphides are virtually absent in sheared and serpentinised dunites from the shear zone.

Figure 6.2. PGE concentrations and sulphide contents in the Hagdale Wick Traverse.

(a) Pt (closed symbols), Pd (open symbols), asterisks mark samples with Pt = Pd.

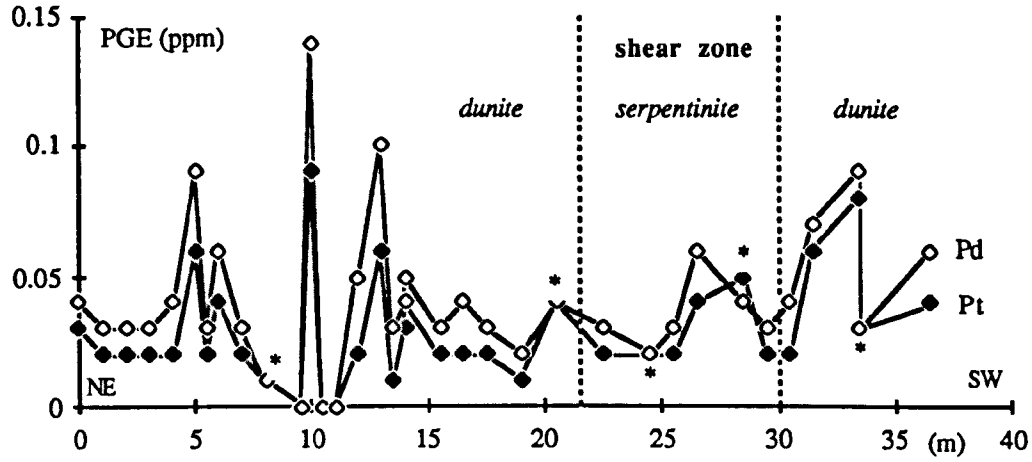

(b) Visual estimates of relative sulphide content.

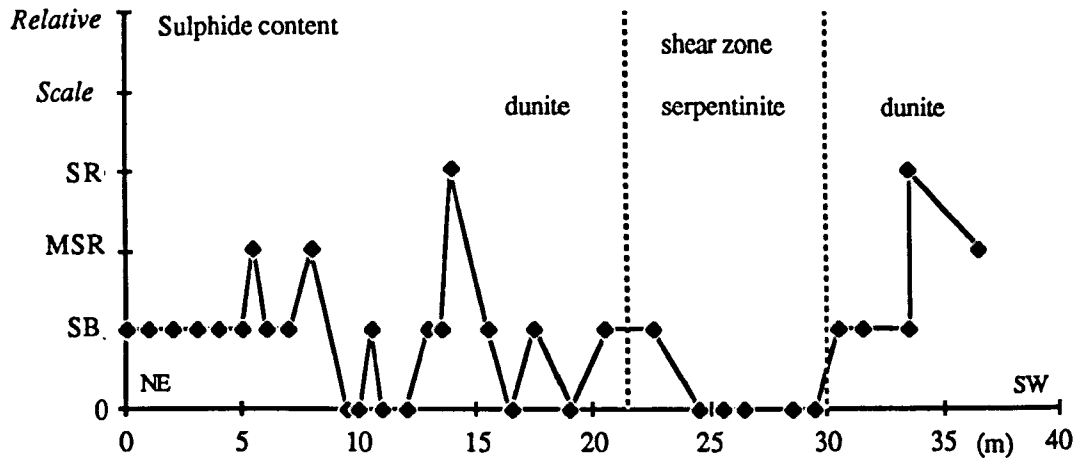

Figure 6.3. Correlation between Pt and Pd in the Hagdale Wick Traverse.

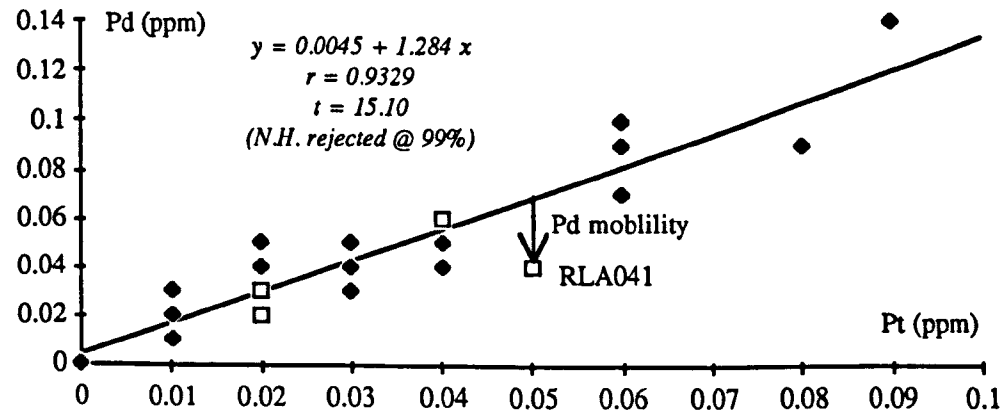

In the fresh parts of the section the Pt and Pd concentrations mirror the sulphide profile, illustrating the association between PGE and sulphide (section 4.5.2).

Individual levels of Pd mirror those of Pt but are consistently higher. This pattern indicates that the two elements are subject to the same genetic controls. A few samples (marked as *) contain levels of Pd equal to those of Pt. These samples occur within the main shear zone or in other zones of alterations. One sample, a highly schistose carbonate-rich serpentinite from the shear zone, contains less Pd than Pt. Graphical comparison of the Pt and Pd concentrations and regression analysis indicates a strong positive correlation and a constant Pt/Pd ratio over most of the traverse (figure 6.3). Departures from this constant ratio are attributed to minor secondary remobilisation of palladium, due to the greater relative mobility of this element (Fuchs and Rose, 1974).

6.2.3 Trace element profiles

Sections have also been drawn showing concentrations of Ni, Cu, Cr and As along the Hagdale Wick traverse (figure 6.4). Levels of PGE are shown for comparison, expressed as the total concentration of Pt and Pd.

Levels of Ni are consistently high across the lowermost 22 m of the traverse. Variations due to differences in sulphide contents are difficult to see since they are numerically small in comparison to the overall concentrations of the element. Sympathetic positive and negative anomalies occur over the shear zone, within which the minimum concentrations are much lower than the background levels across the fresh olivine-rich zone. A sharp drop in total Ni is apparent in the fresh rocks overlying the shear zone, which is consistent with a structural displacement of the original sequence.

Concentrations of copper are highly variable across the traverse with the highest levels occurring only within the fresh dunites. Two broad Cu anomalies are present in the lowermost 22 m. These are related to areas of the traverse with higher relative sulphide contents (e.g. at 5-8 m and 14-15 m on figure 6.2b). Background levels of Cu are very low in comparison to the two anomalies and suggest an underlying trend of increasing levels upwards through the stratigraphy.

Figure 6.4. Variation in PGE, Ni, Cu, Cr and As across the Hagdale Wick Traverse.

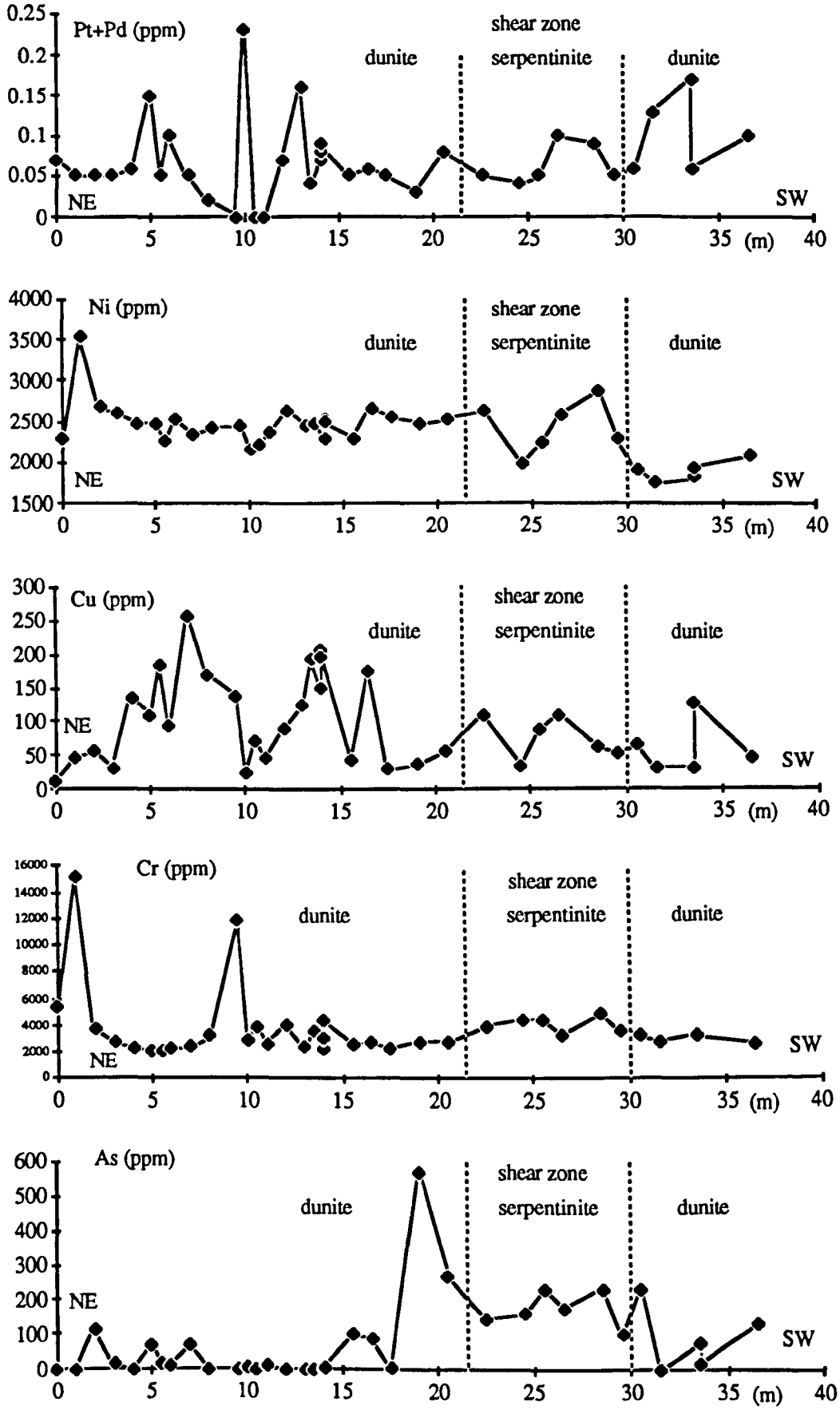

Throughout the traverse there is a background of moderate levels of Cr (c. 3000 ppm), reflecting the presence of accessory chrome-spinel in all of the dunites. The two anomalies correspond to samples collected from minor chromite layers.

A strong As anomaly occurs in the region of the shear zone. Levels of As in the fresh zones are generally an order of magnitude lower. The highest levels of As occur in the slightly altered wall rock adjacent to the shear zone, thus shouldering the main anomaly.

The trace element profiles described above demonstrate the effects of both primary igneous and superimposed secondary processes. Within the fresh areas of the traverse, the control of accessory sulphide phases on the concentrations of chalcophile elements is illustrated by the variable levels of Cu. A similar pattern for Ni is obscured by the relatively high background level, reflecting a significant proportion of the total Ni content within the olivine matrix. Variable amounts of nickel sulphides thus have little impact on the overall form of the profile.

The effects of secondary alteration processes are localised and restricted to the immediate vicinity of the shear zone. These are fingerprinted by high levels of As which result from the introduction of this element by hydrothermal fluids causing the related serpentinisation and talc formation. Sympathetic positive and negative Ni anomalies within the shear zone indicate the release of Ni from olivine and slight remobilisation during extreme serpentinisation. A similar pattern is shown by copper, for which there is a notable absence of anomalies within this zone.

In conclusion, primary igneous concentrations of chalcophile elements are preserved away from localised alteration zones, which may be recognised by their anomalous levels of As but do not contain enhanced levels of Pt or Pd.

6.2.4 Cryptic layering and magmatic cycles

Figure 6.4 summarises the variations in PGE and trace element concentrations across the Hagdale Wick traverse. Each element profile shows the variation between the minimum and maximum recorded concentrations at this locality (table 6.2). For each datum point the minimum level in the traverse has been subtracted from the concentration in the sample. This method of presentation has been used to reduce the extent to which the high constant

Figure 6.5. Trace element cryptic layering in the Hagdale Wick Traverse. The diagram shows on a linear scale the variation between the minimum and maximum recorded levels of each element (see table 6.2).

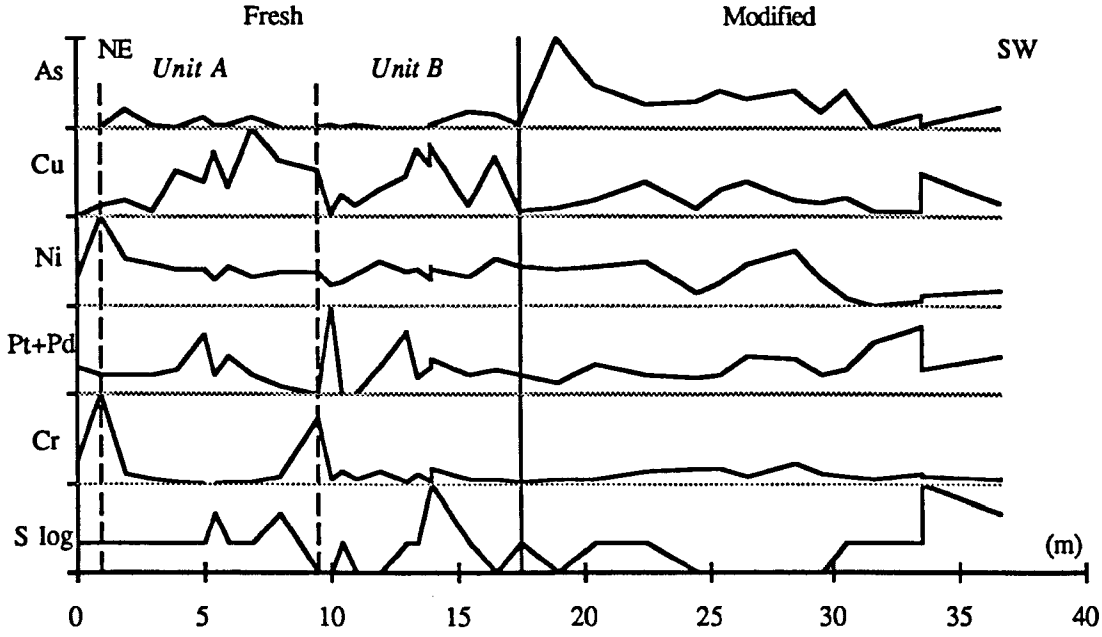

Table 6.2. Range of trace element concentrations shown in figure 6.5.

Element	*As (ppm)*	*Cu (ppm)*	*Ni (ppm)*	*Pt+Pd (ppb)*	*Cr (ppm)*
Minimum	0	13	1749	0	2030
Maximum	573	256	3540	230	15228

background levels of elements such as Ni obscure the relatively small anomalies. The visual field log of relative sulphide content is also shown, plotted in a similar manner.

The fresh and modified areas of the traverse can be recognised by the higher levels of As in the latter. All the element profiles show contrasting textures between these two zones, due in part to different sampling intervals. The fresh zone of the traverse has been further divided using the two chromium maxima as markers. These represent small chromite layers. This divides the other profiles into two symmetrical portions (units A and B). In each unit copper concentrations show a general increases upwards from the stratigraphic base. Background levels of Ni decrease across unit A and are approximately constant over unit B. Anomalies in PGE, Ni or Cu concentrations and visible sulphide contents occur close

together but are mutually displaced. In both cases Pt and Pd anomalies occur near the middle of the unit, slightly below the peak sulphide contents. The maximum concentrations within the broader Cu anomalies occur slightly higher than the peak sulphide contents. A third Pt and Pd anomaly, the highest overall concentration of these elements, occurs close to the junction of the two units at the base of unit B.

The symmetry of the above patterns with respect to the small chromite enrichments indicates that they are cyclic units within the cumulate sequence. These are interpreted as relict igneous cryptic layering resulting from magmatic fractionation processes. In the absence of mineral analyses it is difficult to say whether this alternation results from cyclic variations (e.g. catenary pattern of Cr content in unit A) or from repeated influxes periodically resetting fractionation (i.e. rhythmic sawtooth patterns). The resetting patterns for Cu, the least compatible of this group of chalcophile elements, suggest that the latter interpretation is the most likely.

6.2.5 Strike-length of PGE-enriched horizons

The PGE concentrations located by the three other traverses across the base of the dunite unit are shown in figure 6.6. Although these traverses are only partially exposed, they all contain discrete PGE anomalies of the same order of magnitude as those found in the Hagdale Wick traverse (100-200 ppb). Together all four traverses represent a strike length of approximately 2 km (figure 6.1) and indicate that low level mineralisation is consistently present within this horizon. This suggests that laterally continuous mineralisation might also occur at other stratigraphic levels within the main dunite unit. The identification of stratigraphically controlled mineralisation within such a layered cumulate sequence further confirms that in this environment the PGE were concentrated by igneous processes.

6.2.6 Conclusions

The location of PGE concentrations at the base of the dunite unit validates the igneous fractionation model (section 4.6) which predicted that enrichments should occur at this level. This genetic model suggested that Pt and Pd concentrations occur in association with the

Figure 6.6. Concentrations of PGE in the three other basal dunite traverses. Sample points are extrapolated to half their own concentration at a distance of 1 m, rather than correlated across large zones without exposure, in view of the complex patterns observed in Hagdale Wick.

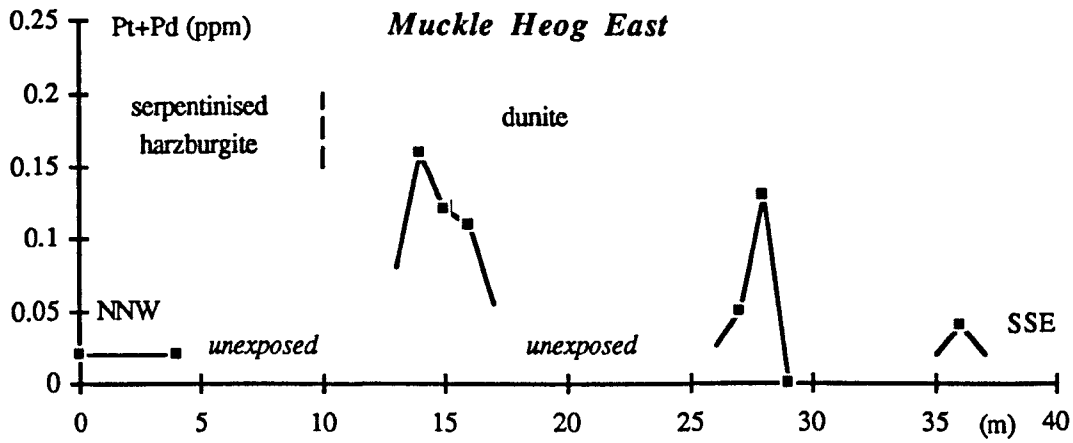

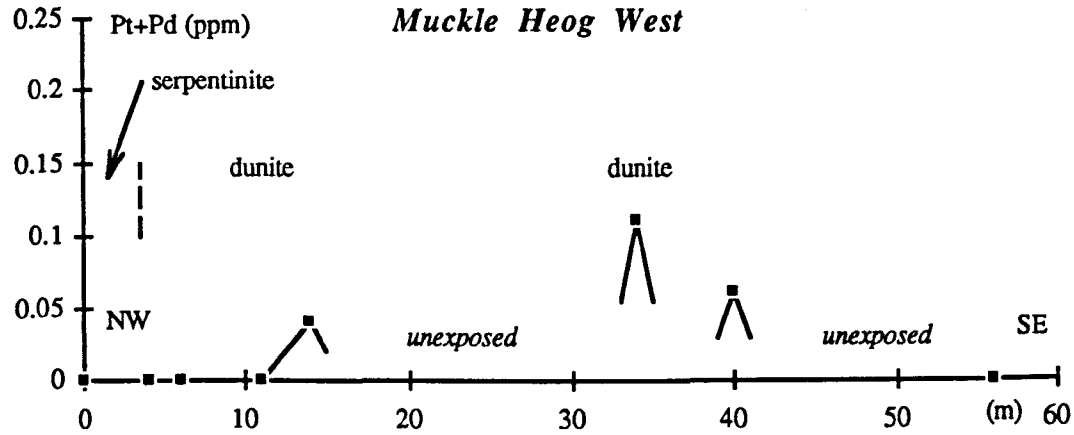

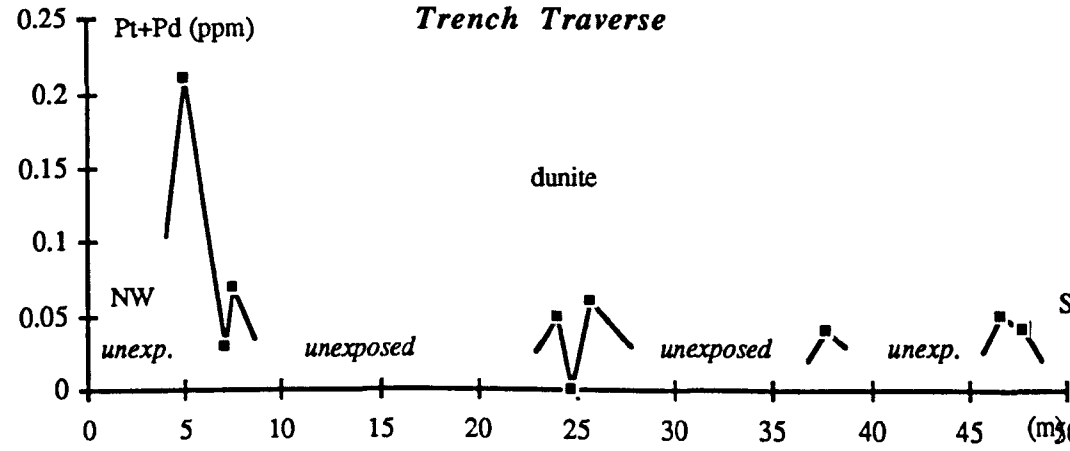

first sulphide phases segregating from the evolving resident magma after each primitive input.

The PGE-enriched horizon at the base of the cumulate sequence exhibits a number of primary igneous signatures. This includes the constant ratio of Pt to Pd and their association with sulphide phases or concentrations of chalcophile pathfinder elements. In fresh rocks magmatic fractionation patterns are preserved within the cumulate sequences. Cryptic geochemical layering indicates that chromite crystallisation preceding sulphide segregation, which in turn scavenged PGE and chalcophile elements from the magma. These sulphide-rich horizons are also fractionated with PGE-rich bases and copper-rich tops.

Although chalcophile element ratios are modified in shear zones by the action of As-rich fluids there is little evidence of hydrothermal enhancement of PGE above magmatic levels. In this environment Pt and Pd appear to be less mobile than Ni or Cu when sulphide phases are remobilised. Some minor remobilisation and loss of Pd is suggested by the lower Pd/Pt ratios of certain samples.

6.3 Chromite quarries

The reconnaisance sampling program (chapter 4) indicated that anomalous levels of Pt and Pd occur in a number of the disused chromite quarries in the area north of Baltasound. Chromite quarries within the cumulate dunite unit all occur in zones of very poor exposure. All of the original chromite-rich dunite has been removed at the surface and the abandoned pits are water-filled and consequently inaccessible. The margins of a few of the quarry faces provide limited exposure of the dunites hosting the original chromite concentrations. These quarry walls were the target of more detailed in situ sampling with the aim of investigating whether PGE concentrations extend into the surrounding dunites.

Sufficient exposures were located at five quarries for the identification of sulphide-bearing horizons. Samples were collected at 1 m intervals along traverses perpendicular to the strike of the extracted orebody at either side of the elongate quarries. End walls were also sampled to infer mineralisation across the extracted volume. Sampling points are shown on scale sketch maps of the quarries (figures 6.7 -6.9). These maps also show the

Plate 6.1. Location of the Hagdale Wick Traverse.

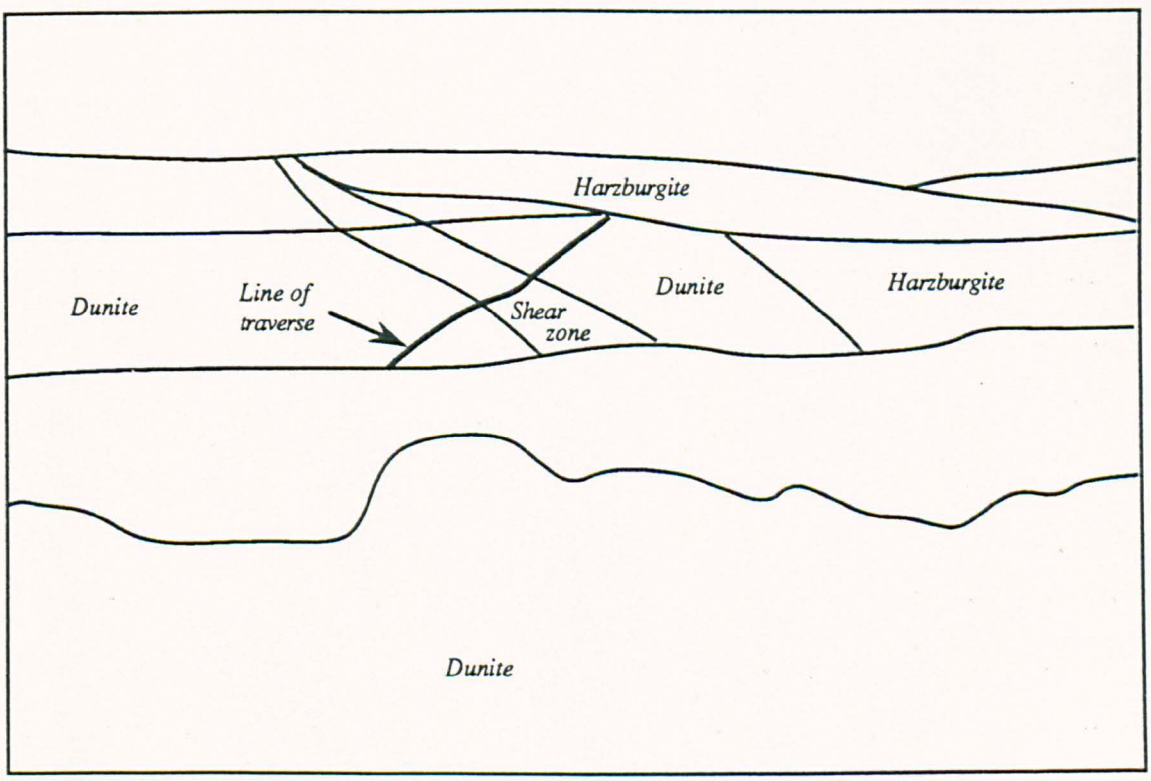

Plate 6.2. Quarry 12 North.

Plate 6.3. Quarry 12 South.

Plate 6.4. Quarry 13.

Plate 6.5. Quarry 10.

Plate 6.6. Quarry West of BX.

Plate 6.7. The adjacent BX Quarry.

Figure 6.7. Location of samples around Quarries 12 North and 12 South.

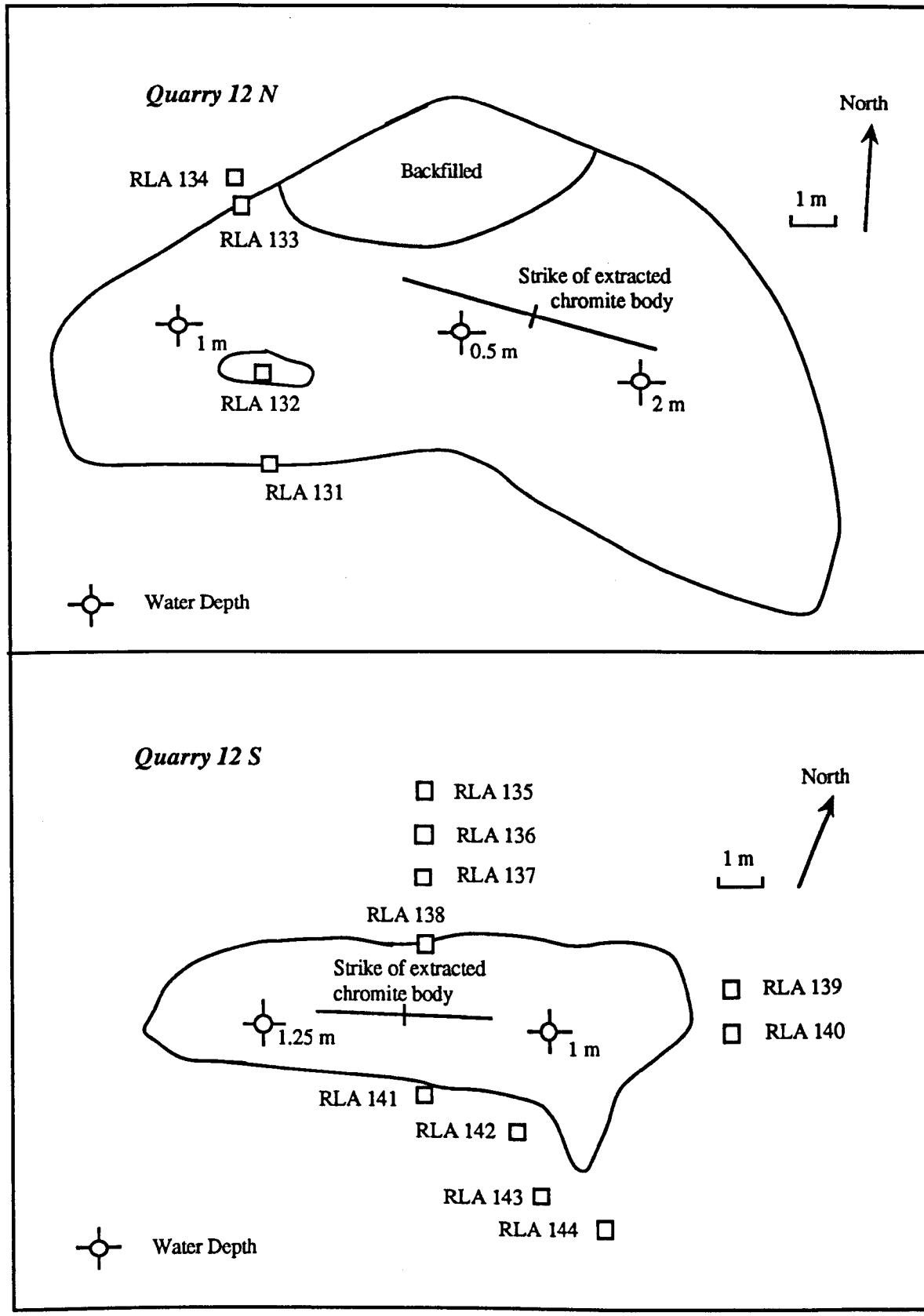

Figure 6.8. Location of samples around Quarry West of BX and Quarry 13.

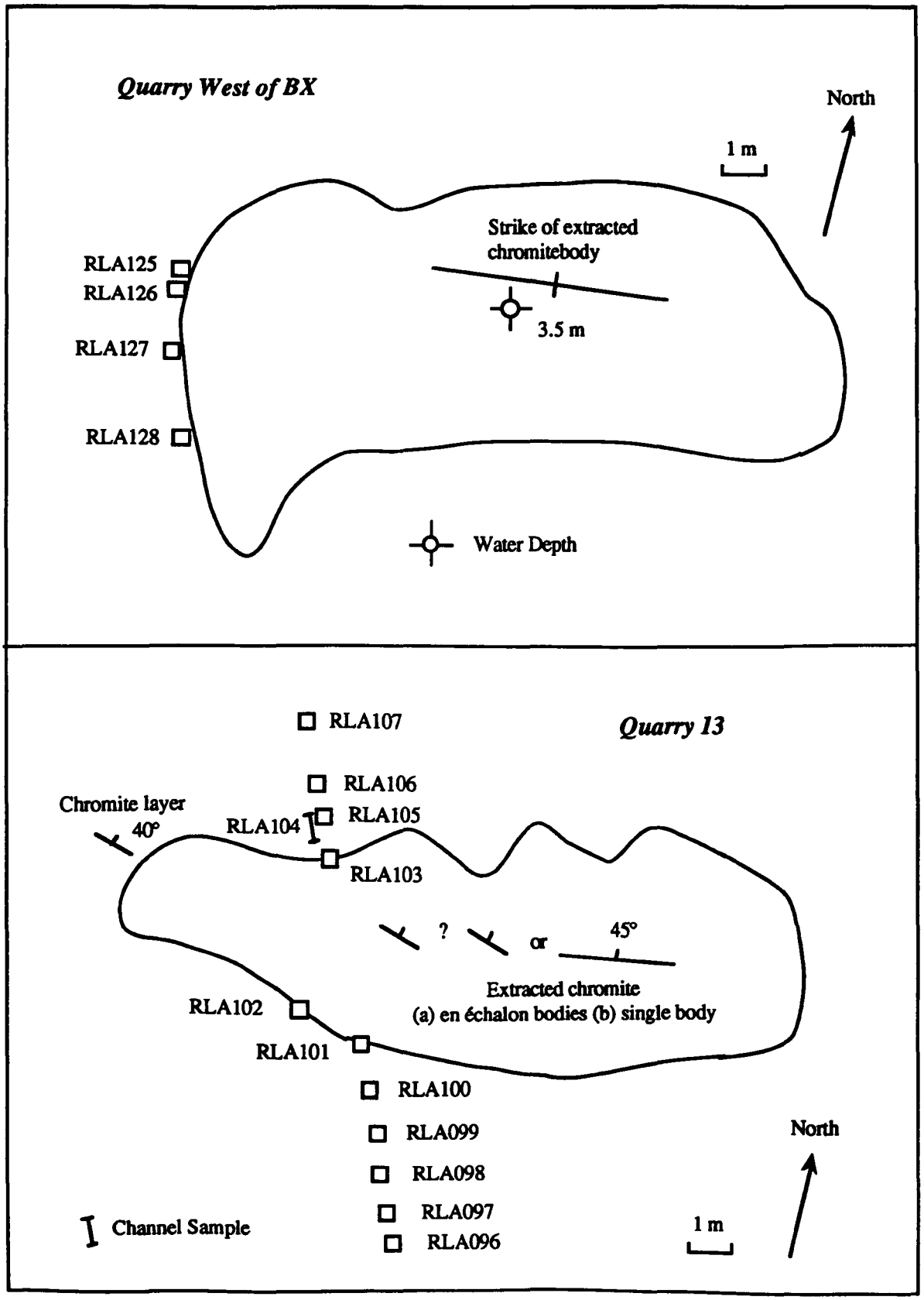

Figure 6.9. Location of samples around Quarry 10.

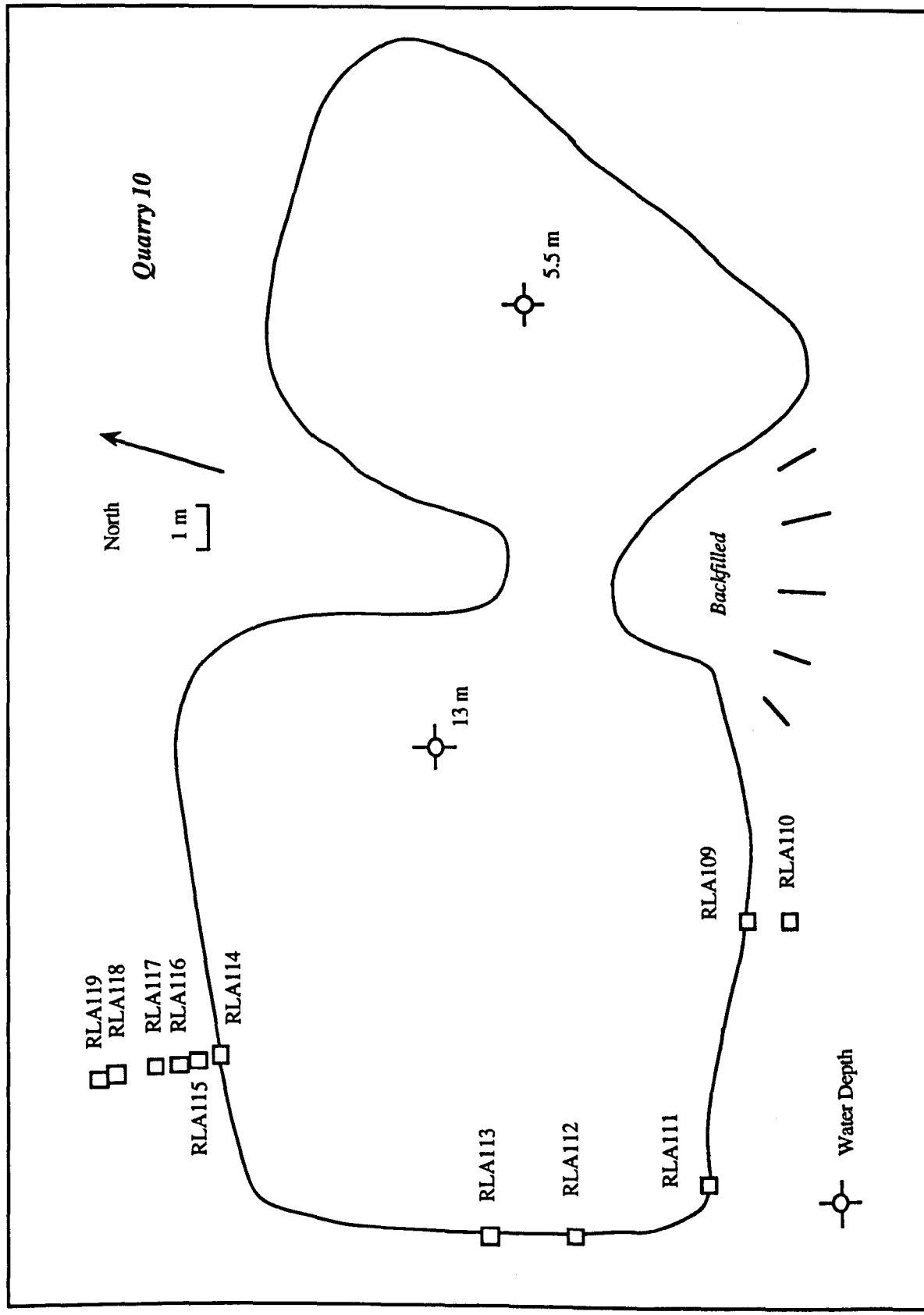

depth of the pits and the approximate original form of the chromite concentrations as inferred from the shape of the voids (plates 6.2 - 6.6).

6.3.1 PGE-enriched horizons

Sections showing PGE concentrations expressed as total Pt+Pd have been plotted for each chromite quarry traverse (figure 6.10). In each case the stratigraphic base of the section is at the origin. The same vertical and horizontal scale has been used in each section to allow visual comparison of the vertical extent and grade of mineralisation. The former position of extracted chromite-rich bodies are shown by dashed vertical lines. Mineralisation within these voids is suggested by extrapolating samples collected off the line of the main traverse in the end walls of the quarries (open circles and dotted profiles).

Anomalous levels of PGE are present in each traverse over stratigraphic thicknesses of 5 to 10 m. These are spatially associated with the former chromite concentrations and generally increase towards the margins of the extracted chromitite bodies. The peak PGE concentrations of over 2.5 ppm are an order of magnitude higher than those recorded from the base of the dunite unit. There is no clear correlation between the size of the chromitite body and either the peak PGE concentration or the overall amount of mineralisation (as represented by the area under the profiles). The largest quarry (10) contains the lowest peak PGE concentrations, which occur in dunites immediately below the chromite body, although the absence of higher levels located by the traverse is probably due to the larger volume of wall rock removed at this locality.

6.3.2 Pathfinder elements

The sample traverses across chromite quarries are shown schematically in figure 6.11. The symbols have been coloured according to the concentrations of PGE the samples contain. This diagram shows the broad zones of anomalous Pt+Pd levels in each traverse and also the close spatial association between the highest PGE concentrations and the chromitite bodies. Figures 6.12 and 6.13 show the same diagram but these have been coloured to represent the levels of Ni and Cu in the samples. Broad zones containing

Figure 6.10. Pseudo-sections showing PGE concentrations in traverses across chromite quarries.

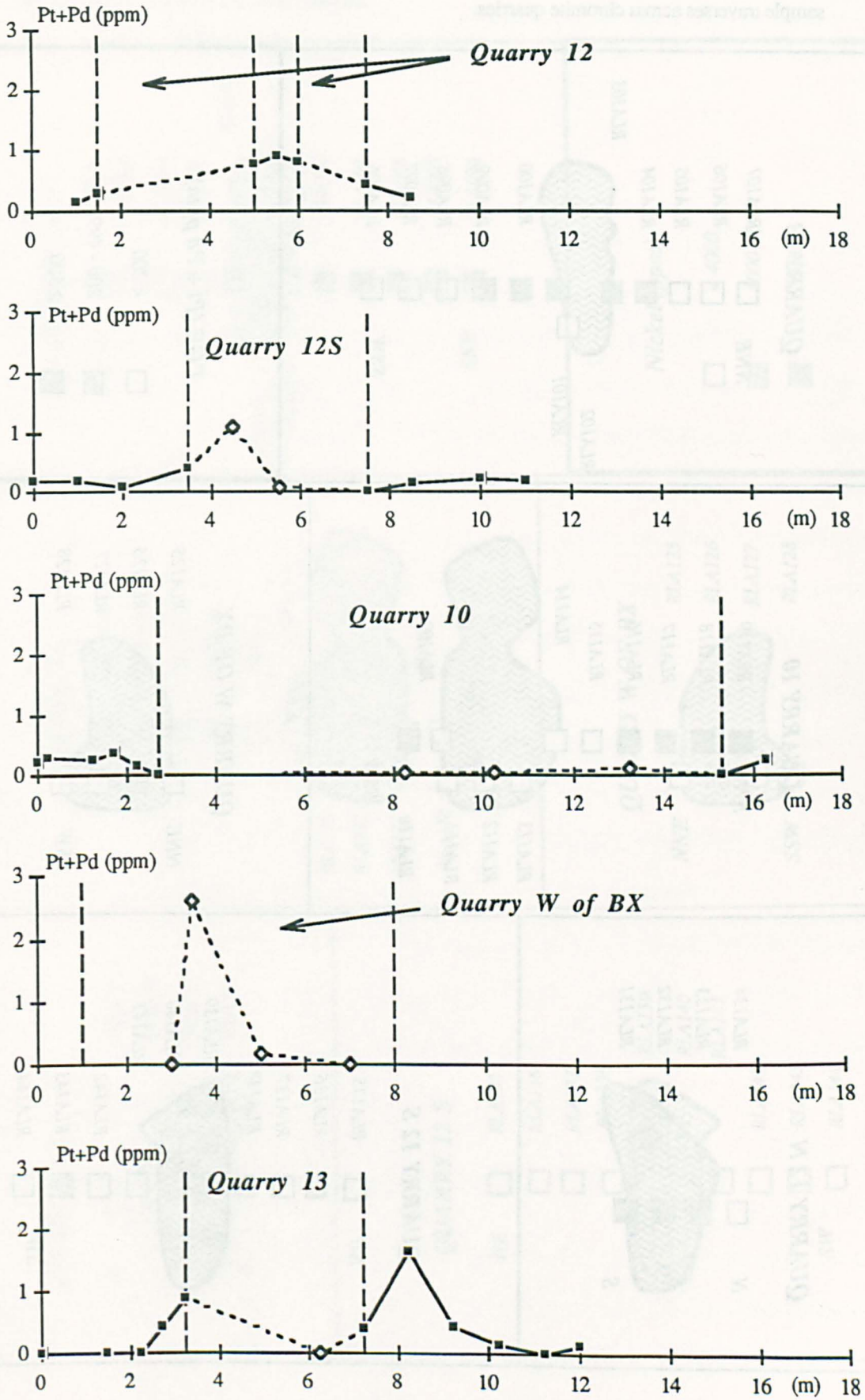

Figure 6.11. Schematic diagram showing sample points and anomalous levels of PGE in sample traverses across chromite quarries.

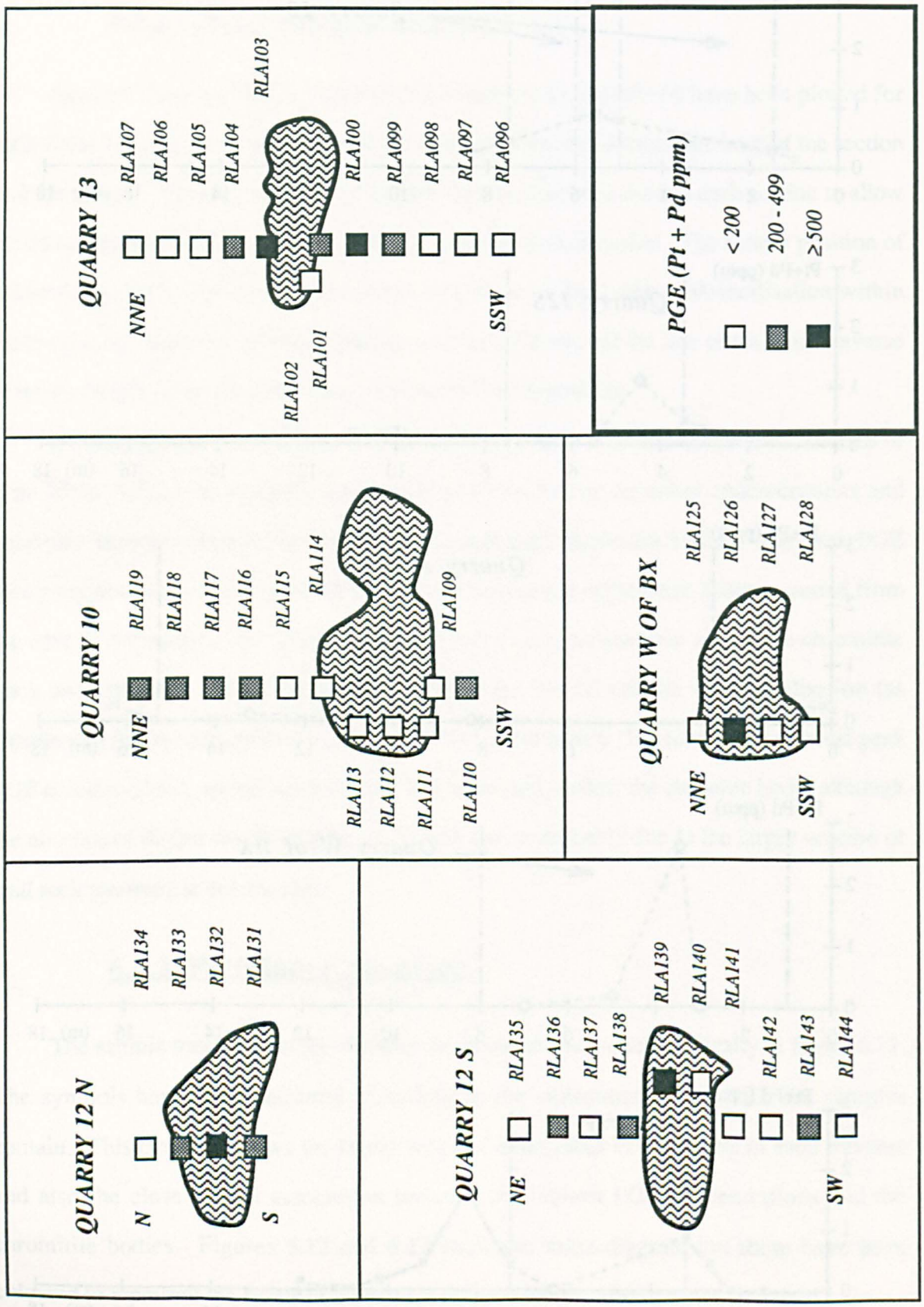

Figure 6.12. Schematic diagram showing sample points and anomalous levels of Ni in sample traverses across chromite quarries.

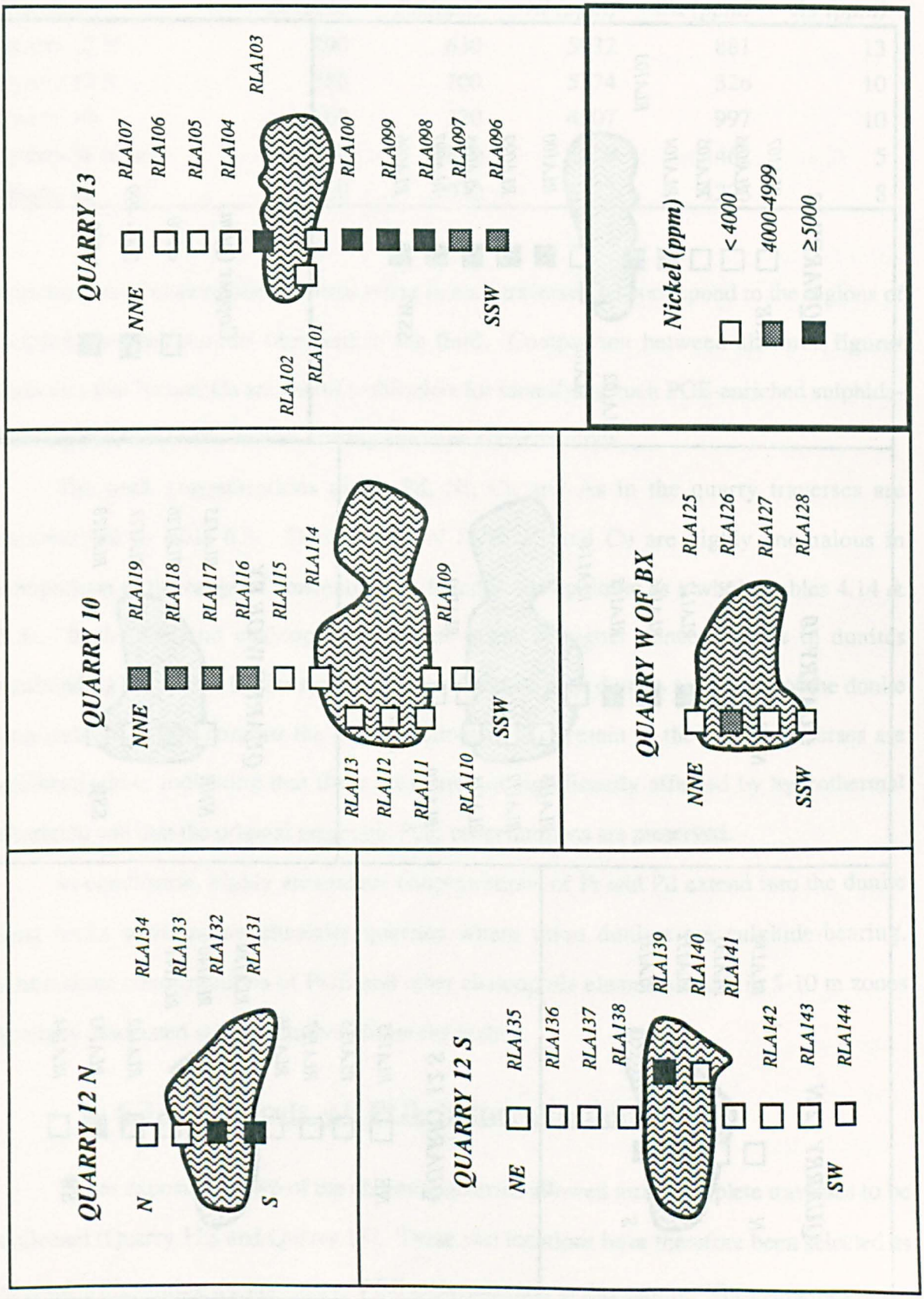

Figure 6.13. Schematic diagram showing sample points and anomalous levels of Cu in sample traverses across chromite quarries.

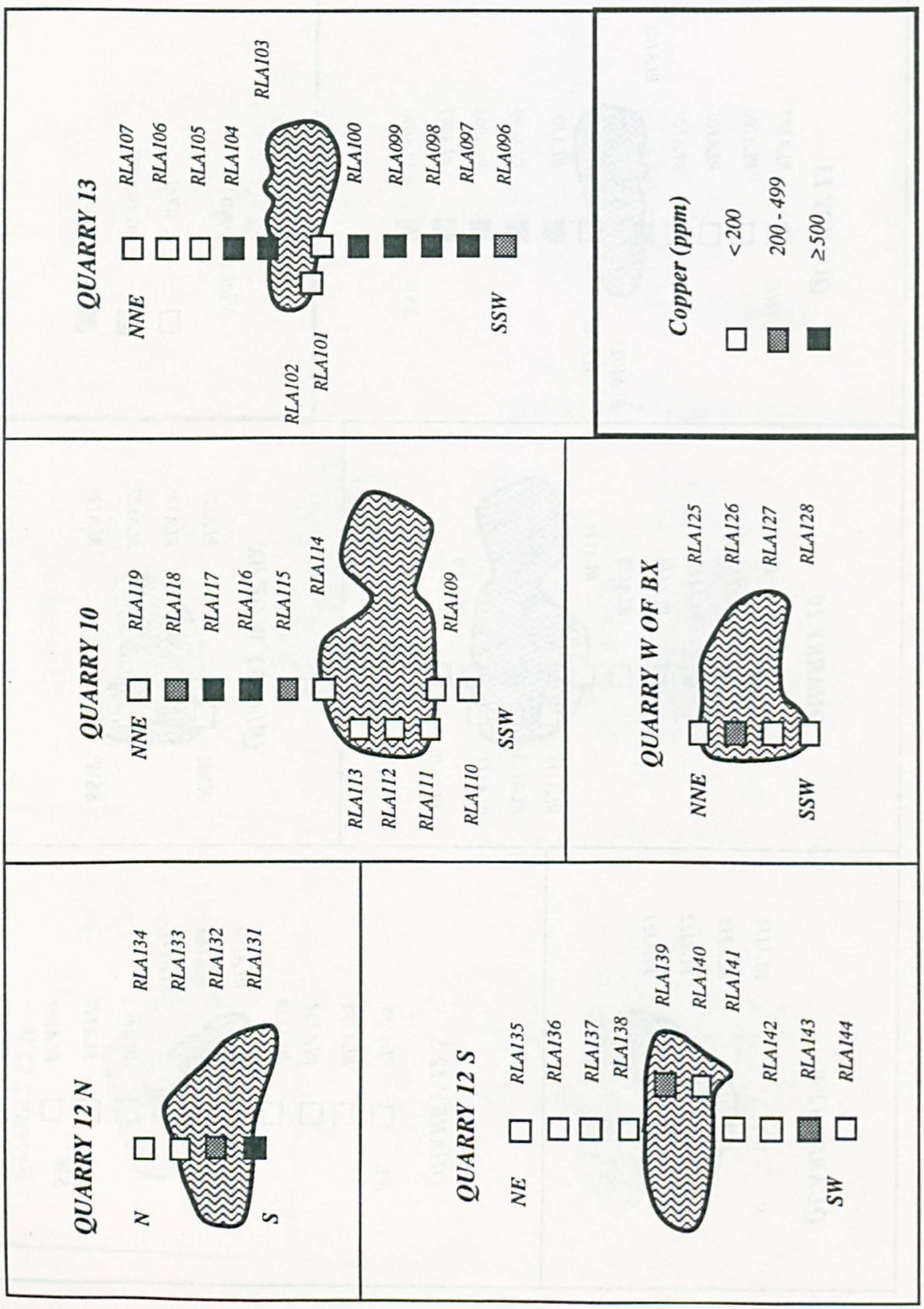

Table 6.3. Peak PGE and pathfinder element concentrations in chromite quarry traverses.

Traverse	*Pt (ppb)*	*Pd (ppb)*	*Ni (ppm)*	*Cu (ppm)*	*As (ppm)*
Quarry 12 N	290	630	5932	881	13
Quarry 12 S	380	700	5274	326	10
Quarry 10	160	220	4507	997	10
Quarry W of BX	780	1810	4226	462	5
Quarry 13	550	1070	6522	1225	8

enrichments of chalcophile elements occur in each traverse and correspond to the regions of sulphide-bearing dunites observed in the field. Comparison between all three figures indicates that Ni and Cu are useful pathfinders for identifying such PGE-enriched sulphide-bearing horizons in the dunites hosting chromite concentrations.

The peak concentrations of Pt, Pd, Ni, Cu and As in the quarry traverses are summarised in table 6.3. These levels of PGE, Ni and Cu are highly anomalous in comparison to the range of concentrations found in the ophiolite as a whole (tables 4.14 & 5.3). Both PGE and chalcophile elements occur at higher concentrations in dunites surrounding chromitite bodies than they do in chromite-poor dunites at the base of the dunite unit (table 6.2). In contrast the concentrations of As present in the quarry traverses are uniformly low, indicating that these areas are not significantly affected by hydrothermal alteration and that the original magmatic PGE concentrations are preserved.

In conclusion, highly anomalous concentrations of Pt and Pd extend into the dunite host rocks surrounding chromite quarries where these dunites are sulphide-bearing. Anomalous concentrations of PGE and other chalcophile elements occur in 5-10 m zones spatially associated with the former chromitite bodies.

6.3.3 Controls of PGE mineralisation

Better exposure at two of the chromite quarries allowed more complete traverses to be collected (Quarry 12S and Quarry 13). These two locations have therefore been selected as examples illustrating the controls of PGE mineralisation in this setting. These quarries occur

at different stratigraphic levels in successive chromite-rich zones (section 2.3.2). Quarry 12 South is located just above the dunite/harzburgite junction and lies within a western extension of chromite zone 1, or alternatively in an even lower stratigraphic zone (figure 2.8). Quarry 13 is situated within zone 2a which is the uppermost zone recognised in the immediate area.

Figures 6.14 and 6.15 show sections drawn for PGE concentrations and the relative contents of accessory sulphides in the Quarry 13 and 12S traverses. In each case the PGE concentrations closely follow variations in sulphide content, but the two profiles are not identical and the differences are consistent for both traverses. The profiles show step-wise increases in PGE and sulphide contents close to the base of the chromite body. Sulphide-rich zones extend vertically above the stratigraphic level of the chromite quarries In contrast the highest PGE concentrations only occur in close proximity to the chromite deposits. This is illustrated by anomalous PGE concentrations in the shaded region of the Quarry 12S traverse (figure 6.14) which represents dunites immediately along strike from the chromite body. The effect of these differences is such that the ratio of PGE to sulphide decreases rapidly upwards away from the chromite body.

The step-like features described above are interpreted as representing the base of major magmatic cycles producing large scale units within the cumulate sequence. Since these occur close to the stratigraphic base of chromitite bodies this confirms that chromite enriched horizons can be used as visual markers for the base of these cycles and hence for potential enrichments in PGE and other compatible elements

Pseudo-sections have also been drawn for the Quarry 12S and 13 traverses showing concentrations of the various pathfinder elements. PGE contents are shown for comparison expressed as the sum of Pt + Pd (figures 6.16 and 6.17). The profiles for Ni and Cu mirror that of Pt+Pd. Concentrations of these chalcophile elements closely follow variations in sulphide content with step-like increases at the base of the chromite body. The relatively low concentrations of As in both traverses also vary in sympathy with the sulphide content and the other chalcophile metals. In contrast Cr anomalies have an antithetic distribution and in both cases occur stratigraphically below zones containing enrichments of chalcophile elements.

Figure 6.14. Pseudo-sections showing levels of PGE and sulphides in the Quarry 12 S Traverse. The stratigraphic base of the section is at the origin in each case. Shaded regions indicate samples extrapolated from along strike of the chromite body. The relative sulphide contents are sulphide-bearing (SB), moderate (MSB), moderately rich (MSR), rich (SR) and very rich (VSR).

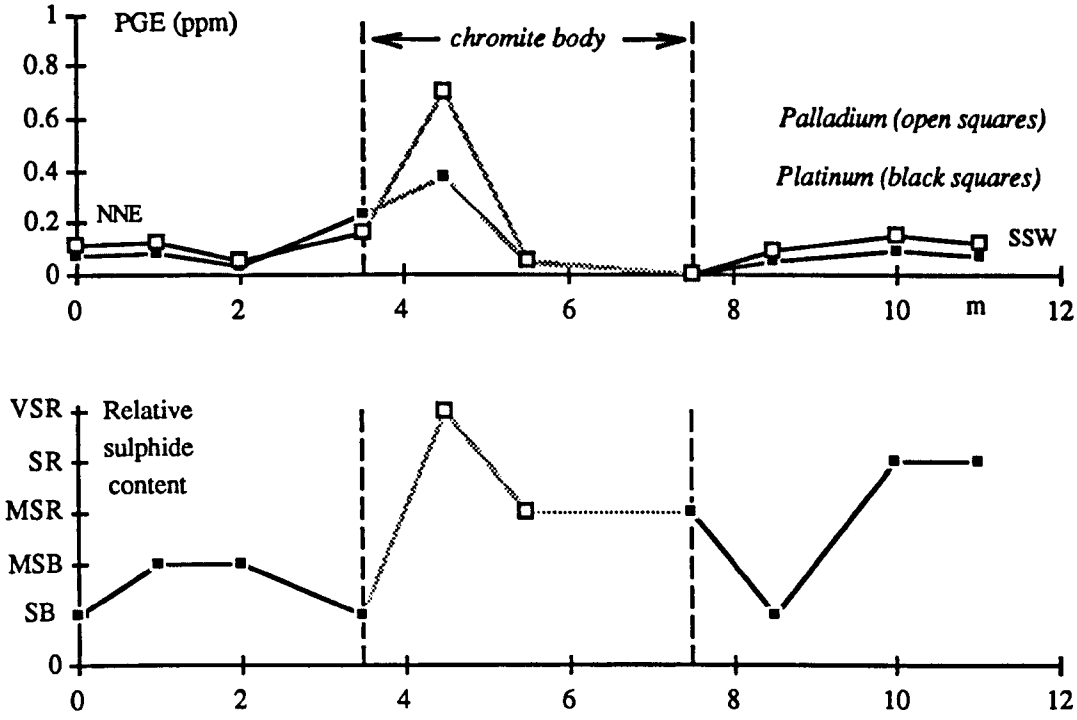

Figure 6.15. Pseudo-sections showing levels of PGE and sulphides in the Quarry 13 Traverse.

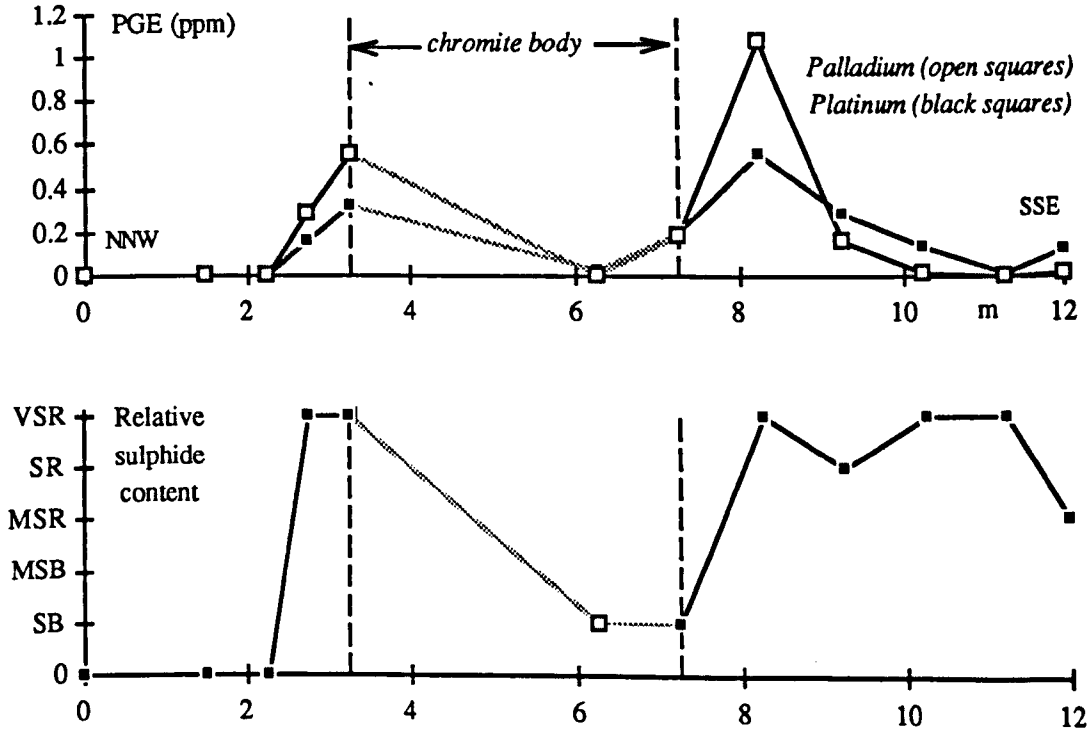

Figure 6.16. Pseudo-sections showing levels of PGE and pathfinders in the Quarry 12 S Traverse.

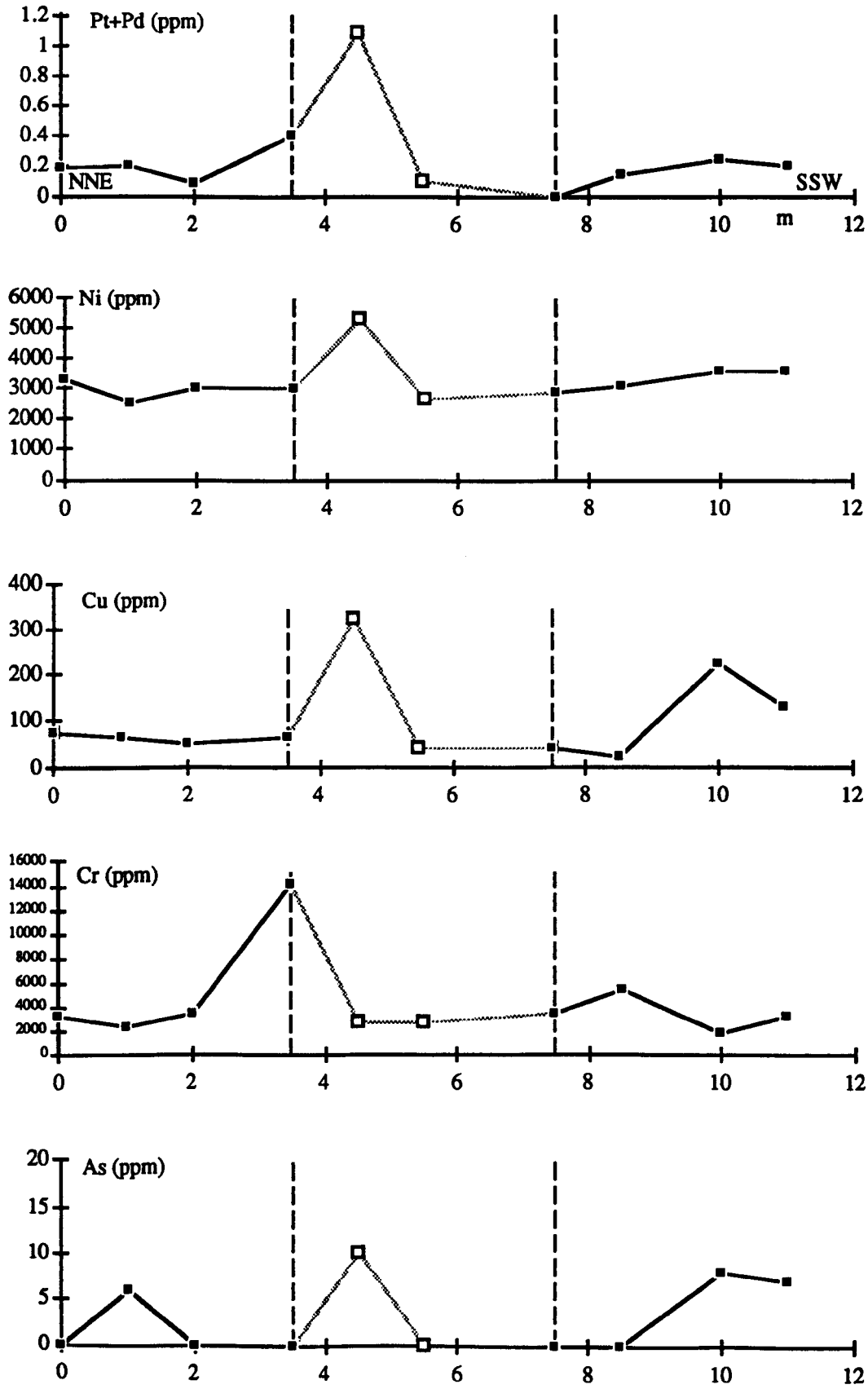

Figure 6.17. Pseudo-sections showing levels of PGE and pathfinders in the Quarry 13 Traverse.

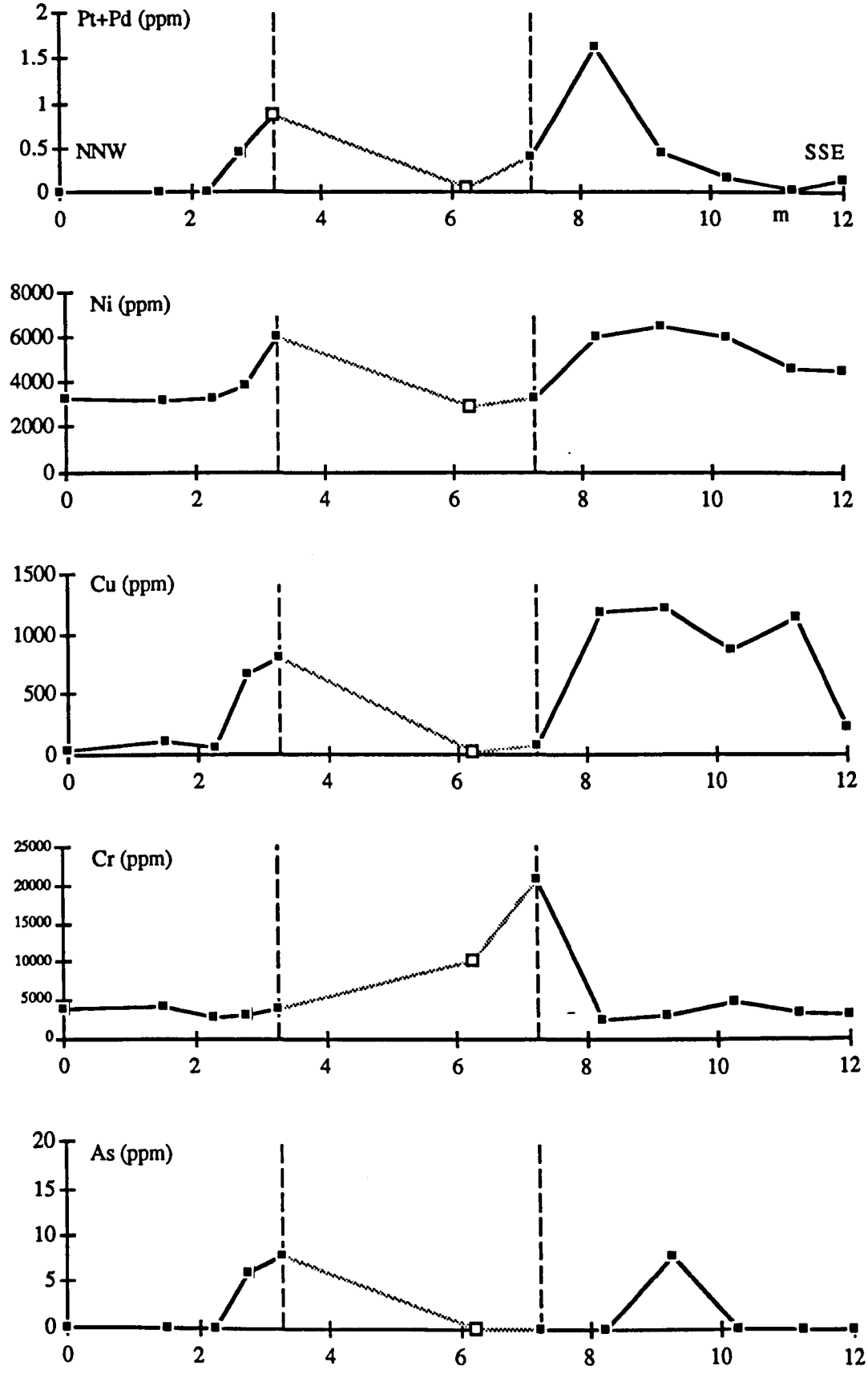

It has been shown that chromium enrichments may be used as markers for the base of cyclic units within magmatic sequences showing cryptic geochemical layering (section 6.2.4). Although the profiles described above are complicated by void spaces left by the extraction of the chromitite they exhibit cryptic layering comparable with that described from the basal dunites. These are best represented in the more complete regions of the traverses above the chromitite bodies. Enrichments of chromite are succeeded by sulphide-rich zones and as a consequence by enrichments of chalcophile elements. These elements do not show constant concentrations across these sulphide-bearing zones. Enrichments of PGE occur only at the base of the zone and decay rapidly upwards. Conversely concentrations of Cu increase progressively across each zone. This fractionation order (PGE, Ni, Cu) is consistent with the order of compatibility predicted by the different partition coefficients (Naldrett & Duke, 1980) between immiscible sulphide liquids and silicate melts for these chalcophile elements (see section 6.4.5). Concentrations of As closely follow those of Cu indicating that very low concentrations of this element (10 - 20 ppm) occur as magmatic background which is distinct in origin and distribution to the much higher levels found in shear zones elsewhere.

6.3.4 Conclusions

The sample traverses described above indicate that chromite concentrations within the cumulate sequence generally have associated sulphide-bearing dunites containing highly anomalous PGE concentrations. These PGE enrichments extend over exposure widths equivalent to a stratigraphic thicknesses in the order of ten metres. Concentrations of PGE were located in all of these traverses and since the chromite concentrations are known to occur at particular stratigraphic horizons (section 2.3.2) this indicates that the PGE mineralisation is also stratigraphically controlled and may extend continuously along strike.

Trace element profiles indicate that sharp changes in the composition of the cumulate sequence are associated with the stratigraphic position of chromite enrichments. A general increase in the concentration of compatible chalcophile elements is found at levels equivalent to the structural base of chromite bodies. This is attributed to influxes of primitive magma during open system fractionation. The scale of layering produced by this process may be as

great as 150-200 m. This is the approximate thickness of the cumulate unit between the two zones of chromite enrichments identified by mapping (section 2.3.2). Sulphide-bearing horizons occur at the base of these units and show internal fractionation. These horizons show metre scale layering and overall fractionation trends, with PGE enrichments at the very base and a progressive increase in Cu contents upwards. This indicates that the sulphide phases within a single horizon have not equilibrated but retain the geochemical signatures imparted by the fractional segregation of immiscible sulphide liquids.

6.4 Pyroxene-bearing sequences

Reconnaissance sampling located anomalous levels of Pt and Pd in sulphide-bearing pyroxenites from close to the base of the pyroxene-bearing layered sequence. Such pyroxenite layers are often well exposed although the surrounding olivine-rich rocks are less resistant to weathering and are usually unexposed. Coastal sections provide the only areas of continuous exposure of both pyroxene-rich and olivine-rich members. Two such sulphide-bearing sequences were identified and samples collected as traverses across the strike of the lithological layering. The structural complexity of this part of the ophiolite sequence (section 2.6) makes it difficult to identify continuous sequences and the original way up of layering is also hard to determine.

6.4.1 The high-level chromite traverse

The first traverse, at the Nev locality (figure 6.1), lies below the cliffs on the north side of the Keen of Hamar and included a zone of minor chromite concentrations (plate 6.8). This chromite mineralisation, although partially extracted by old trial pits, has not previously been described in the literature. It is the only example of in-situ chromitite known in the complex. It occurs within a dunite unit adjacent to pyroxenites and therefore forms another new example of high-level chromite mineralisation (see Prichard et al. 1989).

The chromite and silicate layering strikes NE-SW and dips at approximately 45° to the northwest. The disseminated chromite layering swells laterally into chromite-rich pods and chromitite layers. These are hosted by dunite and lie within a zone which is subparallel to

Figure 6.18. Pseudo-sections showing levels of PGE and sulphides in the Nev traverse.

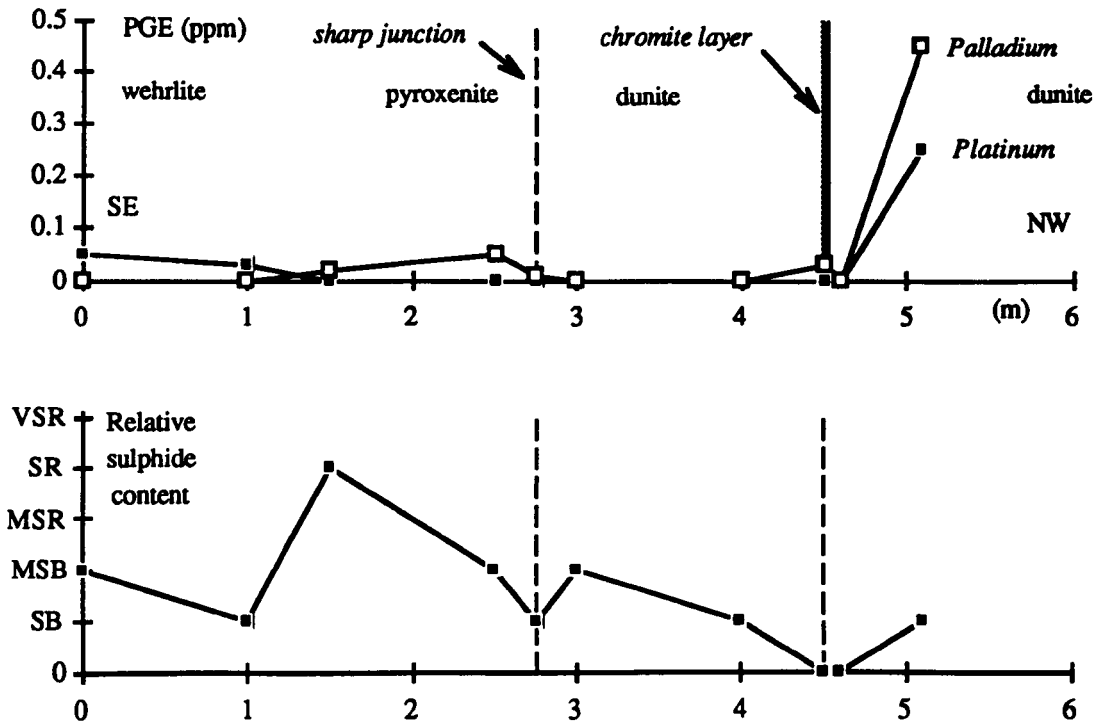

the very sharp junction with pyroxenites 1-2 m below (plate 6.8). Dunites at this junction contain xenoliths of pyroxenite which indicate a NW younging direction. This is supported by modal layering in the pyroxene-bearing member since the cpx content increases from an olivine-rich wehrlite, through typical wehrlites, to pyroxenites immediately below the contact with the overlying dunite unit. Dunites and pyroxene-bearing dunites are exposed for at least 20 m above the chromite layers (plate 2.3.1).

6.4.2 Controls of PGE mineralisation in high-level chromitites

Platinum-group element concentrations and sulphide contents within the high level chromite traverse are shown in figure 6.18. Low levels of Pt and Pd occur within the pyroxene-bearing unit but are absent in the lower part of the overlying dunite unit. Highly anomalous levels of Pt and Pd occur only at the highest level of the traverse, in sulphide-bearing dunites directly above the chromite layers. PGE concentrations are not associated with the pyroxenite/dunite junction.

The relatively low concentrations of PGE in the wehrlites and pyroxenites do not show

Figure 6.19. Pseudo-sections showing levels of major elements in the Nev traverse.

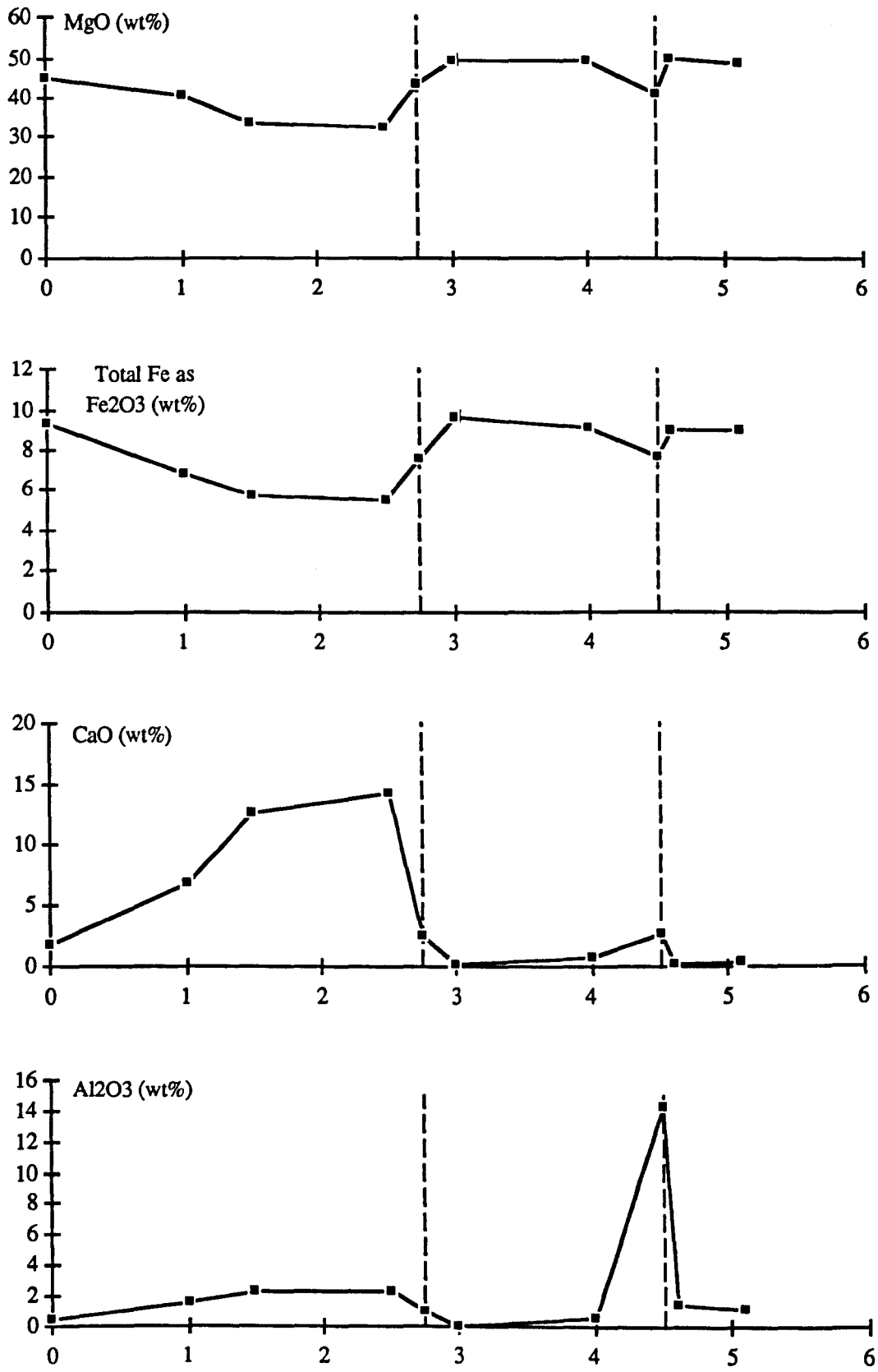

Figure 6.20. Pseudo-sections showing levels of PGE and pathfinders in the Nev traverse.

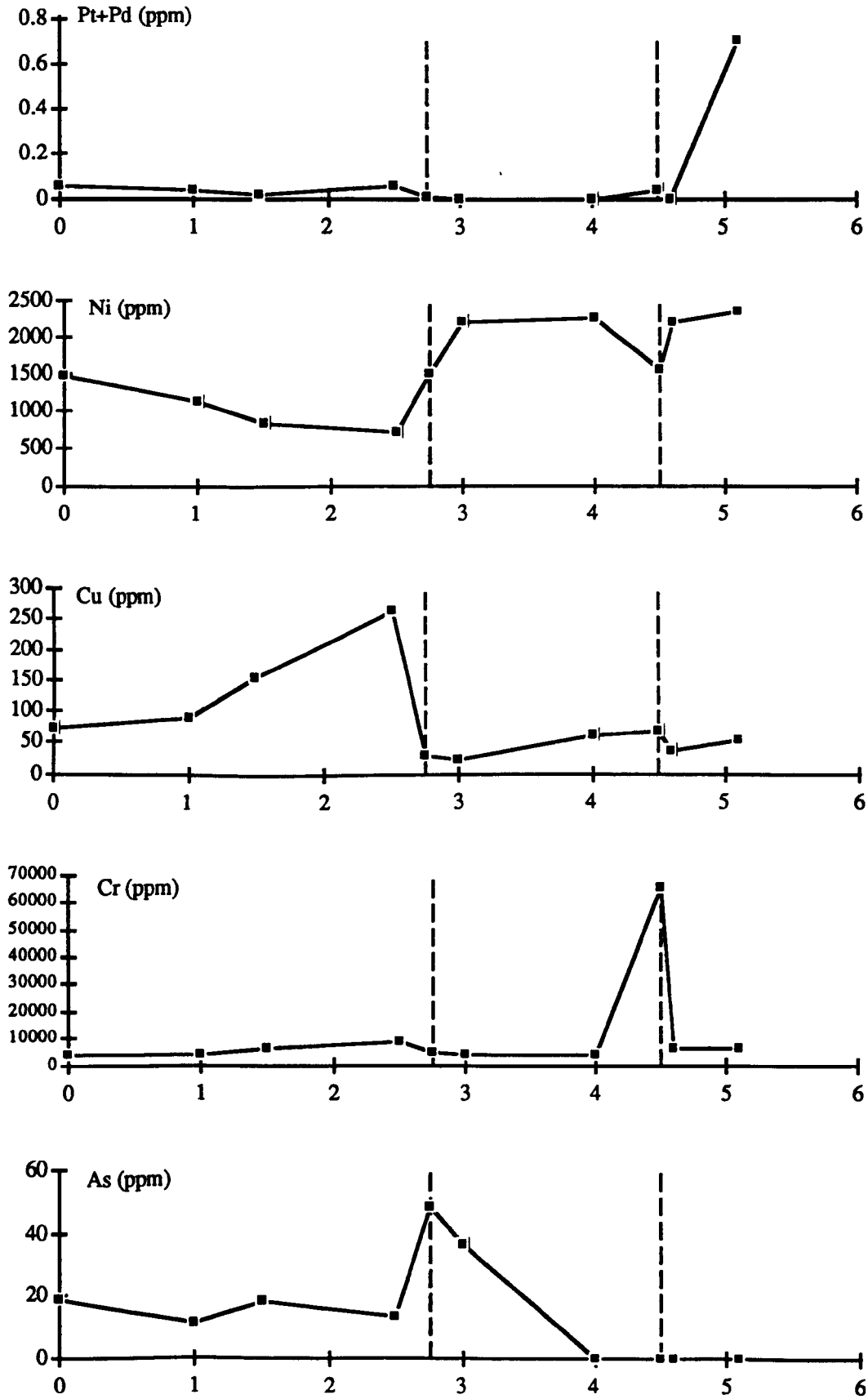

Table 6.4. Peak Pt, Pd, Ni, Cu and As concentrations in pyroxene-bearing traverses.

Traverse	*Pt (ppb)*	*Pd (ppb)*	*Ni (ppm)*	*Cu (ppm)*	*As (ppm)*
The Nev	250	450	2358	266	48
White House	150	230	3861	1507	11

the association and constant ratios of Pt and Pd which is usually found elsewhere. This is probably due to analytical problems or errors. These data indicate that the level of total Pt+Pd across this zone is probably below 100 ppb.

The sulphide contents of the pyroxene-bearing rocks are generally high and decrease rapidly in the overlying dunites. There is a sharp increase in the sulphide content above the chromite layering, marking the appearance of anomalous PGE concentrations.

Figure 6.19 shows profiles drawn for the approximate analyses (by XRF on pellets) of some major element oxides. Whole-rock concentrations of Ca, Al, Mg and Fe depend on the relative proportion of olivine (containing Mg and Fe) and cpx (containing Ca and Al but less Mg or Fe) and hence vary with the rock type. The smooth increase in CaO and Al_2O_3 and decrease in MgO and Fe_2O_3 confirm the field observations of increasing modal cpx towards the junction with dunite. The peak Al_2O_3 concentration is associated with the chromite layer reflecting the chrome-spinel content of this sample.

Trace element profiles (figure 6.20) contain sharp breaks at the pyroxenite/dunite contact and the chromite enriched horizon. Nickel concentrations reflect the olivine content of the samples, decreasing with increases in modal cpx or spinel. Background chromium concentrations increase in proportion to the cpx content, possibly reflecting minor substitution in this mineral. Copper concentrations follow a saw-tooth pattern but in each lithological unit increase smoothly with increasing stratigraphic height. Copper minima occur both at the pyroxenite/dunite contact and in dunites directly above the chromite layers. Overall the concentrations of Cu are significantly higher in the pyroxene-bearing portion of the sequence than in either group of dunites. The relatively low As concentrations also show a similar pattern and are apparently controlled by changes in the primary rock type.

The sequence described above illustrates the geochemical changes occurring near the base of cyclic units at the stratigraphic level at which cpx is crystallising. The top of the underlying unit represents fractionation of a more evolved magma composition and therefore contains increasing levels of Cu and As and low levels of Ni. These evolutionary trends are reset at the base of the overlying olivine-rich unit, which has an intrusive lower contact, indicating input of a batch of a more primitive magma. The high Al content of the spinel phase (figure 6.19) suggests that this mixed with the evolved resident magma.

The sulphide content of the evolved pyroxene-rich cumulates is high although these contain only low levels of Pt or Pd. An increase in sulphide content above the chromite layers of the overlying unit marks a sharp increase in Pt and Pd concentrations. This pattern of PGE enrichments in sulphide-bearing dunites at or above chromite concentrations is identical to that found in the olivine dominant sequences (section 6.3). This provides further illustration of the very compatible behaviour of these elements during open system fractionation of a sulphur saturated magma.

6.4.3 The White House traverse

A continuous sequence of sulphide-bearing wehrlites and pyroxenites was located on the northern side of Balta Sound, SW of the Keen of Hamar (plate 6.9). This is the most easterly exposure of massive pyroxenite in this area and is the first in the ophiolite sequence (enclosure 1). A sample traverse was collected from WSW to ENE across pyroxene-bearing dunites, marginal wehrlites and pyroxenites (plate 6.9). Field evidence for the younging direction of this NNW trending pyroxenite layer is ambiguous. The overall trend in the ophiolite sequence as a whole is from dunites in the NW to wehrlites or pyroxenites further SE. This suggests that the pyroxenite layer that was sampled overlies the dunites at the western end of the traverse. This younging direction is assumed in the following geochemical descriptions.

Plate 6.8. Location of the Nev high level chromite traverse.

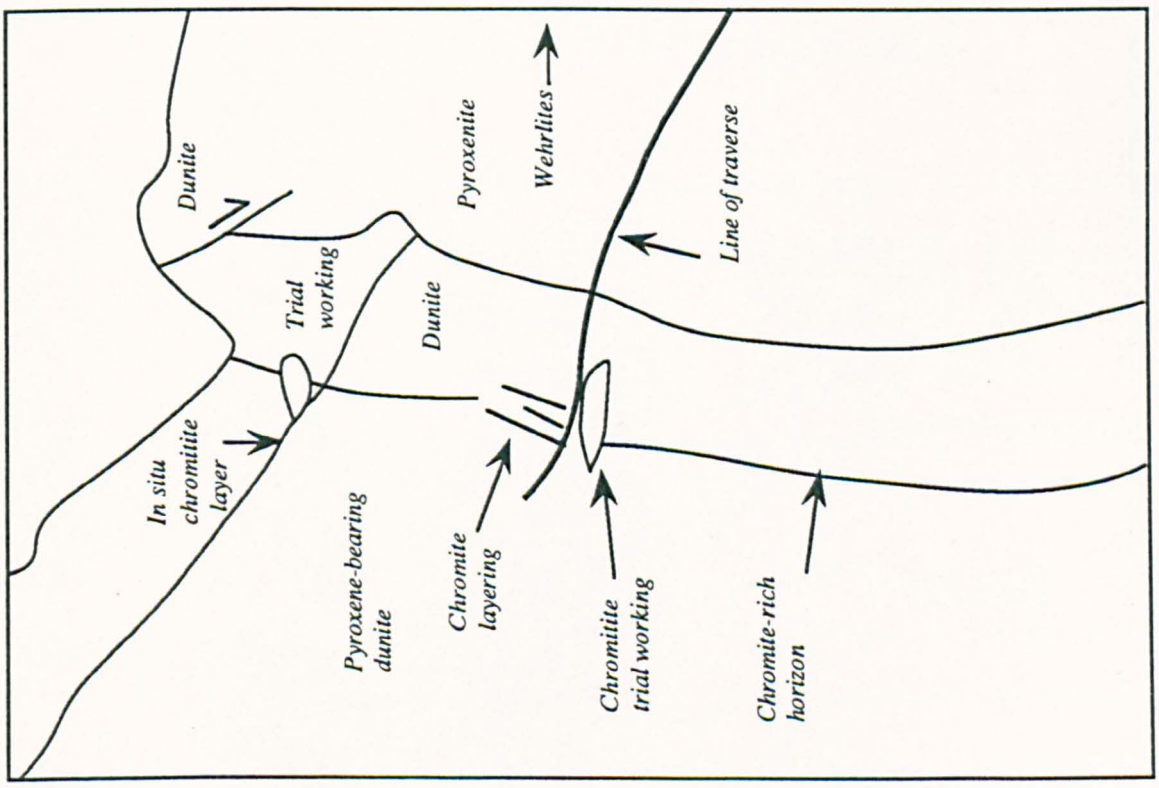

Plate 6.9. Location of the White House basal pyroxenite traverse.

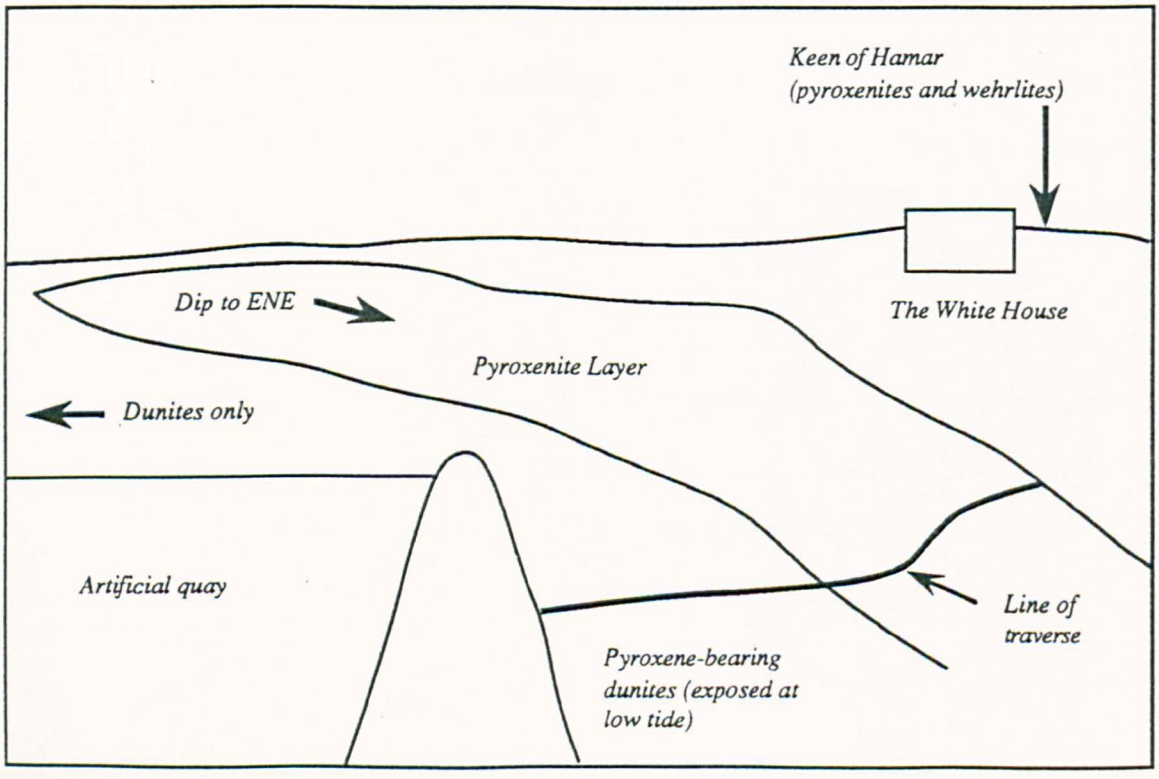

Figure 6.21. Pseudo-sections showing levels of PGE and sulphides in the White House traverse.

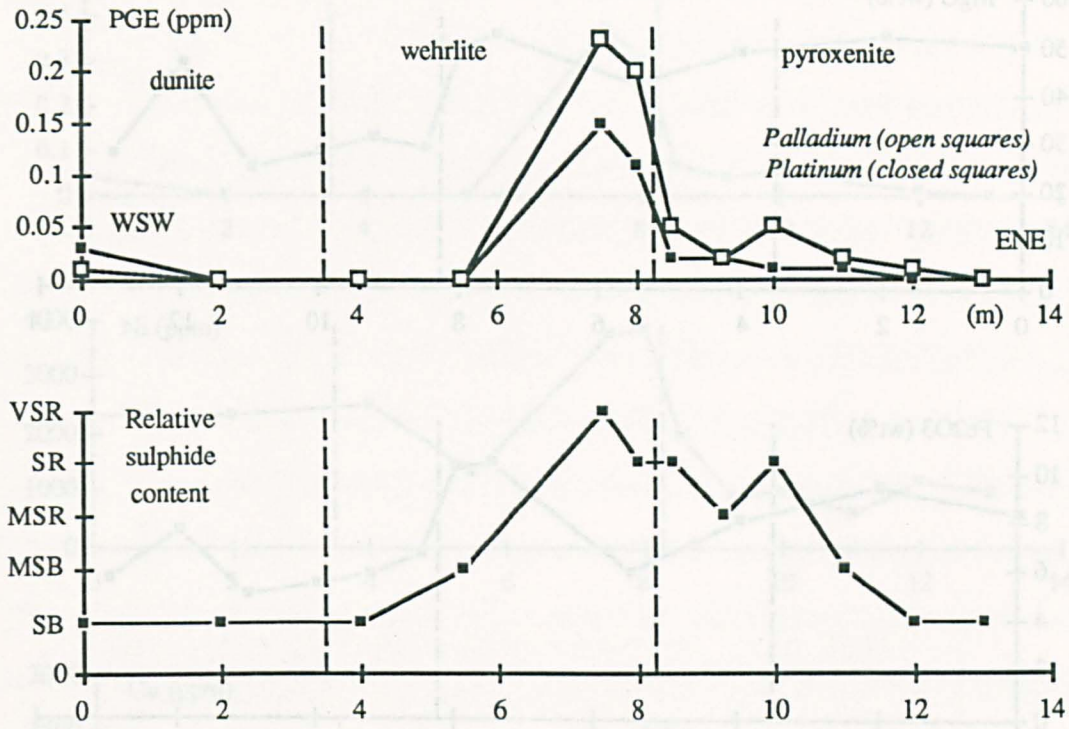

6.4.4 Controls of PGE mineralisation in basal pyroxenites

Platinum-group element concentrations and sulphide contents in the White House traverse are shown in figure 6.21. The concentration of Pt or Pd is clearly related to the amount of sulphide the pyroxene-bearing rocks contain. The maximum levels of PGE occur abruptly within the wehrlitic margin and diminish rapidly into the overlying pyroxenites.The PGE concentrations tail off more rapidly than the sulphide contents so the PGE/sulphide ratio apparently decreases upwards across the pyroxenite layer.

Whole-rock concentrations of Ca, Mg Al and Fe again reflect variations in the relative proportions of modal olivine and cpx (figure 6.22). These profiles confirm the modal layering observed in the field. All contacts are slightly gradational with the cpx content of the dunites increasing towards the pyroxenites producing a wehrlitic margin. The junction between wehrlites and pyroxenites appears quite sharply defined.

Figure 6.22. Pseudo-sections showing levels of major elements in the White House traverse.

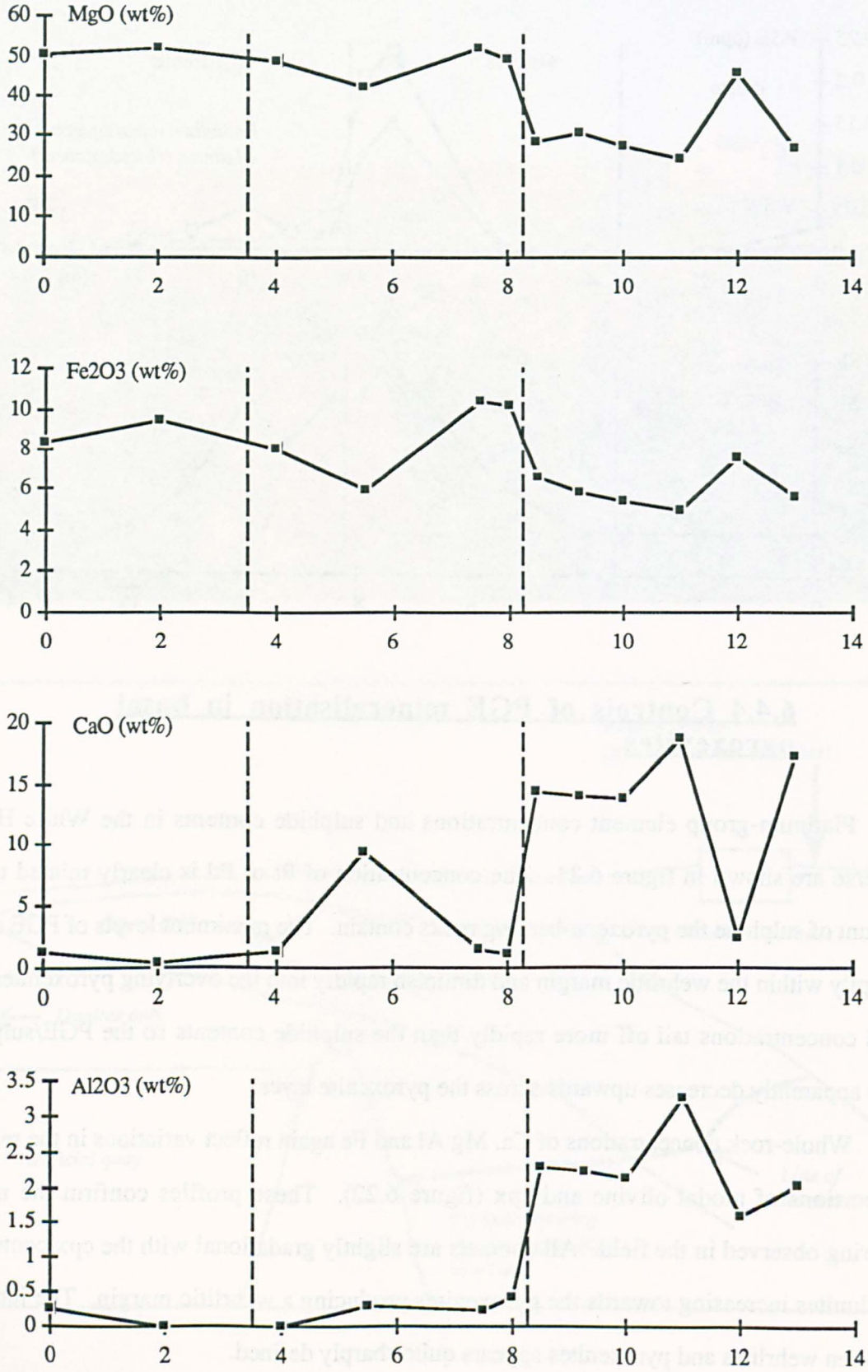

Figure 6.23. Pseudo-sections showing levels of PGE and pathfinders in the White House traverse.

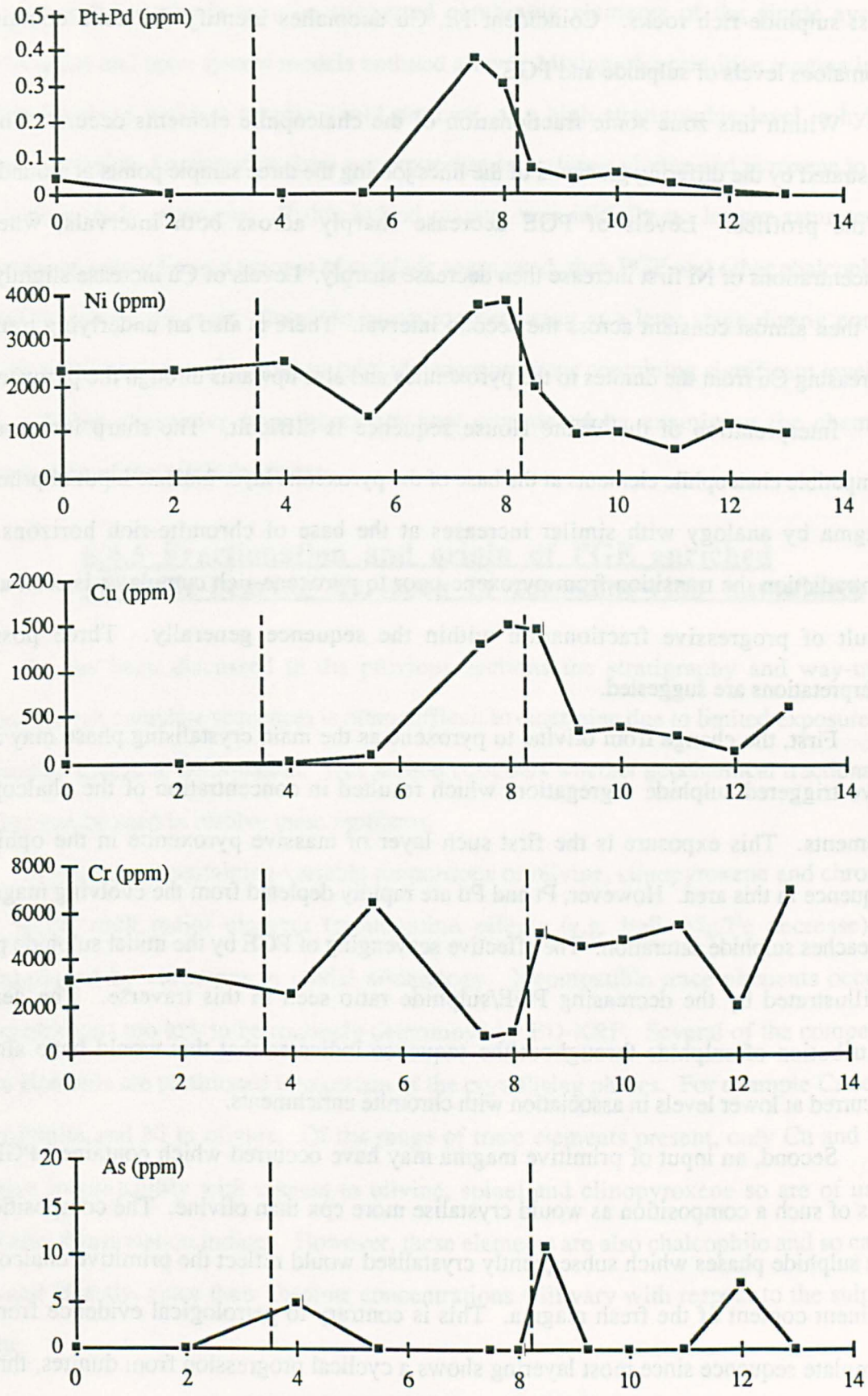

Concentrations of Ni across the traverse are controlled both by the olivine content and the amount of accessory sulphide (figure 6.22). Copper concentrations are highest in the most sulphide-rich rocks. Coincident Ni, Cu anomalies identify the zone containing anomalous levels of sulphide and PGE.

Within this zone some fractionation of the chalcophile elements occurs. This is illustrated by the differing gradients of the lines joining the three sample points at around 8 m in the profiles. Levels of PGE decrease sharply across both intervals, whereas concentrations of Ni first increase then decrease sharply. Levels of Cu increase slightly but are then almost constant across the second interval. There is also an underlying trend of increasing Cu from the dunites to the pyroxenites and also upwards through the pyroxenites.

Interpretation of the White House sequence is difficult. The sharp increases in compatible chalcophile elements at the base of the pyroxenite layer indicate input of primitive magma by analogy with similar increases at the base of chromite-rich horizons. In contradiction the transition from pyroxene-poor to pyroxene-rich cumulates is seen as the result of progressive fractionation within the sequence generally. Three possible interpretations are suggested.

First, the change from olivine to pyroxene as the main crystalising phase may itself have triggered sulphide segregation, which resulted in concentration of the chalcophile elements. This exposure is the first such layer of massive pyroxenite in the ophiolite sequence in this area. However, Pt and Pd are rapidly depleted from the evolving magma if it reaches sulphide saturation. The effective scavenging of PGE by the initial sulphide phase is illustrated by the decreasing PGE/sulphide ratio seen in this traverse. The general distribution of sulphide throughout the sequence indicates that this would have already occurred at lower levels in association with chromite enrichments.

Second, an input of primitive magma may have occurred which contained PGE but was of such a composition as would crystalise more cpx than olivine. The composition of the sulphide phases which subsequently crystalised would reflect the primitive chalcophile element content of the fresh magma. This is contrary to petrological evidence from the cumulate sequence since most layering shows a cyclical progression from dunites, through

wehrlites, to pyroxenites. No pyroxene is observed in the dunite pods within the mantle sequence.

A third hypothesis may be suggested combining elements of the single system fractionation and open system models outlined above. Mixing of a primitive magma input with an evolved resident magma could produce, at a high stratigraphic level, a hybrid capable of rapidly fractionating from a composition crystalising olivine and pyroxene to one crystalising only pyroxene. If this hybrid magma was initially no longer saturated in sulphide, or only a limited amount of sulphide segregated, then PGE and other chalcophiles would remain in the melt. Sulphide saturation occurring at a later stage during normal silicate fractionation could result in sulphide concentrations containing significant levels of PGE. These alternative hypotheses are now considered by examining the chemical fractionation of the sulphide phases.

6.4.5 Fractionation and origin of PGE enriched sulphide-bearing horizons in pyroxene-rich cumulates

As has been discussed in the previous sections the stratigraphy and way-up of pyroxene-rich cumulate sequences is often difficult to determine due to limited exposure and a complex structural deformation. This section considers whether geochemical fractionation indices can be used to resolve these problems.

In sequences containing variable proportions of olivine, clinopyroxene and chromite any whole-rock major element fractionation effects (e.g. bulk Mg/Fe decrease) are camouflaged by variations in modal mineralogy. Incompatible trace elements occur at concentrations too low to be routinely determined by ED-XRF. Several of the compatible trace elements are partitioned into certain of the crystalising phases. For example Cr occurs in chromite and Ni in olivine. Of the range of trace elements present, only Cu and PGE behave incompatibly with respect to olivine, spinel and clinopyroxene so are of use as potential fractionation indices. However, these elements are also chalcophile and so cannot be used directly, since their absolute concentrations will vary with respect to the sulphide tenor.

Table 6.5. Range of estimates of partition coefficients for chalcophile elements between silicate magma and immiscible sulphide liquids.

Element	*Ni*	*Cu*	*Pt*	*Pd*	*Source*
K_D value	275	245	1000	1500	1
	312	250	160000	120000	2

1 References cited by Naldrett & Duke, 1980 including:-
(i) Rajamani & Naldrett, 1978
(ii) Naldrett et al., 1979

2 Campbell & Barnes, 1984 (calculated apparent D value for J-M Reef)

The chalcophile behaviour of PGE has been attributed to the high Nernst partition coefficients (K_D) between immiscible sulphide liquids and silicate magmas (Rajamani & Naldrett, 1978; Naldrett et al., 1979). Estimates of these partition coefficients vary (table 6.5), although by consensus they are thought to be much greater for PGE than for other chalcophiles and roughly similar for individual members of the platinum group (Barnes et al., 1987). The partition coefficients for Ni and Cu are much lower and indicate that the order of decreasing compatibility in immiscible sulphide liquids is PGE >> Ni > Cu. This ranking gives rise to various element ratios which should vary during fractionation. Ratios of either Ni or Cu to any PGE should increase in the melt during sulphide fractionation and hence be higher in any later sulphide phases. Both sulphide fractionation and olivine fractionation will cause an increase in the Cu/Ni ratio of the melt and subsequent sulphide segregations. Since cumulate olivine contains Ni this fractionation index will only be representative of sulphide compositions in whole-rock analyses of olivine-free rocks (i.e. pyroxenites or chromitites). The partition coefficients for Cu and Ni are similar so changes in Cu/Ni ratio due to sulphide fractionation will be small in comparison to those due to olivine fractionation (K_D = 14 for Ni in olivine (Henderson, 1982) whereas K_D for Cu in olivine is assumed to be close to unity). Much greater changes will be seen in ratios between PGE and base metals.

Fractionation indices Cu/(Pt+Pd) and Cu/Ni have been used to show fractionation of sulphide compositions in the Nev and White House traverses (figures 6.24 and 6.25).

Figure 6.24. Sulphide fractionation indices in the Nev high level chromite traverse.

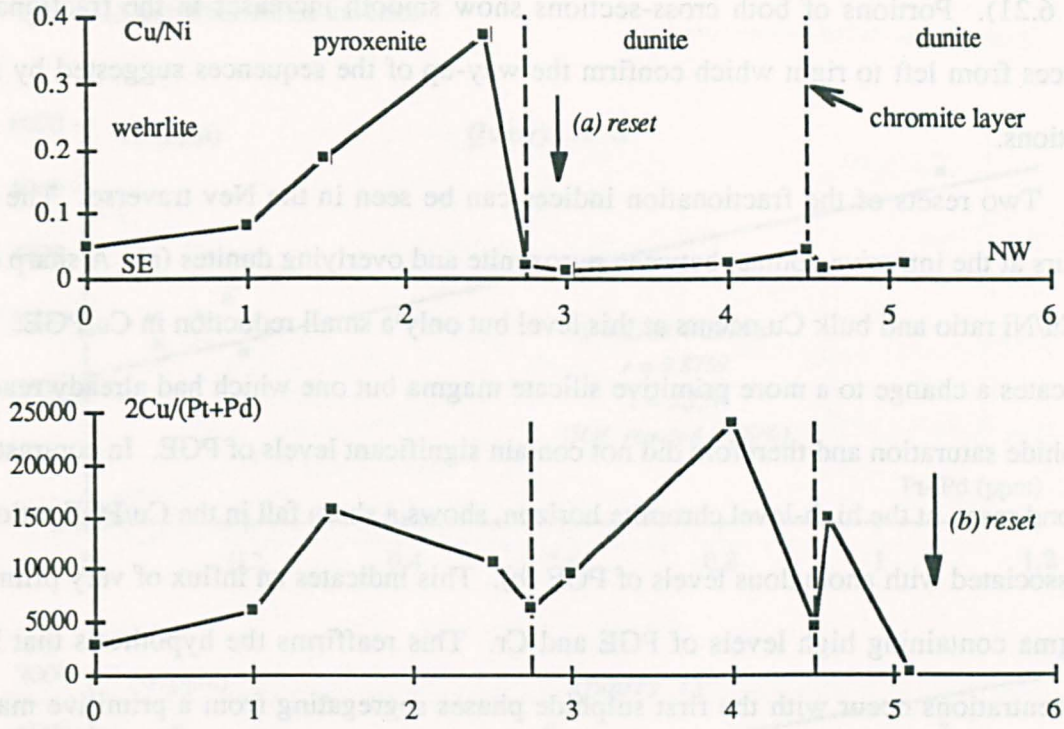

Figure 6.25. Sulphide fractionation indices in the White House traverse.

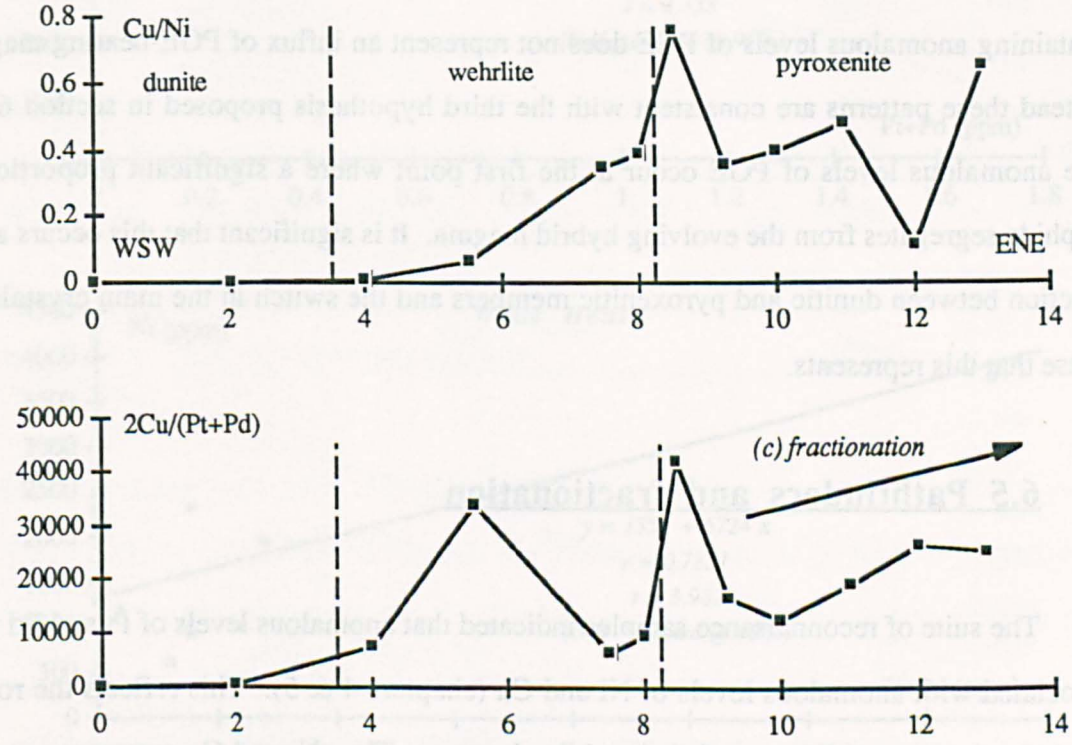

These profiles should be compared to the visual estimates of sulphide tenor (figures 6.18 and 6.21). Portions of both cross-sections show smooth increases in the fractionation indices from left to right which confirm the way-up of the sequences suggested by field relations.

Two resets of the fractionation indices can be seen in the Nev traverse. The first occurs at the intrusive contact between pyroxenite and overlying dunites (a). A sharp drop in Cu/Ni ratio and bulk Cu occurs at this level but only a small reduction in Cu/PGE. This indicates a change to a more primitive silicate magma but one which had already reached sulphide saturation and therefore did not contain significant levels of PGE. In contrast, the second reset, at the high-level chromite horizon, shows a sharp fall in the Cu/PGE ratio and is associated with anomalous levels of PGE (b). This indicates an influx of very primitive magma containing high levels of PGE and Cr. This reaffirms the hypothesis that PGE concentrations occur with the first sulphide phases segregating from a primitive magma which can be visually identified by the associated chromite mineralisation.

In the White House traverse the fractionation indices are not substantially reset but increase progressively from left to right (c). This indicates that the wehrlitic margin containing anomalous levels of PGE does not represent an influx of PGE-bearing magma. Instead these patterns are consistent with the third hypothesis proposed in section 6.4.4. The anomalous levels of PGE occur at the first point where a significant proportion of sulphide segregates from the evolving hybrid magma. It is significant that this occurs at the junction between dunitic and pyroxenitic members and the switch in the main crystalising phase that this represents.

6.5 Pathfinders and fractionation

The suite of reconnaisance samples indicated that anomalous levels of Pt and Pd were associated with anomalous levels of Ni and Cu (chapters 4 & 5). This reflects the role of sulphide phases as collectors of chalcophile elements. Thus Ni and Cu represent potential pathfinders for the PGE. However, only a weak linear dependence was observed over the complete database. From this evidence, it was concluded that this apparent contradiction

Figure 6.26. Regression analysis between PGE and Ni concentrations in the Quarry 12S, Quarry 13 and White House traverses.

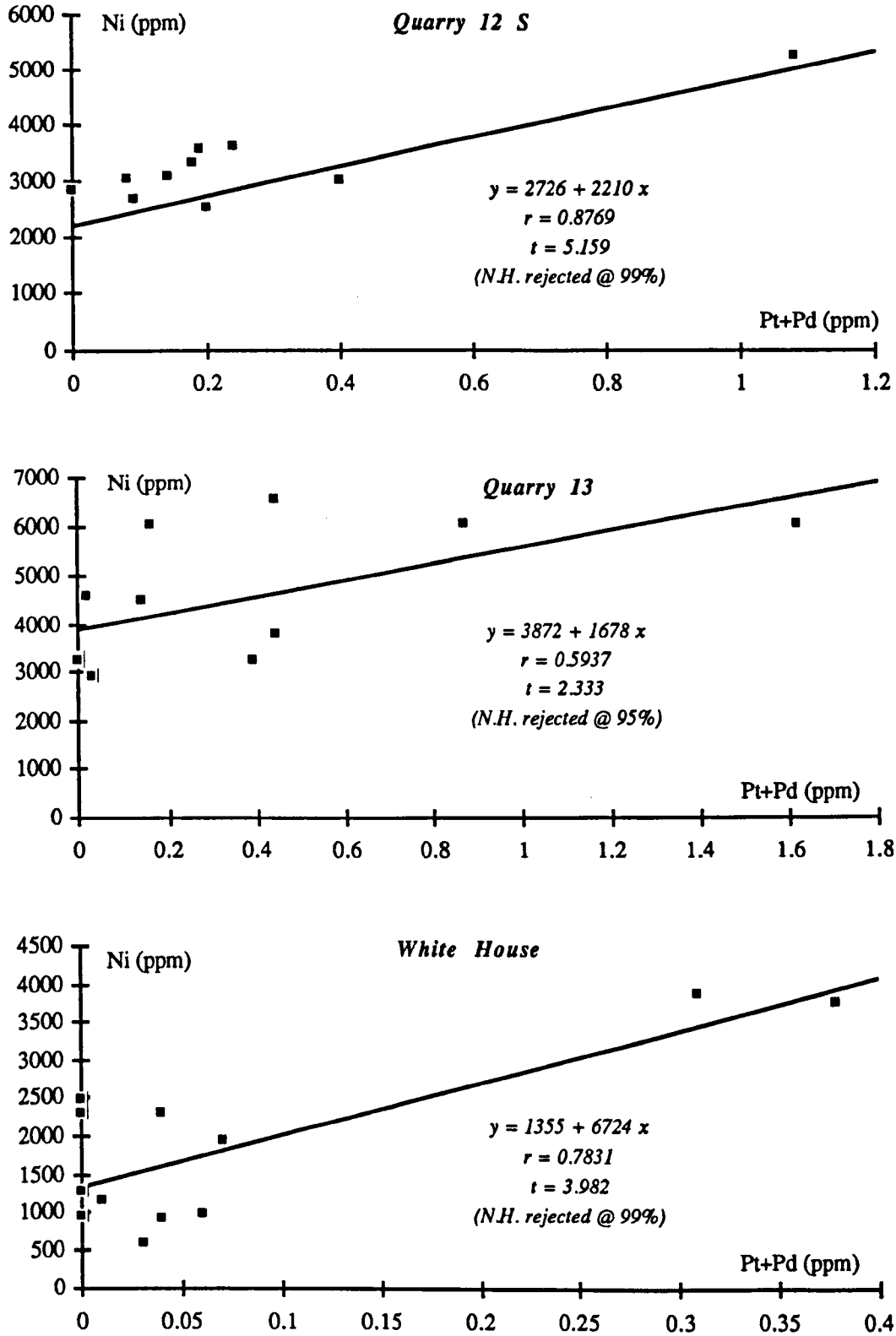

Figure 6.27. Regression analysis between PGE and Cu concentrations in the Quarry 12S, Quarry 13 and White House traverses.

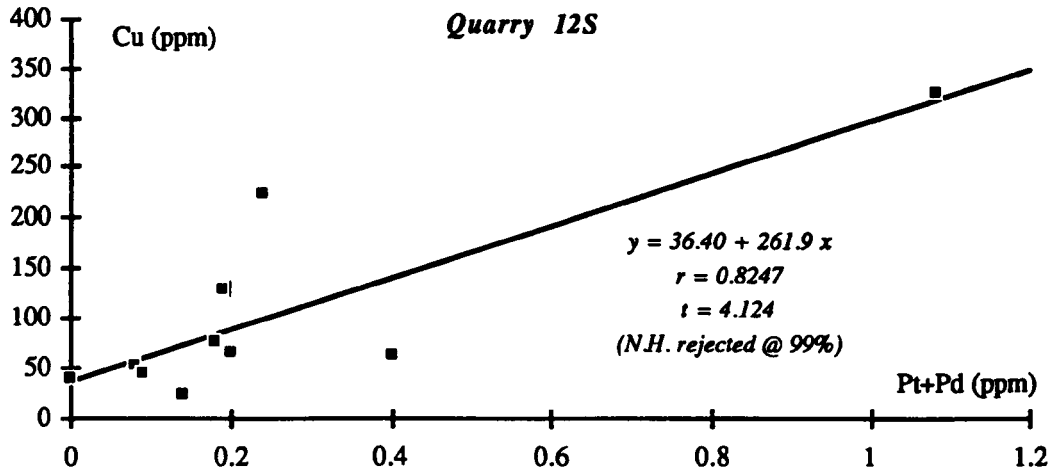

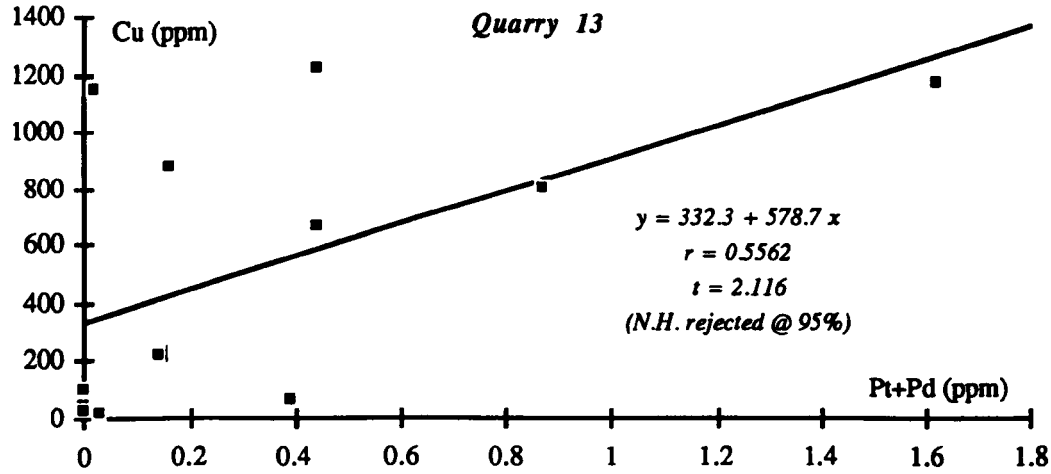

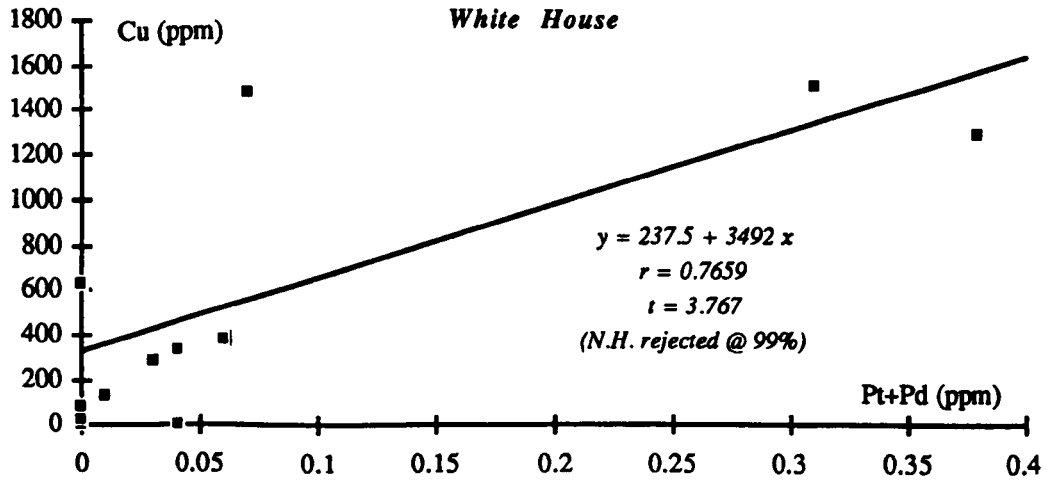

Figure 6.28. Regression analysis between Pt and Pd for the Quarry 12S, Quarry 13 and White House traverses.

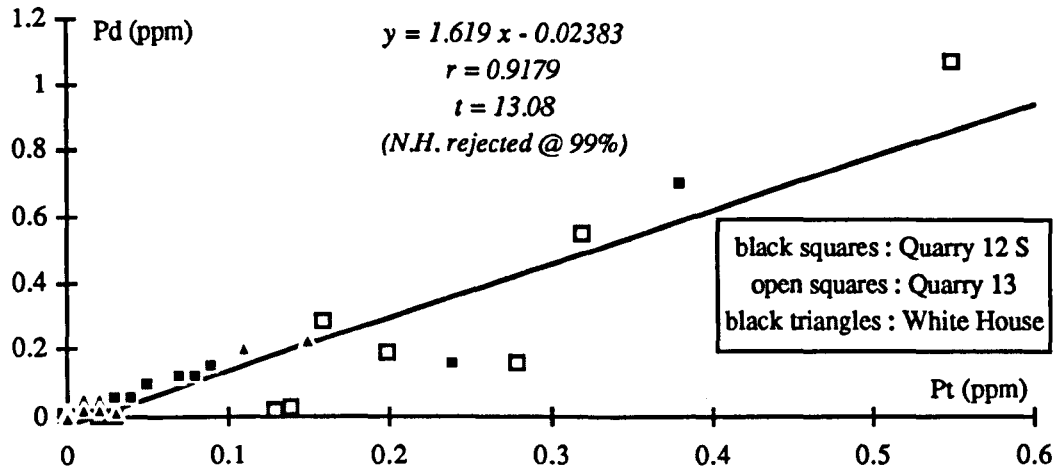

Table 6.6. Summary table of regression coefficients and fractionation indices for the Quarry 12S, Quarry 13 and White House traverses.

Parameter	*Derivation*	*Quarry 12S*	*Quarry 13*	*White House*
Pd/Pt	gradient figure 6.28	1.62	1.62	1.62
Ni background	intercept figure 6.26	2726	3872	1355
Ni/(Pt+Pd)	gradient figure 6.26	2210	1678	6724+
Cu background	intercept figure 6.27	36.4	332	238
Cu/(Pt+Pd)	gradient figure 6.27	262	579	3492
Cu/Ni*	ratio of gradients figures 6.26 & 6.27	0.119	0.345	0.519+

+ Regression of mixed pyroxenites, wehrlites and dunites overestimates Ni/(Pt+Pd) and hence calculated Cu/Ni is a minimum estimate

might be due either to the high imprecision of the PGE analyses or to stratigraphic variations in PGE/pathfinder ratios, assuming that the primary magmatic patterns were preserved (section 5.7). The traverses described in this chapter provide groups of data from the same stratigraphic level allowing these possibilities to be investigated.

Concentrations of Pt and Pd in the Quarry 12S, Quarry 13 and White House traverses were found to be systematically related (via sulphide) contents to Ni and Cu concentrations

(sections 6.3.3 and 6.4.4). These patterns are shown graphically in figures 6.26 and 6.27. For each traverse the total Pt+Pd contents have been plotted against both Ni and Cu concentrations. Regression analysis confirms that a statistically significant correlation occurs between Pt+Pd and Ni or Cu in each group of samples.

A wide variation is seen in the intercept and gradient coefficients of best fit lines for the three traverses (table 6.6). These coefficients have been used to calculate Cu/Ni and Cu/(Pt+Pd) ratios. The three traverses are listed here in order of increasing stratigraphic level, indicating a systematic increase in Cu/(Pt+Pd) and Cu/Ni ratios upwards in the ophiolite cumulate sequence. The use of these ratios as fractionation indices has been discussed in the previous section where it was found that these are also fractionated across sulphide-bearing zones. Since the value of these indices when calculated from regression lines rely most heavily on samples containing the highest PGE concentrations, they give the best indication of the composition of the first sulphide segregating from each magmatic unit.

Concentrations of Pt and Pd in the three traverses have also been compared graphically and subjected to regression analysis. The linear correlation indicates that the Pd/Pt ratio is constant at around 1.6 for all the traverses and does not vary with stratigraphic level. Minor departures from this trend are all towards lower Pd/Pt ratios, indicating some remobilisation and loss of Pd.

The above discussion indicates that during the open-system magmatic fractionation producing the ophiolite layered cumulate sequence the pathfinder elements Ni and Cu are fractionated with respect to Pt, Pd and to one another but that ratios between different members of the platinum-group are unfractionated. This explains why poor correlations are found between PGE and their chalcophile pathfinders in groups of samples from different stratigraphic levels.

6.6 Discussion and conclusions

The detailed traverses indicate that continuous stratigraphically controlled PGE mineralisation is present at several levels in the cumulate sequence. Within these mineralised horizons the concentrations of Pt and Pd are related to sulphide contents and the chalcophile elements Ni and Cu are pathfinders for the PGE. These patterns are indicative of concentration by magmatic processes.

Both Pt and Pd behave compatibly in cumulate sequences derived from magmas which are sulphur saturated. Inherent in this model is the assumption that sulphides originally segregate as immiscible liquids (Naldrett and Duke, 1980). Experimentally derived partition coefficients between such sulphide liquids and silicate magma are so high as to predict effective scavenging of PGE from the melt. Sulphide phases are usually present throughout this ophiolite sequence so PGE enrichments occur at the base of the cumulate sequence. This led to the development of the model suggesting that PGE enrichments occur associated with the first sulphide segregating from the evolving magma (section 4.6).

Repetitions are present in the cumulate sequence. The base of these magmatic cycles are marked by chromite-rich horizons and laterally discontinuous pods of chromitite. Each repetition also has associated PGE-enriched sulphide-bearing zones. The occurrence of these concentrations of early crystal phases (spinels) and compatible elements (Cr, Pt, Pd, Ni) led to the adoption of an open system fractionation model. This allows replenishment of PGE and other compatibles at higher stratigraphic levels at which these elements would otherwise have been depleted by normal fractional crystallisation.

The cumulate sequence as a whole shows a progressive change from dunitic, through wehrlitic to pyroxenitic rocks, with superimposed cyclic repetitions at different scales (section 2.3.3). The initial magma was sufficiently picritic to only crystalise olivine and chromite in the lowermost cyclic units. Structural discontinuities occur below the appearance of gabbro cumulates. The PGE-enriched sulphide-bearing horizons show a progressive increase in Cu/Ni and Cu/PGE ratios at higher stratigraphic levels. The applicability of these fractionation indices has been demonstrated by their increase across

sulphide-bearing horizons where the cumulate stratigraphy and younging directions are well constrained. In contrast the PGE are unfractionated either within a single zone or between successively higher stratigraphic horizons. In either case the Pd/Pt ratios are constant, even between dunite and pyroxenite hosted mineralisation.

These progressive changes may be explained by an open-system fractionation model in which batches of primitive picritic magma mix with an evolving resident magma. The PGE are effectively removed from the hybrid magma by the initial sulphide segregations within the cycle. Unfractionated PGE ratios occur with sulphides at the base of sequences in which the sulphide compositions show progressive evolution with increasing stratigraphic level. Fractionation between the different members of the platinum group of elements is considered further in chapter 7 using high precision analyses of all 6 PGE.

Chapter 7

Magmatic Fractionation of the Platinum-Group Elements

7.1 Introduction

By convention analyses of all six PGE are normalised to chondrite and plotted on a spidergram in the order of decreasing melting point of the native metal (Naldrett et al., 1979). This method produces different characteristic patterns depending on the proportions of the individual PGE in chromite-rich specimens (Page et al., 1982a).

Naldrett et al. (1979) showed that if PGE analyses of sulphide-rich rocks are normalised to the average concentration in chondrite and plotted in the order Ir, Ru, Rh, Pt, Pd & Au smoothly sloping patterns are obtained. In order to compare sulphide-rich and sulphide-poor specimens the analyses may be recalculated to the expected concentrations in 100% sulphide ore. The patterns allow distinction between sulphides segregated from Mg-rich magmas generated by high degrees of melting, such as komatiites (flattish patterns), and those segregating from Mg-poor magmas generated by lower degrees of melting, such as tholeiites (positively sloping patterns; Naldrett & Duke, 1980).

The use of the technique of normalising to chondrite to characterise chromitites from different deposits has already been described (section 1.2.3). The chondrite-normalised patterns of silicate rocks are also diagnostic. Barnes et al. (1985) described flat patterns in upper mantle rocks and Os-, Ir-, Ru-enriched patterns in podiform chromitites but noted that patterns from the non-tectonised portions of ophiolites are not easily distinguishable from those of layered intrusions, ocean-floor basalts, continental flood basalts or alkaline rocks.

The factors influencing noble metal patterns of cumulate rocks have been discussed by Barnes et al (1988) and include the possible content of sulphides, PGM inclusions, cumulate olivine or chromite of the analysed rock and the relative timing of the formation of each of these phases. The usefulness of the spidergram approach to sulphide-poor rocks was

extended by using average mantle compositions as the normalising factor. This allows the inclusion of other chalcophile elements on the diagram and represents a more realistic source material for most PGE deposits. When combined with metal ratio diagrams (e.g. Pd/Ir v Ni/Cu or Ni/Pd v Cu/Ir) these plots provide a powerful tool for characterising and comparing the fractionation history of coeval rock suites.

This final chapter describes, using the above methods, the results of investigations into the processes that fractionate PGE and chalcophile elements during formation of the Shetland ophiolite complex. It begins by describing the chondrite-normalised patterns obtained from the available published analyses. This is complimented by additional high precision re-analysis of selected samples from the new PGE mineralisation parageneses described in earlier chapters. These analyses are used to characterise the processes causing fractionation between different members of the platinum-group which explain the various patterns on chondrite-normalised diagrams. Metal ratio diagrams are then used to suggest trace element models for the observed fractionation history. The final synthesis is an attempt to explain the occurrence and distribution of the different PGE concentrations and assemblages in the ophiolite complex as a whole.

7.2 Previous work

Prichard et al. (1986), in a limited study of ten chromitites, recognised that positively sloping chondrite-normalised patterns are obtained for samples from Cliff which are similar to those found in stratiform intrusions (figure 7.1). Low concentrations with negative slope patterns were obtained from other chromitites, which are similar to those from other ophiolites (section 1.5.4). The authors (Prichard et al., 1986) concluded that the processes responsible for the PGE distribution in stratiform complexes might also be operating in the Shetland ophiolite complex and that a negative slope is the fingerprint of the early cumulate olivine and chromite that becomes separated from the evolving magma as it progresses upwards to the main chamber. More irregular patterns obtained from Harold's Grave chromitites were attributed to hydrothermal alteration but are an artifact of a plotting error. When this data is correctly plotted (figure 7.1) it is clear that these samples follow smooth

Figure 7.1. Chondrite normalised diagram of Shetland chromitites compared to examples from other ophiolites and stratiform intrusions (replotted after Prichard et al., 1986)

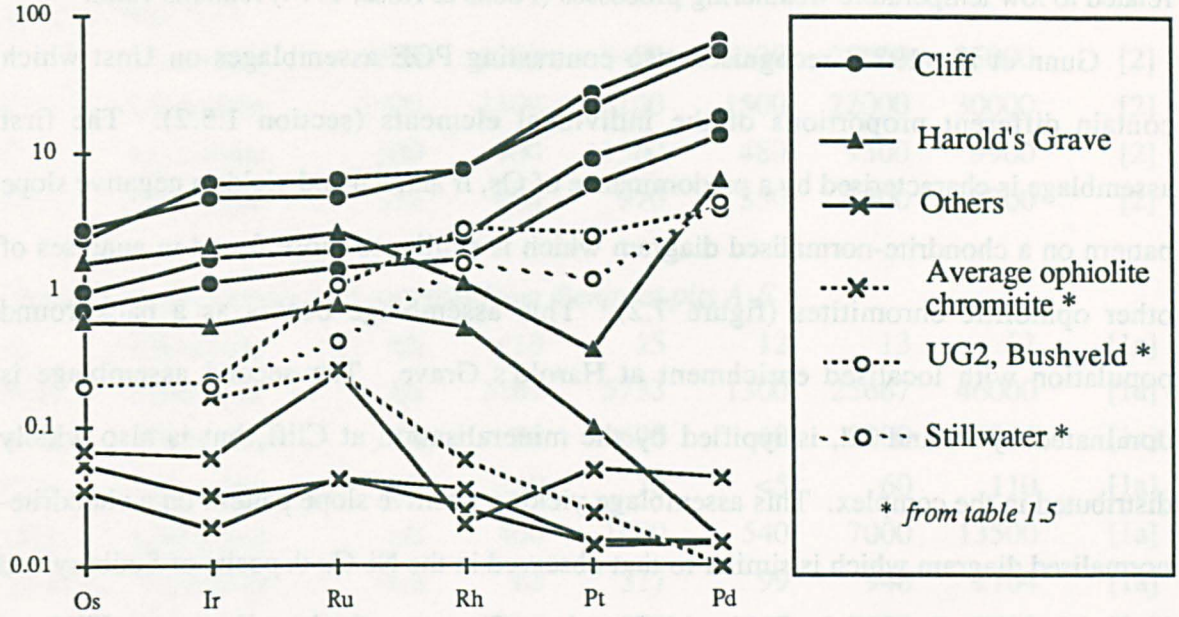

Figure 7.2. Unconventional chondrite-normalised diagram showing the relative proportions of individual PGE (after Gunn et al., 1985).

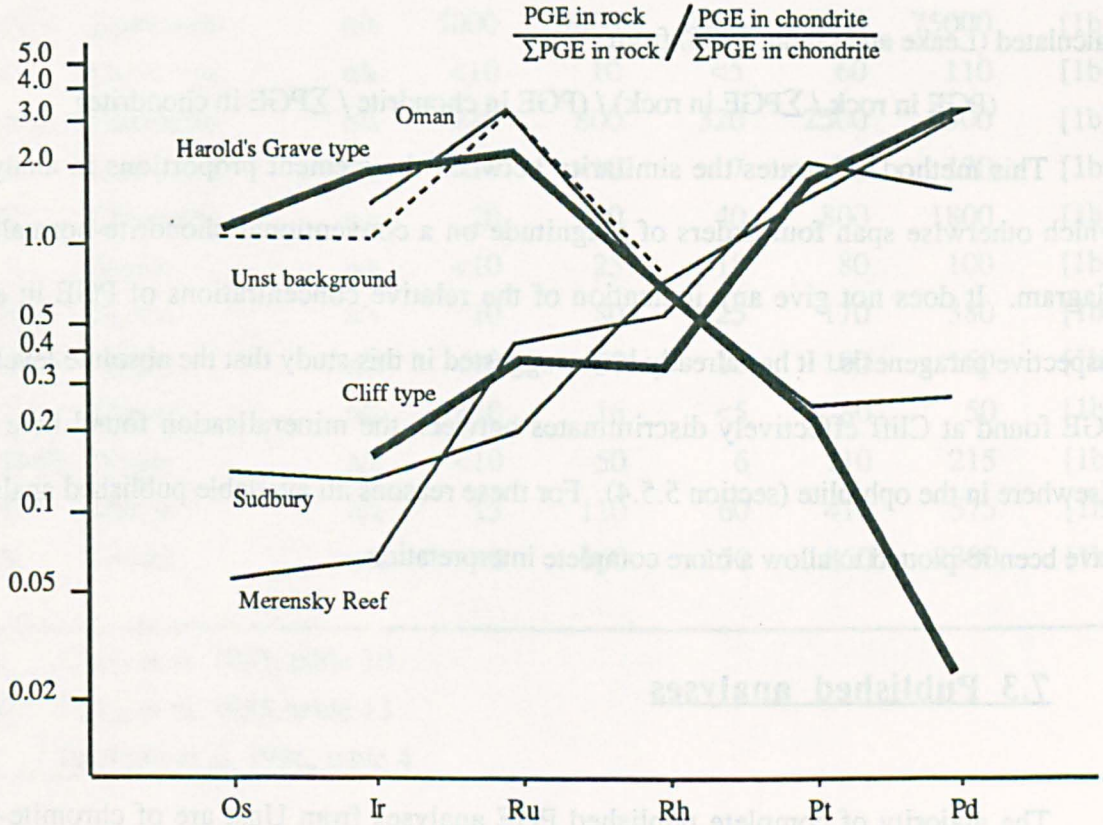

negative slope patterns but in one case include a large positive Pd anomaly (table 1.14). The original observation (Prichard et al., 1986) that such variations in Pt relative to Pd have been related to low temperature weathering processes (Fuchs & Rose, 1974) remains valid.

Gunn et al. (1985) recognised two contrasting PGE assemblages on Unst which contain different proportions of the individual elements (section 1.5.2). The first assemblage is characterised by a predominance of Os, Ir and Ru and yields a negative slope pattern on a chondrite-normalised diagram which is similar to those found in analyses of other ophiolitic chromitites (figure 7.2). This assemblage occurs as a background population with localised enrichment at Harold's Grave. The second assemblage is dominated by Pt and Pd, is typified by the mineralisation at Cliff, but is also widely distributed in the complex. This assemblage yields a positive slope pattern on a chondrite-normalised diagram which is similar to that observed in the Ni-Cu deposits of Sudbury and in the Merensky Reef of the Bushveld Complex. The type of mineralisation at Cliff and elsewhere was assigned to hydrothermal remobilisation from a magmatic source originally within mafic/ultramafic cumulates.

In the highly unconventional diagram used by Gunn et al. (1985) the ordinates are calculated (Leake and Gunn, 1986) from

(PGE in rock / ΣPGE in rock) / (PGE in chondrite / ΣPGE in chondrite)

This method illustrates the similarity between the element proportions in analyses which otherwise span four orders of magnitude on a conventional chondrite-normalised diagram. It does not give any indication of the relative concentrations of PGE in each respective paragenesis. It has already been suggested in this study that the absolute levels of PGE found at Cliff effectively discriminates between the mineralisation found here and elsewhere in the ophiolite (section 5.5.4). For these reasons all available published analyses have been re-plotted to allow a more complete interpretation.

7.3 Published analyses

The majority of complete published PGE analyses from Unst are of chromite-rich material from the Cliff locality (table 7.1). All of the chromitite or chromite-rich spoil

Table 7.1. Published PGE analyses of material from the Cliff locality.

Sample	*Lithology*	*Os*	*Ir*	*Ru*	*Rh*	*Pt*	*Pd*	*Source*
Spoil samples A-D								
A	Chromitite	1200	3200	4400	1500	28000	35000	[2]
B	Chromitite	1400	2500	3100	1500	22000	30000	[2]
C	Chromitite	500	900	1300	480	9300	9900	[2]
D	Chromitite	370	600	970	330	5800	7300	[2]
Chromitites & chromite-rich samples from dumps at pits A-E								
A	Chromitite	n/a	<10	15	12	13	57	[1a]
B(1)	Chromitite	n/a	3167	5733	1300	25667	46000	[1a]
B(2)	Chromitite	n/a	55	600	60	3000	5000	[1a]
C(1)	Chromitite	n/a	<10	10	<5	60	110	[1a]
C(2)	Chromitite	n/a	400	1600	540	7000	13500	[1a]
D+E(1)	Chromitite	n/a	65	317	99	948	2104	[1a]
D+E(2)	Chromitite	n/a	210	800	250	3500	7500	[1a]
Chromitite/dunite pairs from pits A-E								
Pit A	Chromitite	n/a	<10	25	18	20	100	[1b]
Pit B(i)	Chromitite	n/a	1500	3000	1100	20000	25000	[1b]
Pit B(ii)	Chromitite	n/a	5000	9000	1600	32000	75000	[1b]
Pit C	Chromitite	n/a	<10	10	<5	60	110	[1b]
Pit D+E	Chromitite	n/a	210	800	320	2500	5500	[1b]
Pit D	Chromitite	n/a	<10	<10	7	70	120	[1b]
Pit E	Chromitite	n/a	20	200	40	800	1800	[1b]
Pit A	Dunite	n/a	<10	25	18	80	100	[1b]
Pit B(i)	Dunite	n/a	10	80	25	170	380	[1b]
Pit B(ii)	Dunite	n/a	<10	50	10	100	160	[1b]
Pit C	Dunite	n/a	<10	16	<5	80	50	[1b]
Pit D+E	Dunite	n/a	<10	50	6	110	215	[1b]
Pit D	Dunite	n/a	15	110	60	410	575	[1b]
Pit E	Dunite	n/a	40	160	150	850	2300	[1b]

[1a] Gunn et al. 1985, table 10
[1b] Gunn et al. 1985, table 13
[2] Prichard et al. 1986, table 4

Figure 7.3. Chondrite-normalised diagrams showing published analyses of samples from Cliff (from table 7.1).

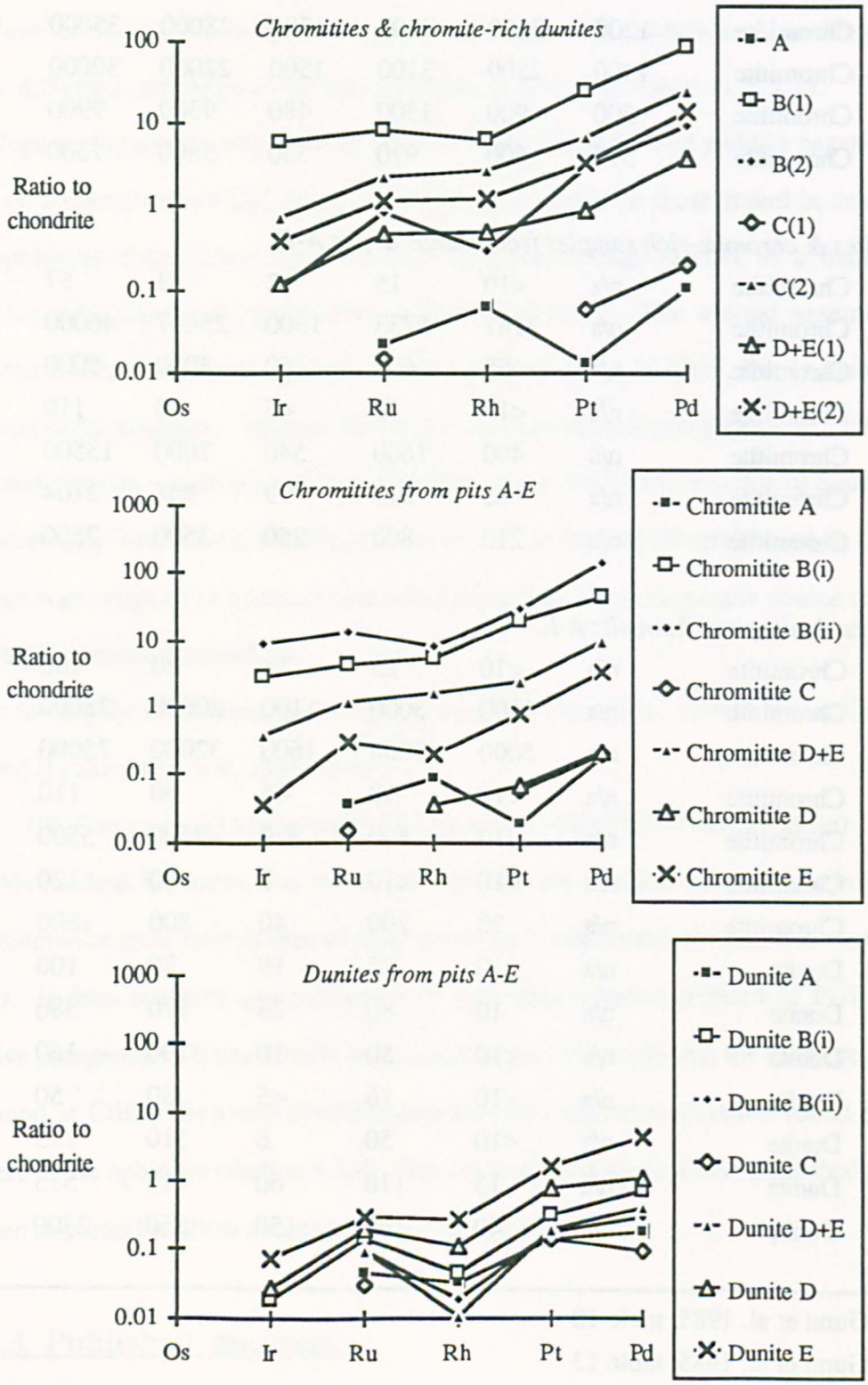

Figure 7.4. Chondrite-normalised diagrams showing published analyses of chromite-rich samples from other areas (from table 7.2).

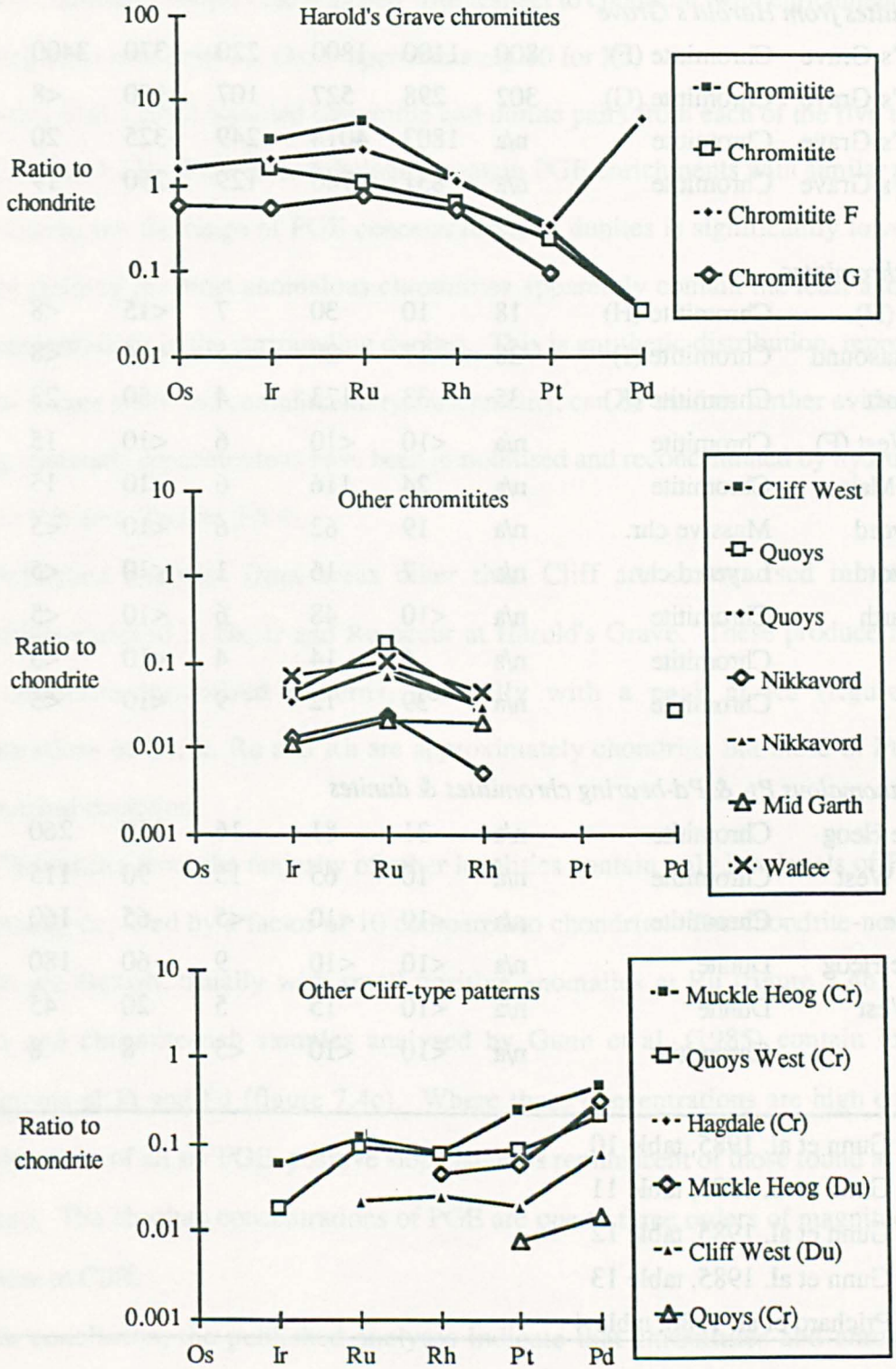

Table 7.2. Published PGE analyses of chromite-rich material from other areas.

Locality	*Lithology*	*Os*	*Ir*	*Ru*	*Rh*	*Pt*	*Pd*	*Key*
Chromitites from Harold's Grave								
Harold's Grave	Chromitite (F)	800	1100	1800	220	370	3400	[2]
Harold's Grave	Chromitite (G)	302	298	527	107	100	<8	[2]
Harold's Grave	Chromitite	n/a	1803	4014	249	325	20	[1c]
Harold's Grave	Chromitite	n/a	831	740	129	250	19	[1c]
Other chromitites								
Quoys (H)	Chromitite (H)	18	10	30	7	<15	<8	[2]
N. Baltasound	Chromitite (J)	28	17	29	5	<14	<8	[2]
Mid-Unst	Chromitite (K)	35	33	173	4	50	23	[2]
Cliff West (F)	Chromitite	n/a	<10	<10	6	<10	15	[1a]
Quoys Main	Chromitite	n/a	24	116	6	<10	15	[1c]
Nikkavord	Massive chr.	n/a	19	62	6	<10	<5	[1d]
Nikkavord	Layered chr.	n/a	7	16	1	<10	<5	[1d]
Mid Garth	Chromitite	n/a	<10	48	6	<10	<5	[1d]
Watlee	Chromitite	n/a	6	14	4	<10	<5	[1d]
Sobul	Chromitite	n/a	39	72	9	<10	<5	[1d]
Other anomalous Pt- & Pd-bearing chromitites & dunites								
Muckle Heog	Chromitite	n/a	31	81	16	250	260	[1d]
Quoys West	Chromitite	n/a	10	65	15	90	115	[1c]
Hagdale	Chromitite	n/a	<10	<10	<5	65	160	[1d]
Muckle Heog	Dunite	n/a	<10	<10	9	60	180	[1d]
Cliff West	Dunite	n/a	<10	15	5	20	45	[1b]
Quoys	Chromitite	n/a	<10	<10	<5	8	8	[1c]

[1a] Gunn et al. 1985, table 10
[1b] Gunn et al. 1985, table 11
[1c] Gunn et al. 1985, table 12
[1d] Gunn et al. 1985, table 13
[2] Prichard et al. 1986, table 4

samples yield smooth positive slope patterns on chondrite-normalised diagrams (figure 7.3). The ratio of the analyses to chondritic concentrations increase steadily from Os through to Pd. The patterns of samples containing lower levels of PGE show minor irregularities. Typically chromitite samples are enriched with respect to chondrite, with enrichment factors increasing from near unity for Os, to approximately 10 for Pd.

Gunn et al. (1985) sampled chromitite and dunite pairs from each of the five trial pits at Cliff (figure 1.11). Both these lithologies contain PGE enrichments with similar positive slope patterns but the range of PGE concentrations in dunites is significantly lower. The trial pits yielding the most anomalous chromitites apparently contain the least anomalous PGE concentrations in the surrounding dunites. This is antithetic distribution, representing depleted source areas and complimentary enrichments, can be used as further evidence that existing magmatic concentrations have been remobilised and reconcentrated by hydrothermal action in this area (section 5.5.4).

Published analyses from areas other than Cliff are summarised in table 7.2. Chromitites enriched in Os, Ir and Ru occur at Harold's Grave. These produce negative slope chondrite-normalised patterns, generally with a peak at Ru (figure 7.4a). Concentrations of Os, Ir, Ru and Rh are approximately chondritic but those of Pt and Pd show marked depletion.

Chromitites from the majority of other localities contain only low levels of PGE and are typically depleted by a factor of 10 compared to chondrite. The chondrite-normalised patterns are flattish, usually with small positive anomalies at Ru (figure 7.4b). A few dunites and chromite-rich samples analysed by Gunn et al. (1985) contain low level enrichments of Pt and Pd (figure 7.4c). Where these concentrations are high enough to allow detection of all six PGE, positive slope patterns reminiscent of those found at Cliff are produced. The absolute concentrations of PGE are one to three orders of magnitude lower than those at Cliff.

In conclusion, the published analyses indicate that chromitites and chromite-rich dunites from the Shetland ophiolite may contain PGE concentrations having either negative or positive slope patterns on a chondrite-normalised diagram. The different patterns occur in samples from different areas and thus appear at first sight to be mutually exclusive. The

possible origin of this geographical division by in situ magmatic fractionation processes is now considered.

7.4 New analyses for all six PGE and Au

The extensive sampling program described in earlier chapters has located further PGE parageneses not covered by the earlier analytical programs described in the previous section. In particular, anomalously high concentrations of Pt and Pd have also been found in sulphide-bearing dunites and pyroxenites from the bases of magmatic cycles within the main cumulate sequence. The chondrite-normalised patterns of pyroxenites, wehrlites and sulphide-bearing chromitites or dunites from this ophiolite have not previously been described. Furthermore, anomalous levels of Pt and Pd in the reconnaisance samples from the disused chromite quarries were shown to be associated with sulphide, whereas anomalous levels of Ir were associated with chromitite (section 4.5). This suggests that different platinum-group elements are concentrated by different processes. Additional high precision PGE analyses are therefore required to fully characterise the types of chondrite-normalised patterns occurring in the complex and to suggest an origin for this fractionation.

A total of 80 of the original reconnaissance samples have been analysed for Os, Ir, Ru, Rh, Pt, Pd and Au (table 7.3). The first 37 of these were collected from nine disused chromite quarries. These included the Cliff and Harold's Grave localities and other quarries from which anomalous Pt, Pd or Ir analyses had previously been obtained. These include chromite quarries from both the dunite and the harzburgite units. A further 31 samples from the Hagdale Wick, Quarry 13 and White House traverses were also re-analysed to establish the PGE ratios of in situ, stratigraphically controlled, mineralisation in both olivine and pyroxene-rich cumulates. The remaining 12 samples were selected from the suite of silicate lithologies because of their unusual PGE contents. They included dunites from several chromite-poor pods, pyroxene-bearing cumulates and sheared lithologies.

Analysis for all six PGE and Au was performed by Analytical Services Ltd., using NiS fire-assay and an ICP-MS analytical finish. Full analytical details and assessment of the reliability of the data have been described earlier (section 4.3.5 & 4.3.6).

Table 7.3. Additional high precision PGE analyses of Shetland samples (ppb).

Locality	Sample	Lithology	Os	Ir	Ru	Rh	Pt	Pd	Au
Cliff	RLC001	Chromitite	50	97	190	55	500	520	6
	RLC002	Chromitite	34	83	170	69	370	180	24
	RLC003	Harzburgite	30	4.5	8.5	1.5	10	13	6
	RLC004	Dunite	290	300	500	230	2400	4000	160
	RLC005	Dunite	6	4	8	1.5	4	4	<2
	RLC006	Serpentinite	4	4	8.5	1.5	5.5	3.5	<2
	RLC007	Dunite/chromite	470	1400	1800	950	10000	8600	80
Harold	RL069	Dunite/chromite	170	180	320	57	170	24	<2
	RL070	Chromitite	520	550	960	140	330	56	<2
Nikka	RLM001	Dunite	2	3.5	9.5	1.5	3.5	5	44
Vord	RLM002	Dunite/chromite	66	66	110	26	210	310	10
South	RLM003	Chromite	90	97	200	20	35	24	<2
	RLM004	Dunite/chromite	46	50	88	34	330	650	18
	RLM006	Dunite/chromite	18	16	39	2.5	3.5	5	<2
Quarry 12	RLM065	Dunite/chromite	24	23	44	20	140	260	20
	RLM066	Dunite/chromite	44	81	150	70	390	260	6
	RLM067	Dunite/chromite	18	16	35	11	120	230	26
	RLM068	Dunite/chromite	44	57	130	60	440	710	22
	RLM070	Dunite/chromite	26	22	43	14	140	340	38
Quarry	RLM059	Dunite/chromite	8	7.5	14	3.5	40	73	<2
12S	RLM063	Dunite	82	77	140	44	370	700	8
	RLM064	Chromitite	32	52	96	37	250	390	6
	RLM069	Dunite	86	82	150	50	360	800	22
Quarry 10	RLM096	Dunite/chromite	40	47	100	32	200	190	4
	RLM097	Chromitite	20	22	58	17	120	190	110
	RLM098	Dunite/chromite	12	14	44	5.5	9	10	2
	RLM099	Chromitite	20	17	58	6.5	21	33	4
Quarry 11	RLM029	Dunite/chromite	38	50	84	30	250	420	62
	RLM030	Dunite/chromite	18	11	41	4.5	8.5	5.5	<2
	RLM082	Dunite/chromite	54	48	110	33	270	410	20
Jimmies	RLM007	Dunite/chromite	98	120	190	110	870	2100	130
	RLM008	Wehrlite	4	4	5.5	2.5	22	48	2
	RLM009	Chromitite	82	90	200	52	170	29	<2
	RLM011	Dunite/chromite	38	35	65	21	160	29	4

Table 7.3 (cont.).

Locality	*Sample*	*Lithology*	*Os*	*Ir*	*Ru*	*Rh*	*Pt*	*Pd*	*Au*
High-	RLA171	Chromitite/Mnt.	30	28	42	6.5	40	21	250
level	RLA172	Chromitite	6	1.5	11	1	2	2.5	14
chromitite	RLA173	Chromitite	8	10	30	3.5	9.5	9	69
Hagdale	RLA025	Dunite	8	12	18	11	73	130	73
Wick	RLA028	Dunite	<2	4.5	12	4	17	23	42
traverse	RLA032	Dunite	8	6	20	5	14	17	42
	RLA033	Dunite	6	4	12	3	6	21	36
	RLA034	Dunite	4	4	14	3	14	20	54
	RLA040	Serpentinite	6	6.5	23	6.5	25	36	48
	RLA041	Serp./breccia	4	7	16	5	25	25	50
	RLA042	Serpentinite	4	4.5	14	4.5	13	21	47
	RLA176	Dunite	12	16	61	6	16	17	70
White	RLA078	Dunite	4	5	13	3	49	40	66
House	RLA079	Dunite	2	2.5	18	1.5	4	6.5	56
traverse	RLA080	Wehrlite	2	2.5	10	1.5	2.5	6.5	44
	RLA081	Wehrlite	6	7	21	4.5	15	20	160
	RLA082	Wehrlite	16	33	32	34	250	410	160
	RLA083	Wehrlite	14	24	37	28	170	340	180
	RLA084	Pyroxenite	6	11	25	7.5	52	78	240
	RLA085	Pyroxenite	4	7	32	5	33	49	240
	RLA086	Pyroxenite	4	6.5	13	4	31	50	200
	RLA087	Pyroxenite	3	5	21	4	21	36	210
	RLA088	Pyroxenite	4	6.5	42	8	27	110	200
	RLA089	Pyroxenite	<2	3.5	15	2	8.5	12	170
Quarry 13	RLA096	Dunite	12	25	38	19	76	86	160
traverse	RLA097	Dunite	24	32	62	45	180	470	160
	RLA098	Dunite	14	18	37	24	110	260	130
	RLA099	Dunite	28	41	88	62	230	670	160
	RLA100	Dunite	21	39	79	49	210	520	98
	RLA101	Dunite/chromite	26	36	75	45	180	250	82
	RLA103	Dunite	20	35	57	51	270	620	110
	RLA104	Dunite	11	20	35	27	150	290	73
	RLA105	Dunite	<2	3	16	3	6.5	15	70
	RLA106	Dunite	<2	2.5	14	1.5	3.5	6	56

Table 7.3 (cont.)

Locality	*Sample*	*Lithology*	*Os*	*Ir*	*Ru*	*Rh*	*Pt*	*Pd*	*Au*
Dunite	RLA149	Dunite	4	6	66	7.5	32	99	70
pods	RLA151	Dunite	4	5	17	4.5	10	26	42
	RLA152	Dunite	12	9	24	6	13	36	110
	RLA153	Dunite	14	15	62	8.5	40	48	160
Transition	RLM040	Dunite/harz.	6	6.5	7.5	3.5	27	36	10
Cumulate	RL060	Pyroxenite	<2	<0.5	0.5	<0.5	95	160	2
sequence	RL104	Wehrlite	2	5	4	5.5	44	42	2
	RLA156	Dunite/wehrlite	4	5	67	3.5	35	110	140
	RLM087	Pyroxenite	12	28	37	23	240	380	18
Shear	RLM088	Chromitite	4	11	19	8.5	73	120	6
zones	RLM071	Dunite	6	4	7	2	12	30	8
	RL050	Serpentinite	<2	1	5.5	0.5	4.5	4	28
Chondrite			514	540	690	200	1025	545	152

Many of the samples analysed in this study contain visible sulphides, although sulphur analyses indicate an overall deficiency of this element and significant remobilisation during secondary alteration (section 5.6). For these reasons all analyses have been presented normalised directly to chondrite, without recalculation to 100% sulphide. The normalisation values used (table 7.3) are those given by Naldrett and Duke (1980). Chondrite-normalised diagrams have been plotted using a standard format to allow comparison of patterns and their slopes. When extremely high or extremely low analyses plot outside the range of this diagram (10^1 to 10^{-3} x chondrite), another four logarithmic intervals have been used so that a valid comparison can be made between the gradients of patterns (i.e. ratios between PGE).

A few samples have also been plotted on mantle normalisation diagrams using the method of Barnes et al. (1988). The normalisation values in this case are Ni 2000 ppm, Cu 28 ppm and 0.00815 x chondrite for the noble metals.

The following section describes the various chondrite-normalised patterns that are characteristic of different rock types or areas of the complex. The origin of these different patterns by internal fractionation of the platinum-group elements during magmatic processes is also discussed.

Figure 7.5. Chondrite-normalised patterns for the chromite-rich and chromite-poor portions sampled from a layered chromitite/dunite boulder at Harold's Grave.

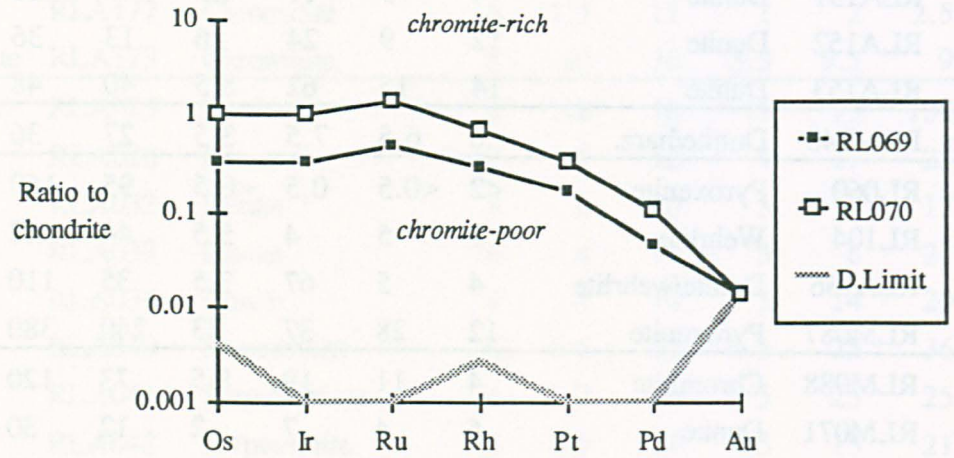

Sample	*Lithology*	*Ni (ppm)*	*Cu (ppm)*	*Cr (ppm)*	*As (ppm)*	*Sb (ppm)*
RL069	Chromite-rich dunite matrix	2346	18	28055	0	1.7
RL070	Chromitite layer	2039	9	79812	3	1.5

Figure 7.6. Harold's Grave type patterns in chromitites from different stratigraphic levels.

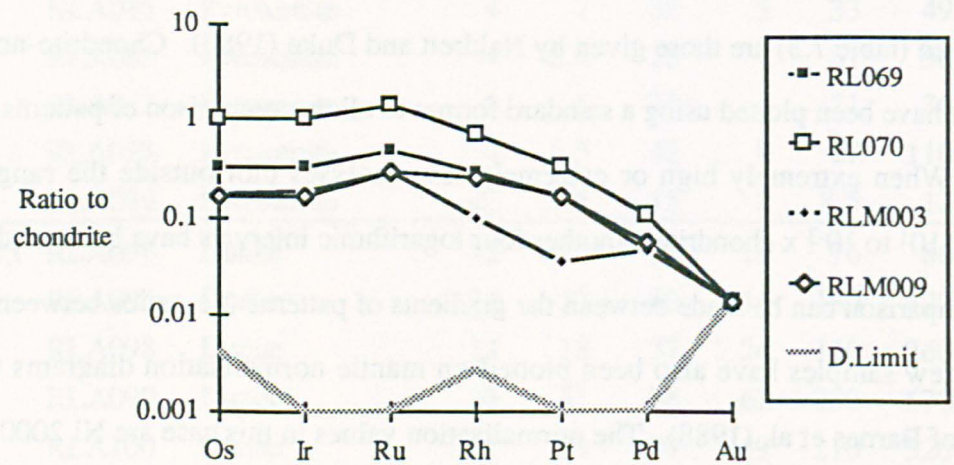

Sample	*Locality*	*Ni (ppm)*	*Cu (ppm)*	*Cr (ppm)*	*As (ppm)*	*Sb (ppm)*
RLM003	Nikka Vord South (Harz. Unit)	1869	0	311457	0	10.7
RLM009	Jimmie's Quarry (Dunite Unit)	1344	0	309513	14	2.3

7.5 Harold's Grave type mineralisation

Analyses of chromitites from the Harold's Grave chromite quarry yield negative slope patterns on chondrite-normalised diagrams which are typical of those obtained from other ophiolitic chromitites (Gunn et al., 1985; Prichard et al., 1986). This locality provides the best example of this type of mineralisation in the Shetland ophiolite complex. Enrichments of PGE in chromitites yielding this type of negative slope pattern are therefore referred to as Harold's Grave type mineralisation. The following sections describe the distribution of this particular geochemical signature and an origin by magmatic fractionation processes is proposed.

7.5.1 Controls of PGE mineralisation in chromitites from the Harold's Grave quarry

New analyses of chromitites and chromite-rich dunites from the Harold's Grave quarry are shown in figure 7.5. Both analyses are of the same boulder, which contained cm scale layers of chromitite. This material was physically separated to allow analysis of the chromite-rich layer and the olivine-rich matrix. Both the analyses yield negative-slope patterns with maxima at Ru. The concentrations of PGE fall off sharply towards Au. Both samples contain enrichments of Os, Ir and Ru but levels of these elements are highest in the most chromite-rich portion. These patterns confirm that this type of Os-Ir-Ru mineralisation is associated with massive chromitite or chromitite layers. A close association between anomalous Ir concentrations and chromite has also been described earlier (section 4.5.1).

These observations are also consistent with the published mineralogical evidence. Prichard et al. (1989) describe euhedral Os-bearing laurites occurring within the chromite matrix. Laurites also occur interstitially to, and on the margins of, chromite grains. These laurites are Os-poor, but contain inclusions of native osmium, attributed to exsolution triggered by an As-rich fluid agent. The occurrence of euhedral laurite grains as inclusions indicates that they formed prior to crystallisation of the enclosing chromite. This suggests that these minerals crystalised directly from the magma at an early stage, nucleated

Figure 7.7. Chondrite-normalised patterns for high-level chromitites from the Nev.

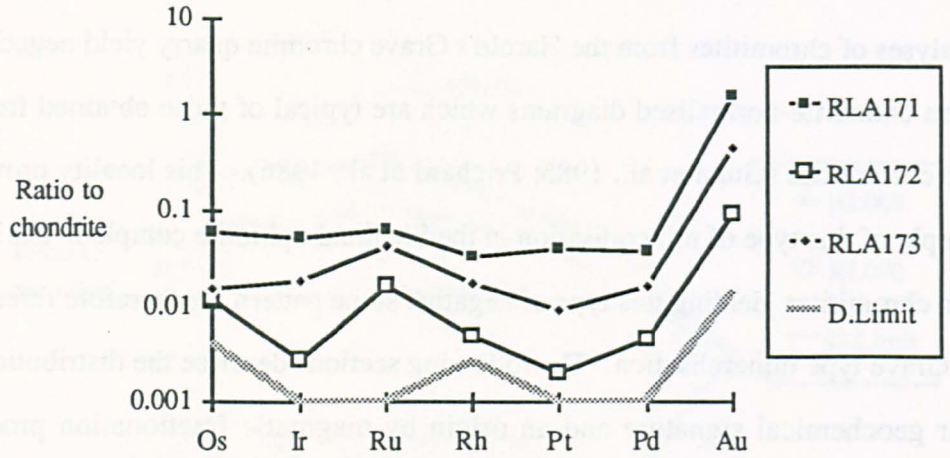

Sample	*Lithology*	*Ni (ppm)*	*Cu (ppm)*	*Cr (ppm)*	*As (ppm)*	*Sb (ppm)*
RLA171	Sheared chromite	1156	19	157262	195	n/a
RLA172	Chromitite (base)	1690	110	132408	31	n/a
RLA173	Chromitite (top)	1771	115	109962	42	n/a

Figure 7.8. Mantle normalised diagram showing chromitites containing Harold's Grave type mineralisation (solid lines) and high-level chromitites from the Nev (dashed lines).

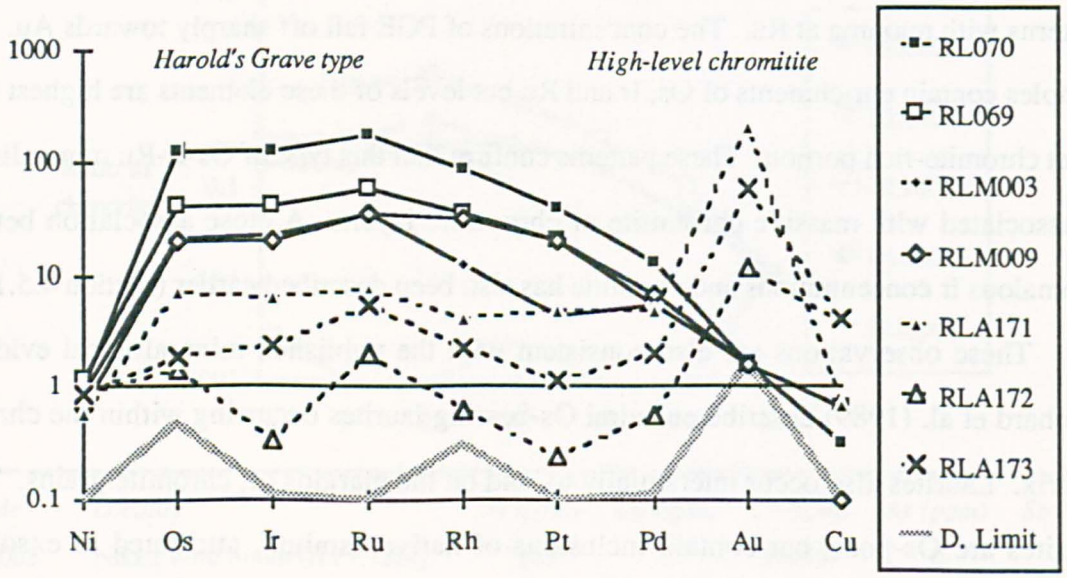

preferentially on chromite, and were fractionally removed by the enclosing chromite-rich cumulates. The suggestion that laurite can fractionally crystalise from a primitive magma saturated in Ru, Os and Ir is consistent with the lower solubilities of Ir than Pt in basaltic melts (Amosse et al. 1990).

7.5.2 Other Harold's Grave type chromitites

Similar negative slope patterns occur in samples from elsewhere, but only in chromite-rich rocks or chromitites (figure 7.6). They occur in chromite concentrations at several stratigraphic levels, including those from dunite pods within the mantle sequence (e.g. Nikka Vord South), from the main dunite unit (e.g. Jimmie's) and from wehrlites in the layered cumulate sequence (chromitite K, table 7.2). The occurrence of chromitites containing fractionally crystalised laurite at high stratigraphic levels indicates that a primitive magma was periodically available at these levels.

7.5.3 High-level chromitites

High-level chromitites from the Nev were found to give chondrite-normalised patterns which are distinct from the Harold's Grave type patterns (figure 7.7). These samples retain the peak at Ru and the negative slope from Ru but both of these features are weaker than in other chromitites. The overall levels of PGE are also an order of magnitude lower. The high-level chromitites also show a pronounced up turn at Pd with large positive Au anomalies. This contrasts with the very low levels of Au in other chromitites which are typically below detection.

Concentrations of pathfinder elements in the Nev chromitites (figure 7.7) indicate that these formed from a more evolved magma than the other chromitites (figures 7.5 & 7.6). They contain lower concentrations of the more compatible elements (i.e. Ni, Cr and PGE) and higher levels of the less compatible elements (i.e. Au, Cu and As) (figure 7.8). This indicates that negative slope patterns are only produced by chromitites crystalising from a very primitive magma, whereas more evolved compositions result in chromitites containing flattish patterns.

Table 7.4. Compositions of chromitites containing Harold's Grave type mineralisation.

Sample	*Locality*	*Type*	*Al_2O_3 (wt%)*	*Al (ppm)*	*Cr (ppm)*	*Cr/(Cr+Al)*	*Ru (ppb)*
RL070	Harold's Grave	HG	3.29	17412	79812	0.82	960
RL069	Harold's Grave	HG	0.29	1535	28055	0.95	320
RLM003	Nikka Vord S.	HG	7.61	40274	311457	0.89	200
RLM009	Jimmie's	HG	9.07	48001	309513	0.87	200
RLC001	Cliff	C	7.79	41227	161943	0.80	190
RLC002	Cliff	C	5.29	27996	128291	0.82	170
RLM064	Quarry 12 S.	C	8.76	46360	248415	0.84	96
RLM097	Quarry 10	C	8.97	47472	272201	0.85	58
RLA171	The Nev HLC	F	10.82	57262	157262	0.73	42
RLA172	The Nev HLC	F	14.61	77320	132408	0.63	11
RLA173	The Nev HLC	F	13.91	73615	109962	0.60	30

HG = Harold's Grave-type, negative slope pattern

C = Cliff-type, positive slope pattern

F = High level chromitite, flattish pattern

Figure 7.9. Covariance of Ru concentrations and Cr/Al ratios of chromitites.

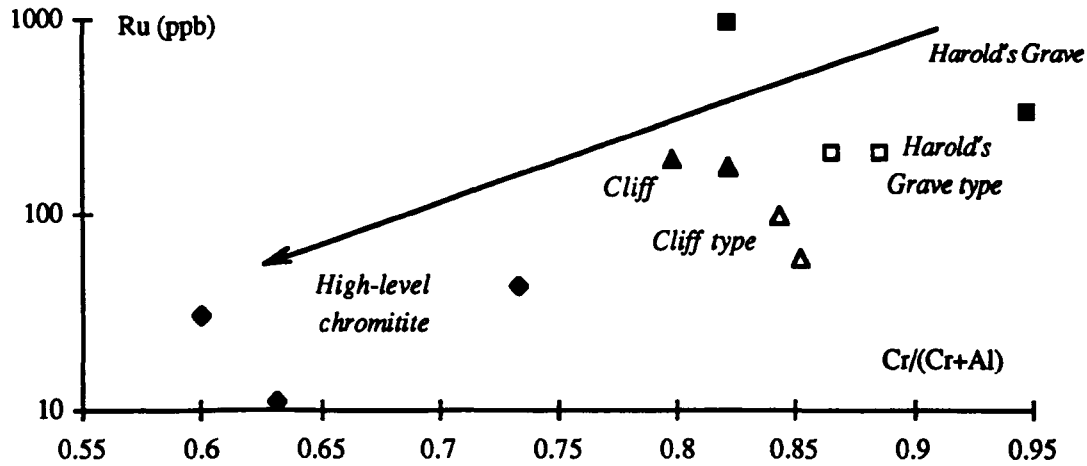

7.5.4 Fractionation of PGE and chromite compositions

All the Harold's Grave type chromitite and high-level chromitite analyses have also been plotted on a mantle normalised spidergram, in order to show the concentrations of the other chalcophile elements (figure 7.8). In this type of diagram PGE enriched samples produce arch shaped patterns (Barnes et al., 1988). In the case of Harold's Grave type mineralisation they show a negative slope from Ru. Although these four chromitites are from different levels in the complex they show very similar patterns and do not form an evolutionary series. This diagram also emphasizes the differences between the patterns for basal and high-level chromitites. The latter are flattish and close to mantle concentrations from Ni to Pd, but show marked enrichments in the less compatible elements Au and Cu. The two patterns can be distinguished by the differing absolute levels of Ru that they contain.

In figure 7.9 the concentrations of Ru in different chromitite samples are compared to the composition of the spinel phase. In the absence of microprobe chromite analyses the Cr/(Cr+Al) ratios used have been derived from XRF pellet analyses*. The high-level chromitites have lower Cr/(Cr+Al) ratios than other chromitites. This is consistent with their formation from a more evolved magma or a mixture of primitive and evolved magma, resulting in more aluminous spinel compositions at higher stratigraphic levels.

The trend of decreasing Ru content with decreasing Cr/(Cr+Al) ratio, and hence evolution of the magma (figure 7.9) is consistent with the proposed mechanism of formation of PGE concentrations of the Harold's Grave type. If laurite and other PGM phases are to crystalise directly from the melt then these elements must reach saturation in the magma prior to or during the crystallisation of the enclosing chromite. Thus Os-Ir-Ru enrichments are only expected to form from the most primitive magmas and only early in the crystallisation history. In more evolved magmas or mixtures from which sulphides have segregated these

---

* These analyses are therefore subject to various inaccuracies due to matrix effects but provide a measure of the relative Cr/(Cr+Al) ratios of the different chromitites. This is apparently an overestimate in comparison to the range of Cr/(Cr+Al) values reported in chapter 3.

elements will not be saturated and thus high-level chromitites will not produce negative slope patterns on a chondrite-normalised diagram.

Finally, the four remaining chromitites for which Ru analyses have been obtained have also been plotted on figure 7.9. Two of these samples are from Cliff and the other two contain Cliff type mineralisation (section 7.5). These analyses fall between the primitive Harold's Grave type and the more fractionated high-level assemblage indicating an intermediate position in the fractionation history for the formation of this type of PGE concentration.

7.6 Cliff-type mineralisation

Analyses of chromitites and chromite-rich dunites from the Cliff quarry produce positive slope patterns on chondrite-normalised diagrams which are reminiscent of those obtained from stratiform intrusions and Ni-Cu sulphide deposits (Gunn et al., 1985; Prichard et al., 1986). The Cliff quarry has been found to contain the highest overall concentrations of Pt or Pd in the Shetland ophiolite and is the best known such example from any ophiolite complex. This type of PGE concentration is therefore referred to as Cliff type mineralisation.

This study has shown that this type of mineralisation is widespread in the complex and also occurs in sulphide-bearing dunites, wehrlites and pyroxenites from the cumulate sequence. The following sections suggest a possible origin for this particular geochemical signature by magmatic fractionation processes within a model which can also account for the distribution pattern.

7.6.1 The Cliff quarry

PGE-enriched samples from Cliff all have relatively smooth positive slope patterns on a chondrite-normalised diagram (figure 7.10). Rocks containing differing absolute levels of PGE produce similar patterns with the same gradients which indicates that the ratios of particular PGE are approximately constant. Similar patterns occur in sulphide-rich dunites, chromitites and chromite-rich dunites. The levels of PGE are apparently independent of the

Figure 7.10. Positive slope chondrite-normalised patterns in PGE-rich samples from Cliff

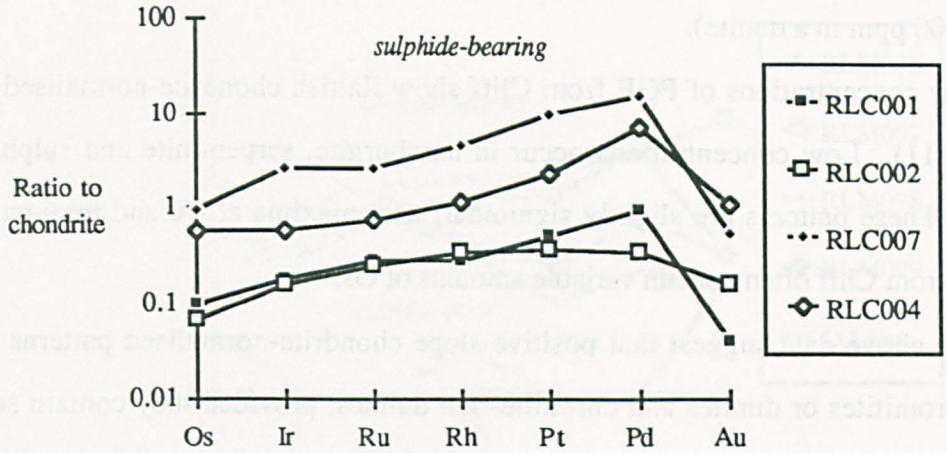

Sample	*Lithology*	*Ni (ppm)*	*Cu (ppm)*	*Cr (ppm)*	*As (ppm)*	*Sb (ppm)*
RLC007	Dunite/chromite	2816	32	79354	121	4.6
RLC004	Dunite (SR)	5667	752	2213	51	11.5
RLC001	Chromitite	1580	0	161943	0	n/a
RLC002	Chromitite	2578	183	128291	123	n/a

Figure 7.11. Flattish chondrite-normalised patterns in PGE-poor samples from Cliff

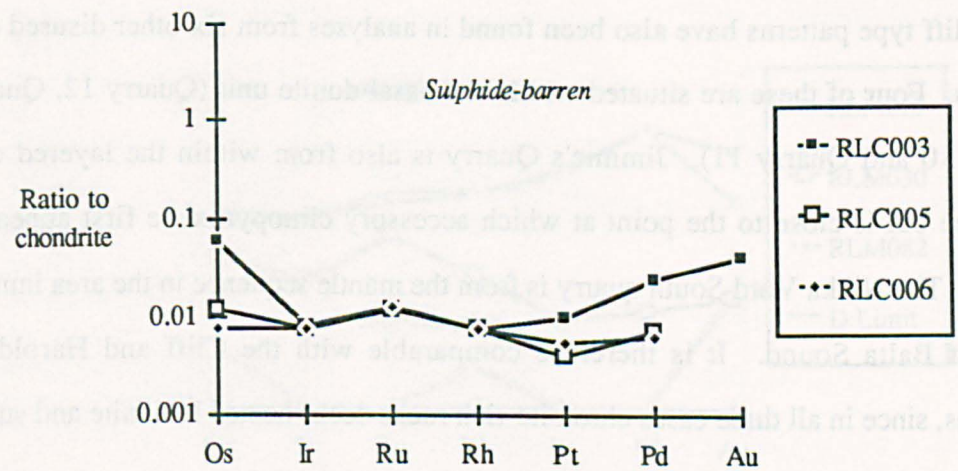

Sample	*Lithology*	*Ni (ppm)*	*Cu (ppm)*	*Cr (ppm)*	*As (ppm)*	*Sb (ppm)*
RLC003	Harzburgite	2363	9	2150	29	1.4
RLC005	Dunite	2676	12	1864	4	0
RLC006	Serpentinite	2233	14	2292	10	1.6

chromite content. Pathfinder analyses indicate that these samples all contain significant amounts of sulphides when allowance is made for the background nickel content of olivine (up to 3500 ppm in a dunite).

Low concentrations of PGE from Cliff show flattish chondrite-normalised patterns (figure 7.11). Low concentrations occur in harzburgite, serpentinite and sulphide-poor dunites. These patterns are slightly sigmoidal, with maxima at Ru and minima near Pt. Samples from Cliff often contain variable amounts of Os.

The above data suggest that positive-slope chondrite-normalised patterns occur in either chromitites or dunites and chromite-rich dunites, provided they contain sulphides. The role of sulphides as a concentration mechanism for the higher contained levels of PGE has been discussed previously (6.4.5). The positive slope pattern appears to be a characteristic of concentrations formed by the collection of PGE by partition into immiscible sulphide liquid. Primary magmatic signatures at Cliff have been extensively modified by secondary processes so the role of sulphide phases is now examined using samples from other less altered areas.

7.6.2 Other chromite quarries

Cliff type patterns have also been found in analyses from six other disused chromite quarries. Four of these are situated within the basal dunite unit (Quarry 12, Quarry 12S, Quarry 10 and Quarry 11). Jimmie's Quarry is also from within the layered cumulate sequence but is close to the point at which accessory clinopyroxene first appears in the dunites. The Nikka Vord South quarry is from the mantle sequence in the area immediately north of Balta Sound. It is therefore comparable with the Cliff and Harold's Grave localities, since in all three cases chromite-rich rocks occur hosted in dunite and surrounded by harzburgites.

7.6.2.1 Cliff type patterns and sulphide phases

Chondrite-normalised diagrams for samples from Quarries 10 and 11 are shown in figures 7.12 and 7.13. In each case Cliff-type patterns occur in sulphide-bearing dunites, chromitites or chromite-rich dunites. The pathfinder analyses have been tabulated in order of

Figure 7.12. Cliff type and sigmoidal patterns from Quarry 10.

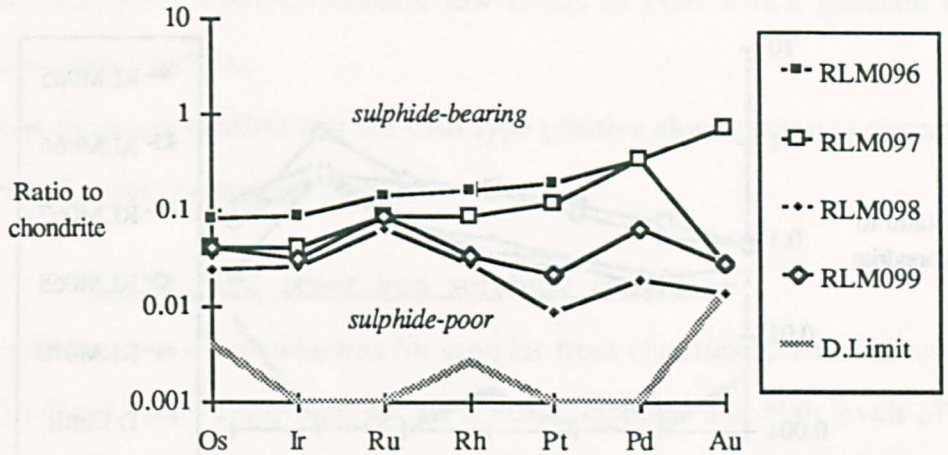

Sample	*Lithology*	*Ni (ppm)*	*Cu (ppm)*	*Cr (ppm)*	*As (ppm)*	*Sb (ppm)*
RLM096	Dunite/chromite	3718	70	220818	10	2
RLM097	Chromitite	3229	633	272201	25	11.3
RLM099	Chromitite	1607	0	310389	0	0
RLM098	Dunite/chromitite	1498	28	241060	0	0

Figure 7.13. Cliff type and sigmoidal patterns from Quarry 11.

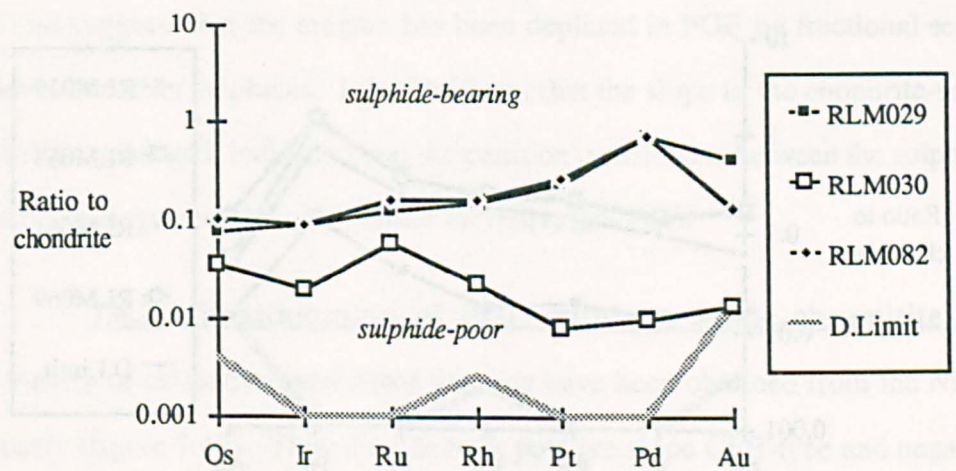

Sample	*Lithology*	*Ni (ppm)*	*Cu (ppm)*	*Cr (ppm)*	*As (ppm)*	*Sb (ppm)*
RLM082	Dunite/chromite	4903	666	232759	0	5.2
RLM029	Dunite/chromite	5068	928	125030	0	0
RLM030	Dunite/chromite	1838	0	174111	0	1.8

Figure 7.14. Cliff type chondrite-normalised patterns from Quarry 12.

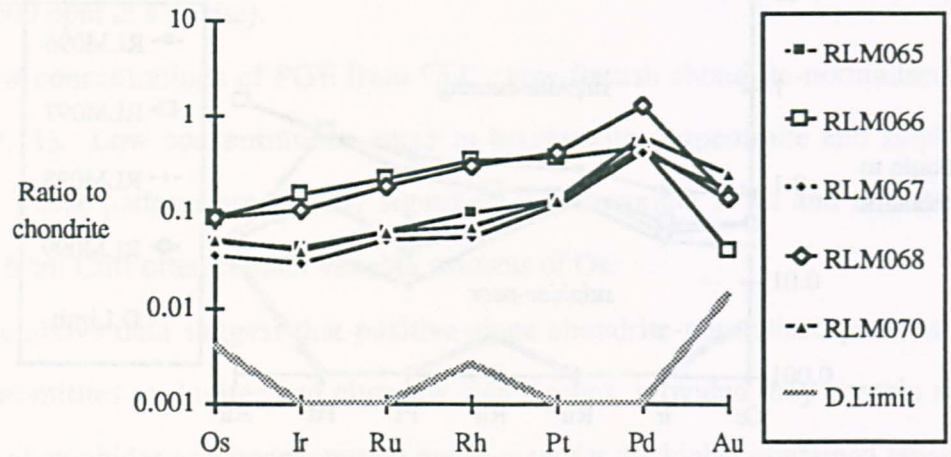

Sample	*Lithology*	*Ni (ppm)*	*Cu (ppm)*	*Cr (ppm)*	*As (ppm)*	*Sb (ppm)*
RLM068	Dunite/chromite	8551	1453	66758	12	3.3
RLM066	Dunite/chromite	2048	49	234168	0	2.2
RLM065	Dunite/chromite	7245	315	86696	15	12.7
RLM067	Dunite/chromite	3794	680	233300	0	1.4
RLM070	Dunite/chromite	6928	1084	81056	10	3.6

Figure 7.15. Cliff type chondrite-normalised patterns from Quarry 12 South.

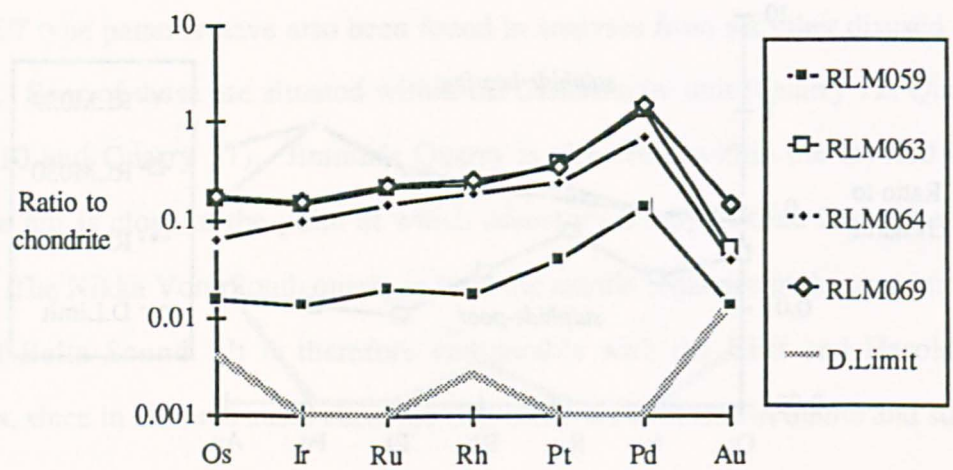

Sample	*Lithology*	*Ni (ppm)*	*Cu (ppm)*	*Cr (ppm)*	*As (ppm)*	*Sb (ppm)*
RLM069	Dunite	6073	899	2004	8	3.3
RLM063	Dunite	5670	847	4107	6	7.8
RLM064	Chromitite	2478	95	248415	18	4.1
RLM059	Dunite/chromite	5039	140	17992	3	1.2

decreasing PGE tenor and indicate that the most PGE-rich samples generally contain higher levels of Ni and Cu, which are indicative of higher sulphide contents. Rocks containing low levels of chalcophile elements contain low levels of PGE which generate sigmoidal "background-type" patterns.

These diagrams confirm that the Cliff type positive slope pattern is characteristic of PGE enriched rocks containing sulphides.

7.6.2.2 PGE tenor and sulphide contents

Chondrite-normalised diagrams for samples from Quarries 12 and 12S are shown in figures 7.14 and 7.15. These samples all contain sulphides and high levels of PGE and accordingly follow Cliff type patterns. It can be seen by comparison of the diagrams with the pathfinder element concentrations listed below that variations in total PGE content do not always follow variations in chalcophile element concentrations. An example of this is the pattern shown by sample RLM0059 (figure 7.15). The shape is similar to that of other sulphide-rich samples but the absolute levels of PGE are lower and more typical of "background-type" analyses. The pathfinder element analyses indicate that this sample does contain a significant amount of sulphide.

This variation in PGE/sulphide ratio indicates disequilibrium between different samples and suggests that the magma has been depleted in PGE by fractional segregation and removal of earlier sulphides. It is significant that the slope of the chondrite-normalised pattern is still unchanged, indicating that the partition coefficients between the sulphide liquid and the silicate magma are broadly similar for individual PGE.

7.6.2.3 Fractionation of PGE within a single chromitite body

A variety of chondrite-normalised patterns have been obtained from the Nikka Vord South quarry (figure 7.16). They include both positive slope Cliff-type and negative slope Harold's Grave-type patterns. These occur in sulphide-bearing chromite-rich dunites and massive chromitites respectively. In both cases the absolute levels of PGE are significantly lower than those at Cliff or Harold's Grave. Sigmoidal "background" patterns occur in sulphide-poor dunites or chromite-rich dunites which contain lower levels of chalcophile elements.

Figure 7.16. Cliff type and Harold's Grave type patterns from the Nikka Vord South Quarry.

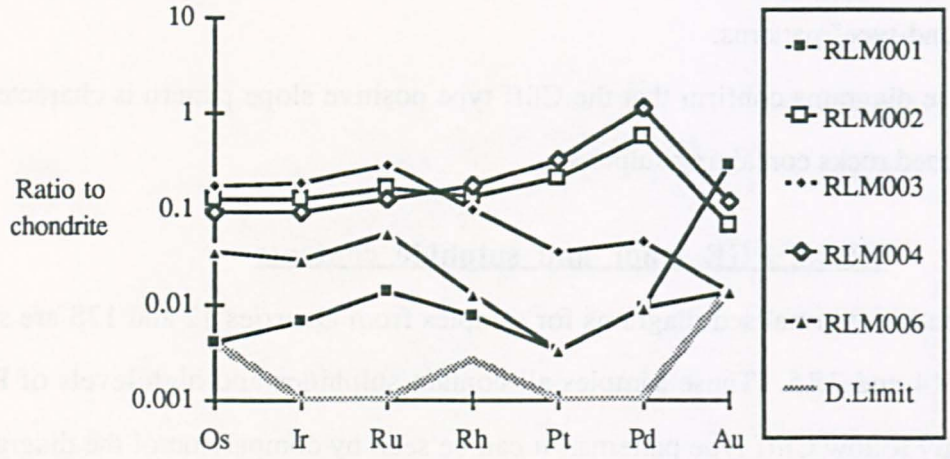

Sample	*Lithology*	*Ni (ppm)*	*Cu (ppm)*	*Cr (ppm)*	*As (ppm)*	*Sb (ppm)*
RLM004	Dunite/chromite	4057	427	126392	6	6
RLM002	Dunite/chromite	3941	63	104229	6	12.9
RLM003	Chromite	1869	0	311457	0	10.7
RLM006	Dunite/chromite	2539	17	150337	10	2.2
RLM001	Dunite	2738	61	1480	0	25.7

Figure 7.17. Cliff type and Harold's Grave type patterns from Jimmie's Quarry.

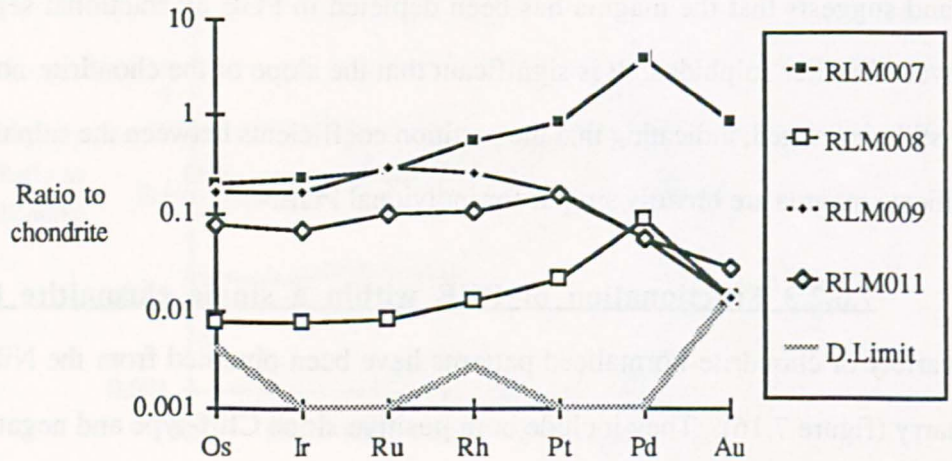

Sample	*Lithology*	*Ni (ppm)*	*Cu (ppm)*	*Cr (ppm)*	*As (ppm)*	*Sb (ppm)*
RLM007	Dunite/chromite	3720	371	98479	9	8.7
RLM008	Wehrlite	2509	99	5831	0	3.2
RLM009	Chromitite	1344	0	309513	14	3.8
RLM011	Dunite/chromite	2323	33	73951	7	2.3

This indicates that both positive and negative slope patterns may occur within the same chromite body. These different patterns are not, therefore, characteristic of particular locations but represent different concentration processes. It has been suggested that these two distinct processes are the fractional crystallisation of PGM and the partitioning of PGE into an immiscible sulphide liquid. Both processes may occur during formation of a single chromite-rich body and its surrounding dunite envelope. Each process causes effective fractionation of the PGE and the resulting rocks inherit different geochemical signatures.

This range of patterns has also been obtained from Jimmie's Quarry (figure 7.17). Positive slope Cliff-type patterns are shown by sulphide-bearing chromite-rich dunites and also by a sulphide-bearing wehrlite. A sample of massive chromitite (RLM009) yielded a negative slope Harold's Grave-type pattern. One sulphide-bearing sample shows a Cliff-type pattern from Os to Pt, but a sharp downturn towards Pd. This is further evidence of the selective remobilisation of Pd as a result of secondary fluid related alteration (section 6.2).

As has been discussed earlier (section 7.4.4) Harold's Grave-type patterns are not restricted to the mantle sequence but may also occur associated with chromitite in the crustal sequence. If this type of mineralisation is the result of fractional crystallisation of PGM then it indicates that primitive magma is available at this level in the sequence which is in turn explained by an open system fractionation model (section 6.6). It is inherent in this model that PGM phases can only crystalise from a magma in which immiscible sulphide liquid has not yet segregated. The very large partition coefficients for all six PGE between silicate magma and such an immiscible liquid predict that the concentrations of PGE will be greatly reduced should a significant amount of sulphide segregate. As a result the solubility of PGM phases such as laurite will no longer be exceeded and these will no longer crystalise.

Since both patterns are seen in the same chromite-rich pod it appears that both processes and the crystallisation of chromite occur within a relatively short time and are in some way related. Direct crystallisation of PGM phases apparently pre-dates or overlaps crystallisation of chromitite bodies, since these minerals are found enclosed by the chromite. Sulphide saturation occurs shortly after formation of the main chromite concentration since sulphide phases are typically seen in the olivine matrix of marginal disseminated chromite-rich dunites as well as in the surrounding dunites. This order is confirmed by the results of

Figure 7.18. Chondrite-normalised patterns of cumulate dunites from the Quarry 13 Traverse.

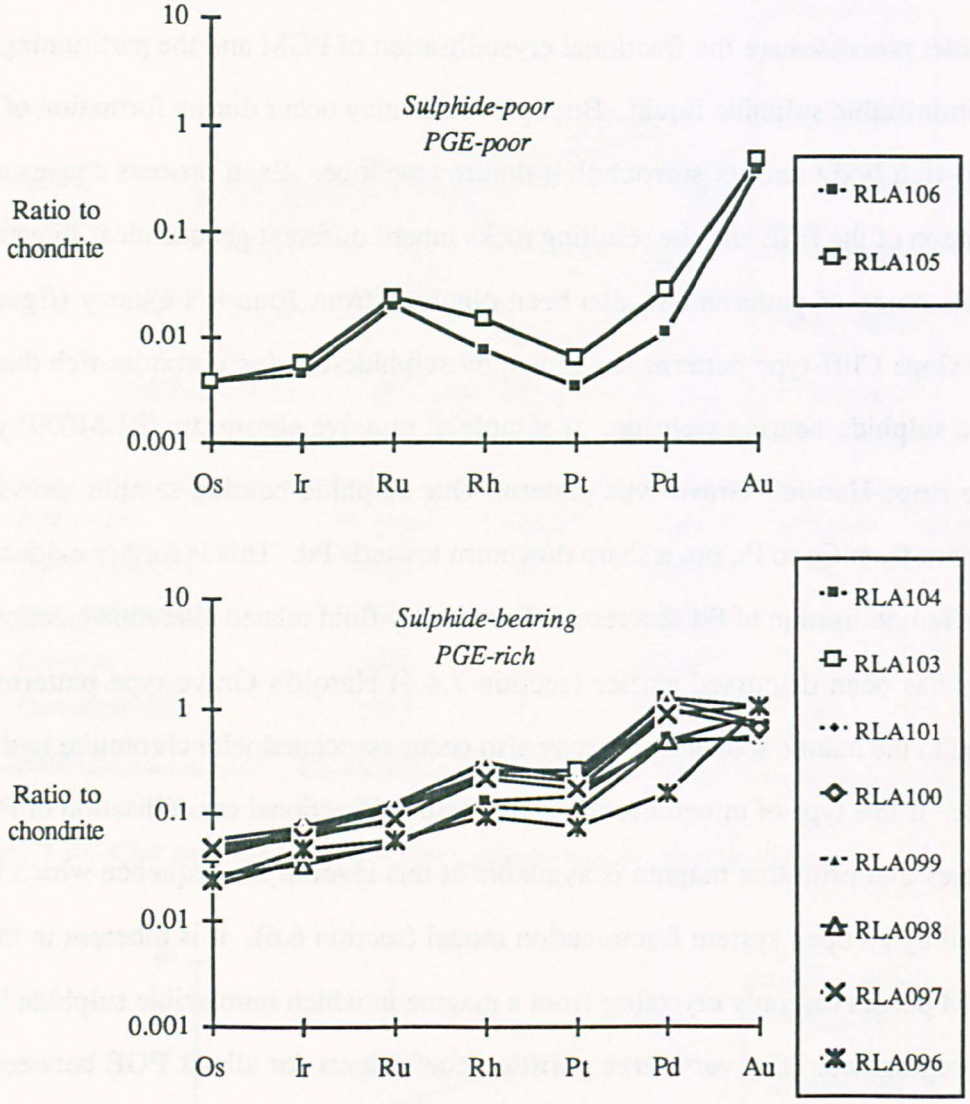

Sample	Metres	Lithology	Sulphide	Ni (ppm)	Cu (ppm)	Cr (ppm)	As (ppm)
RLA106	1.5	Dunite	No S	3193	98	4118	0
RLA105	2.25	Dunite	No S	3295	40	2691	0
RLA104	2.75	Dunite	VSR	3798	663	3023	6
RLA103	3.25	Dunite	VSR	6031	808	3893	8
Position of extracted chromite body							
RLA101	7.25	Dunite/chromite	SB	3232	62	20940	0
RLA100	8.25	Dunite	VSR	6017	1178	2386	0
RLA099	9.25	Dunite	SR	6522	1225	3027	8
RLA098	10.25	Dunite	VSR	6031	881	4690	0
RLA097	11.25	Dunite	VSR	4591	1152	3283	0
RLA096	12	Dunite	MSR	4502	221	3059	0

Figure 7.19. Variation in Os, Ir, Ru, Rh, Pt, Pd and Au across the Quarry 13 Traverse.

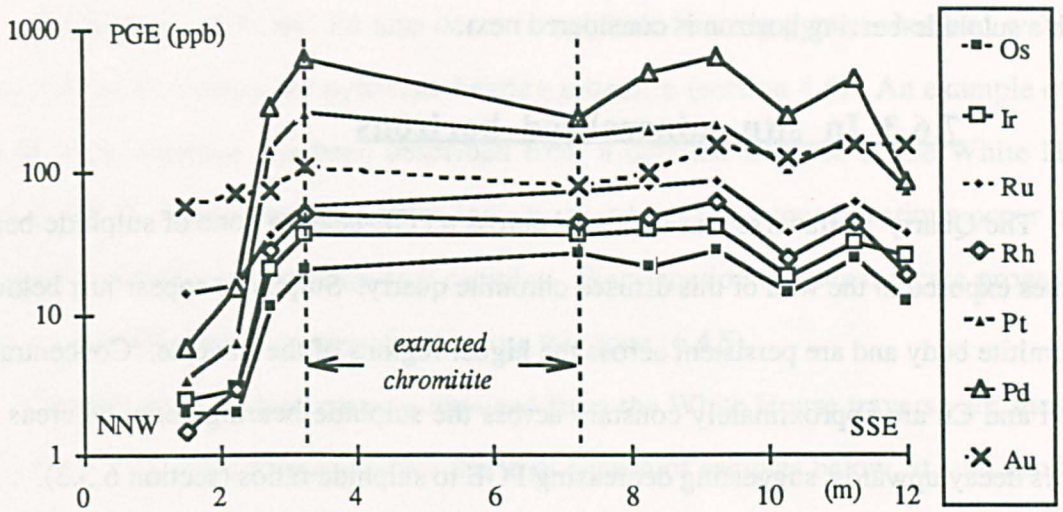

Figure 7.20. Variation in fractionation indices across the Quarry 13 Traverse.

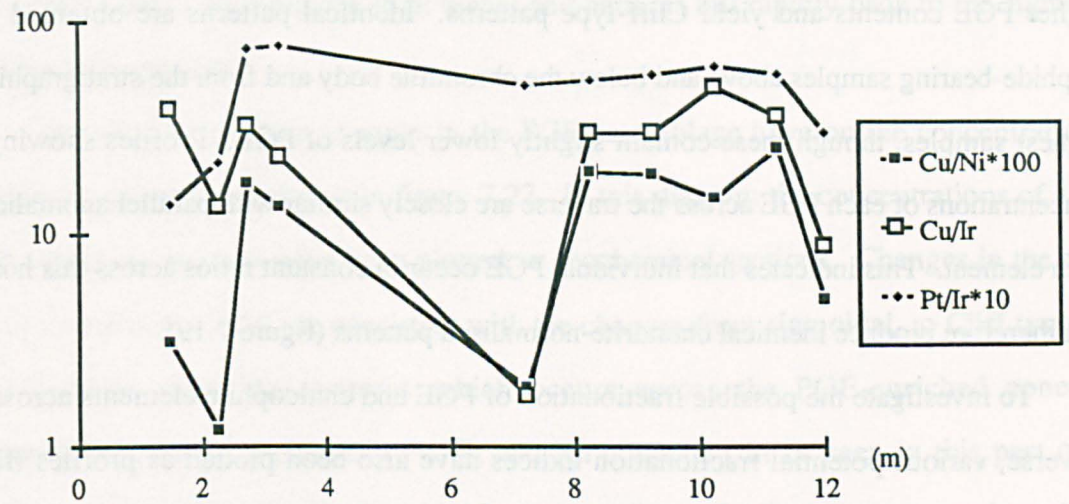

Table 7.5. Variation in fractionation indices across the Quarry 13 Traverse.

Metres	*1.5*	*2.25*	*2.75*	*3.25*	*7.25*	*8.25*	*9.25*	*10.25*	*11.25*	*12*
Cu/Ni*100	3.1	1.2	17.5	13.4	1.9	19.6	18.8	14.6	25.1	4.9
Cu/Ir	39.2	13.3	33.2	23.1	1.7	30.2	29.9	48.9	36.0	8.8
Pt/Ir*10	14.0	21.7	75.0	77.1	50.0	53.8	56.1	61.1	56.3	30.4

sample traverses in which it was found that chromite enrichments give a good indication of the point at which sulphide phases appear. The possible fractionation of the PGE across such a sulphide-bearing horizon is considered next.

7.6.3 In situ mineralised horizons

The Quarry 13 traverse was collected across a PGE-bearing zone of sulphide-bearing dunites exposed in the wall of this disused chromite quarry. Sulphides appear just below the chromitite body and are persistent across the higher regions of the traverse. Concentrations of Ni and Cu are approximately constant across the sulphide-bearing zone, whereas PGE tenors decay upwards, suggesting decreasing PGE to sulphide ratios (section 6.3.3).

The chondrite-normalised patterns clearly reflect the presence or absence of sulphide phases (figure 7.18). The two samples not containing sulphides have lower PGE contents and yield sigmoidal "background" patterns. All the samples containing sulphides have higher PGE contents and yield Cliff-type patterns. Identical patterns are obtained from sulphide-bearing samples above and below the chromitite body and from the stratigraphically highest samples, though these contain slightly lower levels of PGE. Profiles showing the concentrations of each PGE across the traverse are closely similar with parallel anomalies for each element. This indicates that individual PGE occur in constant ratios across this horizon and therefore produce identical chondrite-normalised patterns (figure 7.19).

To investigate the possible fractionation of PGE and chalcophile elements across this traverse, various potential fractionation indices have also been plotted as profiles (figure 7.20). The ratio Pt/Ir was chosen as an indication of the steepness of the chondrite-normalised positive slope patterns. This ratio is nearly constant or decreases sightly across the sulphide-bearing zone. Both the Cu/Ni and Cu/Ir ratios are affected by the anomalously low Cu content of the chromite-rich sample at 7.25 m. Otherwise both indices show a slight increase across the zone.

The variations in fractionation indices across the traverse are consistent with those expected during fractional segregation of immiscible sulphide phases. Since very little change is seen in either the Pt/Ir ratio or the shape of Cliff type patterns it appears that the partition coefficients are similar for individual PGE and in the order Pt > Ir.

7.6.4 Pyroxene-bearing lithologies

Enrichments of Pt and Pd also occur in sulphide-bearing pyroxenites and wehrlites from close to the base of the pyroxene-bearing sequence (section 4.6). An example of this type of mineralisation has been described from a detailed traverse at the White House (section 6.4.3). Geochemical profiles indicate that high PGE concentrations occur in the stratigraphically lowest sulphide-rich samples. Fractionation indices indicate progressive fractionation of sulphide compositions across this zone (6.4.5).

Chondrite-normalised patterns obtained from the White House traverse are shown in figure 7.21. The three diagrams show the PGE pattern of samples below, at, and above the zone of PGE and sulphide enrichment. The basal dunites and wehrlites which contain little sulphide have typical sigmoidal background patterns. These contrast with the Cliff type positive slope patterns shown by the PGE and sulphide-enriched wehrlites. In the pyroxenites above this zone the PGE tenors and patterns fall rapidly back to the sigmoidal background signature.

The effects that these changes in the PGE assemblage have on the concentration of individual elements are shown in figure 7.22. In this diagram the concentrations of all six PGE across the traverse have been plotted as geochemical sections. Changes in the ratios between individual PGE are consistent with the changes from sigmoidal, to Cliff type, and then back to sigmoidal patterns which occurs across the PGE-enriched zone. A proportionally larger increase in Pd, Pt and Rh contents can be seen in this part of the section. As was found in the Quarry 13 traverse (figure 7.19), Au concentrations do not follow those of other PGE. In this traverse the behaviour of Ru is also anomalous.

A striking feature of the chondrite-normalised patterns for sulphide-bearing wehrlites and pyroxenites (figure 7.21) is that they are very similar to those obtained from other sulphide-bearing samples, such as dunites and chromite-rich dunites (figures 7.12 to 7.15). This is consistent with the theory that Cliff type patterns are produced by virtue of the sulphide content of a rock and are thus independent of its silicate mineralogy.

Figure 7.21. Chondrite-normalised patterns from the White House Traverse.

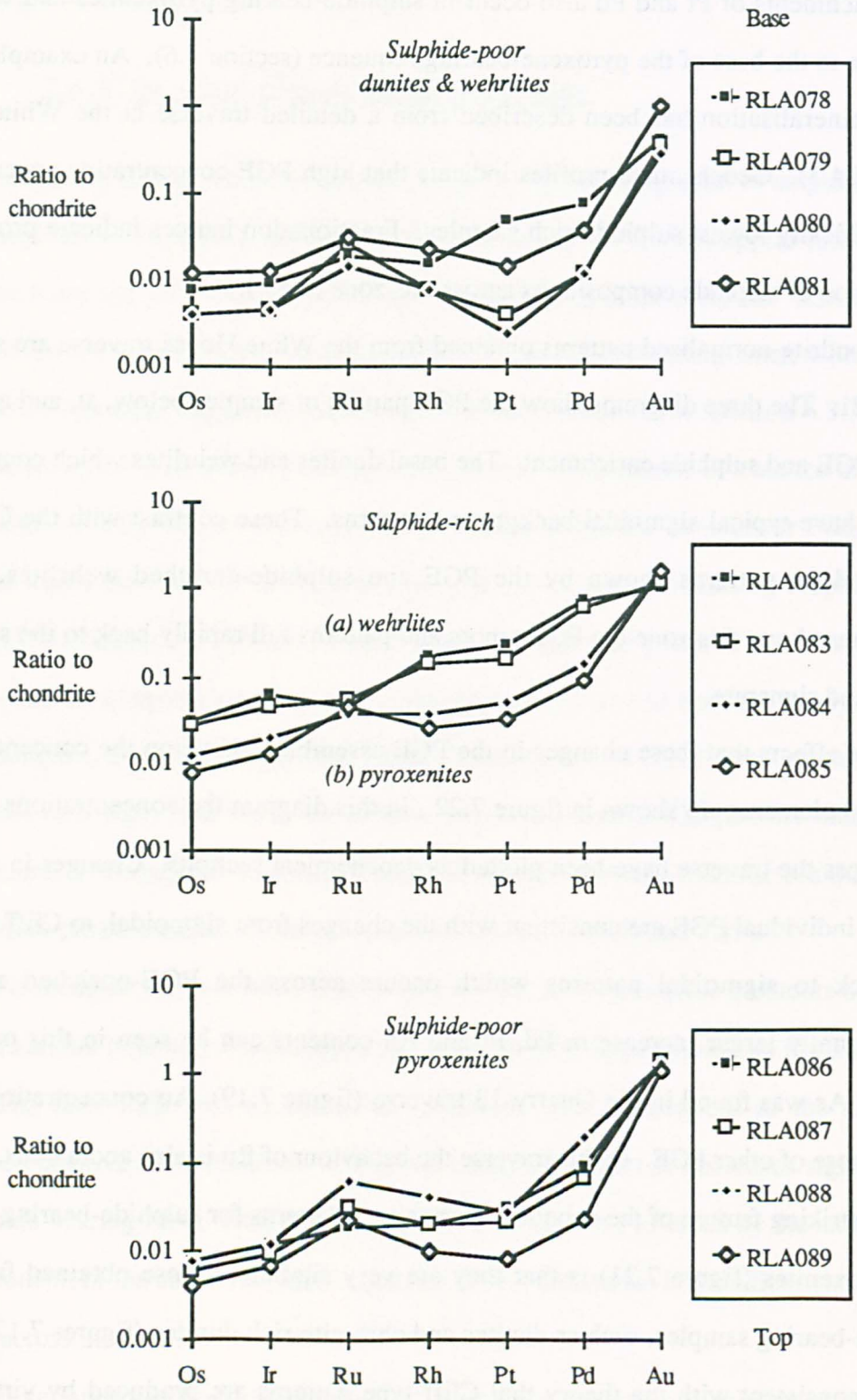

Figure 7.22. Variation in Os, Ir, Ru, Rh, Pt, Pd and Au in the White House Traverse.

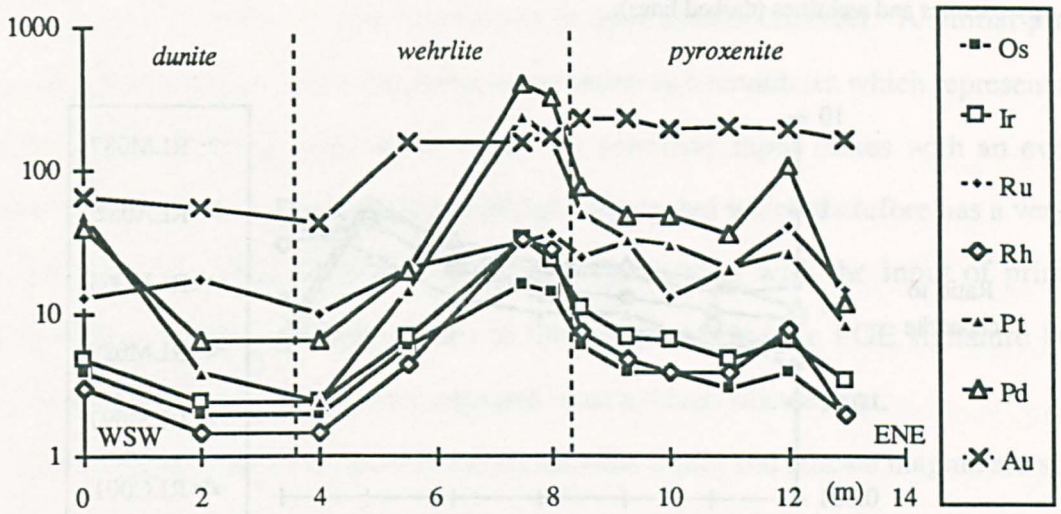

Table 7.6. Details of samples in the White House Traverse.

Sample	*Metres*	*Lithology*	*Sulphide*	*Ni (ppm)*	*Cu (ppm)*	*Cr (ppm)*	*As (ppm)*	*CaO wt%*
Sulphide-poor dunites and wehrlites								
RLA078	0	Dunite	SB	2312	0	3145	0	1.27
RLA079	2	Dunite	SB	2300	0	3409	0	0.32
RLA080	4	Wehrlite	SB	2489	19	2569	5	1.17
RLA081	5.5	Wehrlite	MSB	1296	84	6464	0	9.29
Sulphide-rich wehrlites and pyroxenites								
RLA082	7.5	Wehrlite	VSR	3750	1292	769	0	1.49
RLA083	8	Wehrlite	SR	3861	1507	1003	0	0.97
RLA084	8.5	Pyroxenite	SR	1949	1473	5115	11	14.41
RLA085	9.25	Pyroxenite	MSR	935	330	4616	0	14.05
Sulphide-poor pyroxenites								
RLA086	10	Pyroxenite	SR	967	383	4907	0	13.97
RLA087	11	Pyroxenite	MSB	598	286	5547	0	18.83
RLA088	12	Pyroxenite	SB	1164	131	2112	7	2.25
RLA089	13	Pyroxenite	SB	955	627	7025	0	17.33

Figure 7.23. Cliff-type patterns from various stratigraphic levels and rock types including pyroxenites and wehrlites (dashed lines).

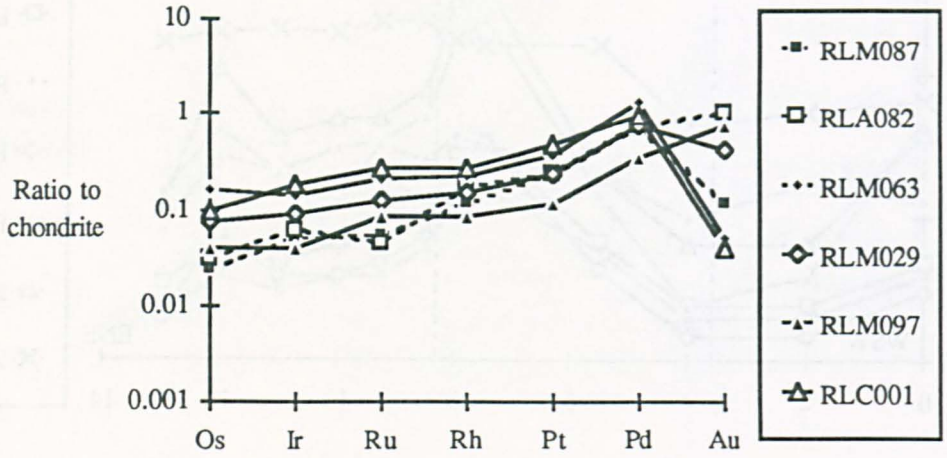

Sample	Locality	Lithology	Σ PGE (ppb)	Pd/Os	Pt/Ir	Pd/Pt
RLM087	Keen of Hamar	Pyroxenite	720	31.7	8.57	1.58
RLA082	White House	Wehrlite	775	25.6	7.58	1.64
RLM063	Quarry 12S	Dunite	1413	8.5	4.81	1.89
RLM029	Quarry 11	Dunite/chromite	872	11.1	5.00	1.68
RLM097	Quarry 10	Chromitite	427	9.5	5.45	1.58
RLC001	Cliff	Chromitite	1412	10.4	5.15	1.04

7.6.5 Stratigraphic variation in Cliff-type patterns

The preceding sections have described positive slope chondrite-normalised patterns occurring in a variety of rock types and at several stratigraphic levels in the ophiolite stratigraphy. Representative examples are shown in figure 7.23. It can be seen from this diagram that identical patterns and hence ratios of PGE are found in chromitites, dunites and chromite-rich dunites from both the mantle and cumulate sequences. Examples from higher stratigraphic levels in pyroxene-rich host rocks are very similar but are slightly depleted in Ru, Ir and Os. This effect can be seen in the higher Pd/Os and Pt/Ir ratios of such samples. In contrast the elements Rh, Pt and Pd occur in the same proportions as in other rock types. This is shown by the similarity of Pd/Pt ratios in all of these samples.

Since the formation of an immiscible sulphide liquid will rapidly deplete PGE from a magma, repetitions of Cliff type mineralisation have been explained as the first sulphides segregating after an influx of primitive melt in an open system chamber. A similar process can be used to explain such mineralisation in pyroxene-rich cumulates which represent more evolved magma compositions. In this case the primitive input mixes with an evolved resident magma from which sulphide has already segregated which therefore has a very low PGE content. This PGE content is replenished by mixing with the input of primitive magma. Thus the first sulphide phases to form have a primitive PGE signature but an evolved sulphide composition and are enclosed in an evolved silicate host.

Since the partition coefficients between sulphide liquid and silicate magma are similar for individual PGE the concentration of these elements in the sulphide phase will reflect their concentration in the magma at the time of sulphide saturation (Barnes et al., 1988). Differences in the chondrite-normalised patterns of pyroxene-rich cumulates indicate that the magma from which these sulphide phases formed was slightly depleted in Os, Ir and Ru (figure 7.23). This is consistent with the field relations and stratigraphic level of this type of assemblage which indicate that sulphide-saturation did not occur immediately after mixing with the input magma (sections 6.4.4 and 6.4.5). This depletion of Os, Ir and Ru can be explained by the prior crystallisation of sulphide-poor ultramafic cumulates more enriched in these particular elements with respect to the PGE content of the magma, which is in turn inferred from the composition of the sulphide phase (figure 7.21a compared to 7.21b).

7.6.6 Effects of hydrothermal reconcentration

Many aspects of the unusually high PGE concentrations at the Cliff quarry indicate that hydrothermal processes were important in generating this style of mineralisation. These include the PGM mineralogy, veining textures, their association with low temperature sulphides and the proximity to major shear zones (Gunn et al., 1985). These are supported by geochemical studies presented here and the correlation between high levels of PGE, As and Sb (section 5.5.4). The high levels of As found here have been related to the hydrothermal overprint by an As-bearing fluid introduced along the basal thrust of the

Figure 7.24. Chondrite-normalised patterns of hydrothermal PGE concentrations (table 7.7).

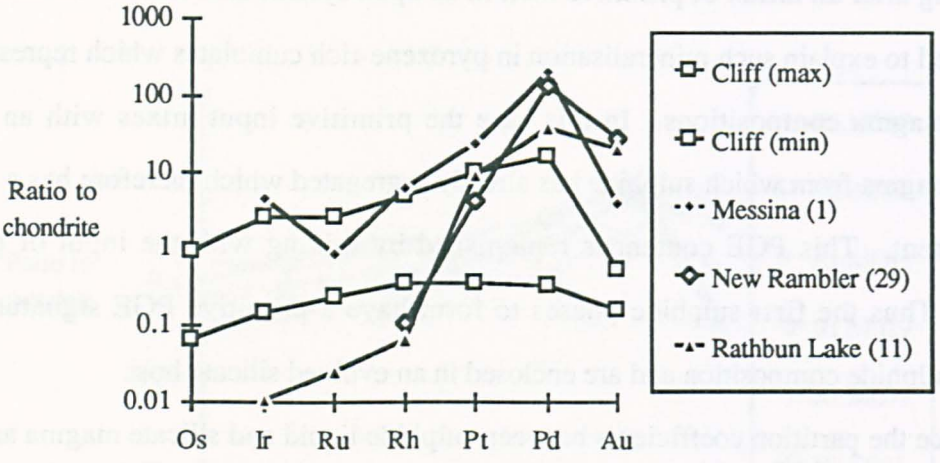

Table 7.7. Average PGE concentrations (in ppb) of hydrothermal PGE deposits.

Deposit (no. samples)	*Os*	*Ir*	*Ru*	*Rh*	*Pt*	*Pd*	*Au*	*Source*
Artonvilla, Messina (1)	n/a	2500	600	1300	24000	116000	600	(1)
New Rambler cpy-py (29)	n/a			21	4400	76000	4300	(2)
Rathbun Lake (11)	< 9	5.8	17	13	9736	20829	3053	(3)

Sources:- (1) Mihálik et al., 1974; (2) McCallum et al., 1976; (3) Rowell & Edgar, 1986

ophiolite complex (Lord & Prichard, 1989). The Cliff quarry also has all the attributes of the magmatic PGE concentrations in other parts of the harzburgite unit, namely it occurs in sulphide-bearing dunites, chromite-rich dunites and dunites hosted in a dunite pod (section 4.5). The unusually high grades are found in the altered, greenish, disseminated chromite-rich dunites marginal to the chromitite body and are therefore thought to arise from the localised hydrothermal enrichment of a magmatic PGE concentration (section 5.5.4).

Pathfinder studies at Cliff (section 5.5.4) and the range of PGE concentrations in the ophiolite as a whole (section 4.4.2) indicate that threshold between magmatic and hydrothermally enhanced levels of PGE is around 1 ppm. It can be seen from figure 7.10 that Cliff samples above and below this threshold have the same overall form and positive slope chondrite-normalised pattern. These are in turn similar to the positive slope Cliff type patterns obtained from a variety of other magmatic occurrences (figure 7.23). Superimposed

on this magmatic pattern are small variations in the relative proportions of Pt, Pd and Au (figure 7.10), although these have a negligible effect on the overall PGE signature.

The mineralisation at Cliff has been compared to hydrothermal PGE deposits of the Pt-Pd-Au type (Gunn et al., 1985; Hulbert et al., 1988). A general feature of such hydrothermal deposits is that they contain concentrations of Pd >> Pt >> other PGE, with highly variable inter-elemental ratios, and they are usually also Au-rich (table 7.7). This leads to very different chondrite-normalised patterns from those found at Cliff (figure 7.24). These geochemical signatures are thought to reflect the differing solubilities of each element, which in turn causes their fractionation during hydrothermal dissolution, transport and precipitation (Hulbert et al., 1988). Similar arguments are used to explain the decoupling of Pt and Pd in the weathering cycle (Fuchs & Rose, 1974).

In the case of the Cliff area, transport by a serpentinisation front for only a few metres is envisaged and in this distance it is unlikely that any significant fractionation between different PGE will occur. The remobilised or enhanced zones will therefore have PGE signatures reflecting those of the magmatic source. This is not without a geological precedent. In the Lac-des-Iles complex magmatic PGE, Cu, Ni sulphide mineralisation has been remobilised and concentrated by late-stage deuteric or greenschist facies metamorphism (Talkington & Watkinson, 1984). This produced a strong secondary enrichment of Pt+Pd and although the resulting Cu/(Cu+Ni) and Pt/(Pt+Pd) ratios are highly variable the magmatic abundance relationship Pd > Au > Pt is preserved in both fresh and altered lithologies.

7.7 Background PGE content of cumulate silicate rocks

7.7.1 Sigmoidal Z-shaped patterns in basal ultramafic cumulates

In the preceding section a number of sulphide-poor samples were shown to contain low concentrations of PGE. When plotted on chondrite-normalised diagrams such analyses display Z-shaped sigmoidal patterns (figures 7.12, 7.13, 7.16, 7.18 and 7.21). Although

Figure 7.25. Chondrite-normalised diagram showing the Z-shaped sigmoidal patterns of dunites from chromite-poor pods.

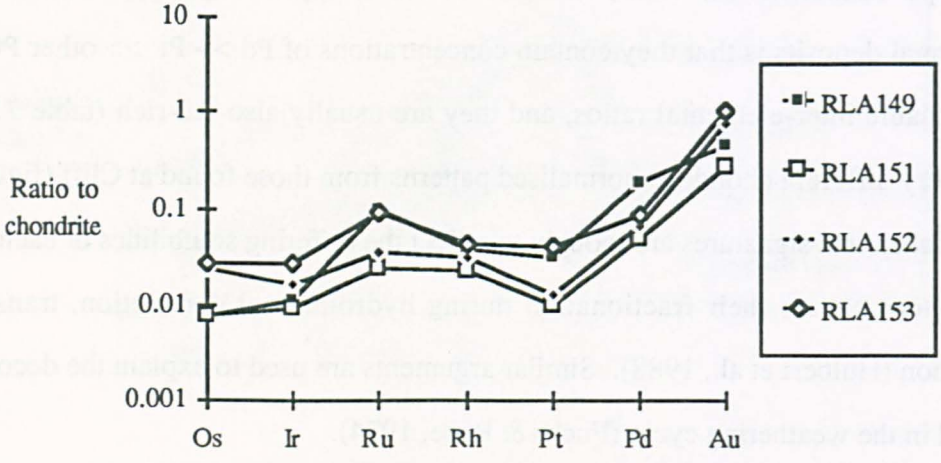

Sample	Lithology	Ni (ppm)	Cu (ppm)	Cr (ppm)	As (ppm)	Sb (ppm)
RLA149	Dunite (S) pod 6	3135	34	3230	0	n/a
RLA151	Dunite (S) pod 6	2926	50	1593	0	n/a
RLA152	Dunite (S) pod 6N	2595	0	1833	0	n/a
RLA153	Dunite (S) pod 1W	2121	27	2210	0	n/a

these analyses are of various rock types the patterns are roughly similar. Compared to chondrite the element concentrations rise from Os, through Ir, to a peak at Ru, before falling through Rh to Pt. They then rise steeply from Pt, through Pd, to an overall maximum at Au. This pattern is therefore distinct from that found in either Harold's Grave or Cliff type mineralisation and appears to occur as a low level background in ultramafic cumulates.

To investigate this assemblage further a variety of sulphide-and chromite-poor lithologies were re-analysed for all six PGE and Au (table 7.3). These include a suite of dunites from chromitite-poor pods within harzburgite and a suite of fresh and altered dunites from the basal dunite unit at the Hagdale Wick traverse. Chondrite-normalised diagrams with these analyses plotted are shown in figures 7.25 & 7.26. These diagrams show that the same sigmoidal patterns are obtained from dunites in both the mantle and crustal sequences. This PGE assemblage is largely unchanged in sheared dunites, now serpentinites, from the

Figure 7.26. Chondrite-normalised diagram showing Z-shaped sigmoidal patterns from fresh and altered basal dunites.

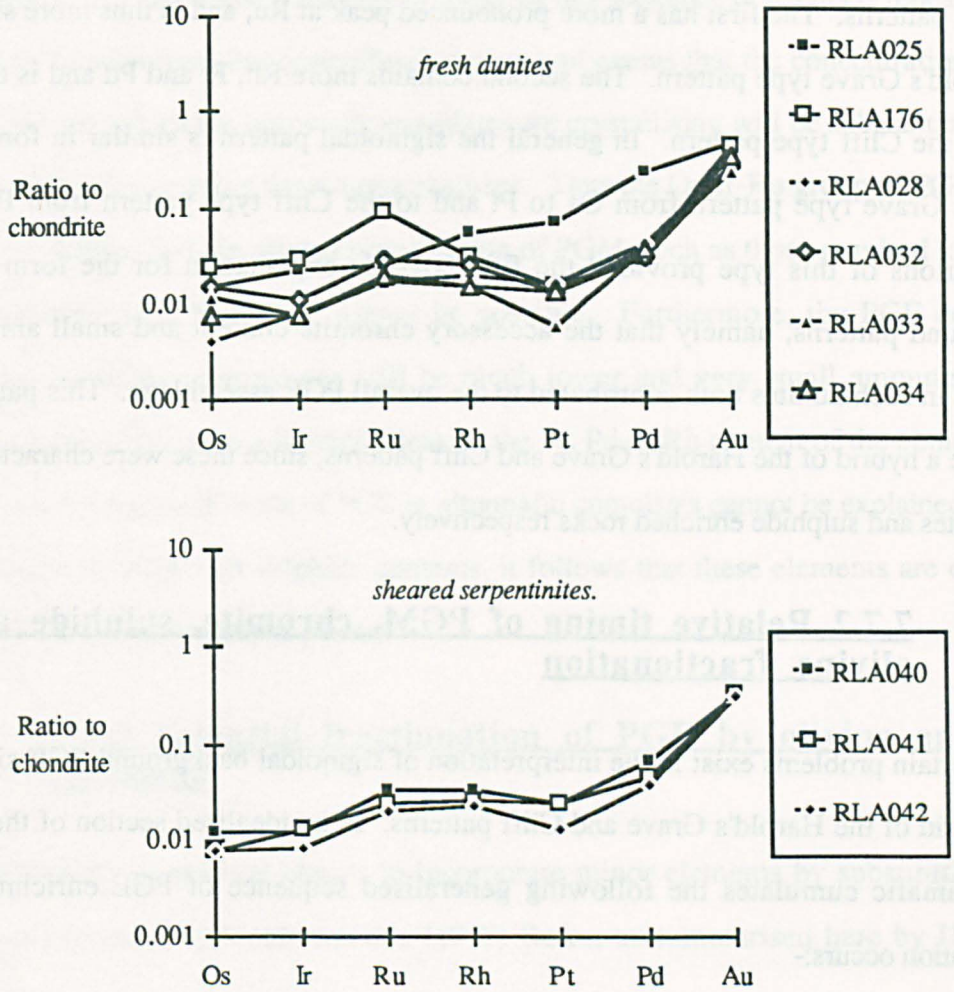

Sample	Lithology	Sulphide	Ni (ppm)	Cu (ppm)	Cr (ppm)	As (ppm)
Fresh dunites						
RLA025	Dunite	No S	2167	23	2841	6
RLA176	Dunite	No S	2366	46	2600	8
RLA028	Dunite	SB	2471	193	3580	0
RLA032	Dunite	SB	2302	43	2608	96
RLA033	Dunite	No S	2673	175	2713	86
RLA034	Dunite	SB	2551	29	2275	6
Shear zone						
RLA040	Serpentinite	No S	2594	110	3285	177
RLA041	Serp./breccia	No S	2871	61	4916	234
RLA042	Serpentinite	No S	2290	52	3577	98

shear zone in Hagdale Wick. This PGE assemblage therefore represents the typical background PGE content of olivine-rich cumulates.

Two dunites from the fresh portion of the Hagdale Wick traverse have slightly different patterns. The first has a more pronounced peak at Ru, and is thus more similar to the Harold's Grave type pattern. The second contains more Rh, Pt and Pd and is therefore close to the Cliff type pattern. In general the sigmoidal pattern is similar in form to the Harold's Grave type pattern from Os to Pt and to the Cliff type pattern from Pt to Au. Observations of this type provided the first possible explanation for the form of such background patterns, namely that the accessory chromite content and small amounts of sulphide in such dunites both contributed to the overall PGE assemblage. This pattern was therefore a hybrid of the Harold's Grave and Cliff patterns, since these were characteristic of chromitites and sulphide enriched rocks respectively.

7.7.2 Relative timing of PGM, chromite, sulphide and olivine fractionation

Certain problems exist in the interpretation of sigmoidal background PGE signatures as a hybrid of the Harold's Grave and Cliff patterns. In an idealised section of the base of the ultramafic cumulates the following generalised sequence of PGE enrichment and fractionation occurs:-

Firstly, chromitites crystalise from the most primitive magmas which also become saturated in Os, Ir and Ru. Thus primary PGM such as laurite crystalise directly from the magma and are enclosed in the chromite grains. This type of cumulate has a Harold's Grave type pattern.

Secondly, sulphide becomes saturated in the magma and immiscible sulphide liquid forms. This occurs only slightly later, since such sulphides are usually found in chromite-rich dunites marginal to chromitite bodies. All the PGE are strongly partitioned into the sulphide phase. These sulphides inherit the PGE signature of the magma at the time of sulphide saturation. The PGE content of the residual silicate magma is reduced considerably, since the magma reservoir is of limited extent (Campbell and Naldrett, 1979; Campbell and Barnes, 1984), but the PGE signature of the magma remains unchanged.

At this point normal silicate crystallisation of the PGE depleted magma continues with the generation of the ultramafic sequence. As has been described above these cumulates typically yield sigmoidal patterns. Fractionation will continue unless an influx of a primitive magma mixes with the resident magma, whereupon this sequence of events is repeated.

It can be seen from this generalised sequence of events that the concentration of PGE in the melt from which the ultramafic cumulates are crystallising will be substantially lower than that originally entering the magma chamber. Thus the Os-Ir-Ru group of PGE will no longer be saturated and the direct crystallisation of PGM, such as those required to give the Harold's Grave pattern, will no longer be possible. Furthermore, the PGE content of subsequent sulphide segregations will be much lower and very small amounts of such sulphides phases will have a limited effect on the Pt, Pd or Rh content of the cumulates. If the very low background levels of PGE in ultramafic cumulates cannot be explained in terms of their PGM or PGE-rich sulphide contents, it follows that these elements are contained within one of the other mineral phases.

7.7.3 Potential fractionation of PGE by olivine or chromite

The ability of mineral phases to incorporate minor elements by substitution in the lattice are governed by Goldschmidt's (1937) Rules, as summarised here by Henderson (1982):-

(1) Ions of similar radii and the same charge will enter into a crystal in amounts proportional to their concentration in the liquid.

(2) An ion of a smaller radius but with the same charge as another, will be incorporated preferentially into a growing crystal.

(3) An ion of the same radius but with a higher charge than another will be incorporated preferentially into a growing crystal.

The relevant ionic radii for the substitution of PGE into the chromite and olivine lattices are given in tables 7.8 and 7.9. Of the various different series of ionic radii those of

Table 7.8. Ionic radii relevant to the substitution of PGE into chromite.

Element	*Ion*	*Coordination & Spin*	*Ionic radii (Å)**		
			S&P	*W&M*	*Ah*
Octahedral sites					
Cr	3+	VI	0.615	0.70	0.63
Al	3+	VI	0.535	0.61	0.51
Ti	4+	VI	0.604	0.69	0.68
Pd	4+	VI	0.615	0.70	0.65
Ru	4+	VI	0.620	0.70	0.67
Ir	4+	VI	0.625	0.71	0.68
Pt	4+	VI	0.625	0.71	[0.65]
Os	4+	VI	0.630	0.71	0.69
Rh	4+	VI	0.60	0.71	n/a
Tetrahedral sites					
Mg	2+	IV	0.57	0.66	n/a
Fe	2+	IV H	0.63	0.71	n/a
Co	2+	IV H	0.58	0.65	n/a

* Ionic radii listed in Henderson (1982) with source abbreviated as follows:

S&P	Shannon and Prewitt (1969, 1970) & Shannon (1976)
W&M	Whittaker and Muntus (1970)
Ah	Ahrens (1952)

Table 7.9. Ionic radii relevant to the substitution of PGE into olivine.

Element	*Ion*	*Coordination & Spin*	*Ionic radii (Å)*		
			S&P	*W&M*	*Ah*
Mg	2+	VI	0.72	0.8	0.66
Fe	2+	VI L	0.61	0.69	-
Fe	2+	VI H	0.78	0.86	0.74
Ni	2+	VI	0.69	0.77	0.69
Ir	3+	VI	0.68	0.81	-
Rh	3+	VI	0.665	0.75	0.68
Ru	3+	VI	0.68	0.76	-
Pd	2+	VI	0.86	0.94	[0.80]

* Sources as in table 7.8

Whittaker and Muntus (1970) appear to best predict the known substitutions of Ti in chromite or of Ni in olivine. The sizes of tetravalent PGE ions indicate that these elements will readily substitute for Cr in octahedral sites of the chromite lattice. Charge balance can be maintained by replacement of octahedral ferric ions by ferrous ions in the same way that tetravalent Ti ions are accommodated in the lattice (Deer et al., 1966). According to Goldschmidt's rules Pd and Ru should preferentially substitute for Cr, whereas substitutions for Os, Ir, Rh and Pt will be less preferred due to the slightly larger ionic radii. In the case of substitution for Mg in olivine the trivalent ions of Rh and Ru are the right size but no obvious substitution can be made to correct this charge excess. Small amounts of trivalent Cr and ferric Fe found in olivine analyses are attributed to exsolved ferric or chromic oxide (Deer et al., 1966), in which case the same arguments apply to the possible substitution of PGE in olivine as do for their substitution in chromite. It appears, therefore, that PGE will not readily be accommodated within the olivine lattice.

The above predictions can be readily tested using the available background PGE analyses. If traces of PGE occur in olivine, then dunites should contain higher concentrations than wehrlites, pyroxenites or chromite-rich dunites. If instead the PGE substitute for Cr in chromite, then dunites, wehrlites and pyroxenites should contain similar levels of PGE, since all three contain accessory chrome spinel. More chromite-rich samples not containing PGM or sulphides should have the same sigmoidal pattern but contain higher PGE concentrations. Evidence for the latter scenario can be seen in the various analyses of background PGE concentrations and their corresponding chondrite-normalised patterns (figures 7.12, 7.13, 7.16, 7.18, 7.21).

Further evidence for this process of substitution in chromite can be seen from the relative proportion of PGE in the Z-shaped sigmoidal pattern (section 7.6.1). From the discussion of the effects of immiscible sulphide segregation from the magma (section 7.6.2) it appears that the later ultramafic cumulates crystalise from a melt containing the same relative proportions of individual PGE as are found in a Cliff type pattern, albeit at considerably lower levels. When the concentrations of elements in sigmoidal patterns are compared to this possible source composition (e.g. by a line through Os, Ir, Rh and Pd) they can be seen to be relatively enriched in Ru but depleted in Pt. This is close to the order

of fractionation of elements predicted by the atomic radii arguments, which suggest that Ru and Pd should substitute more readily for Cr.

The difference between the proportion of individual PGE in chromite-bearing ultramafic cumulates and the magma from which they crystalise has a further implication. The crystallisation of such cumulates will cause additional fractionation of the PGE inter-element ratios. Following the generation of a sequence of cumulates which are relatively enriched in Ru but depleted in Pt, the composition of the melt will show a complimentary pattern of depletion and enrichment. As a result later sulphide segregations, or more evolved cumulates, will be relatively more enriched in Pt and depleted in Ru. In terms of the chondrite-normalised diagram this will give steep positively sloping sigmoidal patterns with an overall S-shape.

7.7.4 Sigmoidal S-shaped patterns in evolved cumulates

Examples of the fourth and final type of chondrite-normalised pattern identified in this study are shown in figure 7.27. This second low concentration PGE assemblage also gives rise to sigmoidal patterns but these are S-shaped in contrast to the Z-shaped patterns from basal ultramafic cumulates. In comparison to chondrite the element concentrations show a minimum at Ir or Ru and a maximum at Pt or Pd. The middle portion of the pattern shows a positive slope, which is steeper than that of Cliff type patterns.

Similar patterns are found in wehrlites and pyroxenites from both the higher levels of the main ultramafic cumulate sequence and from the discrete high-level ultramafic bodies within the gabbro unit. Concentrations of chalcophile elements in these samples indicate that most contain accessory sulphides. The sample with the highest overall levels of PGE contains the highest concentration of Cu, which indicates that it also has the highest sulphide content.

The occurrence of S-shaped sigmoidal patterns in sulphide-bearing ultramafic cumulates at higher stratigraphic levels reflects the progressive fractionation of the PGE signature of the evolving magma. This differential fractionation of particular elements can be related to the differing concentrations of individual PGE in chrome spinel (section 7.2.3). Thus S-shaped sigmoidal patterns represent the relative proportions of PGE remaining in the

Figure 7.27. Sigmoidal S-shaped patterns from high level wehrlites and pyroxenites.

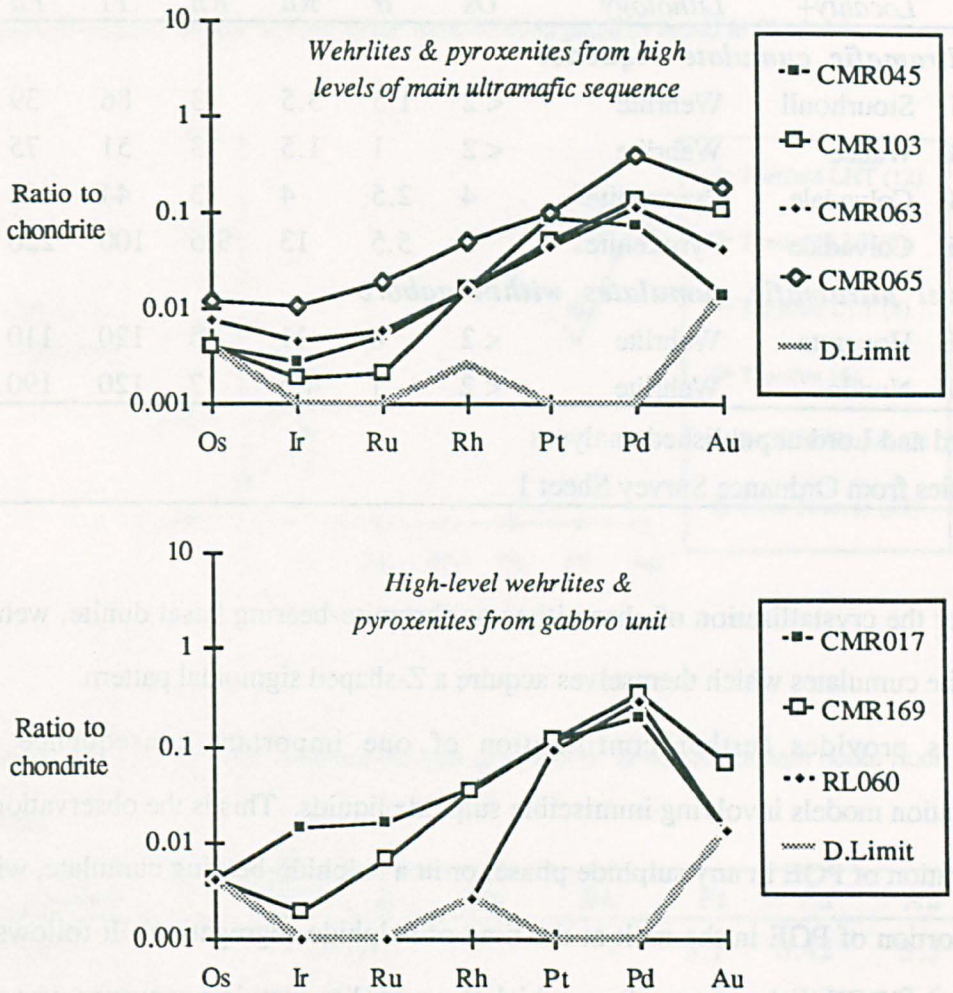

Sample	*Lithology*	*Ni (ppm)*	*Cu (ppm)*	*Cr (ppm)*	*As (ppm)*	*Sb (ppm)*	*CaO wt%*
CMR045	Wehrlite	670	0	3609	0	n/a	9.91
CMR103	Wehrlite	1261	87	1503	0	n/a	2.12
CMR063	Pyroxenite (S)	1000	34	3371	0	n/a	6.35
CMR065	Pyroxenite (S)	742	608	5672	4	n/a	17.66
CMR017	H.L. Wehrlite (S)	729	11	4128	47	n/a	4.91
CMR169	H.L. Wehrlite (S)	806	73	1157	38	n/a	1.92
RL060	H.L. Pyroxenite	627	23	3881	0	0.85	15.24

Table 7.10. Additional PGE analyses of high-level ultramafic cumulates (in ppb).

*Sample**	*Locality+*	*Lithology*	*Os*	*Ir*	*Ru*	*Rh*	*Pt*	*Pd*	*Au*
Main ultramafic cumulate sequence									
CMR045	Stourhoull	Wehrlite	< 2	1.5	3.5	3	86	39	2
CMR103	Watlee	Wehrlite	< 2	1	1.5	3	51	75	16
CMR063	Colvadale	Pyroxenite	4	2.5	4	3	44	62	6
CMR065	Colvadale	Pyroxenite	6	5.5	13	9.5	100	220	28
High-level ultramafic cumulates within gabbro									
CMR017	Hoversta	Wehrlite	< 2	8	11	7.5	120	110	2
CMR169	Nudda	Wehrlite	< 2	1	4.5	7	120	190	10

* Prichard and Lord unpublished analyses

\+ Localities from Ordnance Survey Sheet 1

melt after the crystallisation of chromitites or chromite-bearing basal dunite, wehrlite and pyroxenite cumulates which themselves acquire a Z-shaped sigmoidal pattern.

This provides further confirmation of one important consequence of PGE concentration models involving immiscible sulphide liquids. This is the observation that the concentration of PGE in any sulphide phase, or in a sulphide-bearing cumulate, will reflect the proportion of PGE in the melt at the time of sulphide segregation. It follows that the proportion of PGE in the magma from which the ophiolite cumulate sequence was generated had a PGE signature similar to that found in Cliff type mineralisation and as such contained higher levels of Pd, Pt and Rh than Ru, Ir or Os.

The Shetland ophiolite complex is incomplete compared with the uppermost parts of the Penrose sequence. Exposures of sheeted dykes and pillow lavas are missing or submarine. It has not been possible to analyse these more evolved lithologies and complete the fractionation history of the magma. Very few PGE analyses of dykes or pillow lavas are present in the literature and no complete analyses for all six elements. This is in part due to the very low levels of these compatible elements in such evolved lithologies (typically sub ppb levels). Average compositions from two other ophiolites and some modern ocean floor analogues are summarised in table 7.11. When plotted on a chondrite-normalised diagram these suggest patterns similar to the S-shaped sigmoidal patterns described earlier, albeit at

Figure 7.28. Chondrite-normalised diagram showing PGE analyses of ophiolitic lavas and modern ocean floor basalts (from table 7.9). These incomplete analyses suggest S-shaped sigmoidal patterns similar in form to the most evolved patterns found in Shetland.

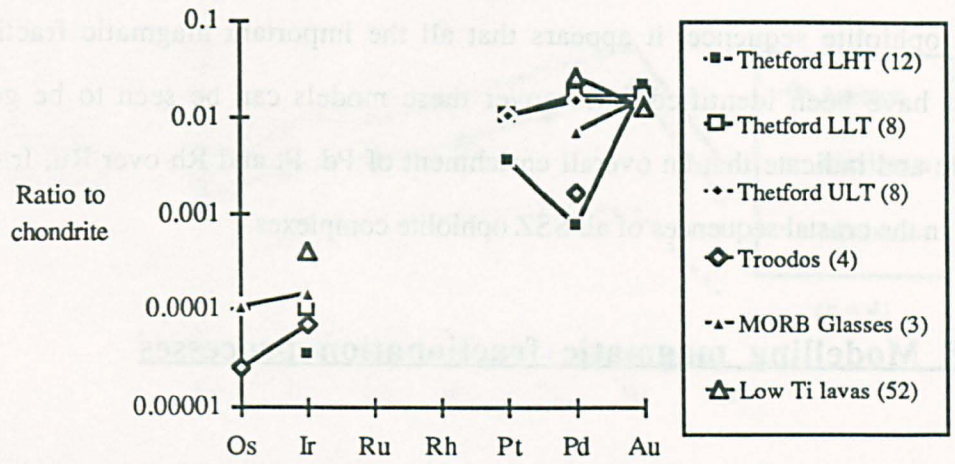

Table 7.11. Average PGE analyses (in ppb) of ophiolitic lavas and modern ocean floor basalts.

Area (n samples)	*Os*	*Ir*	*Ru*	*Rh*	*Pt*	*Pd*	*Au*	*Source*
Thetford LHT (12)	-	0.019	-	-	3.7	0.42	3.5	1
Thetford LLT (8)	-	0.056	-	-	11	9.7	2.6	1
Thetford ULT (8)	-	0.23	-	-	11	8.5	2.2	1
Troodos (4)	0.013	0.039	-	-	-	0.9	-	2
MORB Glasses (3)	0.057	0.082	-	-	-	3.94	2.45	3
Low Ti lavas (52)	-	0.23	-	-	-	15	1.9	4

1 Oshin & Crocket, 1986
2 Becker & Agiorgitis, 1978
3 Hertogen et al., 1980
4 Hamlyn et al.,1985

even lower absolute concentrations (figure 7.28). In particular the gradient of the pattern between Ir and Pt is steeper than either that between Os and Ir or between Pt and Au.

Since the sheeted dykes and pillow lavas of other ophiolites and also modern ocean floor basalts have PGE signatures comparable with the most evolved patterns seen in the Shetland ophiolite sequence, it appears that all the important magmatic fractionation processes have been identified. Moreover these models can be seen to be generally applicable and indicate that an overall enrichment of Pd, Pt and Rh over Ru, Ir or Os is expected in the crustal sequences of all SSZ ophiolite complexes.

7.8 Modelling magmatic fractionation processes

In the preceding three sections the variety of chondrite-normalised patterns generated by different samples from the ophiolite sequence have been described, and their origins discussed. The final section attempts to relate these processes in the framework of the overall magmatic fractionation model for the generation of the ophiolite sequence as a whole.

7.8.1 Summary and range of chondrite-normalised patterns

The various different chondrite-normalised patterns and the range of PGE concentrations they represent are summarised in figures 7.29 to 7.31 and table 7.12. In each case both the number of samples (n) used to calculate the average and the number of localities from which these were collected (x) have been included. The different diagrams in each set have been listed in approximate stratigraphic order. The patterns of sulphide-poor chromite-rich dunites have been included both with the chromitites and the silicate groups since they are obviously related to both end-members.

Sulphide-bearing lithologies containing Cliff type mineralisation have broadly similar smooth positive slope patterns which do not change with stratigraphic level. Harold's Grave type patterns with steep negative slopes are restricted to the basal chromitites. Chromite-rich lithologies from higher stratigraphic levels have flatter near chondritic patterns. The various

Figure 7.29. Average and range of Cliff type patterns from various sulphide-bearing parageneses.

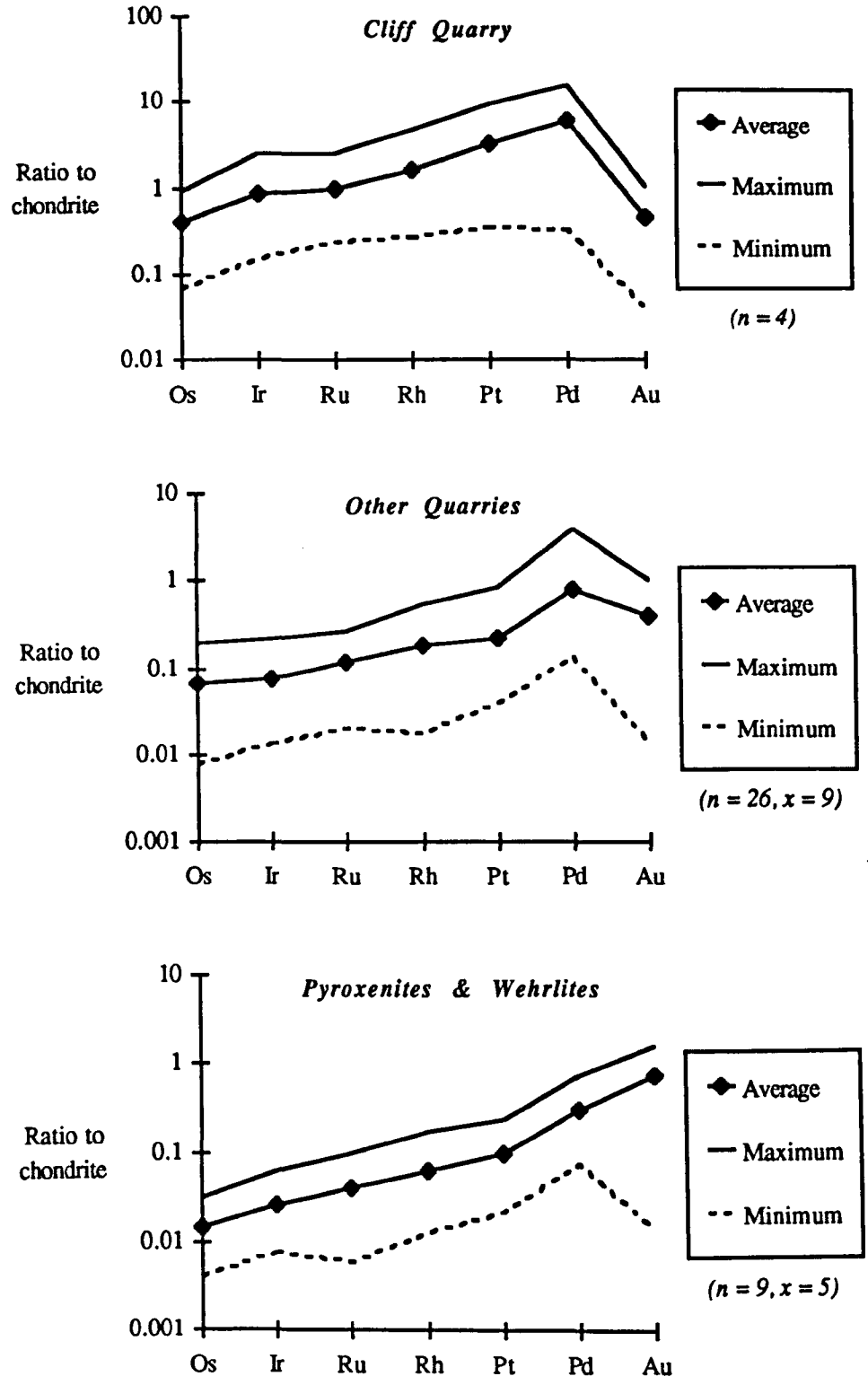

Figure 7.30. Average and range of Harold's Grave type and related patterns from various chromite-rich rocks.

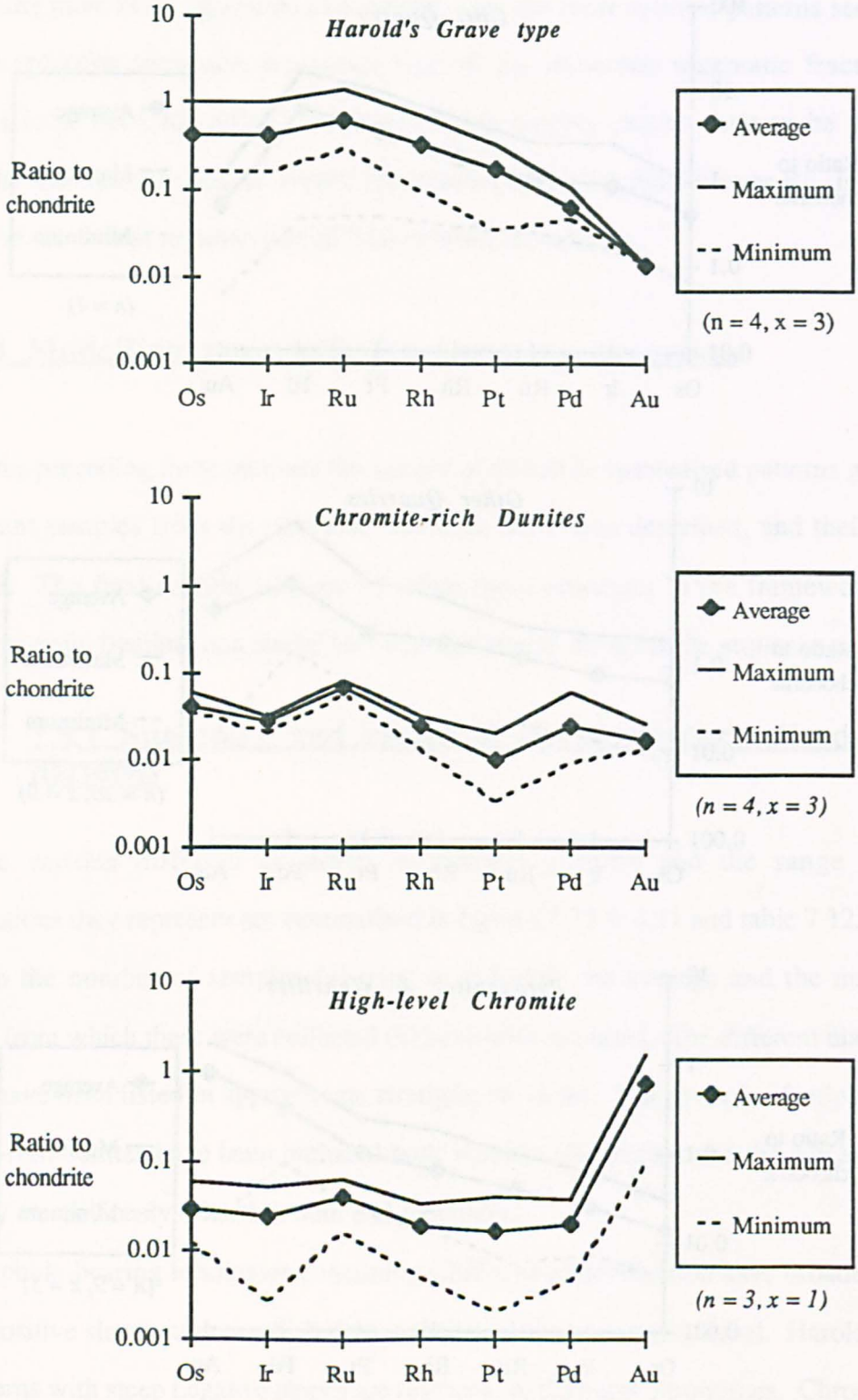

Figure 7.31. Average and range of sigmoidal patterns from various ultramafic cumulates.

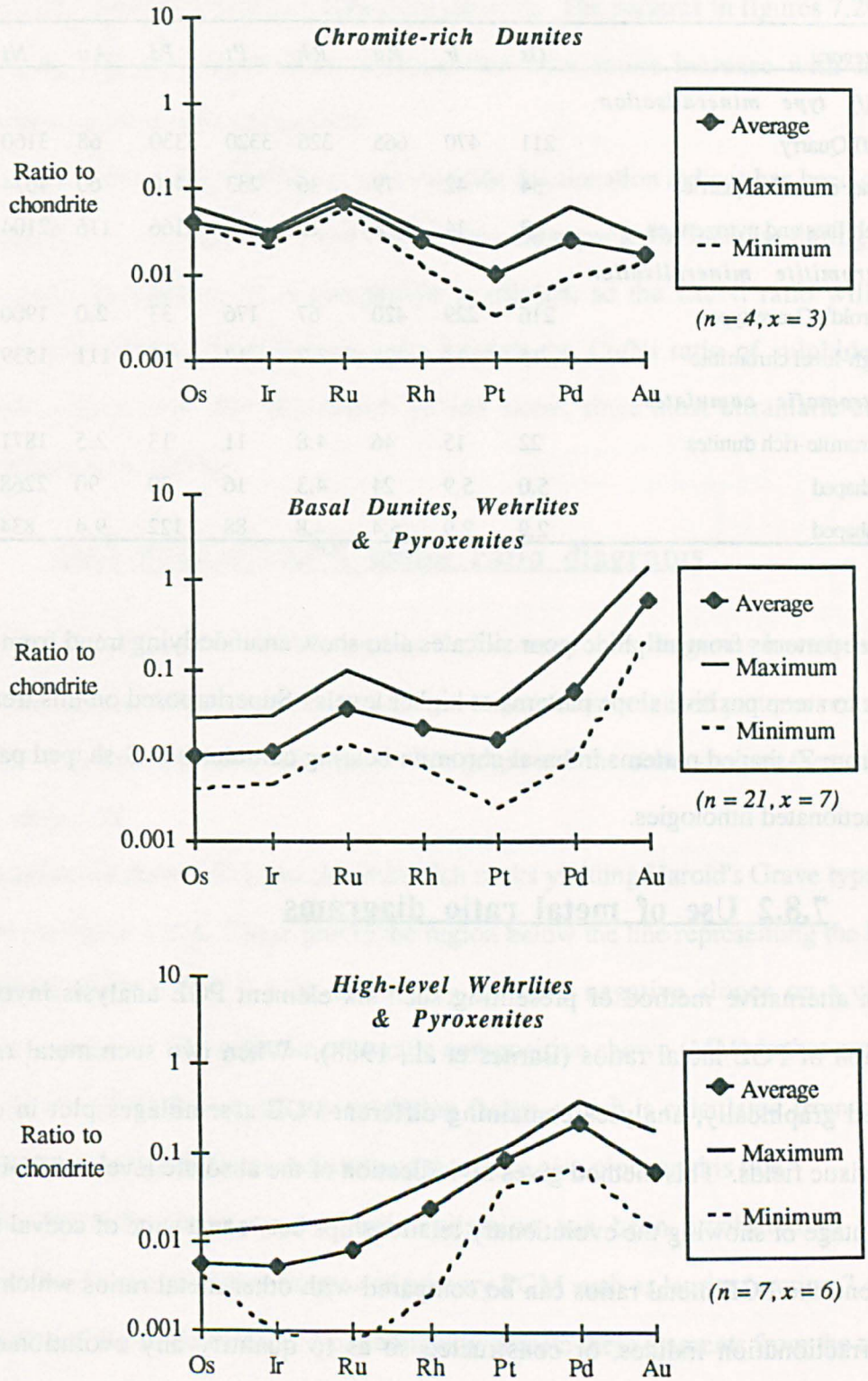

Table 7.12. Average concentrations of PGE (in ppb) and chalcophile elements (in ppm) in different characteristic assemblages. The key refers to symbols used on figures 7.32 to 7.35.

Key	*Category*	*Os*	*Ir*	*Ru*	*Rh*	*Pt*	*Pd*	*Au*	*Ni*	*Cu*
	Cliff type mineralisation									
CC	Cliff Quarry	211	470	665	326	3320	3330	68	3160	242
CT	Other chromite quarries	34	42	79	36	233	440	60	4674	575
CP	Wehrlites and pyroxenites	7.3	14	28	12	99	166	116	2104	557
	Chromitite mineralisation									
HG	Harold's Grave type	216	229	420	67	176	33	2.0	1900	7
HC	High-level chromitite	15	13	28	3.7	17	11	111	1539	81
	Ultramafic cumulates									
SC	Chromite-rich dunites	22	15	46	4.8	11	13	2.5	1871	11
SZ	Z-shaped	5.0	5.9	24	4.3	16	30	90	2268	116
SS	S-shaped	2.9	2.9	5.4	4.8	88	122	9.4	834	119

sigmoidal patterns from sulphide-poor silicates also show an underlying trend from shallow negative to steep positive slope patterns at higher levels. Superimposed on this trend is the switch from Z-shaped patterns in basal chromite-bearing cumulates to S-shaped patterns in more fractionated lithologies.

7.8.2 Use of metal ratio diagrams

An alternative method of presenting such six element PGE analysis involves the calculation of PGE metal ratios (Barnes et al., 1988). When two such metal ratios are compared graphically, analyses containing different PGE assemblages plot in different characteristic fields. This method gives no indication of the absolute levels of PGE but has the advantage of showing the evolutionary relationships between a suite of coeval samples. To this end the PGE metal ratios can be compared with other metal ratios which are also known fractionation indices, or constructed so as to quantify any evolutionary trend recognised within the chondrite-normalised patterns.

In this study two PGE metal ratios have been used in this way. The first ratio gives an indication of the overall slope of the chondrite-normalised pattern. The Pt/Ir ratio has been

used in this case, rather than Pd/Ir or Pd/Os ratios, because of the higher mobility of Pd, or possibly Os, and the lower detection limit for Ir. The second ratio used is Pt/Ru, since this gives an indication of the nature of sigmoidal patterns. The patterns in figures 7.29 to 7.31 and their stratigraphic distribution indicate that both ratios increase with increased fractionation in certain suites of samples.

The use of two further metal ratios as sulphide fractionation indices has been discussed earlier (section 6.4.5). Both Cu/Ni and Cu/Pt ratios are expected to increase during sulphide fractionation. In addition Ni is compatible in olivine, so the Cu/Ni ratio will also be fractionated by olivine crystallisation. As a result the Cu/Ni ratio of sulphide-bearing cumulates is lower than that of sulphide phases alone, since most ultramafic cumulates contain at least some olivine.

7.8.3 Pt/Ir v Cu/Ni metal ratio diagrams

In figure 7.32 a series of Pt/Ir against Cu/Ni metal ratio diagrams have been plotted showing the various fields for the eight different chondrite-normalised patterns recognised in this study. The same symbols are used in each graph and the abbreviations they refer to are listed in table 7.12.

Analyses of chromitites and chromite-rich rocks yielding Harold's Grave type patterns are shown in figure 7.32a. These plot in the region below the line representing the Pt/Ir ratio of chondrite (1025 / 540 = 1.9), since they all have negative slopes on a chondrite-normalised diagram. The estimate of mantle composition shown (MM) is that proposed by Barnes (et al., 1988) for use as a normalising factor, which is calculated from chondritic PGE abundances (0.00815 x chondrite) and therefore also plots on this line.

The Harold's Grave type of mineralisation has been attributed to the direct crystallisation from a primitive magma of primary PGM such as laurite (section 7.4.1). This fractionation of Ru-Ir-Os PGM will preferentially deplete these elements from the magma, so the Pt/Ir ratio of the residual liquid will rise. Conversely the chromite-rich cumulate containing the PGM will have a lower Pt/Ir ratio than the magma from which they formed. The crystallisation of chromite is generally accompanied by the crystallisation of some olivine. This will not affect the Pt/Ir ratio of the melt but will change its Cu/Ni ratio, due to

Figure 7.32. Pt/Ir v Cu/Ni metal ratio diagram showing the fields and fractionation effects of each identified PGE assemblage.

(a) Harold's Grave type mineralisation.

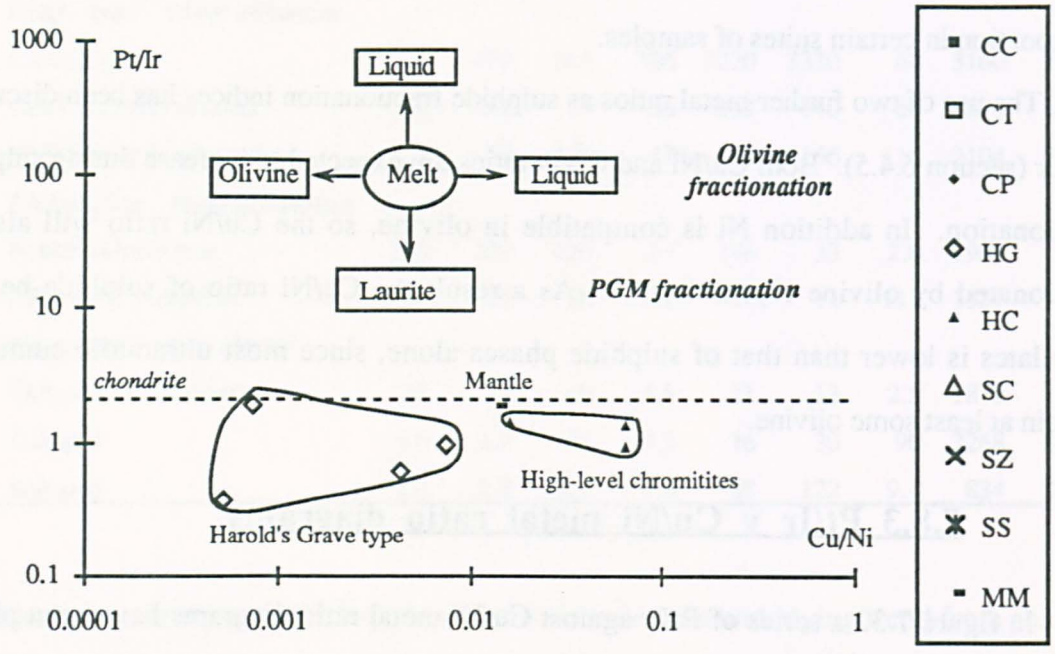

Figure 7.32(b). Cliff type mineralisation.

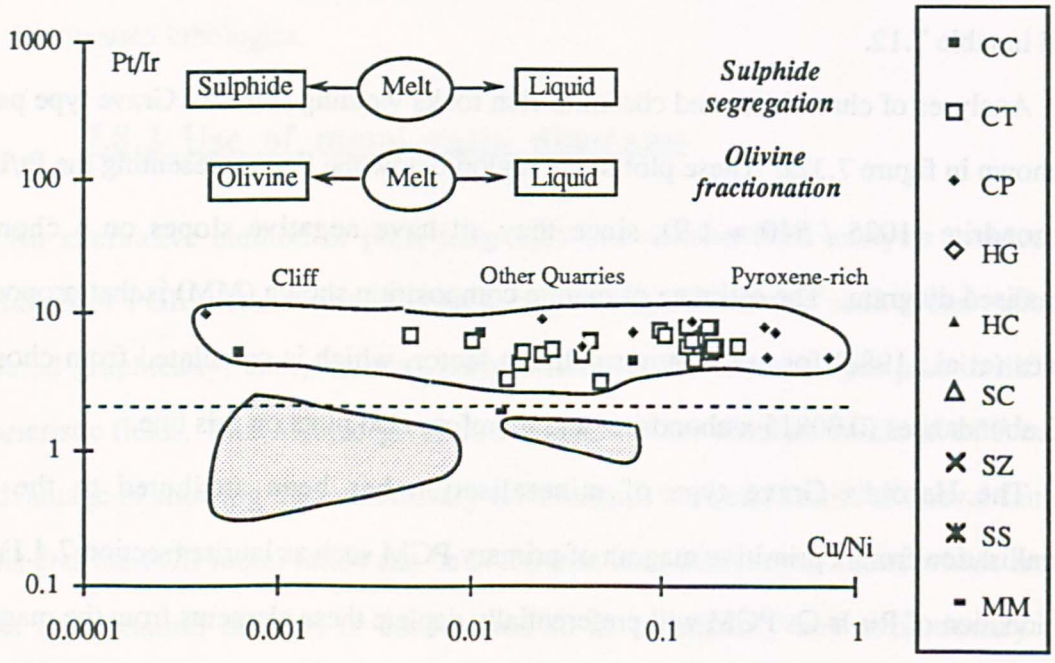

Figure 7.32(c). Silicate lithologies.

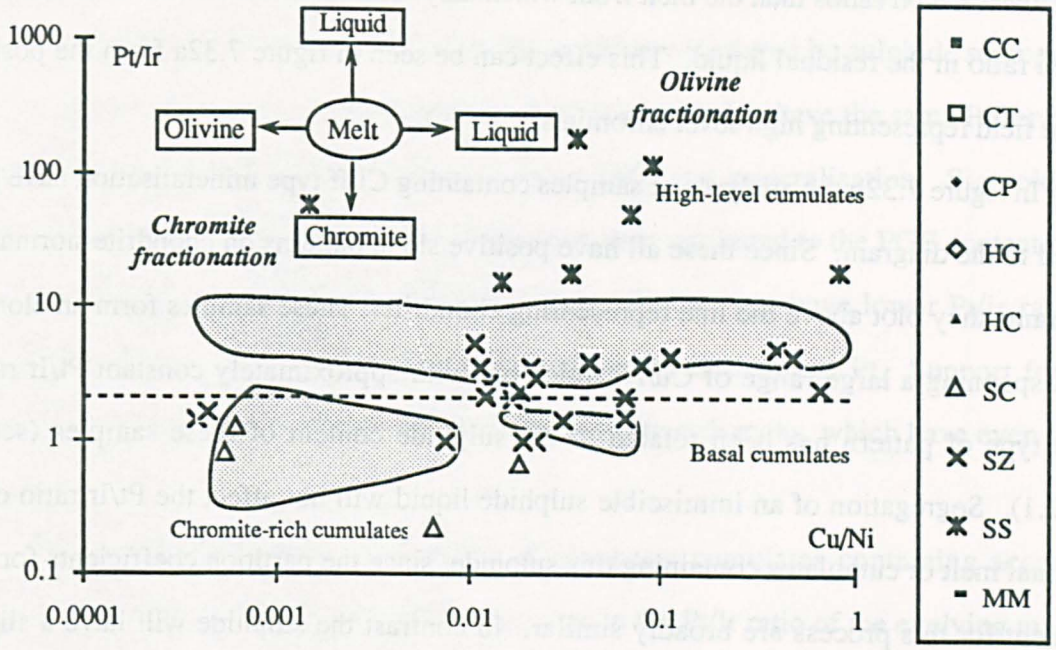

Figure 7.32(d). Resulting evolution (from 1 to 9) of magma compositions (open squares) and cumulates (closed squares) during single system fractionation.

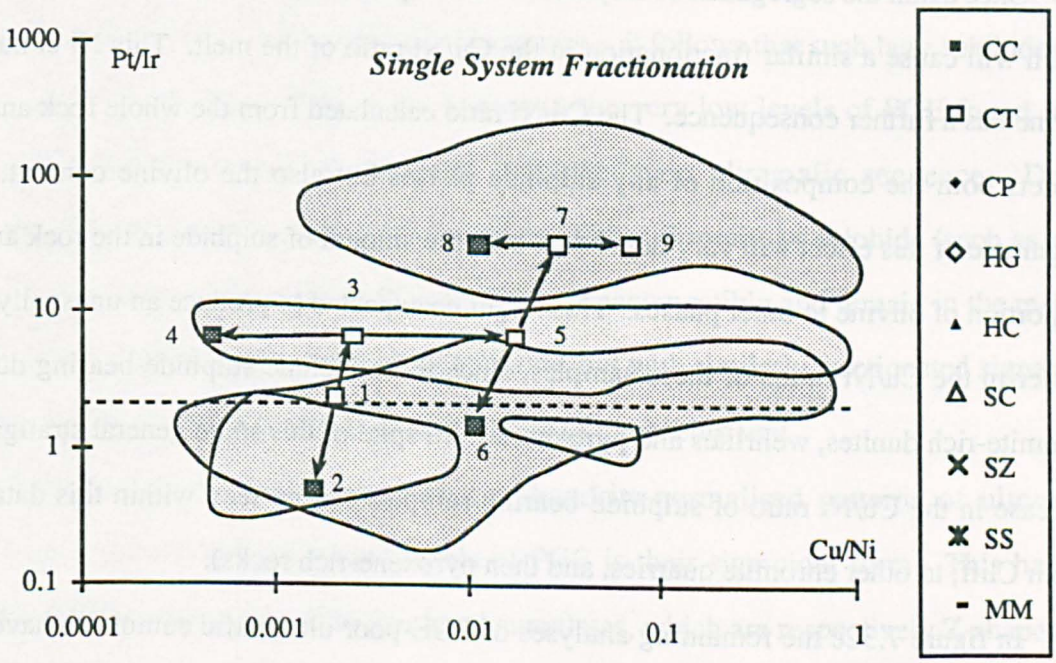

the preferential substitution of Ni in the olivine matrix. Thus olivine-bearing cumulates will have lower Cu/Ni ratios than the melt from which they formed and will result in an increased Cu/Ni ratio in the residual liquid. This effect can be seen in figure 7.32a from the position of the field representing high-level chromites.

In figure 7.32b the analyses of samples containing Cliff type mineralisation have been added to the diagram. Since these all have positive slope patterns on chondrite-normalised diagrams they plot above the line representing chondrite. These samples form an elongate field spanning a large range of Cu/Ni ratios but with approximately constant Pt/Ir ratios. This type of pattern has been related to the sulphide content of these samples (section 7.5.2.1). Segregation of an immiscible sulphide liquid will not affect the Pt/Ir ratio of the residual melt or cumulates containing this sulphide, since the partition coefficients for each element for this process are broadly similar. In contrast the sulphide will have a slightly lower Cu/Ni ratio than the original melt composition and the residual liquid will be displaced to a higher Cu/Ni ratio.

Once again the segregation of sulphides is accompanied by the crystallisation of olivine which will cause a similar fractionation in the Cu/Ni ratio of the melt. This Ni content of olivine has a further consequence. The Cu/Ni ratio calculated from the whole rock analysis reflects both the composition of any sulphide phases but also the olivine content. The magnitude of this effect will vary depend on both the amount of sulphide in the rock and the proportion of olivine to other phases. This might be expected to produce an unusually large scatter in the Cu/Ni ratios of these samples, since these include sulphide-bearing dunites, chromite-rich dunites, wehrlites and pyroxenites. In spite of this some general stratigraphic increase in the Cu/Ni ratio of sulphide-bearing samples can be seen within this data field (from Cliff, to other chromite quarries, and then pyroxene-rich rocks).

In figure 7.32c the remaining analyses of PGE-poor ultramafic cumulates have been added. The podiform dunites, basal cumulate dunites, wehrlites and pyroxenites all plot between the Cliff and the Harold's Grave fields. The more chromite-rich dunites plot just below this group and overlap with the Harold's Grave field. In contrast the higher level cumulates with S-shaped sigmoidal patterns plot towards the top of this diagram. These samples have Pt/Ir ratios significantly higher than the Cliff-type field or any other field.

In the generalised fractionation sequence seen in the ophiolite stratigraphy, the silicate crystallisation producing these cumulates occurs after the initial segregation of sulphide. Since the proportions of individual PGE in the liquid is unchanged by sulphide segregation, the residual liquid from which the cumulates form is expected to have the same Pt/Ir ratio as the sulphide phase, and hence the same ratio as Cliff type mineralisation. Sigmoidal Z-shaped patterns in basal ultramafic cumulates have been attributed to the PGE content of the accessory chromite in these rocks (section 7.2.3). Since these have lower Pt/Ir ratios it appears that Ir more readily substitutes in the chromite lattice than Pt. Support for this argument comes from the position of the more chromite-rich rocks, which have even lower Pt/Ir ratios.

The crystallisation of a thick series of ultrabasic cumulates containing accessory chromite will therefore cause a significant increase in the Pt/Ir ratio of the evolving magma. As a consequence, later sulphide segregations will inherit this more fractionated signature. This explains the very high Pt/Ir ratios of the higher level sulphide-bearing wehrlites and pyroxenites. Since the PGE content of the magma has already been much reduced by the scavenging effect of the initial sulphide segregations, it follows that such later sulphides will have a lower PGE tenor. This effect is seen in the very low levels of PGE found in the higher level wehrlites and pyroxenites from the main ultramafic sequence. During crystallisation of a silicate series which contain neither chromite or sulphide (such as much of the gabbro unit) the remaining PGE will behave incompatibly and remain in the residual liquid. Thus slightly higher PGE concentrations, but with similarly fractionated signatures, are found in the high-level wehrlites near the top of the gabbro unit.

The most significant feature of the chondrite-normalised patterns of ultramafic lithologies containing background levels of PGE is their sigmoidal form. This has two distinct forms in the basal and higher level cumulates, which are respectively Z-shaped and S-shaped. These are thought to represent the complimentary enrichment and depletion of particular PGE by virtue of the differing extents to which each are present by solid solution in accessory chrome spinel (section 7.2.4). Of all the six PGE the most compatible in chromite appears to be Ru, whereas the least incompatible is Pt. The Pt/Ru ratio can

Figure 7.33. Pt/Ir v Pt/Ru diagram showing the fractionation of PGE by the chrome spinel contained in ultramafic cumulates.

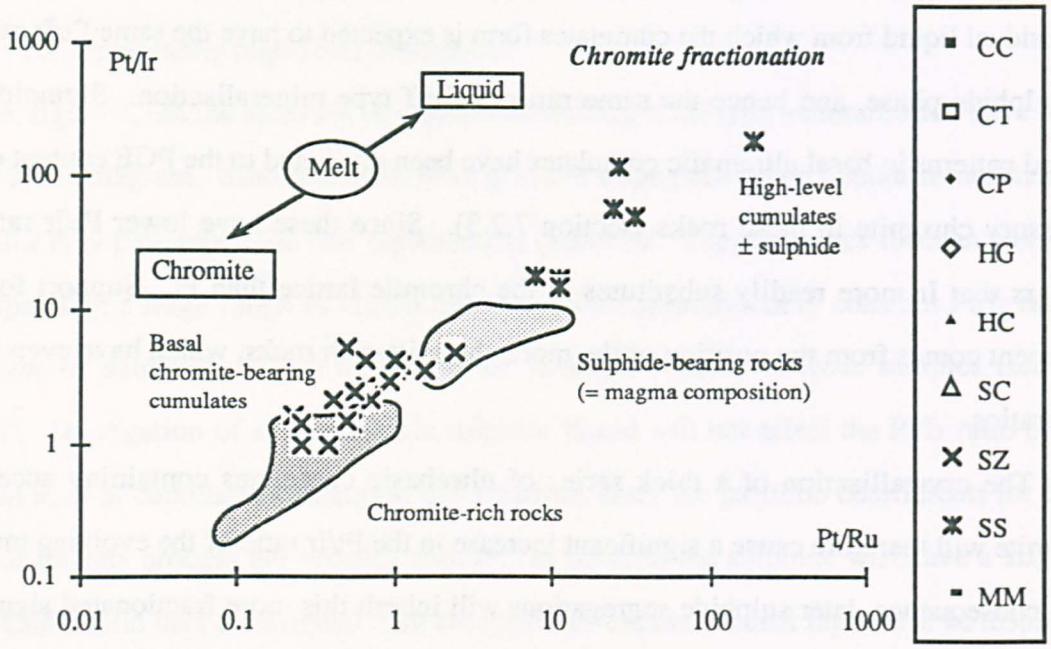

therefore be used to show the extent of this fractionation and to distinguish between the Z-shaped and S-shaped sigmoidal patterns.

The effects of chromite fractionation on Pt/Ir and Pt/Rh ratios are summarised in figure 7.33. The field of sulphide-bearing rocks represent the magma composition at this point in the fractionation history (central shaded field). The basal ultramafic cumulates and the high-level cumulates show complimentary displacements to either side of this field, representing the complimentary enrichment and depletion of Ru and Ir in comparison to Pt. As further proof that this fractionation is due to chromite and not olivine crystallisation, the more chromite-rich samples plot below and to the left of the basal cumulates (lower shaded field).

7.8.4 Single system and open system fractionation models

The overall fractionation history of the magma is summarised in figure 7.32d. This diagram suggests a single system fractionation pathway capable of producing all the observed PGE assemblages in the order inferred from field relations and mineralogical textures (section 7.6.2). Several aspects of the cumulate sequence indicate that an open

system fractionation model is more appropriate (section 3.7, 4.6), with the resulting mixing of primitive melts with an evolved resident magma (section 6.6). The Pt/Ir signatures of successive PGE enrichments in sulphide-bearing horizons are not progressively fractionated at higher stratigraphic levels (figure 7.32). In contrast the Cu/Ni ratios increase from dunite pods and the basal dunite unit to the stratigraphically higher pyroxene-rich cumulates. The higher Cu/Ni ratios of pyroxenites and wehrlites might also be due to the lower levels of olivine (and hence Ni) that these rocks contain. To resolve this ambiguity the Cu/Pt ratios of these samples have also been calculated.

Unlike Cu/Ni, the Cu/Pt ratio is not affected by variations in the olivine content of the different sulphide-bearing samples. There is a general correlation between Cu/Ni and Cu/Pt (figure 7.34), which is expected during sulphide fractionation considering the various partition coefficients of these three elements into immiscible sulphide liquid. Moreover, the field for pyroxene-rich samples falls at generally higher levels of both ratios compared to the field of olivine or chromite-rich specimens. Both fields show broadening in the direction parallel to the x axis due to variations in olivine content and hence Cu/Ni ratios. Three samples plot outside the main fields. These all contain undetected or unusually low levels of Cu. If these low levels are real, and not an analytical artifact, they may indicate some remobilisation of Cu. Significantly two of these samples are from the Cliff quarry. The most PGE-enriched sample analysed by this method also shows a displacement from the main fractionation trend towards lower Cu/Pt ratios, which is consistent with the selective hydrothermal enrichment of PGE (section 5.5.4).

Figure 7.34 indicates that the sulphide phases hosting Cliff type mineralisation in the pyroxene-rich cumulates are more fractionated than those in dunites and chromite-rich dunites. Since the Pt/Ir ratios are unfractionated, this is consistent with the mixing of a primitive sulphur undersaturated PGE-rich magma with a progressively fractionated sulphur saturated resident magma. In terms of the Pt/Ir v Cu/Ni diagram the open system fractionation can be seen as mixing between liquids 3 and 5 (figure 7.35). This hybrid (3') as it becomes saturated will segregate sulphide at 4' and evolve to 5'. With repeated cyclic influxes the compositions of the hybrid magma, the sulphides and the residual magma all move towards higher Cu/Ni ratios.

Figure 7.34. Pt/Ir v Cu/Ni diagram showing the fractionation of sulphide compositions.

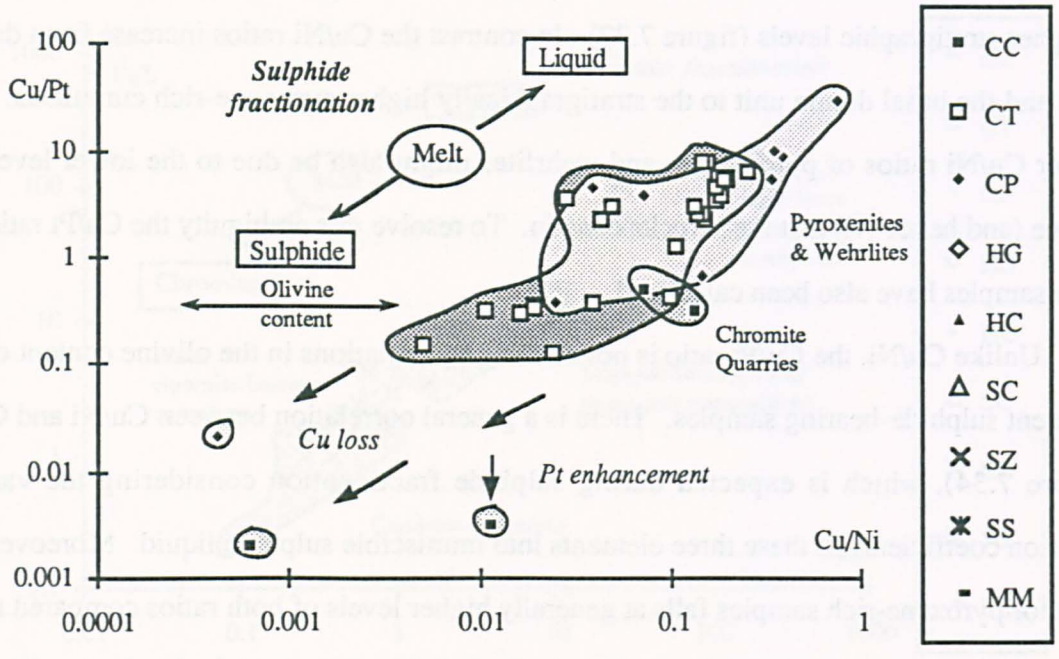

Figure 7.35. Resulting shift of magma (3') and cumulate compositions (4') during open system fractionation with later addition of primitive magma (3) to evolving resident magma (5). With repeated additions of primitive magma (3) to resident magma (5' to 5'") all compositions move to the right of the diagram.

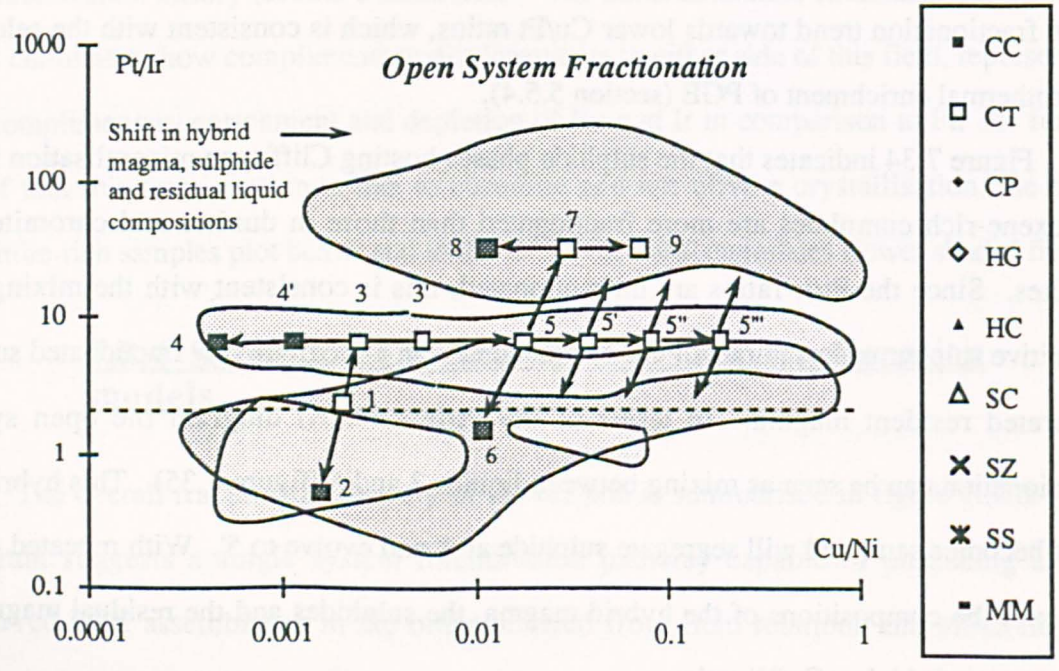

Figure 7.36. Summary diagram showing the envisaged open system fractionation of PGE in terms of the ophiolite silicate stratigraphy and the resulting chondrite-normalised patterns.

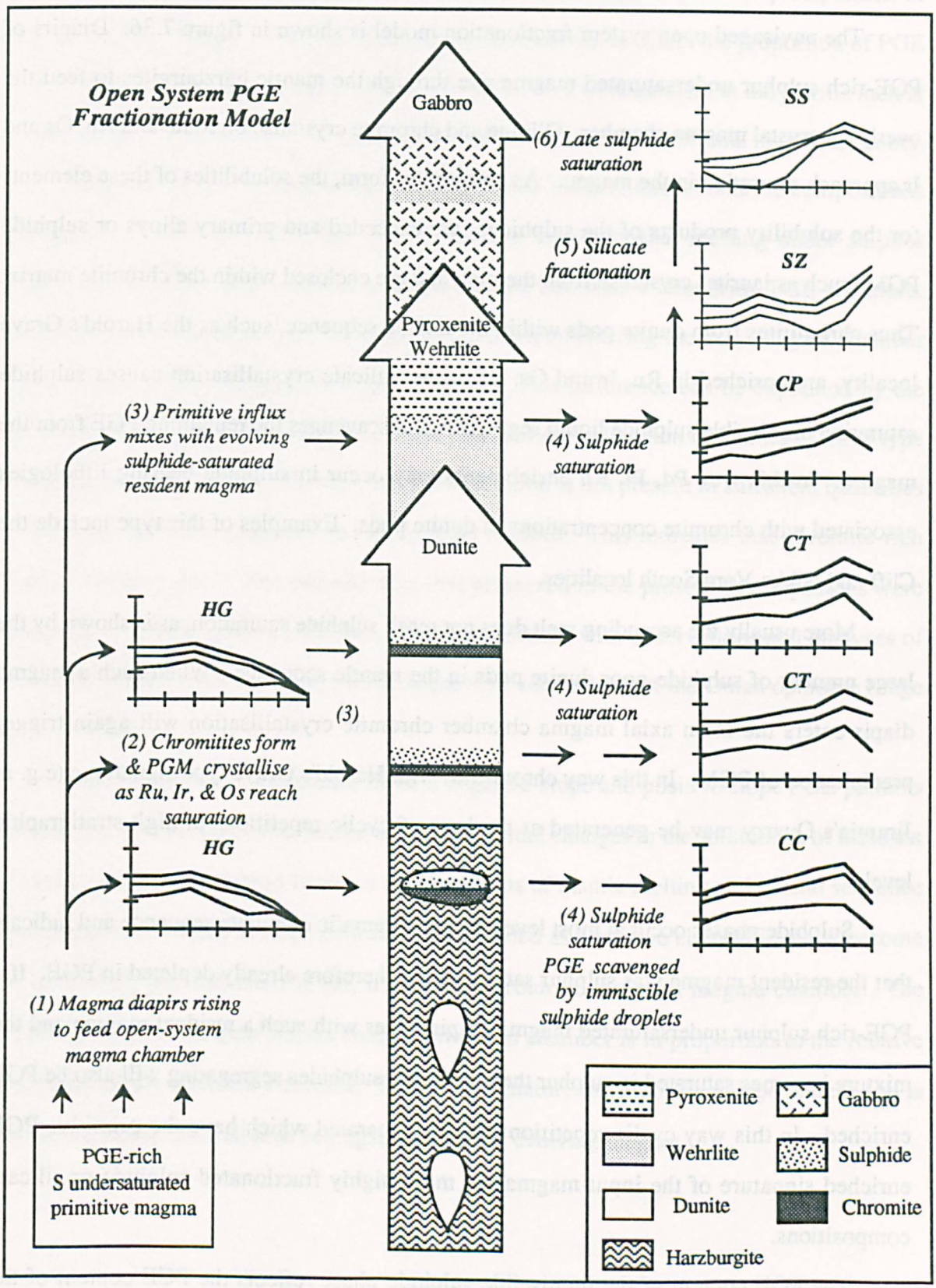

7.8.5 Implications of the open system fractionation model

The envisaged open system fractionation model is shown in figure 7.36. Diapirs of PGE-rich sulphur undersaturated magma rise through the mantle harzburgites to feed the overlying crustal magma chamber. Olivine and chromite crystalise on route and Ru, Os and Ir approach saturation in the magma. As chromitites form, the solubilities of these elements (or the solubility products of the sulphides) are exceeded and primary alloys or sulphide PGM (such as laurite) crystalise from the melt and are enclosed within the chromite matrix. Thus chromitites from dunite pods within the mantle sequence, such as the Harold's Grave locality, are enriched in Ru, Ir and Os. If further silicate crystallisation causes sulphide saturation immiscible sulphide liquid segregates and scavenges the remaining PGE from the magma. In this way Pd, Pt, Rh enrichments may occur in sulphide-bearing lithologies associated with chromite concentrations in dunite pods. Examples of this type include the Cliff and Nikka Vord South localities.

More usually the ascending melt does not reach sulphide saturation, as is shown by the large number of sulphide-poor dunite pods in the mantle sequence. When such a magma diapir enters the main axial magma chamber chromite crystallisation will again trigger precipitation of PGM. In this way chromitites with Harold's Grave type signatures (e.g. at Jimmie's Quarry may be generated at the base of cyclic repetitions at high stratigraphic levels.

Sulphide phases occur at most levels in the ultramafic cumulate sequence and indicate that the resident magma was sulphur saturated and therefore already depleted in PGE. If a PGE-rich sulphur undersaturated magma diapir mixes with such a resident magma and the mixture becomes saturated in sulphur then the initial sulphides segregating will also be PGE enriched. In this way cyclic repetitions can be generated which have the primitive PGE enriched signature of the input magma but more highly fractionated sulphide or silicate compositions.

The PGE content of the immiscible sulphide phase reflects the PGE content of the magma at the time of sulphide saturation. It can be seen from figure 7.36 that the chondrite-

normalised patterns, and hence the PGE contents, of each basal sulphide enrichment are very similar. This indicates that the PGE signature of each input of primitive magma was also similar. In the model shown this is explained as the buffering effect of the precipitation of PGM during formation of Harold's Grave type chromitites. In effect the proportion of PGE in the Cliff type signature reflects the relative solubility of each element in the picritic melt at the temperatures, pressures and fugacities prevailing at the base of the axial magma chamber.

Estimates of the PGE signature of fertile mantle indicate near chondritic compositions (Barnes et al., 1988). Therefore it is reasonable to expect that melting under sulphur undersaturated conditions would produce a magma also with a chondritic PGE signature. As has been argued above the PGE signature of the melt entering the axial magma chamber always has a Cliff-type positive slope signature. This difference can be explained by the depletion of Os, Ir and Ru arising from the previous crystallisation of Harold's Grave type PGM-bearing chromitites. This type of mineralisation is not present in sufficient quantities in the Unst ophiolite sequence to satisfy mass balance. This indicates that chromite-rich pods at lower levels in the ophiolite than that preserved in the present day exposures were generally enriched in these elements. This is consistent with observations and analyses of chromitites from more complete mantle sequences, such as that of the Oman ophiolite (Page et al., 1982b).

In conclusion, the occurrence of both negative-slope and positive slope PGE patterns in ophiolite complexes can be related to the differential changes in the solubilities of these six elements in picritic magmas between the conditions of mantle melting and crustal sequence crystallisation. Negative slope patterns are generated as primitive chondritic melts become progressively oversaturated in Os, Ir and Ru on route to the axial magma chamber. The PGE signature of magma diapirs entering the main chamber is in proportion to the relative solubility of the different elements. This PGE signature has a positive slope pattern and is preserved in the first sulphide segregating from the evolving magma.

7.9 Conclusions

The variety of chondrite-normalised patterns seen in the Shetland ophiolite complex can be explained by magmatic fractionation processes. These patterns are controlled by the following:-

(a) the initial PGE content of the magma

(b) the presence of primary PGM in chromitites

(c) the presence of sulphide phases representing immiscible sulphide liquids

(d) the presence of cumulate chromite containing PGE in solid solution.

(e) the fractionation history of the magma and the relative timing of (b) - (d) in the context of an open system fractionation model.

By the combined use of spidergrams and various metal ratio diagrams the PGE form a useful petrogenetic tool for establishing the early magmatic history of basic-ultrabasic rock sequences and determining their metallogenic potential.

Conclusions

Platinum-Group Element Mineralisation in the Shetland Ophiolite Complex

8.1 Scope of the present study

At the outset of this study considerable debate surrounded the origin of PGE concentrations in the Shetland ophiolite, in particular the unusually high concentrations of Pt and Pd found at Cliff. Contradictory evidence of both magmatic and hydrothermal processes had been described (Prichard et al., 1986; Gunn et al., 1985), although neither fully explained the patterns of PGE concentration which these earlier studies had revealed. Additional detailed work was therefore required to establish the character, distribution and genetic controls of mineralisation and thereby quantify the roles of magmatic and hydrothermal processes both spatially and temporally in the ophiolite complex.

8.2 The ophiolite stratigraphy in the area around Balta Sound

Field mapping has confirmed that the area around Balta Sound contains the lower parts of the Penrose ophiolite sequence. Geochemical data suggest that this is a SSZ ophiolite of Caledonian age. Tectonised mantle sequence harzburgites are overlain by a layered crustal sequence in which dunites grade upwards, with cyclic repetition, through wehrlites into clinopyroxenites. Above this is a gabbroic unit which encloses discrete high-level wehrlite and pyroxenite bodies and is intruded by a dyke swarm at the highest exposed level. These gabbros are separated from the underlying ultramafic sequence by a tectonic junction and comparisons with other more complete ophiolite sequences indicate that a cumulate sequence of layered olivine gabbros is missing at this point. The more complete ultramafic sequence

has near vertical E-W primary foliations and a southerly younging direction. This stratigraphy is increasingly deformed by NE trending high-angle sinistral shear zones further south and east. This culminates in a NE-SW tectonic grain in the pyroxene-rich layered sequence at Ordale.

Small scale mapping on air photographs has revealed much detail of the tectonite and layered cumulate sequences. This allowed samples to be accurately located and placed in context within the igneous stratigraphy. One new aspect of the ophiolite sequence revealed by this detailed mapping is the continuity of stratigraphically controlled zones of chromite enrichment. At least two sub-parallel zones are present within the cumulate dunite unit in the area north of Balta Sound. As a result of these cyclic repetitions, this unit is unusually thick in comparison to the dunite units of other ophiolites. This suggests that the magma composition was unusually picritic and was generated by a higher degree of melting or remelting than in other SSZ ophiolites such as the Troodos complex.

8.3 Chromite mineral chemistry

The Unst chromites show the wide variations in Cr/(Cr+Al) and Mg/(Mg+Fe^{II}) and low Ti or Fe^{III} contents which are characteristic of podiform chromitites. With the exception of subtle changes in Ti content, these differences in major and minor element chemistry are unrelated to stratigraphic level or PGE content. In particular, no chemical uniformity is apparent between podiform chromite concentrations from the same horizon although the stratigraphic continuity of these zones has been established by field mapping. This suggests that individual chromitite bodies may result from magmas with different original compositions or with differing degrees of fractionation. The lack of progressive chemical changes between successively higher chromite horizons suggests that these represent different magma inputs, rather than reversals in a single evolving magma.

The Ti content of chromites from the crustal sequence are significantly higher than those from the mantle sequence. Since chromitites in dunite pods in the mantle sequence represent crystallisation from pockets of magma feeding the overlying chamber, this is possibly related to changes in oxygen fugacity as batches of magma enter the main magma

chamber and mix with the resident melt.

Chromite mineral chemistry distinguishes between chromites from stratiform complexes and ophiolitic complexes. It does not distinguish between ophiolitic chromites containing the positive slope (Pt-, Pd-, Rh- dominant) and negative slope (Os-, Ir-, Ru-dominant) PGE mineralisation, even though these different assemblages are typical of each respective paragenesis. The chromitites from Unst all conform to ophiolitic compositions but may contain either type of PGE concentration. It is apparent that different processes control the composition of the host chromite from those influencing the type of PGE assemblage.

8.4 Magmatic distribution of PGE concentrations

An extensive sampling and analytical program has revealed the widespread occurrence of anomalous PGE concentrations in the ophiolite complex. Anomalous levels of PGE, which were previously known at Cliff and Harold's Grave, have been located in other chromite-rich dunite pods from within mantle harzburgite. More significantly, concentrations of PGE have also been found associated with stratigraphically controlled chromite concentrations within the cumulate dunite unit. These PGE concentrations contain high levels of platinum and palladium, and occur not only in chromitites, but also in the associated dunites and chromite-rich dunites. PGE concentrations have also been located in other chromite-poor rocks within the crustal sequence, including wehrlites and pyroxenites. Anomalous levels of Pt and Pd occur in sulphide-bearing pyroxene-rich lithologies from close to the base of the pyroxene-bearing layered sequence, and also in sulphide-bearing pyroxene-rich ultramafic bodies within the gabbro unit.

Concentrations of Pt, Pd, Ir and Au show similar distribution patterns and the four elements occur together indicating a common origin. The distribution patterns are not related to alteration zones but are lithologically controlled, with PGE concentrations occurring more frequently in certain igneous rock types. Such lithological association is indicative of primary igneous processes, with concentration of the PGE occurring at the same time as the formation of the enclosing silicate rock.

8.5 Controls of PGE mineralisation

Hand specimen description of samples and observation of their accessory sulphide content has provided further evidence of the controls of PGE mineralisation. Anomalous levels of Pt, Pd and Au occur preferentially in sulphide-bearing disseminated chromite-rich dunites, and in sulphide-bearing dunites which are spatially associated with chromite concentrations. Anomalous levels of Ir most commonly occur in chromitites and chromite-rich rocks. These two controls (i.e. chromite and accessory sulphide) form visual pathfinders for PGE mineralisation which can be recognised in the field. The differences in behaviour between Ir and Pt or Pd indicate internal fractionation within the platinum group of elements.

8.6 Exploration guides - The first sulphide model

Anomalous levels of PGE preferentially occur together with sulphides spatially associated with chromite concentrations. These chromite concentrations generally occur close to the base of the layered crustal sequence and in dunite pods within the harzburgite. Chromite enrichments mark the base of each cyclic repetition in the cumulate sequence. This distribution of chromite concentrations indicates that they were formed early in the crystallisation history of the magma. The sulphides associated with the chromite concentrations thus represent the earliest sulphide phases forming within the cumulate sequence. In the case of cyclic repetitions these are the first sulphides segregating from each batch of primitive magma.

A general genetic model for the occurrence of PGE in ophiolites may now be suggested, namely that PGE concentrations occur associated with the first sulphide segregating from the evolving magma. In the Shetland ophiolite this occurred at the same time as, or immediately after chromite crystalised. PGE concentrations therefore occur close to the base of layered cumulate sequences. Repetitions occur representing fresh inputs of magma during open system fractional crystallisation.

8.7 Associated chalcophile elements

Anomalous levels of PGE and Au are associated with anomalous levels of Ni, Cu, Co, Cr, As and Sb. Of these trace elements, Ni, Cu, Co, and Cr show an igneous distribution in the ophiolite sequence. This is illustrated by their patterns of primary lithological association and mineralogical control. Anomalous levels of these elements are associated with chromite-rich lithologies in a similar manner as anomalous Pt, Pd Ir and Au concentrations. The chalcophile elements are fractionated by magmatic processes. This is illustrated by the different relative concentrations of Ni and Cu at different stratigraphic levels in the cumulate sequence. Enrichments of Ni occur in basal olivine-rich lithologies but Cu enrichments also occur in the stratigraphically higher pyroxene-rich rocks. This earlier depletion of Ni is mirrored by decreases in the Ni content of olivine, and possibly the sulphide phases, at higher stratigraphic levels.

Moderate levels of As and Sb show a similar magmatic distribution as Ni, Cu and Co. Superimposed on this pattern are highly anomalous concentrations one or two orders of magnitude higher. These occur in highly altered lithologies associated with shear zones, which is indicative of secondary concentration processes during alteration by hydrothermal fluids.

8.8 Use of pathfinder elements

Anomalous levels of PGE and Au are associated with anomalous levels of Ni, Cu, Co, Cr, As and Sb. The relative strength of these associations is different for each platinum-group element reflecting internal fractionation within the group. Ir shows a particularly strong association with Co and Cr, since both occur in chromite. Pt Pd and Au show a strong association with Ni and Cu, reflecting their connection with sulphide phases.

This relationship between Pt, Pd, Au and chalcophile elements suggests that Ni and Cu are potential pathfinders for PGE mineralisation. Graphically only a weak linear dependence is observed between PGE and chalcophile elements when the whole database is

considered. The reason for this poor correlation is that the ratios of PGE to pathfinder elements vary with stratigraphic level and rock type reflecting igneous fractionation processes. The original primary dependence may also be obscured by secondary processes and remobilisation. Present day sulphur concentrations mostly retain a correlation with chalcophile elements. However, mineral assemblages, calculations of bulk sulphide Ni/S ratios, and field observations of green sulphide alteration rims or Ni-rich serpentinites, all indicate partial remobilisation and a net loss of sulphur. For these reasons whole-rock chalcophile element analyses provide a better indication of original igneous sulphide contents than direct measurements of sulphur concentrations. By chosing different threshold values in different rock types and at different stratigraphic levels, anomalous Ni or Cu concentrations can be used to identify sulphide-bearing zones. These represent target areas for anomalous magmatic PGE mineralisation. These targets can be refined by field observations of igneous stratigraphy, chromite concentrations and accessory sulphide phases, allowing identification of the first sulphide phases in the sequence.

8.9 Localised hydrothermal enhancement of PGE mineralisation at Cliff

PGE mineralisation at Cliff shows all the attributes of other mineralised areas, namely an association with Ni Cu sulphides and chromite. However, the absolute concentrations of PGE at Cliff are one to two orders of magnitude higher than those found elsewhere. Chromitites, disseminated chromite-rich dunites and sulphide-bearing dunites from this locality contain anomalous levels of Ni, Cu and Sb, and highly anomalous levels of Pt, Pd, Ir, Au and As. Furthermore, the higher concentrations of Pt, Pd, Ir and Au show statistically significant correlations with As and Sb. The high levels of As have been attributed to a hydrothermal overprint by As-rich fluids, as a consequence of the proximity of the Cliff area to the basal thrust of the ophiolite (Lord & Prichard 1989). This suggests that the extremely high grades found at Cliff are due to the secondary hydrothermal enhancement of a primary igneous source by serpentinisation and interaction with secondary As-rich fluids.

8.10 Stratiform PGE enriched horizons in the ophiolite ultramafic cumulate sequence

Detailed sample traverses have shown that continuous stratigraphically controlled PGE mineralisation is present at several levels in the cumulate sequence. In spite of the poor exposure of sulphide bearing dunites, and the tectonic disruption of the higher level ultramafic layering, these horizons can be seen to be laterally continuous over a strike length of 2 km. Within these mineralised horizons the concentrations of Pt and Pd are related to sulphide contents, and the chalcophile elements Ni and Cu are pathfinders for the PGE. These patterns are indicative of concentration by magmatic processes.

8.11 Cyclic repetitions - Evidence of open-system fractionation

The cumulate sequence as a whole shows a progressive change from dunitic, through wehrlitic, to pyroxenitic rocks, with superimposed cyclic repetitions at different scales. The base of these magmatic cycles are marked by chromite-rich horizons and laterally discontinuous pods of chromitite. Each repetition also has associated PGE-enriched sulphide-bearing zones. The PGE-enriched sulphide-bearing horizons show a progressive increase in Cu/Ni and Cu/PGE ratios at higher stratigraphic levels. In contrast the PGE are unfractionated either within a single zone or between successively higher stratigraphic horizons, even between dunite and pyroxenite hosted mineralisation.

These progressive changes may be explained by an open-system fractionation model in which batches of primitive sulphur undersaturated magma mix with an evolving resident sulphur saturated magma. The PGE are effectively removed from the hybrid magma by the initial sulphide segregations within the cycle. Thus unfractionated PGE ratios occur with sulphides at the base of sequences in which the sulphide compositions show progressive evolution with increasing stratigraphic level.

8.12 Fractionation of the platinum-group elements

The variety of chondrite-normalised patterns seen in the Shetland ophiolite complex can be explained by magmatic fractionation processes. These patterns are controlled by the following:-

(a) the initial PGE content of the magma

(b) the presence of primary PGM in chromitites

(c) the presence of sulphide phases representing immiscible sulphide liquids

(d) the presence of cumulate chromite containing PGE in solid solution.

(e) the fractionation history of the magma and the relative timing of (b) - (d) in the context of an open system fractionation model.

The occurrence of both negative-slope and positive slope PGE patterns in ophiolite complexes can be related to the differential changes in the solubilities of these six elements in picritic magmas, between the conditions of mantle melting and crustal sequence crystallisation. Negative slope patterns in chromitites are generated as primitive chondritic melts become progressively oversaturated in Os, Ir and Ru on route to the axial magma chamber. These earliest cumulates contain primary PGM, such as laurite, which crystalised directly from the melt. The PGE signature of sulphur undersaturated magma diapirs entering the main axial chamber is thus in proportion to the relative solubility of the different elements. The PGE signature of this magma thus has a positive slope pattern, which is preserved in the first sulphide segregating from the evolving magma. Sulphide saturation occurs after mixing with an evolved resident magma. By this process the PGE composition of primitive inputs is buffered and PGE enriched cyclic repetitions have identical unfractionated patterns.

Background PGE concentrations in chromite-bearing ultramafic cumulates have Z-shaped sigmoidal patterns. This is reflects the differing extent to which individual PGE are accommodated by substitution in the chromite lattice (but not in the olivine lattice). The net effect of the crystallisation of a thick sequence of chromite-bearing dunites, wehrlites and pyroxenites is to produce a complimentary depletion of PGE from the residual melt. This

fractionated liquid has an S-shaped sigmoidal signature with an overall steeper positive slope. This highly fractionated pattern occurs in later sulphide segregations in high-level ultramafic bodies within the gabbro unit. It is also characteristic of the dykes and lavas of other complete ophiolite complexes, and the oceanic basalts representing their modern day analogues.

By the combined use of spidergrams and various metal ratio diagrams, the PGE form a useful petrogenetic tool for establishing the early magmatic history of basic-ultrabasic rock sequences and determining their metallogenic potential.

8.13 The potential for PGE mineralisation in other ophiolite complexes

This study has shown that the PGE mineralisation in the Shetland ophiolite is magmatic in origin, albeit affected to various degrees by later hydrothermal alteration processes. It follows that PGE concentrations should occur in the same overall proportions in other ophiolite complexes and include Pt-Pd-Rh assemblages, as well as the more widely recognised Os-Ir-Ru assemblage. The re-discovery of unusually high Pt concentrations in Shetland chromitites and investigation of the Cliff locality provoked such a degree of interest in the PGE mineralisation potential of other ophiolites that much of this aspect of further work has already begun (table 8.1). In particular, the "first sulphide" exploration model developed here has already been applied, and found to be useful, in locating Pt-Pd-Rh concentrations in the Troodos ophiolite complex (Prichard and Lord, 1990).

It appears that Pt-Pd-Rh concentrations are a general feature of SSZ ophiolites, although the grade and stratigraphic level of this sulphide-hosted mineralisation varies between different complexes and ophiolite belts. Other Caledonian ophiolites contain mineralisation most closely similar to that in Shetland, whereas Tethyan ophiolites typically contain lower levels of PGE. These distinctions can be explained by considering the mantle source history and the conditions and degree of partial melting. It follows from the chalcophile behaviour of PGE that during the generation of sulphur saturated melts these elements will remain in the mantle (Hertogen et al., 1980). Subsequent remelting of this

Table 8.1. Highest concentrations of each PGE (ppb) reported from ophiolite complexes, lithological subunits or related mineralisation (1985-1990).

Ophiolite	*Os*	*Ir*	*Ru*	*Rh*	*Pt*	*Pd*	*Lithology/Association*	*Source*
Shetland Ophiolite								
Cliff, Shetland		5000	9000	1600	32000	75000	Chromitite	Gunn et al., 1985
Cliff, Shetland	1400	3200	4400	1500	28000	35000	Chromitite	Prichard et al., 1986
Baltasound, Shetland	520	550	960	140	330	650	Mantle chromite/dunite	This study
Baltasound, Shetland	98	120	190	110	870	2100	Crustal chromite/dunite	This study
Baltasound, Shetland	28	41	88	62	230	670	Crustal dunite	This study
Baltasound, Shetland	12	28	37	23	240	380	Crustal pyroxenite	This study
Other ophiolites								
Zambales, Philippines		460	1100	759	5958	8351	Crustal chromitites	Bacuta et al., 1988
Zambales, Philippines		120	150	18	66	25	Mantle chromitites	Bacuta et al., 1988
Pole Coral, California		2930	4930	74	2530	15	Chromitite	Moring et al., 1988
Hochgrössen & Kraubath Massifs	250	310	620	130	940	390	Chromitite	Thalhammer et al., 1990
Springers Hill, Bay of Islands	3	10	2	31	520	405	Orthopyroxenites	Edwards, 1990
Springers Hill, Bay of Islands	< 1	< 2	< 1	4	520	190	Clinopyroxenites	Edwards, 1990
Lewis Hills, Bay of Islands	7	9.5	30	3	5	<5	Chromite-rich dunite	Talkington & Watkinson, 1986
Norway av. enriched (incl. Leka)					416	413	Chromitite	Barnes et al., 1988
Osthammeren, Norway	170	667	838	65	320	3	Chromitite	Nilsson, 1990
White Hills, Newfoundland	370	390	690	130	290	90	Chromitite	Talkington & Watkinson, 1986
Thetford Mines, Quebec		6	36	11	130	130	Ultramafic cumulates	Tanguay et al., 1990
Thetford, Quebec	31	32	30	5	10	15	Chromitite	Talkington & Watkinson, 1986
British Columbia Ultramafics	440	450	850	55	110	110	Chromite-rich dunite	Talkington & Watkinson, 1986
Troodos, Cyprus	17	29	150	49	79	69	Crustal chromitite	McElduff & Stumpfl, 1990
Troodos, Cyrprus	2	9	16	6	62	62	Gabbro	Prichard & Lord, 1990
Skyros, Greece	630	780	1210	228	208	22	Chromitite	Economou, 1986
Alpine bodies					15	52	Serpentinites	Burkhard et al., 1988
Vourinos, Greece	18	26	50	10	25	45	Chromitite	Talkington & Watkinson, 1986
10 Greek Ophiolites	70	66	140	12	24	5	Chromitite	Economou, 1986
Associated sulphides & hydrothermal concentrations								
Faeoy, Norway	490	410	480	440	5400	8000	Cu-Ni Sulphide	Boyd et al., 1988
Lillefjellklumpen, Norway	250	290	330	330	5900	4700	Ni-Cu Sulphide	Boyd et al., 1988
Bou Azzer, Morocco					2500		Co-As ores	Leblanc & Fischer, 1989

refractory source produces sulphur deficient PGE-enriched magmas, as exemplified by boninites and the compositionally similar parent magmas proposed for the Bushveld Complex (Hamlyn et al., 1985; Hamlyn & Keays, 1986). The PGE potential of SSZ ophiolite complexes thus depends on a complex balance between the extent of previous source depletion and the degree of second stage melting, so as to generate PGE-rich sulphur-poor magmas which nevertheless become rapidly sulphur saturated on mixing within the axial magma chamber allowing the effective concentration of PGE. In this respect the presence of a thick chromite-bearing cumulate dunite unit (e.g. Shetland, Leka, Zambales) may be a useful indication of the PGE potential of an ophiolite complex.

8.14 The potential for hydrothermal PGE mineralisation

Although the bulk of the PGE mineralisation in the Shetland ophiolite complex has retained its primary magmatic features this is not the case for the unusual concentrations found at the Cliff quarry. The parallel study of magmatic concentrations elsewhere in the complex has highlighted the subtle differences in the mineralisation at this locality and has reconciled the original controversy between magmatists and hydrothermalists (Prichard et al., 1986; Gunn et al., 1985). It has been proposed in this study that magmatic PGE concentrations within the primary sulphide-bearing chromite-rich dunite pod have been locally remobilised and extensively reconcentrated by serpentinising fluids, aided and abetted by the hydrothermal alteration of an As-rich fluid. This theory can be easily tested by investigations of the degree and controls of PGE concentration in a continuous section through the mineralisation (work now in progress). If it is correct then the possibility of further more extensive deposits on Unst remains untested. The extent of the mineralisation at Cliff is naturally limited by the small size of the magmatic source pod. In the cumulate dunite unit volumetrically much larger stratigraphically controlled continuous mineralised horizons have been located by this study. Where these abut against the basal thrust or other hydrothermally altered thrust zones, it is possible that these sub-economic concentrations have been similarly upgraded, with the potential of much larger tonnages. It remains to be

seen whether such wholesale enrichment of magmatic PGE concentrations is geologically feasible or whether the Cliff locality remains in the ore deposit category of "divine joke".

Appendices

Appendix A:- Chromite mineral analyses

Analytical and data correction proceedures are outlined in section 3.2. Data listed on pages 391 to 396. Three analyses (e.g. CL1a, CL1b, CL1c) of each thin section (e.g. CL1).

Appendix B:- Sample list and trace element analyses

Analytical details are given in sections 4.3 and 5.2. Zero signifies that elements were undetected. Data listed on pages 397 to 408. The following abbreviations have been used:-

Sulphides

SB	sulphide-bearing	} *relative scale*	
MSB	moderate sulphide content	} *of amount of*	
MSR	moderately sulphide-rich	} *accessory*	
SR	sulphide-rich	} *sulphide*	
VSR	very sulphide-rich	}	
S	sulphide (Ni?)	YS	yellow sulphide (Cu?)

Chromite

Cr or chr	chromite	mas or mass	massive
dis or diss	disseminated	lay	layer, layered
mult	multiple layer		
Qu	chromite quarry (key to numbers figure 4.1 & table 4.1)		

Rock types

D or dun	dunite	H	harzburgite
pyrox	pyroxenite	harz	harzburgite
WD	wehrlitic dunite	W or wehr	wehrlite
serp	serpentinite or serpentinised	alt%	alteration
H.L.	high-level, i.e. wehrlite or chromite		
CrED	dunite with anomalous accessory chromite		
trans	dunite/harzburgite transitional lithology		
seg	segregated type of transitional harzburgite		

Minerals

mins	minerals	kamm	kammererite
plag	plagioclase	ol	olivine
px	pyroxene	chl	chlorite
mnt	magnetite	Cu	native Cu
CO3	carbonate	antig	platey serpentine
Si	silica-rich/silicified		

Colours & alteration

G or gr	green	}*characteristic*
GM	green matrix	}*alteration colour*
GB	green blotches	}*of sulphides or*
GP	green patches	}*sulphide-rich*
GH	green haloes around sulphides	}*lithologies*
chl R	chlorite rims around chromite grains	

pseuds	pseudomorphs	W	white
Y or yel	yellow	dk	dark
br	brown		

Others

xeno	xenoliths	M	matrix
VF	very fresh	sml	small
lg	large	V	very
nr	near	mod	moderate
?	possible	trav	traverse
exp	exposure	junct.	junction
AS	along strike	STR	stratigraphically
cy	cycle (of cumulates)	na	not analysed
B	bearing, e.g. plag B plagioclase-bearing		
ch or chan	channel sample		

Stratigraphic or lithological tag

H	harzburgite unit	CQ	Cliff chromite quarry
PQ	chromite quarry in dunite pod	DP	dunite pod
DQ	chromite quarry in dunite unit	DU	cumulate dunite unit
C	pyroxene-rich layered cumulates	G	gabbro unit
TH	transitional harzburgite	HLC	high-level cumulates
A	highly altered rocks		
T1 to T13	samples from measured traverses 1 to 13 (see table 6.1, figure 6.1)		

SAMPLE	*CL1a*	*CL1b*	*CL1c*	*CL3a*	*CL3b*	*CL3c*	*CL7a*	*CL7b*	*CL7c*	*1349a*	*1349b*	*1349c*	*Q1a*	*Q1b*	*Q1c*	*Q2a*
Wt.% Oxide																
SiO2	0.08	0.05	0.05	0.11	0.08	0.05	0.11	0.08	0.08	0.08	0.08	0.11	0.08	0.05	0.08	0.11
TiO2	0.15	0.15	0.15	0.15	0.15	0.15	0.17	0.17	0.15	0.17	0.17	0.15	0.17	0.15	0.15	0.15
Al2O3	19.42	19.35	19.37	19.84	20.26	20.34	20.44	20.05	19.95	20.43	20.61	20.1	19.13	19.04	19.44	14.18
FeOT	14.44	15.2	15.62	16.13	14.81	14.63	16.67	16.48	15.89	16.73	15.66	17.63	18.84	19.33	18.71	24.2
MnO	0.09	0.12	0.15	0.16	0.12	0.06	0.13	0.12	0.12	0.13	0.09	0.13	0.12	0.16	0.15	0.32
MgO	15.05	14.76	14.56	14.43	15.45	15.57	14.24	14.3	14.85	14.21	14.84	13.5	12.34	12.06	12.41	9.65
CaO	0.01	0.03	0.01	0.01	0.01	0.01	0.01	0.01	0.01	0.01	0.01	0.01	0.01	0.01	0.01	0.03
Cr2O3	50.49	50.99	50.54	49.39	49.84	49.31	48.92	49.07	48.97	48.45	49.29	48.38	49.78	49.45	48.91	51
NiO	0.1	0.09	0.07	0.06	0.07	0.04	0.1	0.06	0.04	0.06	0.07	0.04	0.09	0.09	0.07	0.14
TOTAL	99.83	100.74	100.52	100.28	100.79	100.16	100.79	100.34	100.06	100.27	100.82	100.05	100.56	100.34	99.93	98.78
Formula Units (32 Oxygens)																
Si	0.020	0.012	0.012	0.027	0.020	0.012	0.027	0.020	0.020	0.020	0.020	0.027	0.020	0.013	0.020	0.029
Ti	0.028	0.028	0.028	0.028	0.028	0.028	0.032	0.032	0.028	0.032	0.031	0.028	0.032	0.028	0.028	0.030
Al	5.67	5.62	5.64	5.79	5.84	5.89	5.93	5.85	5.82	5.96	5.95	5.91	5.66	5.66	5.77	4.42
FeT	2.99	3.13	3.23	3.34	3.03	3.00	3.43	3.41	3.29	3.46	3.21	3.68	3.95	4.07	3.94	5.35
Mn	0.019	0.024	0.031	0.034	0.025	0.013	0.028	0.026	0.026	0.026	0.019	0.027	0.026	0.035	0.033	0.071
Mg	5.55	5.42	5.36	5.32	5.63	5.70	5.22	5.27	5.48	5.24	5.42	5.02	4.61	4.53	4.66	3.80
Ca	0.003	0.008	0.003	0.003	0.003	0.003	0.003	0.003	0.003	0.003	0.003	0.003	0.003	0.003	0.003	0.009
Cr	9.88	9.93	9.88	9.66	9.63	9.57	9.52	9.60	9.58	9.48	9.54	9.53	9.87	9.85	9.73	10.66
Ni	0.020	0.018	0.014	0.012	0.014	0.008	0.020	0.012	0.008	0.012	0.014	0.008	0.018	0.018	0.014	0.030
TOTAL	24.18	24.19	24.20	24.22	24.22	24.23	24.22	24.22	24.25	24.23	24.20	24.22	24.19	24.21	24.20	24.40
Recalculated Analysis																
Si	0.020	0.012	0.012	0.027	0.019	0.012	0.027	0.020	0.020	0.020	0.019	0.027	0.020	0.013	0.020	0.029
Al	5.63	5.58	5.60	5.74	5.79	5.83	5.88	5.79	5.76	5.90	5.90	5.85	5.61	5.61	5.72	4.35
Cr	9.81	9.85	9.79	9.58	9.55	9.48	9.43	9.51	9.48	9.39	9.46	9.45	9.79	9.77	9.65	10.48
FeIII	0.47	0.49	0.52	0.57	0.57	0.60	0.57	0.59	0.66	0.60	0.53	0.59	0.49	0.54	0.52	1.04
Ti	0.028	0.028	0.028	0.028	0.027	0.027	0.031	0.031	0.028	0.031	0.031	0.028	0.032	0.028	0.028	0.029
Mg	5.51	5.38	5.32	5.27	5.58	5.64	5.18	5.22	5.42	5.19	5.37	4.97	4.58	4.49	4.62	3.74
FeII	2.50	2.62	2.68	2.74	2.43	2.38	2.84	2.79	2.60	2.83	2.65	3.05	3.43	3.50	3.38	4.23
Ni	0.020	0.018	0.014	0.012	0.014	0.008	0.020	0.012	0.008	0.012	0.014	0.008	0.018	0.018	0.014	0.029
Mn	0.018	0.024	0.031	0.034	0.025	0.013	0.028	0.026	0.026	0.026	0.019	0.027	0.026	0.034	0.033	0.070
Ca	0.003	0.008	0.003	0.003	0.003	0.003	0.003	0.003	0.003	0.003	0.003	0.003	0.003	0.003	0.003	0.008

SAMPLE	*Q2b*	*Q2c*	*Q3a*	*Q3b*	*Q3c*	*Q3PXa*	*Q3PXb*	*Q3PXc*	*210a*	*210b*	*210c*	*NEV2a*	*NEV2b*	*NEV2c*	*1312a*	*1312b*
Wt.% Oxide																
SiO2	0.19	0.4	0.61	0.08	0.08	0.08	0.11	0.08	0.05	0.05	0.05	0.11	0.08	0.08	0.08	0.24
TiO2	0.18	0.13	0.19	0.21	0.21	0.18	0.18	0.18	0.22	0.22	0.22	0.14	0.14	0.12	0.12	0.14
Al2O3	15.72	14.68	14.02	14.2	14.62	17.34	16.97	16.71	23.1	22.29	22.81	24.52	24.74	24.84	17.57	18.21
FeOT	22.77	24.03	23.65	21.15	20.09	18.7	21.76	22.62	14.73	14.87	14.82	14.85	15	15.48	18.35	16.71
MnO	0.34	0.36	0.29	0.2	0.18	0.1	0.22	0.28	0.1	0.1	0.1	0.13	0.1	0.13	0.18	0.13
MgO	9.41	9.2	8.89	10.61	11.14	12.23	10.21	9.58	15.58	15.28	15.55	15.48	15.61	15.28	13.01	14.01
CaO	0.03	0.04	0.03	0.01	0.01	0.01	0.01	0.01	0.01	0.01	0.01	0.01	0.01	0.01	0.01	0.08
Cr2O3	51.57	51.31	52.2	54.13	54.15	51.11	50.42	50.5	47.09	47.51	46.37	44.85	45.01	44.61	50.28	49.86
NiO	0.01	0.06	0.03	0.04	0.07	0.1	0.06	0.06	0.17	0.17	0.16	0.17	0.12	0.09	0.07	0.07
TOTAL	100.22	100.21	99.91	100.63	100.55	99.85	99.94	100.02	101.05	100.5	100.09	100.26	100.81	100.64	99.67	99.45
Formula Units (32 Oxygens)																
Si	0.049	0.105	0.161	0.021	0.021	0.020	0.028	0.021	0.012	0.012	0.012	0.027	0.019	0.019	0.020	0.060
Ti	0.035	0.026	0.038	0.041	0.041	0.035	0.035	0.035	0.040	0.040	0.040	0.025	0.025	0.022	0.023	0.027
Al	4.82	4.54	4.35	4.34	4.44	5.20	5.17	5.11	6.56	6.39	6.54	6.97	6.99	7.04	5.26	5.40
FeT	4.95	5.27	5.21	4.58	4.33	3.98	4.70	4.91	2.97	3.02	3.01	2.99	3.01	3.11	3.90	3.52
Mn	0.076	0.081	0.065	0.045	0.040	0.021	0.048	0.061	0.021	0.021	0.022	0.027	0.020	0.027	0.039	0.028
Mg	3.65	3.60	3.49	4.10	4.28	4.64	3.93	3.70	5.59	5.54	5.64	5.56	5.58	5.48	4.92	5.26
Ca	0.008	0.011	0.009	0.003	0.003	0.003	0.003	0.003	0.003	0.003	0.003	0.003	0.003	0.003	0.003	0.022
Cr	10.61	10.64	10.87	11.09	11.03	10.28	10.29	10.36	8.96	9.13	8.92	8.55	8.53	8.48	10.10	9.92
Ni	0.002	0.013	0.006	0.008	0.015	0.021	0.013	0.013	0.033	0.033	0.031	0.033	0.023	0.017	0.014	0.014
TOTAL	24.20	24.28	24.19	24.23	24.20	24.20	24.21	24.21	24.19	24.19	24.22	24.19	24.20	24.20	24.28	24.25
Recalculated Analysis																
Si	0.049	0.104	0.159	0.021	0.020	0.020	0.028	0.021	0.012	0.012	0.012	0.026	0.019	0.019	0.020	0.060
Al	4.78	4.49	4.32	4.30	4.40	5.16	5.12	5.07	6.51	6.34	6.48	6.92	6.94	6.98	5.20	5.35
Cr	10.52	10.52	10.78	10.99	10.94	10.20	10.20	10.27	8.89	9.06	8.84	8.48	8.46	8.41	9.98	9.82
FeIII	0.53	0.73	0.51	0.59	0.53	0.53	0.55	0.55	0.49	0.49	0.57	0.50	0.51	0.52	0.73	0.65
Ti	0.035	0.025	0.037	0.041	0.040	0.034	0.035	0.035	0.040	0.040	0.040	0.025	0.025	0.022	0.023	0.026
Mg	3.62	3.55	3.46	4.06	4.24	4.60	3.89	3.67	5.55	5.49	5.59	5.52	5.53	5.43	4.87	5.20
FeII	4.38	4.48	4.66	3.95	3.77	3.42	4.11	4.31	2.45	2.51	2.42	2.47	2.47	2.57	3.13	2.83
Ni	0.002	0.013	0.006	0.008	0.014	0.020	0.012	0.012	0.033	0.033	0.031	0.033	0.023	0.017	0.014	0.014
Mn	0.075	0.080	0.064	0.044	0.040	0.020	0.047	0.061	0.021	0.020	0.021	0.027	0.020	0.027	0.038	0.028
Ca	0.008	0.011	0.008	0.003	0.003	0.003	0.003	0.003	0.003	0.003	0.003	0.003	0.003	0.003	0.003	0.021

SAMPLE	*1312c*	*1301a*	*1301b*	*1301c*	*1408a*	*1408b*	*1408c*	*1316a*	*1316b*	*1316c*	*109a*	*109b*	*109c*	*1392a*	*1392b*	*1392c*
Wt.% Oxide																
SiO2	0.11	0.08	0.08	0.05	0.08	0.08	0.08	0.24	0.08	0.08	0.11	0.13	0.05	0.11	0.08	0.08
TiO2	0.14	0.15	0.15	0.15	0.15	0.17	0.14	0.2	0.18	0.18	0.14	0.14	0.14	0.23	0.22	0.23
Al2O3	17.81	18.83	18.93	18.89	19.16	19.5	17.96	17.24	17.93	17.39	16.2	18.5	19.94	21.15	20.8	21.07
FeOT	19.2	15.55	14.7	14.56	13.76	13.69	13.79	13.21	13.31	13.3	15.08	14.46	14.76	15.79	15.64	15.62
MnO	0.21	0.15	0.13	0.11	0.11	0.08	0.11	0.1	0.11	0.08	0.08	0.11	0.12	0.1	0.12	0.13
MgO	12.39	14.06	14.36	14.26	14.96	15.15	14.73	14.68	15.4	15.32	13.36	14.43	14.78	14.77	14.72	14.65
CaO	0.03	0.01	0.01	0.01	0.01	0.01	0.03	0.03	0.01	0.03	0.03	0.13	0.01	0.01	0.01	0.01
Cr2O3	49.66	50.93	50.67	50.63	51.07	51.4	53.31	51.56	52.63	52.72	53.93	50.42	49.68	47.51	47.52	47.42
NiO	0.06	0.13	0.13	0.13	0.12	0.13	0.1	0.12	0.13	0.09	0.09	0.16	0.17	0.13	0.13	0.1
TOTAL	99.61	99.89	99.16	98.79	99.42	100.21	100.25	97.38	99.78	99.19	99.02	98.48	99.65	99.8	99.24	99.31
Formula Units (32 Oxygens)																
Si	0.028	0.020	0.020	0.013	0.020	0.020	0.020	0.061	0.020	0.020	0.028	0.033	0.012	0.027	0.020	0.020
Ti	0.027	0.028	0.028	0.028	0.028	0.032	0.026	0.038	0.034	0.034	0.027	0.027	0.026	0.043	0.041	0.043
Al	5.35	5.54	5.59	5.59	5.61	5.66	5.25	5.18	5.25	5.13	4.86	5.50	5.83	6.15	6.09	6.16
FeT	4.09	3.24	3.08	3.06	2.86	2.82	2.86	2.82	2.76	2.78	3.21	3.05	3.06	3.26	3.25	3.24
Mn	0.046	0.031	0.027	0.023	0.022	0.018	0.022	0.022	0.023	0.017	0.018	0.023	0.026	0.021	0.025	0.027
Mg	4.70	5.23	5.36	5.34	5.54	5.56	5.44	5.58	5.70	5.72	5.07	5.42	5.46	5.43	5.45	5.41
Ca	0.008	0.003	0.003	0.003	0.003	0.003	0.008	0.008	0.003	0.008	0.008	0.035	0.003	0.003	0.003	0.003
Cr	10.00	10.04	10.02	10.05	10.03	10.00	10.45	10.39	10.33	10.43	10.85	10.05	9.73	9.27	9.33	9.29
Ni	0.012	0.026	0.026	0.026	0.024	0.026	0.020	0.025	0.026	0.018	0.018	0.032	0.034	0.026	0.026	0.020
TOTAL	24.27	24.16	24.15	24.14	24.13	24.12	24.10	24.12	24.15	24.16	24.09	24.17	24.18	24.22	24.23	24.21
Recalculated Analysis																
Si	0.028	0.020	0.020	0.013	0.020	0.020	0.020	0.061	0.020	0.020	0.028	0.033	0.012	0.027	0.020	0.020
Al	5.29	5.50	5.55	5.56	5.58	5.63	5.23	5.16	5.22	5.10	4.84	5.46	5.78	6.09	6.03	6.10
Cr	9.89	9.98	9.96	10.00	9.97	9.95	10.41	10.34	10.27	10.36	10.81	9.98	9.66	9.18	9.24	9.21
FeIII	0.70	0.42	0.39	0.36	0.35	0.32	0.27	0.31	0.41	0.43	0.24	0.44	0.48	0.58	0.60	0.56
Ti	0.027	0.028	0.028	0.028	0.028	0.031	0.026	0.038	0.033	0.034	0.027	0.026	0.026	0.042	0.041	0.043
Mg	4.65	5.19	5.32	5.31	5.51	5.53	5.42	5.55	5.66	5.68	5.05	5.38	5.42	5.38	5.40	5.36
FeII	3.34	2.80	2.67	2.68	2.49	2.48	2.58	2.50	2.34	2.34	2.96	2.59	2.56	2.65	2.62	2.65
Ni	0.012	0.026	0.026	0.026	0.024	0.026	0.020	0.025	0.026	0.018	0.018	0.032	0.034	0.026	0.026	0.020
Mn	0.045	0.031	0.027	0.023	0.022	0.018	0.022	0.022	0.023	0.017	0.018	0.023	0.025	0.021	0.025	0.027
Ca	0.008	0.003	0.003	0.003	0.003	0.003	0.008	0.008	0.003	0.008	0.008	0.035	0.003	0.003	0.003	0.003

SAMPLE	*3683a*	*3683b*	*3683c*	*1332a*	*1332b*	*1332c*	*1320a*	*1320b*	*1320c*	*1386Aa*	*1386Ab*	*1386Ab*	*1400a*	*1400b*	*1400c*	*1395a*
Wt.% Oxide																
SiO2	0.08	0.08	0.08	0.08	0.05	0.05	0.08	0.08	0.08	0.11	0.08	0.11	0.08	0.05	0.08	0.08
TiO2	0.19	0.19	0.19	0.29	0.29	0.29	0.18	0.2	0.18	0.31	0.28	0.32	0.23	0.23	0.26	0.18
Al2O3	28.99	28.55	25.81	18.61	18.74	18.72	17.93	18.01	18.11	21.35	21.25	21.06	17.77	16.05	16.72	12.84
FeOT	13.68	13.85	14.13	15.22	15.14	14.92	16.21	16.63	16.44	16.46	16.44	16.78	18.59	20.16	19.02	20.44
MnO	0.08	0.12	0.09	0.13	0.12	0.13	0.12	0.15	0.15	0.15	0.16	0.13	0.15	0.18	0.19	0.2
MgO	16.61	16.43	15.8	14.51	14.75	14.84	14.23	14.09	14.07	14.68	14.27	14.35	12.17	11.1	11.74	10.85
CaO	0.01	0.01	0.01	0.03	0.03	0.01	0.01	0.01	0.01	0.01	0.01	0.01	0.04	0.03	0.03	0.01
Cr2O3	40.35	40.98	43.27	50.68	50.53	50.68	51.03	49.9	50.77	47.09	46.89	46.76	49.67	51.03	51.09	54.79
NiO	0.15	0.12	0.09	0.12	0.13	0.1	0.12	0.12	0.1	0.09	0.1	0.12	0.09	0.07	0.06	0.04
TOTAL	100.14	100.33	99.47	99.67	99.78	99.74	99.91	99.19	99.91	100.25	99.46	99.64	99.79	98.9	99.19	99.43
Formula Units (32 Oxygens)																
Si	0.019	0.019	0.019	0.020	0.013	0.012	0.020	0.020	0.020	0.027	0.020	0.027	0.021	0.013	0.021	0.021
Ti	0.034	0.034	0.034	0.054	0.054	0.054	0.034	0.038	0.034	0.057	0.052	0.060	0.044	0.045	0.050	0.036
Al	8.04	7.93	7.33	5.48	5.50	5.49	5.30	5.37	5.35	6.19	6.21	6.16	5.37	4.92	5.07	3.98
FeT	2.69	2.73	2.85	3.18	3.15	3.11	3.40	3.51	3.45	3.38	3.41	3.48	3.99	4.39	4.09	4.50
Mn	0.016	0.023	0.018	0.027	0.025	0.027	0.025	0.032	0.031	0.032	0.034	0.028	0.033	0.039	0.041	0.045
Mg	5.83	5.77	5.67	5.40	5.48	5.51	5.32	5.31	5.26	5.38	5.28	5.30	4.65	4.30	4.50	4.26
Ca	0.003	0.003	0.003	0.008	0.008	0.003	0.003	0.003	0.003	0.003	0.003	0.003	0.011	0.008	0.008	0.003
Cr	7.51	7.63	8.24	10.00	9.95	9.97	10.12	9.97	10.07	9.15	9.19	9.17	10.07	10.50	10.39	11.40
Ni	0.028	0.023	0.017	0.024	0.026	0.020	0.024	0.024	0.020	0.018	0.020	0.024	0.019	0.015	0.012	0.009
TOTAL	24.17	24.17	24.17	24.19	24.21	24.20	24.24	24.27	24.24	24.24	24.22	24.25	24.21	24.23	24.20	24.25
Recalculated Analysis																
Si	0.019	0.019	0.019	0.020	0.012	0.012	0.020	0.020	0.020	0.027	0.020	0.027	0.020	0.013	0.020	0.021
Al	7.99	7.88	7.28	5.43	5.46	5.45	5.25	5.31	5.30	6.13	6.16	6.09	5.33	4.88	5.03	3.94
Cr	7.46	7.58	8.18	9.92	9.86	9.89	10.02	9.86	9.97	9.06	9.11	9.07	9.98	10.40	10.31	11.28
FeIII	0.45	0.43	0.44	0.49	0.54	0.52	0.62	0.71	0.62	0.64	0.58	0.65	0.56	0.61	0.51	0.66
Ti	0.033	0.034	0.034	0.054	0.054	0.054	0.034	0.038	0.034	0.057	0.052	0.059	0.044	0.045	0.050	0.035
Mg	5.79	5.73	5.63	5.36	5.43	5.46	5.27	5.25	5.21	5.33	5.23	5.25	4.61	4.26	4.47	4.21
FeII	2.22	2.28	2.39	2.66	2.58	2.56	2.74	2.76	2.80	2.71	2.79	2.79	3.40	3.74	3.55	3.80
Ni	0.028	0.023	0.017	0.024	0.026	0.020	0.024	0.024	0.020	0.018	0.020	0.024	0.018	0.015	0.012	0.008
Mn	0.016	0.023	0.018	0.027	0.025	0.027	0.024	0.032	0.031	0.031	0.034	0.028	0.033	0.038	0.040	0.044
Ca	0.003	0.003	0.003	0.008	0.008	0.003	0.003	0.003	0.003	0.003	0.003	0.003	0.011	0.008	0.008	0.003

SAMPLE	*1395b*	*1395c*	*1333Ba*	*1333Bb*	*1333Bc*	*MIDa*	*MIDb*	*MIDc*	*U83a*	*U83b*	*U83c*	*U403a*	*U403b*	*U403c*	*1364a*	*1364b*
Wt.% Oxide																
SiO2	0.05	0.11	0.11	0.11	0.11	0.08	0.05	0.08	0.05	0.27	0.08	0.08	0.11	0.11	0.08	0.05
TiO2	0.19	0.18	0.29	0.29	0.29	0.23	0.23	0.23	0.2	0.17	0.2	0.26	0.28	0.25	0.17	0.15
Al2O3	13.27	12.76	20.87	20.87	20.62	22.04	21.68	21.67	20.74	19.47	20.55	24.51	24.54	24.37	20.45	19.36
FeOT	19.08	20.39	14.56	14.9	14.39	14.76	15.19	14.79	17.16	21.29	17.16	15.68	16.19	16.58	16.04	15.77
MnO	0.18	0.21	0.09	0.09	0.11	0.1	0.1	0.13	0.16	0.24	0.14	0.14	0.14	0.14	0.12	0.13
MgO	11.57	10.69	15.72	15.53	15.66	15.67	15.34	15.36	13.96	11.22	13.86	15.14	14.93	14.82	14.31	14.03
CaO	0.01	0.01	0.01	0.01	0.01	0.03	0.01	0.01	0.03	0.01	0.03	0.01	0.01	0.03	0.04	0.03
Cr2O3	55.05	54.8	48.95	48.62	48.78	47.08	46.75	46.92	46.91	46.25	47.06	43.71	43.19	43.42	47.55	48.85
NiO	0.09	0.04	0.15	0.16	0.09	0.17	0.16	0.13	0.12	0.1	0.13	0.16	0.16	0.13	0.12	0.1
TOTAL	99.49	99.19	100.75	100.58	100.06	100.16	99.51	99.32	99.33	99.01	99.21	99.69	99.55	99.85	98.88	98.47
Formula Units (32 Oxygens)																
Si	0.013	0.029	0.027	0.027	0.027	0.020	0.012	0.020	0.013	0.069	0.020	0.019	0.027	0.027	0.020	0.013
Ti	0.037	0.036	0.053	0.053	0.054	0.042	0.043	0.043	0.038	0.033	0.038	0.048	0.051	0.046	0.032	0.029
Al	4.08	3.97	5.99	6.01	5.96	6.33	6.29	6.29	6.11	5.88	6.06	7.02	7.05	7.00	6.03	5.76
FeT	4.17	4.50	2.96	3.04	2.95	3.01	3.13	3.05	3.58	4.56	3.59	3.19	3.30	3.38	3.36	3.33
Mn	0.040	0.047	0.019	0.018	0.024	0.021	0.022	0.028	0.034	0.051	0.030	0.028	0.028	0.028	0.025	0.029
Mg	4.50	4.20	5.70	5.65	5.72	5.69	5.63	5.64	5.20	4.28	5.17	5.48	5.42	5.38	5.33	5.28
Ca	0.003	0.003	0.003	0.003	0.003	0.008	0.003	0.003	0.008	0.003	0.008	0.003	0.003	0.008	0.011	0.008
Cr	11.36	11.43	9.42	9.39	9.45	9.07	9.10	9.13	9.26	9.37	9.31	8.40	8.32	8.36	9.40	9.74
Ni	0.019	0.009	0.029	0.031	0.018	0.033	0.032	0.026	0.024	0.021	0.026	0.031	0.031	0.026	0.024	0.020
TOTAL	24.23	24.23	24.21	24.22	24.21	24.23	24.25	24.23	24.27	24.27	24.26	24.22	24.24	24.25	24.23	24.21
Recalculated Analysis																
Si	0.013	0.029	0.027	0.027	0.027	0.019	0.012	0.020	0.012	0.068	0.020	0.019	0.027	0.027	0.020	0.013
Al	4.05	3.93	5.94	5.95	5.91	6.27	6.23	6.23	6.04	5.82	6.00	6.96	6.98	6.93	5.97	5.71
Cr	11.26	11.32	9.34	9.30	9.37	8.99	9.00	9.05	9.16	9.26	9.21	8.32	8.24	8.27	9.31	9.66
FeIII	0.59	0.61	0.56	0.58	0.56	0.61	0.66	0.59	0.69	0.71	0.67	0.58	0.62	0.65	0.61	0.54
Ti	0.037	0.035	0.053	0.053	0.053	0.042	0.042	0.042	0.037	0.032	0.037	0.047	0.051	0.045	0.032	0.028
Mg	4.46	4.16	5.65	5.60	5.67	5.64	5.57	5.58	5.14	4.24	5.11	5.43	5.37	5.32	5.28	5.23
FeII	3.53	3.85	2.38	2.43	2.37	2.37	2.44	2.43	2.85	3.80	2.89	2.58	2.65	2.69	2.71	2.76
Ni	0.019	0.008	0.029	0.031	0.018	0.033	0.031	0.026	0.024	0.020	0.026	0.031	0.031	0.025	0.024	0.020
Mn	0.039	0.047	0.019	0.018	0.024	0.021	0.021	0.027	0.034	0.050	0.030	0.028	0.028	0.028	0.025	0.029
Ca	0.003	0.003	0.003	0.003	0.003	0.008	0.003	0.003	0.008	0.003	0.008	0.003	0.003	0.008	0.011	0.008

SAMPLE	*1364c*	*1361a*	*1361b*	*1361c*	*1365a*	*1365b*	*1365c*	*1366a*	*1366b*	*1366c*	*1368a*	*1368b*	*1368c*
Wt.% Oxide													
SiO2	0.08	0.08	0.08	0.05	0.05	0.05	0.08	0.08	0.08	0.08	0.13	0.13	0.11
TiO2	0.14	0.2	0.2	0.2	0.23	0.22	0.22	0.22	0.22	0.2	0.17	0.18	0.2
Al2O3	15.74	25.06	25.44	25.22	20.94	22.15	21.49	23.5	23.19	22.98	17.8	18.54	18.99
FeOT	17.12	15.95	15.12	15.57	15.22	15.64	15.34	16.74	16.85	18.18	14.96	14.89	15.69
MnO	0.14	0.12	0.12	0.11	0.12	0.14	0.12	0.13	0.14	0.14	0.11	0.11	0.13
MgO	12.79	14.63	15.08	15.02	15.02	14.9	15.1	13.93	14.16	13.25	13.97	14.18	13.98
CaO	0.04	0.03	0.03	0.03	0.01	0.01	0.01	0.03	0.01	0.03	0.03	0.01	0.01
Cr2O3	52.63	42.36	42.46	42.79	47.44	45.76	46.69	44.16	44.39	44.05	52.18	51.39	50.9
NiO	0.09	0.13	0.16	0.13	0.13	0.07	0.12	0.13	0.12	0.1	0.09	0.09	0.09
TOTAL	98.77	98.56	98.69	99.12	99.16	98.94	99.17	98.92	99.16	99.01	99.44	99.52	100.1
Formula Units (32 Oxygens)													
Si	0.021	0.020	0.020	0.012	0.012	0.012	0.020	0.020	0.020	0.020	0.033	0.033	0.027
Ti	0.027	0.037	0.037	0.037	0.043	0.041	0.041	0.041	0.041	0.038	0.032	0.034	0.037
Al	4.78	7.25	7.32	7.24	6.12	6.46	6.27	6.85	6.75	6.75	5.27	5.46	5.57
FeT	3.69	3.27	3.08	3.17	3.16	3.24	3.17	3.46	3.48	3.79	3.14	3.11	3.27
Mn	0.030	0.025	0.025	0.023	0.025	0.029	0.026	0.028	0.030	0.030	0.024	0.024	0.027
Mg	4.91	5.35	5.48	5.45	5.55	5.49	5.56	5.13	5.21	4.92	5.23	5.28	5.18
Ca	0.011	0.008	0.008	0.008	0.003	0.003	0.003	0.008	0.003	0.008	0.008	0.003	0.003
Cr	10.72	8.22	8.19	8.24	9.30	8.95	9.13	8.63	8.67	8.67	10.36	10.15	10.01
Ni	0.019	0.026	0.031	0.026	0.026	0.014	0.024	0.026	0.024	0.020	0.018	0.018	0.018
TOTAL	24.20	24.21	24.19	24.21	24.23	24.24	24.24	24.20	24.23	24.23	24.12	24.12	24.14
Recalculated Analysis													
Si	0.020	0.019	0.019	0.012	0.012	0.012	0.020	0.020	0.020	0.020	0.033	0.032	0.027
Al	4.74	7.19	7.26	7.18	6.06	6.40	6.20	6.79	6.69	6.68	5.24	5.44	5.54
Cr	10.63	8.15	8.12	8.17	9.21	8.86	9.04	8.56	8.59	8.59	10.31	10.10	9.95
FeIII	0.53	0.55	0.50	0.55	0.61	0.63	0.64	0.52	0.60	0.61	0.31	0.33	0.38
Ti	0.027	0.037	0.036	0.036	0.043	0.041	0.041	0.041	0.041	0.037	0.032	0.034	0.037
Mg	4.87	5.30	5.44	5.40	5.50	5.44	5.51	5.09	5.16	4.87	5.20	5.26	5.15
FeII	3.12	2.70	2.56	2.59	2.51	2.57	2.51	2.91	2.85	3.14	2.81	2.77	2.87
Ni	0.018	0.026	0.031	0.025	0.026	0.014	0.024	0.026	0.024	0.020	0.018	0.018	0.018
Mn	0.030	0.025	0.025	0.022	0.025	0.028	0.026	0.028	0.030	0.030	0.024	0.024	0.026
Ca	0.011	0.008	0.008	0.008	0.003	0.003	0.003	0.008	0.003	0.008	0.008	0.003	0.003

TAG	SAMPLE	ROCK	LOCALITY	COMENTS	TRACE ELEMENT ANALYSES (ALL IN PPM)									
					Pt	Pd	Ir	Au	As	Cr	Cu	Ni	Co	Sb
CQ	RL001	chromitite	Cliff	massive, minor GM	0.76	1.12	0.12	0.021	16	148604	0	2298	187	1.4
CQ	RL003	chromitite	Cliff	nodular, sheared, kamm	0.23	0.16	0.03	0	12	176591	0	2441	143	1.2
DU	RL004a	dunite	(d)	typical	0	0	0	0	0	3376	31	2041	138	0
DU	RL005aR	dunite	(a)	S	0	0	0	0	0	1394	14	1775	141	0
DU	RL006a	dunite	(a)	CrED, chl R	0	0	0	0	0	1884	23	1801	139	0
DU	RL007	dunite	(a)	typical	0	0	0	0	0	534	0	1793	138	0
PQ	RL009	chromitite	Harold	v massive	0.14	0	0.38	0	0	263393	0	1404	201	1.2
DU	RL010a	dunite	(b)	CrED, Cr lay	0	0	0	0	0	5458	14	2330	131	0.8
DU	RL011	dunite	(b)	S	0	0	0	0	0	2855	38	2274	140	0
DU	RL013a	dunite	(b)	CrED, chl R, S	0	0	0	0	0	3440	112	2286	134	1
DU	RL016a	dunite	(c)	CrED, chl R, S	0	0	0	0.015	0	5104	70	2153	135	0
DU	RL018a	dunite	(c)	chl R, S	0	0	0	0	0	4023	62	2455	130	0
DU	RL019	dunite	(c)	typical	0	0	0	0	0	4547	23	2231	129	0
DU	RL020	dunite	(d)	CrED, chl R	0	0	0	0	0	4494	27	2165	132	0
PQ	RL021	dunite/chr	Quarries	multiple Cr lay, minor GM	0	0	0	0	0	13826	11	2976	121	0
PQ	RL022	chromitite	drift nr QU 12	massive	0.39	0.63	0.07	0.021	40	299036	261	4174	216	4
DU	RL023	dunite	nr Qu 12	typical	0.02	0	0	0	0	3983	13	2224	123	0
DU	RL024a	dunite	(e)	CrED, Cr lay	0	0	0	0	0	5734	18	2378	105	0
DU	RL025	dunite	(e)	CrED, chl R, S	0	0	0	0	0	3430	135	2137	134	0
DU	RL026	dunite/harz.	(e)	CrED, harz. layer in DU	0	0	0	0	0	3009	76	2207	122	0
DU	RL027a	dunite	(e)	SR, fresh portion	0	0	0	0	0	3149	58	2902	158	0
DU	RL027b	dunite	(e)	SR, weathered portion	0	0	0	0	0	2476	77	3206	151	0
DU	RL028	dunite/vein	(e)	S, Chlorite veins sampled	0	0	0	0	0	4997	38	2607	119	0
DU	RL029a	dunite	(e)	typical	0	0	0	0	0	3823	16	2394	134	0
TH	RL030	dunite/harz.	S. of Little Heog	segregated, (a) harz. layer	0	0	0	0	0	1665	0	2472	107	0
TH	RL031	dunite/harz.	S. of Little Heog	(b) dunite layer, CrED, S	0	0	0	0	0	5571	7	2523	118	0
TH	RL032	dunite	S. of Little Heog	CrED, dunite podlet	0	0	0	0	0	9471	9	2611	119	0
TH	RL033	dunite/harz.	Little Heog pod	seg. above pod (a) harz. lay.	0	0	0	0	0	2111	0	2511	105	0
TH	RLO34	dunite/harz.	Little Heog pod	seg. above pod (b) dunite lay.	0	0	0	0	0	3205	0	2880	110	0
TH	RL035	dunite/harz.	Little Heog pod	patchy (a) dunite lay./dyke	0	0	0	0	0	4309	11	2832	126	0
TH	RL036	dunite/harz.	Little Heog pod	patchy (b) harz. host	0	0	0	0	0	1981	9	2406	117	0
TH	RL037	dunite/harz.	Little Heog pod	seg. below pod (a) dunite lay.	0	0	0	0	0	1589	0	3208	n.a.	n.a.
TH	RL038	dunite/harz.	Little Heog pod	seg. below pod (b) harz. lay.	0	0	0	0	0	1921	0	2448	n.a.	n.a.
DP	RLO41	dunite	Little Heog pod	typical, middle of pod	0	0	0	0	0	1669	8	2718	122	0
DP	RLO43	dunite	Little Heog pod	nr CrED, nr. base of pod	0	0	0	0	0	2214	0	2851	109	0

TAG	SAMPLE	ROCK	LOCALITY	COMENTS	TRACE ELEMENT ANALYSES (ALL IN PPM)									
					Pt	*Pd*	*Ir*	*Au*	*As*	*Cr*	*Cu*	*Ni*	*Co*	*Sb*
DP	RL044	dunite	Little Heog pod	nr CrED, nr. base of pod	0	0	0	0	0	1424	8	2744	128	0.2
DP	RL045	dunite	Little Heog pod	nr CrED, nr. base of pod	0	0	0	0	0	1508	0	2812	118	0
DP	RL046	dunite	Little Heog pod	typical, nr. base of pod	0	0	0	0	0	1593	0	2793	299	0.3
H	RL047	harzburgite	Little Heog pod	above pod	0	0	0	0	0	1989	0	2436	107	0
H	RL048	harzburgite	Little Heog pod	below pod	0	0	0	0	0	2037	19	2442	113	0
TH	RL049	dunite/harz.	Little Heog pod	dunite podlet above pod, S	0	0	0	0	0	1571	19	2945	n.a.	0
A	RL050	serpentinite	Little Heog	Cr/mnt, S	0	0	0	0.042	848	5018	50	1754	336	16.9
G	RL052	gabbro	Ordale	typical	0	0	0	0.015	0	751	16	140	108	0
G	RL054	dyke	Ordale	tourmaline? bearing	0	0	0	0	54	66	42	63	52	1.9
G	RL055	gabbro	Ordale	altered or mafic	0	0	0	0	15	93	82	0	123	0
G	RL056	gabbro	Ordale	altered/mafic, nr. shear zone	0	0	0	0	0	665	8	153	110	0
HLC	RL057	H. L. wehrlite	Ordale	v. altered, 3 opaques, S	0	0	0	0	27	2985	43	2069	220	0.5
HLC	RL058	H. L. wehrlite	Ordale	v. altered	0	0	0	0	9	2789	55	2087	200	0.4
A	RL059	gossan	Ordale	middle of shear zone	0	0	0	0	34	4279	114	2929	n.a.	n.a.
HLC	RL060	H.L.pyroxenite	Ordale	raft in shear zone	0.07	0.12	0	0	0	3881	23	627	61	0.85
G	RL061	gabbro	Ordale	SR, nr serpentinite zone	0	0	0	0	0	188	173	42	50	0
A	RL064	serp. / harz.	Little Heog	sheared, brown, silver mins	0	0	0	0	900	1859	20	2001	123	7.5
A	RL065	serp. / harz.	Little Heog	silicified, red weathering	0	0	0	0	36	2898	17	1728	121	0.8
A	RL066	serp. / harz.	Little Heog	S, CO3, sheared	0	0	0	0	110	5077	365	2245	127	1.6
PQ	RL068	chromitite	Harold's Grave	(a) Cr lay weathered surface	0.31	0.02	0.56	0	10	187899	0	1408	232	1.9
PQ	RL069	dunite/chr	Harold's Grave	(b) dunite host to Cr layer	0.08	0	0.13	0	0	28055	18	2346	119	1.7
PQ	RL070	chromitite	Harold's Grave	(c) fresh	0.18	0.03	0.35	0	3	79812	9	2039	156	1.5
H	RL071	harzburgite	H.G trav. edge of pit	Cr & ol rich	0	0	0	0	0	1721	0	2504	108	0
H	RL072	harzburgite	H.G traverse S +3m	typical	0	0	0	0	0	1842	0	2369	103	0
H	RL073	harzburgite	H.G traverse S +7m	typical	0	0	0	0	0	2077	12	2344	106	0
H	RL074	harzburgite	H.G traverse S +5m	typical	0	0	0	0	0	2201	0	2398	108	0
H	RL075	harzburgite	H.G traverse N +5.5m	typical	0	0	0	0	0	1505	0	2639	114	0
H	RL076	harzburgite	H.G traverse N +5.5m	typical	0	0	0	0	0	2245	0	2467	110	0
H	RL077	harzburgite	H.G traverse N +6m	typical	0	0	0	0.012	0	2223	0	2444	102	0
H	RL078	harzburgite	H.G traverse N +6m	typical	0	0	0	0	0	1929	9	2456	100	0
H	RL080	harzburgite	H.G traverse N +4m	Cr, S, in dunite layer	0	0	0	0.013	0	1913	101	2689	116	0
A	RL082	pyrox. breccia	Skeo Taing, Ordale	fault breccia, mnt, Si, CO3	0.02	0	0	0	23	3935	6	404	482	0.5
C	RL083	pyroxenite	Skeo Taing, Ordale	serpentinised	0	0	0	0	0	4077	0	520	56	0.3
C	RL085	pyroxenite	Skeo Taing, Ordale	serpentinised, coarse	0.02	0	0	0.012	42	5024	15	387	63	2.2
C	RL086	pyroxenite	Skeo Taing, Ordale	serpentinised, S?	0	0	0	0	4	5782	14	354	58	0.7

TAG	SAMPLE	ROCK	LOCALITY	COMENTS	TRACE ELEMENT ANALYSES (ALL IN PPM)									
					Pt	*Pd*	*Ir*	*Au*	*As*	*Cr*	*Cu*	*Ni*	*Co*	*Sb*
A	RL089	serp/pyrox.	Skeo Taing, Ordale	sheared,serp., black, Cr	0	0	0	0	5	4276	11	735	110	1
C	RL090	pyroxenite	Skeo Taing, Ordale	pink/grey	0.03	0	0.02	0	0	4446	0	477	63	2
A	RL093	serp/pyrox.	Skeo Taing, Ordale	yellowy/black, Cr	0	0	0	0	0	2927	8	1150	109	3.6
C	RL095	wehrlite	Skeo Taing, Ordale	layered, pink, S	0.03	0.03	0	0	21	2878	0	637	99	2.2
C	RL096	dun/wehr	Ordale trav. E to W	first exposure	0	0	0	0	0	1440	0	1663	142	0
A	RL097	serp/pyrox.	Ordale	platey dk. green serp.,antig.?	0	0	0	0.015	15	2827	14	1243	122	9
A	RL098	serpentinite	Ordale	S, serp. zone, nr RL061	0	0	0	0.012	6	3954	194	1328	133	5.7
C	RL099	dun/wehr.	Ordale traverse	last WD exposure, large px	0	0	0.03	0	0	2389	0	1393	148	0
C	RL100	wehr/pyrox	Ordale traverse +6m	plag. B	0	0	0	0	0	3122	0	750	68	0.8
C	RL101	pyroxenite	Ordale trav. +0.5m	plag B, fine green px	0	0	0	0	0	4689	0	532	50	0.9
C	RL102	dun/wehr	Ordale trav. +0.5m	typical	0	0	0	0	0	1694	0	1519	100	0.7
C	RL103	pyroxenite	Ordale trav. +100m	typical	0	0	0	0	0	4658	8	381	55	0
C	RL104	wehrlite	Ordale trav. +1.5m	pink	0.05	0.03	0.2	0	0	3039	17	697	103	0
C	RL105	pyroxenite	Ordale trav. +3m	coarse, massive	0	0	0	0.024	26	3173	89	383	40	0
PQ	RLM001	dunite	Nikka Vord S, Qu 6	S, black	0	0	0	0.026	0	1480	61	2738	120	25.7
PQ	RLM002	dunite/chr	Nikka Vord S, Qu 6	S, layered dis. chr, GM	0.08	0.16	0.06	0.012	6	104229	63	3941	236	12.9
PQ	RLM003	chromitite	Nikka Vord S, Qu 6	S, massive	0.05	0	0.07	0	0	311457	0	1869	258	10.7
PQ	RLM004	dunite/chr	Nikka Vord S, Qu 6	S, layered dis. chr, GM	0.17	0.33	0.09	0.033	6	126392	427	4057	159	6
PQ	RLM005	harzburgite	Nikka Vord S, Qu 6	altered, mnt veins	0	0	0	0.027	0	3460	7	2104	99	7.2
PQ	RLM006	dunite/chr	Nikka Vord S, Qu 6	dis chr, no S, yellow matrix	0	0	0	0.029	10	150337	17	2539	168	2.2
DQ	RLM007	dunite/chr	Jimmie's Qu 19	lay dis chr, GM, S	0.58	1.06	0.09	0.135	9	98479	371	3720	154	8.7
DQ	RLM008	wehrlite	Jimmie's Qu 19	S, altered	0	0.03	0	0.015	0	5831	99	2509	95	3.2
DQ	RLM009	chromitite	Jimmie's Qu 19	composite, mass chr or lay	0.09	0	0.05	0.015	14	309513	0	1344	225	3.8
DQ	RLM010	dunite	Jimmie's Qu 19	S, typical	0	0	0	0	0	5050	20	2666	123	3.6
DQ	RLM011	dunite/chr	Jimmie's Qu 19	lay dis chr, no GM, ?S	0.08	0	0.02	0	7	73951	33	2323	154	2.3
PQ	RLM012	dunite/chr	Nikka Vord S, Qu 6	intergrowth texture	0	0	0	0	0	173561	0	1795	200	1.6
C	RLM013	pyroxenite	Keen of Hamar	coarse, massive, S	0	0	0	0	0	6454	23	391	37	3
C	RLM014	wehrlite	Keen of Hamar	px poor, S	0.04	0.04	0	0.043	0	2167	88	1394	165	2.4
C	RLM015	wehr/pyrox	Keen of Hamar	px rich, S,	0	0	0	0	0	3693	337	1126	94	0
C	RLM016	wehr/dunite	Keen of Hamar	px poor, S, layered	0	0	0	0	0	2114	26	1656	122	1.8
C	RLM017	wehr/pyrox	Keen of Hamar	junct. of coarse pyrox. & WD	0	0	0	0	0	3106	27	924	81	1.3
C	RLM018	wehr/dunite	Keen of Hamar	S	0	0	0	0.018	0	1014	147	1801	136	1.2
C	RLM019	wehr/dunite	Keen of Hamar	Cr rich, S	0.02	0.06	0	0.025	0	6362	193	2323	154	2.3
PQ	RLM020	chromitite	Quarry W of Qu 8	massive chr, S, G bloom	0.02	0.03	0	0.021	0	247147	766	4607	209	41
PQ	RLM021	chromitite	Quarry W of Qu 8	massive chr, no S	0	0	0	0	0	284245	0	1605	142	1.5

TAG	SAMPLE	ROCK	LOCALITY	COMENTS	TRACE ELEMENT ANALYSES (ALL IN PPM)									
					Pt	*Pd*	*Ir*	*Au*	*As*	*Cr*	*Cu*	*Ni*	*Co*	*Sb*
PQ	RLM022	dunite	Quarry W of Qu 8	black, few S	0	0	0	0.036	0	3641	32	2707	87	1.3
PQ	RLM023	dunite	Quarry W of Qu 8	black, mod S rich	0	0	0	0.012	4	7287	180	2417	143	2.2
PQ	RLM024	dunite/chr	Quarry W of Qu 8	lay dis chr, no S	0	0	0	0	0	26898	23	2847	134	1
PQ	RLM025	chromitite	Long Quarry, Qu 7	massive chr, no S	0	0	0	0	0	281410	29	1907	197	1.6
PQ	RLM026	dunite	Long Quarry, Qu 7	altered, no S	0	0	0	0	0	11061	20	2712	129	0.6
PQ	RLM027	dunite	Long Quarry, Qu 7	few S	0	0	0	0.019	0	4826	25	2594	111	0.7
DQ	RLM028	dunite	Quarry 11	black, S rich	0	0	0	0	0	3052	73	2458	129	0.8
DQ	RLM029	dunite/chr	Quarry 11	mas/dis chr, S	0.16	0.29	0.04	0.072	0	125030	928	5068	199	0
DQ	RLM030	dunite/chr	Quarry 11	mas/dis chr, no S	0	0	0	0.023	0	174111	0	1838	179	1.8
DQ	RLM031	chromitite	Quarry 11	composite, mas, S rich	0.08	0.14	0.02	0	0	258246	782	4304	231	1.6
DQ	RLM032	chromitite	Quarry 11	composite, mas, S poor	0.29	0.34	0.03	0.021	0	286325	83	1775	196	2.4
DQ	RLM033	dunite	Quarry 14	S	0	0	0	0.026	0	8724	9	2643	102	1.9
DQ	RLM034	dunite	Hagdale Quarry 16	S	0	0	0	0.019	0	6002	343	1790	131	2.5
PQ	RLM035	dunite	Harold's Grave Qu 2	few S	0	0	0	0.021	0	1180	13	2586	87	0
PQ	RLM036	dunite	Harold's Grave Qu 2	typical, no S	0	0	0	0.031	0	2570	9	2563	109	0.7
DU	RLM037	dunite	Quarries area	very S rich	0.02	0.03	0	0.018	0	3853	176	2528	279	1.4
DU	RLM038	dunite	Quarries area	very S rich	0.02	0	0	0.027	0	3217	511	3133	148	9.4
DP	RLM039	dunite	Quarries area	coarse, CrED, nr Qu	0	0	0	0	5	10182	80	2469	133	142
TH	RLM040	dunite/harz	Quarries area	D vein in H, very S & Cr rich	0.03	0.02	0	0.019	0	4105	739	3983	161	8.4
PQ	RLM041	dunite/chr	Nikka Vord East Qu 4	mylonitic fabric, no S	0	0	0	0.01	8	24618	9	2602	142	1.3
PQ	RLM042	dunite	Nikka Vord East Qu 4	typical	0	0	0	0	0	1922	0	2592	113	0
PQ	RLM043	chromitite	Nikka Vord East Qu 4	composite, mas/dis chr	0	0	0	0	0	195042	0	1376	167	0
PQ	RLM044	chromite/mnt	Nikka Vord East Qu 4	minor GP	0	0	0	0.01	13	3273	0	2392	95	0
PQ	RLM045	harzburgite	Nikka Vord East Qu 4	mylonitised, silvery	0	0	0	0.016	10	3043	0	2245	98	0
PQ	RLM046	dunite/chr	Nikka Vord East Qu 4	layered dis chr,	0	0	0	0	4	34224	0	2363	145	0
DQ	RLM047	dunite	Midgarth Quarry 15	one S	0.05	0.06	0	0	5	5702	38	2440	136	0
DQ	RLM048	dunite/chr	Midgarth Quarry 15	dis chr, grey/GM	0	0	0	0.013	5	89503	0	2113	144	0
DQ	RLM049	dunite/chr	Midgarth Quarry 15	junction D/dis chr, GM	0	0	0	0.013	10	61529	20	2407	134	1.1
DQ	RLM050	chromitite	Midgarth Quarry 15	composite, mas/dis, no S	0	0	0	0	0	181066	25	1747	178	0
DQ	RLM051	dunite/chr	Keen of Hamar Qu18N	mas/dis chr, no S, few GB	0	0	0	0.011	0	277434	0	1507	197	0
DQ	RLM052	dunite/chr	Keen of Hamar Qu18N	lay/mas/dis chr, GM, no S	0	0	0	0	0	80219	9	2490	146	0
DQ	RLM053	chromitite	Keen of Hamar Qu18	massive chr, S	0	0	0	0.013	0	320659	0	1582	204	4.3
DQ	RLM054	dunite/chr	Keen of Hamar Qu18	nodular/dis chr, minor GM	0	0	0	0	12	62392	0	2450	129	1
DQ	RLM055	dunite/chr	Keen of Hamar Qu18	layered dis chr, grey/green	0	0	0	0	11	39472	0	2576	127	1.2
DQ	RLM056	dunite/chr	Keen of Hamar Qu18	layered dis chr, green nr Cr	0	0	0	0	7	41698	8	2629	146	0

TAG	SAMPLE	ROCK	LOCALITY	COMENTS	TRACE ELEMENT ANALYSES (ALL IN PPM)									
					Pt	*Pd*	*Ir*	*Au*	*As*	*Cr*	*Cu*	*Ni*	*Co*	*Sb*
DQ	RLM057	dunite	Keen of Hamar Qu18S	S	0	0	0	0	0	6344	16	2744	126	1
DQ	RLM058	dunite/chr	Keen of Hamar Qu18S	mas/dis chr, no S	0	0	0	0	0	248393	54	1755	248	1.8
DQ	RLM059	dunite/chr	Quarry 12 S	S rich & Cr rich dunite, GH	0.05	0.08	0	0.01	3	17992	140	5039	179	1.2
DQ	RLM060	dunite/chr	Quarry 12 S	dis chr,grey/green matrix	0	0	0	0	7	61997	147	3836	145	0
DQ	RLM061	dunite/chr	Quarry 12 S	composite, mas/dis chr, GM	0.03	0.04	0	0	15	148427	229	4112	174	2.3
DQ	RLM062	dunite/chr	Quarry 12 S	composite, dis chr yellow M	0.02	0.03	0	0	11	179901	138	2325	178	1.6
DQ	RLM063	dunite	Quarry 12 S	composite, S rich, fresh, Cu	0.36	0.64	0	0.021	6	4107	847	5670	142	7.8
DQ	RLM064	chromitite	Quarry 12 S	composite, mas chr, S	0.26	0.4	0	0.017	18	248415	95	2478	180	4.1
DQ	RLM065	dunite/chr	Quarry 12	dis chr, S rich, GP	0.18	0.3	0	0.033	15	86696	315	7245	158	12.7
DQ	RLM066	dunite/chr	Quarry 12	dis/mas chr, no S	0.46	0.32	0	0.017	0	234168	49	2048	186	2.2
DQ	RLM067	dunite/chr	Quarry 12	massive Cr nodules in GM, S	0.41	0.8	0	0.038	0	233300	680	3794	181	1.4
DQ	RLM068	dunite/chr	Quarry 12	dis chr, very GM, much S	0.14	0.36	0	0.049	12	66758	1453	8551	163	3.3
DQ	RLM069	dunite	Quarry 12 S	in situ, S rich, GH	0.28	0.59	0	0.032	8	2004	899	6073	167	3.3
DQ	RLM070	dunite/chr	Quarry 12	S & Cr rich dis chr, very GM	0.17	0.42	0	0.066	10	81056	1084	6928	169	3.6
PQ	RLM071	dunite	Nikka Vord N. Qu 5	nr. fault, Cu & S rich, GB	0.02	0.04	0	0.013	8	2284	343	3038	125	1.7
PQ	RLM072	dunite/chr	Layered Quarry	dis chr lay, S, GB	0	0.03	0	0.01	9	19329	59	3195	131	0
PQ	RLM073	dunite/chr	Layered Quarry	dis/lay chr, GM	0	0	0	0	5	108681	12	2195	129	0
PQ	RLM074	dunite/chr	Layered Quarry	sheared, mnt,green/yellow	0	0	0	0	8	139745	14	2119	163	0
PQ	RLM075	chromitite	Quarry 8	composite, S	0.01	0.03	0	0.01	0	279474	0	1509	188	0
PQ	RLM076	chromitite	Quarry 8	composite, little or no S	0	0	0	0	15	293939	0	1626	160	0
PQ	RLM077	dunite/chr	Quarry 8	dis chr, green/brown, S	0.02	0.04	0	0.012	8	131656	25	2590	188	2.4
PQ	RLM078	dunite/chr	Quarry 8	dis chr, no S, GM	0	0	0	0.01	0	94341	0	2737	132	0
DQ	RLM079	dunite	Quarry 13	in situ, S rich, GH, coarse Cr	0.23	0.33	0	0.026	3	6341	340	6307	170	6
DQ	RLM080	dunite/chr	Quarry 13	composite dis chr, GM, no S	0.37	0.34	0	0.018	5	139557	45	1791	188	1.7
DQ	RLM081	dunite/chr	Quarry 13	composite dis chr, yellow M	0.29	0.12	0	0	0	79022	11	2734	153	0
DQ	RLM082	dunite/chr	Quarry 11	S rich, dis chr, very. GM	0.3	0.34	0	0.041	0	232759	666	4903	161	5.2
TH	RLM083	dunite/harz	Muckle Heog	chr & S rich dunite vein	0	0	0	0.022	0	3217	586	2952	150	0
CQ	RLM084	dunite/chr	Cliff Quarry 1	dis chr, fawn/brown M, no S	7.48	7.2	0.95	0.091	181	94325	24	2544	163	5.8
CQ	RLM085	dunite/chr	Cliff Quarry 1	dis chr,yel./rusty, chl, no S	1.45	1.52	0.2	0.088	126	81683	35	2749	170	2.6
CQ	RLM086	dunite/chr	Cliff Quarry 1	composite of very GM, no S,	10.4	64.9	2.7	7.658	525	151344	541	6676	205	24.8
C	RLM087	pyroxenite	White House	S rich, coarse & massive px	0.3	0.42	0.08	0.028	6	6322	164	1130	85	0
A	RLM088	chr/mnt	NW Little Heog	drift, mnt rich sheared harz	0.7	1.18?	0.17	0	17	3232	11	2172	87	0
PQ	RLM089	dunite/chr	in situ pod chromite	mas/dis chr, yellow/GM no S	0	0	0	0	0	244206	0	1677	266	0
PQ	RLM090	dunite/chr	in situ pod chromite	lay/dis chr, no S, rusty	0	0	0	0	7	106267	19	3206	177	0
DQ	RLM091	dunite/chr	Hagdale Wick layers	single lay of multiple, GM	0	0	0	0.02	18	113091	14	2039	143	0

TAG	SAMPLE	ROCK	LOCALITY	COMENTS	TRACE ELEMENT ANALYSES (ALL IN PPM)									
					Pt	*Pd*	*Ir*	*Au*	*As*	*Cr*	*Cu*	*Ni*	*Co*	*Sb*
DQ	RLM092	chromitite	Hagdale Wick layers	layer, mas chr, GM	0	0	0	0	0	145825	0	1711	179	1.6
DQ	RLM093	chromitite	Hagdale Wick layers	layer, mas/dis chr,	0	0	0	0.01	0	190968	0	1371	192	1.8
DQ	RLM094	dunite/chr	Hagdale Wick layers	sheared lay/dis chr, Y/G M	0	0	0	0	0	92151	9	2038	163	1.4
DQ	RLM095	chromitite	Hagdale Wick layers	drift, composite, mas chr	0	0	0	0	22	260003	321	1466	183	0
DQ	RLM096	dunite/chr	Quarry 10	uneven/dis chr, S rich , GM	0.16	0.19	0	0	10	220818	70	3718	177	2
DQ	RLM097	chromitite	Quarry 10	mass chr, S rich, GH	0.08	0.15	0	0.096	25	272201	633	3229	192	11.3
DQ	RLM098	dunite/chr	Quarry 10	uneven/dis chr, no S, GM	0	0	0	0	0	241060	28	1498	182	0
DQ	RLM099	chromitite	Quarry 10	composite, mas chr, no S	0	0	0	0	0	310389	0	1607	164	0
A	RLM100	alteration	E of Little Heog	pink, S rich, sheared Si serp	0	0	0	0	27	5634	98	2733	94	0
DP	RLM101	dunite	dunite pod 1	CrED, chr lay, S	0	0	0	0	0	25355	0	2498	150	6.2
DP	RLM102	dunite	dunite pod 2	weathered, S rich	0	0	0	0	0	2632	9	3411	139	0
DP	RLM103	dunite	dunite pod 2	CrED, chr lay, S	0	0	0	0	0	20419	14	2570	141	0
DP	RLM104	dunite	dunite pod 5 (H.'s G.)	CrED, chr clots	0	0	0	0	0	17212	9	2543	132	0
DP	RLM105	dunite	dunite pod 5	nr Qu, Y/greenish weathering	0	0	0	0	0	2490	0	2498	107	0
PQ	MR28	chr/mnt	Nikka Vord N. Qu 5	black	0.07	0.13	0	0.019	20	215757	28	3058	139	3.5
PQ	MR29	dunite/chr	Nikka Vord N. Qu 5	green matrix, blue Co? bloom	0	0	0	0.012	0	189999	0	1687	212	0
PQ	MR30	dunite	Nikka Vord N. Qu 5	S bearing, S in vein	0	0	0	0	0	14257	17	2673	118	0
PQ	MR31	chromitite	Nikka Vord N. Qu 5	mas chr, one S	0	0	0	0	0	257102	0	1483	220	2
PQ	MR32	chromitite	Nikka Vord N. Qu 5	mas chr, green bloom	0.22	0.4	0	0.022	31	213892	47	3800	260	5.3
PQ	MR33	dunite	Nikka Vord N. Qu 5	altered, red bloom	0.05	0.13	0	0	40	9801	9	3243	84	0
DU	RLA001	dunite	SW of M. Heog	VSR, Cu, dis Cr layer	0.04	0.07	n.a.	n.a.	0	6934	146	3863	n.a.	n.a.
PQ	RLA002	chromitite	Long Quarry	SB, mas Cr	0	0.01	n.a.	n.a.	0	215718	0	1559	n.a.	n.a.
DQ	RLA003	dunite	Fulmar Quarry	SR,	0.03	0.03	n.a.	n.a.	0	9555	348	3421	n.a.	n.a.
DQ	RLA004	dunite	Fulmar Quarry	SR,Cu	0.15	0.28	n.a.	n.a.	0	2483	101	2756	n.a.	n.a.
DQ	RLA005	dunite/chr	Fulmar Quarry	Dis. lay Cr, No S, mod GM	0.01	0.01	n.a.	n.a.	0	73286	62	2427	n.a.	n.a.
DQ	RLA006	dunite/chr	Fulmar Quarry	Mass/diss Cr,patch of GM	0.02	0.03	n.a.	n.a.	0	158068	35	1632	n.a.	n.a.
DQ	RLA007	dunite/chr	Fulmar Quarry	Diss/lay Cr, yellowy GM	0.02	0.12	n.a.	n.a.	0	102212	17	1972	n.a.	n.a.
T1	RLA008	alteration	Pit W of traverse	SB,Mnt/Cr, sheared, grey/br	0.01	0.02	n.a.	n.a.	47	31502	27	2255	n.a.	n.a.
T1	RLA009	dunite	traverse (S to N)	No S, CrED	0.01	0.02	n.a.	n.a.	0	18907	16	2692	n.a.	n.a.
T1	RLA010	dunite	+6m	SB,CrED	0.03	0.04	n.a.	n.a.	0	12976	78	3056	n.a.	n.a.
T1	RLA011	dunite	+5m	MSR,CrED	0	0.01	n.a.	n.a.	0	22808	160	2864	n.a.	n.a.
T1	RLA012	dunite	+5m	SB,CrED	0	0.01	n.a.	n.a.	0	22389	18	2770	n.a.	n.a.
T1	RLA013	dunite/chr	sml pit AS +2m	Diss Cr,mod GM, SB?,	0.03	0.03	n.a.	n.a.	0	135585	29	1845	n.a.	n.a.
T1	RLA014	dunite	trench AS, +19m	SB,CrED	0.01	0.01	n.a.	n.a.	0	31105	69	2348	n.a.	n.a.
T2	RLA015	dunite	Hagdale Wick traverse	SB, (NE to SW)	0.03	0.04	n.a.	n.a.	0	5430	13	2296	n.a.	n.a.

TAG	SAMPLE	ROCK	LOCALITY	COMENTS	TRACE ELEMENT ANALYSES (ALL IN PPM)									
					Pt	Pd	Ir	Au	As	Cr	Cu	Ni	Co	Sb
T2	RLA016	dunite/chr	+1m	SB,dis/lay Cr,GB,weathered	0.02	0.03	n.a.	n.a.	0	15228	45	3540	n.a.	n.a.
T2	RLA017	dunite	2mW AS,+1m STR	SB,GB	0.02	0.03	n.a.	n.a.	109	3649	57	2685	n.a.	n.a.
T2	RLA018	dunite	+1m	SB	0.02	0.03	n.a.	n.a.	14	2698	32	2601	n.a.	n.a.
T2	RLA019	dunite	+1m	SB	0.02	0.04	n.a.	n.a.	0	2231	135	2485	n.a.	n.a.
T2	RLA020	dunite	+1m	SB	0.06	0.09	n.a.	n.a.	68	2079	110	2488	n.a.	n.a.
T2	RLA021	dunite	+0.5m	MSR,fresh	0.02	0.03	n.a.	n.a.	16	2030	185	2280	n.a.	n.a.
T2	RLA022	dunite	+0.5m	SB,fresh	0.04	0.06	n.a.	n.a.	12	2164	92	2536	n.a.	n.a.
T2	RLA023	dunite	+1m	SB, mnt + serp veins, W/GM	0.02	0.03	n.a.	n.a.	65	2391	256	2337	n.a.	n.a.
T2	RLA024	dunite	+1m	MSR,chl R,mnt	0.01	0.01	n.a.	n.a.	0	3143	170	2431	n.a.	n.a.
T2	RLA025	dunite	+2m	No S, mnt	0.09	0.14	n.a.	n.a.	6	2841	23	2167	n.a.	n.a.
T2	RLA026	dunite	+2m	No S, talcy, unsheared	0.02	0.05	n.a.	n.a.	0	4016	90	2641	n.a.	n.a.
T2	RLA027	dunite	+1m	SB, minor GM	0.06	0.1	n.a.	n.a.	0	2356	124	2447	n.a.	n.a.
T2	RLA028	dunite	+0.5m	SB,v altered,CrED,whitish gr	0.01	0.03	n.a.	n.a.	0	3580	193	2471	n.a.	n.a.
T2	RLA029	dunite	+0.5m	SR,altered, GP,GH	0.03	0.04	n.a.	n.a.	0	2207	151	2286	n.a.	n.a.
T2	RLA030	dunite	+1mW AS,	SR,CrED,greenish white	0.03	0.05	n.a.	n.a.	0	3052	208	2543	n.a.	n.a.
T2	RLA031	dunite	+1mE AS	SR,CrED,chl R,mod fresh	0.04	0.05	n.a.	n.a.	6	4301	199	2492	n.a.	n.a.
T2	RLA032	dunite	+1.5m from 029	SB,CrED, rusty green	0.02	0.03	n.a.	n.a.	96	2608	43	2302	n.a.	n.a.
T2	RLA033	dunite	+1m	No S, CrED, chl veins	0.02	0.04	n.a.	n.a.	86	2713	175	2673	n.a.	n.a.
T2	RLA034	dunite	+1m	SB, serp veins	0.02	0.03	n.a.	n.a.	6	2275	29	2551	n.a.	n.a.
T2	RLA035	dunite	+1.5m	No S, serp veins + mnt	0.01	0.02	n.a.	n.a.	573	2766	36	2474	n.a.	n.a.
T2	RLA036	dunite	+1.5m	SB,sheared, greenish grey	0.04	0.04	n.a.	n.a.	266	2677	55	2535	n.a.	n.a.
T2	RLA037	serpentinite	+2m (shear zone+1m)	SB,black,sheared	0.02	0.03	n.a.	n.a.	146	3916	110	2630	n.a.	n.a.
T2	RLA038	talcy serp	+2m	greenish white, CO3 veins	0.02	0.02	n.a.	n.a.	163	4420	35	1975	n.a.	n.a.
T2	RLA039	serp breccia	+1m	black,platey antig?,mnt rich	0.02	0.03	n.a.	n.a.	232	4298	88	2232	n.a.	n.a.
T2	RLA040	serpentinite	+1m	talcy, green antig? mnt rich	0.04	0.06	n.a.	n.a.	177	3285	110	2594	n.a.	n.a.
T2	RLA041	serp breccia	+2m	black,schistose, much CO3	0.05	0.04	n.a.	n.a.	234	4916	61	2871	n.a.	n.a.
T2	RLA042	serpentinite	+1m	silicified, mnt rich,black	0.02	0.03	n.a.	n.a.	98	3577	52	2290	n.a.	n.a.
T2	RLA043	dunite	+1m (host rocks)	SB,CrED,mnt,orangy	0.02	0.04	n.a.	n.a.	231	3160	64	1911	n.a.	n.a.
T2	RLA044	dunite	+3m	?SB, CrED, silicified?	0.08	0.09	n.a.	n.a.	73	3334	29	1821	n.a.	n.a.
T2	RLA045	dunite	-2m (+1m 043)	SB,CrED, Si rich,sheared	0.06	0.07	n.a.	n.a.	0	2741	32	1749	n.a.	n.a.
T2	RLA046	dunite	2m W of RLA044	SR	0.03	0.03	n.a.	n.a.	19	3173	129	1942	n.a.	n.a.
DQ	RLA047	chromitite	S of Setters	SB, mass Cr, few GB	0	0	n.a.	n.a.	164	175802	458	2261	n.a.	n.a.
DU	RLA048	dunite/chr	S of Long Qu 7	SB, CrED, multiple Cr lays	0	0.01	n.a.	n.a.	0	8794	24	3266	n.a.	n.a.
DU	RLA049	dunite	S of Long Qu 7	MSR,	0	0.01	n.a.	n.a.	6	5006	114	2922	n.a.	n.a.
T3	RLA050	serpentinite	M. Heog E Traverse	sheared, dk green, first exp	0.01	0.01	n.a.	n.a.	0	2505	24	2313	n.a.	n.a.

TAG	*SAMPLE*	*ROCK*	*LOCALITY*	*COMENTS*	*TRACE ELEMENT ANALYSES (ALL IN PPM)*									
					Pt	*Pd*	*Ir*	*Au*	*As*	*Cr*	*Cu*	*Ni*	*Co*	*Sb*
T3	RLA 051	harz./serp	+4m SSE	V sheared, whitish yellow	0.01	0.01	n.a.	n.a.	0	2339	0	3250	n.a.	n.a.
T3	RLA052	dunite	+10m	SR, GB	0.06	0.1	n.a.	n.a.	14	1908	1325	3349	n.a.	n.a.
T3	RLA053	dunite	+1m	SR, Cu rich, fresh	0.04	0.08	n.a.	n.a.	12	1685	1288	3771	n.a.	n.a.
T3	RLA054	dunite	+1m	SB	0.03	0.08	n.a.	n.a.	0	2898	19	2518	n.a.	n.a.
T3	RLA055	dunite	+11m	No S, CrED	0.02	0.03	n.a.	n.a.	6	2046	120	2570	n.a.	n.a.
T3	RLA056	dunite	+1m	No S, GB	0.05	0.08	n.a.	n.a.	26	2093	643	4096	n.a.	n.a.
T3	RLA057	dunite	+1m	No S, CrED, few GB	0	0	n.a.	n.a.	9	3809	23	2868	n.a.	n.a.
T3	RLA058	dunite	+7m	No S, CrED, GBs	0.01	0.03	n.a.	n.a.	12	3224	248	2966	n.a.	n.a.
T4	RLA059	serpentinite	M. Heog W Traverse	sheared, green/black	0	0	n.a.	n.a.	5	2840	14	2301	n.a.	n.a.
T4	RLA060	dunite	+4m SE	SB, moderately fresh	0	0	n.a.	n.a.	9	5606	17	2936	n.a.	n.a.
T4	RLA061	dunite	+2m	SB, fresh	0	0	n.a.	n.a.	7	2099	23	2818	n.a.	n.a.
T4	RLA062	dunite	+5m	SB, CrED, chl rims & veins	0	0	n.a.	n.a.	0	4142	64	2414	n.a.	n.a.
T4	RLA063	dunite	+3m	MSR, CrED, few chl veins	0.01	0.03	n.a.	n.a.	5	4150	16	2404	n.a.	n.a.
T4	RLA064	dunite	+20m	SR, lg GBs	0.04	0.07	n.a.	n.a.	8	622	700	3039	n.a.	n.a.
T4	RLA065	dunite	+6m	SB, SR layer	0.02	0.04	n.a.	n.a.	18	2628	51	3457	n.a.	n.a.
T4	RLA066	dunite	+16m	SR, Cr layer, 1 GB	0	0	n.a.	n.a.	6	9731	137	2789	n.a.	n.a.
T5	RLA067	dunite	Trench Traverse	SB	0.12	0.09	n.a.	n.a.	7	3634	16	3165	n.a.	n.a.
T5	RLA068	dunite	+1m SE	SB, CrED	0.01	0.02	n.a.	n.a.	7	4411	62	3533	n.a.	n.a.
T5	RLA069	dunite	+0.5m	MSR, CrED	0.02	0.05	n.a.	n.a.	7	2721	44	2795	n.a.	n.a.
T5	RLA070	dunite	+16.5m	MSR	0.02	0.03	n.a.	n.a.	9	3326	163	3571	n.a.	n.a.
T5	RLA071	dunite	+0.75m	MSR, patchy S	0	0	n.a.	n.a.	0	2416	51	3041	n.a.	n.a.
T5	RLA072	dunite	+2m	MSR, CrED, patchy S	0.02	0.04	n.a.	n.a.	6	2933	140	3927	n.a.	n.a.
T5	RLA073	dunite	+11m	SR, CrED	0.01	0.03	n.a.	n.a.	7	2795	146	2815	n.a.	n.a.
T5	RLA074	dunite	+9m	SB, GBs, fractured	0.02	0.03	n.a.	n.a.	0	3830	739	3894	n.a.	n.a.
T5	RLA075	dunite	+1m	SB, highly fractured	0.02	0.02	n.a.	n.a.	0	3551	32	2865	n.a.	n.a.
DQ	RLA076	dunite/chr	Stream below Trav.	SB, Cr rich dunite	0	0	n.a.	n.a.	0	6851	27	2689	n.a.	n.a.
DQ	RLA077	dunite/chr	+1m SE	No S, diss Cr, fresh	0	0	n.a.	n.a.	5	41990	17	2485	n.a.	n.a.
T6	RLA078	dun/wehr	White House Traverse	SB, WD, much CO3 veining	0.03	0.01	n.a.	n.a.	0	3145	0	2312	n.a.	n.a.
T6	RLA079	dun/wehr	+2m E	SB,WD,W lay serp/CO3	0	0	n.a.	n.a.	0	3409	0	2300	n.a.	n.a.
T6	RLA080	wehrlite	+2m E	SB, px lays	0	0	n.a.	n.a.	5	2569	19	2489	n.a.	n.a.
T6	RLA081	wehr/pyrox	+1.5m	MSB, serp	0	0	n.a.	n.a.	0	6464	84	1296	n.a.	n.a.
T6	RLA082	wehrlite	+2m	VSR, sheared	0.15	0.23	n.a.	n.a.	0	769	1292	3750	n.a.	n.a.
T6	RLA083	wehrlite	+0.5m	SR, fresher	0.11	0.2	n.a.	n.a.	0	1003	1507	3861	n.a.	n.a.
T6	RLA084	pyroxenite	+0.5m	SR,	0.02	0.05	n.a.	n.a.	11	5115	1473	1949	n.a.	n.a.
T6	RLA085	pyroxenite	+0.75m	MSR, typical	0.02	0.02	n.a.	n.a.	0	4616	330	935	n.a.	n.a.

TAG	SAMPLE	ROCK	LOCALITY	COMENTS	TRACE ELEMENT ANALYSES (ALL IN PPM)									
					Pt	*Pd*	*Ir*	*Au*	*As*	*Cr*	*Cu*	*Ni*	*Co*	*Sb*
T6	RLA086	pyroxenite	+0.75m	SB, much YS (=SR)	0.01	0.05	n.a.	n.a.	0	4907	383	967	n.a.	n.a.
T6	RLA087	pyroxenite	+1m	MSB, much dull yellow S	0.01	0.02	n.a.	n.a.	0	5547	286	598	n.a.	n.a.
T6	RLA088	pyroxenite	+1m	SB, fine px, some YS	0	0.01	n.a.	n.a.	7	2112	131	1164	n.a.	n.a.
T6	RLA089	pyroxenite	+1m	SB, YS & bright S	0	0	n.a.	n.a.	0	7025	627	955	n.a.	n.a.
DU	RLA090	dunite	S of Muckle Heog	CrED, S & Cu rich	0.12	0	n.a.	n.a.	5	2271	615	3896	n.a.	n.a.
DU	RLA091	dunite	S of Muckle Heog	CrED, SR, chl rich	0.04	0	n.a.	n.a.	7	3826	336	3307	n.a.	n.a.
TH	RLA092	pyrox vein	E of Setters		0.11	0	n.a.	n.a.	0	3911	266	2773	n.a.	n.a.
TH	RLA093	harz	E of Setters	host to RLA092	0.01	0	n.a.	n.a.	0	1538	12	2696	n.a.	n.a.
C	RLA094	pyrox vein	Keen	px dyke? RLA9- sample	0	0	n.a.	n.a.	0	4524	51	901	n.a.	n.a.
DQ	RLA095	dunite	Hagdale quarry	MSR, in situ HMP's	0.24	0.12	n.a.	n.a.	0	4287	235	2839	n.a.	n.a.
T7	RLA096	dunite	Quarry 13 Trav. S-N	MSR	0.13	0.01	n.a.	n.a.	0	3059	221	4502	n.a.	n.a.
T7	RLA097	dunite	+0.75m	VSR	0.02	0	n.a.	n.a.	0	3283	1152	4591	n.a.	n.a.
T7	RLA098	dunite	+1m	VSR	0.14	0.02	n.a.	n.a.	0	4690	881	6031	n.a.	n.a.
T7	RLA099	dunite	+1m	SR, CrED, GH	0.28	0.16	n.a.	n.a.	8	3027	1225	6522	n.a.	n.a.
T7	RLA100	dunite	+1m	VSR, CrED	0.55	1.07	n.a.	n.a.	0	2386	1178	6017	n.a.	n.a.
T7	RLA101	dunite/chr	+1m Qu edge	SB, dis. Cr, green serp M	0.2	0.19	n.a.	n.a.	0	20940	62	3232	n.a.	n.a.
T7	RLA102	dunite	+1.5mW (+1m)	SB, CrED (HMP's sample)	0.03	0	n.a.	n.a.	0	10042	15	2901	n.a.	n.a.
T7	RLA103	dunite	+4m RLA101 Qu Edge	VSR, CrED	0.32	0.55	n.a.	n.a.	8	3893	808	6031	n.a.	n.a.
T7	RLA104	dunite	+0.5m chan +0.5m	VSR to SR N, CrED +N	0.16	0.28	n.a.	n.a.	6	3023	663	3798	n.a.	n.a.
T7	RLA105	dunite	+1m RLA103, up1m	No S	0	0	n.a.	n.a.	0	2691	40	3295	n.a.	n.a.
T7	RLA106	dunite	+0.75m	No S ,VF	0	0	n.a.	n.a.	0	4118	98	3193	n.a.	n.a.
T7	RLA107	dunite	+1.5m	No S	0	0	n.a.	n.a.	0	3718	23	3246	n.a.	n.a.
DQ	RLA108	dunite	Quarry 11 S edge	MSR, CrED, good GB	0.05	0.08	n.a.	n.a.	8	11121	206	3662	n.a.	n.a.
T8	RLA109	dunite	Quarry 10 S edge	SB, CrED	0	0	n.a.	n.a.	4	27509	23	2892	n.a.	n.a.
T8	RLA110	dunite	+1mS	CrED, No S	0.1	0.17	n.a.	n.a.	0	15104	11	2852	n.a.	n.a.
T8	RLA111	dunite/chr	Qu 10 SW corner	dis Cr, No S	0.08	0.03	n.a.	n.a.	0	138283	169	2717	n.a.	n.a.
T8	RLA112	dunite	+3m N	SB	0.04	0	n.a.	n.a.	0	2731	32	2833	n.a.	n.a.
T8	RLA113	dunite	+2m (edge -2m)	SB	0.04	0	n.a.	n.a.	0	4625	30	2991	n.a.	n.a.
T8	RLA114	dunite	Qu10 edge	CrED, No S, ?1GB	0.02	0	n.a.	n.a.	0	25873	22	3057	n.a.	n.a.
T8	RLA115	dunite	+0.5m N, 1m up	SB	0.05	0.11	n.a.	n.a.	0	7304	272	3876	n.a.	n.a.
T8	RLA116	dunite	+0.5m, 1m up	SR	0.15	0.22	n.a.	n.a.	0	3944	997	4462	n.a.	n.a.
T8	RLA117	dunite	+0.5m, 1m up	SR, Cu, S end of ST's ch	0.15	0.11	n.a.	n.a.	0	10472	681	4507	n.a.	n.a.
T8	RLA118	dunite	+1m, 0.5m up	MSR	0.16	0.12	n.a.	n.a.	10	8842	231	4252	n.a.	n.a.
T8	RLA119	dunite	+0.25m	SB, CrED	0.13	0.09	n.a.	n.a.	10	8743	180	4361	n.a.	n.a.
DQ	RLA120	dunite/chr	Small pit by road	dis Cr, 1 S, rusty specks	0.33	0.51	n.a.	n.a.	0	182576	506	3666	n.a.	n.a.

TAG	*SAMPLE*	*ROCK*	*LOCALITY*	*COMENTS*	*TRACE ELEMENT ANALYSES (ALL IN PPM)*									
					Pt	*Pd*	*Ir*	*Au*	*As*	*Cr*	*Cu*	*Ni*	*Co*	*Sb*
DQ	RLA121	dunite/chr	Small pit by road	dis Cr, GM, No S	0.06	0.17	n.a.	n.a.	0	165991	67	2138	n.a.	n.a.
DQ	RLA122	dunite/chr	Quarry W of BX spoil	mas/dis Cr, MSR, GM, GB	1.7	2.08	n.a.	n.a.	0	219114	1254	6386	n.a.	n.a.
DQ	RLA123	dunite/chr	Quarry W of BX spoil	dis Cr, MSR, GB, No GM	0.13	0.28	n.a.	n.a.	23	64108	1165	7036	n.a.	n.a.
DQ	RLA124	dunite	Quarry W of BX spoil	VSR, V fresh	0.44	0.69	n.a.	n.a.	0	5327	655	5033	n.a.	n.a.
T9	RLA125	dunite	Qu W of BX S, of Cr?	No S	0.01	0.01	n.a.	n.a.	0	6191	12	2967	n.a.	n.a.
T9	RLA126	dunite/chr	+0.5m S	MSR, Cr lay & SR lay	0.78	1.81	n.a.	n.a.	0	16109	462	4226	n.a.	n.a.
T9	RLA127	dunite	+1.5m	SB	0.07	0.11	n.a.	n.a.	5	8048	55	3122	n.a.	n.a.
T9	RLA128	dunite	+2m	No S, CrED	0	0	n.a.	n.a.	0	22837	30	3107	n.a.	n.a.
PQ	RLA129	alteration	Qu 8, S. promontary	SR,trans/alt%, talcy	0	0	n.a.	n.a.	10	2527	150	2732	n.a.	n.a.
PQ	RLA130	alteration	Qu 8, S. promontary	SB, "	0.02	0.02	n.a.	n.a.	20	2227	37	2670	n.a.	n.a.
T10	RLA131	dunite	Qu12 S edge	MSR, SRvein?, 2 sulphides	0.16	0.28	n.a.	n.a.	6	2982	881	5932	n.a.	n.a.
T10	RLA132	dunite	+2m N, middle of Qu	SR, CrED, V green GB	0.29	0.63	n.a.	n.a.	13	5346	284	5313	n.a.	n.a.
T10	RLA133	dunite	+4m N edge	MSR/SB	0.17	0.13	n.a.	n.a.	0	7115	24	3046	n.a.	n.a.
T10	RLA134	dunite	+0.5m, 1m up	SB	0.07	0.09	n.a.	n.a.	0	6789	13	3049	n.a.	n.a.
T11	RLA135	dunite	Qu 12S, N-S	SB	0.07	0.11	n.a.	n.a.	0	3195	76	3313	n.a.	n.a.
T11	RLA136	dunite	+1m S	MSB	0.08	0.12	n.a.	n.a.	6	2350	66	2520	n.a.	n.a.
T11	RLA137	dunite	+1m 1m down	MSB, serp, mnt veins	0.03	0.05	n.a.	n.a.	0	3315	52	3056	n.a.	n.a.
T11	RLA138	dunite	+1.5m, N edge	SD, CrED	0.24	0.16	n.a.	n.a.	0	14178	63	2998	n.a.	n.a.
T11	RLA139	dunite	+10m E, ?+1.5m S	VSR, bulk sample	0.38	0.7	n.a.	n.a.	10	2650	326	5274	n.a.	n.a.
T11	RLA140	dunite	+1m S RLA139	MSR	0.04	0.05	n.a.	n.a.	0	2574	43	2702	n.a.	n.a.
T11	RLA141	dunite	+7m W, ?+1m S	MSR, slightly serp	0	0	n.a.	n.a.	0	3345	39	2864	n.a.	n.a.
T11	RLA142	dunite	+1m S +1m E	SB	0.05	0.09	n.a.	n.a.	0	5404	24	3108	n.a.	n.a.
T11	RLA143	dunite	+1.5m S	SR, GB	0.09	0.15	n.a.	n.a.	8	1697	226	3614	n.a.	n.a.
T11	RLA144	dunite	+1m s +1m E	SR	0.07	0.12	n.a.	n.a.	7	3198	130	3555	n.a.	n.a.
T2	RLA145	dunite	Hag. Wick +3mS 046	MSR, fresh	0.04	0.06	n.a.	n.a.	129	2634	47	2079	n.a.	n.a.
DU	RLA146	pyrox vein	+10m S	SB, vein only	0.07	0.1	n.a.	n.a.	0	4658	421	2650	n.a.	n.a.
DU	RLA147	vein/dunite	as 146	SB, contact, sml veins & cpx	0	0	n.a.	n.a.	18	2698	442	2990	n.a.	n.a.
DU	RLA148	dunite	+ 5-10cm vein	SB, host fresh dunite	0	0	n.a.	n.a.	22	3406	119	2471	n.a.	n.a.
DP	RLA149	dunite	Pod 6	SB middle	0.03	0.08	n.a.	n.a.	0	3230	34	3135	n.a.	n.a.
DP	RLA150	dunite	Pod 6	No S, CrED, Cr clots +Chl R	0	0.01	n.a.	n.a.	0	5823	0	2701	n.a.	n.a.
DP	RLA151	dunite	Pod 6	SB	0.01	0.02	n.a.	n.a.	0	1593	50	2926	n.a.	n.a.
DP	RLA152	dunite	podlet N of Pod 6	SB, v sml S	0.02	0.01	n.a.	n.a.	0	1833	0	2595	n.a.	n.a.
DP	RLA153	dunite	Pod W of pod 1	SB, Nat Cu in veins	0.02	0.02	n.a.	n.a.	0	2210	27	2121	n.a.	n.a.
C	RLA154	pyroxenite	Keen Traverse	plag & ol bearing, 1 SB	0.05	0.05	n.a.	n.a.	0	3661	88	1055	n.a.	n.a.
C	RLA155	pyroxenite	" S of 154	" " MSR	0.05	0.06	n.a.	n.a.	0	7233	348	815	n.a.	n.a.

TAG	SAMPLE	ROCK	LOCALITY	COMENTS	TRACE ELEMENT ANALYSES (ALL IN PPM)									
					Pt	Pd	Ir	Au	As	Cr	Cu	Ni	Co	Sb
C	RLA156	dun/wehr	+3m S of 155	SB, CrED, base of next cy?	0.07	0.19	n.a.	n.a.	0	8585	129	1796	n.a.	n.a.
C	RLA157	pyroxenite	Keen	MSR,plag B, pegmatitic	0.03	0.03	n.a.	n.a.	0	5851	276	782	n.a.	n.a.
C	RLA158	pyroxenite	Keen	MSB, SR patch, no plag	0.07	0.04	n.a.	n.a.	0	7547	265	786	n.a.	n.a.
C	RLA159	wehrlite	Keen	MSR, CrE, W in WD	0.09	0.08	n.a.	n.a.	0	5215	88	2154	n.a.	n.a.
DQ	RLA160	dunite	Jimmies Qu	MSR, Nat Cu rich,	0.13	0.17	n.a.	n.a.	0	5236	1222	3452	n.a.	n.a.
T12	RLA161	dun/wehr	High level Cr Trav.	SB, MSB patch WD	0.05	0	n.a.	n.a.	19	3945	72	1487	n.a.	n.a.
T12	RLA162	wehrlite	+1m NW, 1.5m up	SB, plag?/white pseuds cpx	0.03	0	n.a.	n.a.	11	3862	91	1140	n.a.	n.a.
T12	RLA163	wehr/pyrox	+0.5m	SR, plag B	0	0.02	n.a.	n.a.	18	6261	157	846	n.a.	n.a.
T12	RLA164	pyroxenite	+1m	SB, MSR patch	0	0.05	n.a.	n.a.	13	8207	266	719	n.a.	n.a.
T12	RLA165	dun/wehr	+0.25m	SB, px B, contact	0	0.01	n.a.	n.a.	48	4326	31	1504	n.a.	n.a.
T12	RLA166	dunite	+0.25m	MSB, px xeno? SR+Cr lay	0	0	n.a.	n.a.	36	3797	24	2206	n.a.	n.a.
T12	RLA167	dunite	+1m	SB	0	0	n.a.	n.a.	0	4036	60	2267	n.a.	n.a.
T12	RLA168	dun/chr	+0.5m	dis Cr lay, No S	0	0.03	n.a.	n.a.	0	65179	70	1568	n.a.	n.a.
T12	RLA169	dunite	+0.1m	margin & host of lay, No S ?	0	0	n.a.	n.a.	0	6428	37	2200	n.a.	n.a.
T12	RLA170	dunite	+0.5m	SB, above all Cr layers	0.25	0.45	n.a.	n.a.	0	6324	55	2358	n.a.	n.a.
DQ	RLA171	chr/mnt	Keen H L Cr NE pit	SB, on shear, mnt after Cr	0	0	n.a.	n.a.	195	157262	19	1156	n.a.	n.a.
DQ	RLA172	chromitite	in situ Cr lower part	SB, mass Cr, 1S	0	0	n.a.	n.a.	31	132408	110	1690	n.a.	n.a.
DQ	RLA173	chromitite	in situ Cr top (vert)	mass Cr, dis Cr patch	0	0	n.a.	n.a.	42	109962	115	1771	n.a.	n.a.
T2	RLA174	dunite	0.5m N RLA025	No S, CrED	0	0	n.a.	n.a.	0	11825	138	2442	n.a.	n.a.
T2	RLA175	dunite	0.5m S RLA025	SB, CrED, slightly greenish	0	0	n.a.	n.a.	0	3873	70	2227	n.a.	n.a.
T2	RLA176	dunite	+0.5m S	No S, CrED, serp & sheared	0	0	n.a.	n.a.	8	2600	46	2366	n.a.	n.a.
T13	RLA177	dun/chr	Hagwick M U Trav	mult. dis Cr lay, 0.2m chan	0	0	n.a.	n.a.	0	21109	95	2254	n.a.	n.a.
T13	RLA178	dunite	+1m N	SR, V nat Cu rich, CrED	0	0.01	n.a.	n.a.	0	3573	442	2721	n.a.	n.a.
T13	RLA179	wehr	+1m	cpx lays/veins SB greenish	0.34	0.58	n.a.	n.a.	0	2175	1244	3546	n.a.	n.a.
T13	RLA180	dunite	+1m	SB, CrED, lays	0	0.08	n.a.	n.a.	0	5196	23	2050	n.a.	n.a.
T13	RLA181	dunite	+1m S RLA177	SB,	0	0	n.a.	n.a.	0	3255	53	2734	n.a.	n.a.
T	RLA182	wehr/pyrox	Keen NE pyrox Trav	SB,	0	0	n.a.	n.a.	0	6110	96	764	n.a.	n.a.
T	RLA183	pyroxenite	+6m SE	SR, typical middle of lay	0	0.01	n.a.	n.a.	0	0	0	0	n.a.	n.a.
T	RLA184	pyroxenite	+3m SE edge	SB,	0.01	0.01	n.a.	n.a.	0	5731	151	820	n.a.	n.a.
T	RLA185	pyroxenite	nr middle	SB, pegmatitic	0.02	0.02	n.a.	n.a.	0	8566	402	798	n.a.	n.a.
T	RLA186	wehr/pyrox	N margin	SR, px lays in WD	0.01	0.01	n.a.	n.a.	0	0	0	0	n.a.	n.a.
T	RLA187	pyroxenite	Keen 2nd pyrox trav	MSR, +3m W RLMO87 shear	0.01	0.04	n.a.	n.a.	0	4734	525	607	n.a.	n.a.
T	RLA188	pyroxenite	bulk RLM087		na	na	n.a.	n.a.	0	0	0	0	n.a.	n.a.
T	RLA189	pyroxenite	+1m E	MSR	0.01	0.03	n.a.	n.a.	0	4522	266	782	n.a.	n.a.
T	RLA190	pyroxenite	+9m E	MSR	0.1	0.14	n.a.	n.a.	0	6460	842	1072	n.a.	n.a.

TAG	*SAMPLE*	*ROCK*	*LOCALITY*	*COMENTS*	*TRACE ELEMENT ANALYSES (ALL IN PPM)*									
					Pt	*Pd*	*Ir*	*Au*	*As*	*Cr*	*Cu*	*Ni*	*Co*	*Sb*
TH	RLA191	dunite	S of Haroldswick	dunite dyke host to 192	0.13	0.23	n.a.	n.a.	0	2208	0	2683	n.a.	n.a.
TH	RLA192	pyrox vein	S of Haroldswick		0	0	n.a.	n.a.	0	4160	0	1741	n.a.	n.a.
C	RLA193	dunite	Keen	marked 182	0	0	n.a.	n.a.	0	3650	96	2505	n.a.	n.a.

References

Agiorgitis, G. & Wolf, R. (1977): The distribution of platinum, palladium and gold in Greek chromites. Chemie der Erde **36**, 349-351.

Agiorgitis, G. & Wolf, R. (1978): Aspects of osmium, ruthenium and iridium contents in some Greek chromites. *Chemical Geology* **23**, 267-272.

Agiorgitis, G. & Wolf, R. (1984): Variations of the Os/Ir ratio in terrestrial rocks and minerals. *Chemical Geology* **42**, 277-286.

Ahrens, L.H. (1952): The use of ionisation potentials. Part 1. Ionic radii of the elements. *Geochimica et Cosmochimica Acta* **2**, 155-169.

Allen, C.R. (1975): The petrology of a portion of the Troodos plutonic complex, Cyprus. Unpublished Ph.D. thesis, University of Cambridge, 315pp.

Amin, M.S. (1954): Notes on the ultrabasic body of Unst, Shetland Islands. *Geological Magazine* **91**, 399-406.

Amossé, J., Allibert, M., Fischer, W. & Piboule, M. (1990): Experimental study of the solubility of platinum and iridium in basic silicate melts. Implications for the differentiation of platinum-group elements during magmatic processes. *Chemical Geology* **81**, 45-53.

Anonymous (1972): Ophiolites by Penrose field conference participants. *Geotimes* **17**, 24-25.

Augé, T. (1985): Platinum-group-mineral inclusions in ophiolitic chromitite from the Vourinos complex, Greece. *Canadian Mineralogist* **23**, 163-171.

Augé, T. & Roberts, S. (1982): Petrology and geochemistry of some chromitiferous bodies within the Oman ophiolite. *Ofioliti* **7**, 133-154.

Bacuta, G.C., Gibbs, A.K., Kay, R.W. & Lipin, B.R. (1988): Platinum-group element abundance in chromite deposits of the Acoje ophiolite block, Zambales ophiolite complex, Philippines. *In* Geo-Platinum 87 (H.M. Prichard, P.J. Potts, J.F.W. Bowles & S.J. Cribb, eds.). Elsevier, London, (381-382) (abstract).

Ballhaus, C.G. & Stumpfl, E.F. (1985): Occurrence and petrological significance of graphite in the upper critical zone, western Bushveld complex, South Africa. *Earth and Planetary Science Letters* **74**, 58-68.

References

Barnes S.-J. & Naldrett, A.J. (1987): Fractionation of platinum-group elements and gold in some komatiites of the Abitibi greenstone belt, northern Ontario. *Economic Geology* **82**, 165-183.

Barnes, S.-J., Naldrett, A.J. & Gorton, M.P. (1985): The origin of the fractionation of platinum-group elements in terrestrial magmas. *Chemical Geology* **53**, 303-323.

Barnes, S.-J., Boyd, R., Korneliussen, A., Nilsson, L.-P., Often, M., Pedersen, R.B. & Robins, B. (1988): The use of mantle normalisation and metal ratios in discriminating between the effects of partial melting, crystal fractionation and sulphide segregation on platinum-group elements, gold, nickel and copper: Examples from Norway. *In* Geo-Platinum 87 (H.M. Prichard, J.F.W. Bowles and S.J. Cribb, eds.). Elsevier, London, (113-144).

Bartholomew, I.D. (1983): The primary structures and fabrics of the upper mantle and lower oceanic crust from ophiolite complexes. Unpublished Ph.D. thesis, The Open University, 520 pp.

Becker, R. & Agiorgitis, G. (1978): Iridium, osmium and palladium distribution in rocks of the Troodos complex, Cyprus. *Chemie der Erde* **37**, 302-306.

Bliss, N.W. & Maclean, W.H. (1975): The paragenesis of zoned chromite from central Manitoba. *Geochimica et Cosmochimica Acta* **39**, 973-990.

Boyd, R., Barnes, S.J. & Gronlie, A. (1988): Noble metal geochemistry of some Ni-Cu deposits in the Sveconorwegian and Caledonian orogens in Norway. *In* Geo-Platinum 87 (H.H. Prichard, J.W.F. Bowles and S.J. Cribb, eds.). Elsevier, London, (145-158)

Browning, P. (1982): The petrology, geochemistry and structure of the plutonic rocks of the Oman ophiolite. Unpublished Ph.D. thesis, The Open University, 404 pp.

Brzozowski, T.J. (1977): VLF electromagnetic surveys and associated studies in north Dartmoor and Unst. Unpublished Ph.D. thesis, Chelsea College.

Burkhard, D.J.M., Page, N.J. & Amstutz, G.C. (1988): Platinum-group element analyses of serpentinites in the eastern central Alps, from Davos (Switzerland) to the Valmalenco (Italy). *In* Geo-Platinum 87 (H.M. Prichard, P.J. Potts, J.F.W. Bowles & S.J. Cribb, eds.). Elsevier, London, (165-178).

Campbell, I.H. & Barnes, S.J. (1984): A model for the geochemistry of the platinum-group elements in magmatic sulfide deposits. *Canadian Mineralogist* **22**, 151-160.

Campbell, I.H. & Naldrett, A.J. (1979): The influence of silicate:sulfide ratios on the geochemistry of magmatic sulphides. *Economic Geology* **74**, 1503-1506.

Chang, P.K., Yu, C.M. & Chiang, C.U. (1973): Mineralogy and occurrence of the platinum-group elements in a chromite deposit in northwestern China. *Geochimica* **2**, 76-85.

Cheeney, R.F. (1983): Statistical methods in geology for field and lab decisions. George Allen & Unwin, London, 169 pp.

Clifton, H.E., Hunter, R.E., Swanson, F.J. & Phillips, R.L. (1969): Sample size and meaningful gold analysis. U.S. Geological Survey Professional Paper 625-C, 17 pp.

Constantinides, C.C., Kingston, G.A. & Fisher, P.C. (1980): The occurrence of platinum group minerals in the chromitites of the Kokkinorotsos chrome mine, Cyprus. *In* Ophiolites Proceedings International Ophiolite Symposium Cyprus (A. Panayiotou, ed.). Ministry of Agriculture and Natural Resources, Geological Survey Department, Nicosia, (93-101).

Craig, J.R. & Scott, S.D. (1974): Sulphide phase equilibria. *In* Sulphide Mineralogy (P.H. Ribbe, ed.). Mineralogical Society of America Short Course Notes 1, (CS1-110).

Craig, J.R., Naldrett, A.J. & Kullerud, G. (1968): The Fe-Ni-S system: 400° C isothermal diagram. *Carnegie Institute Washington Yearbook* **66**, 440-441.

Crocket, J.H. (1981): Geochemistry of the platinum-group elements. *In* Platinum-Group Elements; Mineralogy, Geology, Recovery (L.J. Cabri, ed.), *Canadian Institute of Mining and Metallurgy Special Volume* **23**, 47-64.

Crocket, J.H. & Chyi, L.L. (1972): Abundances of Pd, Ir, Os and Au in an alpine ultramafic pluton. *24th International Geological Congress (1972)* Section **10**, 202-209.

Crocket, J.H. & Teruta, Y. (1977): Palladium, iridium, and gold contents of mafic and ultramafic rocks drilled from the Mid-Atlantic Ridge, Leg 37, Deep Sea Drilling Project. *Canadian Journal of Earth Sciences* **14**, 777-784.

Currie, L.A. (1968): Limits for qualitative detection and quantitative determination. Application to radiochemistry. *Analytical Chemistry* **40**, 586-593.

Curtis, C.D. & Brown, P.E. (1969): The metasomatic development of zoned ultrabasic bodies in Unst, Shetland. *Contributions to Mineralogy and Petrology* **24**, 275-292.

Deer, W.A., Howie, R.A. & Zussman, J. (1966): An introduction to the rock forming minerals. Longman, Harlow, 528 pp.

Dickey, J.S., Jr. (1975): A hypothesis of origin for podiform chromite deposits. *Geochimica et Cosmochimica Acta* **39**, 1061-1074.

Economou, M.I. (1986): Platinum group elements (PGE) in chromite and sulphide ores within the ultramafic zone of some Greek ophiolite complexes. *In* Metalogeny of basic and ultrabasic rocks (M.J. Gallagher, R.A. Ixer, C.R. Neary and H.M. Prichard, eds.). Institute of Mining and Metallurgy, London, (441-454).

References

Edwards, S.J. (1990): Harzburgites and refractory melts in the Lewis Hills massif, Bay of Islands ophiolite complex: The base-metals and precious-metals story. *Canadian Mineralogist* **28,** 537-552.

Embrey, P.G. & Fuller, J.P. (1980): A manual of new mineral names 1892-1978. British Museum (Natural History), Oxford University Press.

Flinn, D. (1958): On the nappe structures of north-east Shetland. *Quarterly Journal of the Geological Society of London* **114,** 107-136.

Flinn, D. (1970): Some aspects of the geochemistry of the metamorphic rocks of Unst and Fetlar. *Proccedings of the Geologists' Association* **81,** 509-527.

Flinn, D. (1985): The Caledonides of Shetland. *In* The Caledonide orogen - Scandinavia and related areas (D.G. Gee and B.A. Sturt, eds.). Wiley, New York, (1159-1172).

Flinn, D., Frank, P.L., Brook, M. & Pringle, I.R. (1979): Basement-cover relations in Shetland. *In* The Caledonides of the British Isles-reviewed (A.L. Harris, C.H. Holland & B.E. Leake, eds.). Scottish Academic Press, Edinburgh, (109-115).

Forminykh, V.G. & Khvostova, V.P. (1970): Platinum content of Ural dunite. *Doklady Akademii Nauk SSSR* **191,** 185-187.

Fuchs, W.A. & Rose, A.W. (1974): The geochemical behaviour of platinum and palladium in the weathering cycle in the Stillwater complex, Montana. *Economic Geology* **69,** 332-346.

Garson, M.S. & Plant, J. (1973): Alpine type ultramafic rocks and episodic mountain building in the Scottish Highlands. *Nature Physical Science* **242,** 34-38.

Gass, I.G. (1968): Is the Troodos massif of Cyprus a fragment of Mesozoic ocean floor. *Nature* **220,** 39-42.

Gass, I.G. (1980): The Troodos massif: Its role in the unravelling of the ophiolite problem and its significance in the understanding of constructive plate margin processes. *In* Ophiolites Proceedings International Ophiolite Symposium Cyprus (A. Panayiotou, ed.). Ministry of Agriculture and Natural Resources, Geological Survey Department, Nicosia, (23-35).

Gass, I.G. (1990): Ophiolites and oceanic lithosphere. *In* Ophiolites: Oceanic Crustal Analogues Proceedings of the Symposium "Troodos 1987" (J. Malpas, E.M. Moores, A. Panayiotou, C. Xenophontos, eds). Geological Survey Department, Cyprus, (1-10).

Gass, I.G. & Smewing, J.D. (1981): Ophiolites: obducted oceanic lithosphere. *In* The Sea: 7. Oceanic lithosphere (C. Emiliani, ed.). Wiley, New York, (339-362).

Gass, I.G., Neary, C.R., Prichard, H.M. & Bartholomew, I.D. (1982): The chromite of the Shetland ophiolite. A reappraisal in the light of new theory and techniques.. A report for the Commission of European Communities. The Open University, Milton Keynes, 264 pp..

Greenbaum, D. (1977): The chromitiferous rocks of the Troodos ophiolite complex, Cyprus. *Economic Geology* **77**, 1175-1194.

Gregory, R.T. (1984): Melt percolation beneath a spreading ridge: Evidence from the Semail peridotite, Oman. *In* Ophiolites and Oceanic Lithosphere (I.G. Gass, S.J. Lippard and A.W. Shelton, eds.). Geological Society Special Publication No. 13, Blackwell Scientific Publications, Oxford, (55-62).

Gunn, A.G. (1989): Drainage and overburden geochemistry in exploration for platinum-group element mineralisation in the Unst ophiolite, Shetland, U.K. *Journal of Geochemical Exploration* **31**, 209-236.

Gunn, A.G., Leake, R.C., Styles, M.T. & Bateson, J.H. (1985): Platinum-group element mineralisation in the Unst ophiolite, Shetland.. Mineral Reconnaissance Programme Report No. 17, British Geological Survey, Keyworth. 116 pp.

Haggerty, S.E. (1976): Opaque mineral oxides in terrestrial igneous rocks . *In* Oxide Minerals (D. Rumble, III, ed.). Mineralogical Society of America Short Course Notes 3, (Hg 101-300).

Hamlyn, P.R. & Keays, R.R. (1986): Sulfur saturation and second stage melts: Application to the Bushveld platinum metal deposits. *Economic Geology* **81**, 1431-1445.

Hamlyn, P.R., Keays, R.R., Cameron, W.E., Crawford, A.J. & Waldron, M. (1985): Precious metals in magnesian low-Ti lavas: implications for metallogenesis and sulfur saturation in primary magmas. *Geochimica et Cosmochimica Acta* **49**, 1797-1811.

Heddle, M.F. (1878): The county geognosy and mineralogy of Scotland. Orkney and Shetland. *Mineralogical Magazine* **2**, 9-35.

Henderson, P. (1982): Inorganic Geochemistry. Pergamon, Oxford, 353 pp.

Hertogen, J., Janssens, M.-J. & Palme, H. (1980): Trace elements in ocean ridge basalt glasses: Implications for fractionations during mantle evolution and petrogenesis. *Geochimica et Cosmochimica Acta* **44**, 2125-2143.

Hey, M.H. (1975): An index of mineral species and varieties arranged chemically with an alphabetical index of accepted mineral names and synonyms. British Museum (Natural History), London.

Hibbert, S. (1821): Discovery of chromate of iron in Shetland. *Transactions of the Society for the encouragement of Arts, Manufacture and Commerce* **38**, 23-26.

Hitchen, C.S (1929): Unst and its chromite deposits. *Mining Magazine* **40**, 18-24.

Hulbert, L.J., Duke, J.M., Eckstrand, O.R., Lydon, J.W., Scoates, R.F.J. & Cabri, L.J. (1988): Geological environments of the platinum-group elements. Geological Survey of Canada Open File 1440, 148 pp.

Ixer, R.A. & Prichard, H.M. (1989): The mineralogy and paragenesis of Pt, Pd, Au and Ag-bearing assemblages at Cliff, Shetland. *Bulletin of the Geological Society of Finland* **61**, 40 (abstract).

Jen, Y.-C. & Teng, Y.-J. (1973): Isomorphous system RuS2-OsS2-IrS2 and the mineral system PdS-PtS. *Geochimica* **4**, 254-263.

Johan, Z. & Augé, T. (1986): Ophiolitic mantle sequences and their evolution: mineral chemistry constraints. *In* Metalogeny of basic and ultrabasic rocks (M.J. Gallagher, R.A. Ixer, C.R. Neary and H.M. Prichard, eds.). Institute of Mining and Metallurgy, London, (305-318).

Keays, R.R., Nickel, E.H., Groves, D.I. & McGoldrick, P.J. (1982): Iridium and palladium as discriminants of volcanic-exhalative, hydrothermal, and magmatic nickel sulfide mineralisation. *Economic Geology* **77**, 1535-1547.

Keith, T.E.C & Foster, H.L. (1973): Basic data on the ultramafic rocks of the Eagle quadrangle, east-central Alaska. U.S. Geological Survey open-file report, 4 sheets.

Khvostova, V.P., Golvnya, S.V., Chernysheva, N.V. & Bukhanova, A.I. (1976): Distribution of the platinum group metals in chromite ores and ultramafic rocks of the Raz-Iz massif (Polar Urals). *Geochemistry International* **13**, 35-39.

Kullerud, G. (1963): The Fe-Ni-S system. *Carnegie Institute Washington, Yearbook* **62**, 175-189.

Leake R.C. & Gunn, A.G. (1986): Exploration for platinum-group element mineralisation in the Unst ophiolite complex, Shetland. *In* Geology in the real world- the Kingsley Dunham volume (R.W. Nesbitt and I. Nichol, eds.). Institute of Mining and Metallurgy, London, (253-266).

Leblanc, M. & Fischer, W. (1989): Noble metals in cobalt-arsenide ores: Hydrothermal concentration from a serpentinite source-rock (Bou-Azzer, Morocco). *Bulletin of the Geological Society of Finland* **61**, 36 (abstract).

Legendre, O. (1982): Minéralogie et géochimie des platinoids dans les chromitites ophiolitiques. Comparaison avec d'autres types de concentrations en platinoides. Thèse de doctorat de troisième cycle, Université de Paris, France 171 pp.

Legendre, O. & Johan, Z. (1981): Minéralogie des platinoides dans les chromites massives de séries ophiolitiques.. Rapport Annuel d'Activité CNRS Juillet 1980-Juillet 1981, 32-33.

Loney, R.A., Himmelberg, G.R. & Coleman, R.G. (1971): Structure and petrology of the alpine-type peridotite at Burro Mountain, California, U.S.A.. *Journal of Petrology* **12,** 245-309.

Lorand, J.P. & Pinet, M. (1984): L'orcelite des péridotites de Beni Bousera (Maroc), Ronda (Espagne), Table Mountain et Blow-Me-Down Mountain (Terre-Neuve) et du Pinde septentrional (Grèce). *Canadian Mineralogist* **22,** 553-560.

Lord, R.A. & Prichard, H.M. (1989): An igneous source for gold in the Shetland ophiolite. *Transactions of the Institution of Mining and Metallurgy (Section B: Applied earth science)* **98,** B44-46 (abstract).

Lord, R.A. & Prichard, H.M. (1989b): Magmatic fractionation of PGE in the Shetland ophiolite complex. *Bulletin of the Geological Society of Finland* **61,** 38 (abstract).

McCallum, M.E., Loucks, R.R., Carlson, R.R., Cooley, E.F. & Doerge, T.A. (1976): Platinum metals associated with hydrothermal copper ores of the New Rambler mine Medicine Bow Mountains, Wyoming. *Economic Geology* **71,** 1429-1450.

McElduff, B. & Stumpfl, E.F. (1990): Platinum-group minerals from the Troodos ophiolite, Cyprus. *Mineralogy and Petrology* **42,** 211-232.

Menzies, M.A. & Allen, C. (1974): Plagioclase lherzolite residual mantle relationships within two eastern Mediterranean Ophiolites. *Contributions to Mineralogy and Petrology* **45,** 197-213.

Mihálik, P., Jacobsen, J.B.E. & Hiemstra, S.A. (1974): Platinum-group minerals from a hydrothermal environment. *Economic Geology* **69,** 257-262.

Miller, J.A. & Flinn, D. (1966): A survey of the age relations of Shetland rocks. *Geological Journal* **5,** 95-116.

Moring, B.C., Page, N.J. & Oscarson R.L. (1988): Platinum-group element mineralogy of the Pole Corral podiform chromite deposit, Rattlesnake Creek Terrane, northern California. *In* Geo-Platinum 87 (H.M. Prichard, P.J. Potts, J.F.W. Bowles & S.J. Cribb, eds.). Elsevier, London, (257-258) (abstract).

Montain, B.W. & Wood, S.A. (1988): Solubility and transport of platinum-group elements in hydrothermal solutions: thermodynamic and physical chemistry constraints. *In* Geo-Platinum 87 (H.M. Prichard, P.J. Potts, J.F.W. Bowles & S.J. Cribb, eds.). Elsevier, London, (57-82).

Murton, B.J. (1986): Anomalous oceanic lithosphere formed in a leaky transform fault: evidence from the Western Limassol Forest Complex, Cyprus. *Journal of the Geological Society of London* **143,** 845-854.

Murton, B.J. (1989): Tectonic controls on boninite genesis. *In* Magmatism in the Ocean Basins (A.D. Saunders & M.J. Norry, eds.), *Geological Society Special Publication No.* **42,** 347-377.

Naldrett, A.J. (1981): Platinum-group element deposits. *In* Platinum-Group Elements; Mineralogy, Geology, Recovery (L.J. Cabri, ed.), *Canadian Institute of Mining and Metallurgy Special Volume* **23**, 197-232.

Naldrett, A.J. & Barnes, S.-J. (1986): The behaviour of platinum group elements during fractional crystallisation and partial melting with special reference to the composition of magmatic sulphide ores. *Fortschritte der Mineralogie* **64**, 113-133.

Naldrett, A.J. & Cabri, L.J. (1976): Ultramafic and related mafic rocks: Their classification and genesis with special reference to the concentration of nickel sulphides and platinum-group elements. *Economic Geology* **71**, 1131-1158.

Naldrett, A.J. & Duke, J.M. (1980): Platinum metals in magmatic sulphide ores. *Science* **208**, 1417-1424.

Naldrett, A.J., Hoffman, E.L., Green, A.H., Chou, C.-L. & Naldrett, S.R. (1979): The composition of Ni-sulfide ores, with particular reference to their content of PGE and Au. *Canadian Mineralogist* **17**, 403-415.

Neary, C.R. (1974): Chromitiferous ultrabasic rocks in the northern Hijaz of Saudi Arabia. Unpublished Ph.D. thesis, University of Leeds 380 pp.

Neary, C.R. & Brown, M.A. (1979): Chromite from the Al'Ays complex, Saudi Arabia, and the Semail complex, Oman. *In* Evolution and mineralisation of the Arabian Shield (A.M.S. Al-Shianti, ed.), *I.A.G. Bulletin* **2**, 193-205.

Neary, C.R. & Prichard, H.M. (1985): Molybdenum mineralisation on Unst, Shetland Isles. *Scottish Journal of Geology* **21**, 197-204.

[Neary, C.R., Prichard, H.M. & Potts, P.J.] (1984): Chromite, platinoids, gold and moly in the Shetlands. *In* Panorama (anon.). *Mining Magazine* **151**, 559-560.

Nilsson, L.P. (1990): Platinum-group mineral inclusions in chromitite from the Osthammeren ultramafic tectonite body, south central Norway. *Mineralogy and Petrology* **42**, 249-263.

Oshin, I.O. (1981): The abundances and geochemistry of some noble metals in Thetford Mines ophiolites, P. Q. Unpublished Ph.D. thesis, McMaster University, 391 pp.

Oshin, I.O. & Crocket, J.H. (1982): Noble metals in Thetford Mines ophiolites, Quebec, Canada. Part I: Distribution of gold, iridium, platinum, and palladium in the ultramafic and gabbroic rocks. *Economic Geology* **77**, 1556-1570.

Oshin, I.O. & Crocket, J.H. (1986): Noble metals in Thetford Mines ophiolites, Quebec, Canada. Part II: Distribution of gold, silver, iridium, platinum, and palladium in the Lac de l'Est volcano-sedimentary section. *Economic Geology* **81**, 931-945.

Page, N.J. (1969): Platinum content of ultramafic rocks. *In* U.S Geological Survey Heavy Metals Program, Progress Report 1968 - Topical Studies. U.S. Geological Survey Circular 622, (5).

Page, N.J. & Talkington, R.W. (1984): Palladium, platinum, rhodium, ruthenium and iridium in peridotites and chromitites from ophiolite complexes in Newfoundland. *Canadian Mineralogist* **22**, 137-149.

Page, N.J., Johnson, M.G., Haffty, J. & Ramp, L. (1975): Occurence of platinum-group metals in ultramafic rocks of the Medford-Coos Bay 2° quadrangles, southwestern Oregon. U.S. Geological Survey Miscellaneous Field Studies Map MF-694.

Page, N.J., Rowe, J.J. & Haffty, J. (1976): Platinum metals in the Stillwater complex, Montana. *Economic Geology* **71**, 1352-1363.

Page, N.J., Engin, T. & Haffty, J. (1979a): Palladium, platinum, and rhodium concentrations in mafic and ultramafic rocks from the Kizildag and Guleman areas, Turkey and the Faryab and Esfandagheh-Abdasht areas, Iran. U.S. Geological Survey Open-File Report 79-840.

Page, N.J., Pallister, J.S., Brown, M.A., Smewing, J.D. & Haffty, J. (1979b): Platinum-group metals in chromite-rich rocks from two traverses through the Semail ophiolite, Oman. *American Geophysical Union Transactions* **60**, 963 (abstract).

Page, N.J., Haffty, J. & Ahmad, Z. (1980): Palladium, platinum, and rhodium concentrations in mafic and ultramafic rocks from the Zhob Valley and Dargai complexes, Pakistan. *In* Shorter Contributions to Mineralogy and Petrology, 1979. U.S. Geological Survey Proffesional Paper 1124-F (F1-F6).

Page, N.J., Cassard, D. & Haffty, J. (1982a): Palladium, platinum, rhodium, ruthenium, and iridium in chromitites from the Massif du Sud and Tiébaghi Massif, New Caledonia. *Economic Geology* **77**, 1571-1577.

Page, N.J., Pallister, J.S., Brown, M.A., Smewing, J.D. & Haffty, J. (1982b): Palladium, platinum, rhodium, iridium, and ruthenium in chromite-rich rocks from the Samail ophiolite, Oman. *Canadian Mineralogist* **20**, 537-548.

Page, N.J., Aruscavage, F.J. & Haffty, J. (1983): Platinum-group elements in rocks from the Voikar-Syninsky ophiolite complex, Polar Urals, U.S.S.R. *Mineralium Deposita* **18**, 443-455.

Page, N.J., Engin, T., Singer, D.A. & Haffty, J. (1984): Distribution of platinum-group elements in the Bati Kef chromite deposit, Guleman-Elazig area, eastern Turkey. *Economic Geology* **79**, 177-184.

Pearce, J.A. (1980): Geochemical evidence for the genesis and eruptive setting of lavas from Tethyan ophiolites. *In* Ophiolites Proceedings International Ophiolite Symposium Cyprus (A. Panayiotou, ed.). Ministry of Agriculture and Natural Resources, Geological Survey Department, Nicosia, (261-272).

References

Pearce, J.A., Alabaster, T., Shelton, A.W. and Searle, M.P. (1981): The Oman ophiolite as a Cretaceous arc-basin complex: Evidence and implications. *Philosophical Transations Royal Society London A* **300**, 299-317.

Pearce, J.A., Lippard, S.J. & Roberts, S. (1984): Characteristics and tectonic significance of supra-subduction zone ophiolites. *In* Marginal Basin Geology (B.P. Kokelaar and M.F. Howells, eds.). Blackwell Scientific Publications, Oxford (77-94).

Philips, F.C. (1927): The serpentinites and associated rocks and minerals of the Shetland Islands. *Quarterly Journal of the Geological Society of London* **41**, 358-367.

Potts, P.J. (1984): Neutron activation-induced beta autoradiography as a technique for locating minor phases in thin section: Application to rare earth element and platinum-group element mineral analysis. *Economic Geology* **79**, 738-747.

Potts, P.J. (1986): Neutron activation induced beta autoradiography as a technique for locating minor phases in thin section: Emulsion response characteristics. *Materials Science Forum* **7**, 35-44.

Potts, P.J. (1987): A handbook of silicate rock analysis. Blackie & Sons, London, 622 pp.

Potts, P.J. & Prichard, H.M. (1986): Mineralogical applications of neutron activation-induced beta autoradiography: the search for gold mineralisation in thin section.. *In* Metalogeny of basic and ultrabasic rocks (M.J. Gallagher, R.A. Ixer, C.R. Neary and H.M. Prichard, eds.). Institute of Mining and Metallurgy, London, (455-465).

Potts, P.J., Webb, P.C. & Watson, J.S. (1984): Energy dispersive x-ray fluorescence analysis of silicate rocks for major and trace elements. *X-ray Spectrometry* **13**, 2-15.

Potts, P.J., Williams Thorpe, O., Isaacs, M.C. & Wright, D.W. (1985): High-precision instrumental neutron-activation analysis of geological samples employing simultaneous counting with both planar and coaxial detectors. *Chemical Geology* **48**, 145-155.

Prichard, H.M. (1985): The Shetland ophiolite. *In* The Caledonide orogen - Scandinavia and related areas (D.G. Gee and B.A. Sturt, eds.). Wiley, New York, (1173-1184).

Prichard, H.M. & Lord, R.A. (1988): The Shetland ophiolite: evidence for a supra-subduction zone origin and implications for platinum-group element mineralisation. *In* Mineral Deposits within the European Community (J. Boissonnas and P. Omenetto, eds.). *Special Publication No.6 of the Society for Geology Applied to Mineral Deposits*, Springer-Verlag, Berlin, (289-302)

Prichard, H.M. & Lord. R.A. (1989): Magmatic and secondary PGM in the Shetland ophiolite complex. *Bulletin of the Geological Society of Finland* **61**, 39 (abstract).

Prichard, H.M. & Lord, R.A. (1990): Platinum and palladium in the Troodos ophiolite complex, Cyprus. *Canadian Mineralogist* **28**, 607-617.

Prichard, H.M. & Neary, C.R. (1981): Chromite in the Shetland Islands ophiolite complex.. *In* An international symposium on metalogeny of mafic and ultramafic complexes (1980). UNESCO, Athens, (343-360).

Prichard, H.M. & Neary, C.R. (1982): Some observations on chromite in Shetland ophiolite complex. *Ofioliti* **2**, 455-465.

Prichard, H.M. & Tarkian, M. (1988): Platinum and Palladium minerals from two PGE-rich localities in the Shetland ophiolite. *Canadian Mineralogist* **26**, 979-990.

Prichard, H.M., Potts, P.J. & Neary, C.R. (1981): Platinum group element minerals in the Unst chromite, Shetland Isles. *Transactions of the Institute of Mining and Metallurgy (Section B: Applied earth science)* **90**, 186-188.

[Prichard, H.M., Potts, P.J. & Neary, C.R.] (1984): Platinum and gold in the Shetland ophiolites. *In* Industry in action: Exploration (anon.). *Mining Journal* **303**, 77.

Prichard, H.M., Neary, C.R. & Potts, P.J. (1986): Platinum group minerals in the Shetland ophiolite. *In* Metalogeny of basic and ultrabasic rocks (M.J. Gallagher, R.A. Ixer, C.R. Neary and H.M. Prichard, eds.). Institute of Mining and Metallurgy, London, (395-414).

Prichard, H.M., Potts, P.J., Neary, C.R., Lord, R.A. & Ward, G.R. (1989): Developement of techniques for the determination of the platinum-group elements in ultramafic rock complexes of potential economic significance: Mineralogical studies.. European Communities Commission report EUR 11631, Luxembourg, 163 pp.

Rajamani, V. & Naldrett, A.J. (1978): Partitioning of Fe, Co, Ni, and Cu between sulfide liquid and basaltic melts and the composition of Ni-Cu sulfide deposits. *Economic Geology* **73**, 82-93.

Ramdohr, P. (1967): A widespread mineral association, connected with serpentinisation. *Neues Jahrbuch fur Mineralogie Abhandlungen* **107**, 241-265.

Reed, H.H. (1934): The metamorphic geology of Unst, in the Shetland Islands. *Quarterly Journal of the Geological Society of London* **90**, 637-628.

Read, H.H. (1936): The metamorphic history of Unst, Shetland. *Proceedings of the Geological Association of London* **47**, 283-293.

Rivington, J.B. (1953): Recent chromite exploration in Shetland. *Mining Magazine* **89**, 329-337.

Roberts, S. (1986): The role of igneous processes in the formation of ophiolitic chromitite. Unpublished Ph.D. thesis, The Open University 261 pp.

Rowell, W.F. & Edgar, A.D. (1986): Platinum-group element mineralisation in a hydrothermal Cu-Ni sulfide occurrence, Rathbun Lake, northeastern Ontario. *Economic Geology* **81,** 1272-1277.

Shannon, R.D. (1976): Revised effective ionic radii and systematic studies of interatomic distances in halides and chalcogenides. *Acta Crystallographica A* **32,** 751-767.

Shannon, R.D. & Prewitt, C.T. (1969): Effective ionic radii in oxides and fluorides. *Acta Crystallographica B* **25,** 925-946.

Shannon, R.D. & Prewitt, C.T. (1970): Revised values of effective ionic radii. *Acta Crystallographica B* **26,** 1046-1048.

Spray, J.G. (1988): Thrust-related metamorphism beneath the Shetland Islands oceanic fragment, northeast Scotland. *Canadian Journal of Earth Sciences* **25,** 1760-1776.

Steel, T.W., Levin, J. & Copelowitz, I. (1975): Preparation and certification of a reference sample of a precious metal ore. Report No. 1696 of the National Institute for Metallurgy, Johannesburg, RSA.

Stevens, R.E. (1944): Composition of some chromites of the western hemisphere. *American Mineralogist* **26,** 1-34.

Stockman, H.W. & Hlava, P.F. (1984): Platinum-group minerals in alpine chromitites from southwestern Oregon. *Economic Geology* **79,** 491-508.

Stumpfl, E.F. (1962): Some aspects of the genesis of platinum deposits. *Economic Geology* **57,** 619-623.

Stumpfl, E.F. & Tarkian, M. (1976): Platinum genesis: New mineralogical evidence. *Economic Geology* **71,** 1451-1460.

Talkington, R.W. (1981): The geology, petrology, and petrogenesis of the White Hills Peridotite, St. Anthony Compex, northwestern Newfoundland. Unpublished Ph.D. thesis, Memorial University of Newfoundland, St. John's.

Talkington, R.W. & Watkinson, D.H. (1984): Trends in the distribution of the precious metals in the Lac-des-Iles complex, northwestern Ontario. *Canadian Mineralogist* **22,** 125-136.

Talkington, R.W. & Watkinson, D.H. (1986): Whole rock platinum-group element trends in chromite-rich rocks in ophiolitic and stratiform igneous complexes. *In* Metalogeny of basic and ultrabasic rocks (M.J. Gallagher, R.A. Ixer, C.R. Neary and H.M. Prichard, eds.). Institute of Mining and Metallurgy, London, (427-440).

Tanguay, S., Hérbert, R. & Bergeron, M. (1990): Distribution of PGE in pyroxene-bearing ultramafic cumulates in the Thetford Mines ophiolitic complex, Quebec. *Canadian Mineralogist* **28,** 597-605.

Tarkian, M. & Prichard, H.M. (1987): Irarsite-hollingworthite solid-solution series and other associated Ru-, Os-, Ir-, and Rh-bearing PGMs from the Shetland ophiolite complex. *Mineralium Deposita* **10,** 71-85.

Thalhammer, O.A.R., Prochaska, W. & Mühlhans, H.W. (1990): Solid inclusions in chrome-spinels and platinum group element concentrations from the Hochgrössen and Kraubath ultramafic massifs (Austria): Their relationships to metamorphism and serpentinisation. *Contributions to Mineralogy and Petrology* **105,** 66-80.

Thayer, T.P. (1960): Some critical differences between Alpine-type and stratiform peridotite-gabbro complexes. 21st International Geological Congress, Copenhagen 1960, Report (13), 247-259.

Thayer, T.P. (1969): Gravity differentiation and magmatic re-emplacement of podiform chromite deposits. *In* Magmatic Ore Deposits (H.D.B. Wilson, ed.), *Economic Geology Monograph* **4,** 132-146.

Thayer, T.P. (1970): Chromite segregations as petrogenetic indicators. *In* Symposium on the Bushveld Igneous Complex and other Layered Intrusions (Visser and von Gruenewaldt eds.) *Geological Society of South Africa, Special Publication* **1,** 380-390.

Ulmer, G.C. (1974): Alteration of chromite during serpentinisation in the Pennsylvania-Maryland district. *American Mineralogist* **59,** 1236-1241.

Von Gruenewaldt, G. (1977): The mineral resources of the Bushveld complex. *Minerals Science Engineering* **9,** 83-95.

Westland, A.D. (1981): Inorganic chemistry of the platinum-group elements. *In* Platinum-Group Elements; Mineralogy, Geology, Recovery (L.J. Cabri, ed.), *Canadian Institute of Mining and Metallurgy Special Volume* **23,** 5-18.

White, R.W., Motta, J. & Araújo, V.A. de (1971): Platiniferous chromitite in the Tocantins complex, Niquelândia, Goiás, Brazil. U.S. Geological Survey Professional Paper 750-D, (D26-D33).

Whittaker, E.J.W. & Muntus, R. (1970): Ionic radii for use in geochemistry. *Geochimica et Cosmochimica Acta* **34,** 945-956.

Whittaker, P.J. & Watkinson, D.H. (1985): Platinum-group minerals from chromitite in alpine-type peridotite of the Cache Creek group, British Columbia. *Canadian Mineralogist* **23,** 320 (abstract).

Williams, H. & Smyth, W.R. (1973): Metamorphic aureoles beneath ophiolite suites and alpine peridotites: Tectonic implications with west Newfoundland examples. *American Journal of Science* **273,** 594-621.

References

Wylie, A.G., Candela, P.A. & Burke, T.M. (1987): Compositional zoning in an unusual Zn-rich chromite from the Sykesville district of Maryland and its bearing on the origin of "ferritchromit". *American Mineralogist* **72,** 413-422.

Yu, T. & Chou, H. (1979): Ruarsite, a new mineral. *Science Bulletin (Ko'Hsueh Tu'ng Pao)* **24,** 310-316.

ENCLOSURES